THE INFLUENCE OF FABRICATION EFFECTS ON THE STRENGTH OF FIRED CLAY PRODUCTS

Vedananda Tilakasiri Loku Bogahawatta
B.Sc. (Ceylon), B.Sc. (Sheffield), M.Sc. (London), M.I.Ceram.

A thesis submitted for the degree of Doctor of Philosophy of the University of London

Geomaterials Unit, School of Engineering, Queen Mary and Westfield College

University of London

July 1990

Text cut off in original

ABSTRACT

A study has been made of the enhancement of the mechanical strength of bricks fabricated from five Sri Lankan Quaternary and post-Quaternary brick clays with the objective of identifying and optimising those factors which control the quality and performance characteristics of fired clay products of this type.

Mineralogical investigations have shown that the clays are predominantly kaolinitic. Of the accessory minerals, feldspars and gibbsite are the chief constituents.

The experimental programme involved the development of feasible processing techniques for clay bodies, the establishment of optimum heat treatments for their firing, and the testing and evaluation of material properties of the fired products. The microstructures of fired materials have been characterized using optical and electron microscopical techniques, as well as X-ray diffraction, electron probe microanalysis and chemical analysis. A limited study was also made of the durability of laboratory fired specimens. Methods of strength enhancement included use of the reactions of phosphates with natural clays, use of mineralizers to induce mullitization and surface coating by an efflorescence process.

A kinetic analysis based on the first order kinetics is proposed for the estimation of optimum firing conditions for kaolinitic clays.

The study has shown that surface coating of bricks increases the load at the elastic limit by up to 30% and the ultimate failing load by 19% in the clays examined. The measured increases in modulus of rupture and modulus of elasticity are over 33% and 40% respectively.

A fabrication technique which requires the incorporation of phosphates has been developed. This provides the possibility of lowering the peak temperature of firing to 500°C. Flexural strength increase of up to 60% over the normally fired unbonded specimens can be achieved using this technique. Relevant compatibility relations in the ternary system SiO_2-P_2O_5-Al_2O_3 at 500°C are proposed.

The presence of an optimum amount of mineralizer in a clay body may alter its sintering characteristics resulting in an increase in modulus of rupture up to 55%. However, uncontrolled additions exceeding 4 wt% cause deleterious effects. Microstructural analysis provides evidence that liquid phase sintering, development of mullite, development of pores and bloating are the dominant strength determining features in these clays. An empirical equation correlating the functional relation between modulus of rupture, mullite content and porosity is proposed. Mechanisms of strength development are discussed in the light of these findings.

ACKNOWLEDGEMENTS

I wish to express my deep appreciation to the British Council for the award of a scholarship to carry out this programme of research. I wish to thank my supervisor Dr.A.B. Poole for his support and guidance and Prof.P.G. Fookes for the inspiration to undertake this study.

I am indebted to members of the staff of the Geomaterials Unit, particularly Kevin Schrapel, Chris Mole, Archie McLachlan and Stuart Adams for valuable discussion and help. The assistance given by Anne Austen is also thankfully acknowledged.

In conclusion I wish to thank my wife, Sumana, and my daughter, Manique, for their continued patience, encouragement and assistance throughout my years of study.

CONTENTS

LIST OF TABLES

LIST OF FIGURES

LIST OF PLATES

CHAPTER 1

INTRODUCTION

1.1 GENERAL CONSIDERATIONS

Clay bricks have a long history of use worldwide in a diverse range of climates. They have a range of strengths and durabilities depending upon the clay from which they are made and their process of manufacture.

Poor transport facilities available in many areas limited the early brick industry to indigenous materials and to craftsmen, whose experience with these materials was handed down over the years. Today's transport system and technology has improved the situation but the evaluation and processing of clay resources still require careful consideration in brickmaking in order to create lasting and durable buildings. Today brick has increasingly become an important load bearing material. This necessitates widely different properties in bricks according to their intended use but in every case one of the most important quality criteria is their strength.

The specific factors affecting the strength of ceramic materials can be grouped into two broad categories; those that are the result of the preparation and manufacturing techniques, and those that pertain to the type of applied loading and operating environment of the component. In evaluating the performance of the structural components, the first category has a strong influence on their fracture characteristics, while the other has only a secondary influence on strength.

Increasing interest in the use of ceramics as engineering materials has led to a large number of investigations on relatively pure ceramics. Commercial, multiphase clay bricks, however, constitute a much more complex problem particularly since the behaviour of less pure brick clays is only partially known and is not fully understood. Consequently few workers have attempted to investigate the material properties of these structural clay

products in a similar manner. In many instances, methods based on experience provided solutions to industrial problems.

If we wish to understand the behaviour of bricks in service and to make maximum use of their potential as a structural material, a systematic approach must be made to the assessment of properties of raw materials and products. Only then can appropriate steps be taken to optimise the use of clay and associated energy resources.

1.2 CURRENT PROBLEMS

By far the greater proportion of the clay bricks produced in Sri Lanka is used in cottage and low-rise type of construction. Structural brickwork failed to win a wider acceptance in the building industry for the following reasons.

(i). Bricks are too variable in their properties to be relied upon as a structural material. Wide variability results from both non uniformity in firing and of the raw materials.

(ii). The present criteria of acceptability require conformity with Sri Lankan standard specifications (SLS 39:1978-Specification for Common Burnt Clay Building Bricks). While these standards set forth strength requirements, no durability criteria are proposed at the present time. In situations where durability is of prime concern, necessary guidelines are usually inferred from compressive strength data. Consequently the lack of a standard basis to remove faulty bricks from sale is the prime reason why occurrence of durability failures persist, particularly in structures exposed to the weather.

(iii).Compressive strength of bricks manufactured by the cottage industry is very low and the vast majority of bricks do not satisfy the standard strength requirements. Use of inappropriate processing techniques together with scant attention to the optimising of materials and processing

conditions greatly contribute to the generally poor quality of bricks.

(iv). Fuel wood, once available in abundance is used almost exclusively in the cottage brick industry. But as wood supplies dwindle, brickmakers are inclined to low temperature firing aimed at conserving fuel at the expense of quality, notably the strength.

1.3 SCOPE OF INVESTIGATION

General concern within the brick industry has highlighted the need for research into cost-effective methods of improving the strength of clay products and related energy conservation considerations. The question which arises is how far it is possible to influence the sintering behaviour in local clays by changing the body composition so that the desired properties in the ceramic body, particularly the strength, are improved or are obtained at lower firing temperatures. The means of achieving this objective remains obscure as a result of the limited research concerning the relationship between raw material properties and the fired structures of tropical soils.

This research study was designed to investigate the intrinsic properties of Sri Lankan brick clays in order to gain a better insight into their behaviour in relation to strength development in fabrication. Particular emphasis has been placed on the following issues.

(i). The establishment of optimum firing conditions required to obtain a technically acceptable product.

(ii). The effect of firing on the physical and mechanical properties of clays.

(iii).The changes in internal morphology, microstructure, mineralogy and constitution of clays on firing.

(iv). Relationship between mechanical strength, porosity and mullite content of the fired product.

(v). The possibility of improving strength by the development of a surface coating on clay products.

(vi). The influence of mineralizers on the material properties, constitution, extent of vitrification and strength development of fired clay products.

(vii).The use of the reactions of phosphates with clay minerals for low-temperature strengthening of clay products.

The research project was concerned with five brick clays of diverse origin representative of five soil groups from wet and intermediate zones of Sri Lanka.

The information developed through the study is aimed at providing a basis for the design of raw material mixtures and processes to give desired firing characteristics of the clay products. The strategies devised are intended for the application of cost-effective techniques for the improvement of the materials performance and bulk material strength of clay products.

CHAPTER 2
REVIEW OF LITERATURE

2.1 BACKGROUND

Clay bricks must compete with other structural materials such as concrete in load-bearing applications. In such instances, selection criteria are usually based on properties such as strength, toughness, unit weight, durability and other considerations such as relative cost and ease of handling.

One of the serious drawbacks of clay products compared to other materials is their brittleness, that is, their susceptibility to catastrophic failure. Bricks like concrete, are strong in compression but weak in tension and as such are used in the construction industry in situations where the tensile strength is of secondary importance. In applications which preclude the use of bricks, reinforced concrete of acceptable tensile characteristics is commonly used. Although failure load of brickwork does not depend on the strength of the brick component alone, its mechanical properties are contributory to overall stability.

According to Davidge and Evans (1970), although there appears little that can be done to improve the toughness of conventional ceramics, they can be strengthened. However, the literature deals mostly with ceramics which involve relatively pure materials. Methods of increasing strength of fired clay products based on natural less pure clays have received little attention in the past. Nevertheless in the manufacture of such products the high cost of raw material selection and adjustment have made processing techniques a major concern. Therefore, it is essential to elucidate the strength concepts and also fabrication effects controlling the mechanical strength of clayware ceramics.

CHAPTER 2

2.2 FACTORS AFFECTING THE STRENGTH OF CLAYWARE CERAMICS

The factors, cited in the literature, which are most likely to contribute to the strength developed by a clay body in the fired condition may be grouped into two broad categories; those that are the result of the forming techniques and those that pertain to the type of applied loading and operating environment of the structural component (Weil 1963). Designating the first group as "fabrication effects" and the other as "environmental and stressing effects", the important factors that fall into the two categories can be listed as follows.

2.2.1 Fabrication effects

(i). Grain size of the raw materials
(ii). Porosity
(iii).Mullite formation
(iv). Composition and sintering additives
(v). Surface condition
(vi). Heat treatment
(vii).Texture

2.2.2 Environmental and stressing effects

(i). Atmospheric environment
(ii). Imposed temperatures
(iii).Rate of loading (static/cyclic)
(iv). State of stressing (uniaxial/biaxial)
(v). Stress gradients

The fabrication effects develop a texture (micro-structure) upon which the fracture strength and other properties of the fired product intrinsically depend. The microstructure thus represents a key feature which links fabrication and properties of clay products. Fig. 2.1 indicates some of the important textural features which are controlled by the fabrication effects and that affect both the flow stress and fracture stress of the material.

The present investigation was concerned mainly with the fabrication effects. Some of the most important of these effects are reviewed in the ensuing text and are considered in the order given above.

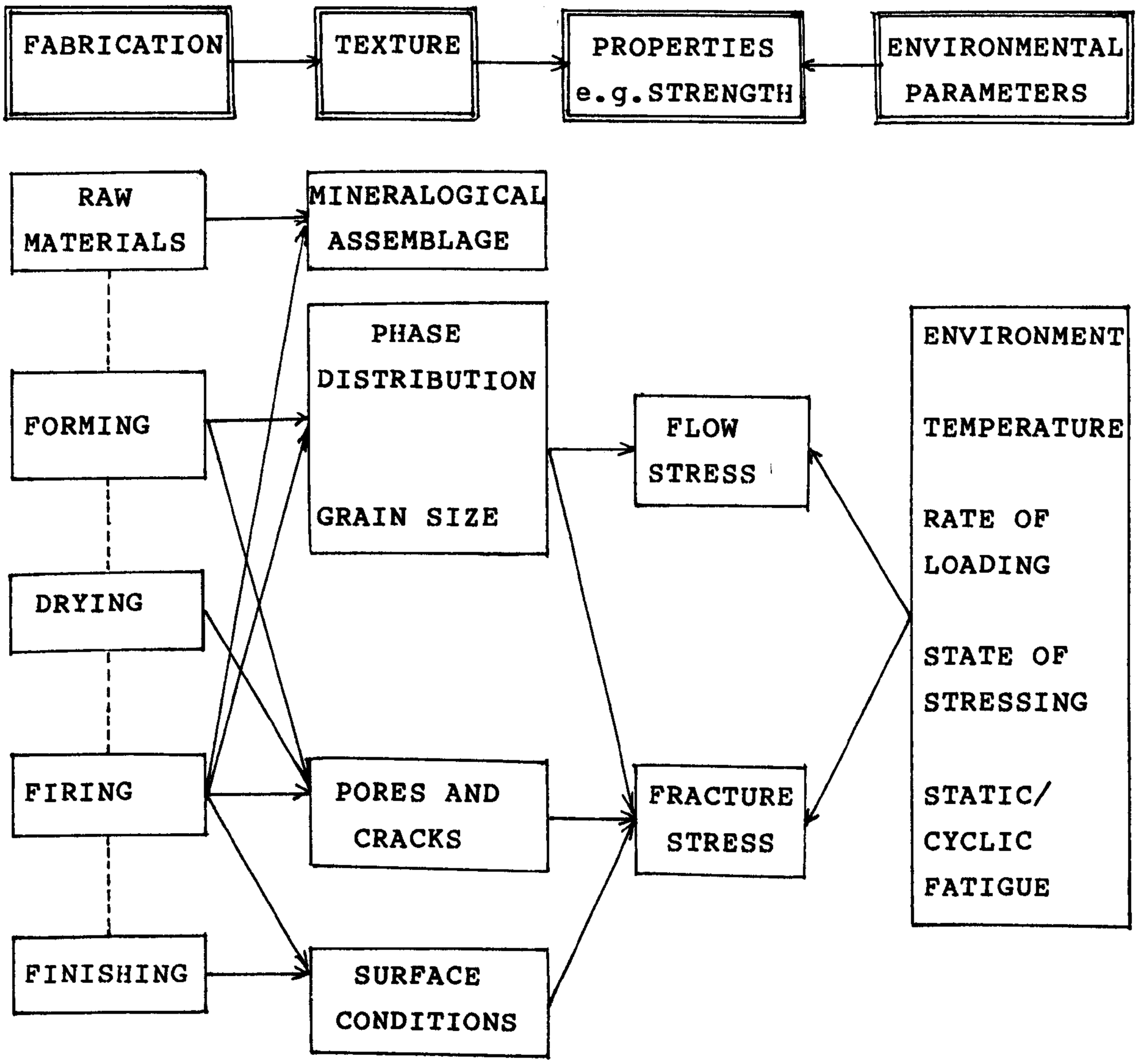

Fig. 2.1-The interrelationships between effects and features affecting strength.

2.3 THE CONCEPTS OF STRENGTH AND FRACTURE

The strength of any material represents the net balance between the attractive and repulsive forces exerted between its atoms. At rest the net interatomic force acting between two adjacent atomic planes in a crystal is zero. As tension is applied, the repulsive forces diminish more rapidly than the attractive forces; therefore, the net interatomic force balancing the applied external load will increase to a maximum and then decreases as shown in Fig. 2.2.

CHAPTER 2

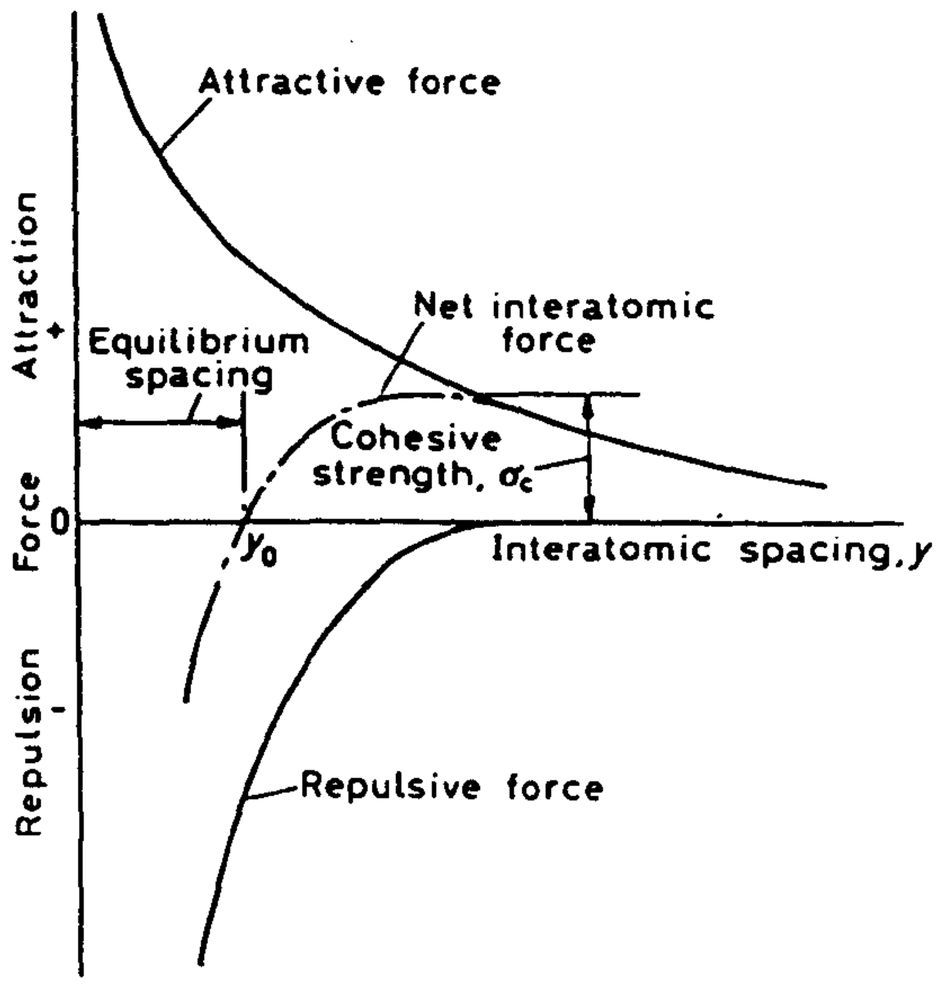

Fig. 2.2-Variation of interatomic forces with atomic distances.

On an atomistic level, fracture occurs when the interatomic forces or bonds between the atoms in a material are stretched past the maximum. The fracture strength or stress required for fracture (σ_c) can be calculated from a knowledge of the nature of the stress-displacement (net strength) curve. For this purpose, the stress-displacement curve is usually approximated to a sine curve having a wave length a as shown in Fig. 2.3 (Uhlman and Kreidl 1980).

The corresponding expression derived for the fracture strength is of the form:

$$\sigma_c = (E\gamma_s/a_o)^{\frac{1}{2}}$$

Where E is the Young's modulus, γ_s is the surface energy and a_o is the equilibrium atomic energy.

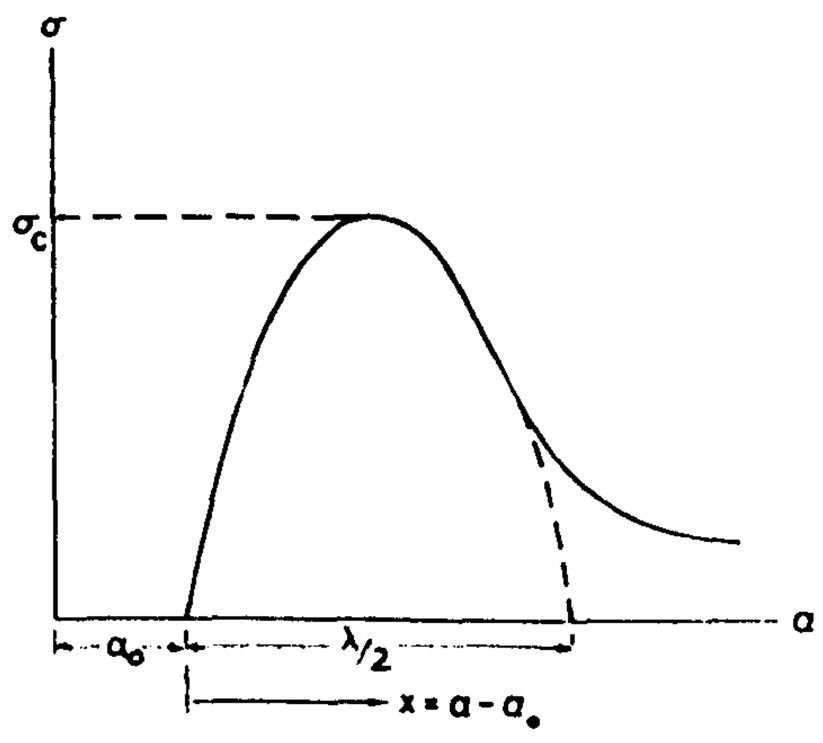

Fig. 2.3-Stress required to separate atomic planes: a_o is the equilibrium separation at zero stress.

However, strengths of common ceramic materials are 10-100 times lower than the value calculated using the above equation. This discrepancy is considered to be due to the presence of processing-induced flaws. These defects usually occur in the form of small surface cracks. The intensification of the applied load by such flaws was shown to lead to stresses of 10^4 MPa or greater in the vicinity of the crack tip.

Inglis (1913) showed that when a load is placed on a structure a stress concentration is produced at a crack tip. He demonstrated that the maximum tensile stress at the tip of an elliptical crack, having length 2c and minor axis 2h is given by

$$\sigma_{max} = \sigma \left[1 + (2c/h) \right] ,$$

σ = applied stress

σ_c = fracture stress

When $\sigma_{max} = \sigma_c$, crack growth will occur. This means that cracks will propagate, and fracture will occur at much lower applied stresses than those theoretically required.

CHAPTER 2

Griffith (1921), working with glass rods, calculated the elastic energy stored in the vicinity of an elliptical flaw oriented with the major axis perpendicular to the applied stress and determined the decrease of this energy with increasing flaw size. Equating this decrease of elastic energy with energy needed to form the fracture surface resulted in the critical stress, that is, macroscopic strength, σ , required for failure. For a flat plate containing an elliptical flaw the expression for σ becomes:

$$\sigma = (2E\gamma_s/\pi c)^{\frac{1}{2}}$$

This inverse square root relation between strength and flaw size has been confirmed for glasses. In Griffith's analysis, it was the thermodynamic surface energy of the material that was considered to be important. It is now known that, due to the use of energy in processes other than the formation of new surface, the energy required for rapid failure is about a factor of 10 greater than the thermodynamic surface energy estimated by extrapolation of liquid surface energy. However, the above form of the expression is still widely used.

2.4 FABRICATION EFFECTS RELEVANT TO THE STUDY

2.4.1 Grain size

The dependence of strength on grain size has been studied in the past in relation to whiteware products. Krause et al. (1942) claimed that 15 to 30 μ quartz grains added to a body produced the highest strength. Dietzel (1953) and Mattyasovszky-Zsolnay (1957) interpreted this in terms of prestresses induced in the matrix. Wiedmann (1959) on the other hand, obtained results which do not confirm the prestress theory. Genin (1958) studied the microstresses resulting from the mismatch of the expansion of the quartz and glassy phase and indicated that the tensile strength of whitewares decreased with increase in grain size. Subsequently, Warshaw and Seider (1967) studied triaxial porcelain containing alumina and silica and observed an inflection in the strength-grain size curve (Fig. 2.4) as

the grain size decreases to 25 μ. This was considered to be the result of the transition of fracture type from extensive interconnected matrix to internal, peripheral and some noninterconnected matrix fracture. Although it appears that the work reported to date is inconclusive, the general picture which emerges is that a decrease in grain size produces higher rupture strengths in ceramics at least within limits. Such dependence has also been extensively studied with oxide ceramics such as alumina (Spriggs et al. 1964, Passmore et al. 1965), magnesia (Vasilos et al. 1964, Carniglia 1965, 1972) and devitrified glass (Emrich 1964).

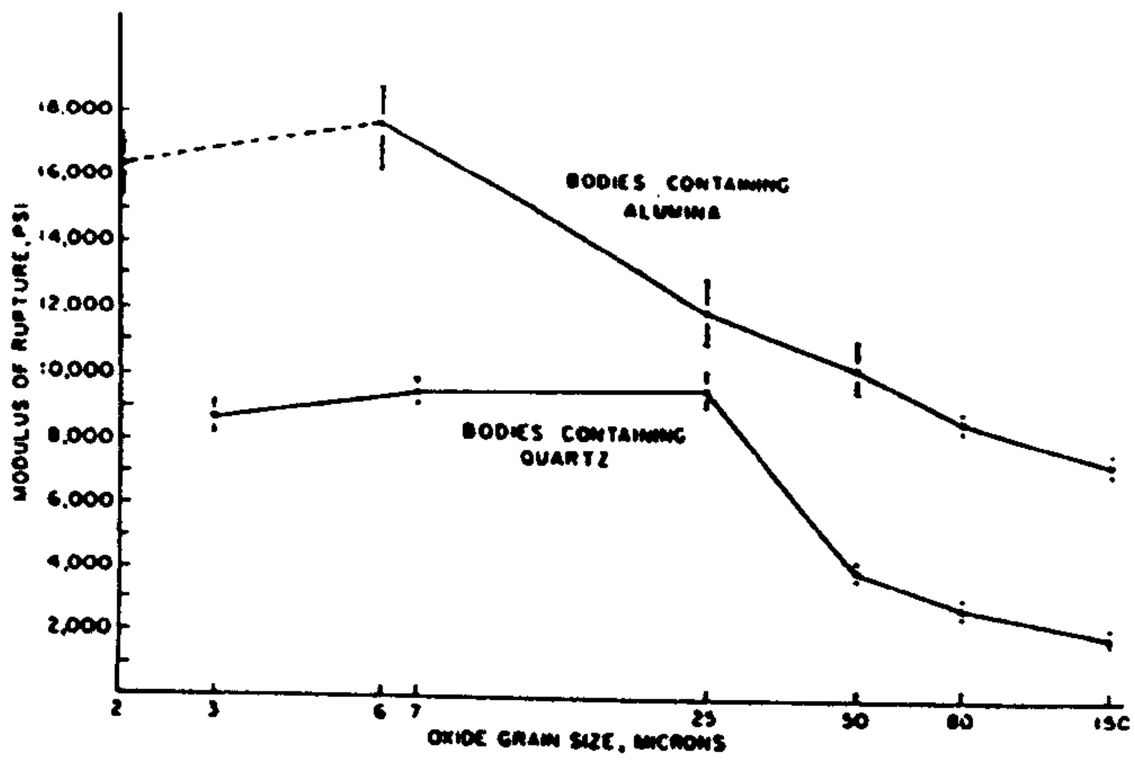

Fig. 2.4-Modulus of rupture vs. diameter of oxide grains.

Equations relating the tensile strengths of brittle polycrystalline ceramic materials to their grain size have been proposed by Orowan (1948), by Petch (1953) and by Knudsen (1959). The Orowan and Petch equations have some foundation in brittle fracture, whereas Knudsen equation is purely empirical. These data indicate that the flexural strength decreases with increasing grain size (Fig. 2.5) for relatively non-porous bodies in which the crystals are well bonded. The grain size dependence of strength can be described by

$$S = S_o G^x$$

in which S is the strength at grain size G, S_o the strength at unit grain size, and x the grain size exponent. The observed grain size exponents vary widely. No satisfactory explanation has been established for this variation.

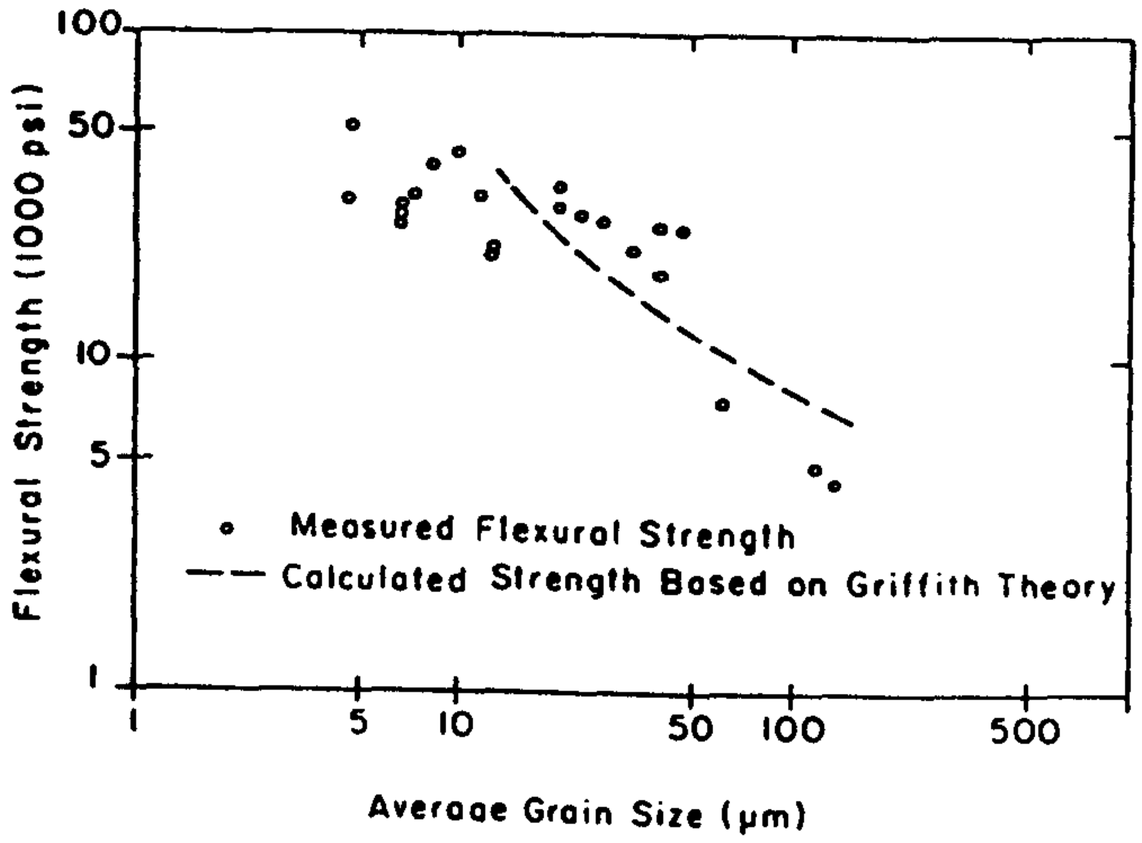

Fig. 2.5-Strength vs. average grain size for TiO_2

Several working models have also been proposed to describe the combined effects of porosity and grain size on the uniaxial strength of ceramics. The Orowan-Petch treatment of data uses the relation:

$$S_{g,p} = (S + S_1 G^{-\frac{1}{2}}) \exp(-bp)$$

where $S_{g,p}$ is the mean strength of several specimens of mean grain size G and porosity p. The quantities S , S_1 and b are all empirically determined.

At very fine grain sizes, however, expected rupture strengths are often not attained and the strength dependence discussed above may not be obeyed. This may be due to impurities present in grain boundaries which produce a bulk weakening effect (Kriegel 1965). Harrison (1964) noted that surface finish is much more effective in increasing the strength. In view of the above and fairly well established nature of grain size dependence of strength of ceramics which possibly permits its application to structural ceramics irrespective of the composition of materials, the

grain size aspect has been given a limited attention in this investigation.

2.4.2 Porosity

The strength decreases with increasing porosity. Ceramics in which this effect was found include alumina (Passmore et al. 1965), magnesia (Stokes et al. 1963), fused silica (Gannon et al. 1965) glass (Hasselman et al. 1964) and composites of a glass matrix with alumina and mullite (Studt et al. 1962).

Two aspects of pores come into play in weakening of ceramic bodies by pores. One is the bulk weakening effect associated with the volumetric removal of material by the presence of pores. The other is the stress concentration effect leading to nucleation of cracks at low stress. At high temperatures in more ductile materials (MgO), pores at boundaries may limit strength by promoting grain boundary sliding (Day et al. 1966). Several workers (Spriggs 1962, Hasselman 1962) have suggested that the effects of pores on strength may depend on:

(i). pore shape
(ii). pore orientation
(iii). whether the pores are open or closed, and
(iv). the location of pores (that is, in grain boundaries or within grains)

However, little information is presently available to prove these potential effects. Nevertheless it is the stress concentration effect which prevents the application of rigorous theories for the porosity-strength dependence.

Various expressions have been proposed to describe the effect of porosity upon elastic modulus. These expressions are briefly identified in Table 2.1, where E, G and K denote the tensile, shear and bulk moduli of elasticity, p stands for porosity, v is Poisson's ratio, the subscript o identifies the non-porous material, while the symbols a, b and k designate experimental constants.

Table 2.1-Proposed expressions for the effect of porosity on elastic constants

Author	Nature of expression	Proposed relationship
McKenzie	Analytical	$\frac{G}{G_o} = 1 - \frac{5(3K_o - 4G_o)}{9K_o + 8G_o} p + bp^2$ $\frac{K_o}{K} = \frac{1}{1 - p} + \frac{3K_o\ p}{4G_o(1 - p)} + ap^2$
Spriggs	Empirical	$E/E_o = e^{-bp}$
Chandler and Fryxell	Empirical	$E/E_o = 1 - bp$
Chung	Semi-empirical	$E/E_o = G/G_o = K/K_o = 1 - ap - bp^2$
Hasselman	Semi-empirical	$E/E_o = G/G_o = K/K_o = 1 - \frac{ap}{1 + (a - 1)p}$
Weil-Hashin	Analytical	$\frac{E}{E_o} = \frac{1-p}{1-k_1p}$, $k_1 = \frac{(1-v_o)(13-15v_o)}{2(7-5v_o)}$ $\frac{G}{G_o} = \frac{1-p}{1-k_2p}$, $k_2 = \frac{2(4-5v_o)}{7-5v_o}$ $\frac{k}{K_o} = \frac{1-p}{1-k_3p}$, $k_3 = \frac{1-v_o}{2(1-2v_o)}$

According to Weil (1963), the equations should satisfy the boundary conditions:

$E/E_o = G/G_o = K/K_o = 1$ when $p = 0$

$E/E_o = G/G_o = K/K_o = 0$ when $p = 1$

The empirical expressions proposed by Spriggs (1961), and Chandler and Fryxell (1963) fail to satisfy the latter requirements, while those of McKenzie (1950) and Chung (1963) meet this boundary condition only for special values of a and b. Both Hasselman (1962) and Weil-Hashin (1963) relationships satisfy boundary conditions. Detailed investigations on this subject are lacking. Chandler and Fryxell (1963) carried out a review of the adequacy of the relationships and their results are summarised in Table 2.2.

Table 2.2-Comparison of equations for effect of porosity on Young's modulus in sintered beryllium oxide; after Chandler and Fryxell

				Linear equation $E = E_0 (1 - bp)$			Spriggs equation $E = E_0 e^{-bp}$			Hasselmann equation $E = E_0[1 + \frac{Ap}{1 - (A + 1)p}]$		
Material	Grain size range (u)	Porosity range (%)	No. of obs-ervations	E_0 (10^6 p.s.i.)	b	Std.devn. (%)	E_0 (10^6 p.s.i.)	b	Std. devn. (%)	E_0 (10^6 p.s.i.)	A	Std. devn. (%)
UOX plus 0.5% MgO by wt.	2-5	4-17	150	54.9	1.72	2.34	55.7	2.06	2.35	55.3	-1.99	2.08
	7-10	2-16	150	57.3	1.82	1.19	58.2	2.21	1.35	58.2	-2.24	0.76
	15-20	2-15	150	59.2	1.80	1.09	59.9	2.14	1.28	59.9	-2.16	0.70
	35-50	2-14	150	62.8	2.25	1.86	63.7	2.71	1.77	63.7	-2.81	11.36
AOX	5-100	2-15	450	56.1	1.86	1.83	56.7	2.20	1.77	56.6	2.19	1.27

CHAPTER 2

As regards the effect of porosity upon strength is concerned, the first empirical relationship was suggested by Duckworth (1953) in the form

$$S = S_o e^{-bp}$$

where S is the strength of the porous material, S_o the strength of the non-porous material, p is the absolute porosity and b is a constant. The objection to this equation is that it does not satisfy boundary conditions; at p = 1, it predicts a finite value of strength ($S=S_o e^{-b}$), rather than the correct value of S = 0.

The value of b depends on the material and its technique of preparation. It commonly varies from 4 to 9. In view of the necessity of renewed determination of b not only for each material but also for each change in preparation technique considered, a semi-empirical relationship analogous to his expression for elastic constants (see Table 2.2) was developed by Hasselman (1963). This is of the form:

$$S = S_o \left[1 - \frac{Ap}{1+(A-1)p} \right]$$

This expression satisfies both boundary conditions, that is, $S = S_o$ at p = 0 and S = 0 at p = 1.

Relatively few investigations have been reported in the literature which were concerned with the adequacy of the strength-porosity relationships in ceramic bodies. A study reported by Weil (1963) for porous alumina shows the close agreement between theory (continuous line in Fig. 2.6) and test results (scatter of points).

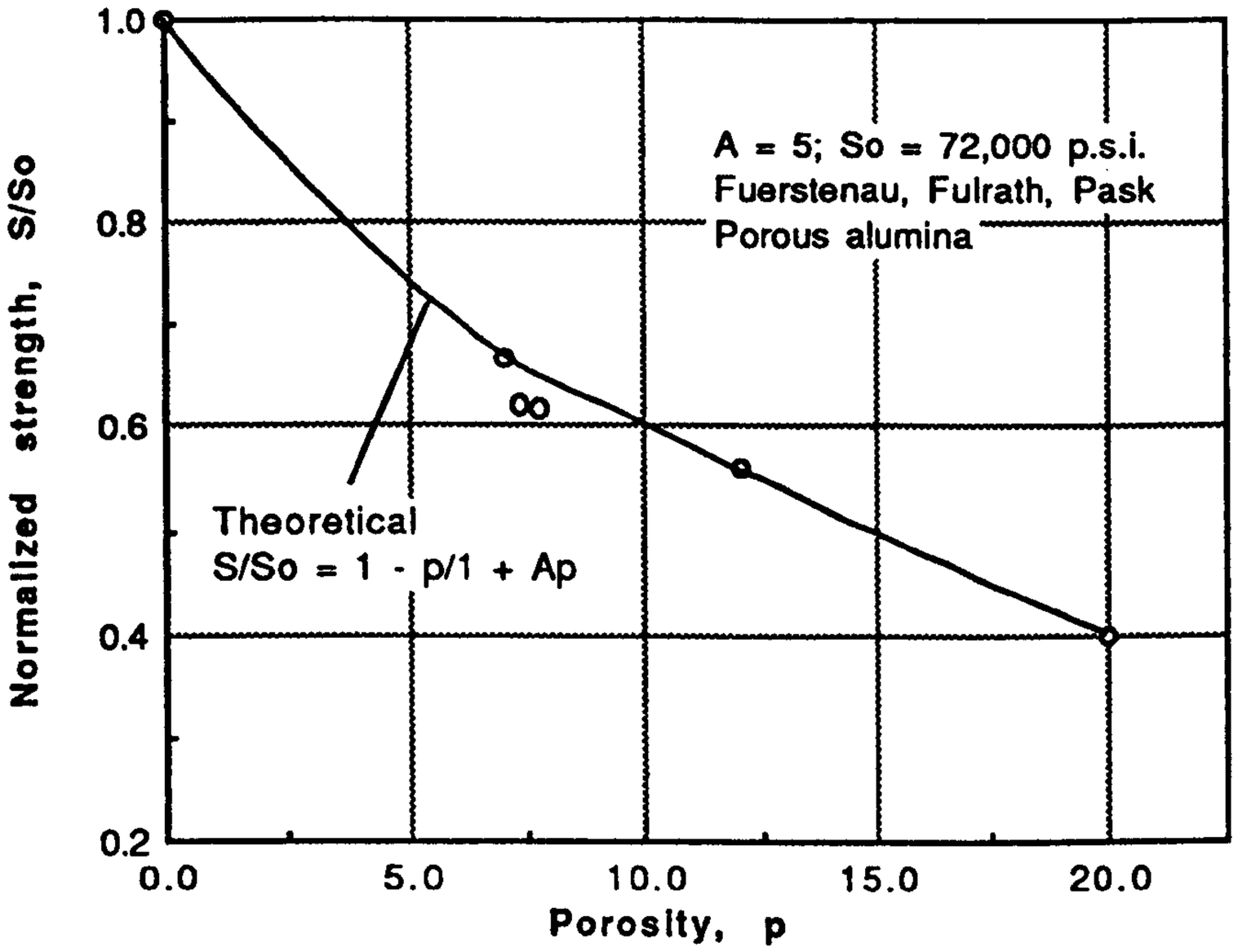

Fig. 2.6-Comparison of theory and experiment for the effect of porosity upon strength.

2.4.3 Mullite formation

Mullite is the most stable crystalline constituent of aluminosilicates fired to high temperatures. It is widely accepted that the development of interlocking mullite needles in a clay body on firing increases its mechanical strength though this hypothesis is not free from controversy. Mattyasovszky-Zsolnay (1957) disputed the strengthening action of mullite on the grounds that the mechanical strength of porcelain was influenced mainly by stresses set up in the glassy phase rather than by the morphology or amount of mullite crystals. Presumably, the weakening action due to microcracks arising from the volume expansion of quartz played a more important role than the strengthening action of mullite in the quartz-rich body considered by him. Schuster et al. (1972) examined a stoneware body made from illite and other raw materials by various analytical techniques. The presence of primary and secondary mullite phases and also sub-microscopic crystals of mullite in glassy phase, formed by thermal decomposition of illite, was observed. Homogeneously dispersed illitic clay and intense fluxing action of alkali ions in the

lattice caused uniform distribution of mullite in the glassy phase. It is likely that the uniformly distributed mullite crystals contributed to the development of strength in the stoneware body. Lach (1974) reported that the presence of a viscous glassy phase aids diffusion of cations facilitating the formation of regular mullite crystals; alternatively, higher temperatures are necessary to obtain well developed mullite crystals in the absence of glassy phase. Grofcsik (1966) reported that strength and other mechanical properties of porcelain insulators could be improved by promoting the mullite formation. According to Koch (1970), a porcelain body should be subjected to a firing schedule favourable for the development of a structure containing alumina, some plate-like primary mullite and a high proportion of fine acicular secondary mullite concentrated in the glassy phase and also at the grain boundaries. Abdel-Fata et al. (1972) used comparatively more pure forms of china clay and fireclay with γ-Al_2O_3 for preparing mullite and corundum porcelain. They observed that best results were obtained with 39% china clay or 20% fireclay with γ-Al_2O_3 fired at 1550°C.

Most previous workers in this field studied vitreous ceramic bodies constituted with pure clays. So far as is known, no work has yet been published on the significance of high temperature phase development on mechanical strength in less pure ceramics of the type used in structural clay products.

2.4.3.1 Induced mullitization by mineralizers

Because of the industrial importance of mullite as a heavy duty material, the effects of mineralizers and firing atmospheres on the mullitization of kaolinite have also been investigated (Parmelee et al. 1942, Skinner et al. 1953, Mackenzie 1969). Bien et al. (1962) observed that 30% aluminium fluoride was effective in producing mullite in pure kaolinite at temperatures lower than 1000°C. The work of Segnit et al. (1971) is particularly noteworthy in view of the use of abundant and relatively inexpensive $CaCO_3$ as

the mineralizer. However, the amount of $CaCO_3$ used by them (52 wt%) corresponded to the composition of the anticipated product zoisite ($Ca_2Al_3Si_3O_{12}OH$) although this phase was not detected in the system. Moreover, their work was mainly concerned with the investigation of the nature of the kaolinite-$CaCO_3$ reaction. The excessive amount of $CaCO_3$ used by them can hardly be expected to promote the development of mullite in kaolinite.

Previous work on mullitization of kaolinite was subjected to the following limitations.

(i). The studies were aimed at either investigating the nature of reactions of certain cations with clay minerals or determining the role of mineralizers in inducing mullite formation.

(ii).The clays used were almost exclusively pure or standard minerals from known sources.

(iii).The temperatures employed were above 1200°C (temperature corresponding to the zero free energy of formation of mullite from pure clay).

(iv).None of the studies was concerned with the quantitative aspects of the significance of mullite formation on the strength development of fired clay bodies.

The survey of the literature has also shown that there is very little information relating properties with microstructure. However, it is well-established that two microstructural forms of crystalline mullite can exist. These are the 'primary' mullite with a granular habit and 'secondary' mullite possessing a needle-like structure. It is possible that the two forms of mullite affect the mechanical strength in different ways. In view of the excellent properties of mullite as reported by Metcalfe et al. (1975) [for example, strength of 172 MN/m^2 (25,000 p.s.i) at a density of 95% of the theoretical value (3.16 $g.cm^{-3}$)] it is plausible to assume that the increased mullite content adds to the mechanical strength of a fired clay body.

2.4.4 Composition and sintering additives

A potential means of increasing the rate of densification and therefore the strength of ceramics is to use suitable additives. Smothers and Reynolds (1954) were the first to describe work on the addition of magnesia to alumina to effect crystallization at lower temperatures. Since then, it has been noted by various workers that small additions (ranging from 1 to 10%) of another material can have a marked effect on the densification, grain growth and other characteristics of the major material. However, not all additives are necessarily effective in promoting sintering (Coble and Aitken 1966). The additive systems magnesium oxide, calcium oxide and titanium oxide are effective in strengthening alumina (Mckee et al. 1963, Jorgensen et al. 1964, Bannerjee et al. 1964, Jorgensen 1965) whereas iron oxide, and titanium oxide are suitable for magnesia (Jones et al. 1958, Layden et al. 1959).

In addition, additives may react chemically with the matrix particles, thus increasing bonding strength. An important aspect of this bonding is that sintering can be accomplished at lower temperatures to achieve equal or higher strengths. Another effect which additives may have is the prevention of grain growth so that grain size finer than normal can be maintained. However, if the additive forms a liquid in sintering, grain growth may be accelerated. Examples of growth inhibition include alumina or silica in the MgO-FeO system (Van Vlack et al. 1962). Examples of grain growth in liquid phase sintering include titania, iron oxide, manganese oxide and copper oxide in alumina (Vernetti and Cook 1966) and lithium fluoride in magnesium aluminium spinel investigated by Barnes et al. (1966).

Sometimes additives may also segregate in grain boundaries after sintering. This may affect strength and ductility especially when present as a continuous film. At low testing temperatures, such a film may increase or decrease strength, but is likely to prevent ductile behaviour. At high temperatures, such boundary phases are

likely to be weak and lead to fracture at low strain. (Copley and Pask 1965). Thus, sintering additives must be used with care. The reactive additive system involving phosphates used in the investigation is described in detail below.

2.4.5 The reactions of phosphates with clay minerals

2.4.5.1 Phosphate bonding

It is economically desirable to reduce the sintering temperature of structural clay products which partially or fully vitrify at relatively high temperatures used in manufacture. In this respect, the use of bonding materials which react chemically with the matrix particles at low temperatures is attractive for many applications in ceramics.

The literature indicates that phosphoric acid and certain phosphates offered good prospects as bonding agents (Kingery 1950, Hill 1953). The bonding property of phosphates with refractory oxides (Bartha et al. 1971) and silicates (Forest 1964, Robinson et al. 1967, Tauber et al. 1972) is widely used in the production of refractories of high pyrometric cone equivalent and strength, refractory cements and mortars (Kingery 1952), slags and glasses (Sudakas and Sinina 1971) etc. However, additive systems involving phosphoric binders are unknown in fired clay products presumably because of the ease at which strengths are achieved by extensive heat treatment. The energy conservation is still a low priority concept in the processing of such products.

In spite of many applications, the properties of refractory bonds employing phosphates have not been systematically studied. Kingery (1950), Sudakas et al. (1971) and Robinson and McCartney (1964) ascribe the formation of cold-setting and heat-setting bonds in refractory oxide-phosphate systems to:

(i). chemical reaction of phosphoric acid or acidic phosphates with oxides at normal or high temperature,

(ii) thermal reaction by dehydration of glassy meta-phosphates.

However, unlike the uniform metal oxide surfaces, clay minerals are characterized by edge and face interactions which make the above mentioned models hard to apply to clay minerals (Secor and Radke 1985, Bar Yosef et al. 1988).

2.4.5.2 Reactions with natural clays

Reactions between phosphates and soil minerals have received considerable attention from soil scientists but no attempt has yet been made by material scientists to exploit beneficially the wealth of knowledge accumulated over the last two decades.

As early as 1934 Paver and Marshall presented evidence that supposedly hydrogen saturated clays were in reality mixed hydrogen and aluminium clays with the exchangeable Al resulting from the replacement of crystal lattice Al by hydrogen. Schofield (1939) suggested that by keeping the clay in a concentrated solution of strong electrolyte at pH 3, the exchangeable Al (and Fe) could be maintained at a minimum. Laws and Page (1946) found that grinding of kaolinite produced new mineral species and increased the solubility of alumina in solutions of acid and base. Perkins (1948) presented similar evidence to show that grinding of kaolinite significantly altered the thermal curves, indicating the loss of water; greatly increased the amount of acid required to lower the pH, indicating the liberation of a cation. Again in 1948, Mukherjee et al. showed that clay minerals yielded Fe^{3+} upon repeated washing with salt solution. Subsequently Harward and Coleman (1954) and Low (1955) confirmed by potentiometric and conductometric titration and heat of neutralization studies that H-clays (prepared by electrodialysis or by leaching with dilute acids) were actually H-Al clays and that the aluminium originated from the clay lattice.

CHAPTER 2

Phosphate ions have been reported to enhance the decomposition of clay minerals at low pH values. Stout (1940) demonstrated that ground clay minerals would react with phosphates reversibly, changing the lattice structure of the clay mineral as the phosphate ions were alternately exchanged with hydroxyl ions. Black (1941) observed the gradual dissolution of aluminium from kaolinite in concentrated acid phosphate solutions (0.1 to 1.0 M) and attributed it to the lattice disruption by substitution of phosphate ions for internal structural hydroxyl groups in kaolinite. Coleman (1944) was the first soil scientist to postulate that phosphate fixation by clay minerals was due to the aluminium content of the clays.

Low and Black (1948) using 10^{-4} M phosphate solution, found that addition of phosphate to kaolinite precipitated the dissociated Al ions, thus upsetting the dissociation equilibrium of kaolinite and accelerating its decomposition. They suggested replacement of surface hydroxyl groups and silicate tetrahedra in the kaolinite crystals by phosphate tetrahedra as mechanisms for the initial rapid absorption of phosphate, and subsequent recrystallization of the surface phosphate to aluminium phosphate for the slow uptake of phosphate from solution. Since that time Haseman et al. (1950), Cole and Jackson (1950), Russell and Low (1954) have presented additional evidence for this concept. Wild (1953) showed that the exchangeable ions in Al resins when made to react with orthophosphates, increased the level of "fixation" as the pH was raised and Al hydrolysed more completely. Finally Kittrick and Jackson (1956) investigated the effect of 1.0 M phosphate solutions on kaolinite at 90°C and demonstrated the presence of variscite ($AlPO_4.2H_2O$) like compounds. Their work is especially noteworthy because they showed that in kaolinite-variscite systems the solubility product of variscite is unaltered, and that kaolinite will decompose in the presence of rather high phosphate concentrations to form variscite. Hemwall (1957) found that exchangeable Al ions on kaolinite participate in phosphate sorption reactions and suggested that decomposition

reactions of the sort considered by Kittrick and Jackson would occur only where the amount of soluble phosphate present was larger than the supply of exchangeable Al. Coleman et al. (1957) showed that phosphate binding depends upon the acidity and chloride salts which served to displace Al from exchange sites. It was also suggested that phosphate binding reactions which involve exchangeable Al ions lead to the formation of a substance with the overall composition of variscite, and that 2 moles of H ions are produced for each mole of product which is formed.

2.4.5.3 Products of reactions

Much attention has been focussed on the study of insoluble aluminium and iron phosphates as end products of the reaction of phosphates in acid soils. Most of these studies have necessarily been concerned with the preparation and characterization of aluminium and iron phosphate minerals.

Haseman et al. (1950) identified several complex Al and Fe phosphates formed upon treatment of clay minerals gibbsite and goethite with phosphate solutions. Koji Wada (1959) showed that phosphates react rapidly with allophane and halloysite at room temperature to form an insoluble phosphate and that interlayer complex formation is possible between halloysite and ammonium phosphate. Kittrick and Jackson (1955) showed that minerals of the variscite-strengite isomorphous series may form as a result of reaction of added phosphate with clay minerals and oxides of aluminium and iron. The determination of solubility product of variscite by Cole et al. (1951) and Lindsay et al. (1959) and strengite by Chang et al. (1957) made it possible to apply solubility criteria in the study of phosphate reaction products in soils, and such studies have been carried out by Clark and Peech (1955) who showed that reaction between added phosphates and soils is time dependent and that variscite was probably one of the ultimate reaction products. Hemwall (1957) also applied solubility criteria in his study of reactions of clay minerals with phosphate and

suggested that variscite was formed. Wright et al. (1960) again by the application of solubility criteria showed that some crystalline phosphate mineral of the variscite-strengite isomorphous series was the ultimate reaction product of applied phosphate in the acid soils studied. Lindsay et al. (1959) by solubility studies identified amorphous aluminium phosphate among the products that are formed directly when solutions derived from water soluble phosphates react with aluminium hydroxide and aluminium ions in the soil. Subsequently Taylor et al. (1961) by solubility studies concluded that several complex crystalline aluminium phosphates are formed similarly and that their subsequent hydrolysis may lead to the precipitation of amorphous aluminium phosphate in the soil. Veith et al. (1977) demonstrated the formation of amorphous analogs of variscite and sodium-montebrasite when allophanic soils were reacted with sodium orthophosphates. The presence of amorphous compounds in the products was demonstrated using solubility and stability criteria and also from analysis of their formation curves.

A remarkable contribution was made by material scientists who were investigating a possible substitute for scarce quartz crystals in wartime electronic applications. They studied the inversions between the various crystalline forms of aluminium orthophosphate and showed the resemblance of the crystalline forms and inversion temperatures to those of silica. According to Beck (1949) the analogous inversions occur at lower temperatures in aluminium orthophosphate than in silica, so that it is not surprising to find alumino-phosphate glasses with comparatively low softening temperatures.

Despite intensive research for the last 50 years, our understanding of phosphate-soil reactions is inadequate. The general consensus is that phosphates react with aluminium containing minerals to form surface compounds as well as insoluble Al-phosphates. However, the details of the

mechanisms involved and of the phosphate phases formed are matters of continuing discussion.

2.4.6 Surface condition

2.4.6.1 Surface coatings and strength

Ceramics are brittle materials which tend to have rupture strengths which are very sensitive to surface conditions. The studies of glass (Symmers et al. 1962, Brearley et al. 1963, Fletcher et al. 1964), magnesia (Miles et al. 1961, Harrison 1964, Stokes et al. 1965), and alumina (Parikh 1966) systems showed that the presence of surface defects lower their mechanical strength. In glass, the mechanism of failure is believed to be the introduction of cracks or other surface flaws such as inclusions. Surface preparation which minimized or removed defects caused a strength increase in glass rods from as low as 15,000 p.s.i. to values as high as 400,000 p.s.i.. In magnesia or alumina, fresh dislocations are introduced by stresses which reduce strength. The strength increase by the surface removal of defects was, however, less dramatic in magnesia.

Preliminary experiments by Westwood (1960) on lithium fluoride crystals indicated that surface coatings produced by chemical reaction minimized imperfections and caused a substantial increase in the mechanical strength of crystals. Other investigators (Morley et al. 1962, Mallinder et al. 1966) have demonstrated that reacted surface coatings can exert a profound influence on the rupture strength of sapphire crystals, sometimes causing a tenfold increase in this property. These results help to extend the above concept to brittle materials in general although the previous investigations were limited mainly to single component systems involving pure materials.

2.4.6.2 Theoretical considerations on strengthening

A surface coating can be expected to play a dual role in strengthening a ceramic body.

(i). Stress considerations show that the presence of voids and flaws have a stress raising effect giving rise to

localized stress concentration near the imperfections. The stress increase induces crack propagation and weakens the body.

The effect of surface flaws on the mechanical strength can be understood using the stress-raising concept applied to a surface microcrack in a body under stress (Fig. 2.7).

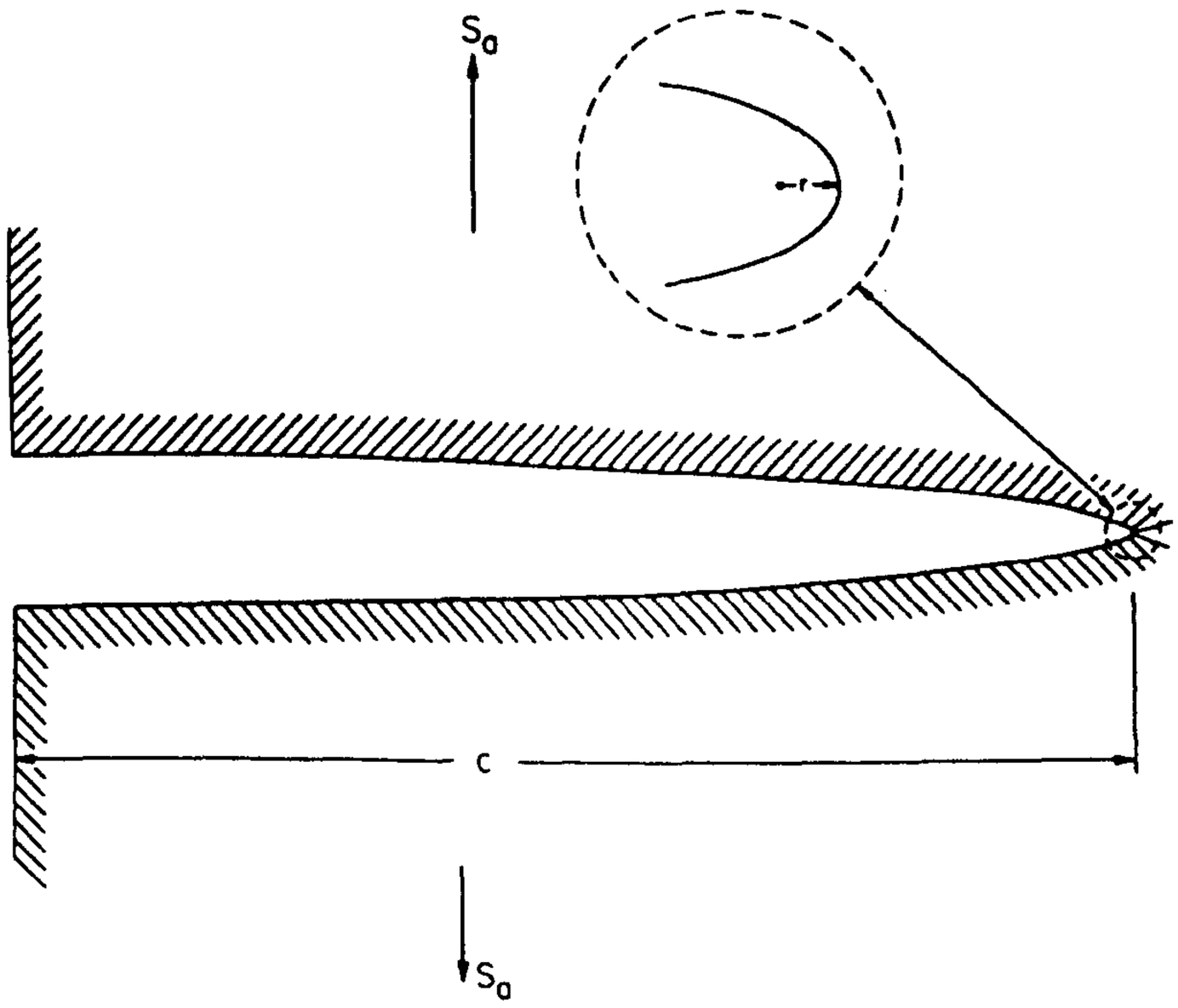

Fig. 2.7-Surface microcrack in a body under stress.

For a crack with a semi major axis ℓ and a radius p at the axis extremity,

The stress-raising factor(applied = $2\sqrt{\ell/p}$
on one half of a flat crack pore)

For a hypothetical microcrack with a depth of 1μ and a width of 2 interatomic distances (4 Å),

that is, if ℓ = 10,000 Å and p = 2 Å ,

the stress raising factor = $100\sqrt{2}$

The probability of a 1μ microcrack is fairly high and it becomes apparent from the magnitude of the stress raising

factor that this defect has a catastrophic effect on the strength (Duckworth 1953).

A coating which fills the microcracks and other surface imperfections reinforces the weak points where stress raising defects are localized. This clearly increases the overall mechanical strength of the body. In addition, if the coating is of compressive nature, it enhances the strengthening effect according to the following considerations.

(ii).Ceramic materials are weak in tension. A surface compressive stress imparted by a coating develops a compensating tensile stress in the interior of the body. An external load therefore has to overcome these forces in addition to initial body strength before failure occurs.

The magnitude of these stresses can be estimated on the basis of a method proposed by Duke et al. (1968) for glass ceramics.

In a rectangular bar as shown in Fig. 2.8,

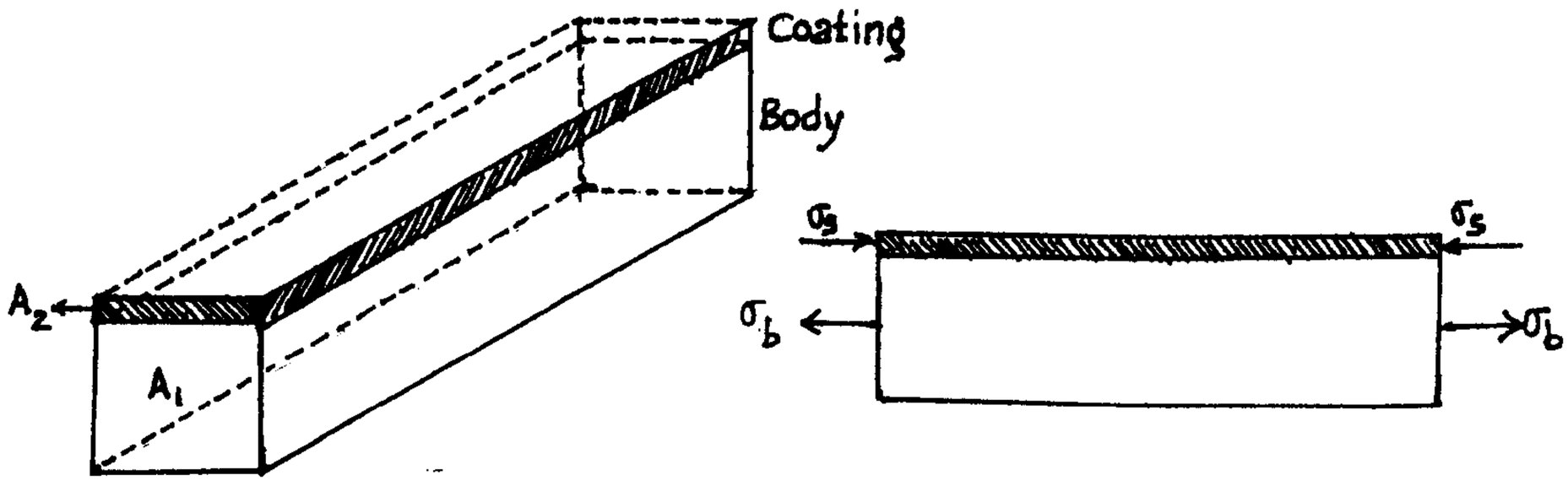

Fig. 2.8-Schematic representation of stresses in a laminated rectangular bar.

if we assume that:

(i). both the surface layer and the body are isotropic and elastic,

(ii). the temperature distribution is uniform, and

(iii). the elastic moduli and the Poisson's ratios are the same for the coating and the body, then

surface compressive stress, $\sigma_s = -(a_1-a_2)\Delta T \frac{E}{1-v} \frac{A_1}{A}$

body tensile stress, $\sigma_b = (a_1-a_2)\Delta T \frac{E}{1-v} \frac{A_2}{A}$

a_1 and a_2 = linear expansion coefficients for the body and coating respectively.

ΔT = temperature difference between the setting point of the coating and the temperature where the stress is measured.

E = Young's modulus

v = Poisson's ratio

A, A_1 and A_2 = cross-sectional areas of the bar, body and coating respectively.

The total strain, $(a_1-a_2)\Delta T$, can be obtained from the plot of expansion curves of both coated body and coating. Since the elastic modulus, Poisson's ratio (usually 0.3 for ceramics), A, A_1 and A_2 can be measured for the body and coating, the stresses σ_s and σ_b can be calculated directly.

In a modulus of rupture test, both the surface compression and the initial strength of the body must be overcome before failure occurs. It is evident from the above that the greatest increase in strength is obtained with the greatest mismatch in expansion. Consequently, a surface coating which develops a compressive stress in the surface owing to its lower thermal contraction can be expected to have a strengthening effect on the body.

2.4.7 Heat treatment

2.4.7.1 Firing schedule

Norton and Hodgdon (1931) studied the quantitative relations between the two factors, peak temperature and soaking time of the firing schedule of variously heat treated triaxial bodies. They found that each ten tenfold

increase in soaking time permitted lowering of peak temperature by 23°C. Accordingly, the application of Arrhenius equation:

$$\log \frac{k_1}{k_2} = A \left[\frac{1}{T_2} - \frac{1}{T_1}\right]$$

where k_1 = reaction rate at temperature T_1

k_2 = reaction rate at temperature T_2

A = constant

to the vitrification process of feldspathic bodies was suggested by them on the assumption that the vitrification is the result of a chemical reaction. Shelton and Meyer (1938) investigated feldspathic whiteware bodies and reported that the optimum heating rate and minimum soaking time governed the shortest firing schedule productive of the best microstructure and physical properties. Meyer (1938) based on this study proposed a chart and expressions for the calculation of heat treatments for whiteware bodies. However, his indirect method of using data on pyrometric cones to calculate the exponential constant (A) of the Arrhenius equation is questionable. According to Barrett (1976), Meyer's expressions are cumbersome and previous methods of approaching the problem of estimating the amount of reaction in a given time are rather empirical.

The present trend in manufacture is to impart fast firing to ceramic ware. The question to be answered is how fast can the firing cycle be to bring about suitable texture and bulk properties in the fired bodies. Norton (1931) made a study of microstructure on several triaxial bodies subjected to various heat treatments. He reported that bodies soaked at peak temperature for a longer time showed more quartz solution and more mullite development than rapidly fired bodies. However, there is a lack of agreement among investigators concerning the effect of shortening the heat treatments. Some showed that for time-temperature combinations which produce the same body maturity, short firing gave more fluid glass thus improving physical properties; on the other hand, fast firing produced more sealed pores. Moreover, it was observed that starting

materials with finer particle size permitted fast firing since they produced fewer closed pores. Trials were cited by German (1952) to prove that both normal firing and fast firing produced ware of similar mechanical properties.

2.4.7.2 The influence of firing

Liquid-phase sintering in clayware ceramics

The processes of strengthening of fine-grained ceramic bodies through the effect of elevated temperature is attributed to sintering. During sintering, individual mix components react to form new crystalline phases in which the particles are mutually strongly bound. A liquid phase is also usually formed which solidifies into a glass, or into a mixture of fine crystals.

Several theoretical models have been proposed for the sintering process, representing conditions in which no vitreous phase is present (Kuczinski 1949, Mackenzie and Shuttleworth 1949) as well as conditions involving vitreous phases (Kingery 1959). Real systems differ from these models in a number of ways. The sintering mechanism of practical significance in traditional clayware ceramics is liquid-phase sintering. Kingery (1960) investigated the mechanism of this process (Fig. 2.9). The surface tension of the liquid phase is the major driving force. Three separate densification processes are believed to occur:

(i). rearrangement of solid particles to give increased density

(ii). solution precipitation in which material is dissolved away from contact points, allowing the centres of the particles to approach each other; and finally,

(iii).coalescence of the solid particles.

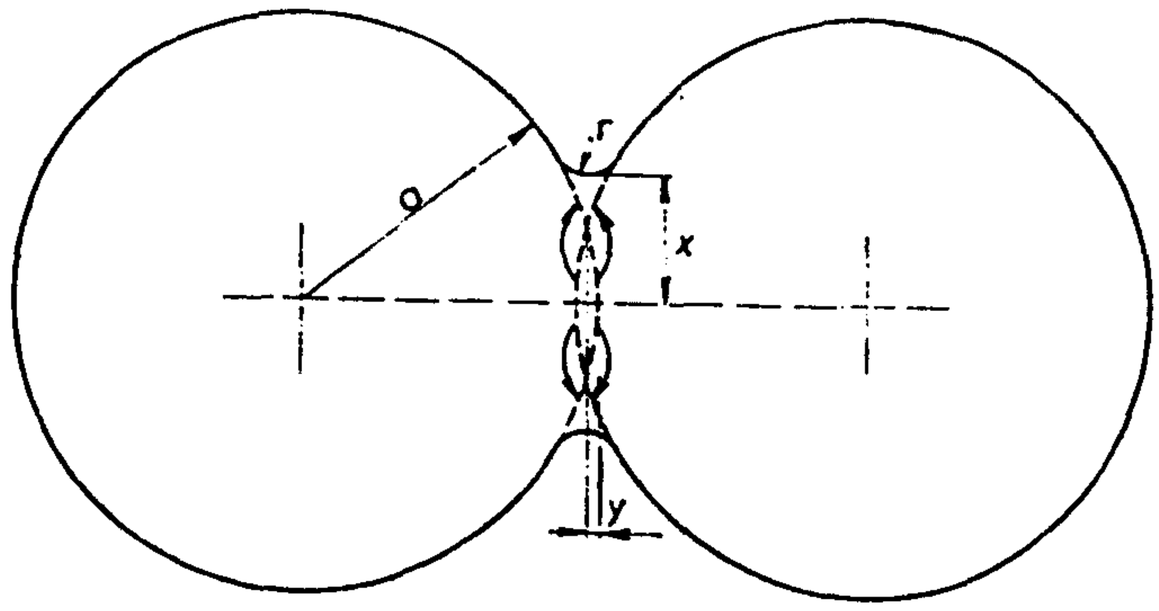

Fig. 2.9-The Kingery-Berg model.

On heating to temperatures of about 1000°C and higher the clay particles and fluxes begin to react together to form a predominantly glassy mass and at this stage sintering and densification occur. This sintering process is complete at typically 1200°C. The filler (quartz) particles being more refractory play a relatively minor chemical role in the sintering process, although some dissolution into the glassy phase occurs.

2.4.7.3 Processes occurring during firing

When temperature of a clay body is gradually increased, reactions and transformations take place in stages. The first stage entails the removal at about 200°C of water largely adsorbed on the surface. Oxidation of organic matter occurs between 200° and 700°C. The first crystalline change in kaolinite, dehydroxylation, occurs at 450°C with the formation of metakaolinite ($Al_2O_3.2SiO_2$). Quartz undergoes polymorphic transformation at a temperature of 573°C. At a temperature of about 980°C, metakaolinite crystallizes first into a spinel and then into extremely fine mullite (Brindley and Nakahira 1957).

The most significant processes will begin to take place at temperatures above 1000°C, namely:

(i). formation of the glassy melt from feldspar which initiates sintering,

(ii). formation of mullite, either directly from the clay mineral, or by reaction between feldspar and clay (primary and secondary mullite),

(iii). dissolution of quartz grains in the melt.

Table 2.3 gives the probable events in firing a triaxial body. Fig. 2.10 illustrates how the various constituents of the body change with the temperature of firing.

Table 2.3-Reactions in firing a triaxial body

Temperature (°C)	Reaction
Up to 100	Loss of moisture
100 - 200	Removal of adsorbed water
450	Dehydroxylation; increased porosity
500	Oxidation of organic matter
573	Quartz inversion; little overall volume damage
950	Spinel forms from clay; start of shrinkage
1000	Primary mullite forms
1050 - 1150	Glass forms from feldspar, mullite grows, shrinkage continues
1200	More glass formation, mullite grows, pores closing, some quartz dissolution

CHAPTER 2

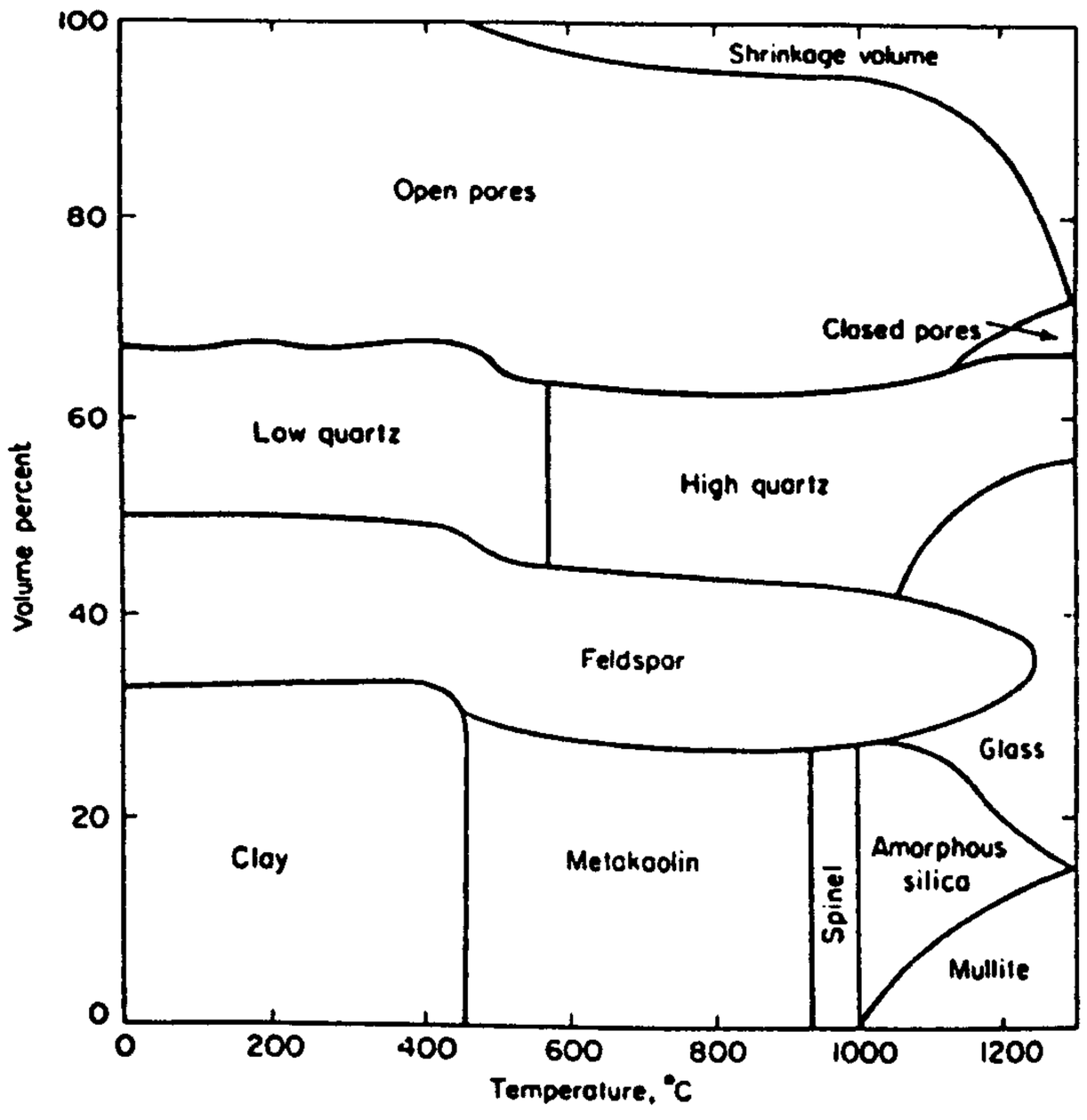

Fig. 2.10-Constituents in a triaxial body on firing (after Norton 1970).

If the brick bodies under consideration are assumed to be of composition within the ternary system K_2O-Al_2O_3-SiO_2 (Fig. 2.11) for the sake of simplicity, the high temperature processes occurring within the bodies can be predicted from the respective phase equilibrium data (Osborn and Muan 1964).

The average composition of the bodies is represented by the point P in the phase diagram. The diagram shows that the first eutectic melt may form at 950°C. However, since interaction of the individual components at this temperature is very slow, little eutectic melt forms and melting of feldspar occurs at 1050-1150°C. At the same time, primary mullite will begin to form at about 1000°C. The melt composition is given by the intersection of the mullite-P connecting line with the isotherm corresponding to the temperature in question.

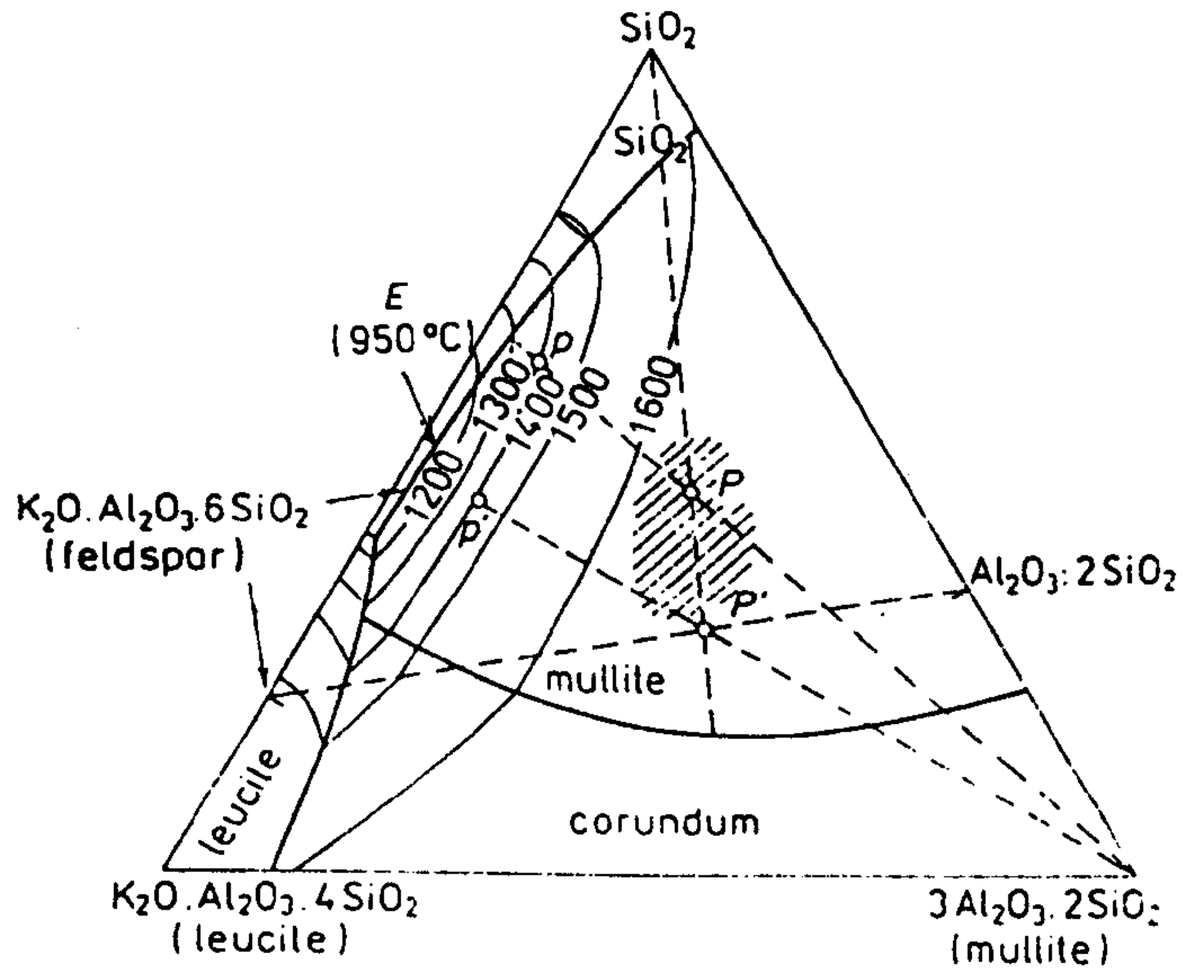

Fig. 2.11-Phase diagram of the system K_2O-Al_2O_3-SiO_2 (high silica part, after Osborn and Muan 1964).

In comparison with the original feldspar melt, the final glassy phase will be richer in Al_2O_3 and SiO_2. An increase in firing temperature produces more SiO_2 in the glass which in turn increases the already high viscosity of the glass. This widens the sintering range of the body. However, it is necessary to control quite precisely the firing temperature to attain optimum mechanical properties. If the temperature is too high, dissolved gases may be released from the glassy matrix creating pores and impairing the properties. Moreover, bodies having more glassy phase tend to deform easily at elevated temperatures due to viscous flow. It is well known that the effect of higher firing temperature is the same as that of longer soaking time at slightly lower temperature (Norton 1970).

2.4.7.4 The influence of microstresses

Microstresses arise inside the material as a result of the thermal expansion mismatch of the glass and the quartz grains. Inversion of quartz also contributes to this adverse effect. The stresses usually arise at the quartz-glass interfaces producing sometimes microcracks within the grains

or at their periphery. The structure of traditional ceramics thus contains weak points which enhance the development of fracture on loading. Srbak et al. (1972) developed a high strength porcelain by incorporating up to 30% Al_2O_3 into the body. The introduction of Al_2O_3 apparently reduced the glass content in the body. A bonding strength of the order of 200 MPa was achieved. Binns (1965) investigated the changes in fracture strength and Young's modulus of glass and alumina grain, within the concentration range 0-40% alumina. The mixtures attained maximum density at 600° to 700°C. It was concluded from this work that elasticity and strength of the composite can be increased markedly beyond that of the glass. The rate of increase in elasticity is independent of the grain size of the alumina, and indicates that the composite solid behaves partly as a constant-strain system. The resulting uneven stress distribution is believed to be responsible for the observed increase in strength.

2.4.8 Texture

The properties of ceramic products are determined not only by the composition and structure of the phases present but also by the arrangement of those phases. The phase distribution or microstructure in the final ware depends on the fabrication factors illustrated in Fig. 2.1.

Kingery (1960) classified the characteristics of microstructure that can be determined as

(i). the number and identification of phases present, including porosity,
(ii). the relative amounts of each phase present, and
(iii). characteristics of each phase, such as size, shape and orientation.

Both fracture and deformation characteristics of ceramic materials are strongly affected by the above micro-structural features. For single phase polycrystalline materials, the amount and distribution of porosity together with the grain size often determine the observed mechanical properties. However, all aspects of these simple systems are not quantitatively understood. Therefore, it is not

surprising that the mechanical properties of complex, multi-phase microstructures have not been analysed in detail.

For ceramic systems that consist of a crystalline phase dispersed in vitreous matrix the deformation characteristics are largely determined by those of the vitreous phase rather than the properties of the crystals (Kingery 1962).

An example of a microstructural effect was given by Van Vlack (1960) who found that crystals in silica brick form a continuous self-bonded structure since the liquid phase present under operating conditions does not penetrate grain boundaries. In contrast, the siliceous phase present in magnesia refractory brick completely penetrates grain boundaries and separates them. As a result contamination is much more significant for basic brick than it is for silica. Silica bricks have a substantial load bearing capacity at temperatures within 50°C of their melting point, at which time they contain a large proportion of liquid phase. In contrast, magnesia bricks have poor load-bearing capacity at temperatures about half their melting point even though they have a much smaller fraction of liquid phase present.

According to Van Vlack, for complex ceramics a precise description of the number of phases present (including porosity), morphology and relative orientation is essential in evaluating their properties. Measurements or analyses which do not precisely define the microstructural characteristics are impossible to compare with other data or interpret in terms of the controlling variables.

CHAPTER 3

GEOLOGY AND MINERALOGY OF THE CLAYS

3.1 OUTLINE OF GEOLOGY IN RELATION TO CLAY DEPOSITS

The island of Sri Lanka can be divided into two main physiographic divisions (Herath 1973):

(i). The coastal lowlands with elevations from sea level to 270 m with little relief and traversed by rivers which have reached their base level of erosion in the coastal plain.

(ii).The highlands with elevations from 270 to 2,420 m with immature drainage pattern and marked relief abounding in mountains and ridges.

The general level varies from sea level to about 130 m and some erosion remnants rise to 300 m. The central highlands rise steeply from the coastal plain. The coastal plain is widely exploited for clays and provides nearly 90 percent of the industrial requirement. The rivers of the island have a radial distribution. The upper reaches are mainly confined to the hill country. Seasonal floods in low-lying areas cause extensive development of alluvium along the lower reaches of the major river systems. The alluvial clay deposits are thus concentrated in the lower reaches of the major river systems and in other low-lying areas.

Four-fifths of the island is made up of Precambrian crystalline rocks. Consequently the island is devoid of true consolidated clays except for a few shale formations. Nevertheless Sri Lanka is well provided with structural clays suitable for brickmaking occurring in many areas of the country, although brickmaking is more concentrated in several areas, notably in the south-west and north-west sectors.

A wide range of structural clays, mostly kaolinitic but differing in origin, mineralogy and properties are being used at the present time. Deposits of kaolinitic clay in Sri Lanka can be broadly classified into three categories as follows:

(i). Transported (alluvial) deposits.
(ii). Residual deposits.
(iii).Shale deposits.

Of these, alluvial deposits have provided the bulk of cottage brick and tile production. Those which occur in the flood plains of the major rivers are the most exploited. An industrial classification of structural clay deposits is given in Table 3.1, where the structural clays are listed according to their industrial uses and the age of parent material. A geological map of Sri Lanka showing the distribution of formations important to the clay industry is presented in Fig. 3.1.

Table 3.1-Industrial classification of structural clay deposits

Transported alluvial kaolin	Holocene (recent) river and lake deposits used in brick and tile and ceramic manufacture.
Residual kaolin	Pleistocene (quaternary) kaolinized gneiss and granite deposits extending up to recent periods. Deposits worked for the production of handmade bricks. Red earths belong to this principal formation.
Kaolinitic shales	Jurassic shales (predominantly carbonaceous) overlying mainly limestone. Limited mining is carried out purely for handmade bricks.

The features of these formations important to the clay industry are discussed in the ensuing text. Much of the following data has been collected during the field study. Relevant geological information has also been included.

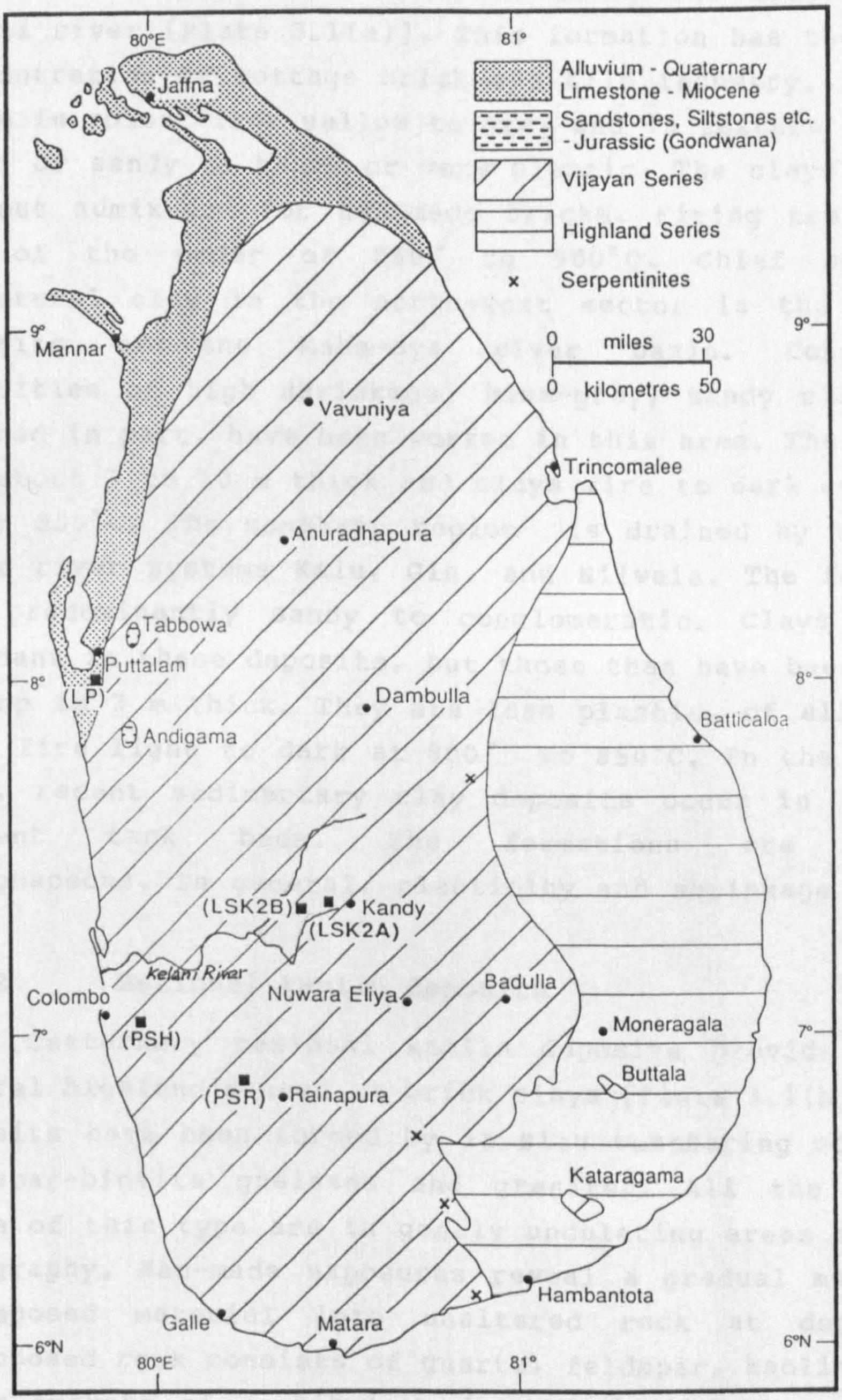

Fig. 3.1 Location of samples examined. (Collecting sites shown as black dots)

3.1.1 Transported kaolin deposits

Very extensive deposits of alluvial clays occur in the south-west sector of the island along the course of the Kelani river [Plate 3.1(a)]. This formation has the highest concentration of cottage brick and tile industry. The clays range in colour from yellow to grey and in texture from very light or sandy to heavy or very plastic. The clays are used without admixture for handmade bricks. Firing temperatures are of the order of 850° to 900°C. Chief source of structural clay in the north-west sector is the alluvial deposits of the Maha-oya river basin. Considerable quantities of high shrinkage, blue-grey, sandy clay, iron-stained in part, have been worked in this area. The deposits are about 3 to 10 m thick and clays fire to dark colours at about 850°C. The southern region is drained by the three major river systems Kalu, Gin, and Nilwala. The formations are predominantly sandy to conglomeratic. Clays are not abundant in these deposits, but those that have been located are up to 3 m thick. They are less plastic, of all colours and fire light to dark at 800° to 850°C. In the dry zone area, recent sedimentary clay deposits occur in abandoned ancient tank beds. The formations are commonly carbonaceous. In general, plasticity and shrinkage are very low.

3.1.2 Residual kaolin deposits

Quaternary residual kaolin deposits provide much of central highland's need of brick clays [Plate 3.1(b)]. These deposits have been formed by in situ weathering of quartz-feldspar-biotite gneisses and granites. All the residual clays of this type are in gently undulating areas of mature topography. Man-made exposures reveal a gradual merging of decomposed material into unaltered rock at depth. The decomposed rock consists of quartz, feldspar, kaolinite, and minor amounts of amphiboles with vermiculite and magnetite as the principal accessory minerals. Depth of alteration ranges from 10 to 15 m, but workable thickness is less due to iron staining or incomplete alterations.

CHAPTER 3

a

b

Plate 3.1-Brick clay formations.
(a)-Alluvial clay exposed in the pit (2-3 m deep).
(b)-Residual soil exposed in 3-4 m face.

CHAPTER 3

The kaolin horizon being worked has a thickness ranging from 2 to 5 m, averaging about 3 m, with a variable overburden of loose sand, gravel and gritty clay, 3 to 6 m thick. All the kaolin beds in the sequence are lenticular. There is a considerable variation in the mineralogy and properties of the clays. Although of high kaolin content the clay has little strength. Firing temperature is about 900°C.

3.1.3 Shale deposits

Jurassic shale deposits are of limited occurrence. Tabbowa, Andigama, and Pallama formations consisting of thin, discontinuous lenses of shale provide a limited supply of clays. The lenses are generally 5 m thick. The clays of the shale lenses comprise kaolinite and quartz with occasional accessory minerals. They are commonly somewhat silty or sandy and generally carry sufficient iron oxides to give a distinct red colour to the fired product.

Most of the mining operations of the three types of deposits are open cut. Because of their small scale nature, little attempt has been made to utilize sophisticated excavation and treatment processes. At many pits the production of high grade material is carried out by selective mining. The public and private sectors including the cottage industry consume nearly 1.4×10^6 m^3 of clay per annum. The annual clay brick production is close to 500 million.

3.2 MATERIALS

The five clays examined in this study were taken from four principal brickyards located within the wet and intermediate zones of the island. The present day climate of the areas is characterized by a tropical seasonal regime of rainy and dry spells. The total annual rainfall in the wet and intermediate zones is below 320 mm and 250 mm respectively. The average mean temperature of the wet zone lies between 21 -29°C and in the intermediate zone it is approximately 32°C.

CHAPTER 3

After visits to the brickyards and reference to the geological map, each of the clay formations and their weathered sequences was systematically sampled from open clay pits. The clay samples were sealed in the field to prevent drying and lattice dehydration. The samples collected were representative of three soil groups distinguishable on the basis of colour and texture. In the Sri Lankan soil classification system, the soils would be classed as Red-yellow podzolic soils, Reddish brown lateritic soils and Red-yellow latosols.

In all 52 samples from 13 representative pits were collected. Of these 28 samples were obtained from residual soil pits in the central region, 20 alluvial clay samples from pits in the western and south-western provinces, and 4 latosol samples from a weathered profile in the north-western province. The sampling was based on the changing stages of the weathered profile, or on other physical differences which were visually apparent.

The samples collected whilst not representing all the potentially valuable brick clays of the island generally provide a cross section of those now worked. The results obtained from these samples will indicate the variation in mineralogy and ceramic properties that could be expected in deposits of different formations.

The approximate position of the five sampling sites is shown in Fig. 3.1. Locations and descriptions of individual samples are given in Table 3.2.

The clay samples obtained from the pits were representative of the strata presently used for winning. The overburden, which had a depth of 0.5-1.0 m was removed manually prior to sampling. The bulk sample size was approximately 25 kg. Small grab samples of each clay type were also collected for testing the plastic properties.

Table 3.2-Description of samples

Location	Designation	Description	Uses
Kandy	LSK2A	Moderately well drained, brownish yellow (10YR 6/6) ferruginous lateritic soil derived from the feldspar of the quartz-feldspar-biotite gneisses and granites belonging to the crystalline complex. Depth 3 m. Soil contained hard and soft nodular concretions.	Bricks, sun-baked blocks
Katugas-tota	LSK2B	Moderately well drained pale yellow (2.5Y 6.5/4) kaolinized soft lateritic soil belonging to the lateritic soil group from a 3-4 m weathering profile of quartz-feldspar-biotite gneisses and granites.	Bricks, sun-baked blocks
Hanwella	PSH	Fluviatile sedimentary clay; dark grey (10YR 3/1.5) from the flood plains of Kelani river; 3-4 m.	Bricks, tiles,
Ratnapura	PSR	Imperfectly drained, grey (5Y 8/1) podzolic clay occurring in association with meta sediments	Bricks, tiles, pottery
Puttalam	LP	Well drained, yellowish brown (10YR 5/5.3) latosol from the north-west coastal plain; 0.5-1.0 m.	Fill and base material

CHAPTER 3

3.3 ANALYTICAL PROCEDURES

Chemical, physical and mineralogical analyses along with descriptions were made in order to characterize the soils and provide a better basis for their classification. The methods employed in clay mineral identification were X-ray diffraction, differential thermal analysis and infrared absorption analysis. The major and trace constituents of the soils were determined by both spectrometric method and X-ray fluorescence analysis. Where possible, electron probe microanalysis has also been used. The mineralogical composition was calculated from the results of chemical analyses and X-ray analysis. In addition to the above mentioned analyses, detailed particle size analysis was also made of the samples.

3.3.1 Qualitative mineralogical analysis

3.3.1.1 X-ray diffraction analysis

X-ray diffractograms for the raw clays and their clay fractions were obtained using unorientated and orientated specimen mounts, respectively. The raw clay samples were ground in an agate mortar before packing in a sample holder. The clay fractions were sedimented on glass slides from dispersed suspensions and dried. In both cases X-ray diffractograms were obtained using a Philips diffractometer set with CuK_{α} radiation and the minerals present were identified according to the d-spacings of the reflections. The results of X-ray analysis (Appendix 1) are discussed in Section 3.4.

3.3.1.2 Differential thermal analysis

Differential thermal analysis of the clays was carried out with a Stanton Redcroft STA-780 Series simultaneous DTA-TG-DTG thermal anlyser linked to a computer. DAPS-2 programme was used for the acquisition and analysis of data. A heating rate of 10°C/min and sample weight of about 30 mg were maintained in all cases. Coarse clay (2.0-0.2 um) samples were analysed with calcined alumina as the inert reference material. The range investigated was from ambient temperature to 1100°C. Both the DTA and TG curves and in

some cases DTG curves were recorded. The results (Appendix 2) are presented in Section 3.4.

3.3.2 Determination of chemical constituents

3.3.2.1 ICP Spectrometric analysis

The major and trace constituents of the soils were determined by the inductively coupled plasma (ICP) emission spectrometric method suggested by Walsh and Howie (1980) for silicate rocks and minerals. The methods of sample preparation and analysis are given below.

A sample of soil (0.5 g) passing through the 125 μm BS sieve was evaporated to dryness with 5 ml of perchloric acid ($HClO_4$) and 15 ml of 40% hydrofluoric acid (HF). The residue was treated with 25 ml of conc. hydrochloric acid, heated on a water bath for 30 minutes and cooled. The contents were then transferred to a conical flask and the solution was made up to 50 ml with distilled water.

The solution to be analysed was automatically sprayed into a high temperature flame in the spectrometer; the flame was of sufficient temperature to rupture the chemical bonds and excite a large number of intense spectral lines. The light emitted was then focussed into a conventional air path 1.5 m spectrometer, in which the spectral lines diffracted from the main grating were detected by fixed photomultipliers. The signal from the photomultipliers was analysed by the computer linked to the system with respect to the intensity readings obtained from solutions containing known concentrations of the elements stored in it. The results were obtained in a computer print-out of concentrations (Appendix 3).

The detection limits for the major elements by this method were below 0.01% and the precision was better than 1-2% and the ICP analysis was free from chemical interferences. The results are summarised in Table 3.3.

3.3.2.2 X-ray fluorescence analysis

Since the spectrometric analysis described in Section 3.3.2.1 does not allow direct determination of SiO_2, clays have been quantitatively analysed for major constituents, SiO_2, Al_2O_3, Fe_2O_3, TiO_2, and CaO by X-ray fluorescence.

In this technique the specimen is bombarded by X-rays of a wide spectrum of wavelengths. This causes fluorescent X-rays which are characteristic of the elements in the sample to be emitted by excitation of elements of lower atomic numbers. A suitable spectral line from a given element is selected by means of an analysing crystal and the intensity of the scattered radiation is measured by a counter. The count ratio (that is, number of counts/sec of sample ÷ number of counts/sec of standard) is proportional to the concentration of the element to be determined.

Samples for analysis were prepared by powder pressing clay (-100 mesh) into tablets as described by Poole (1970) for geological samples. A Philips X-ray spectrograph set up with a LiF analysing crystal was used. A number of reference standards similar in type to the unknowns were selected. The data for standards and unknowns corrected for background were used to prepare calibration curves. The unknown sample values were obtained from these curves.

The elemental analyses of coarse clay fractions of clays thus accomplished by spectrometric analysis in conjunction with fluorescence analysis are presented in Table 3.3.

Table 3.3-Chemical analyses of clays

Oxide constituent	LSK2A	LSK2B	PSH	PSR	LP
SiO_2	41.18	41.76	43.05	43.74	47.33
Al_2O_3	25.06	24.46	24.85	24.83	22.77
Fe_2O_3	16.43	16.73	12.34	11.79	11.12
MgO	1.56	0.90	0.82	0.50	0.41
CaO	1.30	0.82	0.43	0.46	0.50
Na_2O	0.32	0.14	0.29	0.28	0.19
K_2O	0.41	0.26	1.29	1.21	1.04
TiO_2	1.41	1.32	1.14	1.13	3.19
P_2O_5	0.17	0.12	0.18	0.15	0.07
MnO	0.11	0.19	0.07	0.09	0.16
Loss on ignition	12.05	13.30	15.54	15.82	13.22

The elemental analysis shows that the residual soils (LSK2A and LSK2B) are low in silica and high in iron. The total flux content ($RO + R_2O + Fe_2O_3 + TiO_2$) is substantially higher in these soils than in the others. This is of importance in the consideration of fusion characteristics of the soils at high temperatures. The K_2O content shows at least a three fold increase from the residual soils to the podzolic clays. The presence of sodium and potassium in all the soils examined indicates traces of feldspar (and micas).

3.3.3 Quantitative mineralogical analysis

3.3.3.1 Estimation of kaolinite

The amount of kaolinite was determined in the raw clays by the method of known additions (Brindley and Brown 1980) using pure kaolinite as the standard.

The raw clays were ground in an agate mortar to pass through 325 mesh sieve in order to minimize orientation

effects. 1 g of each sample was mixed with 0.1 g of standard kaolinite in a mechanical vibratory mixer. The prepared mixture packed in an aluminium sample holder was then scanned in the Philips diffractometer with filtered CuK_α radiation at 60 kV and 30 mA. The number of counts corresponding to the reflection of kaolinite at 3.56 A was measured before and after the addition. Necessary corrections were made for background scattering. Three sets of counts were taken for each sample and the procedure was repeated for prepared mixtures containing 0.15 g, 0.175 g, and 0.20 g additions of standard kaolinite. The intensity ratio given by the relation:

$$I_1/I_2 = \frac{W_p(1 + W_t)}{W_p + W_t}$$

where W_p = weight proportion of kaolinite in the clay mineral

W_t = amount of standard kaolinite added to 1 g of sample

I_1 = intensity of kaolinite peak before the addition

I_2 = intensity of kaolinite peak after the addition.

was used to construct calibration curves for the determination of kaolinite in the raw clays. Table 3.4 presents the analyses of the clays for kaolinite.

Table 3.4-Kaolinite and quartz contents of raw clays determined by XRD

Clay	% Kaolinite	% Quartz
LSK2A	46	31
LSK2B	74	15
PSH	59	21
PSR	55	18
LP	36	48

3.3.3.2 Estimation of quartz

The quartz content was determined for the five raw clays by XRD using pure quartz as the standard. The same counting technique as was used for the determination of kaolinite was used. Since the clays examined contain mica which interferes with the strongest quartz reflection at 3.34 Å, the interference free reflection of quartz at 1.82 Å was used for the estimation of quartz. Table 3.4 presents the quartz content of raw clay samples determined using the calibration curves constructed from intensity data.

3.3.3.3 Mineralogical balance sheet

The mineralogical balance sheet of the five raw brick clays was derived by a combination of analytical techniques. Kaolinite and quartz contents were estimated from quantitative XRD. Having detected the presence of feldspars by XRD, their relative amounts were calculated by rational analysis from bulk chemistry. The following factors were used for the calculation:

percentage K_2O x 5.913 = potash feldspar

percentage Na_2O x 8.435 = soda feldspar

Feldspars were assumed to have ideal stoichiometric formulae. Accessory minerals were estimated by subtracting the total amount of kaolinite, quartz and feldspars from 100%. The mineralogical balance sheet for the raw clays based on feldspar convention is shown in Table 3.5.

Table 3.5-Mineralogical balance sheet for raw brick clays

Clay	% Kaolinite	% Na feldspar	% K feldspar	% Quartz	% Minor accessory minerals
LSK2A	46	3	2	31	18
LSK2B	74	1	1	15	9
PSH	59	2	8	21	10
PSR	55	2	7	18	18
LP	36	1	6	48	9

Table 3.5 shows that the raw brick clays vary quite considerably in mineralogy. LSK2B has the highest kaolinite content (74%) and LP the lowest (36%). The highest feldspar content was found in PSH (10%) and the lowest in LSK2B (2%). The undesirable properties of latosol (LP) are evident from its high quartz content (48%) and low kaolinite content. Residual soil, LSK2B has a favourable mineral assemblage compared to widely used podzolic clays, PSH and PSR.

3.3.4 Infrared absorption analysis

The constituent atoms of a mineral have vibrations with frequencies in the infrared region of the spectrum. When the mineral is irradiated by a range of monochromatic frequencies, absorption occurs at several bands. The resultant spectrum of absorption frequencies is a characteristic property of the mineral which not only serves as a finger print for its identification, but also provides, useful information on structural features, including the differentiation of chemically combined water from constitutional hydroxyl, the degree of order of the structure, the nature of isomorphic substituents and an indication of the family of minerals to which an unknown mineral is related.

The absorption spectra were used for supplementing the finding from XRD, DTA and TGA and also for determining the crystallinity index of kaolinite.

The method of sample preparation for infrared absorption analysis is as follows. A small amount of the sample (~1.5 mg) was ground and mixed with potassium bromide in an agate mortar. The mixture was placed in a 12.5 mm die cavity and pressed at a pressure of 8 tons. The infrared spectrum of the sample between 400 to 4000 cm^{-1} was then recorded using a Pye Unicam SP 1100 spectrophotometer. The infrared spectra of the clays (Appendix 4) are presented Section 3.4.

3.3.4.1 Infrared spectra of clay minerals

The infrared spectra of clay minerals yield useful information supplementary to that given by X-ray and thermal studies. The sensitivity of infrared spectroscopy to components of a clay mixture is often very different from other methods. Gibbsite, goethite, quartz, kaolinite and halloysite have all been recognized by infrared where their presence was uncertain from X-ray diffraction (Farmer 1974). The absorption of kaolin minerals near 3700 cm^{-1} is uniquely distinctive, and allows their identification when other constituents interfere with the 7 Å signal of the anhydrous kaolinites or the 10 Å peak of hydrated species (Kodama and Oinuma 1963). Kaolinite and gibbsite can be detected at lower levels by their OH stretching bands than by X-ray techniques (Wilson 1966).

As each layer of a silicate absorbs infrared radiation independently, their detection does not depend on the regular successive stacking required to give a distinctive X-ray pattern. Thus hydrothermal conversion of montmorillonite to kaolinite is detectable at a very early stage, before three-dimensional order has been achieved (Poncelot and Brindley 1967).

Infrared spectra appear to be particularly sensitive to disorder in crystal structures. The rather diffuse spectra of many fireclays and ball clays indicate that the disorder in the structure of these kaolinitic minerals does not consist solely of stacking faults (Beutelspacher and Marel 1961). The high sensitivity of infrared methods to such well ordered species as kaolinite can, however, be a disadvantage, as the sharp absorption bands of kaolinite often obscure the more diffuse bands of more poorly ordered species, although the latter may be from the major part of the sample (Farmer 1974).

Infrared absorption of both amorphous compounds and crystalline compounds depend on the atomic composition and bonding; the presence of amorphous compounds in admixtures is therefore, easily recognizable in infrared spectra than

in X-ray traces. This allows resolution of, for example, discrete silica phase in association with a silica-alumina phase, and structural differences between allophane and silica-alumina gels of similar composition (Mitchell, Farmer and McHardy 1964; Wada 1967). On the other hand, vermiculite which produces diffuse absorption due to weak OH stretching bands in allophane soils is more readily detected by X-ray methods (Wada 1967).

The identification of clay minerals by infrared spectra is greatly facilitated by reference to spectra of well characterized specimens. Valuable collections of layer-silicate spectra have been published by Farmer (1974), Oinuma and Hayashi (1968), Marel (1966) and Stubican and Roy (1961).

The infrared spectrum of a well crystallized kaolinite presents four OH stretching bands. It has been shown by deuteration of intercalated kaolinite (Ledoux and White 1964) that the band around 3625-3620 cm^{-1} is due to the hydroxyl groups located inside the sheet (inner hydroxyl). The three other bands, observed around 3697, 3669 and 3652 cm^{-1}, are due to hydroxyl groups constituting one side of the sheet, sometimes referred to as inner-surface hydroxyls. The in-plane bending vibrations of surface hydroxyl groups in the kaolinite minerals lie at 936 cm^{-1} and that of inner hydroxyl at 915 cm^{-1}. The relative intensities of these bands depend not only upon the nature of the kaolinite but also upon the shape of the particles, their orientation and the angle of incidence of radiation upon the specimen examined in the spectrometer.

The spectral features presented in the foregoing paragraphs were used in the interpretation of absorption spectra of five brick clays (Section 3.4).

3.3.4.2 Crystallinity index

Several methods of measuring the crystallinity index of kaolinite have been described in the literature. These methods have proved satisfactory for well crystallised kaolinite, but problems due to interference arise when

dealing with samples containing a mixture of disordered kaolinite and illite.

In an attempt to classify kaolinites by infrared spectroscopy, Parker (1969) plotted the ratio of the absorption of the two bands at 3695 and 3620 cm^{-1} of orientated samples against the corresponding ratio from randomly orientated samples of various types of kaolinite; concentration of points occurred in certain areas, a single type of kaolinite being dominant in each area. He concluded that changes in the ratio of absorption bands for a randomly orientated sample were related to the degree of order of kaolinite present, that is, whether it was well-crystallized or disordered. However, illite which gives an absorption band at 3640 cm^{-1} overlapping that of kaolinite limits the scope of the method.

Neal and Worral (1977) determined the crystallinity index of kaolinite in fireclays on the basis of the absorption ratio (A_{3695}/A_{910}) ascertained from the interference free absorption band at 910 cm^{-1} of the spectrum instead of the conflicting band at 3640 cm^{-1}. This approach was used in the present study to determine the crystallinity index of kaolinite present in the soils under investigation. The values of crystallinity index of kaolinite in the coarse clay fraction (2.0-0.2 μm) are given in Table 3.6.

Table 3.6-Crystallinity index of kaolinite in coarse clay fraction of raw clays

Clay fraction	Crystallinity index
LSK2A	0.64
LSK2B	0.58
PSH	2.33
PSR	0.43
LP	0.62

3.3.5 Particle size analysis

The particle size distribution of the raw clay samples were determined by wet-sieving according to BS 1377:1975 (Methods of test for soils for civil engineering purposes). The percentage of material in the -63 um size range was determined by pipette method with sodium hexametaphosphate as the dispersing agent. The size distribution curves for the five clays are given in Fig. 3.2.

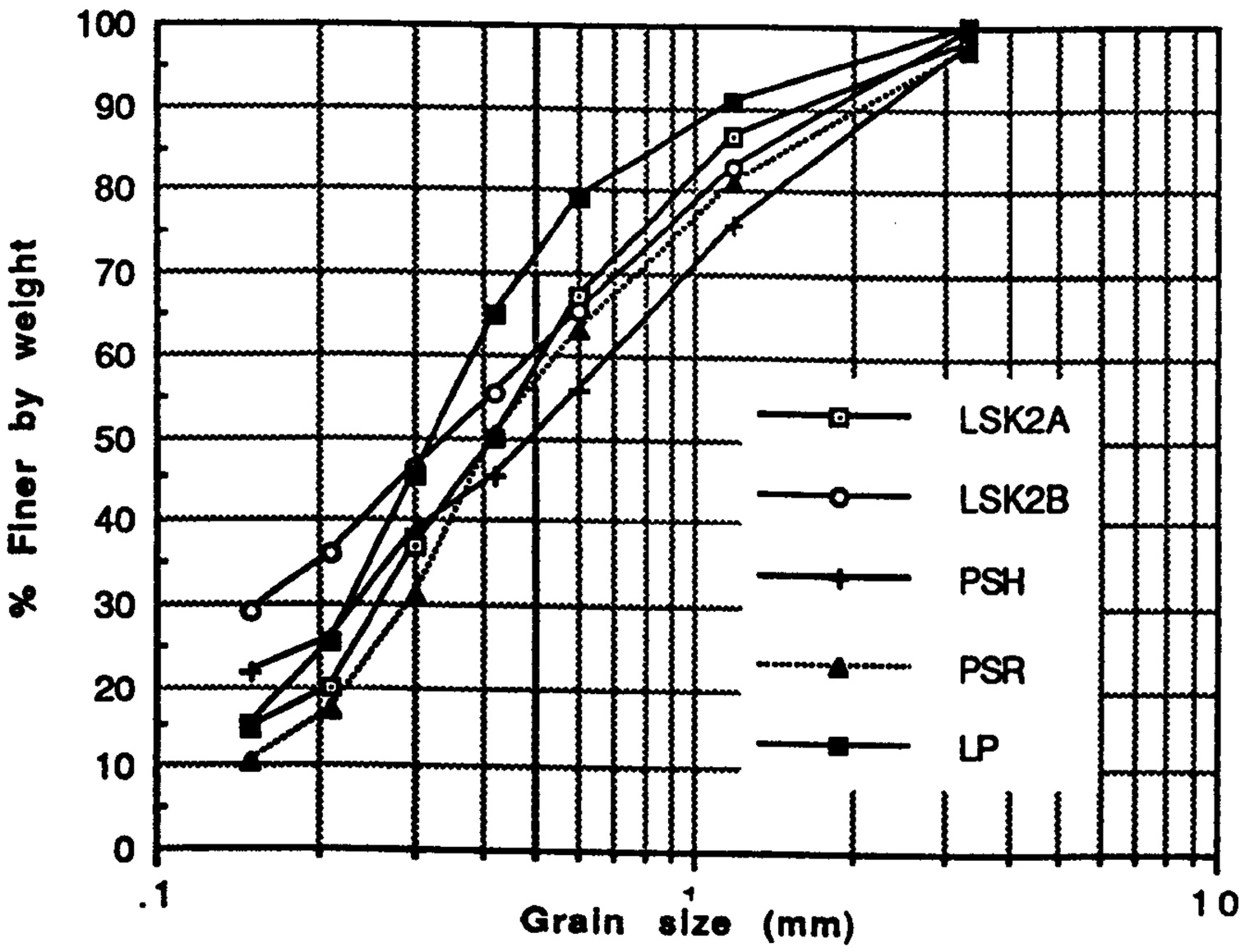

Fig. 3.2-Particle size distribution curves of the clays.

The soils were characterized in terms of sand, silt and clay fractions according to the scheme recommended by Shepard (1954) for intermediate and fine-grained sediments by plotting the percentages on a triangular diagram (Fig. 3.3).

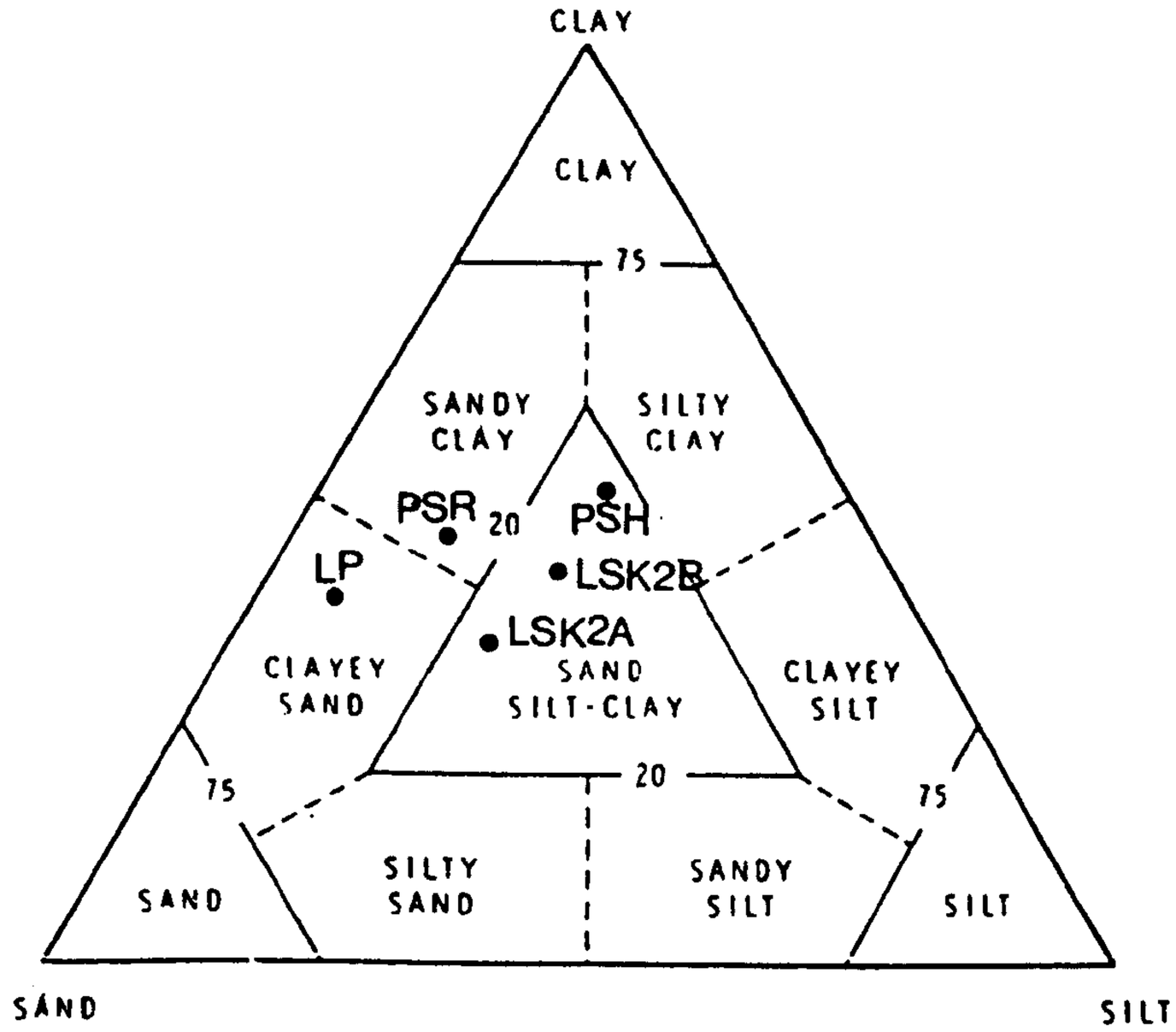

Fig. 3.3-Classification of soils (after Shepard 1954).

The two residual soils, LSK2A and LSK2B, and the podzolic clay, PSH, occupy the sand-silt-clay region of the grading triangle. The podzolic clay, PSR, can be classified as a sandy clay whereas the latosol, LP, can be classified as a clayey sand.

It has been found that acceptable plastic properties correlate with specific granulometric compositions. The generalized limiting ranges of favourable granulometric composition proposed by Winkler (1954) and Niesper (1958) were used to determine the suitability of clays for brickmaking (Fig. 3.4).

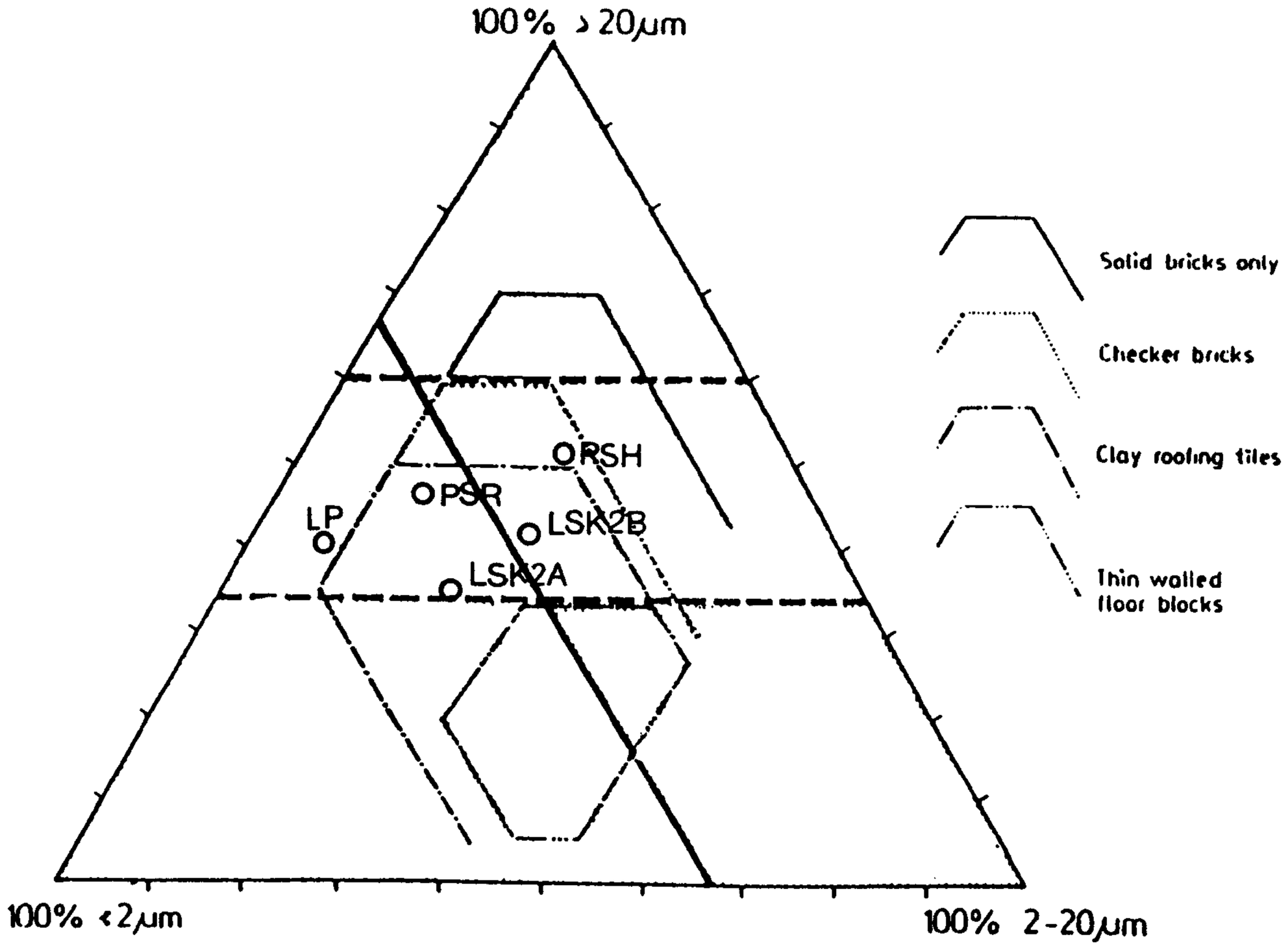

Fig. 3.4-Grading triangle for classification of clays according to their end uses (after Niesper 1958).

Latosol fails to satisfy the limiting particle size criterion because of its coarseness. Residual soils and podzolic clays are suitable for brickmaking. This triangular diagram also shows clearly the relationships of three size groups-sand (>20u), silt (20 to 2u), and clay (<2u)-which exert significant control on the properties of the clay material. Examination of Fig. 3.4 shows the high silt content of latosol. Much of the silt fraction seems to be due to fine-grained quartz and accessory minerals. As weathering proceeds there is a significant reduction in particle size. Those materials highest in clay size particles are the podzolic clays. However, they are much more variable than residual soils in their particle size range, reflecting the differences in pedogenesis.

CHAPTER 3

3.4 CLAY MINERALOGY

The X-ray diffractograms of the coarse clay fractions (2.0-0.2 μm) of the clays are shown in Fig. 3.5. The predominant constituents identified in the two residual soils (LSK2A and LSK2B) were kaolinite as evidenced by peaks at 7.2 and 3.56 Å and the absence of characteristic chlorite peaks, quartz (3.34 Å) and K, Na, Ca-feldspars (4.24, 4.12, 3.77, 2.99 and 2.93 Å). The accessory minerals included vermiculite (14.34 Å) and amphiboles (8.39 Å). The appearance of a continuous band, instead of triplets in the 2.25-2.56 Å range probably indicate the presence of halloysite or the low degree of order of kaolinite in the two clays. The fine-grained soil LSK2B contained no vermiculite.

The two podzolic clays (PSH and PSR) from the wet zone differ from the residual soils in containing gibbsite as indicated by the 4.8 and 4.37 Å peaks. The other dominant minerals present were kaolinite, feldspars, quartz and vermiculite. The podzolic clay PSH was shown to be high in feldspars by the presence of strong reflections at 3.77, 3.23 and 3.18 Å. They probably arise from two different feldspars.

The intermediate zone soil latosol (LP) contained less-ordered kaolinite (4.46 Å). Quartz and K-feldspars were also present with only a trace of goethite (2.69 Å).

X-ray diffraction analysis of the fine clay fractions (<o.2μm) of the soils showed them to be composed predominantly of kaolinite. Table 3.7 summarizes the minerals present in the coarse and fine clay fractions of the five clays.

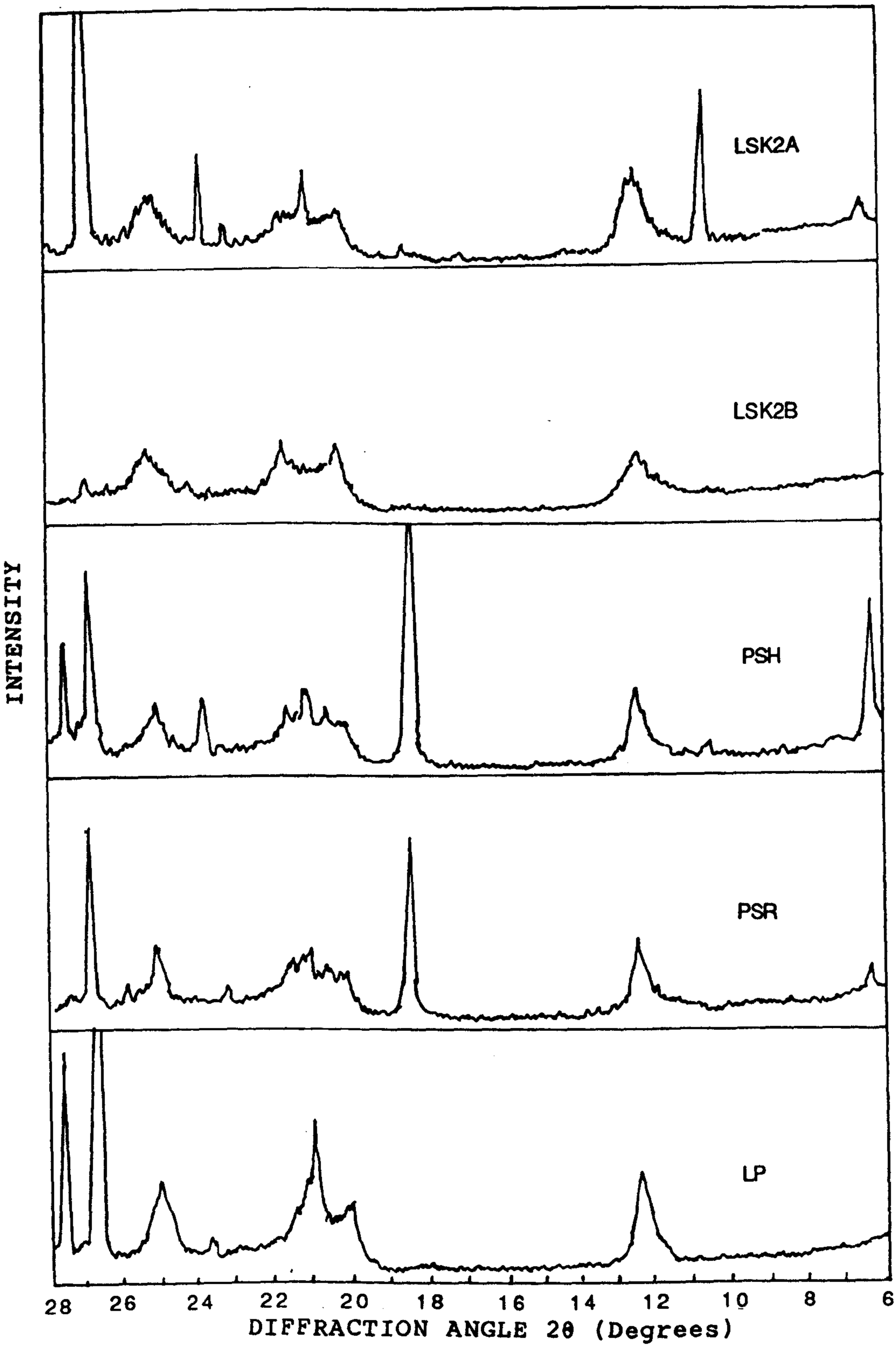

Fig. 3.5-X-ray diffraction patterns of the coarse clay fractions of clays.

Table 3.7-Mineralogical constituents present in raw brick clays

Clay	Geat soil group	Major constituents	Minor constituents
LSK2A	Reddish brown lateritic soils	quartz, kaolinite, K-feldspar, Na and Ca-feldspars	vermiculite, amphiboles
LSK2B	Reddish brown lateritic soils	quartz, kaolinite, K-feldspar, Na and Ca-feldspars	amphiboles
PSH	Red-yellow podzolic soils (Sub-group with Plinthite)	quartz, kaolinite, K-feldspar, Na and Ca-feldspars	gibbsite, vermiculite
PSR	Red-yellow podzolic soils (Modal)	quartz, kaolinite, K-feldspar	gibbsite, vermiculite
LP	Red-yellow latosols	quartz, kaolinite (disordered), K-feldspar	traces of goethite

It is evident from the above that the clay fractions of the samples studied differ from each other in mineralogical composition. The residual soils with a low degree of weathering are characterised by the presence of minerals such as vermiculite and amphiboles. The podzolic clays on the other hand, are developed on sedimentary materials which are relatively more weathered. They contain an appreciable amount of gibbsite indicating that they are the most weathered of the samples studied. Latosol, devoid

of accessory minerals and gibbsite represents an intermediate weathering profile.

DTA diagrams for the coarse clay fractions of the five clays are reproduced in Fig. 3.6. In general the DTA curves confirm and supplement the conclusions drawn from the X-ray analysis. They revealed the presence of kaolinite which had endothermic peaks in the 470°to 490°C range and exothermic peaks at 870°to 950°C. The exothermic peak attributed to kaolinite-mullite transformation of the residual soil LSK2B (926.2°C) is quite sharp. Mullite nucleation is of a lesser magnitude in other soils indicated by subdued exothermic peaks. Exothermic response is in the form of a very small upward inflection in the podzolic clay PSR. Diffuse endothermic peaks in the region of 70°C are attributed to physically adsorbed water. The DTA curves for the three clays LSK2A, PSH and PSR show a distinct endothermic reaction between 260° and 280°C probably caused by vermiculite (Smykatz-Kloss 1974). The weak endothermic deflection at 572°C produced by the two quartz-rich soils LSK2A and LP represents the inversion of quartz.

The thermogravimetric (TG) curves (Appendix 2) show a rapid weight loss up to about 70°C followed by a slow but steady weight loss up to about 250°C. A rapid loss due to the evolution of combined water starts at about 320-350°C and proceeds to about 550°C. The weight-loss curves flatten out above a temperature of approximately 700°C.

The kaolinite content of the clays was estimated by thermogravimetry using the weight loss associated with the evolution of combined water on dehydroxylation. According to Bain and Morgan (1970), this is more reliable than utilizing the peak areas on DTA curves, where the position of the line defining the base of the peak is often uncertain, and the area might be slightly enhanced by the thermal energy released by the polymorphic transition of quartz. However, distinct quartz transition occurred evidently at a higher temperature (572°C) than the dehydroxylation of the clays

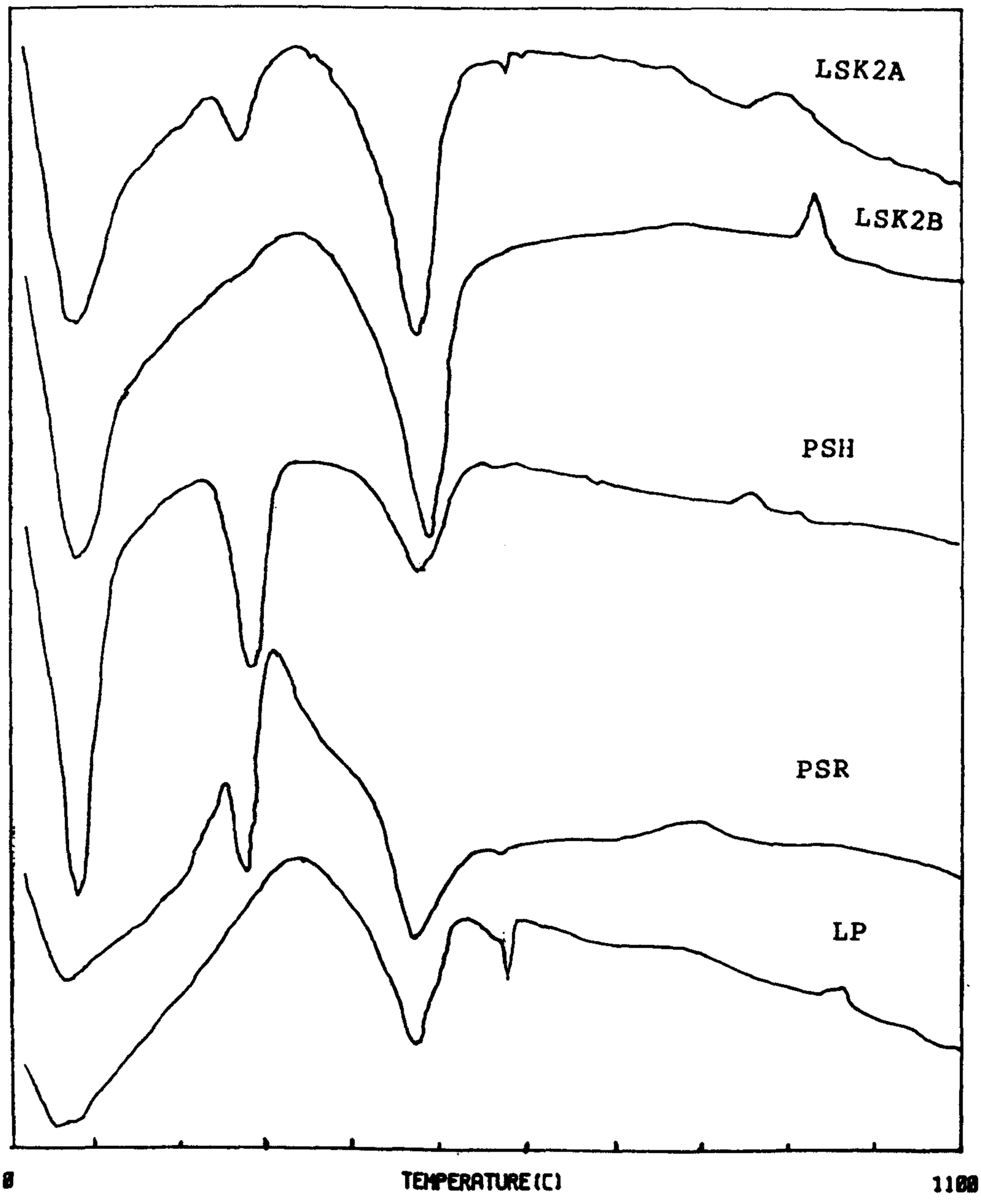

Fig. 3.6-Differential thermal curves of the clays.

(480°C) examined. Nevertheless weight loss data were used for the quantitative estimation of kaolinite in the clays. Analyses were made by reference to the TG data of standard kaolinite from Dixie Rubber Pit, South Carolina, U.S.A., obtained under the same conditions. The weight-loss values and the corresponding kaolinite contents of the clays are listed in Table 3.8.

Table 3.8-Kaolinite contents of raw clays determined by TGA in conjunction with DTA

Clay	% Weight loss (dehydroxylation)	% Kaolinite
LSK2A	4.77	38
LSK2B	7.06	56
PSH	5.69	45
PSR	6.60	53
LP	2.11	17

The results from XRD and DTA (Tables 3.4 and 3.8) analyses differ widely, DTA generally giving the lowest figures.

The infrared absorption spectra of the -125 μm fraction of the soils are given in Fig. 3.7. The characteristic spectral features of the five soils include:

(i). The presence of a very broad band in the 3450-3500 cm^{-1} region accompanied by two distinct shoulders at approximately 3640 and 3710 cm^{-1}. These are assigned to OH stretching frequencies for adsorbed water, inner hydroxyls and free hydroxyls respectively of kaolinite. The presence of two low frequency bands at 1100 and 910 cm^{-1} corresponding to Si-O and H-O---Al stretching is again clear evidence for the kaolinitic nature of the soils.

(ii). The weak band near 1630 cm^{-1} can be correlated with the bending vibration of OH due to adsorbed water. However, this is also indicative of the adsorption bonds of amorphous materials with high surface area which are insensitive to X-ray analysis.

(iii).The band of medium intensity at 462 cm^{-1} and a weaker absorption at 800 cm^{-1} correspond to quartz.

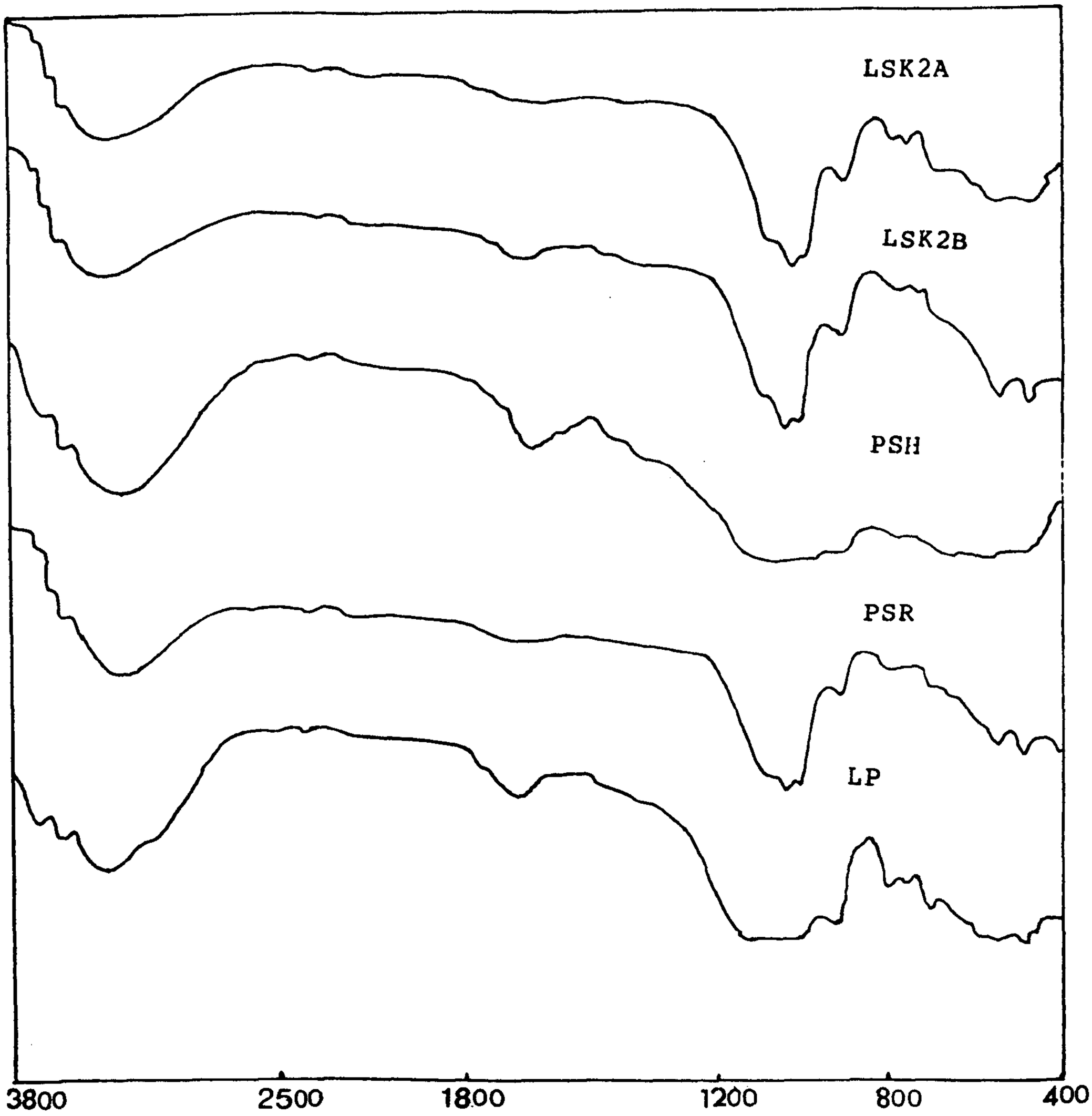

Fig. 3.7-Infrared absorption spectra of the clays.

(iv). The strong doublet at 1030 and 1000 cm^{-1} is due to microcline and muscovite in the two residual clays (LSK2A and LSK2B). Taken in conjunction with the X-ray analyses, the absorption band at 1030 cm^{-1} correspond to gibbsite present in the two podzolic clays (PSH and PSR). The additional band at 530 cm^{-1} is consistent with the presence of traces of muscovite not detected in the X-ray analysis.

CHAPTER 4

EXPERIMENTAL METHODS

Mineralogical and field studies described in Chapter 3 were aimed at obtaining information on the clay mineralogy and physico-chemical characteristics of the clay materials, and thus to evaluate the relationships of the various types, and to arrive at an understanding of the practices employed in their utilization.

The experimental programme involved a series of techniques designed for strengthening the clay bodies under consideration. Particular emphasis was placed at each stage to effect strengthening at low firing temperatures than those currently employed in practice. The first experimental system outlined below dealt with a kinetic analysis for the computation of optimum heat treatments. The other systems were concerned with techniques of improving structural strength of fired clay products. Critical problem areas were outlined. The experimental methods are summarised below.

4.1 ESTIMATION OF OPTIMUM FIRING CONDITIONS FOR CLAYS

4.1.1 Introduction

An investigation into the properties of five brick clays was conducted to establish the optimum firing conditions required to obtain a technically acceptable product.

4.1.2 Method

Five clay mixes were isostatically pressed at 500 p.s.i. to form discs (diameter-30 mm, thickness-4 mm). Each disc contained 8.00 g of material. The discs were subjected to different heat treatments at peak temperatures from 1025° to 1100°C, under a range of isothermal firing times. Physical properties of fired specimens indicative of the degree of vitrification viz. bulk density, apparent porosity, water absorption and volume contraction were measured. The critical time of vitrification corresponding

to optima of properties for each heat treatment was ascertained from the observed property trends.

The kinetic analysis involved the application of Arrhenius equation ($k = Ae^{-Ea/RT}$) for the vitrification of the ceramic bodies examined. The 'logarithmic time of vitrification' method of treatment of isothermal data yielded the exponential factor (Ea/R) from the reasonably well-correlated linear plots of log. time of vitrification vs. reciprocal firing temperature. Empirical relationships between rate of vitrification and firing temperature for clay bodies were thus developed, based on the experimentally determined values of the exponential factor. These relationships were used to determine the heat treatments productive of the maximum mechanical strength of the clay bodies.

Chapter 5 deals with the experimental technique used in this study.

4.2 STRENGTH ENHANCEMENT BY SURFACE COATING

4.2.1 Introduction

This study dealt with the development of a clay product with an in situ coating which minimizes surface imperfections where the stress raising effects are localized. The coating was produced by an efflorescence deposition technique.

4.2.2 Methods

Fusibility study of clays

Each clay was ground to pass through 63 μm BS sieve and dispersed in water. A slip coating prepared from ground clay was applied on the top surface of dried moulded bars. Coated bars were then air dried for 24 h and fired in an electric furnace according to a fixed firing schedule. After firing, the maturing characteristics of the surface coatings were investigated in relation to the SiO_2/Al_2O_3 ratios of the clays.

CHAPTER 4

Effect of fluxing materials on the fusibility of clays

The chemical analyses were the starting points for experimental procedure which consisted in adjusting the silica and alumina proportions and also the RO (CaO + MgO) and R_2O (K_2O + Na_2O) contents in the mixes with admixtures involving the following materials;

(i). wood ash
(ii). lime
(iii) sodium carbonate
(iv). sodium chloride

Electron microprobe analysis of wood ash was made and other materials were assumed to be of stoichiometric composition for the purpose of formulation. Eight different series were made with the clay-flux constituents. The materials in powder form were dry mixed in a plastic tube mill for 5 min. The experimental mixes applied on green ware were fired at 900°C in an electric furnace for 2 h.

The maturing characteristics of the mixes were studied in relation to the total flux content and the SiO_2/Al_2O_3 ratio.

Compositions in the binary system SiO_2-Na_2O

Four experimental mixes were prepared with analar grade Na_2CO_3 and silica powder ground to pass through 63 μm sieve. Compositions were chosen to represent the two known binary eutectics of the system. Dry mixing of materials was carried out in a vibratory mill for 10 min. The experimental bars made from residual soil LSK2A were thinly covered with both dry and wet mixes and fired at 900°C for 2 h in an electric furnace. Evaluation of compositions were made with respect to body-coating interaction.

CHAPTER 4

Conventional multi-component systems

The data available on the recent analyses of coatings used in antiquity and also the details reported on the state-of-the-art of conventional technology were used as starting points for experiments. The following procedure was adapted in formulating batch compositions.

(i). the reported analyses of the compositions were expressed in terms of oxide constituents.

(ii). the raw materials were allocated in molecular ratios to satisfy the quantities of oxides.

(iii). percentage batch composition was then deduced from the molar composition using molecular weights of raw materials.

The compositions discussed above did not prove satisfactory for the desired firing range.

Coating based on the ternary system Na_2O-Al_2O_3-SiO_2 produced by efflorescence technique

A series of experiments were made with the two clay bodies, latosol (LP) and residual soil (LKS2A); analar grade Na_2CO_3 was used to activate the formation of self-coated layer.

The fraction of soil passing through 1.18 mm test sieve was used. A pre-determined quantity of Na_2CO_3 was dissolved in optimum amount of distilled water sufficient to bring clay mass into moulding consistency. The ingredients were then intimately mixed and rectangular bars (160 mm x 30 mm x15 mm) were moulded at a pre-moulding moisture content of 13-29% depending on the type of clay. The moulded specimens were first air dried at room temperature (20°C) for a period of 4 days to promote efflorescence deposition and then oven dried at 50°C to a final moisture content of about 3%. The top surfaces of dried specimens were then sprinkled with silica sand ground to pass through 63 μm BS sieve and the specimens were fired in an electric furnace at 900°C for 2 h to obtain a self-coated clay product.

A series of trials were conducted to establish the optimum conditions for the following processing variables.

(i). Granulometric composition of clay
(ii). Source of Na_2O
(iii).Concentration of salt
(iv). Rate of drying (temperature and period of air and oven drying)
(v). Schedule of firing

4.2.3 Evaluation

The effects of the surface coating on the mechanical strengths (modulus of rupture and modulus of elasticity) of clay bodies were investigated. Step-wise microprobe analysis across the profile of the coating in thin section was carried out to examine the characteristics of coatings and the mechanism of interface reactions. Simplified calculations of the stresses generated by the coating based on expansion data and microprobe analyses were used to determine the factors underlying the strength enhancement of the coated clay bodies.

An accelerated durability test was designed to suit the climatic conditions of Sri Lanka in order to evaluate the performance of clay bricks. The test was also intended to induce thermal stresses which tend to craze the surface coating of brick. The details of experiments and results are presented in Chapter 6.

4.3 THE INFLUENCE OF $CaCO_3$ MINERALIZER, MULLITE, HEMATITE AND POROSITY ON THE STRENGTH

4.3.1 Introduction

The objective of this section of research was to examine the influence of $CaCO_3$ mineralizer on the high temperature phase development and strength improvement of clays and to determine the quantitative relations among the modulus of rupture, porosity, hematite content and mullite content in fired clay bodies.

4.3.2 Method

Three brick clay samples (LSK2A, PSH and LP) covering different formational types, localities of origin, degrees of order and particle sizes were employed. The minus 1.40 mm fraction of clay was oven dried (105°C, 24 h) and then mixed with 2, 3 and 4 wt% of lime in a mechanical mixer. An optimum amount of water was added in order to bring each sample to the correct consistency for wet moulding. The clay mixes were allowed to mature for at least 20 h and then compacted into 160 mm x 30 mm x 15 mm bars at a moulding moisture content of 25-30%. A minimum of 6 bars to represent each sub- sample (and a total of 144 bars to represent 6 firing trials of each clay mix) were made. The experimental bars were air dried and then oven dried (105°C, 24 h) before firing in an electric furnace; the bars were heated at a rate of 5°C/min, held for 2 h at the peak temperatures of 700°, 800°, 1000° and 1150°C and then cooled naturally to simulate the normal manufacturing conditions.

The fired bars produced under different experimental conditions were tested for

(i). Modulus of rupture
(ii) Linear drying shrinkage
(iii) Linear firing shrinkage
(iv). Water absorption
(v). Porosity
(vi). Relative density
(vii).Efflorescence

The trends of property variation were established with respect to the mineralizer content. Mineralogical changes which occurred during firing were followed by XRD analysis. The effect of firing on the internal morphology of the clays was examined by SEM. Constitution of high temperature phases was studied by electron probe microanalysis.

In order to determine the dependence of modulus of rupture on the textural characteristics, the mean of the modulus of rupture of specimens fired at each temperature was plotted against the integrated intensity of:

(i). mullite (110) reflection
(ii). common mullite and hematite (220) reflection
(iii).hematite (110) reflection

The experimental values were initially fitted to two constant equations by the least squares method. Regression equations with high degree of correlation were chosen. In addition, a quantitative relationship between modulus of rupture and porosity was established from the relevant property trend. An empirical relation which well represents the combined effects of mullite content and porosity on the modulus of rupture of the clay bodies was then obtained.

Mechanisms whereby development of strength occurs in both raw clays and clay-$CaCO_3$ compositions were elucidated from the microstructural features and phase relations. The experimental method and the results are presented in Chapters 7 and 8.

4.4 THE USE OF THE REACTIONS OF PHOSPHATES WITH CLAY MINERALS FOR LOW TEMPERATURE STRENGTHENING

4.4.1 Introduction

The purpose of this investigation was to explore the possibility of utilizing the reactions of phosphates with clay minerals which are known to occur at low temperatures from the viewpoint of strengthening clay products at low temperatures of firing.

4.4.2 Method

The investigation consisted of experiments designed to:

(i). Ascertain the preparation criteria of clay mixes such as the equilibrium pH, optimum concentration of phosphate and time of maturing,
(ii). Establish conditions most favourable for the suppression of the possible formation of harmful products of phosphate-silicate reaction,
(iii).Utilize undesirable reaction products, if any, by making them react with admixtures,

(iv). Study the variation of properties such as modulus of rupture, porosity, bulk density, and shrinkage of the bonded clay bodies with the temperature of firing,

(v). Examine the changes in constitution and microstructure of bonded clay bodies by XRD, SEM, IRS and DSC studies,

(vi). Evolve a possible mechanism for the reaction leading to bonding of phosphates with clay minerals.

The clay used was the residual soil (LSK2A) and the details of the method of fabrication and product evaluation are given in Chapter 9.

4.4.3 Evaluation of the durabilty

Laboratory tests were designed to evaluate the durabilities of the samples in relation to the performance of samples of engineering brick satisfying standard specifications.

CHAPTER 5

ESTIMATION OF OPTIMUM FIRING CONDITIONS FOR CLAYS

This chapter describes an investigation into the properties of five brick clays to establish the optimum firing conditions required to obtain a technically acceptable product.

5.1 INTRODUCTION

Firing is the most important process in the manufacture of structural clay products that determines the physical properties of the final product. The properties of the product such as strength, porosity, frost resistance, thermal expansion, thermal conductivity and hardness are determined by the relative abundance and textures of the various phases resulting from the firing process. Firing also accounts for a major part of the cost of producing clay products. Considerations of the firing schedule [rate of heating, peak temperature and isothermal holding (soaking) time] are therefore very important to the efficiency and economy of the firing process. Acceleration of firing brings about increased kiln output, together with reduced energy consumption. Although these aspects have been applied for centuries by trial and error, there has long been a need for a scientific method of determining the optimum firing conditions. A major difficulty in developing such a method is in the assessment of the extent of completion of reactions occurring in heat-treated ware. In the past this has been attempted rather empirically.

The method of computation of heat treatment for whiteware bodies proposed by Meyer and Shelton (1938) is particularly noteworthy. They derived a cumbersome expression for feldspathic compositions to determine the compatible heat treatments on the basis of the value of A_z (area under the reaction rate-temperature curve) associated with a certain degree of vitrification. It appears, however, that a simple and practical approach to estimate the extent of firing in relation to the degree of vitrification is

imperative for the effective use of correlative expressions in technological practice.

The purpose of the investigation is to establish optimum firing conditions for the brick clays based on the first order kinetics applied to the reactions leading to the vitrification of these kaolinitic clays. This was undertaken as a prerequisite for work on the strength improvement of clays. In order to establish data for the kinetic analysis, it was necessary to evolve physical property relationships with the degree of firing and to establish criteria for ascertaining the optimum state of firing.

5.1.1 Physical property relationships

Very little information has been published on the manner in which the intrinsic properties of tropical ferruginous soils vary according to the conditions of firing. This has important practical implications, for example can the critical stresses that arise in the firing of clay bodies be modified by the control of firing schedule; are the physical properties which characterize the degree of sintering or body maturing time-temperature related ? The lack of such information necessitated investigations to determine and correlate the effects of heat treatment on the physical properties of clay bodies.

5.1.2 Optimum state of firing

The effect of firing temperature on the porosity and linear shrinkage of a triaxial body is depicted in Fig. 5.1. The diagram indicates that apparent porosity decreases with increasing firing temperature up to a minimum beyond which bloating occurs. An opposite trend is followed by linear shrinkage. This phenomenon is ascribed to the growth of pores caused by the evolution of gases dissolved in the melt or liberated by decomposition, for example, of Fe_2O_3 (Maniatis and Tite 1975). It is associated with a loss of mechanical strength. Thus both strength and durability (characterized by porosity) improve with the degree of heat treatment up to a point beyond which further heat treatment

impairs the properties. This effect remains unaltered irrespective of the variation in time of soaking.

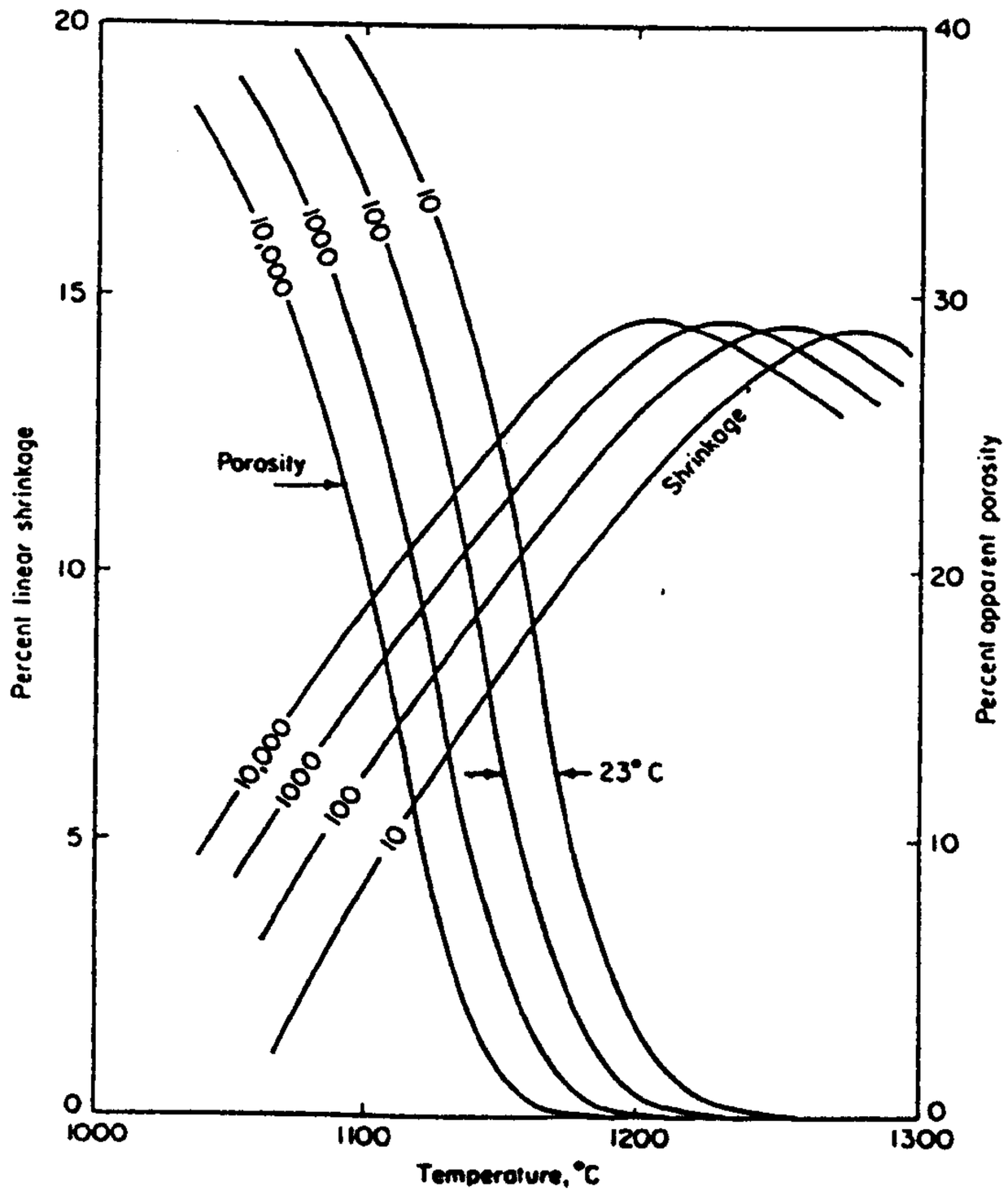

Fig. 5.1-Effect of time and temperature on a triaxial body. Numbers on curves are holding times in minutes (after Norton 1970).

The optimum firing refers to the extent to which a clay body must be fired in order to have an acceptable range of properties. In current technological practice, firing conditions appropriate to a particular product are usually determined by trial and error. A technological parameter such as strength or water absorption specified for the end use of the product are determined on specimens subjected to a series of firing schedules. A schedule which yields a desirable product irrespective of its heat work requirement is finally chosen. This procedure, however, does not permit subsequent transformation to alternative schedules for optimization of firing. Moreover, methods based on experience have disadvantages. When more than one product specification criteria are considered important, for example

volume shrinkage to represent body maturity and saturation coefficient to guarantee durability, a satisfactory compromise is difficult to achieve. Therefore a method based on the degree of vitrification as the criterion for determining the optimum state of firing was considered in the study. The method of determination of the optimum state of firing is described in the following paragraphs.

The effect of heat treatment on the degree of vitrification is characterized by a property such as porosity, water absorption or dry-to-fired shrinkage. The following changes in properties beyond the point of complete vitrification are well recognized.

(i). volume shrinkage ceases and swelling begins.
(ii). apparent porosity and water absorption increase and bloating occurs.
(iii).bulk density decreases and deformation begins.

Within the context of this investigation, the point of complete vitrification was assumed to lie midway between incipient vitrification and fusion where critical changes in properties occur (Ries 1947). This was ascertained by the optima of physical properties. Specimens were considered to have optimum physical properties when bulk density and volume contraction were maximum and apparent porosity and water absorption were minimum; the optimum heat treatment was identified as coincident with the state of optimum properties.

It was observed in the investigation, however, that apparent porosity and bulk density (also indicative of the mechanical strength of material) were the most useful in identifying the optima precisely. Nevertheless the other trends in properties were similar and volume contraction and water absorption were used to resolve ambiguities arising from experimental errors and to confirm judgements based on the other parameters.

The present investigation relates to optimum firing consistent with the maximum mechanical strength of fired material. In a situation where durability is of prime

concern, the less stringent saturation coefficient and the corresponding degree of vitrification are considered to be applicable more favourably from the viewpoint of energy conservation.

5.2 KINETIC ANALYSIS

The kinetics of kaolinite decomposition have been studied extensively and the results interpreted in terms of a diffusion model as well as first order kinetics (White and Murray 1949).

Norton and Hodgdon (1931) suggested the application of Arrhenius equation for the vitrification of triaxial ceramicware bodies. Meyer (1938) applied the Arrhenius equation to the vitrification of feldspathic whiteware bodies and calculated the exponential factor (Ea/R) from known properties of pyrometric cones. The calculated value was used to derive expressions for estimating heat schedules for whiteware bodies. However, Meyer's somewhat ambiguous assumption that the data obtained from properties of pyrometric cones are applicable to whiteware bodies of different characteristics is likely to limit the accuracy of his analysis. The present investigation employs the 'logarithmic time' method of kinetic analysis of isothermal data based on the Arrhenius equation.

The temperature dependence of the rate of vitrification is expressed by the Arrhenius equation as:

$$k = A \exp(-Ea/RT) \qquad (1)$$

where k = rate of reaction (rate of vitrification), Ea = activation energy, R = Boltzmann constant, T = absolute temperature, and A = a constant.

The logarithmic form of the equation for k is

$$\ln k = -(Ea/RT) + \ln A \qquad (2)$$

Redfern (1987) in his studies on the decomposition of kaolinite showed that the time required to attain a certain degree of vitrification (t) under isothermal conditions is proportional to 1/k.

i.e., $t = c/k$ where c = a constant

Therefore, from (1):

$$t = (1/A') \exp (Ea/RT) \quad \text{where } A' = A/c$$

The logarathmic form of the equation for t is

$$\ln t = (Ea/RT) - \ln A'$$

Therefore, a plot of ln t versus 1/T gives Ea/R as the gradient.

The equation (2) can be rearranged as:

$$\ln(k_1/k_2) = (Ea/R)[(1/T_2)-(1/T_1)] \qquad (3)$$

where k_1 and k_2 are the rates of vitrification at temperatures T_1 and T_2 (°K) respectively.

It was found during the present research study that the incipient vitrification of the clays under consideration did not commence below 850°C. Consequently the rate of vitrification of a clay at a temperature above 850°C relative to that at 850°C was considered to be a measure of the overall rate of vitrification at that particular temperature.

Therefore, if K_t is the rate of vitrification at t° C relative to that at 850°C (1123°K),

i.e., if $k_1 = k_t$ and $k_2 = k_{850} = 1$,

the equation (3) reduces to

$$\ln k_t = Ea/R\ [(1/1123)-(1/t+273)] \qquad (4)$$

For each clay, isothermal firing trials were performed at four temperatures by varying the soaking period. The soaking period corresponding to the optimum degree of vitrification as shown by the critical changes in properties (Section 5.1.2) was used in the construction of ln t-reciprocal temperature plots. The exponential factor calculated from the plots was used in equation (4) to determine the relative rates of vitrification at different temperatures of firing.

CHAPTER 5

The first stage of the kinetic analysis involves the calculation of the amounts of reaction taking place in a clay body during heating to the maximum temperature and during soaking at the maximum temperature. The amount of reaction taking place during cooling was considered negligible and therefore disregarded in this analysis.

As given in the foregoing equation, if k_t is the relative rate of reaction (degree of vitrification) of a clay body at t°C,

(a) the degree of vitrification (V) attained during heating is given by :

$$V_{\text{heating}} = \int_{ho}^{h} k_t \, dh$$

where h denotes time and (h-ho) represents the time interval during which the temperature was raised from T_o (1123°K) to the maximum firing temperature T (°K) at a constant rate. This also represents the curvilinear area under the k_t-time diagram (Fig. 5.2).

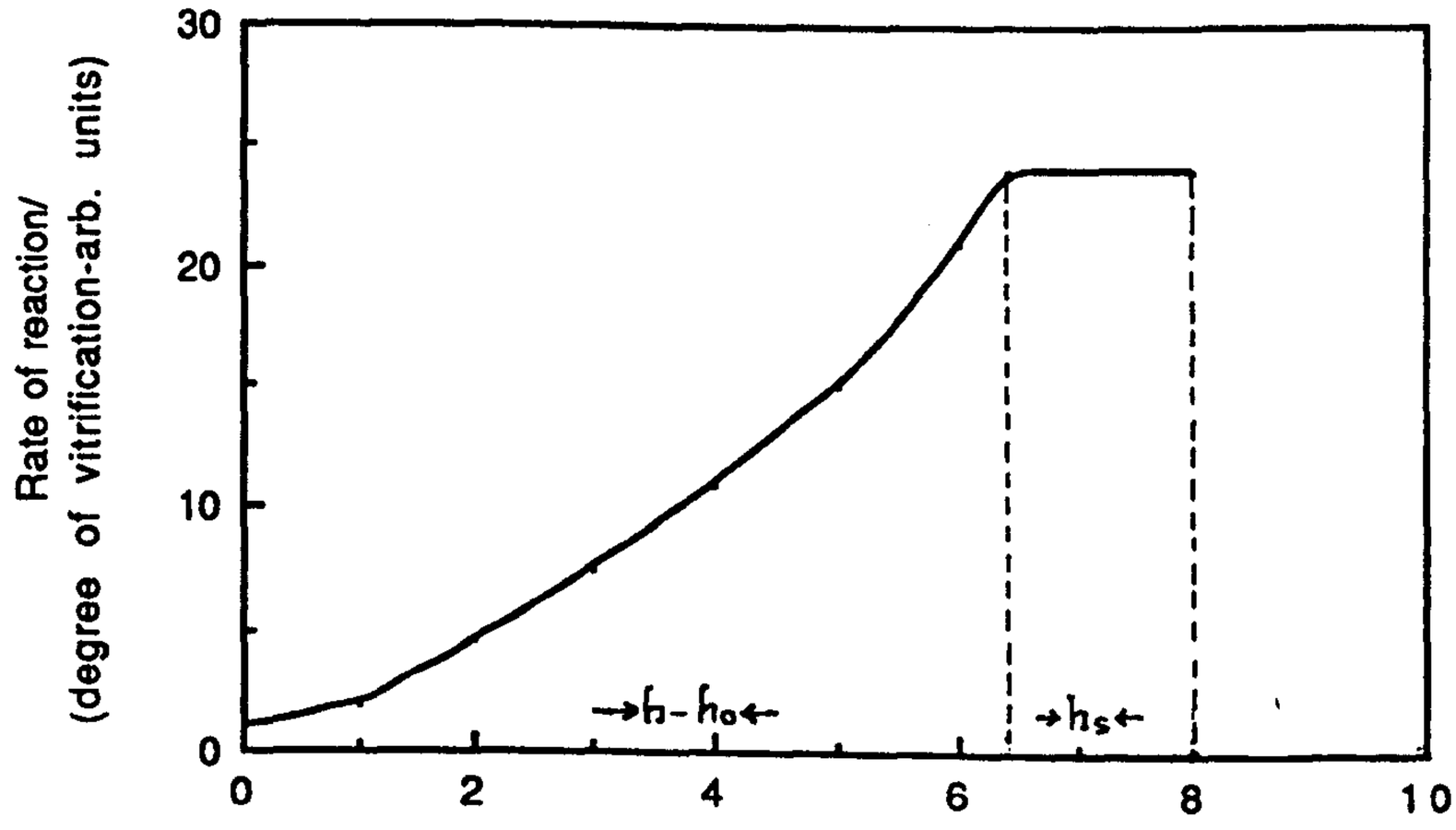

Fig. 5.2-Schematic representation of the reaction rate-time of firing dependence for the clays.

(b) The degree of vitrification attained during soaking is given by:

$$V_{soaking} = k_t \times h_s \qquad \text{where } h_s = \text{soaking time}$$

This represents the rectangular area under the k_t-time diagram (Fig. 5.2).

The overall degree of vitrification attained during heat treatment of a clay body according to a fixed firing schedule is thus given by:

$$V_{total} = \int_{h_o}^{h} k_t \, dh + k_t \times h_s$$

5.3 EXPERIMENTAL TECHNIQUE

The five clays studied are listed in Table 5.1 together with some relevant mineralogical data. (Chemical, mineralogical and mechanical analyses of the clays are given in Chapter 3). They ranged from two kaolinitic clays of residual origin (LSK2A, LSK2B) to two podzolic clays (PSH, PSR) and included the latosol (LP). The clays were ground to pass 125 μm sieve and dried to a pre-pressing moisture content of about 10%. Samples of clays weighing 8.00 g each were then pressed in an hydraulic press at a pressure of 500 p.s.i. into discs of 40 mm diameter and 4 mm thickness (Plate 5.1).

Table 5.1-Mineralogical data for clays

Clay	Code letters	Mineralogical composition Q	K	F	RO content	R_2O content	Total flux content
Residual	LSk2A	a	a	s	2.86	0.73	21.43
Residual	LSK2B	a	a	s	1.72	0.40	20.17
Podzolic	PSH	a	s	m	1,25	1.58	16.31
Podzolic	PSR	a	s	m	0.96	1.49	15.37
Latosol	LP	a	m	m	0.91	1.23	16.45

[RO = CaO + MgO, $R_2O = Na_2O + K_2O$]

[Total flux content = RO + R_2O + Fe_2O_3 + TiO_2]

a = abundant>30% Q = Quartz

s = subsidiary>15%<30% K = Kaolinite

m = minor>5%<15% F = Feldspars

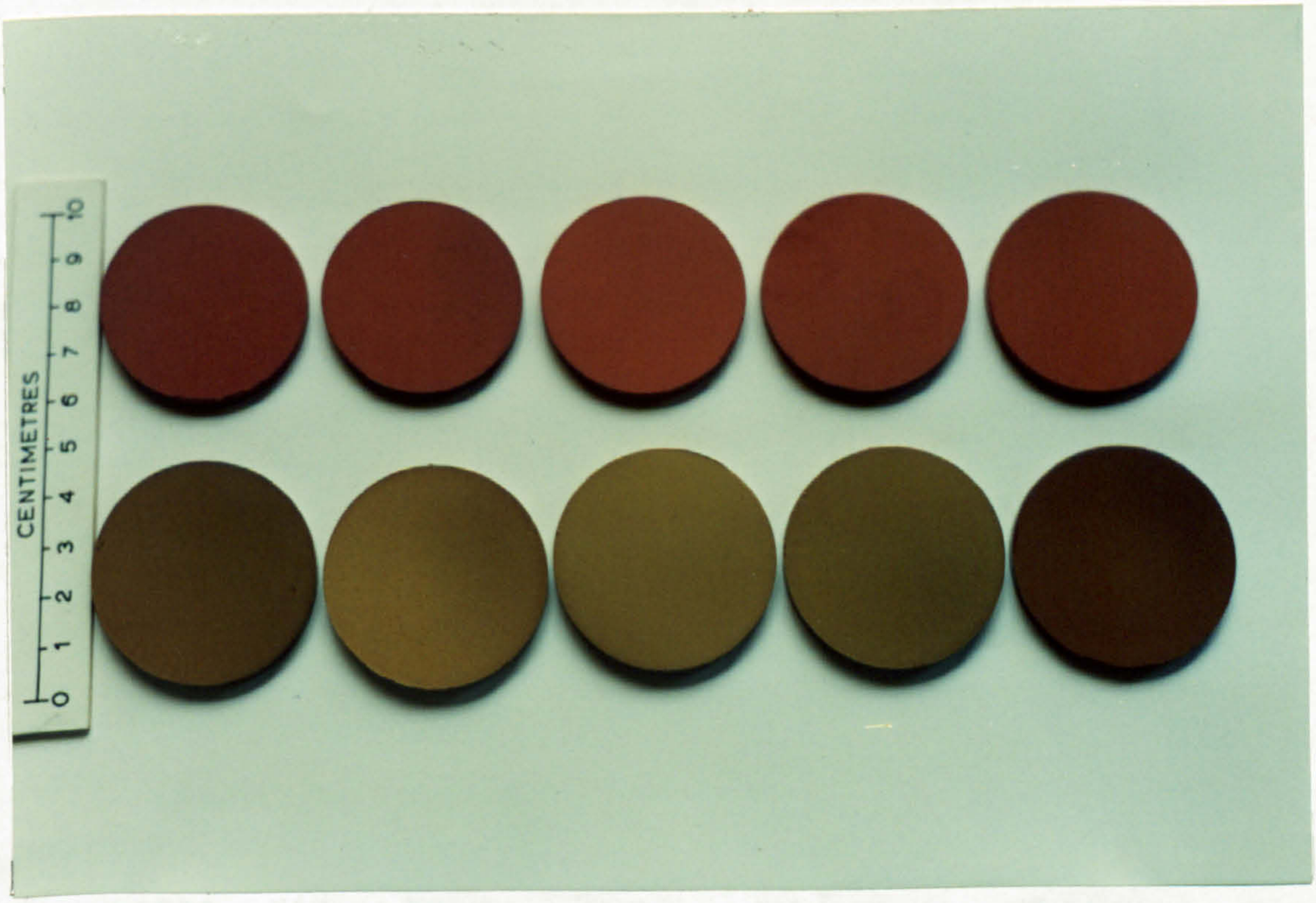

Plate 5.1-Discs made by iso-static pressing.
From left to right- fired/green discs-
LSK2A, LSK2B, PSH, PSR and LP.

After oven-drying (110°C, 24 h), the discs were fired in an electric muffle furnace in air at temperatures from 1025° to 1100°C, the temperature intervals between the different firings being 25°C. The heating rate was 5.6°C/min. A range of soaking times at peak temperatures from 30 min. to 5½ h depending upon the maturing characteristics of clays, was used. The time-temperature conditions used in firing of different clays are given below.

Peak temperature(°C)	Isothermal holding time(h)
1025	1.0
1025	2.0
1025	3.0
1025	4.0
1025	5.0
1025	5.5
1050	1.0
1050	1.5
1050	2.0
1050	3.0
1050	4.0
1050	4.5
1075	1.5
1075	2.0
1075	3.0
1075	3.5
1075	4.0
1100	0.5
1100	1.0
1100	1.5
1100	1.75
1100	2.0

After the completion of firing trials, the properties which determine the degree of vitrification of fired specimens viz. bulk density, apparent porosity, water absorption and volume contraction were measured.

5.3.1 Test methods

5.3.1.1 Bulk density

The test procedure specified in ASTM designation C373-72 (Standard Test Method for Water Absorption, Bulk Density, Apparent Porosity and Apparent Specific Gravity of Fired Whiteware Products) was followed in the measurement. Bulk density (in g/cm^3) of fired material was obtained by calculating the volume of cylindrical disc from the external dimensions and dividing its dry mass by the exterior volume.

5.3.1.2 Apparent porosity

Apparent porosities were determined according to ASTM designation C373-72 by impregnation of fired bodies by boiling in distilled water for 5 h followed by further immersion for 24 h. The saturated sample was then weighed and the apparent porosity calculated as:

$$\text{Apparent porosity} = [M-D/V] \times 100$$

where M = Saturated mass

D = Dry mass

V = Exterior volume (in cm^3)

5.3.1.3 Water absorption

Water absorption was calculated according to ASTM designation C373-72 from the ratio of mass of water absorbed to the mass of the dry specimen as follows.

$$\text{Water absorption} = [M-D/D] \times 100$$

5.3.1.4 Volume contraction

Dry-to-fired volume contraction was measured by calculating the external volume of oven-dried specimens and fired specimens. The lengths were measured by vernier calliper to the nearest 0.01 mm. The change in volume divided by the original volume was used to determine percentage volume contraction. An average of three values was used for each reported value.

CHAPTER 5

5.4 EVALUATION

5.4.1 Effect of isothermal heating on physical properties

The results of determinations of various physical properties of the five clays are given in Tables 5.2-5.6. The effects of isothermal soaking on the physical properties of fired specimens are illustrated in Figs. 5.3-5.6.

A definite relation of physical properties and of isothermal soaking period at firing temperatures 1025°, 1050°, 1075°, and 1100°C was observed for the five clays studied. Increasing the soaking period resulted in increased bulk density, volume contraction, decreased water absorption and apparent porosity. The increased amount of interstitial glass and fewer pores undoubtedly influenced the variation in physical properties. The changes became marked as the beginning of the vitrification range was approached. In general, a reversal of the properties occurred beyond a certain optimum soaking period with increase in degree of heat treatment. At this stage, the deleterious effects of bloating presumably had counteracted the favourable effects caused by increased amounts of mullite. At low temperatures of firing (1025° and 1050°C) the properties changed slightly until an optimum soaking period was reached at which the reversal of properties occurred. At high temperatures of firing (1075° and 1100°C) the properties changed rapidly as the optimum soaking period was approached; heat treatments exceeding the optimum produced a marked deterioration of properties.

Table 5.2-Heat treatments and physical properties of fired specimens: (1) Residual soil - LSK2A
(Average value of property determined from 6 specimens subjected to each schedule of heat treatment)

Heat treatment (Rate of heating-338°C/h)		Properties			
Max.firing temp. (°C)	Soaking period (h)	Bulk density (g/cm^3)	% Apparent porosity	% Water absorption	% Volumete contraction
1025	1.0	1.67	37.94	23.84	14.33
	2.0	1.65	40.17	23.70	15.21
	3.0	1.71	40.80	23.34	18.15
	4.0	1.70	39.02	22.25	18.38
	5.0	1.79	32.28	17.66	17.28
	5.5	1.76	37.33	20.78	19.44
1050	1.0	1.76	36.86	20.25	18.33
	1.5	1.80	36.42	19.56	20.06
	2.0	1.76	35.42	20.22	20.72
	3.0	1.82	36.25	19.75	23.13
	4.0	1.77	34.31	18.71	20.72
	4.5	1.70	36.30	21.52	20.34
1075	1.5	1.74	36.09	20.90	20.10
	2.0	1.75	35.74	20.12	20.53
	3.0	1.85	33.62	17.69	24.37
	3.5	1.81	33.06	18.30	22.42
	4.0	1.75	34.48	19.69	21.37
1100	0.5	1.81	36.18	19.50	23.28
	1.0	1.79	33.00	17.79	21.58
	1.5	1.89	30.28	15.84	22.61
	1.75	1.76	33.93	18.48	21.37
	2.0	1.79	34.97	19.00	23.69

Table 5.3-Heat treatments and physical properties of fired specimens: (2) Residual soil - LSK2B
(Average value of property determined from 6 specimens subjected to each schedule of heat treatment)

Heat treatment (Rate of heating-338°C/h)		Properties			
Max. firing temp. (°C)	Soaking period (h)	Bulk density (g/cm^3)	% Apparent porosity	% Water absorption	% Volume shrinkage
1025	1.0	1.64	39.63	23.71	18.06
	2.0	1.72	37.49	21.11	21.75
	3.0	1.71	34.75	19.94	19.50
	4.0	1.71	34.78	19.71	20.81
	5.0	1.63	36.81	22.41	20.13
	5.5	1.65	36.30	21.64	20.54
1050	1.0	1.73	38.18	21.60	24.66
	1.5	1.77	30.54	16.64	21.80
	2.0	1.80	30.76	16.64	25.16
	3.0	1.90	26.96	14.01	27.00
	4.0	1.91	26.19	13.19	27.40
	4.5	1.83	28.27	15.29	26.63
1075	1.5	1.78	25.41	14.08	22.94
	2.0	1.81	26.12	14.13	25.39
	3.0	1.95	21.66	10.95	30.45
	3.5	1.92	20.44	10.17	30.29
	4.0	1.92	24.04	12.64	33.78
1100	0.5	1.96	23.00	11.38	29.83
	1.0	2.16	20.37	9.10	35.96
	1.5	2.19	19.21	7.97	38.39
	1.75	2.06	18.04	8.28	34.41
	2.0	1.98	18.37	8.94	32.04

Table 5.4-Heat treatments and physical properties of fired specimens: (3) Podzolicclay -PSH
(Average value of property determined from 6 specimens subjected to each schedule of heat treatment)

Heat treatment (Rate of heating-338°C/h)		Properties			
Max. firing temp. (°C)	Soaking period (h)	Bulk density (g/cm^3)	% Apparent porosity	% Water absorption	% Volume contraction
1025	1.0	1.47	47.07	31.27	10.66
	2.0	1.49	44.34	29.27	13.35
	3.0	1.50	44.81	29.77	14.27
	4.0	1.55	44.09	27.91	15.27
	5.0	1.56	42.12	26.58	15.27
	5.5	1.49	43.89	29.37	17.07
1050	1.0	1.50	45.51	29.58	17.19
	1.5	1.54	42.68	27.27	16.48
	2.0	1.60	42.56	26.04	19.96
	3.0	1.62	40.27	24.57	20.82
	4.0	1.63	41.00	24.54	20.86
	4.5	1.63	41.05	24.85	20.40
1075	1.5	1.63	40.49	24.96	22.80
	2.0	1.68	39.50	23.11	23.41
	3.0	1.64	39.41	23.96	21.71
	3.5	1.75	37.30	21.11	24.46
	4.0	1.69	39.41	22.94	24.24
1100	0.5	1.65	41.70	24.96	24.00
	1.0	1.66	40.90	24.04	24.04
	1.5	1.76	39.40	21.76	26.75
	1.75	1.67	38.77	23.03	24.87
	2.0	1.72	37.71	21.64	25.43

Table 5.5-Heat treatments and physical properties of fired specimens: (4) Podzolic clay -PSR
(Average value of property determined from 6 specimens subjected to each schedule of heat treatment)

Heat treatment (Rate of heating-338°C/h)		Properties			
Max. firing temp. (°C)	Soaking (h)	Bulk density (g/cm^3)	% Apparent porosity	% Water absorption	% Volume contraction
1025	1.0	1.55	44.53	28.02	8.16
	2.0	1.48	44.18	29.65	8.95
	3.0	1.52	45.43	29.15	9.02
	4.0	1.58	41.12	25.97	10.04
	5.0	1.59	43.68	26.73	10.04
	5.5	1.55	45.35	29.52	12.70
1050	1.0	1.57	41.71	26.48	12.52
	1.5	1.59	42.36	26.20	13.42
	2.0	1.62	38.40	23.12	14.77
	3.0	1.67	40.58	23.40	15.35
	4.0	1.67	40.00	23.58	15.39
	4.5	1.57	41.31	26.82	14.66
1075	1.5	1.67	39.18	23.22	15.39
	2.0	1.64	39.28	23.47	15.69
	3.0	1.69	38.23	22.13	15.85
	3.5	1.70	38.43	22.58	19.03
	4.0	1.66	39.17	23.24	18.84
1100	0.5	1.64	39.22	24.15	18.40
	1.0	1.66	38.10	22.47	16.58
	1.5	1.76	36.71	20.68	19.66
	1.75	1.61	38.82	23.40	13.67
	2.0	1.72	37.26	21.35	17.17

Table 5.6-Heat treatments and physical properties of fired specimens: Latosol - LP
(Average value of property determined from 6 specimens subjected to each schedule of heat treatment)

Heat treatment (Rate of heating-338°C/h)		Properties			
Max. firing temp. (°C)	Soaking period (h)	Bulk density (g/cm^3)	%Apparent porosity	%Water absorption	%Volume shrinkage
1025	1.0	1.71	39.26	22.43	10.20
	2.0	1.73	35.53	20.12	8.20
	3.0	1.68	37.81	22.05	8.49
	4.0	1.69	37.53	22.06	8.98
	5.0	1.65	32.69	19.44	6.00
	5.5	1.70	32.63	18.52	8.76
1050	1.0	1.72	36.80	21.06	11.26
	1.5	1.70	36.51	21.02	12.32
	2.0	1.67	31.92	18.35	8.29
	3.0	1.79	30.26	16.15	11.89
	4.0	1.79	33.46	18.35	14.28
	4.5	1.77	25.39	14.02	12.52
1075	1.5	1.79	25.25	13.80	12.97
	2.0	1.74	24.11	13.54	10.37
	3.0	1.84	23.15	14.37	19.25
	3.5	1.89	24.00	12.42	19.85
	4.0	1.99	24.32	11.93	22.77
1100	0.5	1.78	25.68	14.01	11.16
	1.0	1.81	28.87	16.05	15.32
	1.5	1.83	27.70	14.50	17.07
	1.75	1.84	27.97	14.60	14.21
	2.0	1.83	30.15	15.68	19.38

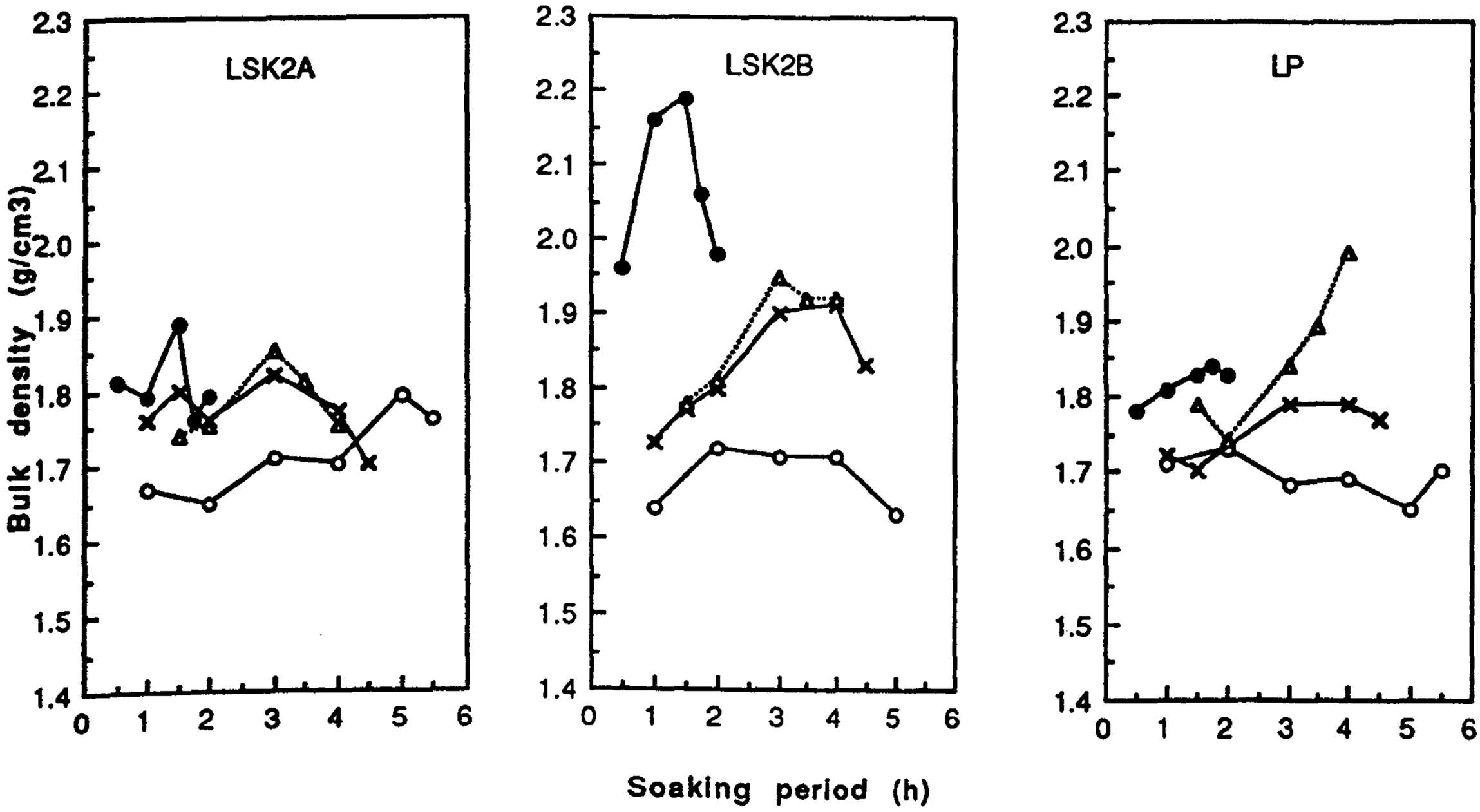

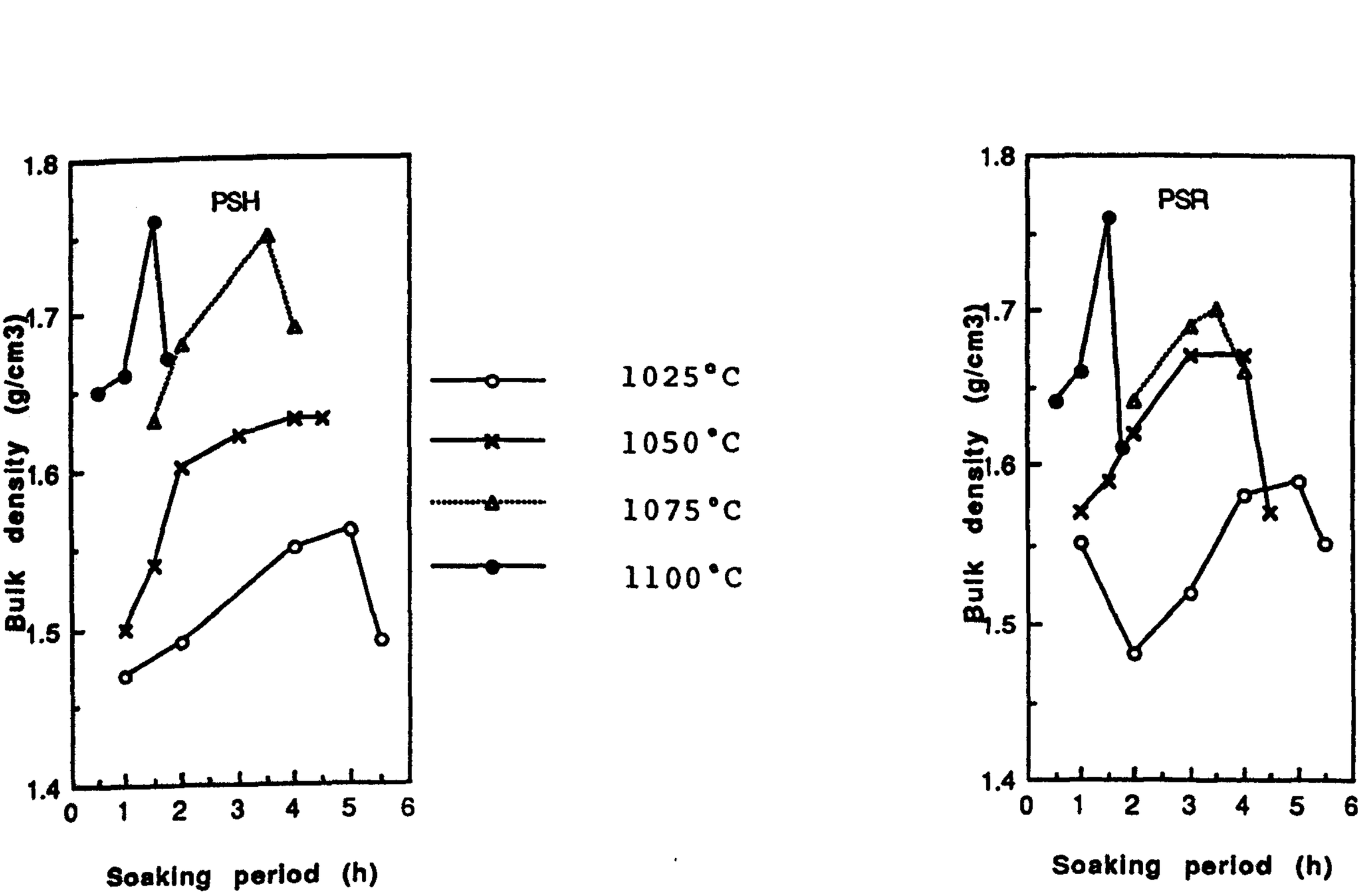

Fig. 5.3-Variation of bulk density with soaking period at different temperatures of firing for various clays.

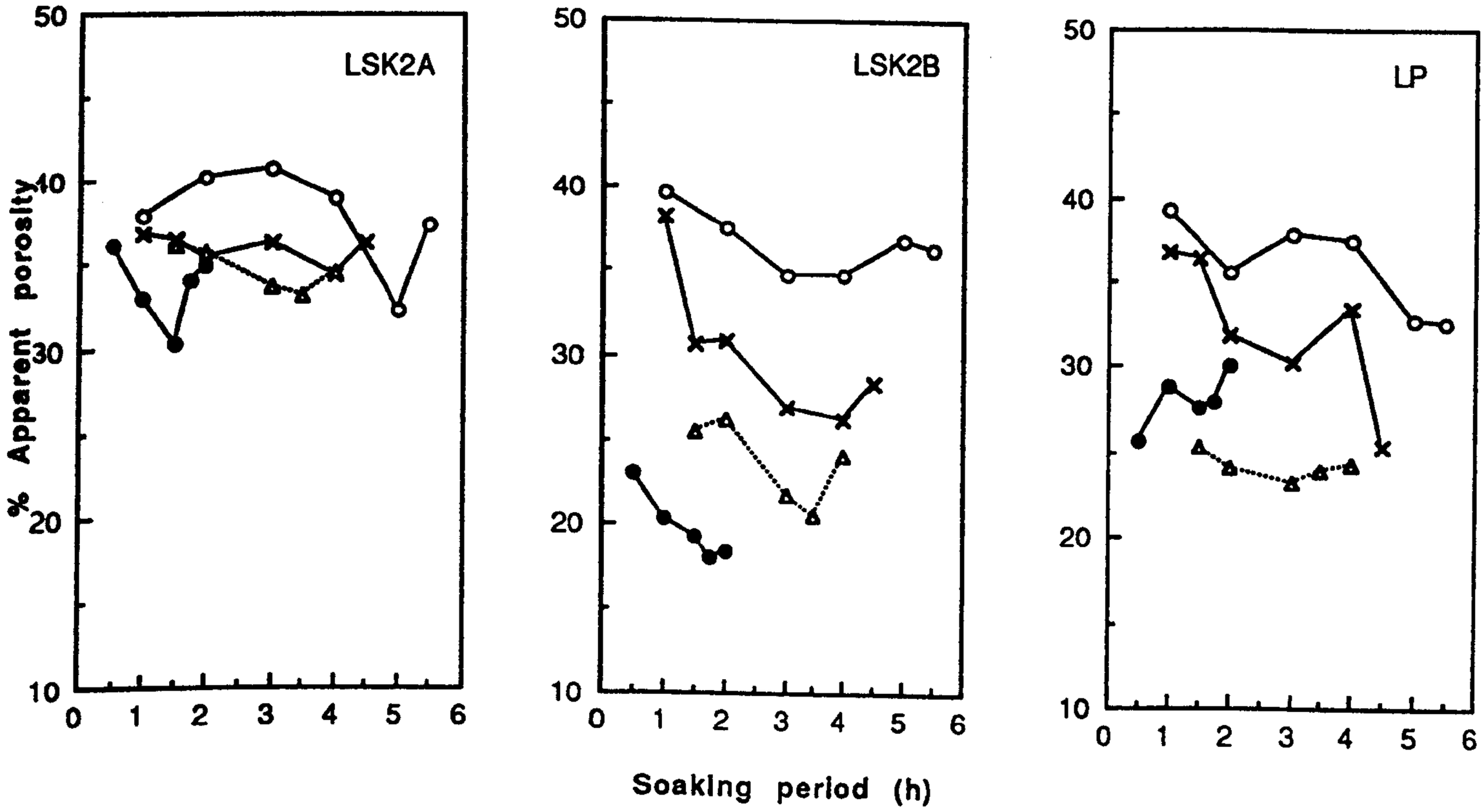

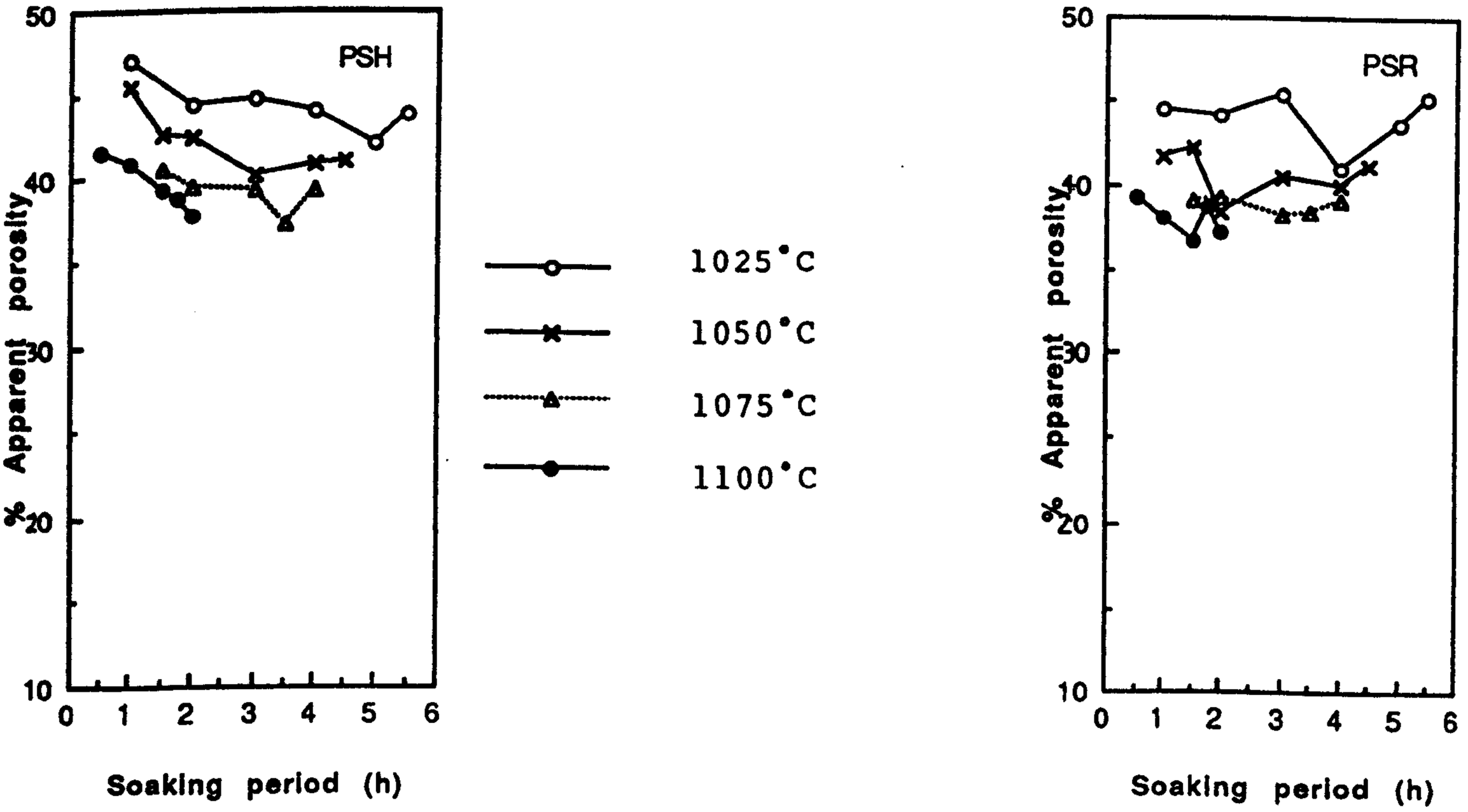

Fig. 5.4-Variation of apparent porosity with soaking period at different temperatures of firing for various clays

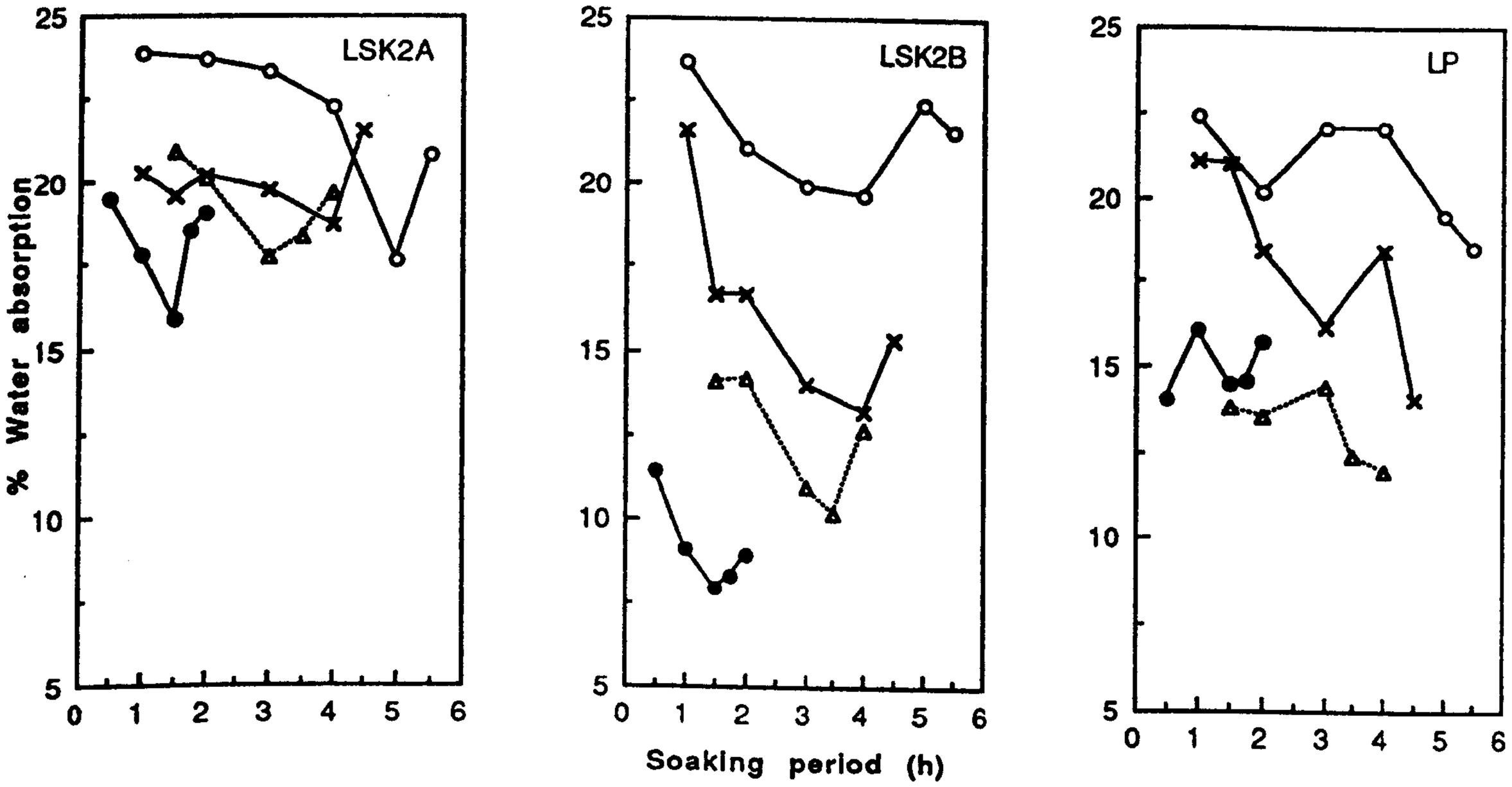

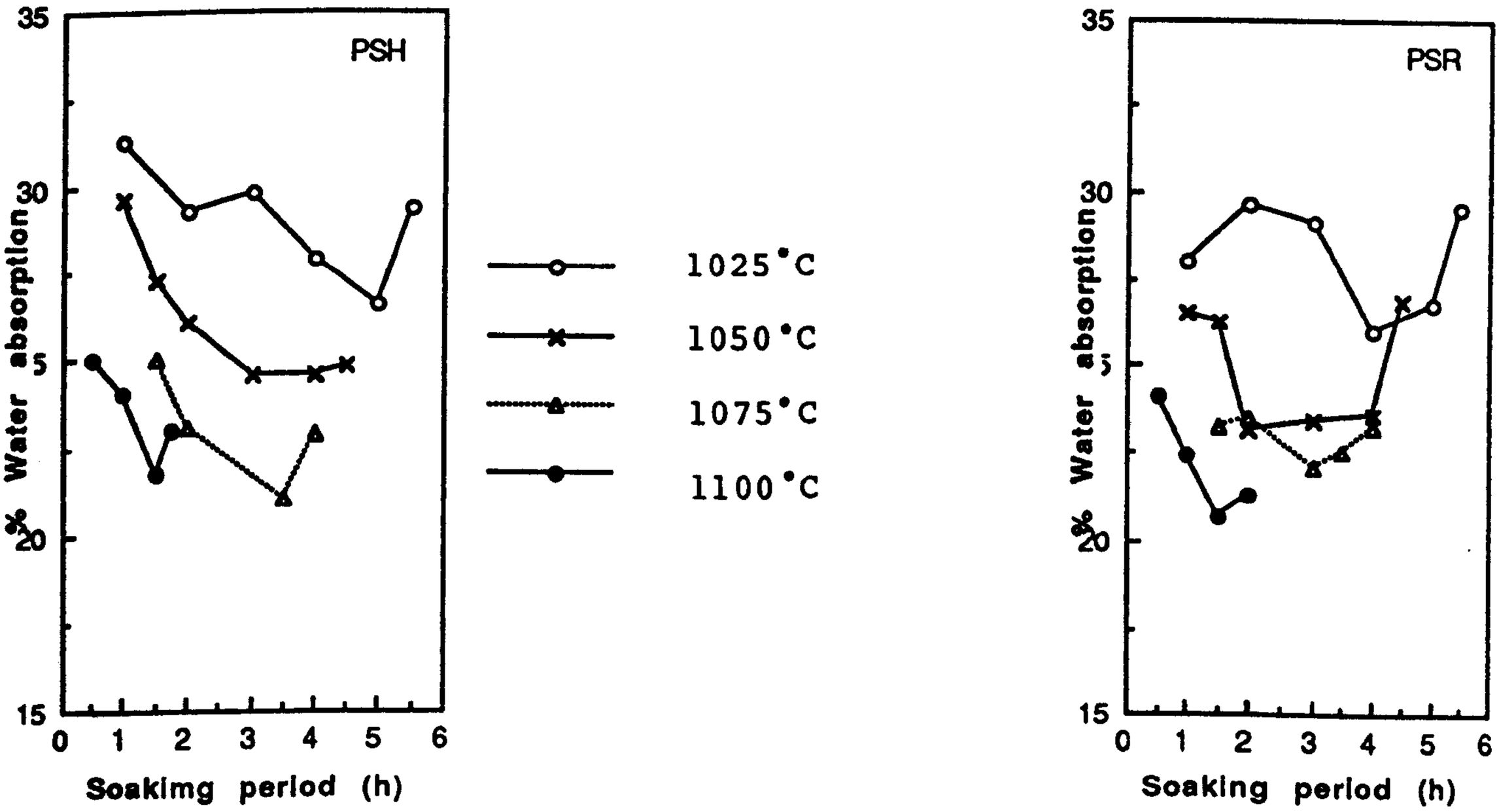

Fig. 5.5-Variation of absorption with soaking period at different temperatures of firing for various clays.

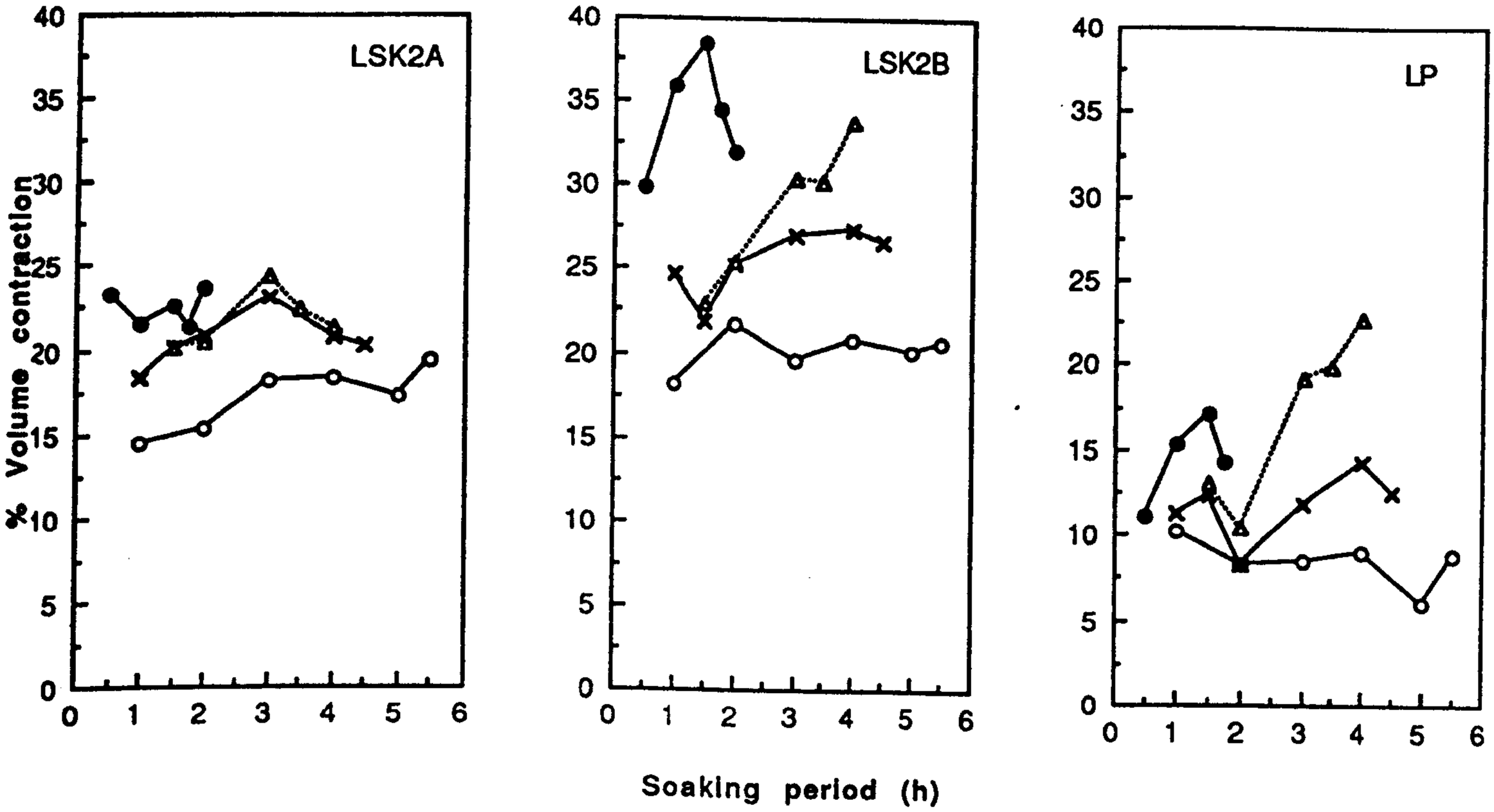

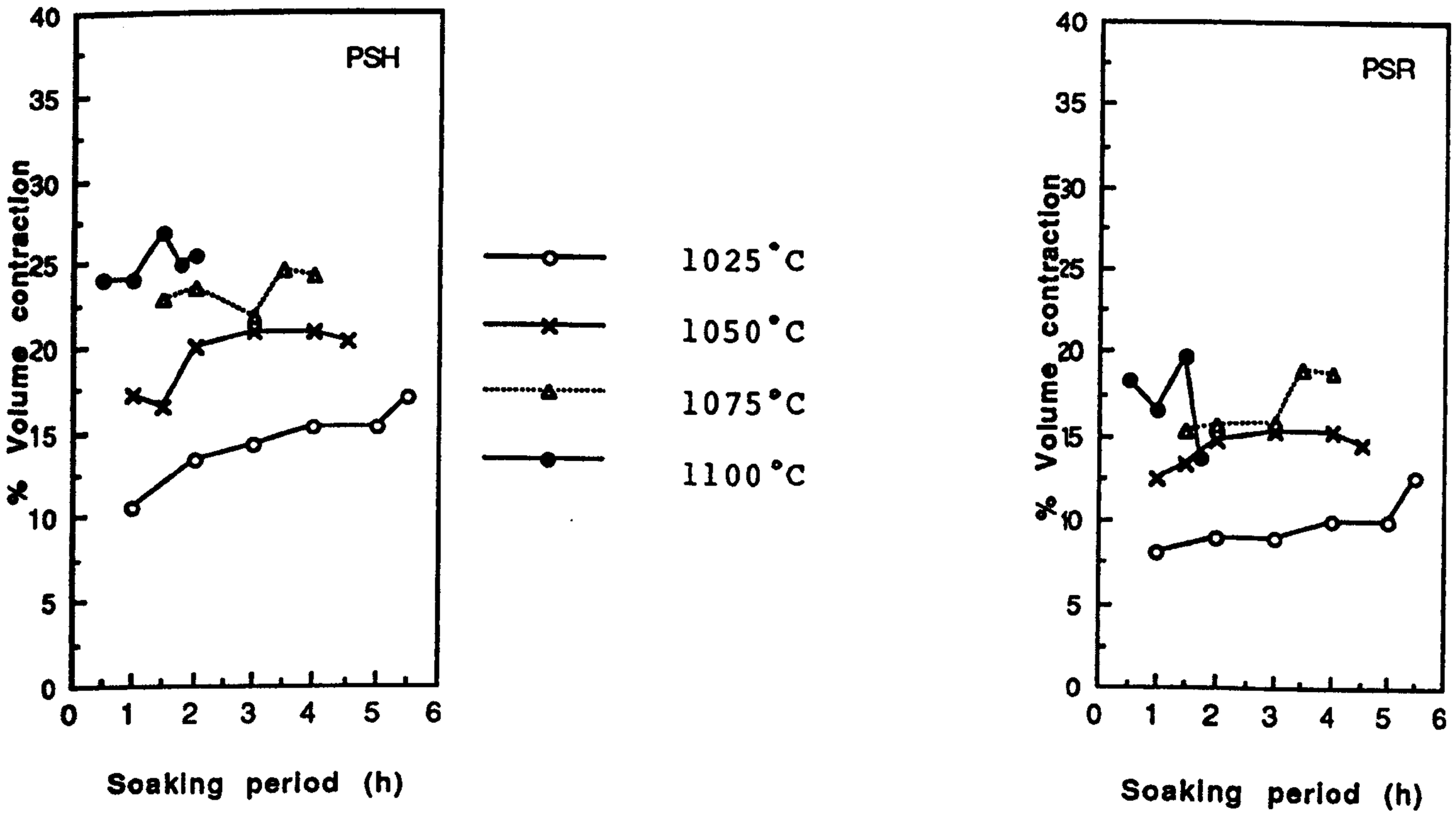

Fig. 5.6-Variation of volume contraction with soaking period at different temperatures of firing for various clays.

5.4.2 ln t - reciprocal temperature plots

The physical property relationships (Figs. 5.3-5.6) based on the experimental data given in Tables 5.2-5.6 were used to determine the optimum soaking periods at different temperatures of firing. These data on optimum heat treatments for various clays are given in Table 5.7. In Fig. 5.7 the data on the optimum heat treatments are plotted as ln t against 1/T.

Table 5.7-Data on optimum heat treatments for clays

Clay	Optimum soaking period (in h) for firing temperatures shown (Rate of heating - 5.6°C/min)			
	1025°C	1050°C	1075°C	1100°C
Residual soil LSK2A	5.0	4.0	3.0	1.5
Residual soil LSK2B	4.5	4.0	3.5	1.5
Podzolic clay PSH	5.0	4.0	3.5	1.5
Podzolic clay PSR	4.5	4.0	3.25	1.5
Latosol LP	5.5	4.5	4.0	1.75

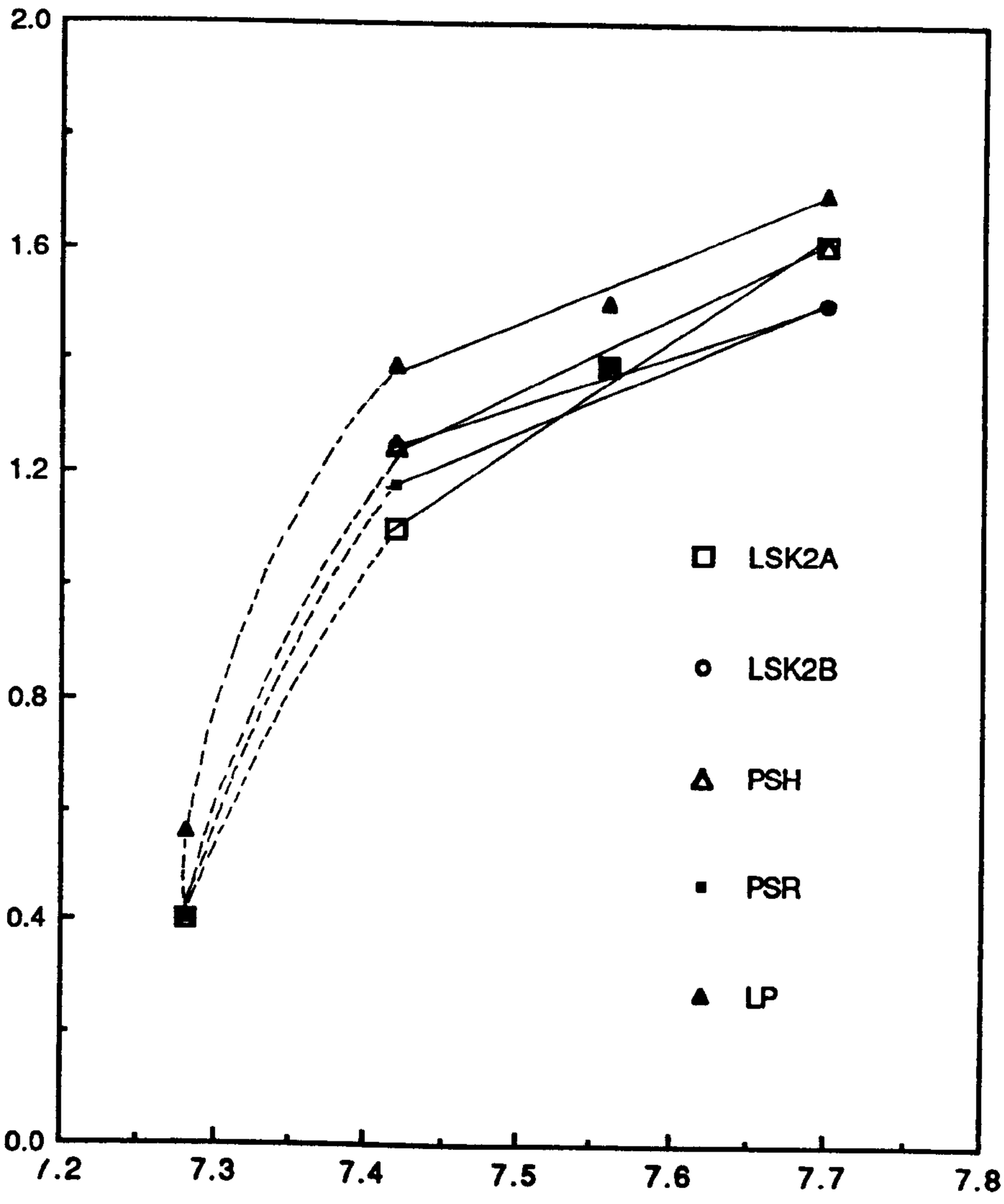

Fig. 5.7-ln t-1/T plots for isothermal heating of clays.

The graphs deviate from linearity at high temperatures, due to non-isokinetic behaviour (Redfern 1987). Between 1025° and 1075°C, however, the mechanism approaches isokinetic behaviour and the plots show linearity with a high degree of correlation (correlation coefficient-0.984-0.997). Therefore, exponential factors (Ea/R) have been calculated from the linear dependence obeyed below 1075°C. The exponential factors calculated for the five clays are given in Table 5.8.

5.4.3 Rate equation for the residual soil LSK2A

The exponential factor (Ea/R) calculated from the ln t -reciprocal temperature plot (Fig. 5.7) for the residual soil LSK2A is 18,214 (Table 5.8). The equation (4) given in Section 5.2 thus reduces to:

$$\ln k_t = 18{,}214[(1/1123)-(1/t+273)] \quad (5)$$

$$= 16.22-[18{,}214/t+273]$$

k_t can therefore be expressed as

$$k_t = \frac{e^{16.22}}{e^{18{,}214/t+273}} \quad (6)$$

The equation (6) gives the temperature dependence of the rate of vitrification (k_t). The integration of this with respect to time gives a measure of the degree of vitrification attained during heating. However, it appeared that the solution of this would be made simple by the use of an empirical equation. Therefore, an empirical equation which adequately describes the kinetic behaviour of the clay was deduced from the equation (6) as follows.

The equation (5) can be rewritten as

$$\ln k_t = \frac{18{,}214(t-850)}{1123(t+273)}$$

$$= F(t-850) \quad \text{where } F = \frac{18{,}214}{1123(t+273)}$$

The factor F calculated for the practical range of firing temperatures between 1000° and 1100°C varied within 0.0120±0.0007. The assigning of the value 0.012 for F yields the empirical equation:

$$\ln k_t = 0.012(t-850)$$

This can be transformed to the exponential form as:

$$k_t = e^{0.012(t-850)} \quad (7)$$

$$\text{or } k_t = e^{0.012rh} \quad (8)$$

where r = constant rate of heating (°C/h)

and h = heating time above 850°C

The rate equations for the clays are given in Table 5.8.

Table 5.8-Exponential factors and rate equations for the clays

Clay	Exponential factor (Ea/R)	Rate equation	
		Exact (Theoretical treatment-Eq.6)	Empirical (Exptl. derivation-Eq.7)
Residual soil LSK2A	18,214	$k_t = \frac{e^{16.22}}{e^{18,214/t+273}}$	$k_t = e^{0.012(t-850)}$
Residual soil LSK2B	8,928	$k_t = \frac{e^{7.95}}{e^{8,928/t+273}}$	$k_t = e^{0.006(t-850)}$
Podzolic clay PSH	12,857	$k_t = \frac{e^{11.45}}{e^{12,857/t+273}}$	$k_t = e^{0.008(t-850)}$
Podzolic clay PSR	11,428	$k_t = \frac{e^{10.18}}{e^{11,428/t+273}}$	$k_t = e^{0.0076(t-850)}$
Latosol LP	11,071	$k_t = \frac{e^{9.86}}{e^{11,071/t+273}}$	$k_t = e^{0.0073(t-850)}$

5.4.4 Calculation of the degree of vitrification

The relative degree of vitrification of the heat treated clay body was determined in two steps:

(1) Calculation of the degree of vitrification resulting from heating ($V_{heating}$)-

The integration of the empirical rate equation for the clay within the required time limits and under conditions of constant rate of heating yielded $V_{heating}$.

(2) Calculation of the degree of vitrification resulting from soaking ($V_{soaking}$)-

The rate of vitrification (k_t) at the maximum temperature of firing obtained by the exact rate equation when multiplied by the soaking period gave $V_{soaking}$.

The sum of two partial degrees of vitrification gave the total degree of vitrification. Table 5.9 presents the calculations for the residual soil LSK2A and shows the higher degree of vitrification imparted by the 1050°C heat treatment with a soaking period of 4 h. The resulting specimens had superior physical properties compared to those subjected to other forms of heat treatment. The correlation thus serves as a guide to maintaining product quality.

Table 5.9-Calculation of degree of vitrification for residual soil subjected to various heat treatments

Firing schedule [Rate of heating (r)-338°C/h]			Relative degree of vitrification for each stage of firing		Total relative degree of vitrification (arb. units)	% Contribution of heating to overall vitrification
Maximum firing temp. (°C)	Soaking period-h_s (h)	Heating time above 850°C-h (h)	Heating Calculated from: $V_{heating}=\int_{h_o}^{h} k_t dh=\int_{h_o}^{h} e^{0.012rh}$	Soaking Calculated from: $V_{soaking}=\frac{e^{16.22}}{e^{18,214/t+273}} \times h_s$		
1025	5.0	0.52	$\frac{[e^{0.012x338h}]}{0.012r}$ = 1.8	$\frac{e^{16.22}}{e^{14.03}}$ x5 = 44.6	46.4	3.9
1050	4.0	0.59	$\frac{[e^{0.012x338h}]}{0.012r}$ = 2.4	$\frac{e^{16.22}}{e^{13.77}}$ x4 = 46.4	48.8	4.9
1075	3.0	0.66	$\frac{[e^{0.012x338h}]}{0.012r}$ = 3.3	$\frac{e^{16.22}}{e^{13.51}}$ x3 = 45.1	48.4	6.8
1100	1.5	0.74	$\frac{[e^{0.012x338h}]}{0.012r}$ = 4.7	$\frac{e^{16.22}}{e^{13.26}}$ x1.5 = 28.9	33.6	14.0

5.4.4.1 Order of error in the calculation of the degree of vitrification

The empirical rate equation (8) was used in ascertaining the degree of vitrification attained during heating ($V_{heating}$) whereas the exact rate equation (6) was employed in calculating the degree of vitrification attained during soaking ($V_{soaking}$). The values for the residual soil LSK2A are shown in Table 5.9 which also gives the contribution made by heating to the overall vitrification process. In order to estimate the error involved in using equation (8) in place of equation (6), both equations were converted to the time dependence form using the relation rh = t-850. The resulting expressions for k_t:

$$k_t(\text{exact}) = \frac{e^{16.22}}{e^{18,214/rh+1123}}$$

$$k_t(\text{empirical}) = e^{0.012rh}$$

gave two sets of values of k_t which were plotted for values of h from 0 to 0.74; these limits of h corresponded to temperatures of firing of 850°and 1100°C respectively. The plots are shown in Fig. 5.8. The percentage variation of the degree of vitrification resulting from heating ($V_{heating}$) estimated from the areas under the two curves for different temperatures of firing are presented in Table 5.10.

Table 5.10-Variation in the assessment of the total degree of vitrification

Maximum firing temperature (C)	% Variation in Vheating	% Contribution of Vheating to Vtotal	% Variation in Vtotal
1025	-8.3	3.9	-0.32
1050	-6.2	4.9	-0.30
1075	-4.1	6.8	-0.28
1100	-3.3	14.0	-0.46

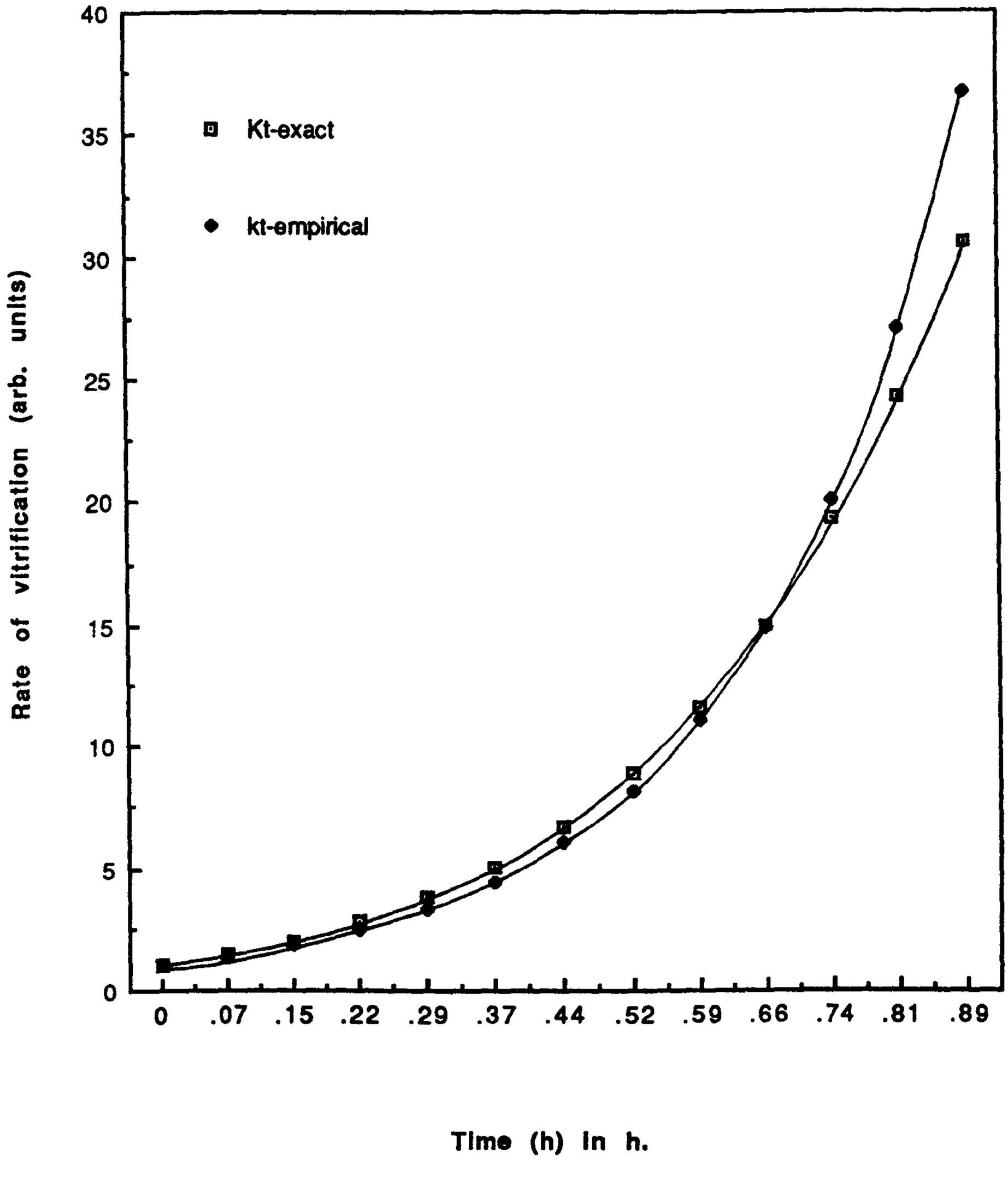

Fig. 5.8-Rate of vitrification-time plots for residual soil LSK2A.

Since the contribution of heating to the overall vitrification is small at all temperatures of firing (see Table 5.9), the order of error involved in the assessment of the total degree of vitrification is relatively insignificant. It is evident from the data given in Table 5.10 that the error involved is well within the limits of experimental tolerances.

It is also apparent from the above that the degree of vitrification predicted from the empirical equation is slightly lower than that calculated from the exact rate equation over the range of temperature between 850° and 1075°C. However, the actual reaction rates in practical ceramics are always much slower at any given temperature than those predicted by the exact rate equation. Therefore the empirical rate equation can be expected to provide a more realistic picture of the extent of completion of reactions in fired brick clay bodies examined. The degree of vitrification calculated using data given in Tables 5.7 and 5.8 for the clays subjected to the experimental firing schedules are summarised in Table 5.11.

Table 5.11-Degree of vitrification for the five clays subjected to various heat treatments

Maximum firing temp. (°C)	Total relative degree of vitrification for clays shown (soaking period in h at the maximum firing temperature is given in parenthesis)				
	LSK2A	LSK2B	PSH	PSR	LP
1025	46.4 (5.0)	14.0 (4.5)	23.4 (5.0)	18.9 (4.5)	21.8 (5.5)
1050	48.8 (4.0)	14.4 (4.0)	24.2 (4.0)	20.0 (4.0)	21.9 (4.5)
1075	48.4 (3.0)	14.6 (3.5)	25.4 (3.5)	19.5 (3.25)	22.5 (4.0)
1100	33.6 (1.5)	8.1 (1.5)	14.5 (1.5)	11.8 (1.5)	12.7 (1.75)

5.5 IMPLICATIONS OF KINETIC ANALYSIS

The variation of total degree of vitrification implies that

(1) The most favourable heat treatment for attaining the highest degree of vitrification and therefore the maximum mechanical strength for the clays LSK2B, PSH and LP is accomplished at 1075°C; for the clays LSK2A and PSR, the heat treatment at 1050°C for 4 h seems adequate.

(2) Heat treatments exceeding the optimum cause catastrophic effects probably due to bloating of clays.

(3) The clay fraction of LSK2B is less susceptible to increase in firing temperature, attaining near optima of properties at 1025°C; for this clay, high firing above 1025°C is unproductive.

(4) The clay fraction of LSK2A attains the highest degree of vitrification at all temperatures indicating its relative ease of densification and strengthening.

5.5.1 Extension of the analysis for the estimation of firing conditions

If the degree of vitrification of a clay body satisfying a particular property specification is known from a knowledge of its thermal history, any combination of two of the following conditions of firing:

(i). maximum temperature (sufficient to initiate incipient vitrification of clay material),

(ii). soaking period of the firing schedule,

(iii).rate of heating of the firing schedule

can be transposed to a desirable combination as follows

(1) Partial degrees of vitrification are calculated using known conditions of firing and total degree of vitrification.

(2) The appropriate partial degree of vitrification and correlative expression are then used in conjunction to arrive at the unknown condition of firing.

It is conceivable that suitable firing conditions consistent with low energy consumption or satisfying plant requirements could also be determined on the basis of the above for a given raw material.

CHAPTER 6

DEVELOPMENT OF A SELF-COATED CLAY PRODUCT

6.1 GENERAL CONSIDERATIONS

The literature reviewed in Chapter 2 gives information on strengthening of glass products by vacuum deposition and flame polishing techniques of surface preparation. In this experimental study, the objective was to develop a low-maturing, self-coated clay product utilizing the ternary eutectic compositions of the system Na_2O-Al_2O_3-SiO_2 so that the mechanical strength of the bulk material can be enhanced by the surface effects of coating. Apparently, there have been no previous attempts to establish the validity of the concept of strengthening by surface coating and to develop an 'in-situ' forming technique for surface coating of structural clay products. It was anticipated that a low temperature fired coated clay product satisfying technical strength criteria would also find application as a glazed facing brick. The conventional manufacture of glazed bricks suffer from several disadvantages which are listed below.

6.1.1 Salt glazing and other conventional glazing systems

The method of producing salt glaze invented in 1671 (Patent No.164, John Dwight) involves placing the dried ware in the kiln and vapourizing common salt in the kiln fires at the height of the firing process. The salt vapour enters the kiln chamber and forms the glaze in combination with the clay on the surface of the ware. The following reaction series occurs at the surface of brick:

$$2NaCl + H_2O = Na_2O + 2HCl$$

$$Na_2O + Al_2O_3.2SiO_2 + xSiO_2 = Na_2O.Al_2O_3(2+x)SiO_2(glass)$$

$$Overall: 2NaCl+H_2O+Al_2O_3.2SiO_2+xSiO_2=Na_2O.Al_2O_3(2+x)SiO_2+HCl$$

The evolution of HCl vapour in the process has adverse environmental effects. The corrosive vapours also have disastrous effects on the heating elements of electric furnaces. In view of this, the last of the open-vent kiln in

Germany was shut down in mid-1983 and research is being conducted in Europe on alternative, less-corrosive glazing systems (Kingery 1986).

The salt glaze cannot be applied successfully to clays which are either too aluminous or too siliceous; since the glaze is formed by the reaction between salt vapour and clay, the composition of the clay must be favourable to the formation of a glaze, and the clay must also withstand a kiln temperature of about 1200°C. At a temperature of this order of magnitude, some clays become overfired as indicated by bloating or by deforming under the load of kiln setting (Stull et al. 1942).

Normal salt glazing cannot be undertaken below 1200°C and the volatalising of salt requires large amount of heat which makes the process less attractive from the viewpoint of energy conservation.

The conditions controlling firing are difficult to maintain but are vital in securing a good glaze.

Salt glazes on silica-poor bodies are very prone to crazing. Remedying of this is accomplished by altering the body composition which may also increase the cost of production (Singer and Singer 1963).

There are often higher losses of ware due to irregular glazing in the various parts of the kiln, non-uniformity of different batches, warpage, etc., due to higher kiln temperature leading to higher unit and labour costs.

The other types of ceramic glazes applied to structural clay products entail higher production costs. The glaze is usually applied on the unfired ware by spraying or by dipping and is either fritted or formulated with lead compounds.

The nature of the body-glaze interfacial layer in conventional glazes can have a profound effect on the nature of the ware. For example excessive mullite development may cause peeling since its expansion coefficient is lower than that of either body or glaze. On cooling the mullite is

compressed from all sides and eventually cracks through the centre to relieve the stress, thereby separating the glaze from the body (Smith 1954).

6.2 PROCESSING TECHNIQUES

The two low-grade Sri Lankan brickmaking clays, viz. latosol (LP) and residual soil (LSK2A) with widely varying particle size distribution and amounts of clay mineral content and fluxes were chosen for the main investigation. Initial experiments were limited to these two clays in view of the wide scope of the investigation. For the fusibility studies and formulation of eutectic compositions up to five clays (two podzolic clays, two residual soils and a latosol) were employed. The properties of the clays are given in Chapter 3.

The techniques of processing used in the development of the self-coated clay product are outlined in Sections 6.2.1, 6.2.2 and 6.2.3.

6.2.1 Formulation of fusible clay mixes

Consideration of the structure of ceramic glazes shows that the basic glass former is silica, and that its properties are varied by the addition of other constituents. Also, study of phase rule data shows that the addition of one substance to another always lowers the melting point. In general the more different substances present the greater the lowering. By combination of structural and phase rule data sufficient directive for the formulation of fusible clay mixes were obtained. The methods of sample preparation are described below. The details of the systems investigated are given in Sections 6.4.1 and 6.4.2.

(i). Direct application of finely ground clays of different amounts of clay mineral content and fluxes on the surface of green ware in slip form to explore the potential fusibility of clays.

(ii). Direct application of mixtures of finely ground clay and fluxing materials (wood ash, lime, Na_2CO_3 and $NaHCO_3$) incorporated to improve the fusibility of clays. The application was carried out in both wet and dry form.

6.2.2 Compounding of eutectic mixes

Excluding other considerations, increase of the O/Si ratio loosens the silica network and lowers the melting point. This, coupled with structural considerations given in Section 6.2.1 formed the basis of the next series of trials outlined below. The details of the systems investigated are given in Sections 6.4.3 and 6.4.4.

(i). Direct application of coating mixtures based on the compositions of the SiO_2-Na_2O binary system on the surface of green ware.

(ii). Coating the surface of green ware with multicomponent low-melting formulations.

6.2.3 Efflorescence coating

This method involves the use of an efflorescence technique in which a coating component (Na_2CO_3) in solution is mixed with dried clay.

Surface deposition of the component was induced by controlled air-drying. The surface material was subsequently made to react with an externally applied layer of ground silica to form a vitreous coating on firing. A low surface concentration of Al_2O_3 of the clay body was thus utilized to obtain the required eutectic composition of the ternary system Na_2O-Al_2O_3-SiO_2. The development of the surface-coated clay product is described in Section 6.5.

A summary of the materials investigated and methods employed to develop a low-maturing surface coating for clay products is presented in Table 6.1.

Table 6.1-Materials investigated and methods employed to develop a low-maturing surface coating

(Heat treatment - maximum firing temperature 900°C, soaking time 2 hours)

Materials	Methods employed/governing factors for coating composition
Residual soil-LSK2A Residual soil-LSK2B Podzolic clay-PSH Podzolic clay-PSR Latosol-LP	Fusibility study based on SiO_2/Al_2O_3 ratio of different clays.
Clays: Residual soil-LSK2A Podzolic clay-PSH Latosol-LP Fluxes: Wood ash Na_2CO_3 (anhydrous) K_2CO_3	Fusibility study involving fluxes and raw clays based on the effect of lowering the melting point by alkaline/alkaline earth constituents used as network modifiers.
Ground silica Na_2CO_3	Low-maturing eutectic compositions of the Na_2O-SiO_2 binary system.
Podzolic clay-PSH Ground silica Wood ash Na_2CO_3 (anhydrous) K_2CO_3	Formulation of batch compositions based on analytical data of low-maturing glazes.
Residual soil-LSK2A Latosol-LP	Development of a coating of eutectic composition in the Na_2O-Al_2O_3-SiO_2 ternary system based on an efflorescence surface deposition technique.

CHAPTER 6

6.3 HEAT TREATMENT

The samples were subjected to a schedule of heat treatment in an electric furnace simulating as nearly as possible the exact firing conditions employed in practice. Firing was carried out in an oxidizing atmosphere in air. The temperature and time schedule convenient for nucleation and phase separation to produce a satisfactory coating was dependent on the composition. The schedule of heat treatment employed for the compositions are shown schematically in Fig. 6.1.

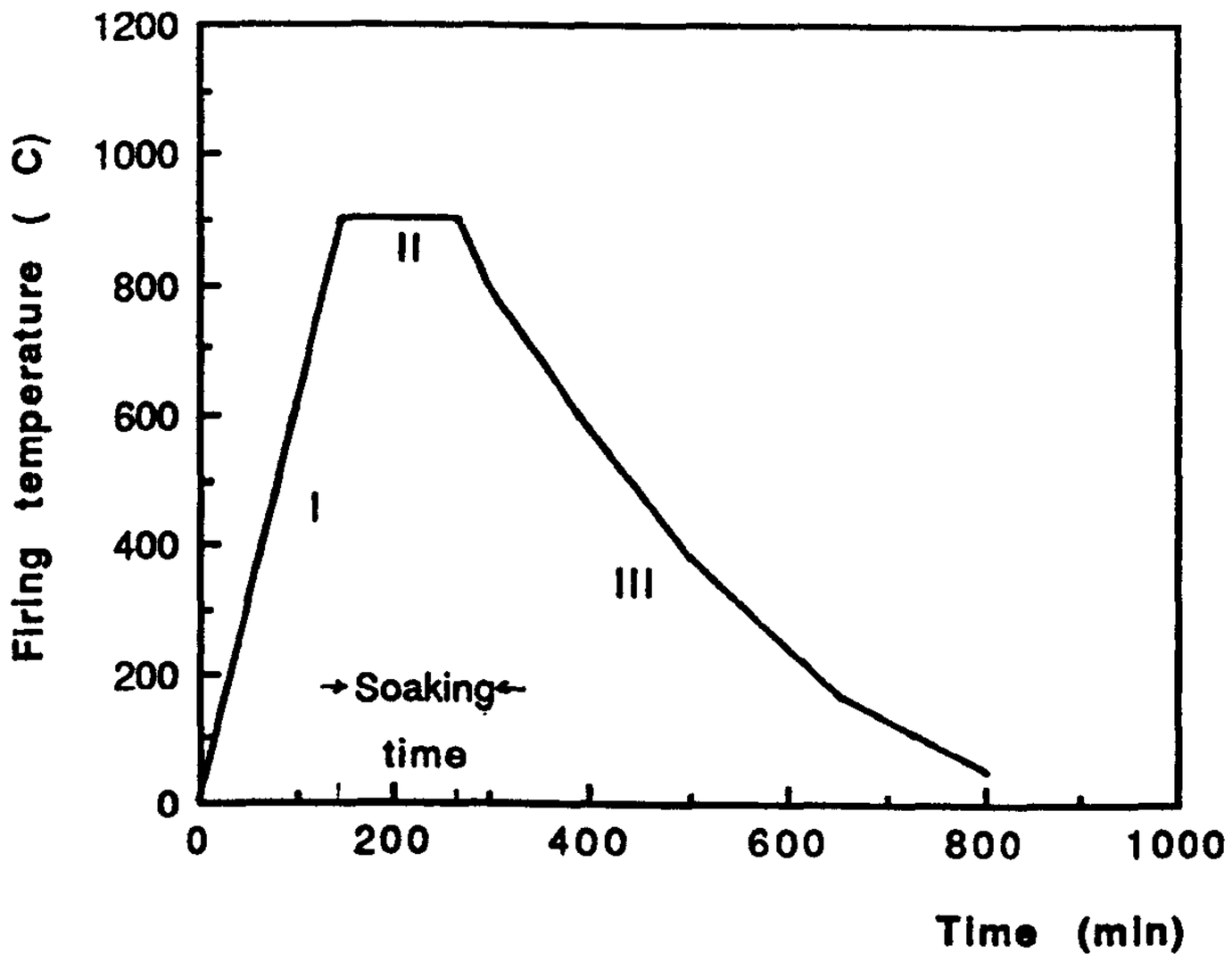

Fig. 6.1-Schematic representation of firing schedule.

Part I of the curve indicates the rate of rise of temperature (6°C/min). Part II, which is the most important part of the schedule indicates the nucleation temperature (900°C) and soaking time (2 h). Part III of the curve indicates the rate of cooling (0.6°C/min).

6.4 DETAILS OF THE SYSTEMS INVESTIGATED

6.4.1 Fusible clay mixes

Five clays (LSK2A, LSK2B, PSH, PSR and LP) of different mineralogical and granulometric composition were examined in the first series of investigations for their potentiality as low fusion point materials to produce a vitreous coating on fired clay products.

Each clay was ground by a mechanical mortar to pass 63 μm BS test sieve and then dispersed in water. The consistency of the slip was adjusted to suit its application as a coating. The slip coating was then applied on the top surface of dried bars made from clay mixes of latosol (LP) and residual soil (LSK2A). The coated bars were finally air-dried for 24 h and fired in the electric furnace according to the firing schedule described in Section 6.3. The identification numbers of each clay, its oxide constituents and technological parameters important from the viewpoint of determining its fusibility are presented in Table 6.2.

Table 6.2-Pertinent fusibility data on clays

Description		Technological parameters						Empirical formula
Clay	Designation	SiO_2	Al_2O_3	SiO_2/Al_2O_3	RO	R_2O	Total flux	
Residual	LSK2A	41.18	25.06	1.64	2.86	0.73	20.02	$RO.R_2O.4Al_2O_3.11SiO_2$
Residual	LSK2B	41.76	24.46	1.71	1.72	0.40	18.85	$RO.R_2O.8Al_2O_323SiO_2$
Podzolic	PSH	43.05	24.85	1.73	1.25	1.58	15.17	$RO.R_2O.6Al_2O_318SiO_2$
Podzolic	PSR	43.74	24.83	1.76	0.96	1.49	14.24	$RO.R_2O.8Al_2O_324SiO_2$
Alluvial	ACB	49.79	21.30	2.34	1.81	1.80	13.67	$RO.R_2O.4Al_2O_316SiO_2$
Latosol	LP	47.33	22.77	2.08	0.91	1.23	13.26	$RO.R_2O.7Al_2O_326SiO_2$

From Table 6.2 it is seen that the values of SiO_2/Al_2O_3 ratios are close for the two residual soils and two podzolic clays ranging from 1.64 to 1.76. The value for the latosol is appreciably high (2.08). All are within limits for good matt coatings proposed by Stull and Johnson (1942). However, the coatings formulated from these compositions did not prove satisfactory for the desired firing range, and the next step in the search for a coating was to incorporate fluxing materials to lower the melting point further.

6.4.2 Compositions involving clay and other raw materials

The purpose of this part of the study was to ascertain whether the fusion points unattained in the foregoing study could be lowered by the incorporation of fluxes to raw clays.

The use of fluxes to improve the maturing behaviour of bodies and glazes is not uncommon in the ceramics industry. For centuries, the oriental ceramists, notably the Chinese and later the Japanese have used wood ash and lime as fluxing materials (Thurn 1945, Turner 1956, Leach 1976, Tichane 1986, Taylor et al. 1986).

The chemical analyses were the starting points for the experimental procedure which consisted in adjusting the silica and alumina proportions and also the RO and R_2O contents in the mixes with admixtures involving fluxing materials. The fluxes used in this series of trials were:

(1) Wood ash

(2) Lime

(3) Na_2CO_3-anhydrous

(4) K_2CO_3

Wood ash used in the experiment was prepared by burning twigs at 400°C for 2 h in an electric furnace. Particles of charcoal present in the residue were removed by sieving through 1.70 mm sieve. The microprobe analyses of wood ash

are presented in Table 6.5. The industrial lime used was pre-calcined at 600°C for 2 h. Sodium carbonate (anhydrous) and potassium carbonate used were of the analar grade.

6.4.2.1 Structural considerations

Consideration of the fusibility of ceramic glazes shows that:

(i). A higher O/Si ratio achieved by increasing the amount of network modifiers (for example, RO, R_2O type of oxides) loosens the silica network and lowers the melting point.

(ii). A relatively higher ratio of SiO_2/Al_2O_3 makes the network co-former Al_2O_3 which is unable to form glass by itself hold the network less strongly, lowering the melting point.

Previous investigators (Stull 1942, Parmelee 1973) have reported that the SiO_2/Al_2O_3 ratio for low-maturing compositions is generally above 4. Examination of the analyses of a wide range of low-maturing compositions reveal that RO and R_2O contents and also the total flux content play an important role in the fusion and that the RO content in such compositions is generally lower than 5 while the total flux content is generally between 25 and 30. These guidelines were used in the formulations described below.

Eight different series were made with the clay-flux constituents. Three types of clay (LSK2A, PSH and LP) representing different soil groups were used. The materials in powder form were dry mixed in a plastic tube mill for 5 min. The consistency of the mix dispersed in water was carefully adjusted before it was applied to green ware with a brush. The experimental batches were fired at 900°C in an electric furnace for 2 h. The compositions of the experimental mixes compounded on the above basis and their maturing characteristics are presented in Table 6.3.

Table 6.3-Composition and maturing characteristcs of clay-flux bodies

Mix designation	Composition in wt%					Maturing characteristics
	Clay-LSK/ PSH/LP	Wood ash	Lime	Na_2CO_3 (anhyd.)	NaCl	
K/H/P 1	95	5	-	-	-	No noticeable softening
K/H/P 2	90	10	-	-	-	Slight tendency to interact
K/H/P 3	88	10	-	-	2	Colour changed to dark grey
K/H/P 4	85	10	-	-	5	Colour changed to dark grey
K/H/P 5	85	13	2	-	-	Immature
K/H/P 6	90	6	4	-	-	Immature
K/H/P 7	90	9	-	1	-	No noticeable softening. Good adherence
K/H/P 8	88	13	-	2	-	Signs of body-coat interaction

The compositions did not prove satisfactory for the desired firing range, and the next step in the search for a coating was to investigate low-melting binary systems.

6.4.3 Compositions in the binary system SiO_2-Na_2O

Having failed to secure a stable coating in the initial series of tests, the analysis of a number of binary compositions of known melting points were studied as starting points for further studies.

The Na_2O-SiO_2 system chosen is characterized by low-melting point eutectics. The two lowest eutectics at 799° and 840°C are composed of 28% and 37% Na_2O respectively.

Four experimental mixes were prepared with analar grade Na_2CO_3 and silica powder ground to pass through 63 μm sieve. Dry mixing of materials was carried out in a vibratory mill for 10 min. The experimental bars made from residual soil LSK2A were thinly covered with both dry and wet mixes before firing. The compositions of the experimental mixes and their maturing characteristics are given in Table 6.4.

Table 6.4-Composition and maturing characteristics of binary mixes fired at 900°C for 2h

Mix designation	Composition in wt%		Maturing characteristics (coating applied on LSK2A)
	Ground SiO_2	Anhyd. Na_2CO_3	
S1	95	5	Immature.
S2	90	10	No noticeable maturing.
S3	80	20	Slight tendency toward maturing.
S4	70	30	Signs of localized maturing.

The mix 80/20 showed a tendency towards melting and the mix 70/30 partially melted showing a matt surface texture; body-coating reaction layer was relatively insignificant. The other compositions were immature. In general, the series also did not produce satisfactory results.

6.4.4 Conventional multi-component systems

A combination of phase rule considerations given in Section 6.2.1, and structural considerations given in Section 6.4.2.1 formed the basis of the next series of trials.

The data available on the recent analyses of coatings used in antiquity and also the details reported on the state-of-the-art of conventional technology were used as

starting points for experiments. The following procedure was adopted in processing data to deduce batch compositions.

6.4.4.1 Formulation of batch compositions

(i). The analysis of the low-maturing composition under consideration was expressed in terms of the relative quantities of oxide constituents.

(ii). The raw materials were allocated in molecular ratios to satisfy the quantities of oxides.

(iii).Percentage batch compositions were then computed from the molecular composition by multiplying by the molecular weights.

Six compositions were formulated after successive evaluation of maturing characteristics of each coating. The chemical analyses of the coatings used as the starting compositions and of the raw materials used in the compounding of experimental mixes are listed in Table 6.5. The batch compositions of the mixes are presented in Table 6.6.

The results of the fusibility of the compositions studied (Table 6.6) were far from satisfactory. The results showed clearly that the heat treatment (that is, either maximum firing temperature or soaking time) employed was inadequate to initiate nucleation in the compositions studied.

Table 6.5-Compositions used as starting points for experiments

Material	Source	Chemical composition												Empirical formula
		SiO_2	Al_2O_3	Fe_2O_3	TiO_2	CaO	MgO	K_2O	Na_2O	RO	R_2O	Total flux	SiO_2/Al_2O_3	
Babylonian brick glaze	Kingery (1986)	60.00	1.60	1.10	0.15	7.00	3.50	3.60	17.00	10	21	32	37.5	$RO.R_2O.0.25R_2O_3.1.90RO_2$
Babylonian low-fire composition	Kingery (1986)	62.30	1.51	1.14	-	6.00	3.88	4.03	16.95	10	21	22	41.2	$RO.R_2O.0.04R_2O_3.2.04RO_2$
Chinese brick and tile glaze	Shanghai Inst. Ceram. (1986)	69.63	4.51	0.73	0.13	11.35	1.42	0.72	9.90	14	10	26	15.4	$RO.R_2O.0.11R_2O_3.2.55RO_2$
Egyptian glaze-1	Dayton (1978)	64.11	1.52	1.36	-	6.19	5.59	2.37	13.98	12	16	29	42.2	$RO.R_2O.0.04R_2O_3.2.16RO_2$
Egyptian glaze-2	Dayton (1978)	66.50	1.10	4.20	-	7.50	3.12	2.98	12.14	11	15	30	60.4	$RO.R_2O.0.09R_2O_3.2.58RO_2$
Egyptian glaze-3	Dayton (1978)	56.32	7.56	0.80	-	12.12	5.53	2.84	9.44	18	12	31	7.4	$RO.R_2O.0.13R_2O_3.1.74RO_2$
Wood ash	-	3.21	0.72	0.94	0.14	68.82	5.12	9.92	0.41	74	10	85	4.4	$RO.R_2O.0.01R_2O_3.0.04RO_2$

Table 6.6-Composition and maturing characteristics of multicomponent mixes

Designation	Composition					Maturing characteristics
	Clay (PSH)	SiO_2	Wood ash	K_2CO_3	Na_2CO_3	
1	5.45	52.45	12.92	2.82	26.32	Slight tendency toward maturing. Localized fused areas are covered with a powdery layer.
2	3.81	54.41	11.90	-	29.86	Signs of localized maturing.
3	16.19	54.41	16.55	-	12.85	No noticeable maturing.
4	3.76	59.92	14.08	-	22.22	Good surface adherence, but no maturing.
5	2.83	61.81	13.47	-	21.88	Immature.
6	20.54	42.00	22.00	-	15.43	Immature.

6.5 FABRICATION OF THE SELF-COATED CLAY PRODUCT

The system Na_2O-Al_2O_3-SiO_2 offered a number of advantages in the formulation of the composition of the coating. The liquidus of many compositions are appreciably low; two ternary eutectics exist at 732° and 740°C, with the lowest eutectic corresponding to a mixture of 26 parts Na_2O, 13 parts Al_2O_3 and 61 parts SiO_2 (Fig. 6.2).

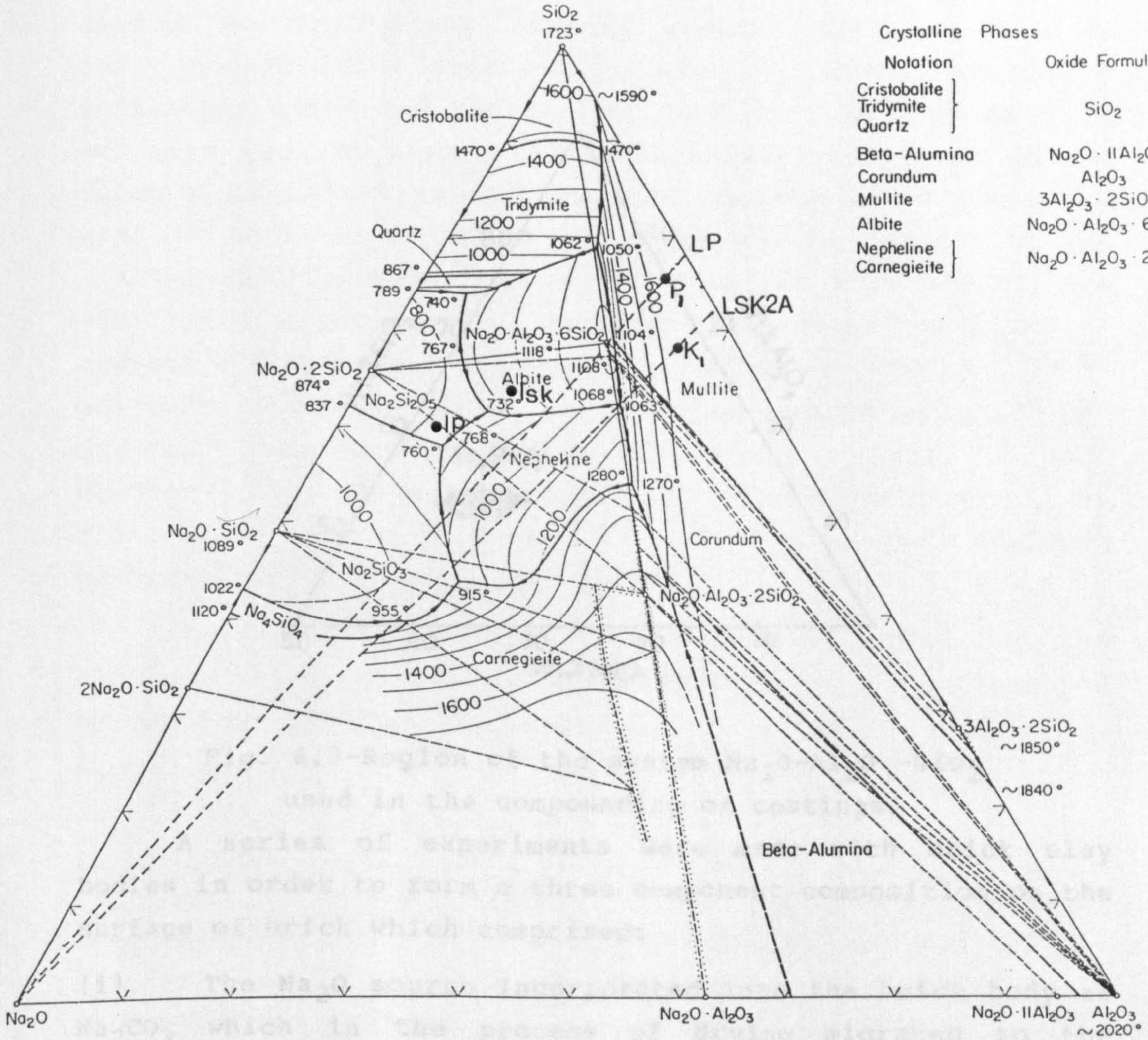

Crystalline Phases	
Notation	Oxide Formula
Cristobalite, Tridymite, Quartz	SiO_2
Beta-Alumina	$Na_2O \cdot 11Al_2O_3$
Corundum	Al_2O_3
Mullite	$3Al_2O_3 \cdot 2SiO_2$
Albite	$Na_2O \cdot Al_2O_3 \cdot 6SiO_2$
Nepheline, Carnegieite	$Na_2O \cdot Al_2O_3 \cdot 2SiO_2$

Fig. 6.2-The ternary system Na_2O-Al_2O_3-SiO_2 (after Osborn and Muan 1964).

Moreover, commonly available salts such as sodium carbonate and sodium bicarbonate can act as cheap sources of Na_2O. The region in this system considered suitable for preparing the low-maturing coating is indicated in Fig. 6.3.

CHAPTER 6

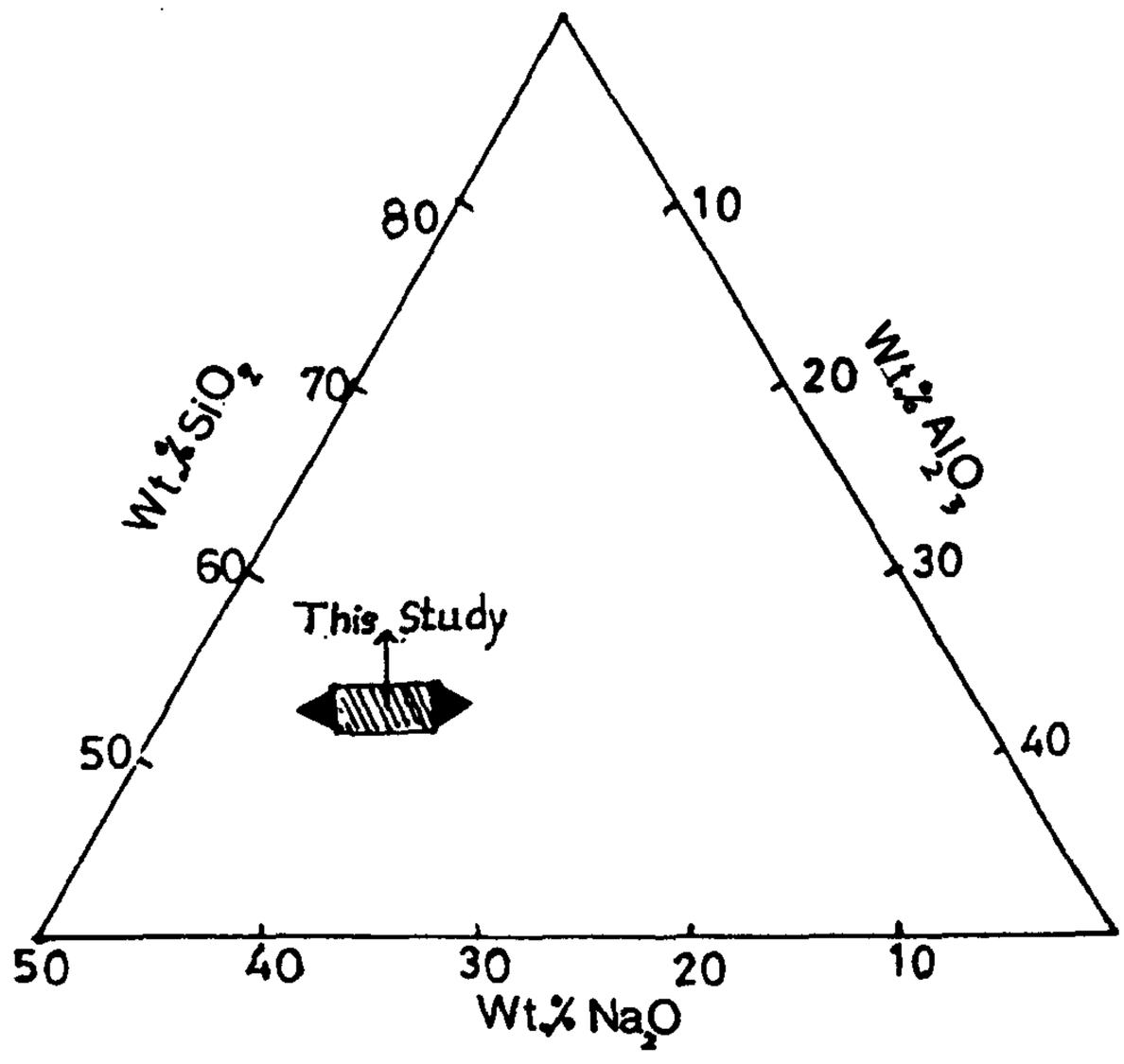

Fig. 6.3-Region of the system Na_2O-Al_2O_3-SiO_2 used in the compounding of coatings.

A series of experiments were made with brick clay bodies in order to form a three component composition on the surface of brick which comprised:

(i). The Na_2O source incorporated into the brick body as Na_2CO_3 which in the process of drying migrated to the surface as an efflorescence.

(ii). The SiO_2 enriched external layer obtained by sprinkling the surface with ground silica (-63 μm) which provided the required proportion of SiO_2 to the system.

(iii). The surface layer of green body which contributed a low proportion of Al_2O_3 originating from clay minerals.

The clays used were latosol (LP) and residual soil (LSK2A). Analar grade Na_2CO_3 (anhydrous) was used to activate the formation of self-coated layer.

The fraction of soil passing through 1.18 mm test sieve was used in the initial series of experiments. Pre-determined quantities of Na_2CO_3 were dissolved in the

optimum amount of distilled water required to bring the clay mass into moulding consistency. The ingredients were then intimately mixed and rectangular bars (160 mm x 30 mm x 15 mm) were cast at a pre-moulding moisture content of 13-29% depending on the type of clay. The composition of the mixes used in the investigation are presented in Table 6.7. The moulded specimens were first air dried at room temperature (20°C) for a period of 4 days to leatherhard condition to promote efflorescence and then oven dried at 50°C to a final moisture content of about 3%. The top surface of the dried specimens was sprinkled with silica sand ground to pass through 63 μm sieve. The specimens were then fired in an electric furnace at 900°C for 2 h. The firing cycle employed is similar to that presented in Fig. 6.1.

The successive stages of processing involved in the development of the self-coated clay product are represented by the flow chart in Fig. 6.4.

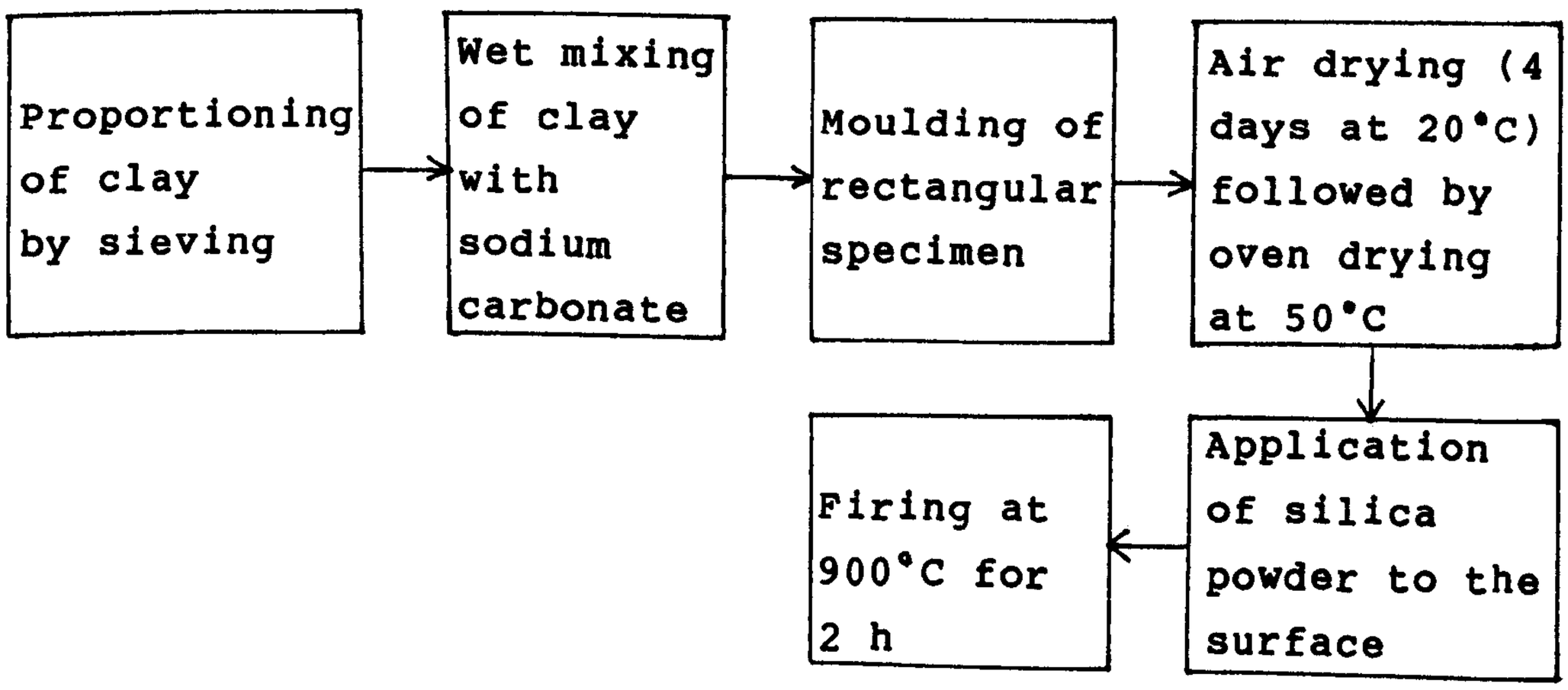

Fig. 6.4-Flow diagram of the process of development of self-coated clay product.

CHAPTER 6

A number of the processing conditions were found to have a profound influence on the development of the coating. A series of trials were therefore conducted to establish the optimum conditions favourable for the development of the self-coated product. The most important conditions considered are discussed below.

6.5.1 Source of Na_2O

Sodium carbonate (anhydrous), sodium bicarbonate (hydrated) and sodium chloride were all used as the source materials of Na_2O. The salts used were of the analar grade. The effectiveness of the salts was assessed with respect to both the extent of surface deposition and the state of maturity of the fired coating. From a comparative study involving 9 series of trials, it was apparent that sodium carbonate (anhydrous) was the most effective in producing a thick surface deposition on the green body and in developing a well matured coating on the fired body. Sodium bicarbonate produced a poor yield of surface crystallisation and a faint reaction zone in the fired product. Moreover, its poor solubility in water gave rise to processing problems and therefore the material was considered inappropriate. On the other hand, no surface efflorescence was discernible with sodium chloride and the fired product showed a black non-uniform surface discolouration. Sodium chloride thus also seemed ineffective. The results are summarised in Table 6.7.

Table 6.7-Characteristics of surface coatings

Designation	Composition (Pre-pressing M.C-18%)		Texture of coating developed on LSK2A	
	Material	Wt% in raw clay	Unfired surface (After drying for 72 h)	Fired surface (After firing at 900°C for 2 h)
KS1	Anh. Na_2CO_3	1.0	Surface crystallization on top surface.	Thin dark brown, rough, mat surface layer with a fair degree of maturity.
KS3	"	3.0	Surface crystallization on top surface.	Dark brown, rough, matt surface layer. Fair degree of maturity.
KS5	"	5.0	Extensive surface crystallization on all external surfaces.	Dark brown, rough, matt, mature surface layer. Coating-core interaction zone visible.
KSB1	$NaHCO_3$	1.0	No noticeable change.	No noticeable change.
KSB3	"	3.0	Faint surface scum on the outer periphery.	Very thin dark brown, matt surface layer.
KSB5	"	5.0	Poor yield of surface crystallization.	Thin dark brown matt surface layer.
KC1	NaCl	1.0	No visible surface crystallization.	No noticeable change.
KC3	"	3.0	No visible surface crystallization.	No surface effects. Slight change in body colour.
KC5	"	5.0	No visible surface crystallization.	Overall body colour changed to dark brown. No coating-core interaction zone.

6.5.2 Concentration of salt

Six series of trials were conducted with the two clays (LSK2A and LP) at 3 levels of concentration of sodium carbonate. It was apparent that, a salt concentration of 1 wt% produced a smooth lustrous coating on the fired body of high coarse fraction (LP). A coating with a mottled texture resulted on the surface of fine clay body (LSK2A). The lustrous coating, however, showed signs of crazing. Since lustre is not of primary importance for the final product, although it enhances its aesthetic value, another three series of trials were conducted in an attempt to improve the hardness of the surface coating as follows:

(i). by reducing the concentration of alkali salt in the body mix.
(ii). by increasing the amount of silica on the surface.
(iii). by adjusting the granulometric composition of the clay mix.

The low-cost option (i) led to a surface coating with low brilliance but free of crazing on the fired latosol (LP). The optimum salt concentration was 0.75 wt%. The coating was of ash-grey colour and contained filled up craters which minimized surface deformities. The fine clay produced a dark brown coating with a satisfactory texture free of defects (Plate 6.1). Table 6.8 presents a subjective assessment of the quality of coating produced on specimens made from two types of clay at 3 levels of concentration of alkali salt.

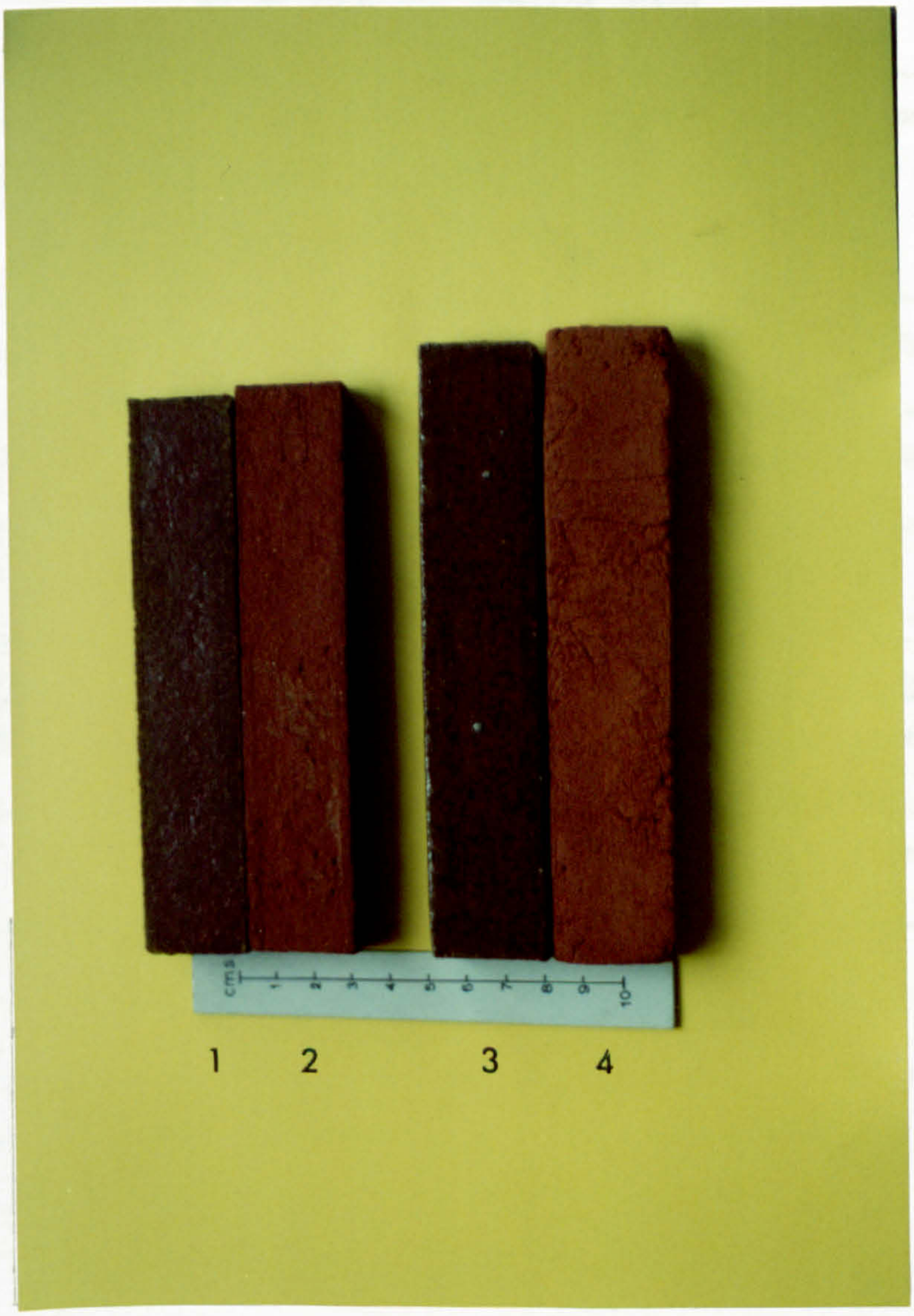

Plate 6.1-Bars fired at 900°C.
From left to right: (1) Residual soil-coated
(2) Residual soil-normal
(3) Latosol-coated
(4) Latosol-normal

Table 6.8-Mix composition and degree of maturity of coating for different clays

Mix designation	Composition (Pre-pressing M.C.-13-29%)		Degree of maturity of coating (Firing-900°C for 2 h)
	Clay	Wt% addition of $NaCO_3$	
K1	Residual soil LSK2A	0.5	Low degree of maturity.
K2	"	0.75	High degree of maturity. Mottled texture.
K3	"	1.00	Matured with mottled texture.
P1	Latosol-LP	0.5	Low degree of maturity.
P2	"	0.75	High degree of maturity. Somewhat lustrous.
P3	"	1.00	Matured but was glassy.

An optimum alkali salt concentration of 0.75 wt% was thus found adequate to obtain a satisfactory coating on the two types of clay used in the investigation.

6.5.3 Rate of drying

It was apparent that the rate of drying played an important role in promoting the efflorescence of clay bodies. Four series of trials were therefore designed to investigate the effect of the rate of drying. These were carried out with 2 clays treated with 1 wt% Na_2CO_3 under the conditions given below.

(i). Air drying for 24 h at room temperature after demoulding, followed by oven drying at 110°C for 24 h.

(ii). Air drying for 24 h at room temperature after demoulding, followed by oven-drying at 50°C to a constant weight.

(iii). Air drying at room temperature for 6 days.

(iv). Air drying to leatherhard condition at room temperature followed by oven-drying at 50°C to a constant weight.

The drying trials were performed with individual bars resting on the 50 mm x 150 mm surface. The examination of the fired specimens revealed that the drying procedure (iii) produced the best results. The mode of drying (iv) which roughly simulated the industrial practice was also found satisfactory. The drying conditions given in (i) was unfavourable for efflorescence coating. Both procedures (i) and (ii) tended to produce warped items. It was concluded therefore that continuous air drying or air drying to leatherhard moisture content followed by oven-drying at 50°C must be adopted in drying of green ware.

6.5.4 Granulometric composition of clay

The grain size distribution of the clay had a significant effect on the development of efflorescence coating as was evident from the foregoing series of experiments on parametric effects. The observations pointed to the fact that the granulometric composition of the latosol (LP) was the most favourable for the formation of a uniform surface layer. The coating on this fired body was smooth and well matured. The residual soil (LSK2A) which developed a uniform surface layer possessed a less vitreous texture with a high degree of maturity. The podzolic clay on the other hand produced no surface coating and the fired product showed no distinct reaction layer; the surface with a faint brown colouration still contained unreacted silica. The grain size distribution of the 3 brickmaking clays and the state of maturity of the respective surface coatings are represented in the triaxial diagram (Fig. 6.5).

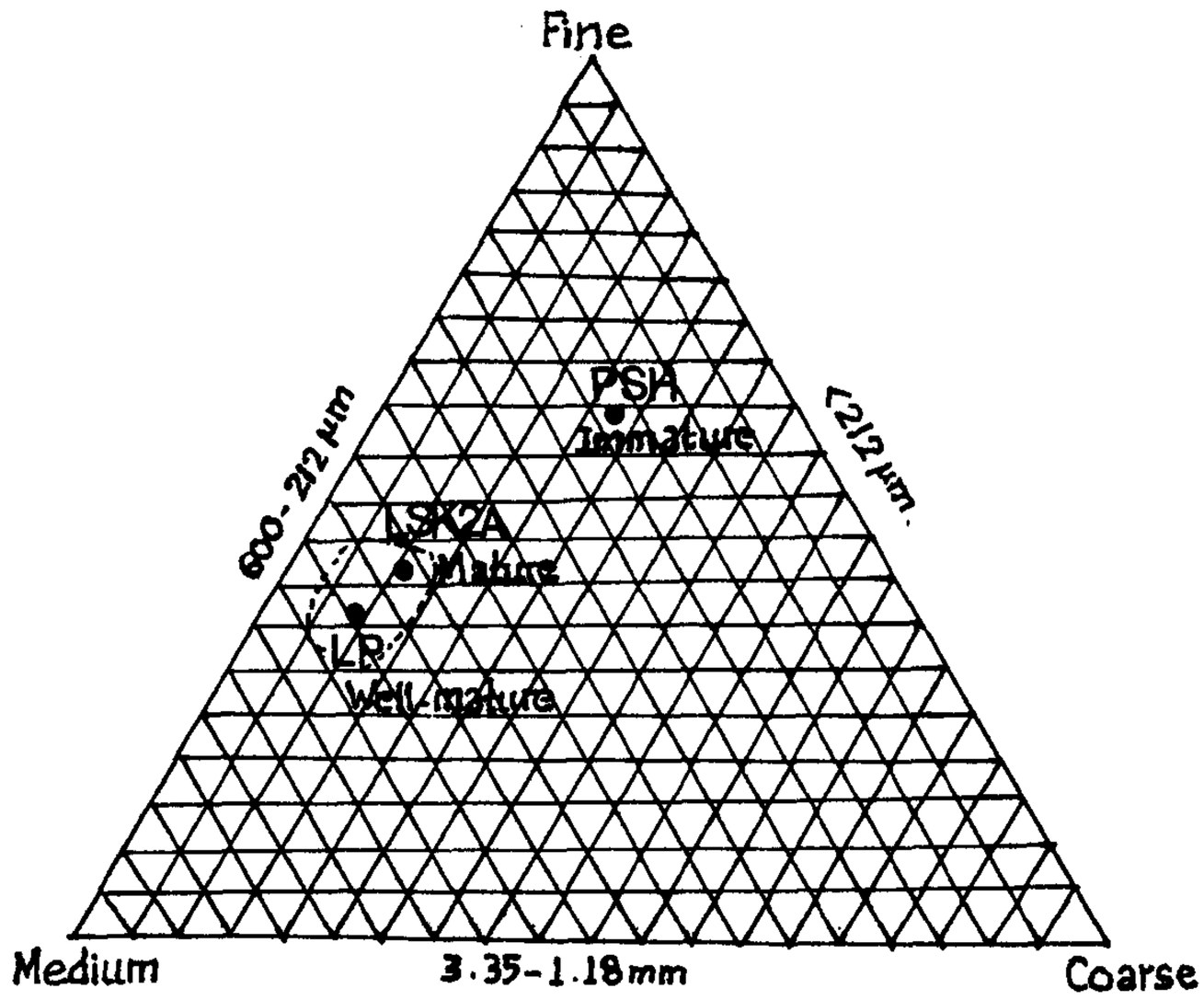

Fig. 6.5-Granulometric composition of the three soils. (LP-latosol, LSK2A- residual soil, PSH-podzolic clay)

The limiting ranges of favourable grain size compositions required to obtain a satisfactory coating could be deduced from the diagram. These are marked by a dotted line in Fig. 6.5. The size gradation of the starting materials determined by mechanical sieve analysis thus becomes a prerequisite for the adjustment of their granulometric composition to the optimum range.

6.6 THE MECHANICAL CHARACTERISTICS OF THE COATED PRODUCTS

6.6.1 Yielding behaviour

Load-deflection curves of both control (normal) and coated specimens were recorded using a 3-point bending attachment on a Schenck-Trebel programmable universal testing machine at a cross-head speed of 1 mm/min. Computer plots of deflection at mid-span relative to the ends of the span as a function of the mid-span load were obtained for each specimen (Appendix 5). The typical load-deflection curves are reproduced in Fig. 6.6.

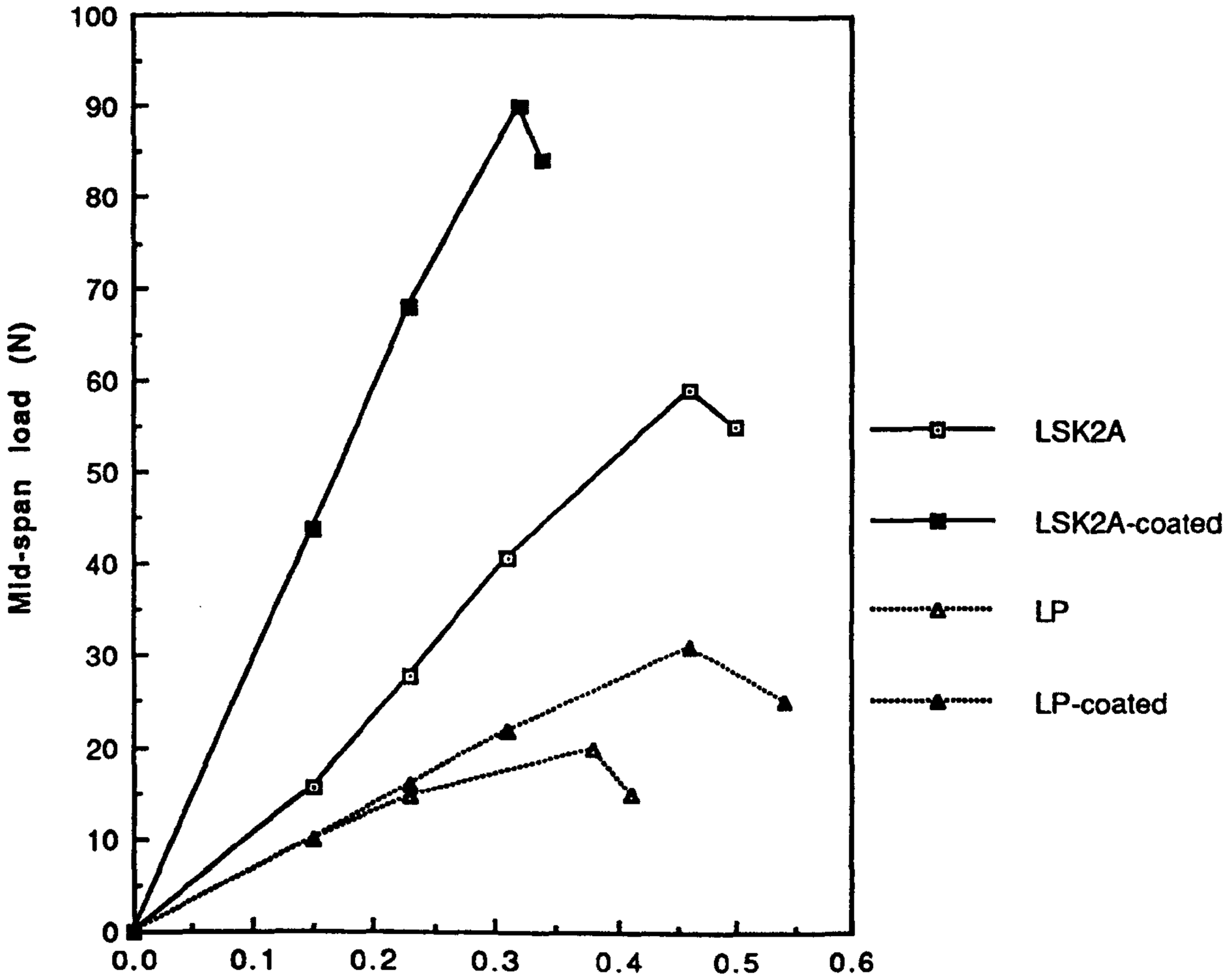

Fig. 6.6-Load-deflection curves for flexural tests on bars.

Coatings on both residual clay and latosol affected all stages of the deformation behaviour of the experimental bars when subjected to load tests. Table 6.9 displays the results of tests on specimens in the coated and uncoated conditions. The numerical values quoted are averages from tests on several specimens (3-6) in each condition and the figures in brackets are the percentage increase in value caused by the presence of the coating.

Table 6.9-The effect of coating on the yielding behaviour of fired bars produced from: (1) Residual soil (LSK2A) (2) Latosol

(Change in property indicated in brackets)

Clay body	Average load at the elastic limit (N)	Average ultimate failing load (N)
Normal LSK2A	46.9	61.0
Coated LSK2A	61.2 (+39%)	72.8 (+19%)
Normal LP	15.3	22.5
Coated LP	19.9 (+30%)	27.3 (+21%)

Experimental inaccuracies due to errors in the measurement of lengths and dimensional variation along bars, and errors in load measurement led to an estimated error ±1% on the strength results quoted.

The coating on LSK2A increased the load at the elastic limit by 39% and the ultimate failing load by 19%. The coating on LP exhibited a similar yielding behaviour. The increase in values of the limiting loads were 30% and 21% respectively. In both cases, the difference in behaviour of uncoated and coated specimens were particularly revealing. The load-deflection curves for flexural tests on bars demonstrate that the coating improved the mechanical strength of both clays within the accuracy of observations.

6.6.2 Strength

6.6.2.1 Modulus of rupture

The test was carried out according to ASTM designation C674-77 (Standard test methods for flexural properties of ceramic materials).

The rectangular test specimen was placed on the bearing edges, spaced 102 mm between centres, with the specimen overhanging at each end by at least 6.4 mm. The

load was applied at right angled to the 25.4 mm surface of the specimen and midway between the supporting edges at a uniform rate of 454±68 kg/min until failure occurred. The width and the thickness at the break was measured to the nearest 0.01 mm.

The modulus of rupture (M) of each rectangular specimen was calculated as follows.

$$M = 3WL/2bd^2$$

where;

M = Modulus of rupture, N/mm^2

W = load at rupture, N

L = distance between supports, 102 mm

b = width of specimen, mm

d = thickness of specimen, mm

The effect of the surface coating on the modulus of rupture of the clay bodies are listed in Table 6.10.

Table 6.10-Modulus of rupture and calculated dispersion values for coated and normal residual soil and latosol bars fired at 900°C for 2 h

Material	M.O.R. (mean) N/mm^2	Std. deviation N/mm^2	Coeff. of variation (%)
Normal residual soil LSK2A	1.73	0.09	5.0
Coated residual soil LSK2A	2.41	0.09	4.0
Normal latosol LP	0.48	0.03	6.0
Coated latosol LP	0.64	0.03	5.0

Coefficient of variation (V_c) calculated from,

$$\%V_c = \frac{r \times 100}{n}$$

r = std. deviation

n = mean of values

6.6.2.2 Modulus of elasticity

The modulus of elasticity of uncoated and coated fired rectangular clay bars was determined using a 3-point bending attachment on a Schenck-Trebel programmable universal testing machine fitted with a 2 kN load cell (Plate 6.2). The determinations were carried out according to ASTM designation C674-81 (Test Methods for Flexural Properties of Ceramic Whiteware Materials).

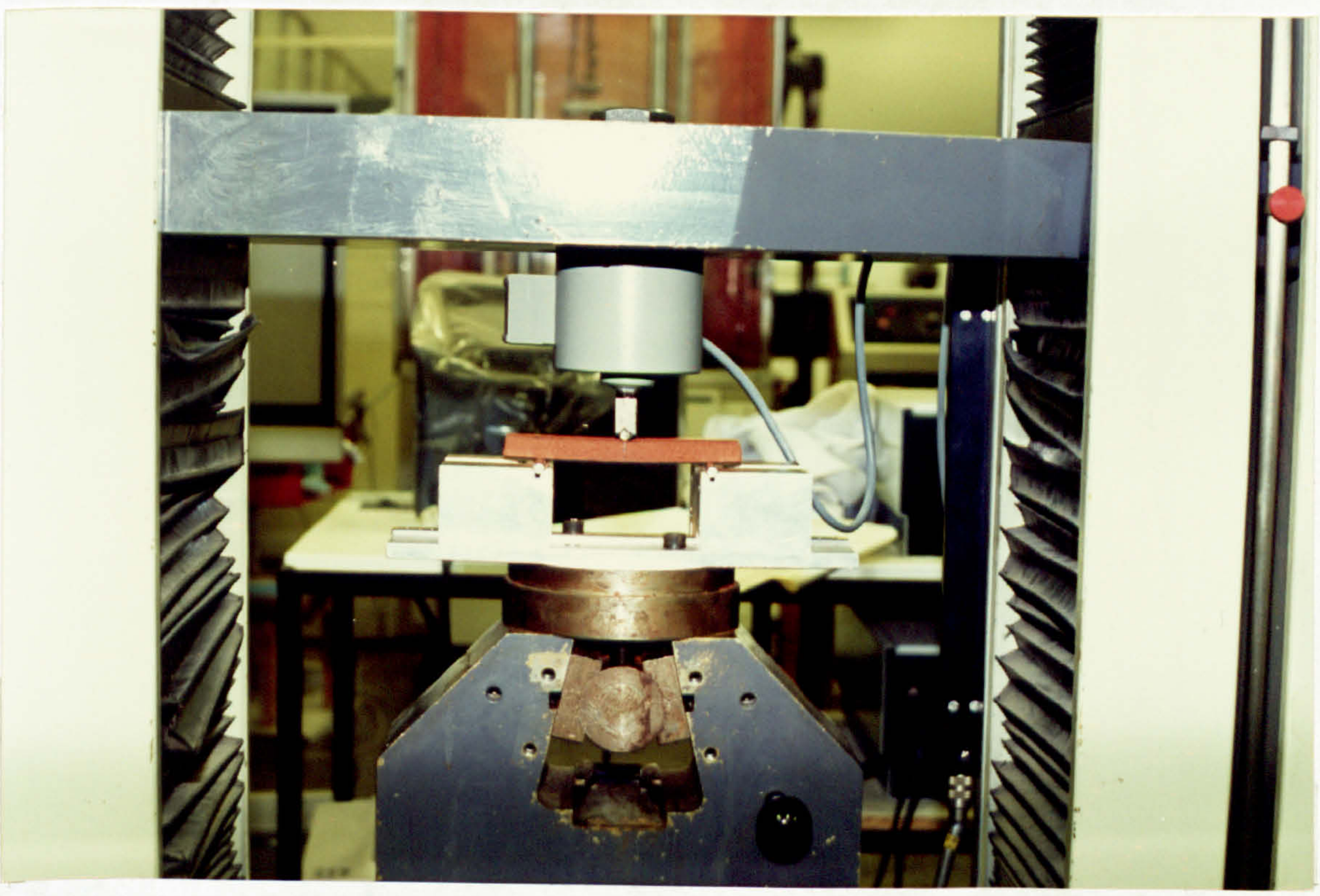

Plate 6.2-Arrangement of 3-point test assembly.

The specimen was supported in the same way as for the M.O.R determination and the machine was set to record automatically the load-deflection chart to a convenient scale at a cross-head speed of 1 mm/min. The stress-strain line representative of each curve was drawn to cover the elastic range and the M.O.E was calculated as follows:

$$E = WL^3 / 4\Delta bd^3$$

where;

W = load coordinate of the selected point,(N)

L = length of span, (mm)

Δ = deformation coordinate of the selected point, (mm)

b = width of specimen at the centre, (mm) and

d = thickness of specimens at the centre, (mm)

The effect of the surface coating on the modulus of elasticity of the clay bodies are given in Table 6.11.

Table 6.11-Modulus of elasticity and calculated dispersion values for coated and normal residual soil and latosol bars fired at 900°C for 2 h

Material	M.O.E. (mean) N/mm^2	Std. deviation N/mm^2	Coeff. of variation (%)
Normal residual soil LSK2A	533.0	19.0	3.5
Coated residual soil LSK2A	787.0	147.0	18.0
Normal latosol LP	181.0	12.0	6.0
Coated latosol LP	253.0	35.0	14.0

The coating increased both the M.O.R and the M.O.E significantly. The measured M.O.R and M.O.E values were at least 33% and 40% higher than those of the initial clay bodies.

6.6.3 Thermal expansion

It was evident from the consideration given in Section 2.4.6 that the mechanical strength of a ceramic material is increased if the coating is in a state of compression and this could be achieved with a coating of lower coefficient of expansion than the body.

Factors for calculating the coefficient of expansion of coatings from their compositions have been proposed by several workers (Singer et al. 1963). The calculation is based on an approximate relationship:

$$\frac{E}{100} = a_1p_1 + a_1p_2 + \ldots\ldots + a_np_n = \frac{10^6\Delta l}{l\Delta t}$$

found between the overall thermal expansion coefficient of a composite and its composition. a_1, a_2,.....,a_n denote the expansion coefficients and p_1, p_2,.....,p_n denote the molecular or cationic percentages of the components.

The coefficients of expansion of coatings and clay bodies were calculated using the above relationship in order to estimate the role played by coatings in strengthening the clay bodies under consideration. For this purpose, the surface coatings developed on the two clay bodies were mechanically removed and their electron microprobe analyses with those of uncoated bodies were obtained using polished specimens. The normalized overall composition of each specimen was ascertained by analyses performed at a minimum of three different locations. The factors used for the calculation of the coefficients of expansion are given in Table 6.12. The analyses of coatings and their coefficients of expansion are given in Table 6.13.

Table 6.12-Factors for the linear expansion coefficient

(after Singer et al. 1963)

[Given as weight% factor x molecular weight / 100]

Group	English and Turner	Hall	Takahashi (cationic not molecular percentages)	
			0-100°C	>100°C
SiO_2	0.15	60% 2.40		
		70% 2.04	0.50	0.60
		80% 1.56		
		90% 0.90		
TiO_2			-3.5	
Al_2O_3	1.43	5.1	$AlO_{1.5}$ 2.7	3.1
Fe_2O_3			$FeO_{1.5}$ 3.2	5.0
MgO	1.8	0.81	3.3	6.0
CaO	9.1	8.4	13.0	14.5
MnO			10.0	13.4
Na_2O	26.8	23.6	$NaO_{0.5}$ 26.9	29.5
K_2O	36.7	28.3	$KO_{0.5}$	33.3

Expansion calculated from $\frac{E}{100} = a_1p_1 + a_1p_2 + ...+ a_np_n = \frac{10^6 Al}{At}$ where a is the factor,

p the molecular or cationic percentages.

Table 6.13-Electron microprobe analyses (normalized) and calculated coefficients of expansion of coatings and clay bodies

Material	Composition in wt%									Coeff. of expansion ($x10^{-6}/°C$)
	SiO_2	TiO_2	Al_2O_3	Fe_2O_3	MnO	MgO	CaO	Na_2O	K_2O	
Bulk mat. LSK2A	64.44	1.10	19.46	7.70	0.07	1.47	1.82	3.43	0.49	6.31
Coating LSK2A	53.13	0.62	12.77	5.89	0.10	1.07	1.71	24.46	0.24	8.53
Bulk mat. LP	82.26	2.24	9.83	3.67	0.01	-	0.09	1.51	0.41	4.18
Coating LP	55.27	2.38	7.67	3.92	0.14	-	0.25	30.06	0.31	8.66

6.6.3.1 Role of stresses in strength improvement

The measured parameters for the residual soil are:

a_1(expansion coefficient for the body) = $6.31x10^{-6}/°C$

a_2(expansion coefficient for the coating)= $8.53x10^{-6}/°C$

ΔT(setting point of the coating)= 550°C (approximate)

E(Young's modulus)= 787 N/mm^2

v(Poisson's ratio)= 0.22 (Duke et al. 1968)

$A_1/A = 0.97$, $A_2/A = 0.03$ (based on the determination of coating thickness by electron microprobe analysis)

Then, according to the theoretical treatment given in Section 2.4.6.2:

$$\sigma_s = 1.19\ N/mm^2, \quad \sigma_b = -0.04\ N/mm^2$$

The corresponding values for the latosol are:

$$\sigma_s = 0.76\ N/mm^2, \quad \sigma_b = -0.02\ N/mm^2$$

In a modulus of rupture test, both the surface compression and the initial strength of the body must be overcome before failure occurs. It appears from the above that the magnitude of the stresses for the clays are very low compared to the body strength and therefore the contribution of stresses to the improvement of strength is relatively insignificant. It is therefore reasonable to assume that the minimization of surface defects rather than the surface compression is the major factor contributing to the strength improvement in the two clay bodies studied.

6.6.4 Interface reactions

Sections of fired specimens through the coatings into the bulk material and mechanically removed surface coatings were used in the examination and analysis. After resin impregnation and polishing, these sections were examined with the scanning electron microscope. The electron microprobe analysis was carried out using a Link Systems energy dispersive system attached to the scanning electron microscope. The sections used in the examination and electron microprobe analyses were made of the following:

(i). The surface coating developed on the fired specimen of residual soil-LSK2A.

(ii). The body-coating interaction core of the residual soil -LSK2A.

(iii).The surface coating developed on the fired specimen of latosol- LP.

(iv). The body-coating interaction core of the latosol- LP.

Step-traverse electron probe microanalyses were made across the profile of the coating in thin section in order to investigate the chemical characteristics of coatings and bodies and the mechanism of interface reactions. For this purpose, a spot analysis of the surface was first carried out at several locations. An electron microprobe beam was then adjusted to raster an area 2000x1500 μm^2 underlying the coating to give an average area analysis. The beam was moved in 2000 μm steps or intervals across the profile to obtain successive area analyses. The movement of the beam was from

the exterior surface, across the area representing the interior and into the uncoated boundary in the body of the bar containing the coating. Tables 6.14 and 6.15 give variation of chemical composition through sections and Fig. 6.7 shows chemical profile of the structure of coating for the two types of clay. They illustrate characteristics of the two coatings and show similarities and differences between them.

Table 6.14-Variation of chemical composition through section of profile of coated clay body

(1) Residual soil - LSK2A

Material	% Oxide								
	SiO_2	TiO_2	Al_2O_3	Fe_2O_3	MnO	MgO	CaO	Na_2O	K_2O
Coating on LSK2A	55.96	2.35	7.50	3.81	0.10	-	0.21	29.40	0.34
Area: 2000 u from surface	62.36	0.86	18.98	7.61	0.01	1.56	1.99	6.05	0.43
Area: 2000x2 u from surface	59.82	0.89	21.19	8.48	0.10	1.91	1.85	5.38	0.35
Area: 2000x3 u from surface	58.93	0.93	23.05	8.59	0.01	0.87	1.69	5.47	0.39
Area: 2000x4 u from surface	60.59	1.12	21.58	9.06	0.05	1.26	1.34	4.55	0.37
Area: 2000x5 u from surface	60.29	0.90	22.68	8.55	0.12	0.80	2.27	3.99	0.29
Area: 2000x6 u from surface	60.78	1.30	21.85	8.61	0.02	1.16	1.76	3.83	0.57
Area: 2000x7 u from surface	64.40	1.10	19.45	7.69	0.07	1.47	1.82	3.43	0.49

Table 6.15-Variation of chemical composition through section of profile of coated clay body

(2) Latosol - LP

Material	% Oxide								
	SiO_2	TiO_2	Al_2O_3	Fe_2O_3	MnO	MgO	CaO	Na_2O	K_2O
Coating on LP	55.12	2.37	7.65	3.91	0.14	-	0.25	29.98	0.31
Area: 2000 u from surface	80.42	1.75	9.53	3.69	0.04	0.39	0.21	3.62	0.28
Area: 2000x2 u from surface	80.74	2.34	10.82	4.18	0.02	-	0.14	1.27	0.41
Area: 2000x3 u from surface	70.51	3.72	14.85	5.90	0.09	0.47	0.37	3.43	0.52
Area: 2000x4 u from surface	79.35	2.45	11.09	3.95	-	0.43	0.12	2.19	0.37
Area: 2000x5 u from surface	82.09	2.23	9.81	3.66	0.01	-	0.09	1.51	0.41
Area: 2000x6 u from surface	84.29	0.87	9.54	2.50	0.02	0.65	0.12	1.70	0.28
Area: 2000x7 u from surface	80.82	2.03	9.90	3.78	0.12	0.02	0.14	2.19	0.77

The coating developed on the residual clay is 75-100 µm thick, whereas that on the latosol is much wider (350-375 µm). The other major difference in the profiles shown is the sharp concentration of Na_2O on the coating on latosol. In both cases, the glassy coating is characterized by the enrichment of Na and Al and deficiency of Si as is evident from the analyses given in Tables 6.14 and 6.15. The correspondence of peaks for alumina, iron oxide and sodium oxide marks the boundary of the reaction interface. Beyond the reaction zone, concentrations of Na and Al fall off and Si rises.

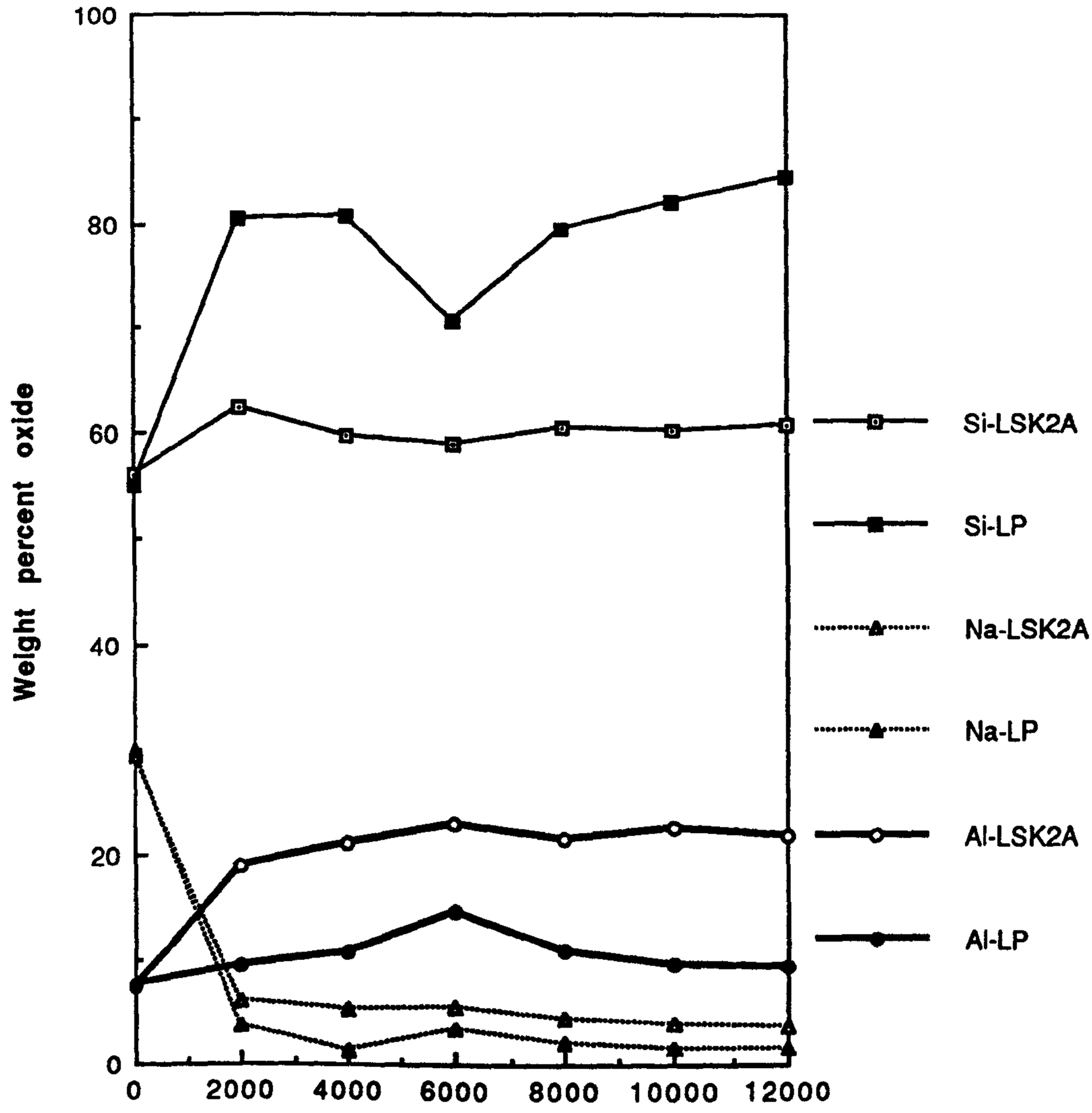

Fig. 6.7-Chemical profile of the coatings on residual soil and latosol.

6.6.5 Microstructure

The electron microscopic examination showed that the development of the coating transformed the original granular texture of the surfaces of both fired bodies into a smooth homogenous layer which greatly minimized the surface flaws and pits (Plate 6.3). The surface of fired residual clay, however, contained a fine irregular crack pattern showing evidence of crazing presumably arising from the mismatch of the coefficients of thermal expansion of coating and body. The surface layer of latosol is characterized by a high degree of homogeneity; the crack propagation is less widespread in this clay although the underlying, less conspicuous crack pattern is identifiable in the section (Plate 6.3). In both cases, the fresh surfaces with greatly minimized surface defects can be expected to cause a favourable influence on the mechanical strength of fired bodies provided they can overcome the negative effect of the induced thermal stresses.

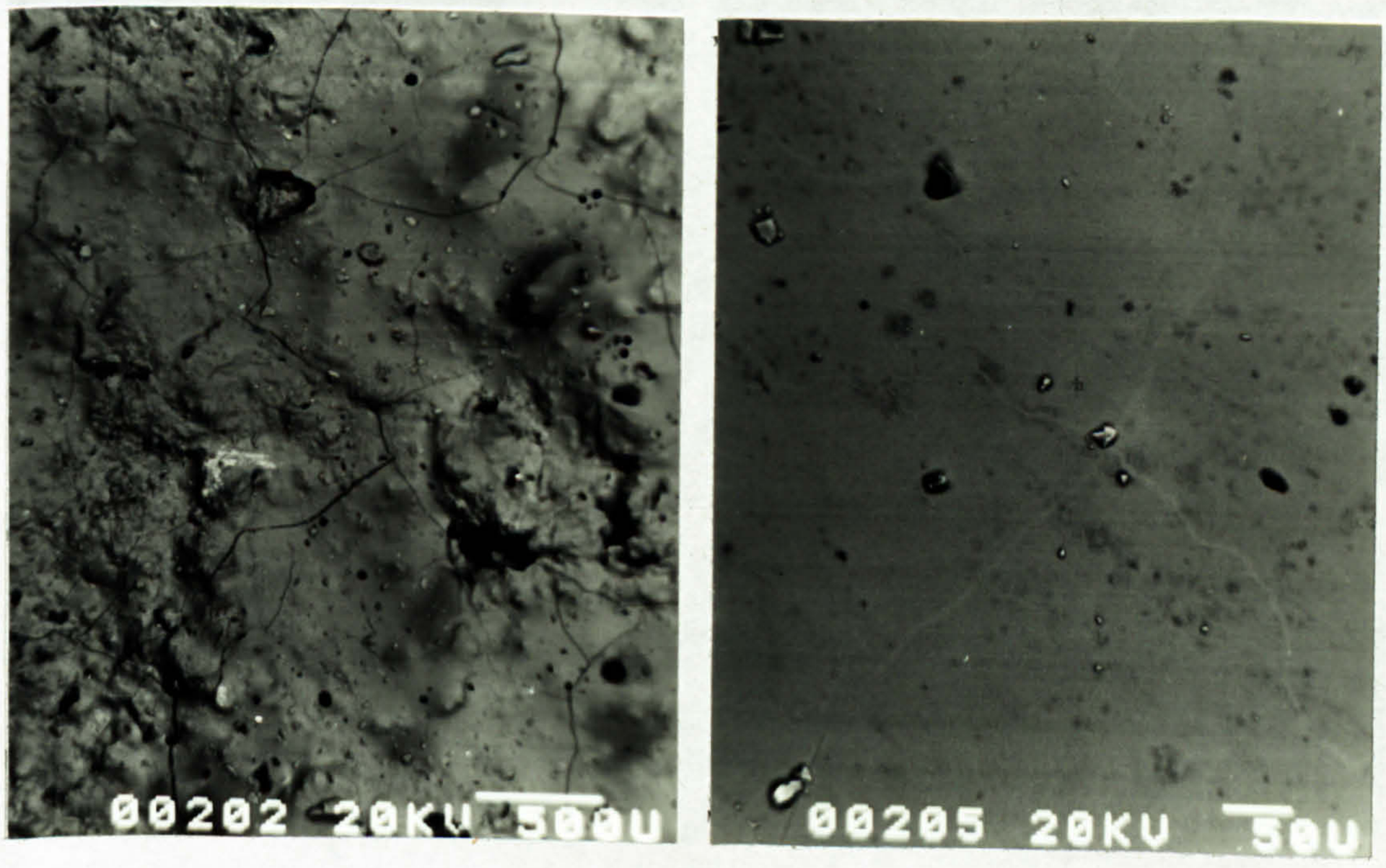

1 2

Plate 6.3-Photomicrograph of surface coating developed on (1) Residual soil LSK2A (2) Latosol LP

CHAPTER 6

The microstructure of the section through the coating typically consists of a granular ceramic core containing varying amounts of interstitial glass (Plate 6.4). The core is encased in a vitrified layer which is essentially a continuous matrix of glass containing some residual pores. The microstructure of the fired clay bodies can therefore be defined in terms of:

(i). thickness of the surface coating.
(ii). composition of the surface coating.
(iii). extent of any interstitial glass phase within the ceramic core.

The surface vitrified zone is quite distinct in both specimens. It is approximately 100 μm thick in the residual soil specimen which has a poorly defined boundary between the interface and the core. The interface and the bulk core of this specimen contain sufficient interstitial glass to produce a high degree of interparticle bonding within the core and to effect coalescence of the coating and the core.

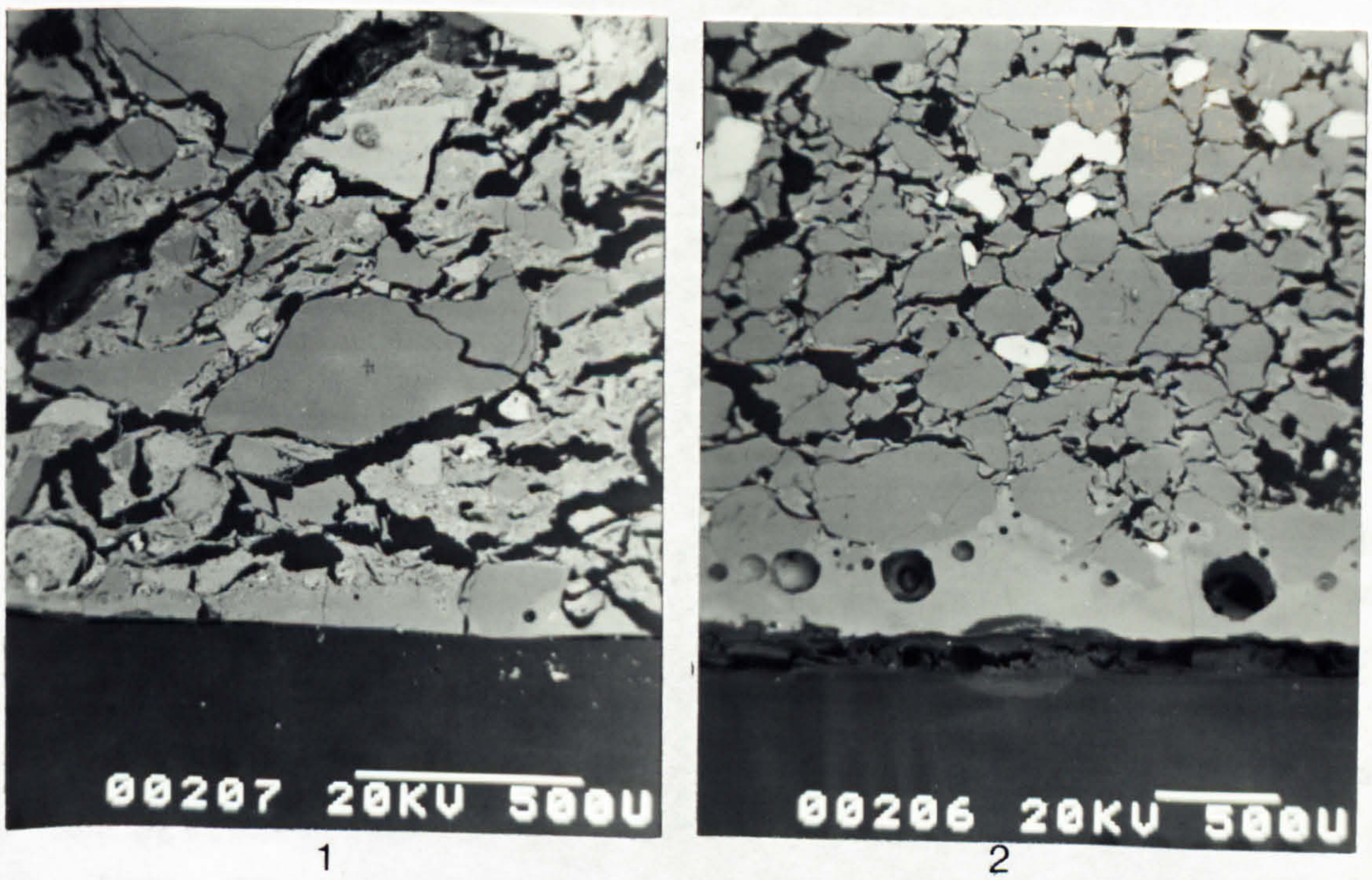

1 2

Plate 6.4-Photomicrograph of section through coating of (1) Residual soil LSK2A (2) Latosol LP.

The alkaline component (Na_2O) is less mobile in the structure to produce a thick coating. Nevertheless, the effects of the minimized surface defects and the high degree of interparticle bonding can be expected to play a dual role in counteracting the unfavourable thermal stresses. The specimen of latosol is characterized by a thick surface coating (350-375 μm) which contains some residual spherical pores, and by a ceramic core containing significantly low amount of interstitial glass. The boundary between the body-coating interface is clearly defined. This is consistent with a structure in which the alkaline component (Na_2O) is potentially mobile and can therefore be transported into the external surface. In this specimen, the migration of Na_2O and the consequent development of a vitrified glass layer made the surface hardening effect more predominant than the fusion of grains. The presence of pores on this coating, however, exerted a negative effect. Consequently, the more significant surface hardening effect and the obscure internal fusion of grains may have contributed to the improvement of the mechanical strength of fired latosol.

The variability in microstructure thus reflects differences in the extent to which the two clay bodies are strengthened by the combined effects of minimization of surface defects and enhancement of inter-particle bonding.

6.6.6 Infrared spectroscopic analysis of the unfired coatings

The coating developed on latosol showed a high degree of maturity, brilliance and smoothness of the surface when compared to that on the residual soil. The infrared spectra of surface material formed on green specimens as an efflorescence were therefore obtained in order to examine the preferential migration of body constituents to the surface. The analysis was carried out with a Unicam SP 1100 Infrared Spectrometer and the region of spectra covered was 400 to 4000 cm^{-1} (Appendix 6).

The spectra of the two surface materials are presented in Fig. 6.8. The two materials show very similar spectra

except for the appearance of a weak absorption band at 682 cm^{-1} in the spectrum of the surface material of latosol. It seems likely that this is due to v_4 vibrations of CO_3^{-2}. The intense absorption band at 3500 cm^{-1} observed in both spectra is assigned to stretching vibrations of OH groups. The broadening of this band to lower frequencies (3000cm^{-1}) in latosol is indicative of increase in bond strength of this surface material (Farmer 1974). The 1450 and 862 cm^{-1} bands are indeed representative of characteristic CO_3^{-2} vibrations from carbonate. The two spectra thus basically differ with respect to the degree of hydration of the carbonate phase. It is plausible, therefore, to assume that the difference in characteristics of the fired coating material is due to participation of mineral phases originating from clays in solid state reactions.

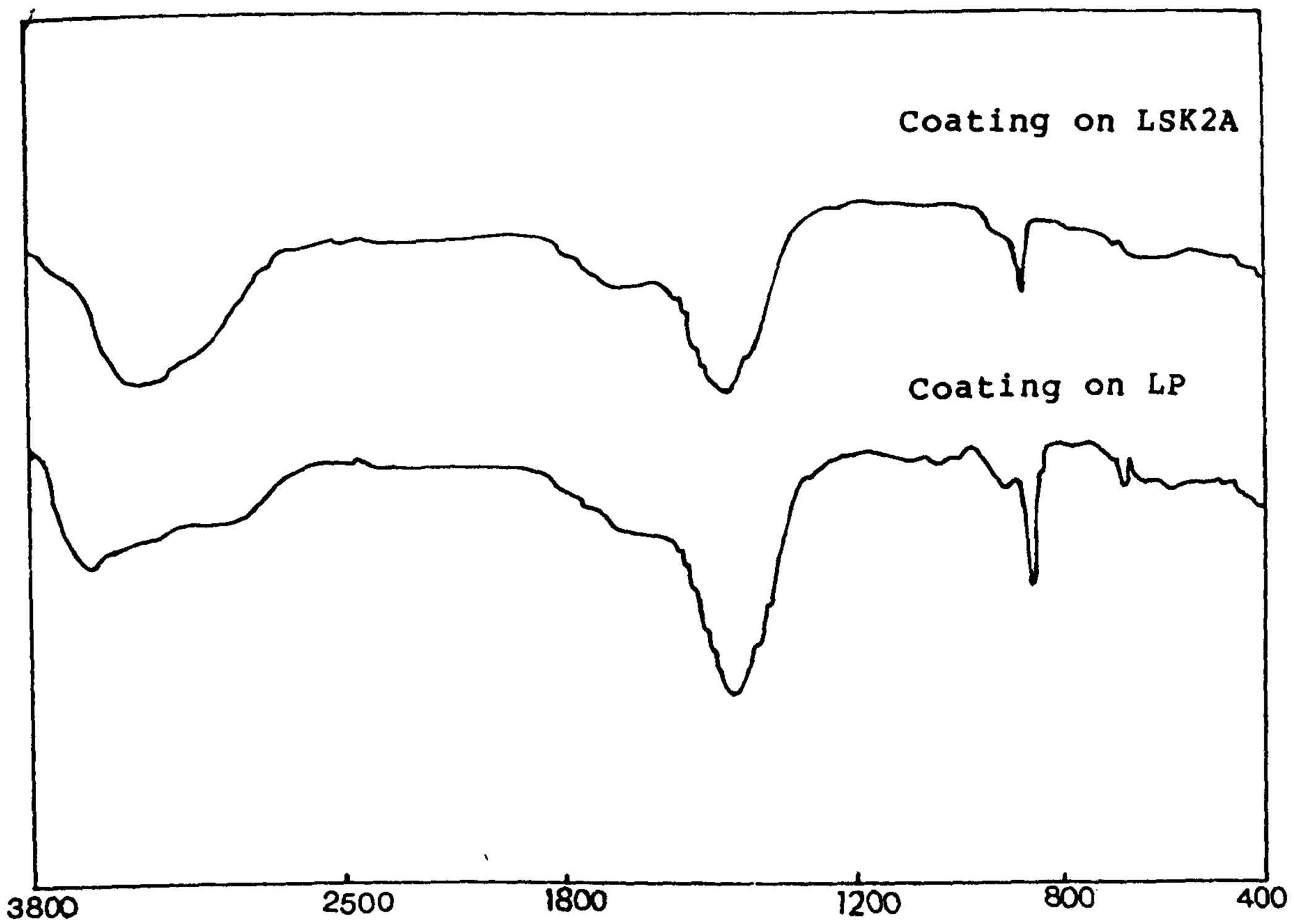

Fig. 6.8-Infrared spectra of unfired coatings.

6.6.7 Durability

Climate in Sri Lanka is too mild for frost action to cause damage in building materials. The principal causes of deterioration are:

(i). the moisture movement and erosion due to rain
(ii).air borne sea salts, the action of which is limited to the coastal areas.

An accelerated durability test was therefore designed to suit the climatic conditions in Sri Lanka. The method of test consisted of a 10 cycle heat-quench procedure on specimens with recording of the weight losses. The test was found to give reproducible results. The correlation of these test results with those of long term natural exposure could form the basis for future studies. This test was also intended to induce thermal stresses which tend to craze the surface coating of brick.

6.6.7.1 Test procedure

The dry weight of each specimen (140 mm x 27 mm x 13.5 mm) was determined after drying at 110°C to a constant weight. Three weighed specimens representing each lot of uncoated and coated brick along with three samples of approximately the same weight of a clay brick (LBC) conforming to BS specification were allowed to remain for 8 h in an oven pre-heated to 60°C. (The temperature at which the specimens were maintained was approximately twice the average day temperature and the time of heating corresponded to the average number of hours of daily sunshine in Sri lanka). The specimens were then quenched immediately by transferring them to a water container maintained at 20±3°C. They were soaked for 16 h and examined for surface defects. The 16 h time of immersion reaching near saturation simulated extreme conditions of rainfall which are too rigorous and less likely to be met in practice since the brick wall, usually plastered is not fully exposed to elements of weather. However, the experimental conditions were chosen in order to accelerate the deterioration of brick specimens.

The heat-quench cycle was repeated ten times. After the tenth cycle each specimen was weighed after drying to a constant weight at 110°C, and the weight loss recorded as a percentage of the dry weight. The specimens were also carefully examined taking care to distinguish between body cracks and craze marks. The results of the accelerated durability test are shown in Table 6.16.

Table 6.16-Results of laboratory accelerated durability test on coated bricks and engineering bricks

Batch No.	Type of brick	Percentage loss in weight after 10 cycles	Mean
A1	LSK2A	-0.12	
A2	"	-0.24	-0.15
A3	"	-0.09	
AC1	Coated LSK2A	-0.04	
AC2	"	-0.05	-0.04
AC3	"	-0.04	
P1	LP	-0.03	
P2	"	-0.03	-0.03
P3	"	-	
PC1	Coated LP	-0.05	
PC2	"	-0.09	-0.06
PC3	"	-0.03	
PCC1	Coated LP	-0.05	
PCC2	(Remedied for	-0.03	-0.04
PCC3	crazing)	-0.03	
LBC1	Engineering	1.51	
LBC2	brick-LBC	0.23	1.04
LBC3		1.38	

6.6.7.2 Results of laboratory durability tests

The experimental specimens of bricks showed a slight gain in weight during the test. In contrast, the samples of engineering brick showed a marked loss in weight of more than 1 percent. The slight gain in weight observed in both coated and uncoated specimens is probably attributed to the absorption of carbon dioxide by the lime rich clays during drying in the oven. Neither the coating nor the body of coated specimens was affected by the heat-quench procedure; no specimen disintegrated after 10 cycles of test. Thus the coating does not appear to have any detrimental effect on the overall durability of the brick specimens as determined by these laboratory durability tests.

6.7 MECHANISM OF FORMATION OF COATING

Electron probe microanalysis of the surface coatings (Table 6.13) shows that the composition of the surface coating on LP lies at a point close to the 760°C eutectic of the system Na_2O-Al_2O_3-SiO_2 whereas that of the surface coating on LSK2A lies at a point close to the 732°C eutectic within the primary phase field of nepheline (Fig. 6.2). The probable course of the reaction series can thus be predicted as follows.

(i). The initiation of reaction with a low amount of Na_2CO_3 changes the surface layer to a composition such as P1 on the Na_2O-LP join or K1 on the Na_2O-LSK2A join in the primary phase field of mullite. These being in the triangle mullite-albite-silica would begin to melt at the temperature of the eutectic (1050°C). Since this temperature has not been reached in the firing trials, no glass formation would occur initially.

(ii). As more Na_2CO_3 reacts with clay, the composition of the surface layer of the body shifts to the mullite-albite-nepheline triangle. The minimum temperature at which liquid can form in the compositions within this area is 1063°C.

(iii).Further reaction brings the surface layer of LP very close to the lowest eutectics and that of LSK2A to the primary phase field of nepheline. This would result in the formation of a substantial amount of liquid phase, particularly in LP. Such a liquid phase presumably absorbs further Na_2CO_3, resulting in a new trend of composition change along the respective joins. However, it is possible that the participation of Fe_2O_3 brings the composition into the quaternary system Na_2O-Al_2O_3-Fe_2O_3-SiO_2 making it more complicated than expected.

6.8 SUMMARY OF RESULTS

(i). Appropriate compositions in the Na_2O-Al_2O_3-SiO_2 system developed according to the mineralogy of clays are suited for strength improvement of clay bodies when produced as efflorescence surface coatings. A chemical reaction probably took place at the coating-body interface with solution and diffusion of chemical species.

(ii). The fabrication requirements necessary to develop the surface coating are:

(a) The SiO_2/Al_2O_3 ratio of clay must be within the range 1.5-2.0.

(b) The optimum granulometric composition of clay:
3.35-1.18 mm fraction- 9-11%.
600-212 μm fraction- 47-54%.
<212 μm fraction- 20-25%.

(c) The optimum amount of additive required to activate the efflorescence deposition and subsequent sintering of coating- 1 wt% solution of Na_2CO_3(anhydrous).

(d) Pre-moulding moisture content of clay mix- 13-29%.

(e) Air-drying of moulded specimens at room temperature for 6 days followed by oven-drying at 50°C for 24 h.

(f) Firing at a peak temperature of 900°C for 2 h.

(iii).Surface coating improved both the yielding and strength behaviour of fired clay bodies; the load at the elastic limit and the ultimate failing load were increased by approximately 30% and 19% respectively. The measured increases in modulus of rupture and modulus of elasticity were over 33% and 40% respectively.

(iv). Simplified calculations of the coefficients of thermal expansion of body and coating showed that the minimization of surface defects rather than surface compression was the underlying factor for the observed improvement in strength of the clays examined.

(v). Crazing occurred on surface coating of latosol (LP) probably as a result of the large expansion mismatch between the body and the coating. Remedying of this at the expense of surface lustre was possible by increasing the amount of silica on the surface.

(vi). Mineralogical analysis carried out in conjunction with microscopic analysis afforded a close insight into the mechanism of formation of coating.

(vii).Coating developed on the surface of clay bodies does not appear to have any detrimental effect on the overall durability of the brick specimens.

CHAPTER 7

THE INFLUENCE OF CALCIUM CARBONATE MINERALIZER ON THE STRENGTH, CONSTITUTION, AND PROPERTIES OF FIRED CLAY PRODUCTS

7.1 BACKGROUND OF STUDY

Little is known about the behaviour of lime in Sri lankan brick clay bodies although the fluxing ability of lime is well known (Section 2.4.3.1). This investigation is concerned with the use of calcium carbonate as a mineralizer in three brick clay bodies with particular emphasis placed on:

(i). the physical and mechanical properties of fired product, particularly the strength,

(ii). the relationship between the mechanical strength of fired product and high temperature crystalline phases,

(iii).the textural characteristics favourable from the viewpoint of strength development,

(iv). the mechanism of strength development in the systems under consideration.

7.2 EXPERIMENTAL

7.2.1 Materials

The three brick clay samples covering different formational types, localities of origin, degrees of order and particle sizes used in the investigation were:

(i). Residual soil-LSK2A,

(ii). Podzolic clay-PSH,

(iii).Latosol-LP.

The properties of the clays are given in Chapter 3. The mineralizer used was analar grade calcium carbonate.

7.2.2 Specimen preparation

The minus 1.40 mm fraction of each clay was oven-dried (105°C) and then mixed with 2, 3, and 4 wt% of calcium carbonate in a mechanical mixer. An optimum amount of water was added in order to bring each sample to the correct consistency for wet moulding. The wet moulding technique was

employed in view of its effectiveness in dispersing the mineralizer. The clay mixes were allowed to mature for at least 20 h and then compacted into 160 mm x 30 mm x 15 mm bars at a moulding moisture content of 25-30%. A minimum of 6 bars to represent each sub-sample and control sample and a total of 144 bars to represent six firing trials of each clay mix were made. The experimental bars were air-dried and then oven-dried at 105°C for 24 h. The composition of the experimental mixes are presented in Table 7.1. The nominal positions of these compositions are plotted on the ternary system $CaO-Al_2O_3-SiO_2$ in Fig. 7.1.

Table 7.1-Composition of experimental mixes

Clay	Designation of clay mix	$CaCO_3$ content (wt%)	Water content (wt%)
Podzolic clay	H	-	37.3
	HCA	2.0	37.1
	HCB	3.0	40.0
	HCC	4.0	40.0
Residual soil	K	-	38.3
	KCA	2.0	39.1
	KCB	3.0	39.6
	KCC	4.0	38.0
Latosol	P	-	18.3
	PCA	2.0	18.3
	PCB	3.0	18.5
	PCC	4.0	18.5

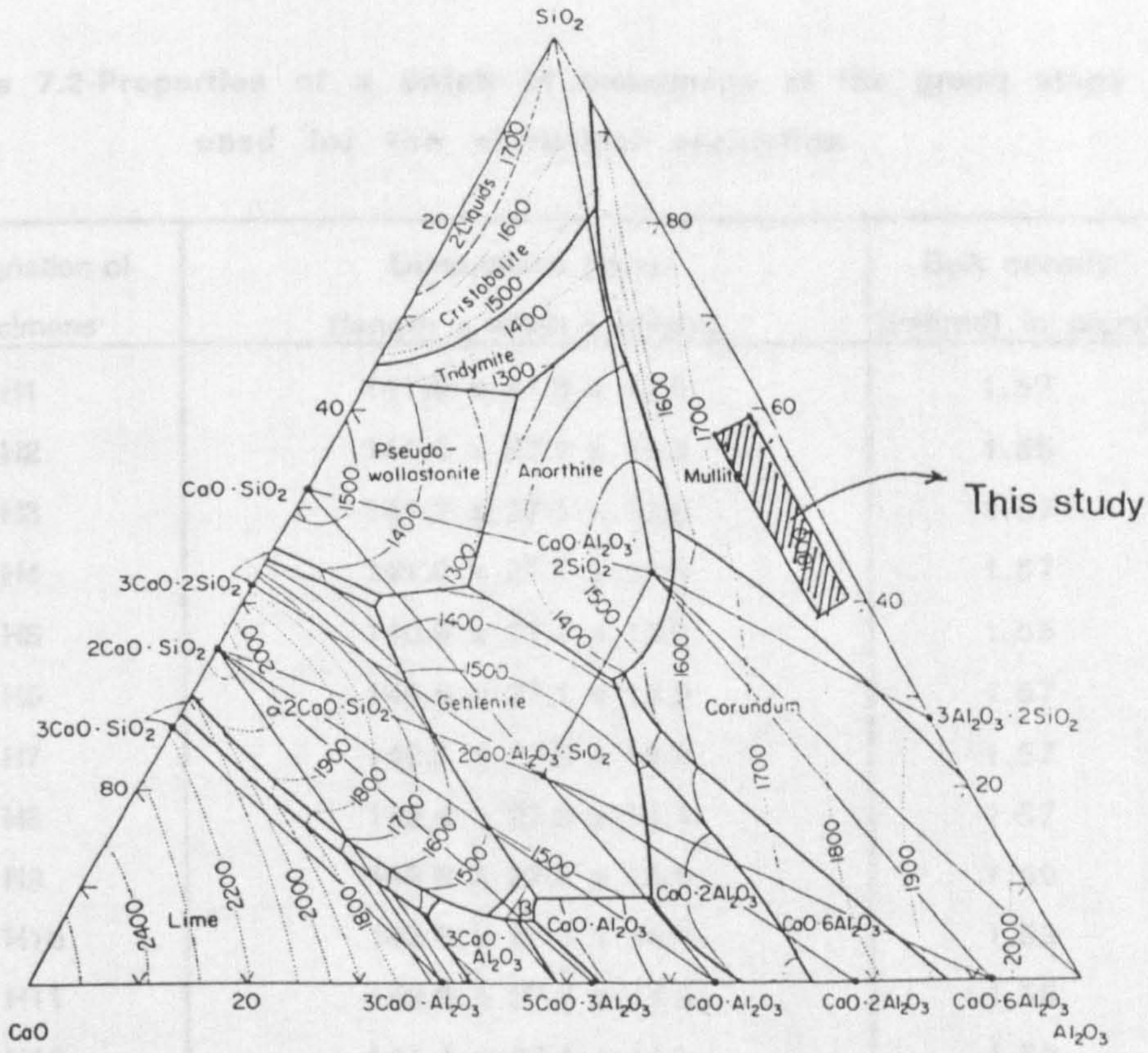

Fig. 7.1-The ternary system $CaO-Al_2O_3-SiO_2$ (Gentile and foster) showing the positions of the compositions used in this work.

The statistical spread of extent of compaction and of dimensional stability of the specimens were assessed with respect to the bulk density and length at the original green stage. A typical set of data used for the statistical analysis is given in Table 7.2.

Table 7.2-Properties of a batch of specimens at the green stage used for the statistical evaluation

Designation of specimens	Dimensions (mm) (length x width x height)	Bulk density (unfired) in g/cm^3
H1	141.6 x 27.0 x 13.9	1.57
H2	141.6 x 27.1 x 14.0	1.55
H3	141.2 x 27.1 x 13.9	1.57
H4	141.6 x 27.1 x 13.8	1.57
H5	140.9 x 27.1 x 13.9	1.55
H6	140.6 x 27.1 x 13.5	1.57
H7	142.3 x 27.6 x 13.9	1.57
H8	142.4 x 27.3 x 14.1	1.57
H9	142.6 x 27.4 x 14.0	1.59
H10	142.6 x 27.4 x 14.0	1.59
H11	142.5 x 27.2 x 14.5	1.58
H12	141.4 x 27.4 x 14.5	1.58

(i). Bulk density:

Process A.M.($\bar{x}$) = 1.57

Sample S.D.(σ_{n-1})= 0.01

Coefficient of variation = 0.63

(ii).Length:

Process A.M.($\bar{x}$) = 141.8

Sample S.D.(σ_{n-1})= 0.69

Coefficient of variation = 0.48

The reproducibility of sample preparation seemed satisfactory, but, as is normal with brickmaking materials, depended on the homogeneity of the clays used for the investigation.

7.2.3 Firing of specimens

An electric muffle furnace was used for firing the specimens. The experimental bars were heated at a rate of 5.6°C/min, held for 2 h at the temperatures of 700°, 800°, 1000°, 1100° and 1150°C and then cooled naturally to simulate as far as possible the normal manufacturing conditions.

7.3 PROPERTIES INVESTIGATED

7.3.1 Physical properties

The compacted bars processed under different experimental conditions were tested for:

(i). Modulus of rupture- carried out in accordance with ASTM designation C674-77.

(ii). Linear firing shrinkage

(iii). Water absorption

(iv). Apparent porosity } determined according to ASTM designation C373-72.

(v). Bulk density

(vi). Efflorescence- carried out in accordance with BS 3921:1985.

The test procedures used in the determination of bulk density and modulus of rupture are described in Sections 5.3.1.1 and 6.6.2.1 respectively. The methods of determination of apparent porosity and water absorption are briefly described in Sections 5.3.1.2 and 5.3.1.3. Details of the other test procedures are given below.

7.3.1.1 Linear firing shrinkage

The linear firing shrinkage was determined by measuring the length of the bars before and after firing. The lengths were measured by vernier calliper to the nearest 0.01 mm. The change in dimension divided by the original dimension was used to determine percentage linear shrinkage. An average of three values was used for each reported value.

7.3.1.2 Water absorption and apparent porosity

Water absorption and apparent porosities were determined on all fired bodies according to the procedure described in ASTM designation C373-72 (Standard test method

for water absorption, bulk density, apparent porosity and apparent specific gravity of fired whiteware products). A pycnometer was used in obtaining measurements. The oven-dried sample was weighed and immersed in distilled water for 24 h and weighed again. The saturated sample was transferred to a pycnometer filled with water which was weighed with and without the sample and the water absorption and apparent porosity were calculated as:

$$\text{Water absorptiom} = \frac{(A-D)}{D} \times 100$$

$$\text{Apparent porosity} = \frac{\text{Volume of open pores}}{\text{Exterior volume}} \times 100 = \frac{A-D}{A-(B-C)} \times 100$$

where A = Mass of saturated surface-dry sample in air
B = Mass of pycnometer filled with water and with sample
C = Mass of pycnometer filled with water only
D = Mass of oven-dry sample in air

The apparent porosity determined in this way refers to the volume fraction of accessible pores- $V_{open}/V_{impervious}+V_{open}$ and was used to measure the progress of vitrification of fired clay bodies.

7.3.1.3 Efflorescence

The test for efflorescence was carried out as described in BS 3921:1985 (Specification for clay bricks).

All faces of the specimen (except one flat surface) was covered with polythene sheet to prevent evaporation. The exposed surface was then placed in contact with the mouth of an inverted bottle containing deionised water. The rim of the bottle was sealed. The face of the specimen was then allowed to remain in contact with deionised water for 48 h. After saturation, the specimen was removed from the bottle and allowed to dry from its exposed face in the laboratory for 7 days. The procedure was repeated for 14 days and the dried specimen was examined for deposit of salts and powdering of the surface.

7.3.2 Constitution and microstructure

7.3.2.1 X-ray diffraction analysis

Representative samples of fired specimens subjected to the modulus of rupture (M.O.R.) test were ground initially in a mechanical agate mortar for 15 min. Grinding was continued manually for another 30 min. The X-ray spectrum was then run on a Philips diffractometer using CuK_{α} radiation (50 kV, 30 mA) to detect any new phases formed. Randomly packed powder samples were used to minimize preferred orientation of the particles.

A quantitative assessment of phases was made by the measurement of intensities of the appropriate peaks. The diffraction peaks used in the identification of phases were, for mullite at 5.39 Å , for hematite at 2.51 Å , for δ-Al_2O_3 at 2.08 Å and for cristobalite at 4.05 Å .

7.3.2.2 Scanning electron microscopy

Microstructures of selected samples representative of the optimum compositions of the mixes were examined by a Hitachi electron microscope fitted with an energy dispersive analysis system. The surfaces of the specimens were vacuum coated with a thin film of carbon prior to examination. Fracture surfaces of both unetched samples and samples etched in 40% HF for 5 seconds were examined.

The effect of firing on the internal morphology and microstructure of the clays is described in Chapter 8.

7.4 GENERAL PROPERTY TRENDS

7.4.1 Modulus of rupture

Excerpts from the modulus of rupture test results are shown in Tables 7.3, 7.4 and 7.5. Modulus of rupture as a function of firing temperature is shown for the pure clays and their compositions in Fig. 7.2. On the basis of statistical analyses of the results, several conclusions were drawn.

Table 7.3-Effect of addition of calcium carbonate on properties of clay bodies (1) Podzolic clay compositions

Designation of clay mix	Property	Average value of property of bars fired at temperatures shown (°C)					
		700	800	900	1000	1100	1150
H	Modulus of Rupture (N/mm^2)	2.31	6.39	8.71	11.88	17.56	24.82
HCA		3.00	4.72	9.15	12.60	13.26	13.96
HCB		3.13	7.75	3.88	12.90	12.55	14.39
HCC		3.62	5.96	8.24	11.12	12.41	15.35
H	% Linear firing shrinkage	1.41	3.11	4.29	6.85	6.94	10.56
HCA		1.35	1.70	5.40	7.53	8.01	8.26
HCB		0.80	4.01	3.09	5.44	7.45	7.64
HCC		0.94	2.93	5.13	5.87	7.02	7.81
H	% Water absorption (24 h immersion)	31.00	27.24	25.40	22.15	17.20	9.77
HCA		30.13	29.25	23.35	17.78	11.49	13.72
HCB		30.18	25.21	23.91	21.07	14.17	16.11
HCC		29.43	26.57	22.26	19.88	14.00	13.17
H	% Apparent porosity	45.44	43.78	41.02	38.10	31.40	19.54
HCA		43.20	44.27	39.21	31.89	22.00	25.97
HCB		44.88	40.77	38.91	36.39	26.16	29.14
HCC		43.94	41.09	37.68	33.94	24.92	23.75
H	Bulk density (g/cm^3)	1.37	1.44	1.48	1.60	1.69	1.86
HCA		1.39	1.40	1.53	1.67	1.72	1.75
HCB		1.39	1.48	1.48	1.59	1.68	1.67
HCC		1.39	1.43	1.56	1.58	1.64	1.67
H	Efflorescence	----------Nil----------					
HCA							
HCB							
HCC							

Table 7.4-Effect of addition of calcium carbonate on properties of clay bodies (2) Residual soil compositions

Designation of clay mix	Property	Average value of property of bars fired at temperatures shown (°C)					
		700	800	900	1000	1100	1150
K	Modulus of Rupture (N/mm^2)	2.16	2.28	1.91	1.59	1.86	1.82
KCA		2.19	2.28	2.02	1.71	1.95	1.78
KCB		2.11	2.34	2.01	1.88	1.88	1.69
KCC		2.18	2.38	2.15	2.16	1.91	1.75
K	% Linear firing shrinkage	0.71	0.72	0.98	1.57	3.30	1.44
kCA		0.82	1.34	1.13	2.18	2.90	2.52
KCB		0.34	1.03	1.23	1.74	1.68	2.13
KCC		0.31	1.31	1.75	1.82	2.03	2.31
K	% Water absorption (24 h immersion)	20.12	18.72	19.06	18.45	15.08	15.55
KCA		19.41	18.93	17.64	16.11	15.25	15.06
KCB		19.57	19.36	19.17	15.90	15.43	15.35
KCC		19.73	19.19	18.76	16.29	16.12	15.52
K	% Apparent porosity	33.81	32.33	33.29	31.90	27.47	27.63
KCA		33.23	32.49	30.87	29.13	27.02	26.96
KCB		34.46	33.59	33.29	28.28	27.24	27.02
KCC		33.90	34.39	33.20	28.82	28.11	27.08
K	Bulk density (g/cm^3)	1.54	1.58	1.57	1.58	1.65	1.63
KCA		1.58	1.60	1.56	1.61	1.64	1.60
KCB		1.57	1.60	1.59	1.60	1.64	1.61
KCC		1.58	1.59	1.60	1.62	1.65	1.63
K KCA KCB KCC	Efflorescence	----------Nil----------					

Table 7.5-Effect of addition of calcium carbonate on properties of clay bodies (3) Latosol compositions

Designation of clay mix	Property	Average value of property of bars fired at temperatures shown (°C)			
		800	900	1000	1150
P	Modulus of rupture (N/mm^2)	0.11	0.49	0.38	0.08
PCA		0.45	0.52	0.58	0.39
PCB		0.48	0.48	0.61	0.37
PCC		0.54	0.53	0.48	0.28
P	% Linear firing shrinkage	-	-0.51	-0.38	-
PCA		-0.26	-0.32	-0.45	-0.32
PCB		1.29	-	-0.38	-0.32
PCC		-0.45	-1.02	0.32	0.64
P	% Water absorption (24 h immersion)	10.95	11.22	11.35	11.81
PCA		11.80	11.36	11.47	10.92
PCB		11.89	11.60	11.17	11.10
PCC		11.93	11.33	10.83	10.92
P	% Apparent porosity	21.91	22.20	22.75	23.80
PCA		22.66	22.40	22.48	21.61
PCB		23.12	22.48	21.84	21.35
PCC		22.88	21.90	21.39	20.96
P	Bulk density (g/cm^3)	-	1.77	1.75	-
PCA		1.77	1.75	1.74	1.75
PCB		1.77	-	1.73	1.74
PCC		1.76	1.79	1.72	1.76
P	Efflorescence	----------Nil----------			
PCA					
PCB					
PCC					

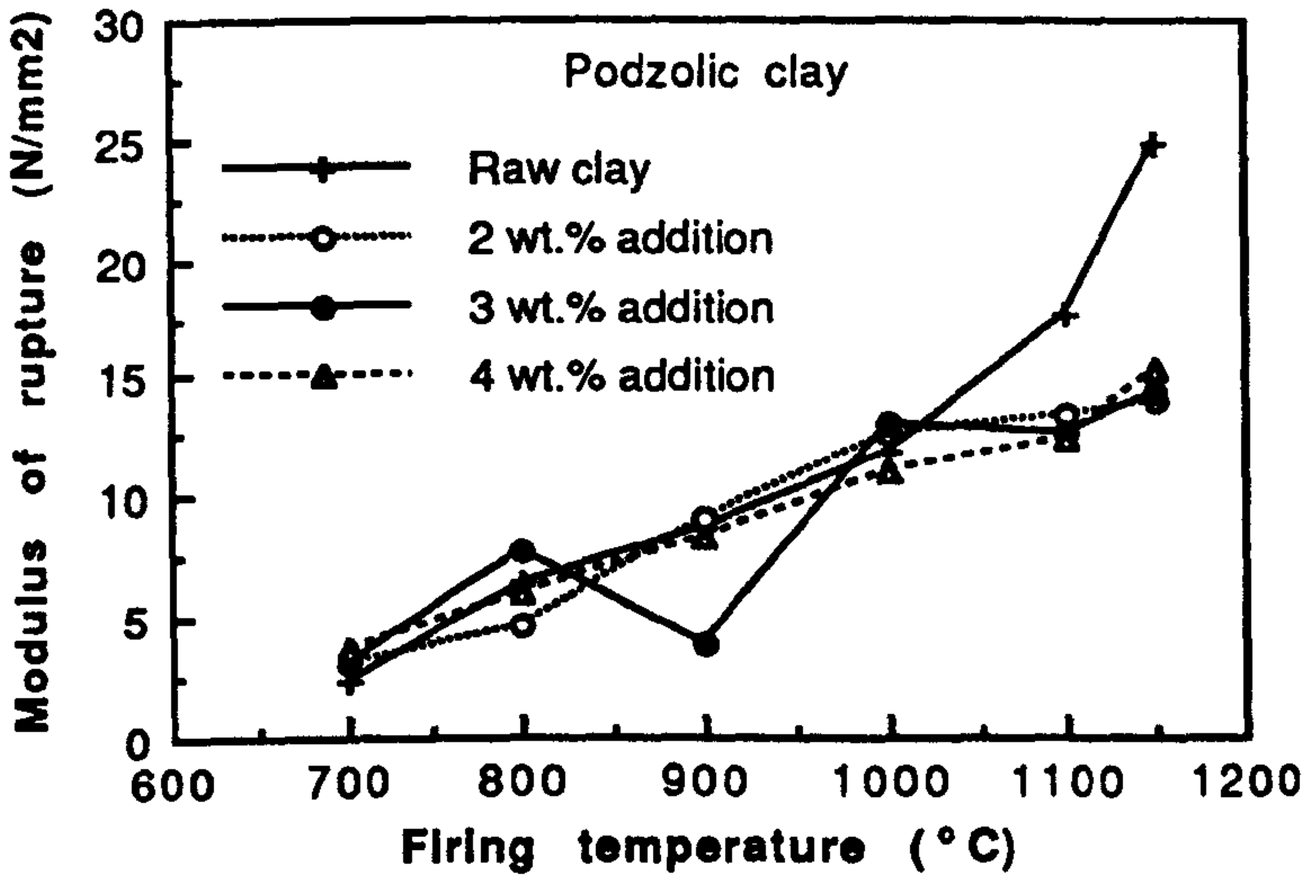

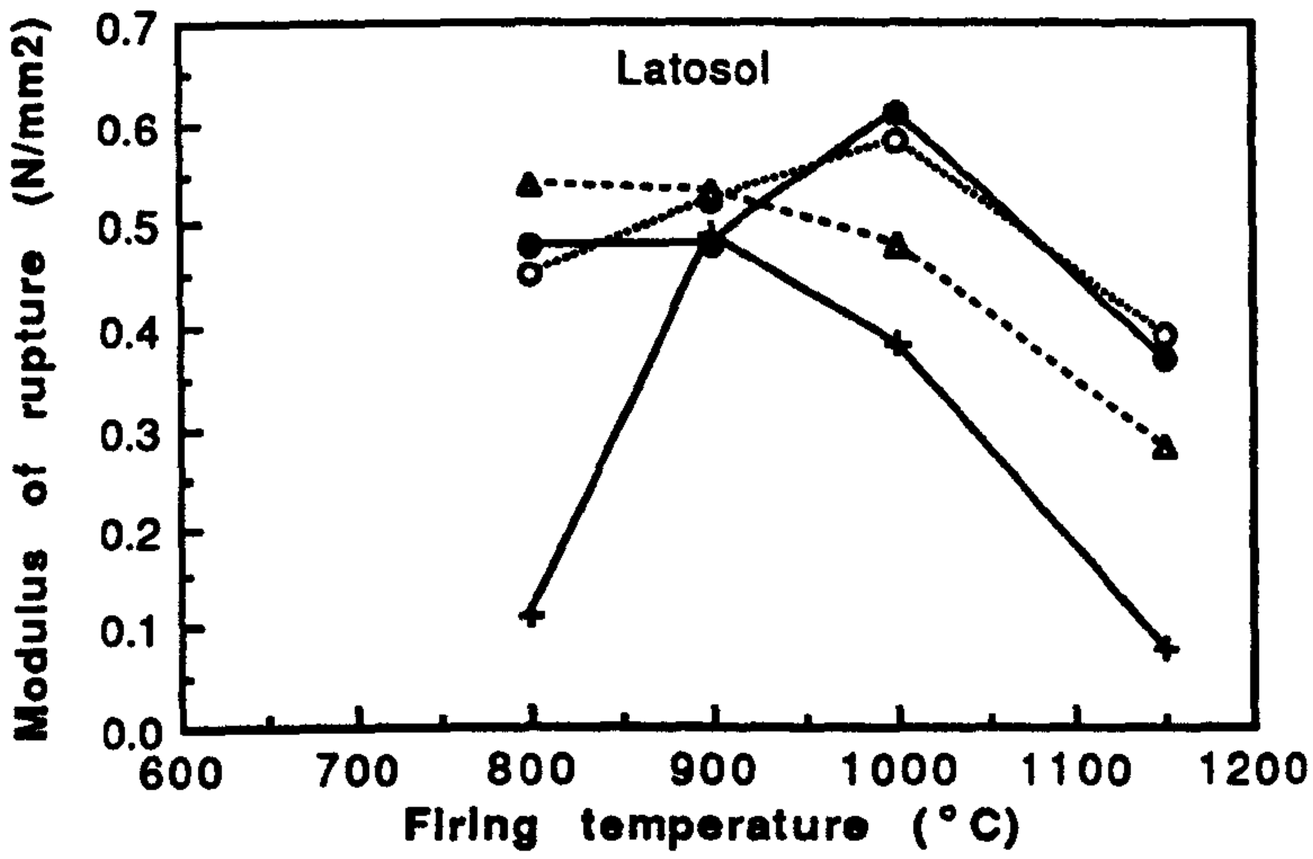

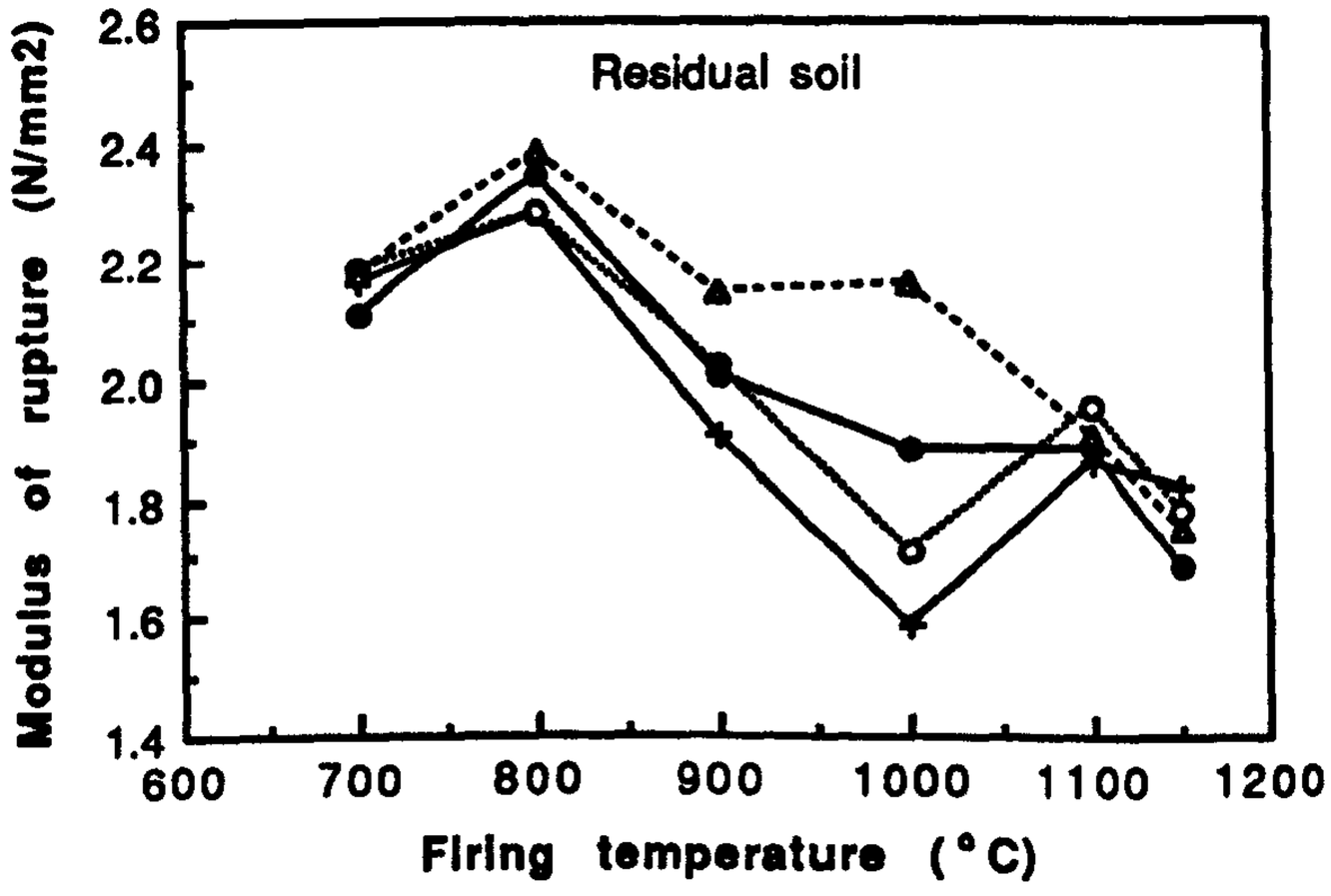

Fig. 7.2-Variation of Modulus of rupture as a function of firing temperature and $CaCO_3$ content for clay compositions.

Calcium carbonate additions exert considerable influence on the strength increase of coarse-grained residual soil and poor quality, less plastic latosol than on fine-grained, plastic podzolic clay. A progressive strength increase with increasing amount of additive was seen in the residual soil; the gain in strength was at a maximum (36%) for compositions containing 4 wt% $CaCO_3$ fired at 1000°C. On the other hand, a fluctuation in strength was discernible in the residual soil and its compositions with the M.O.R. attaining a maximum of 2.38 N/mm^2 when fired at 800°C. Maximum gain in strength of latosol (55%) was obtained at 3 wt% in compositions fired at 1000°C. The 2 wt% addition produced only a marginal strength increase in podzolic clay in the firing range between 900°and 1000°C. But a deterioration in strength resulted in compositions fired between 1000°and 1150°C. For this clay, additions exceeding 2 wt% were ineffective, if not detrimental. In all cases the firing temperature appeared to be a significant factor.

7.4.2 Apparent porosity

Up to 1100°C, the fine-grained podzolic clay bodies showed the highest change in porosity and therefore the greatest vitrification (Fig. 7.3). The porosity of residual soil compositions dropped less rapidly between 800°and 1100°C. These bodies with a high coarse fraction showed intermediate vitrification characteristics. Originally insensitive coarse-grained latosol showed a significant change with the incorporation of mineralizer indicating an improvement of its performance. In general, porosity decreased up to 1100°C when the amount of $CaCO_3$ was increased and when the firing temperature was raised. Above 1100°C, the increase in porosity of the podzolic clay bodies suggested a bloating process, evidence of which could be seen on the fired specimens. The gradual reduction in porosity of this clay over the range 800°to 1000°C correlates rationally with the increase in M.O.R (Fig. 7.2), indicating a probable interdependence of the two factors. In the case of quartz-rich residual soil and latosol, however, microcracks were probably developed on cooling which

drastically reduced their strength and obscured the porosity dependence of strength.

7.4.3 Dry-to-fired contraction

The variation in the linear firing shrinkage of clay bodies as a function of firing temperature is given in Fig.7.4. In general, contraction of bodies increased with temperature over the firing range from 700° to 1150°C, but the latosol exhibited an anomalous behaviour in producing an overall expansion in the compositions except in the one containing 4 wt% $CaCO_3$. High quartz content of latosol evidently caused permanent volume expansion due to the inversion of quartz.

The examination of the set of firing shrinkage curves for podzolic clay showed a general increase in shrinkage of the clay body containing 2 wt% $CaCO_3$ between 900° and 1000°C. This is probably attributed to the development of liquid phase by eutectic composition containing the optimum amount of mineralizer. The 3 and 4 wt% additions, however, made the bodies more refractory and rigid; rigidity of all $CaCO_3$ compositions increased above 1100°C as was strikingly apparent from their low shrinkage values. Thus it is evident that the firing rigidity limits, to a large extent the maximum firing temperatures of fired clay products are clearly influenced by the $CaCO_3$ addition. The subsidence of shrinkage above 1100°C indicates the formation of closed pores in the body. This change, reflected as bloating was a remarkable feature in the porosity curves of the podzolic clay mixes (Fig. 7.3). For practical considerations, it is well to have a flat shrinkage region extending over a long temperature range. Such conditions would ensure the uniformity of the fired product. To this end, the vertical dashed lines on Fig. 7.4 indicate the maturing ranges for the three clay mixes. Clay compositions containing 4 wt% $CaCO_3$ imparted the longest maturing range to both residual soil and latosol whereas the 2 wt% addition extended the maturing range of the podzolic clay appreciably.

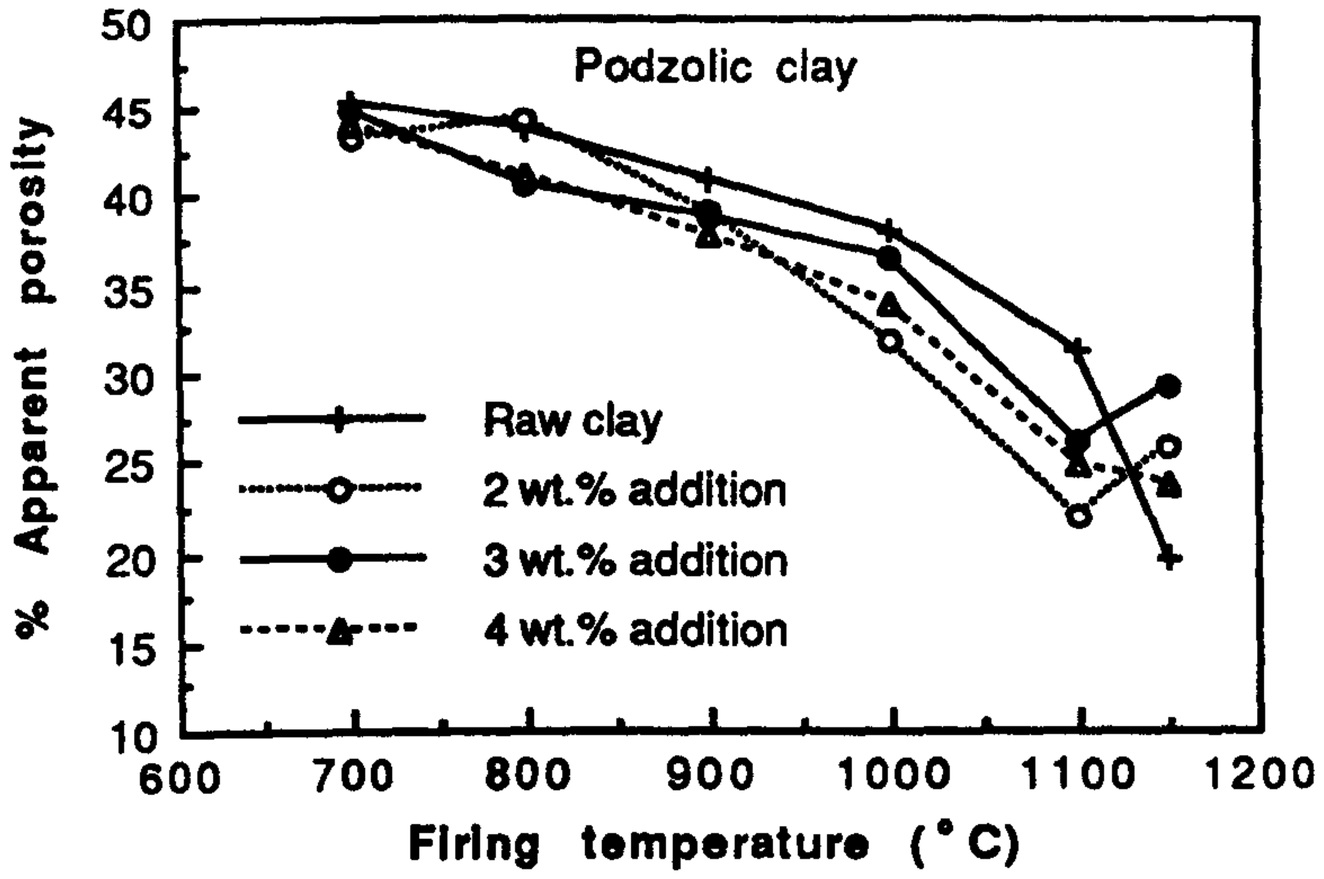

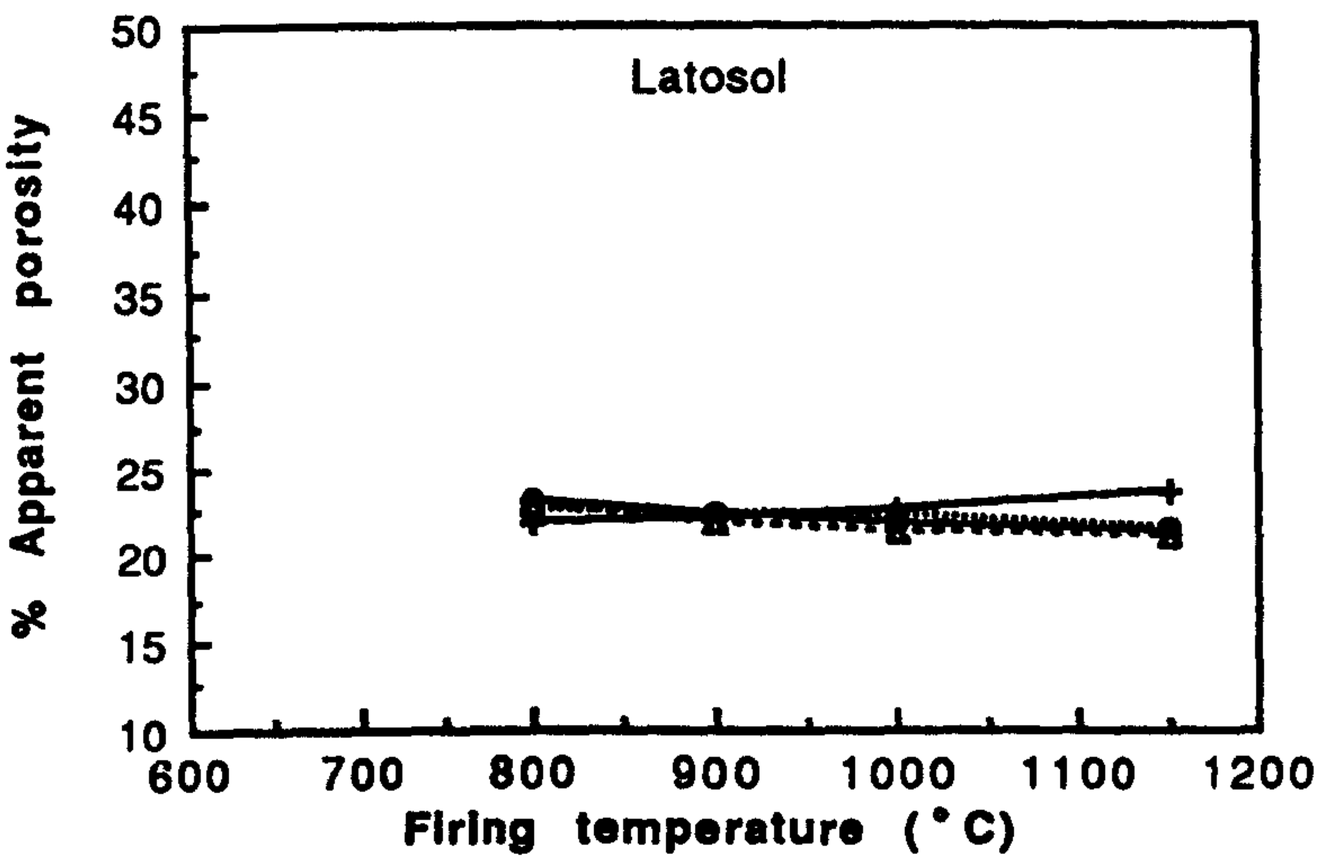

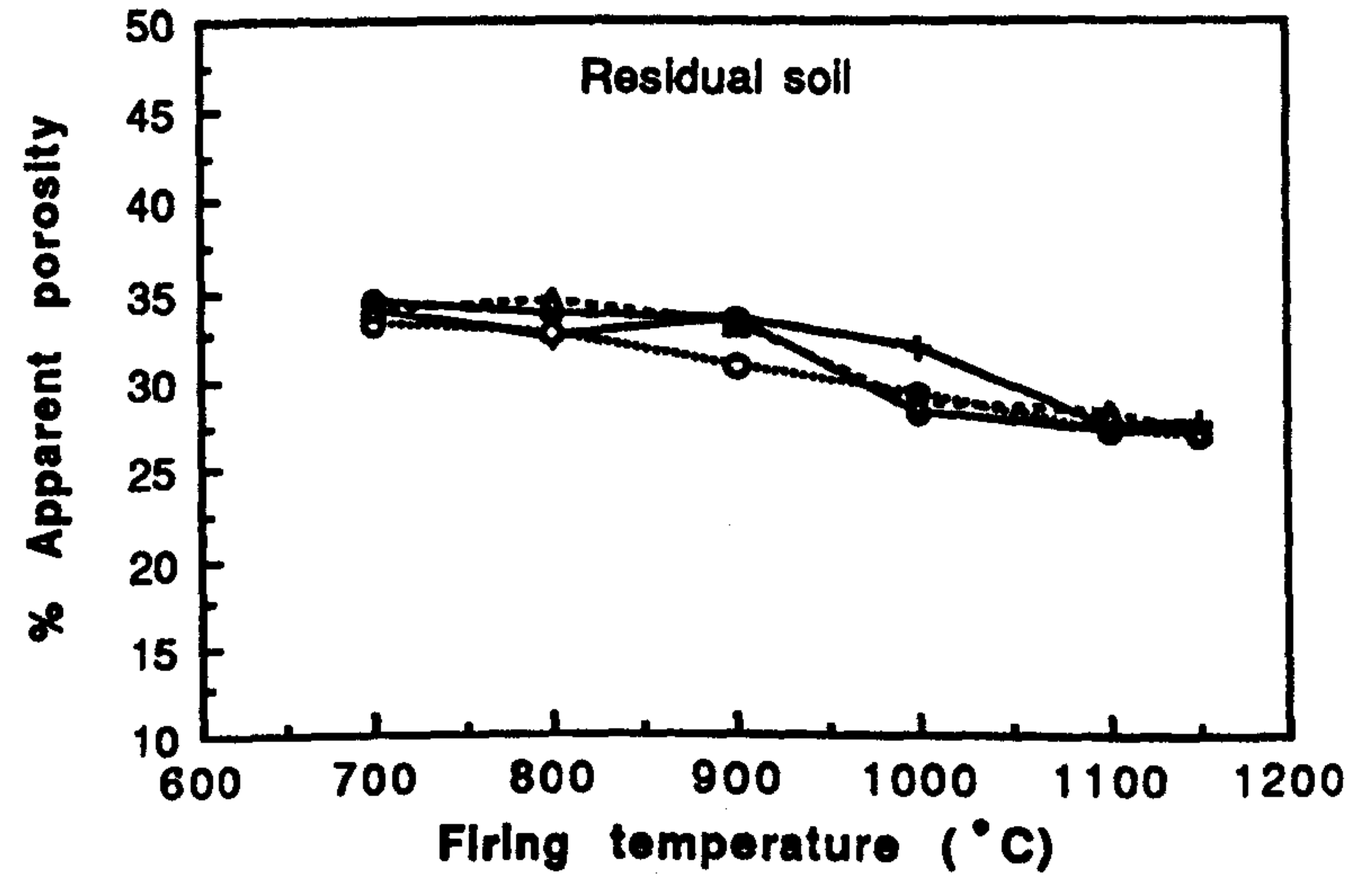

Fig. 7.3-Variation of porosity as a function of firing temperature and $CaCO_3$ content for clay compositions

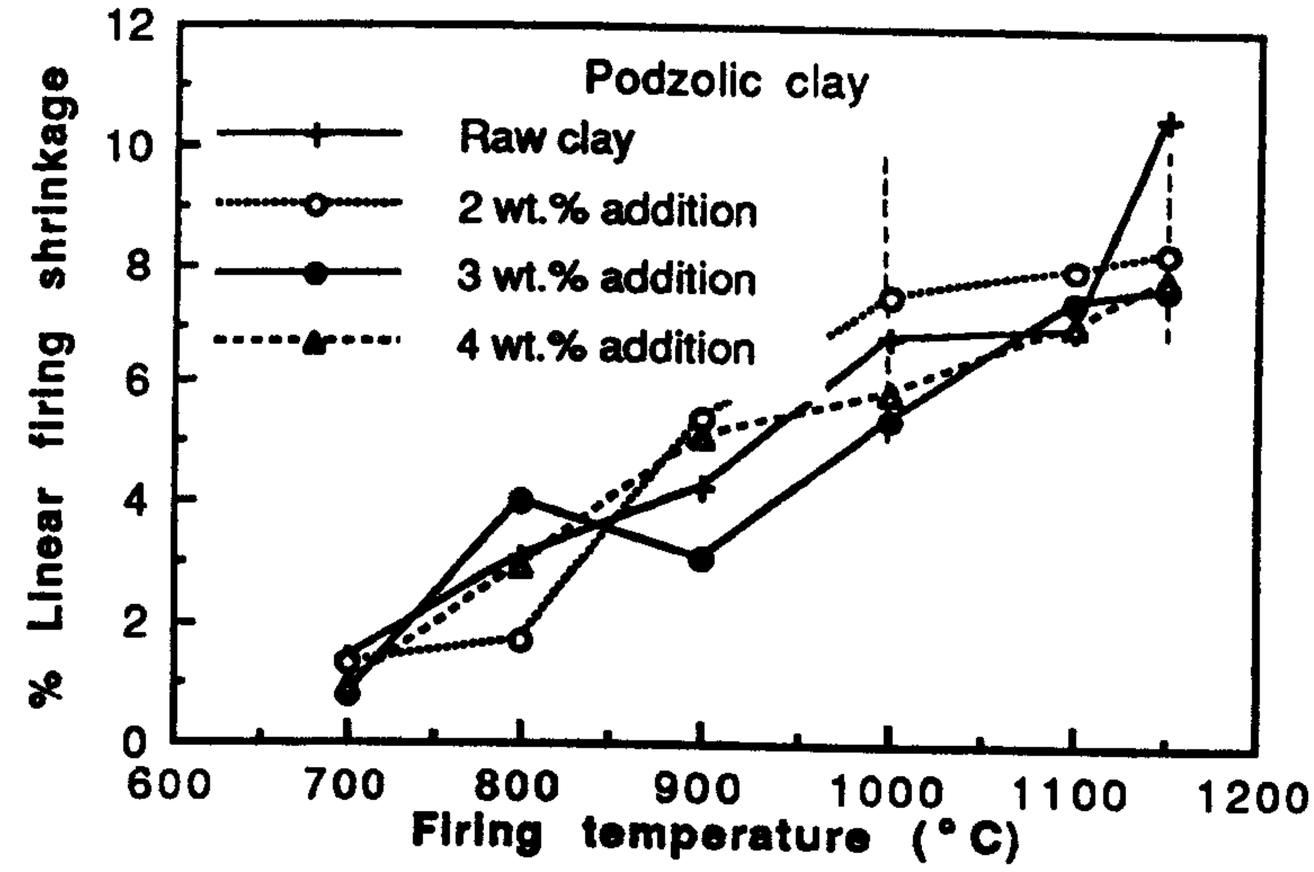

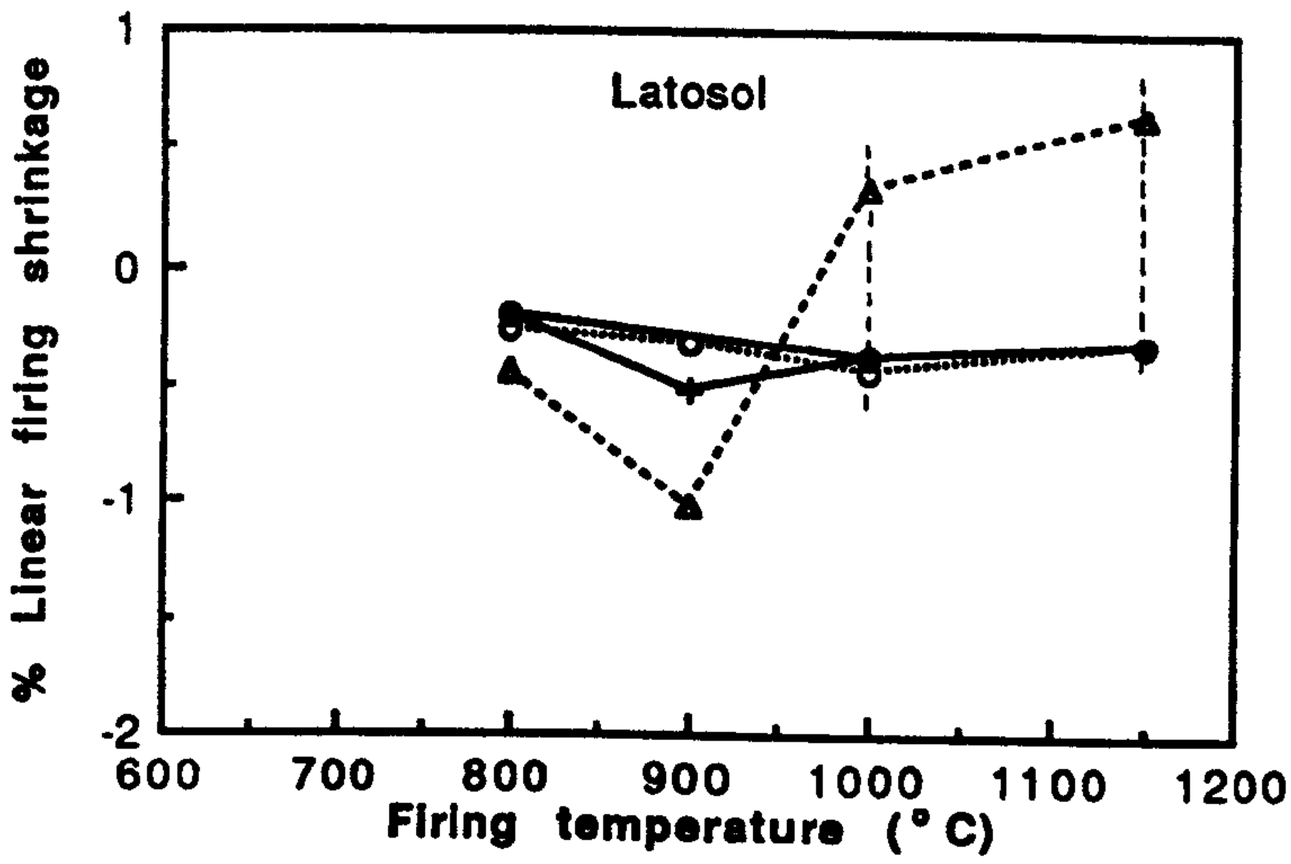

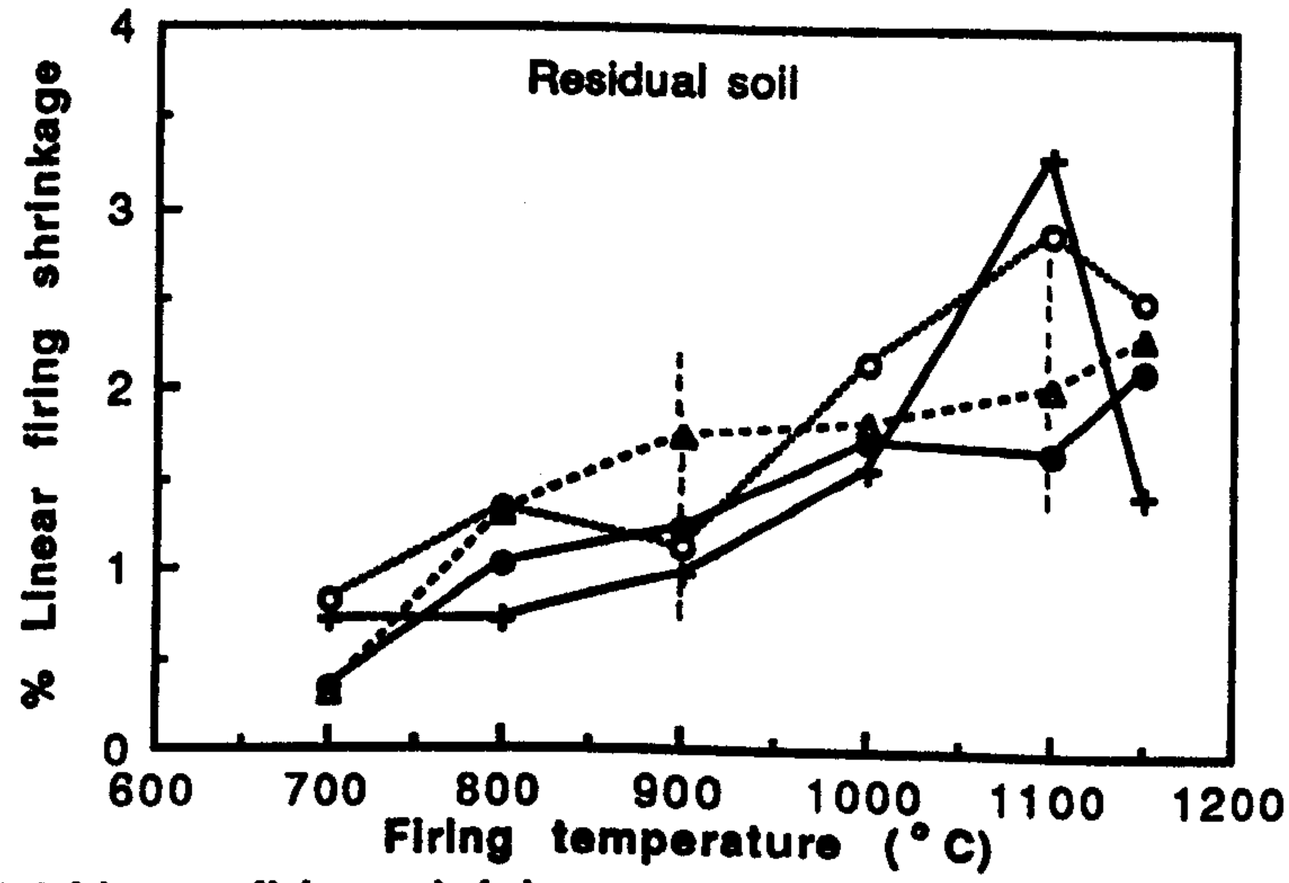

Fig. 7.4-Linear firing shrinkage curves of the clay compositions.

CHAPTER 7

7.5 EFFECT OF $CaCO_3$ ON THE PROPERTIES

7.5.1 Strength

The much lower porosity and higher shrinkage of $CaCO_3$ compositions fired to about 1050°C illustrated in Figs. 7.3 and 7.4 are clear indications of the effects of improved sintering. The improvement of strength by $CaCO_3$ is most likely the result of the enhancement of the sintering rate probably through liquid-phase formation. The microstructural features of fired specimens substantiate this mechanism. It is conceivable that optimum amounts of $CaCO_3$ determined by the type of clay promoted liquid-phase sintering. At higher temperatures, however, excessive liquid formation caused warping and consequent loss of strength of the fired material. This condition was reached at a firing temperature of about 900°C in the residual soil and at a somewhat higher firing temperature of about 1000°C in both podzolic clay and latosol.

7.5.2 Porosity

It is evident from the foregoing details of porosity trends that the fineness of the starting material has a considerable influence on the rate of vitrification of the body. The addition of $CaCO_3$ probably had an interactive influence: reactions were more vigorous in fine-grained bodies. Consequently the initial liquid formation in the podzolic clay compositions was significantly higher at the relevant eutectic temperatures resulting in higher changes in porosity. The reversal or subsidence of porosity of the $CaCO_3$ compositions of podzolic clay and residual soil at a temperature of about 1100°C indicates the development of closed pores. This implies that the maximum firing temperature for the above compositions is 1100°C. Limiting conditions of firing, however, were not approached in the latosol. Morphological changes associated with the above phenomenon are clearly observable in the microstructures (Chapter 8).

7.5.3 Firing shrinkage

The firing shrinkage of a material at a particular temperature is primarily dependent upon the particle size distribution and the amount of fluxes. The shrinkage curve for podzolic clay indicates strong fluxing activity at firing temperatures above 800°C. Taken in conjunction with the mineralogical data (Section 3.3.3.3), it appears likely that the combined effect of high feldspar content (10%) and finer particle size contributed to its low shrinkage. Differential shrinkage behaviour of the other two clays of feldspar content between 5 and 7% was determined mainly by their particle sizes. The addition of low amounts of $CaCO_3$ to the clays enhanced their fluxing activity. Additions exceeding the optimum, however, made the compositions refractory. The beneficial effects of $CaCO_3$ additions on the maturing range of the compositions are given in the Section 7.4.3.

7.6 MINERALOGICAL CHARACTERISTICS

7.6.1 Podzolic clay

The X-ray diffraction analyses (Appendix 7) of the fired samples are summarised in Table 7.6. Raw podzolic clay consisted of a mixture of quartz, feldspars and kaolinite together with small quantities of gibbsite and vermiculite (Section 3.4). The X-ray pattern of the clay fired at 800°C was similar to that of the unfired clay except for the absence of characteristic kaolinite reflections indicating the collapse of the structure. Faint hematite peaks were also observed at 2.69 and 2.51 Å. The prominent reflections at 3.33 and 3.23 Å corresponding to quartz and microcline were still present. The basal reflections of the major phases persisted up to a firing temperature of 900°C. Samples fired at 1000°C showed strong reflections for mullite (5.37, 3.40, 2.88, 2.54, 2.41 and 2.13 Å) and hematite (3.66, 2.69, 2.51 and 2.21Å). Accessory minerals have almost completely disappeared. First traces of cristobalite (4.07 Å) and ŏ-Al_2O_3 (2.09 Å) were detected at 1100°C. An increase in mullite and hematite contents was

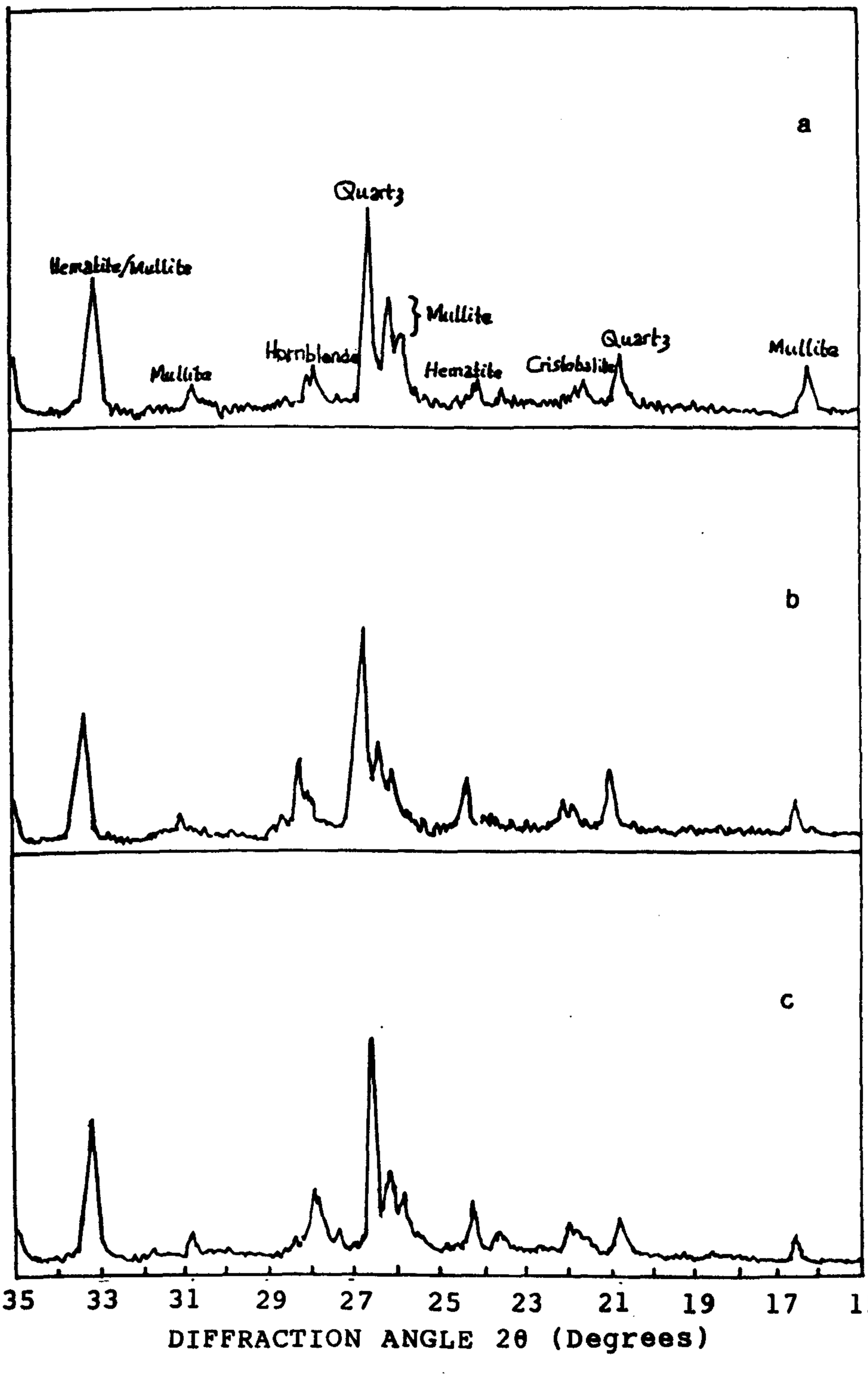

Fig. 7.5-X-ray diffraction patterns of podzolic clay compositions fired at 1150°C for 2 h. a-PSH + 2% $CaCO_3$, b-PSH + 3% $CaCO_3$, c-PSH + 4% $CaCO_3$

also discernible. Firing at 1150°C significantly increased both the mullite and hematite contents as was evident from their relatively intense reflections (Fig. 7.5). Cristobalite and ŏ-Al_2O_3 reflections increased in strength showing their progressive development as the firing temperature was increased.

Table 7.6-XRD analyses of fired clays

Clay	Temperature at which phase first or last* observed (°C)			
	Mullite	Cristobalite	Corundum	Hornblende*
Podzolic clay	1000	1100	1100	-
Podzolic clay+2wt% $CaCO_3$	1000	>1000	-	-
Podzolic clay+3wt% $CaCO_3$	1000	1000	>1150	-
Podzolic clay+4wt% $CaCO_3$	1000	1000	>1150	-
Residual soil	1000	1000-1100	-	>1000
Residual soil+2wt% $CaCO_3$	1000	1000-1100	1000	>1000
Residual soil+3wt% $CaCO_3$	1000	1000-1100	-	>1000
Residual soil+4wt% $CaCO_3$	1000	1000-1100	1000-1100	>1000
Latosol	1000-1150	1000-1150	-	-
Latosol+2wt% $CaCO_3$	1000-1150	1000-1150	-	>1150
Latosol+3wt% $CaCO_3$	1000-1150	1000-1150	-	>1150
Latosol+4wt% $CaCO_3$	1000-1150	1000-1150	-	>1150

An analogous set of diffraction patterns of podzolic clay-$CaCO_3$ compositions provided evidence for the probable suppression of the formation of cristobalite and ŏ-Al_2O_3 in the compositions containing 2 wt% $CaCO_3$. No ŏ-Al_2O_3 but only traces of cristobalite were detected in these compositions fired at 1150°C. In compositions containing 3 and 4 wt% $CaCO_3$, however, the first signs of crystallization of ŏ-Al_2O_3 were seen in the specimens fired at 1150°C. Thus there is circumstantial evidence to suggest that $CaCO_3$ in amounts exceeding 2 wt% preferentially increased the nucleation temperature of ŏ-Al_2O_3 and cristobalite by

approximately 50°C in the podzolic clay compositions examined. It is probable that $CaCO_3$ hindered the breakdown of metakaolinite into these constituents.

7.6.2 Residual soil

X-ray diffraction results (Appendix 8) showed that quartz, feldspars and kaolinite are prominent constituents of the residual soil coarse clay fractions along with the amphiboles. For the residual soil, the main differences noted between the diffraction patterns of the unfired and the 800°C fired specimens were the disappearance of the characteristic kaolinite reflections and the reduced intensity of the remaining reflections of the latter. Quartz, feldspars and amphibole peaks were the most intense, followed closely by hematite (2.69 and 2.51 Å). In specimens fired at 1000°C, mullite was identified; feldspar and amphibole reflections were less intense. At 1100°C, notable changes in constitution were strong reflection (4.07 Å) attributed to cristobalite, faint reflection (2.07 Å) attributed to δ-Al_2O_3 and the disappearance of the characteristic reflections of amphiboles (8.20 and 3.09 Å). Major mullite and hematite peaks increased in strength significantly as the firing temperature was increased from 1000°to 1100°C. Specimens fired at 1150°C yielded X-ray patterns containing mullite, cristobalite and hematite as the major phases. Traces of δ-Al_2O_3 were detected at temperatures above 1100°C.

Diffraction patterns of compositions containing up to 4 wt% $CaCO_3$ fired below 900°C were basically similar to the corresponding patterns of raw clays. However, the specimens fired above 1000°C showed evidence for the suppression of mullite reflections. Mullite could only be identified in these compositions at 1100°C. On the other hand, evidence of crystallization of δ-Al_2O_3 was seen in specimens fired at 1000°C. It is conceivable, therefore, that the addition of up to 4 wt% $CaCO_3$ inhibits the mullite formation and diverts the kaolinite transformation to yield δ-Al_2O_3 and probably cristobalite in the residual soil. This contrasts with the

situation for podzolic clay compositions having different phase assemblages. A summary of the mineralogical changes occurring in the residual soil with increasing firing temperatures is presented in Fig. 7.6.

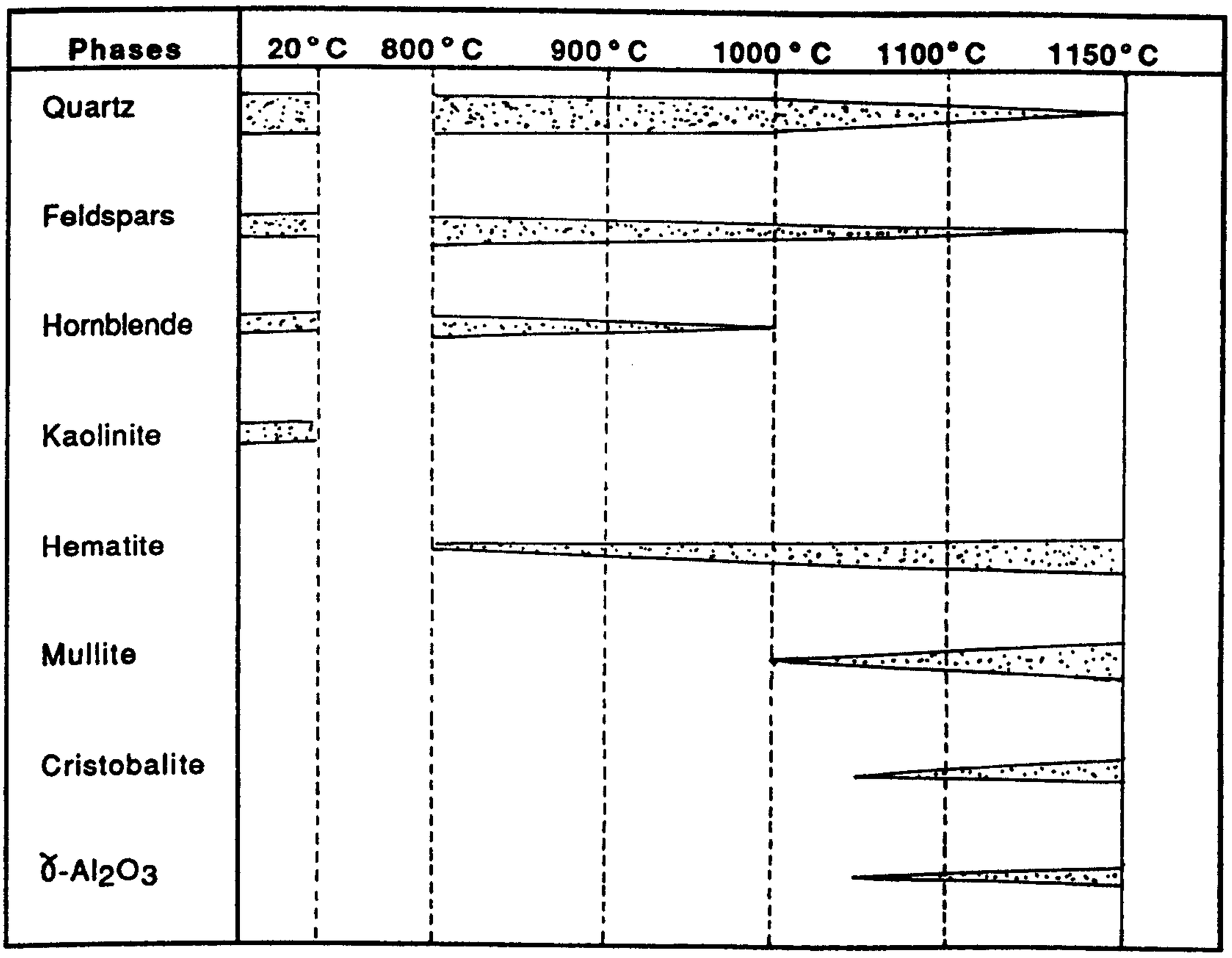

Fig. 7.6-Summary of the mineralogical changes occurring in residual soil with increasing firing temperatures.

7.6.3 Latosol

The major phases present up to 1100°C in the raw clay specimens were quartz, feldspars and accessory minerals. At 1100°C, there was faint evidence for the presence of mullite. The weakly present peak at 4.09 Å is probably due to tridymite (low) formed as a product of inversion of quartz. No ϑ-Al_2O_3 was detected, nor did there appear to be any change in the original minerals (Appendix 9).

Diffraction traces of specimens containing 2, 3 and 4 wt% $CaCO_3$ all contained peaks attributed to cristobalite (4.05 Å) at 1150°C, instead of tridymite. No ϑ-Al_2O_3 was detected. There were no significant differences between samples with different contents of $CaCO_3$.

7.6.4 Phase relations

The presence of other impurities precludes use of simple phase equilibria for interpretation, although at the higher temperatures equilibrium conditions are probably approached.

The nominal positions of the clay compositions are shown plotted on the ternary system $CaO-Al_2O_3-SiO_2$ in Fig. 7.1. No calcium alumino-silicate phases were detected up to 1150°C with the experimental compositions of low $CaCO_3$:kaolinite ratio. (Low ratios were employed to accelerate the kaolinite transformation). The equilibrium phases expected at 1000°C, viz. mullite, SiO_2 and Fe_2O_3 solid solution were all detected by XRD analyses and SEM examination. Evidence for the presence of δ-Al_2O_3 in the residual soil at 1000°C and in the podzolic clay at 1100°C was also found. However, the three clays contain other interactive constituents such as Fe_2O_3, TiO_2, K_2O, Na_2O and MgO in appreciable amounts to shift the equilibrium compositions to the phase field of mullite + Al_2O_3 $_{ss}$ + Fe_2O_3 $_{ss}$ in the $Fe_2O_3-Al_2O_3-SiO_2$ diagram. No single ternary phase diagram such as $CaO-Al_2O_3-SiO_2$ is, therefore, particularly applicable in the interpretation of results.

7.6.5 Microstructure vs. heat treatment

Microstructural changes taking place in clay bodies during firing are described in Chapter 8. Scanning electron microscopy of fired clays showed the progressive vitrification and final bloating of the material. Etching of the vitrified clay revealed the morphology of phases such as mullite and hematite. Microstructures indicate that low-silica bodies have higher mullite content after firing. This was anticipated since such bodies are richer in both Al_2O_3 and alkalies resulting in more mullite formation.

Up to 4 wt% $CaCO_3$ was not effective in the mullitization of the three kaolinitic soils over the range of firing temperature from 700° to 1150°C. Nucleation of mullite started in the three raw clays at relatively low temperatures between 900° and 1000°C. The first development

of primary speckled mullite were in the feldspar grains. At 1150°C, mullite crystallized out as interlocking needles. The relative amount of mullite present in fired podzolic clay at this temperature is low, despite the 12-fold increase in the modulus of rupture (from 2.31 N/mm^2 at 700°C to 24.82 N/mm^2 at 1150°C). It is difficult to justify this order of development of strength as being solely due to the presence of interlocking mullite needles. It is conceivable that porosity, which is a measure of the extent of glass formation may also account partly for the strength development of the clays examined.

7.7 STRENGTH RELATIONSHIPS

7.7.1 Effect of mullite on the modulus of rupture

In Fig. 7.7, the effect of temperature and mineralizer content on the development of mullite is shown in the form of plots of integrated intensity of the 110 reflection of mullite versus temperature for clay bodies. Of particular interest was that the addition of up to 4 wt% $CaCO_3$ mineralizer had a negative effect in inducing mullitization of the three brick clays, over the range of temperature from 800° to 1150°C.

Similar plots of integrated intensity of the common 220 reflection of mullite and hematite (Fig. 7.8) indicate the possibility that the 2 wt% addition is effective in promoting the development of hematite below 1000°C particularly in residual soil and podzolic clay compositions.

An attempt has also been made to study the part that mullite plays in strengthening fired clay bodies. Since the presence of quartz in the pure clays is a source of microstresses and cracks, the fine-grained podzolic clay, PSH, of low quartz content (21%), which showed uniform variation in modulus of rupture and porosity on firing was chosen for this study.

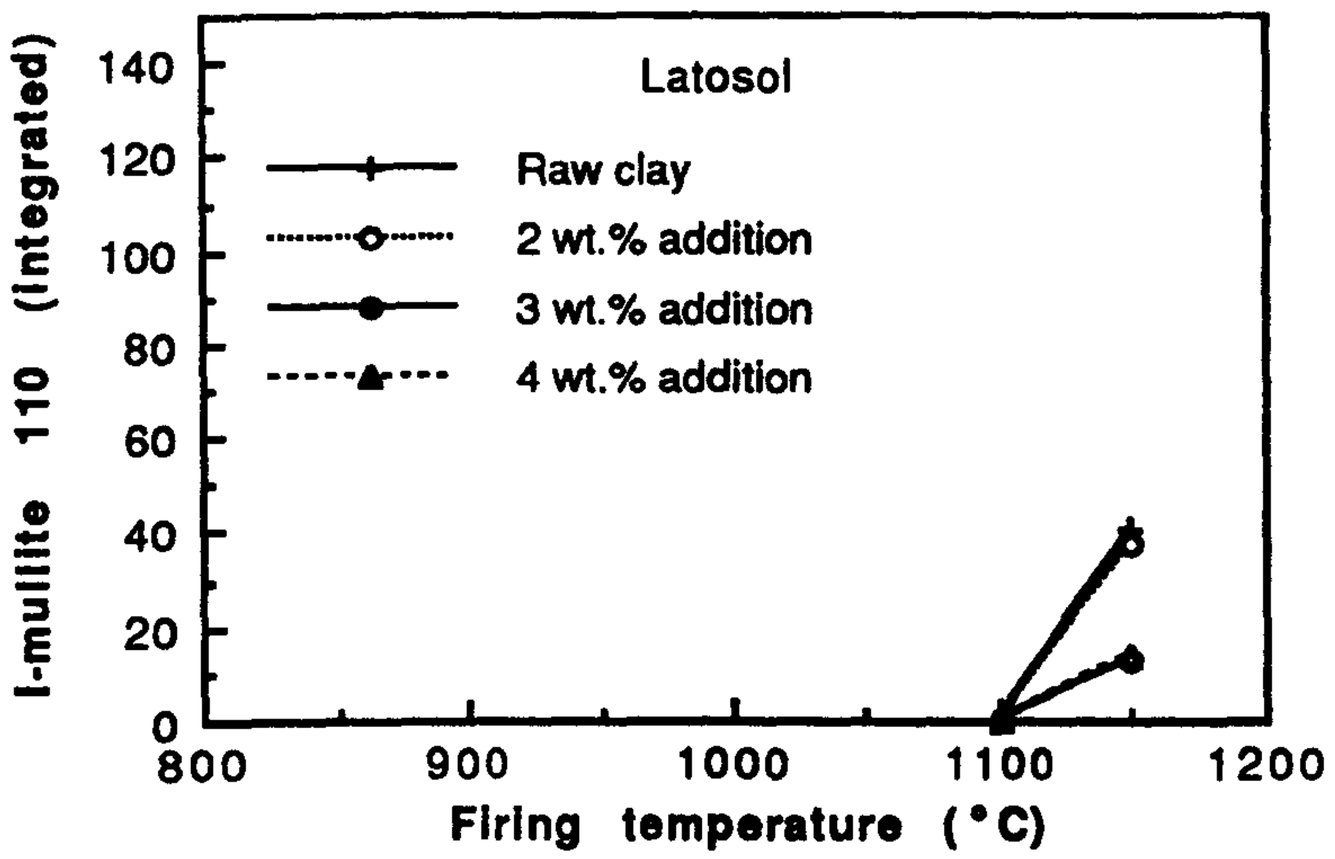

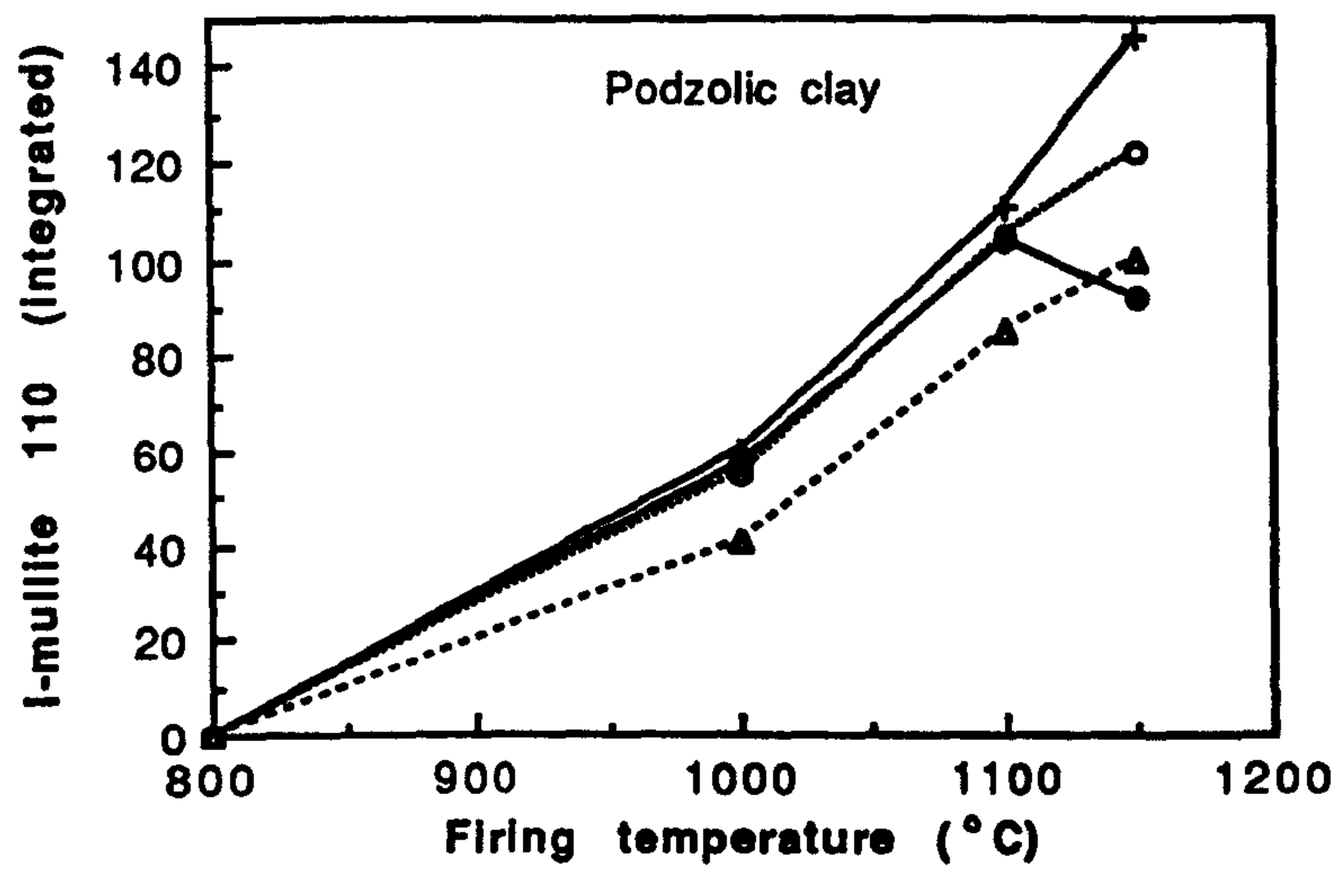

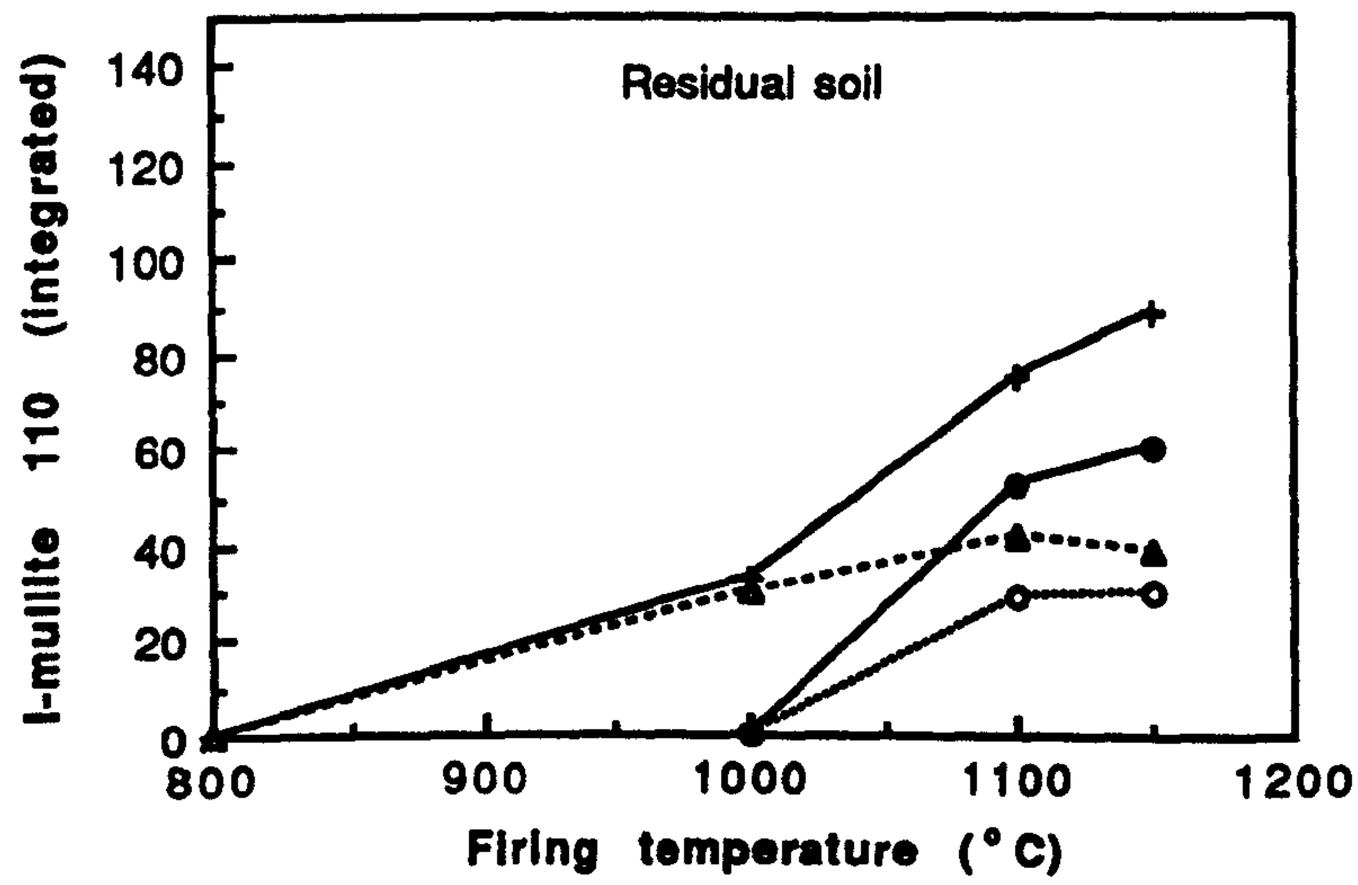

Fig. 7.7-Integrated intensity of mullite 110 reflection (area under peak) as a function of firing temperature.

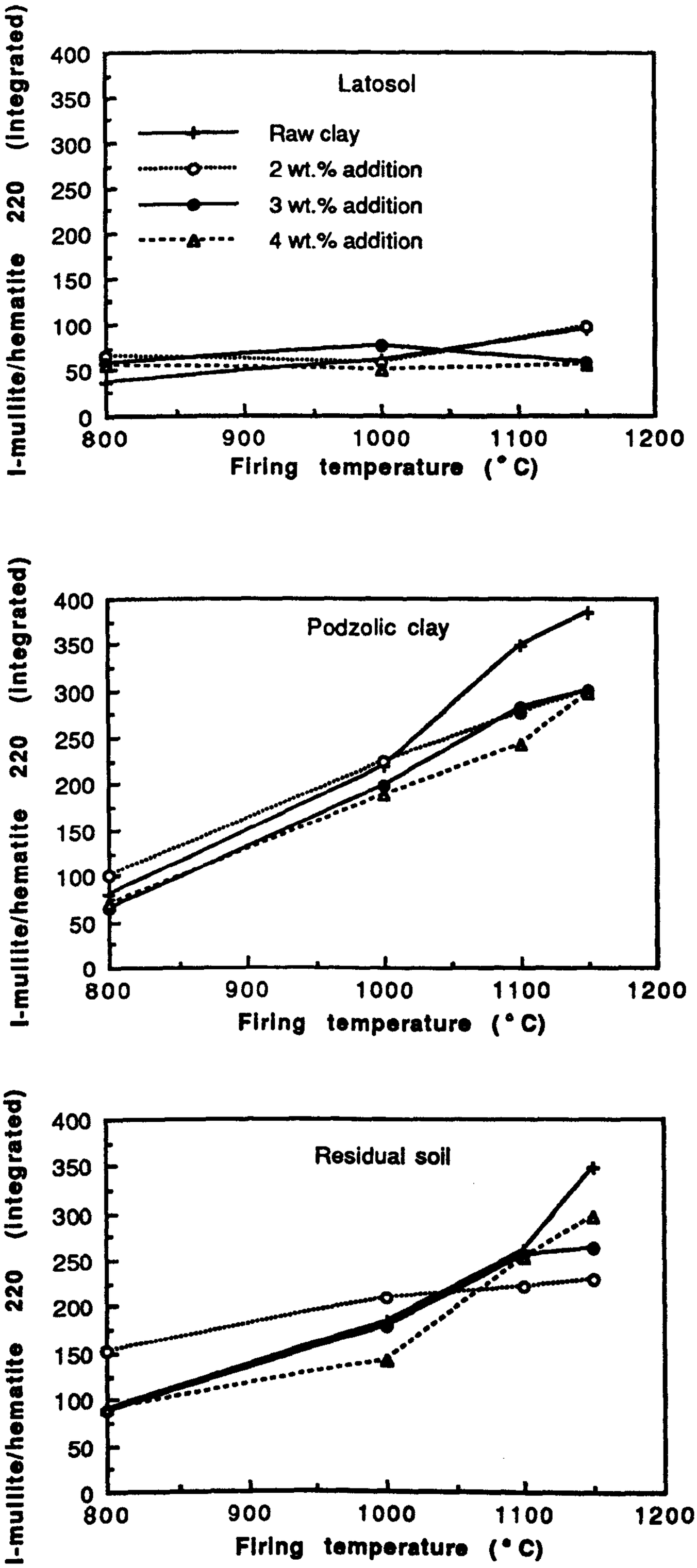

Fig. 7.8-Integrated intensity of mullite/hematite 220 reflection (area under peak) as a function of firing temperature

CHAPTER 7

From the 144 specimens of podzolic clay tested, the test results of modulus of rupture of 36 specimens representing the untreated clay fired at temperatures between 900° and 1150°C were considered in the data. Standard X-ray procedures using CuK_{α} radiation and scanning at 1°(2θ)/min were used to obtain the integrated intensity of the 110 reflection of mullite. The integrated intensity was measured by taking the product of the maximum peak height and the peak width at maximum height. The mean of the modulus of rupture of specimens fired at each temperature was plotted against the integrated intensity of mullite 110 reflection (Fig. 7.9).

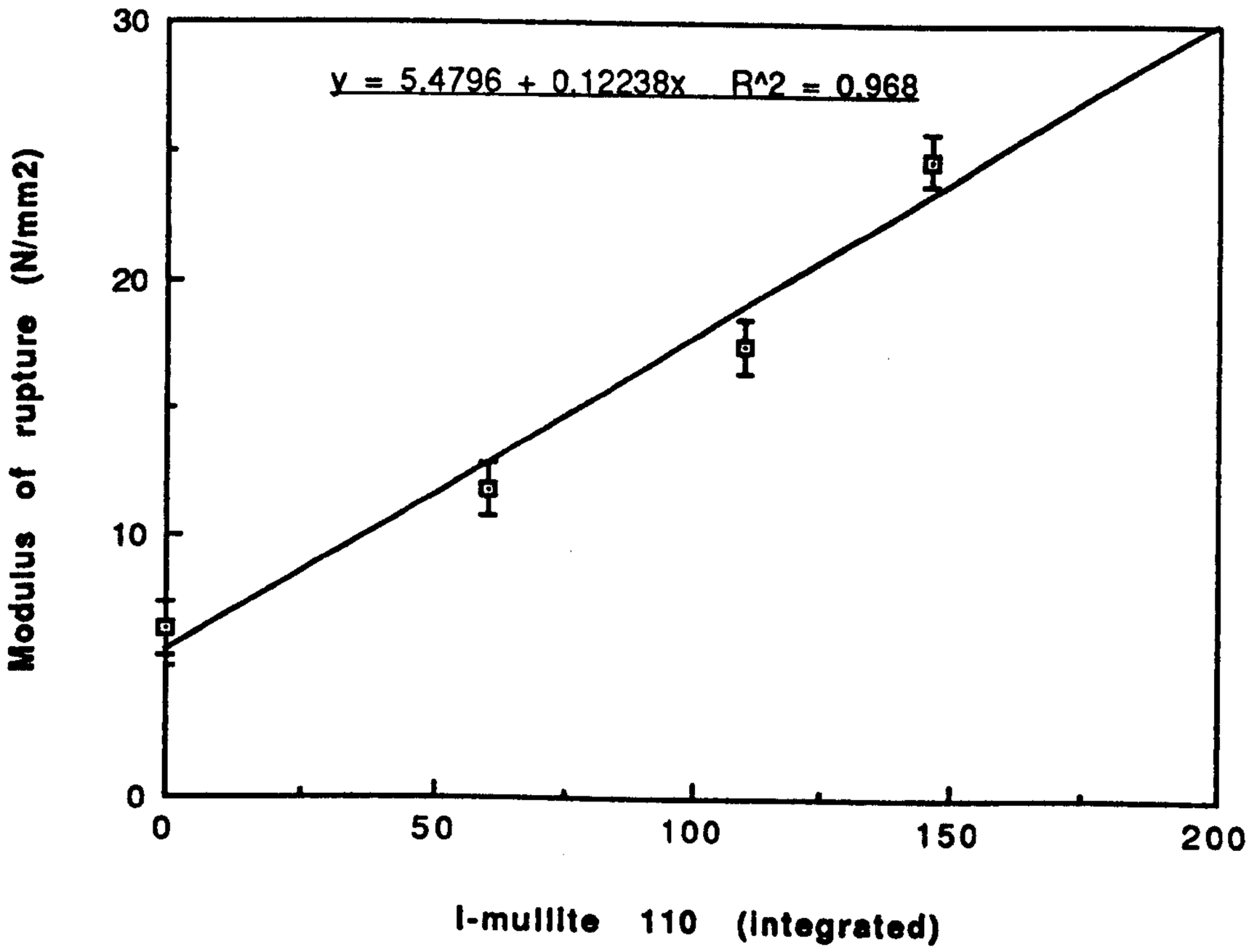

Fig. 7.9-Integrated intensity of mullite 110 reflection as a function of modulus of rupture for podzolic clay

Fig. 7.9 shows the ± 2S (S= estimate of the standard deviation) range of the modulus of rupture (M.O.R.) values for each set of six bars tested. In general there was good reproducibility of results within each set. Over 90% of the bars broke near the centre where the maximum bending moment occurred. The mean values of each set are given by the circles. A regression analysis was made to find the appropriate regression equation and to determine the degree of dispersion. The experimental values were fitted to a two constant equation by the least squares method. The regression equation is:

$$M.O.R = 0.12\ I_m + 5.48$$

where I_m = Integrated intensity of the mullite 110 reflection

The correlation coefficient,

$$r = \frac{n\Sigma xy - \Sigma x \Sigma y}{[n\Sigma x^2 - (\Sigma x)^2]^{\frac{1}{2}}\ [n\Sigma y^2 - (\Sigma y)^2]^{\frac{1}{2}}} = 0.984$$

indicates a high degree of correlation between modulus of rupture and integrated intensity of mullite 110 reflection.

7.7.2 Effect of hematite on the modulus of rupture

The relationship derived for the modulus of rupture and mullite content showed good agreement above the temperature of initial recrystallization of mullite. However, it appeared that the strength development of clay bodies at relatively low firing temperatures (from 2.3 N/mm^2 at 700°C to 8.7 N/mm^2 at 900°C) is not well accounted for by the above equation.

The microstructures of clay bodies fired at various temperatures and their changes in constitution (Chapter 8) provided evidence for the gradual enrichment of hematite in the glassy matrix. X-ray analysis confirmed the progressive crystallization of hematite with increase in temperature (Fig. 7.5). As a simple hypothesis the development of hematite was considered to be a measure of the extent of the glassy phase and hence relates to strength development below

900°C. Values of modulus of rupture were plotted against the hematite content for the podzolic clay over the range of temperature from 700°to 1000°C as shown in Fig. 7.10.

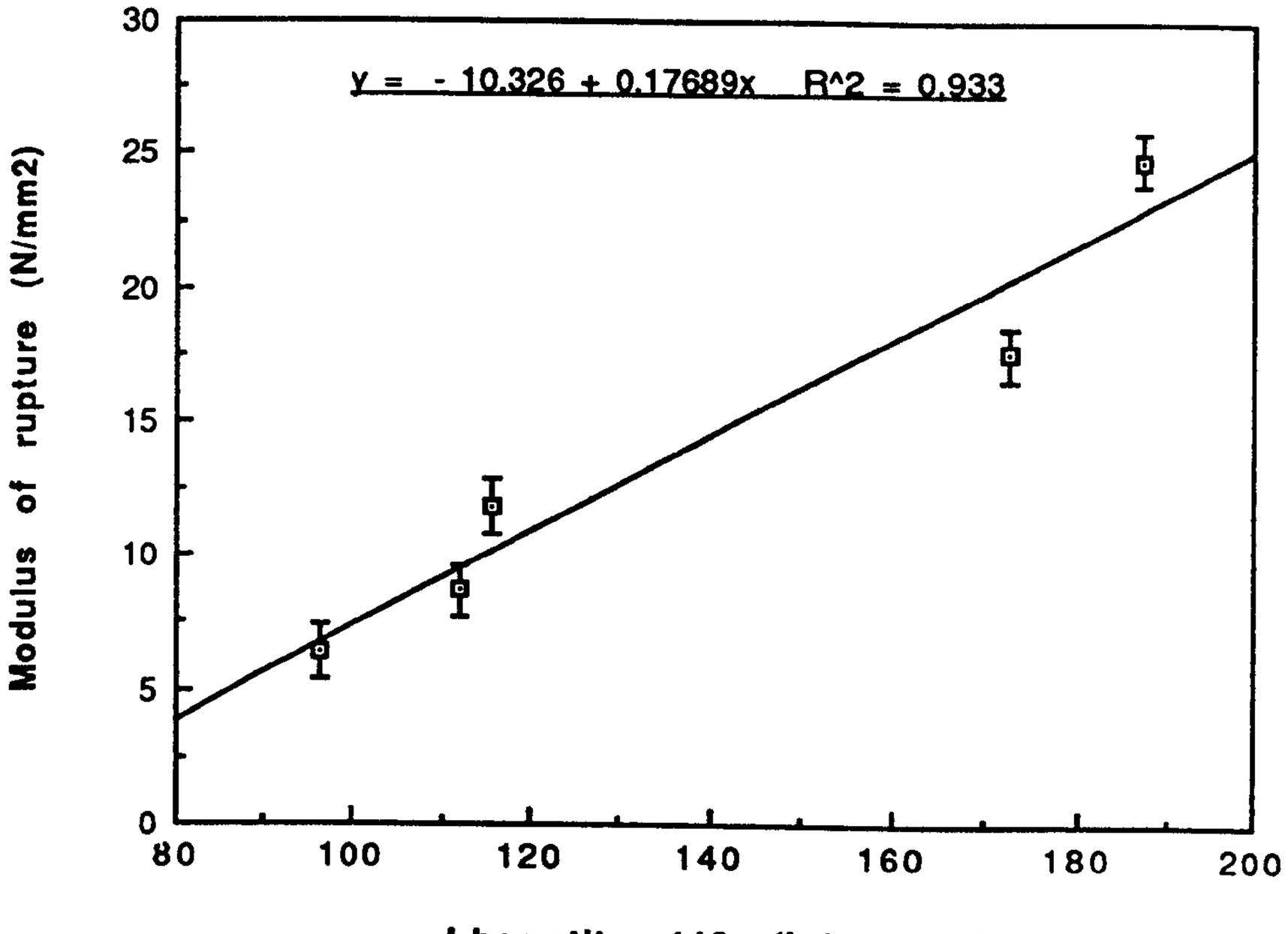

Fig. 7.10-Integrated intensity of hematite 110 reflection as a function of modulus of rupture for podzolic clay

The regression equation and correlation coefficient for the dependence are:

$$M.O.R = 0.18\ I_h - 10.33,\ r = 0.966$$

where I_h = Integrated intensity of the hematite 110 reflection.

It is apparent from the above that the modulus of rupture and hematite content are fairly well-correlated between 700°and 1000°C for the podzolic clay.

X-ray analysis provided additional evidence for the progressive increase in total mullite and hematite content with increase in firing temperature from 800°C (Fig. 7.8). Therefore, the overall effect of mullite and hematite on the modulus of rupture over the range of temperature from 800° to 1150°C, was investigated using the mullite 220 reflection which coincides with the hematite 110 reflection at 2.69 Å (Fig. 7.11).

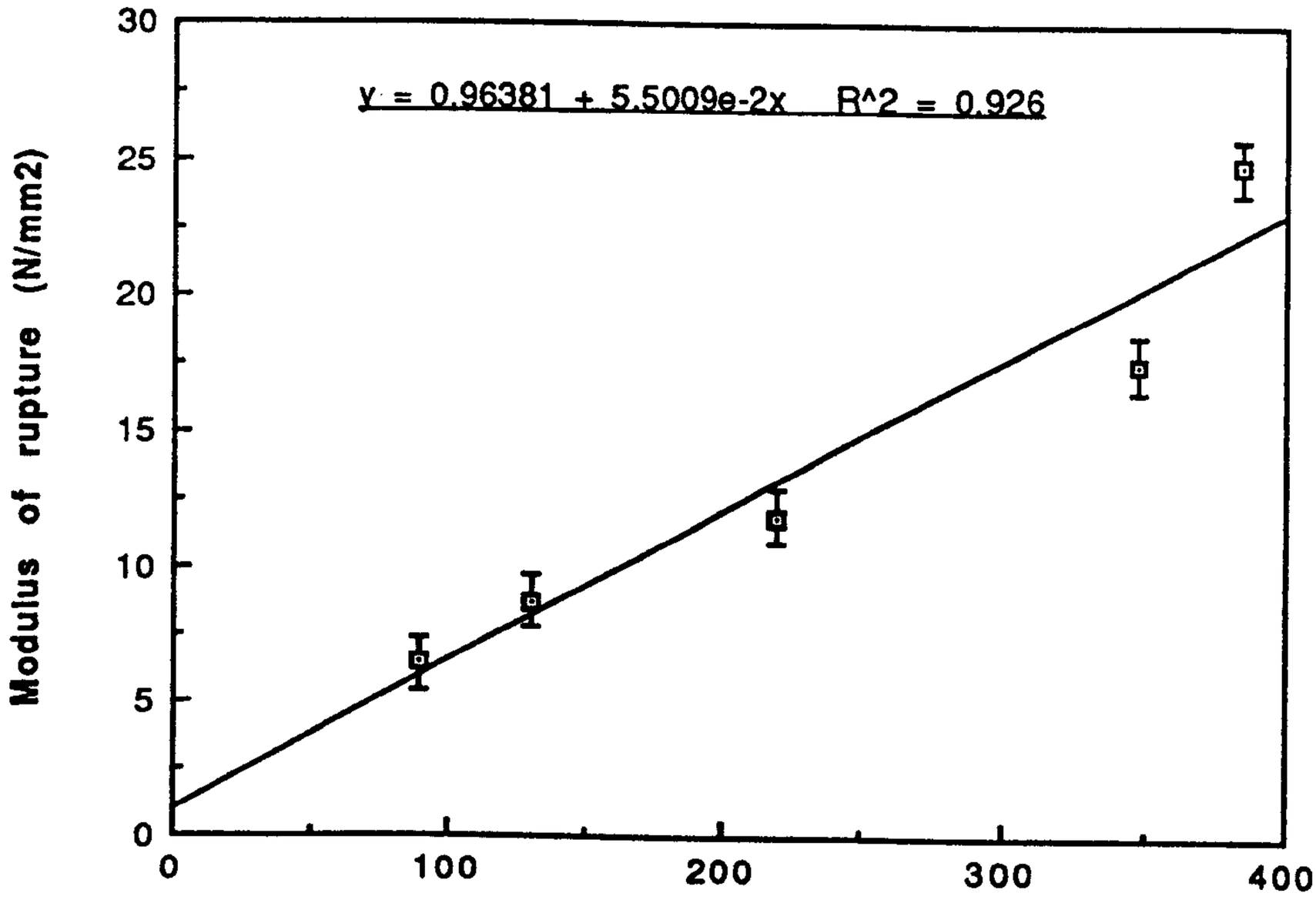

Fig. 7.11-Integrated intensity of mullite/hematite 220 reflection as a function of modulus of rupture for podzolic clay

The regression equation and correlation coefficient for the dependence are:

$$M.O.R = 0.05\ I_{m+h} + 0.96,\ r = 0.962$$

where I_{m+h} = Integrated intensity of the common hematite and mullite reflection

The dependence of highest correlation viz. modulus of rupture and mullite content was used in conjunction with the porosity dependence discussed in the following Section.

7.7.3 Effect of porosity on the modulus of rupture

Fig. 7.12 shows the measured porosity dependence of modulus of rupture for podzolic clay bodies.

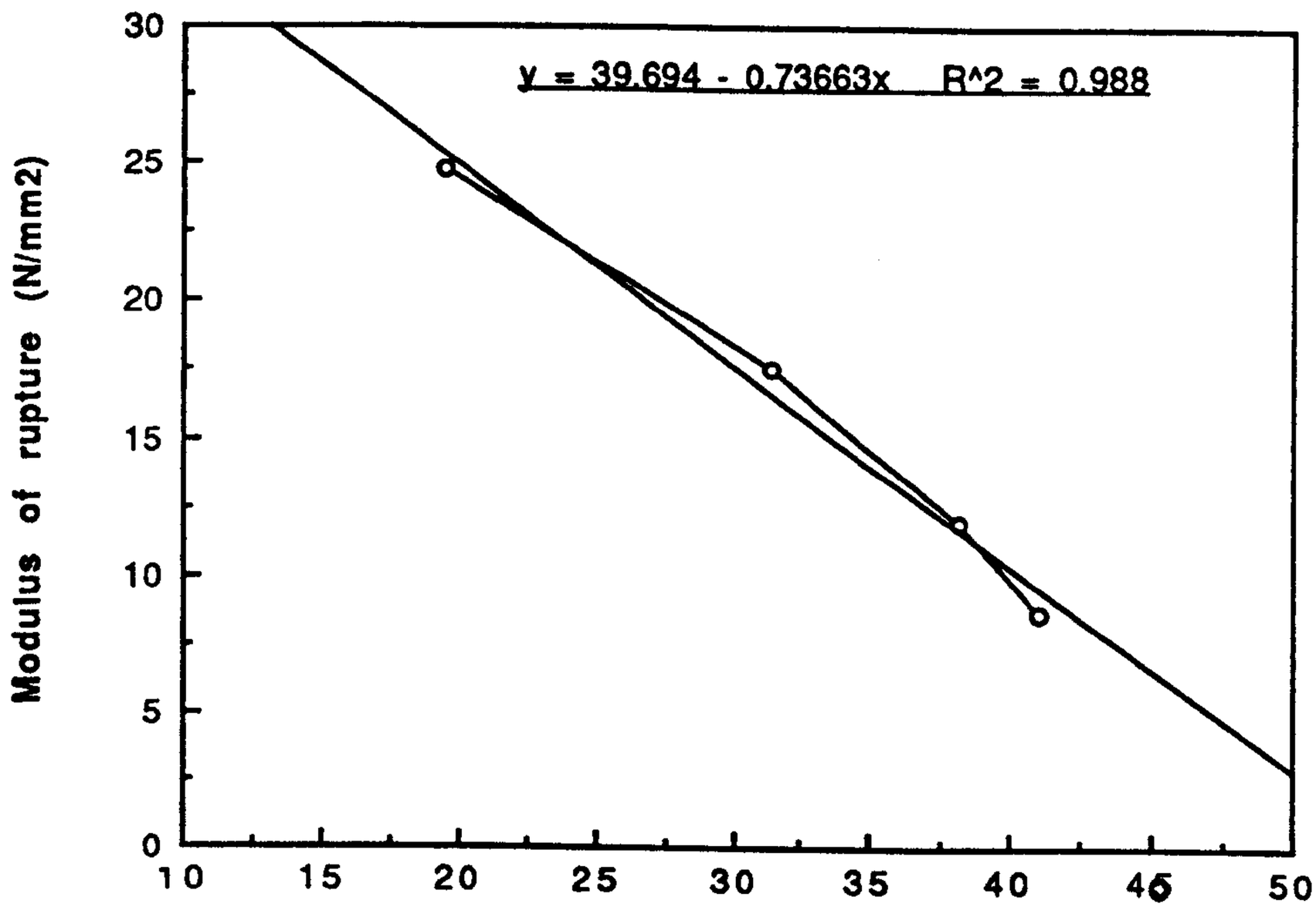

Fig. 7.12-Variation of modulus of rupture with porosity for podzolic clay.

The modulus of rupture increases linearly with decrease in apparent porosity over the range of 20-40% apparent porosity, beyond which departure from linearity is seen. The modulus of rupture does reach zero as porosity approaches the original porosity of the unfired material. This behaviour accords the model of Eudier (1962) which postulates that the reduction of strength with porosity is a direct consequence of the reduction in low-bearing cross-sectional area. The modulus of rupture and apparent porosity are reasonably well correlated over the above range by a straight line:

$$M.O.R = -0.74\ A.P. + 39.69,\ r = 0.994$$

or $M.O.R = M_{op} [1 - 0.019 A.P.]$

where M_{op} = M.O.R. at zero porosity

The region of linear dependence corresponds to the temperature interval 900-1150°C.

7.7.4 Combined effects of both mullite and porosity on the modulus of rupture

From Sections 7.7.1 and 7.7.2 it was evident that the correlation between the mullite content and modulus of rupture is the most significant of all the dependences. The regression equation obtained for this dependence:

$$M.O.R = 0.12 I_m + 5.48$$

can be rearranged as:

$$M.O.R = M_{om} [1 + 0.022 I_m]$$

where M_{om} = M.O.R at zero mullite content

The porosity dependence for the podzolic clay body is:

$$M.O.R = M_{op} [1 - 0.019 A.P.]$$

The combined effects of both mullite and porosity on modulus of rupture of the podzolic clay body are thus well represented by the equation:

$$M.O.R = M_o [(1 + 0.022 I_m)(1 - 0.019 A.P.)]^{\frac{1}{2}}$$

Here M_o represents M.O.R of a body of zero porosity and free from mullite. A compacted body fired at a temperature below the nucleation of mullite (1000°C) to the point of complete vitrification approximates to this ideal product.

The above relationship yields a value of 15 N/mm^2 for M_o within experimental error. This indicates that the maximum strength (M.O.R) attainable in the podzolic clay body fired to temperatures below the nucleation of mullite is 15 N/mm^2.

CHAPTER 7

7.8 STRENGTHENING MECHANISMS

An attempt has been made to elucidate the mechanisms whereby development of strength occurs in both raw clays and clay-$CaCO_3$ compositions on the basis of microstructural features (Chapter 8) and phase relations.

7.8.1 Normal clay bodies

(i).At firing temperatures below 1000°C

The texture of low-fired (800-1000°C) specimens is characterized by numerous large voids undergoing changes in size and shape. Traces of liquid phase arising from fluxes can also be seen. The limited amount of liquid phase initiates intergranular contact. It is postulated, therefore that the strength development in the experimental clay bodies is mainly due to a low degree of liquid-phase sintering. Schematic representation of the mechanism of strength development of experimental clay bodies is given in Fig. 7.13(a).

(ii).At firing temperatures between 1000°and 1150°C

The microstructures of specimens fired between 1000°and 1150°C provide evidence for the coalescence of grains. Porosity is in the form of small holes. The formation of a small amount of liquid phase at high temperatures assists greatly the intergranular contact and accelerates the growth of mullite needles which reinforces the matrix. Both processes contribute to the enhancement of strength. Therefore, primarily the liquid-phase sintering coupled with matrix reinforcement by recrystallization and to a lesser extent the solid-state sintering are assumed to be operative over the above range of firing temperature [Fig. 7.13(b)].

7.8.2 Clay-$CaCO_3$ compositions

Since the eutectic temperature corresponding to the group of phases involving CaO is appreciably low (1150°C), some liquid phase will always be formed at optimum firing temperatures (1000-1150°C). The presence of significant amount of fluxes aids the liquid phase formation. These

conditions are favourable for the liquid-phase sintering [Fig.7.13(c)].

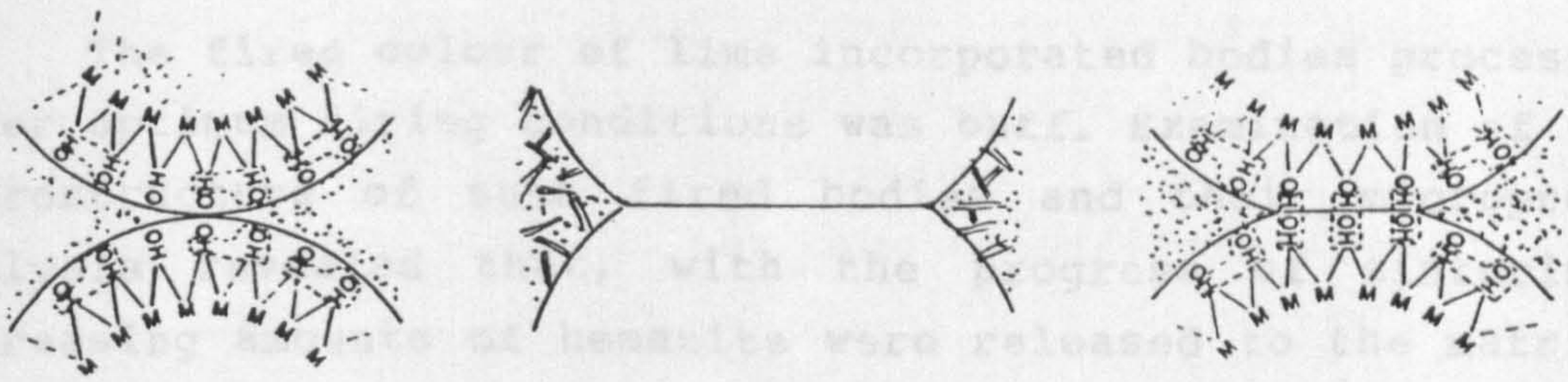

(a)-Solid state sintering and some liquid-phase sintering. (Dehydroxylation nearing completion).

(b)-Liquid-phase sintering and matrix reinforcement. (Dehydroxylation complete).

(c)-Liquid-phase sintering. (Dehydroxylation nearing completion).

Fig. 7.13-Schematic representation of the mechanism of strength development of experimental clay bodies.

Supporting evidence for the liquid-phase sintering mechanism is summarized below and includes:

(i). relatively high firing shrinkage of compositions containing optimum amounts of $CaCO_3$ over the range of temperature between 900°C and 1000°C.

(ii).rapid decrease in porosity of the optimum compositions over the range of temperature between 900°C and 1000°C.

(iii).microstructural effects which indicate morphological characteristics consistent with the enhanced vitrification of $CaCO_3$ compositions.

(iv).electron microprobe analyses of the glassy phase that showed its enrichment with Ca^{2+}, as opposed to Fe^{3+} which exists both as matrix inclusions and discrete particles.

(v).optical observation of glass-like second phase regions uniformly dispersed throughout the fracture surfaces.

CHAPTER 7

The experimentally determined values of modulus of rupture of different bodies are in reasonable agreement with the proposed mechanisms of strengthening.

7.9 INDUSTRIAL IMPLICATIONS

The fired colour of lime incorporated bodies processed under optimum firing conditions was buff. Examination of the microstructure of such fired bodies and their microprobe analysis revealed that, with the progress of sintering, increasing amounts of hematite were released to the matrix. The isolation of hematite into pockets within the body presumably caused the visible lightening in colour of the fired body which in turn depends on the relative concentration of hematite and on its grain size.

It was seen that the enhancement of vitrification of a clay was possible with an optimum amount of $CaCO_3$ and that the excessive amounts increased the rigidity of fired product. Both these effects can be used beneficially depending on whether the raw material is of high-lime or low-lime content. The detrimental effect of $CaCO_3$ on the strength of 'over-fired' bodies, however, must not be overlooked.

For practical considerations it is advantageous to have the maturing range of a clay as long as possible since there is a temperature differential within the kiln. The potential use of $CaCO_3$ in widening the maturing range of the three types of clay was amply demonstrated in this investigation.

7.10 SUMMARY OF RESULTS

(i). From the point of view of producing fired clay products with desirable properties, the amount of mineralizer, particle size of clays and the heat treatment are all important variables which must be strictly controlled. These influences seem to be interactive.

(ii). Up to 4 wt% addition of $CaCO_3$ was not effective in accelerating the mullitization of the three kaolinitic soils over the firing temperature range of 700 -1150°C; there is

circumstantial evidence to suggest that the 2 wt% addition suppressed the nucleation of cristobalite and ϑ-alumina in the podzolic clay while the 4 wt% addition had an opposite effect on the residual soil.

(iii).Optimum compositions of $CaCO_3$ (2-4 wt%) improved the modulus of rupture of clay bodies fired at 900°to 1000°C. The gain in strength of compositions fired at 1000°C over pure clay bodies fired at the same temperature were:

6% - for podzolic clay

36% - for residual clay

60% - for latosol

The strength improvement was most promising in the coarse-grained soils. However, the strength of bodies deteriorated after being fired above 1000°C. Nevertheless the additions had a beneficial effect on the maturing range of the clays.

(iv).The strength enhancement of clay-$CaCO_3$ compositions is probably attributed to liquid-phase sintering.

(v).The modulus of rupture of fine-grained plastic podzolic clay with low silica content increased in proportion to the amount of mullite present. In the case of silica-rich soils, the strain induced by the α-β transformation of quartz probably more than outweighed the strengthening effect of mullite.

(vi). The modulus of rupture of fine-grained plastic podzolic clay increased linearly with decrease in apparent porosity over the range of 20-40% apparent porosity.

(vii). The combined effects of both mullite content and porosity on the modulus of rupture of the fine-grained clay bodies are well represented by the equation:

$$M.O.R. = M_o\,[(\,1-0.03\ A.P.)(\,1+0.02\ I_m\,)]^{\frac{1}{2}}$$

According to this relationship, the maximum strength (M.O.R.) attainable with a clay compact of podzolic clay fired to temperatures below the nucleation of mullite is 15 N/mm^2. This relationship shows promise as a basis for

evaluation of clays for the manufacture of structural clay products.

(viii).Scanning electron microscopy of fired clays and clay compositions provided supporting evidence for the mechanisms involved in strength enhancement that are postulated here.

CHAPTER 8

TEXTURE OF FIRED CLAY PRODUCTS

8.1 MICROSTRUCTURAL AND MORPHOLOGICAL CHANGES DURING FIRING

The phases present after firing structural clays have been studied using X-ray diffraction techniques and the microstructural changes have also been investigated by optical microscopy. These studies are reported in the literature and have revealed only limited information about the internal morphological changes related to the development of properties such as porosity and strength of the fired product. Segnit and Anderson (1972) reported a limited study on the vitrification of illite at 1100°C. According to Freeman and Rayment (1975), no work has been published up until 1975 on the application of scanning electron microscopy to less pure ceramics of the type used in structural clay products. They provided a general description of the micrographs of four fired clays (London clay, Lower Oxford clay, Gault clay and Carboniferous shale). Following this work, Tite and Maniatis (1975) reported a morphological study on five fired clays (London clay, Gault clay, Dorset ball clay, Keuper marl and Weald clay). Since then, no studies have been reported in the literature except for a few on unfired clays published abroad. The features observed in raw clays by previous investigators include morphology, fabric, texture and growth mechanisms of crystals. These have been mostly dealt with from the point of view of characterisation of clays in relation to their pedogenesis. As regards Sri Lankan clays, no work has yet been published on their microscopy.

The present research was concerned with

(i). the changes in internal morphology of the two types of clay discussed in Chapter 7, in sequential stages of firing,

(ii). the texture, extent of vitrification and interparticle bonding of crystals in the above fired materials,
(iii).the influence of calcium carbonate mineralizer on the internal morphology of the two clay bodies, and
(iv). the changes in constitution and growth of mullite, widely accepted as important parametric effects contributing to the strength of fired clay products.

The objective of investigation was to elucidate information on the above in relation to the development of properties, particularly porosity and strength in the fired product. The morphological and microstructural changes were followed by both optical and scanning electron microscopy in conjunction with electron probe microanalysis.

8.2 SCANNING ELECTRON MICROSCOPY

8.2.1 Samples examined

Clay bodies representative of two major brickmaking clays (Podzolic and Residual) were chosen for the study. Latosol with poor vitrification characteristics was not considered. The specimens used in the scanning electron microscopic examination were:

(i). Podzolic clay - -1.40mm fraction, unfired and unetched.
(ii). Podzolic clay - fired at 800°C for 2 h, unetched.
(iii).Podzolic clay - fired at 850°C for 2 h, unetched and etched.
(iv). Podzolic clay - fired at 1150°C for 2 h, unetched and etched.
(v). Podzolic clay - added with 3 wt% $CaCO_3$ and fired at 800°C for 2 h, unetched.
(vi). Podzolic clay - added with 2 wt% $CaCO_3$ and fired at 1100°C for 2 h, unetched and etched.
(vii).Residual soil - -1.40mm fraction, unfired and unetched
(viii).Residual soil- fired at 800°C for 2 h, unetched and etched.
(ix). Residual soil - fired at 850°C for 2 h, unetched.
(x). Residual soil - added with 4 wt% $CaCO_3$ and fired at 1000°C for 2 h, unetched and etched.

8.2.2 Preparation and examination of samples

Samples were prepared by wet moulding bars. The bars were fired in a laboratory electric muffle furnace in an oxidizing atmosphere at temperatures from 800° to 1150°C. A heating rate of 5.6°C/min with a soaking time of 2 h at the peak temperature was employed for the firings. The freshly broken samples were vacuum coated with a thin film of carbon prior to examination. Selected samples were etched in 40% hydrofluoric acid for 5 seconds before being coated and examined.

A Hitachi electron microscope was used to examine fracture surfaces. The specimens introduced into the microscope fitted with an energy dispersive X-ray analysis system were analysed using a Link Systems programme which corrects iteratively for background and overlap.

8.2.3 Morphological characteristics - Podzolic clay compositions

Plates 8.1-8.12 show photomicrographs of the samples of raw and lime-containing podzolic clay subjected to increasing heat treatment.

8.2.3.1 Podzolic clay unfired (Plate 8.1)

The unfired moulded body is composed of an aggregate of thin crystallites of kaolinite and featureless relatively large grains of quartz and feldspar (1-5 μm). Careful examination of the micrograph shows the needle-like morphology of the kaolinite crystallites. However, characteristic hexagonal shape of crystallites can seldom be seen. Most of the crystallites are of the order of 2 μm in length. These may have been derived from the plates of disordered kaolinite.

8.2.3.2 Podzolic clay fired at 800°C (Plate 8.2)

On firing at 800°C, the most significant change observed at first was the development of liquid phase. The photomicrograph clearly shows the evidence of fusion of small grains in clusters of glassy ground mass. However, the

amount of melt formed was insufficient to effect complete sintering resulting in residual porosity.

The porosity is mainly due to approximately spherical intergranular voids. The sub-micron particles are probably quartz.

8.2.3.3 Podzolic clay fired at 850°C (Plates 8.3-8.5)

At this firing temperature, sintering at the contacts of individual crystallites became more intensified. This is clearly seen in the thin poorly formed crystallites probably of metakaolinite. A marked increase in glass formation was evident (Plate 8.3).

Etching caused preferential dissolution of glass revealing a random matrix of metakaolinite crystallites and feldspar and quartz grains (Plate 8.4). The back scattered photomicrograph taken at low resolution (Plate 8.5) indicates that the porosity is made up of fine pores.

8.2.3.4 Podzolic clay fired at 1150°C (Plates 8.6-8.8)

By 1150°C, a major change in morphology had taken place. The continuous vitrified layer containing large pores formed over the fracture surface obliterated the characteristic morphology previously observed in the specimen. Large grains were dissolved and the body was almost completely vitrified (Plate 8.6).

The porosity is made up of voids between adjacent sintered aggregates. These voids which are isolated have changed from spherical to irregular shape. The gradual decrease in porosity with coalescence of partially vitrified grains which persisted up to 1000°C has now been reversed with the enlargement of voids. The extension of void volumes indicated the evidence of bloating in the body at this firing temperature.

Plate 8.1-Fracture surface of wet-moulded podzolic clay, unfired.

Plate 8.2-Podzolic clay fired at 800°C. Partial coalescence of grains.

Plate 8.3-Podzolic clay fired at 850°C. Discontinuous vitrification.

Plate 8.4-Podzolic clay fired at 850°C: etched with 40%HF.

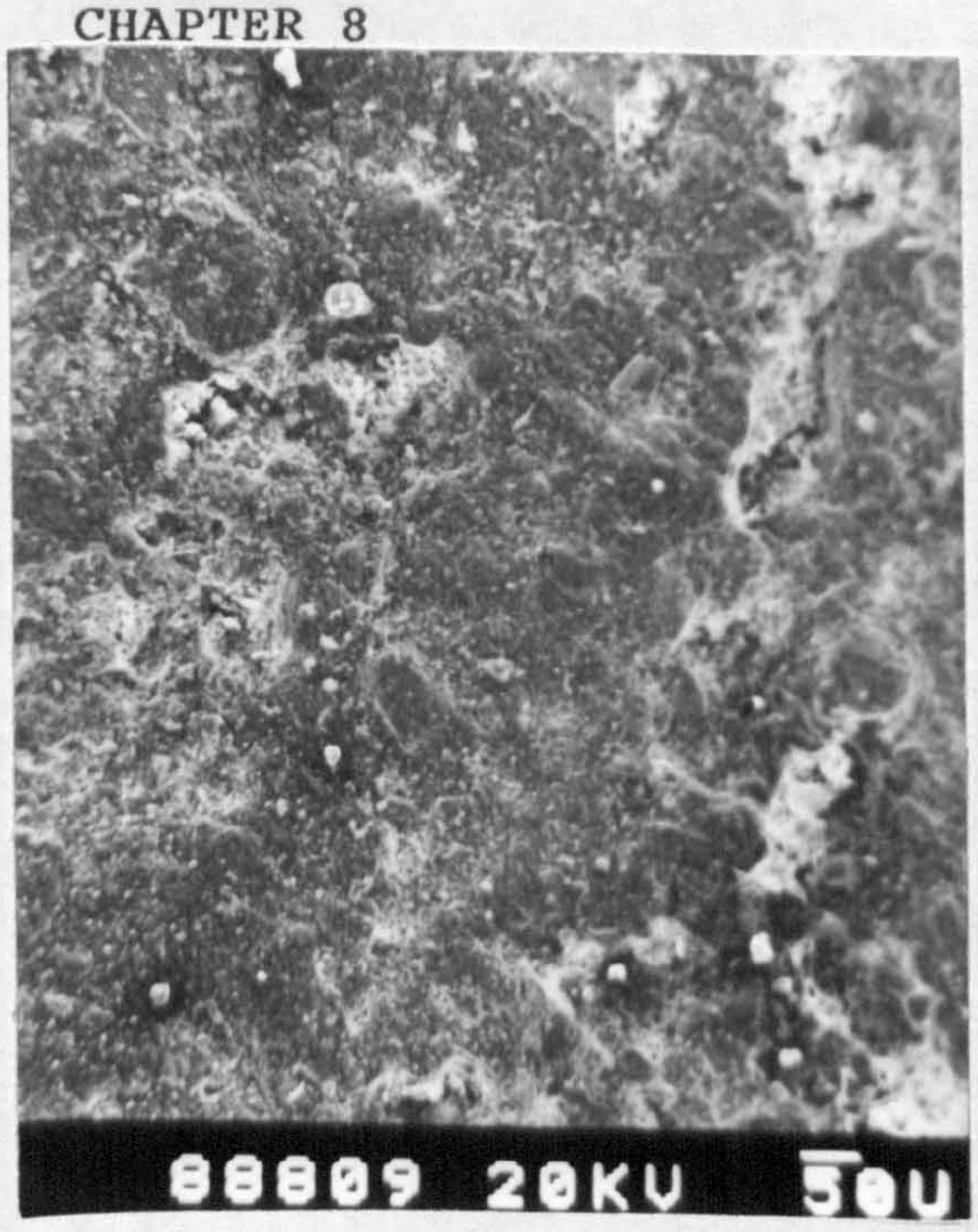

Plate 8.5-Back scattered photomicrograph of podzolic clay fired at 850°C. Low concentration of fine pores.

Plate 8.6-Podzolic clay fired at 1150°C. Continuous vitrified surface. Partial bloating.

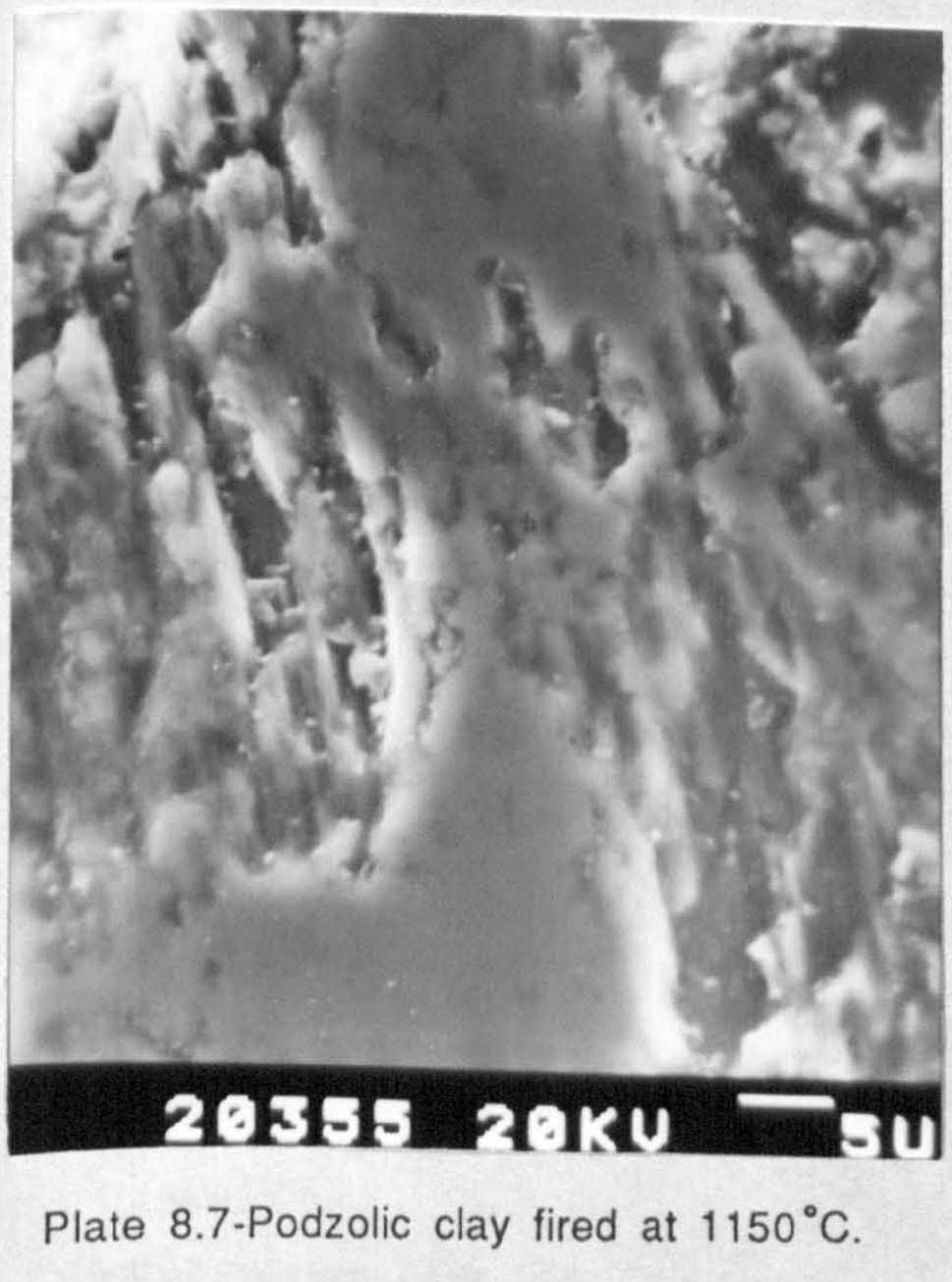

Plate 8.7-Podzolic clay fired at 1150°C. Mullite needles embedded in glass.

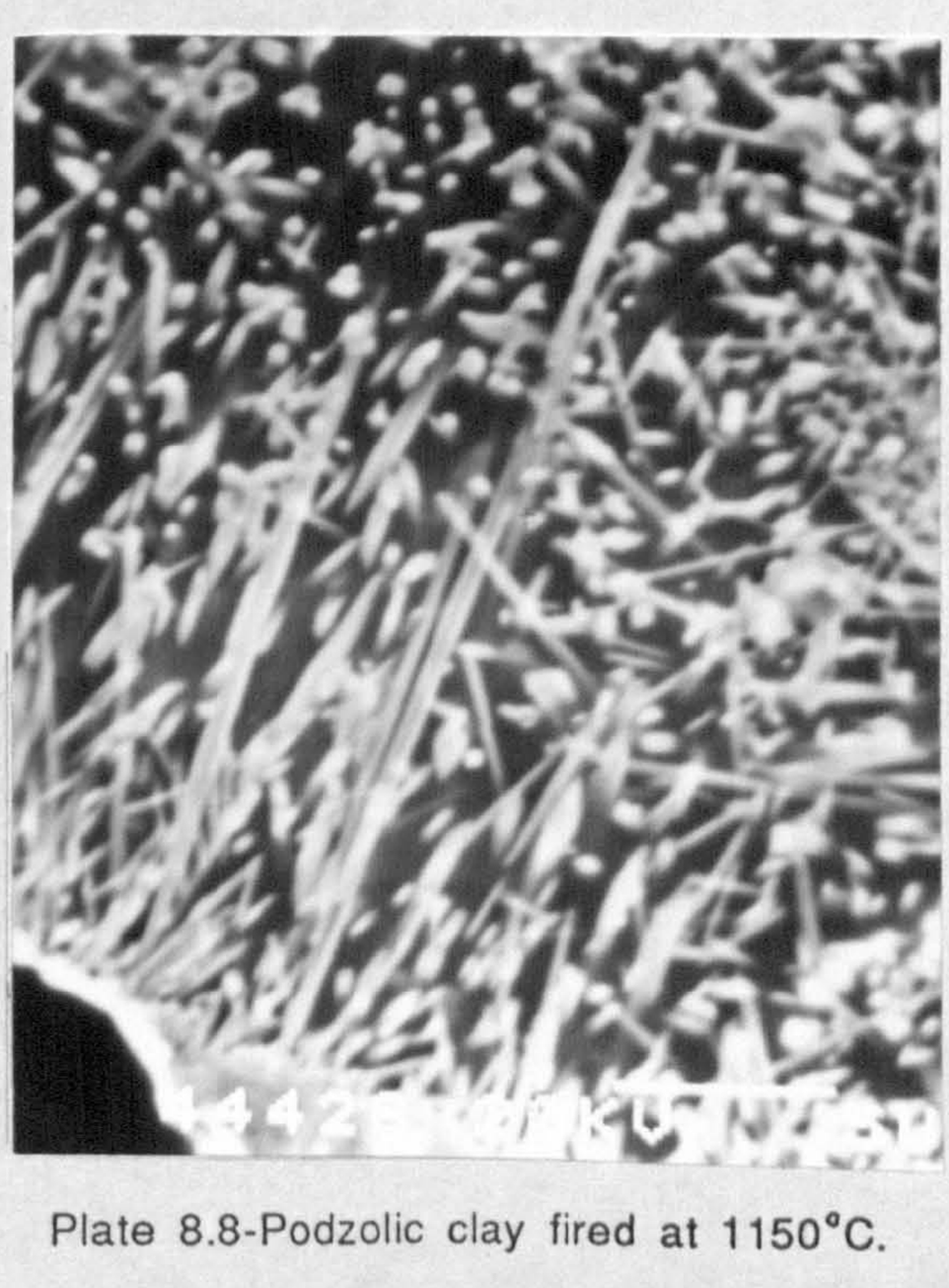

Plate 8.8-Podzolic clay fired at 1150°C. Interlocking secondary mullite needles and primary mullite on etched surface.

X-ray diffraction indicates the presence of mullite at 1150°C. The skeletal structure of needle-shaped mullite crystals reinforcing the glassy phase is clearly observable even at low resolution (Plate 8.7). Etching caused preferential dissolution of glass leaving well developed interlocking acicular mullite needles standing out in relief (Plate 8.8). It seems probable that mullite needles grow into the feldspar relicts from the surface. The maximum length of mullite needles is 12-15 μm. Extensive interlocking among both fine and well developed needles is common.

The microprobe analyses of mullite, intergranular glassy phase and bulk fired material are presented in Table 8.1.

Table 8.1-Electron probe microanalyses (normalized) of:
(1) Bulk fired material
(2) Secondary mullite
(3) Intergranular glassy phase
for podzolic clay

Material	% Oxide								
	SiO_2	Al_2O_3	Fe_2O_3	Na_2O	K_2O	CaO	MgO	TiO_2	MnO
Secondary mullite	34.57	64.08	1.29	-	0.01	0.01	-	0.02	0.02
Glassy phase	13.65	40.96	39.47	0.54	0.33	0.09	3.63	1.12	0.16
Bulk material	46.67	32.62	15.26	0.55	1.62	0.69	0.81	1.15	0.18

Mullite developed in the podzolic clay contains a small proportion of Fe_2O_3 in solid solution. The composition of mullite approximates to an Al_2O_3:SiO_2 ratio 2:1. The associated energy dispersive X-ray trace for the analysis of mullite is given in Fig. 8.1

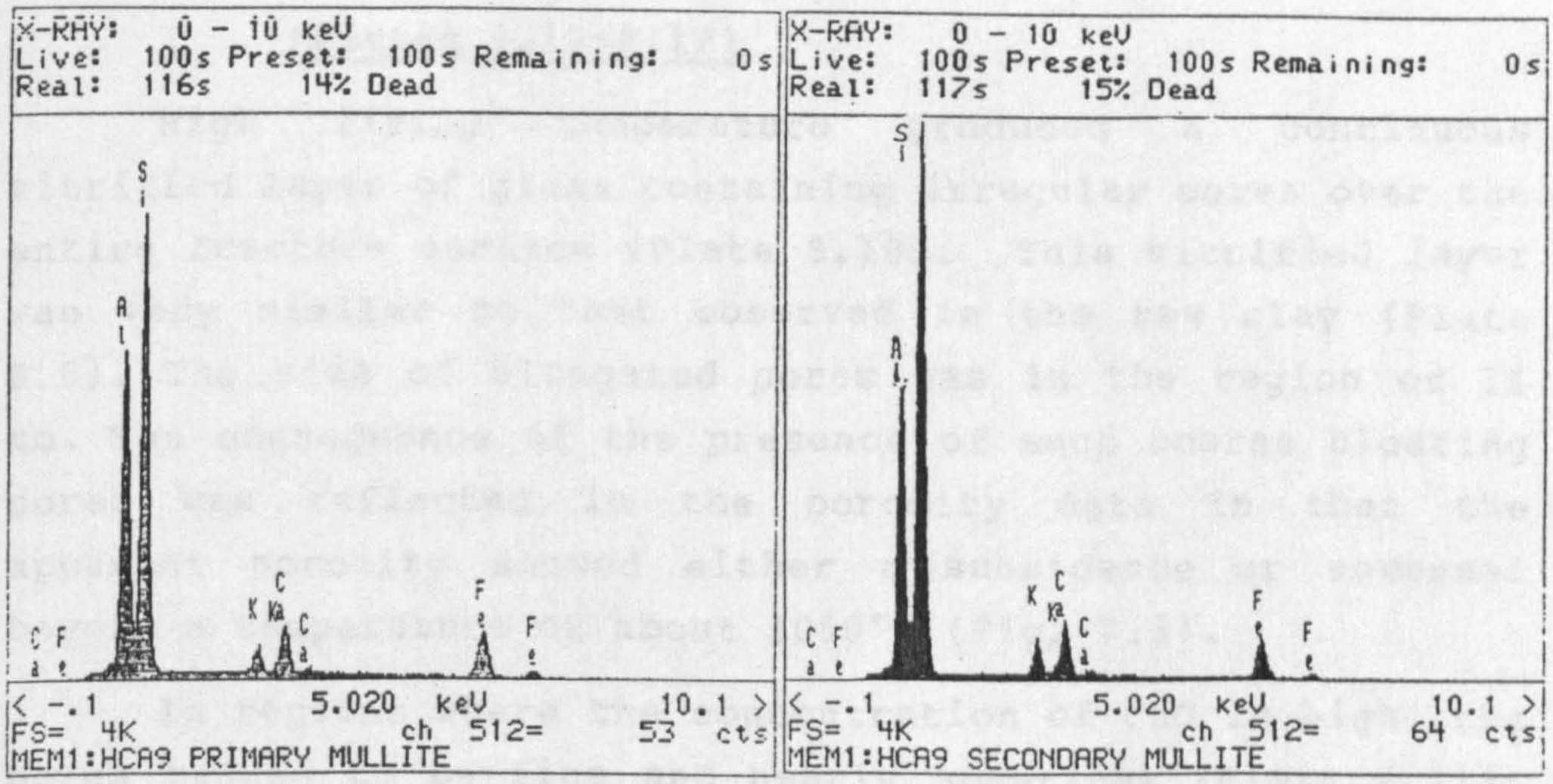

Fig. 8.1-X-ray energy dispersive analysis.
(1) Primary mullite (2) Secondary mullite

8.2.3.5 Podzolic clay with 3 wt% $CaCO_3$ fired at 800°C (Plate 8.9)

The most striking feature of the microstructure of podzolic clay with 3 wt% $CaCO_3$ fired at 800°C compared with the microstructure of raw podzolic clay fired at the same temperature (Plate 8.2) is the high degree of sintering which enhanced the interparticle bonding. This suggests the lowering of the onset temperature of vitrification in the clay body containing $CaCO_3$. The appearance of glass was in the form of smooth-surfaced layers. There seems to have been some collapse of the spherical voids. Indefinite outlines of original clay grains can still be seen but for the most part they have been dissolved in the feldspathic glass.

When compared with the fracture surface of raw clay fired at 800°C (Plate 8.2), this morphological structure appears to be more uniform. In addition, extensive diffusion has resulted in complete reconstitution of bulk material to a less porous body. Consequently, the fired body is much stronger (Fig. 7.2).

8.2.3.6 Podzolic clay with 2 wt% $CaCO_3$ fired at 1100°C (Plates 8.10-8.12)

High firing temperature produced a continuous vitrified layer of glass containing irregular pores over the entire fracture surface (Plate 8.10). This vitrified layer was very similar to that observed in the raw clay (Plate 8.6). The size of elongated pores was in the region of 15 µm. The consequence of the presence of such coarse bloating pores was reflected in the porosity data in that the apparent porosity showed either a subsidence or reversal beyond a temperature of about 1050°C (Fig. 7.3).

In regions where the concentration of CaO is high, the pores tended to be fine and nearly spherical (Plate 8.11). This shows the importance of uniformity of dispersion of the additive in controlling the porosity as well as the mechanical strength of the fired body.

A representative micrograph of mullite needles formed in the $CaCO_3$ containing clay is depicted in Plate 8.12. The specimen was characterised by:

(i). the presence of well developed large crystals of mullite of maximum grain size 25 µm.

(ii). the absence of globular primary mullite, in contrast to the lime free specimen (Plate 8.8) which showed the coexistence of both types of mullite.

The grain size of mullite crystals formed in the clay appeared to be influenced by the presence of $CaCO_3$ which probably made the glassy phase less viscous facilitating the mobility of ions. It seems probable that although $CaCO_3$ interfered with the nucleation of mullite, the presence of it favoured the direct formation and grain growth of secondary mullite.

Plate 8.9-Podzolic clay containing 3 wt% $CaCO_3$ fired at 800°C. Extensive glass formation.

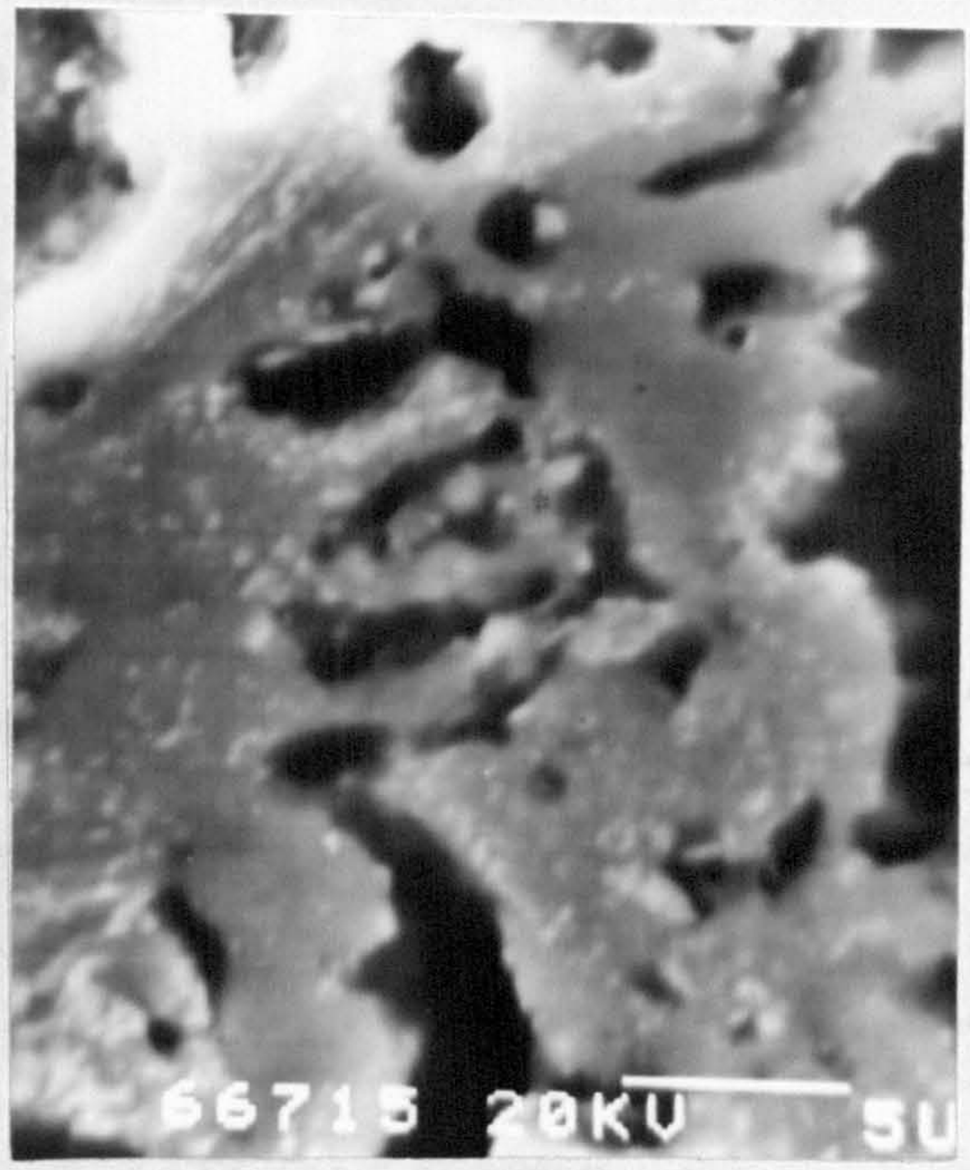

Plate 8.10-Podzolic clay containing 2 wt% $CaCO_3$ fired at 1100°C. Continuous vitrified surface with coarse bloating pores.

Plate 8.11-Podzolic clay containing 2 wt% $CaCO_3$ fired at 1100°C. Fine spherical pores in regions of high concentration of CaO.

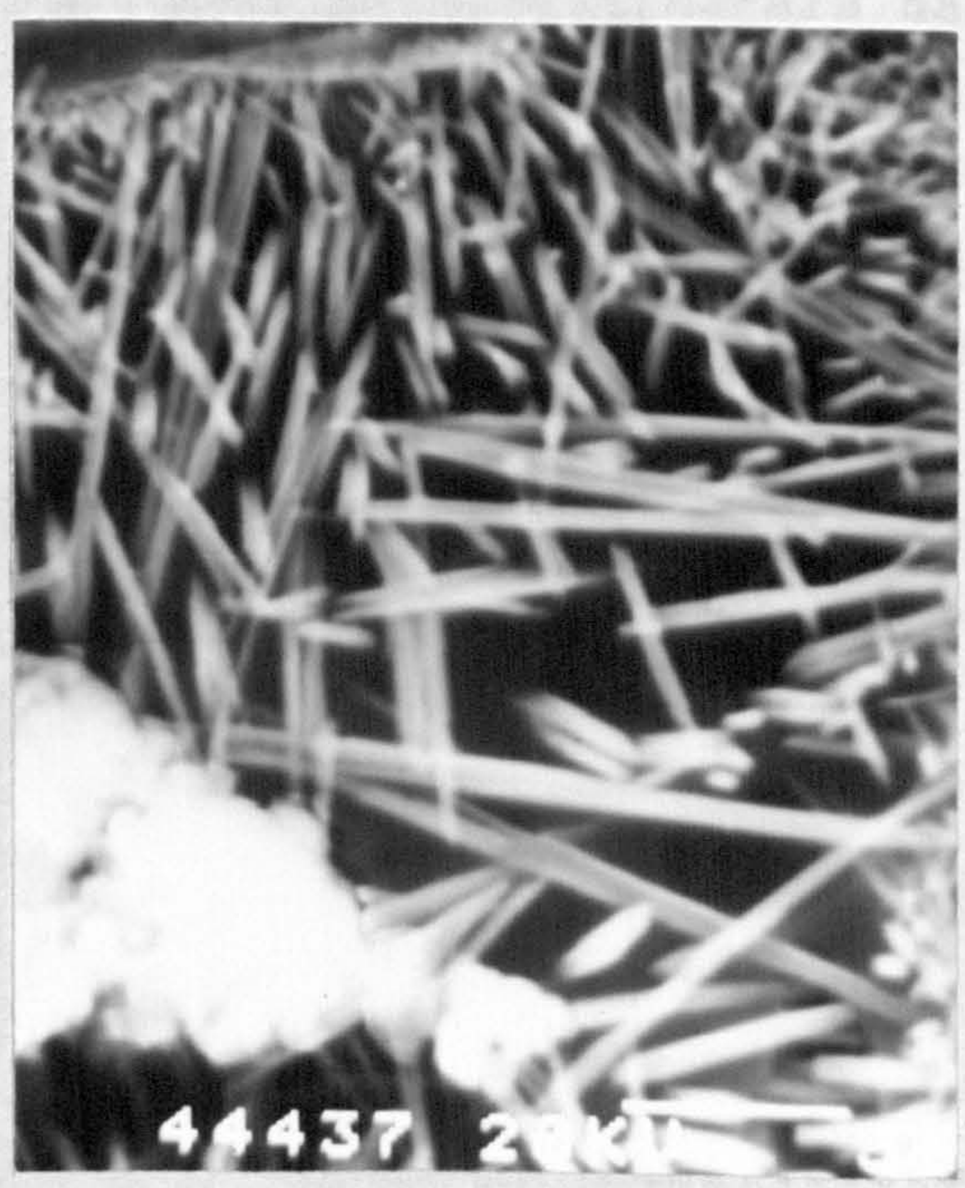

Plate 8.12-Podzolic clay containing 2 wt% $CaCO_3$ fired at 1100°C. Well-developed interlocking mullite needles on etched surface. Absence of primary mullite.

8.2.4 Morphological characteristics - Residual soil compositions

The micrographs depicted in Plates 8.13-8.19 are a series showing the effects of increasing heat treatment on residual soil and its compositions.

8.2.4.1 Residual soil unfired (Plate 8.13)

The unfired body at low magnification shows a featureless mass. The average size of abundant and loosely packed coarse aggregate in the dispersed matrix of sub-micron size clay particles is about 25 μm. The well dispersed nature of the structure compared to that of the podzolic clay is strikingly apparent.

8.2.4.2 Residual soil fired at 800°C (Plates 8.14-8.15)

Coalescence of the crystallites has occurred on firing at 800°C. Traces of glass can also be detected (Plate 8.14). The relative abundance of the liquid phase is higher than in the podzolic clay fired at the same temperature (Plate 8.2). It is probable that the dehydroxylation of clay minerals has taken place in the specimen although the overall morphology is still largely determined by the coarse aggregate. The particles of fine aggregate were partially sintered whilst the coarse aggregate remained as discrete grains retaining their rough outlines. Isolated ovoid pores are abundant.

Etching revealed a skeletal structure with fibrous matrix showing a high degree of interparticle bonding even at this relatively low firing temperature (Plate 8.15). Small crystallites mostly seen on edge with a platy crystal habit are probably hematite.

8.2.4.3 Residual soil fired at 850°C (Plates 8.16-8.17)

At 850°C thin individual platelets with a low degree of intergranular contact can be seen. Although vitrification had begun, the original clay mineral flakes are still clearly visible (Plate 8.16). The vitrified regions are, however, less continuous than those for the raw podzolic clay (Plate 8.3) indicating the sluggishness of

vitrification of this clay. The porosity is significantly high as was evident from the micrograph taken in back scattered mode at low resolution (Plate 8.17). Residual soil thus differs from podzolic clay in developing a high concentration of coarse pores at 850°C. This is probably attributed to the high lime content originally present in the residual soil (Table 3.3).

8.2.4.4 Residual soil with 4 wt% $CaCO_3$ fired at 1000°C (Plates 8.18-8.19)

Coalescence of the crystallites became more pronounced at 1000°C. Extensive sintering of clay aggregates is evident (Plate 8.18). The overall size of the clusters of sintered aggregates (approximately 3 μm) observed at 800°and 850°C has reduced considerably. The particulate character of the unfired material has now been completely obliterated. This change in morphology is matched by the recrystallization of mullite and cristobalite as shown by X-ray analysis.

The etched specimen (Plate 8.19) showed no evidence of the existence of needle-like secondary mullite although the correlative X-ray diffractogram clearly indicated the presence of mullite. It seems probable that mullite exists in primary globular form at 1000°C in this specimen. The surface of the sample fired at 1000°C is uniform and structureless with a low proportion of fine pores (diameter:0.5-1 μm). There is no evidence of the occurrence of bloating at this temperature.

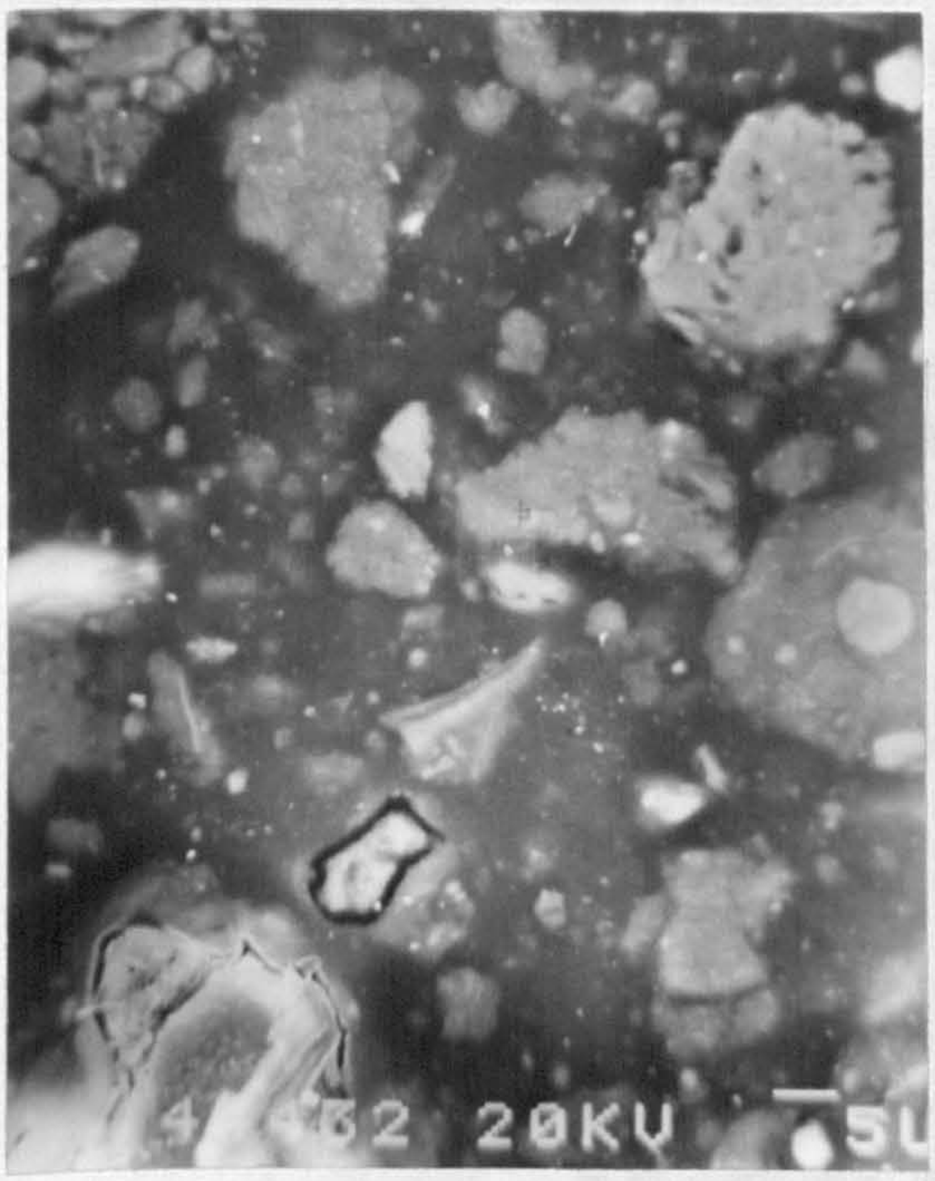

Plate 8.13-Fracture surface of wet-moulded residual soil, unfired.

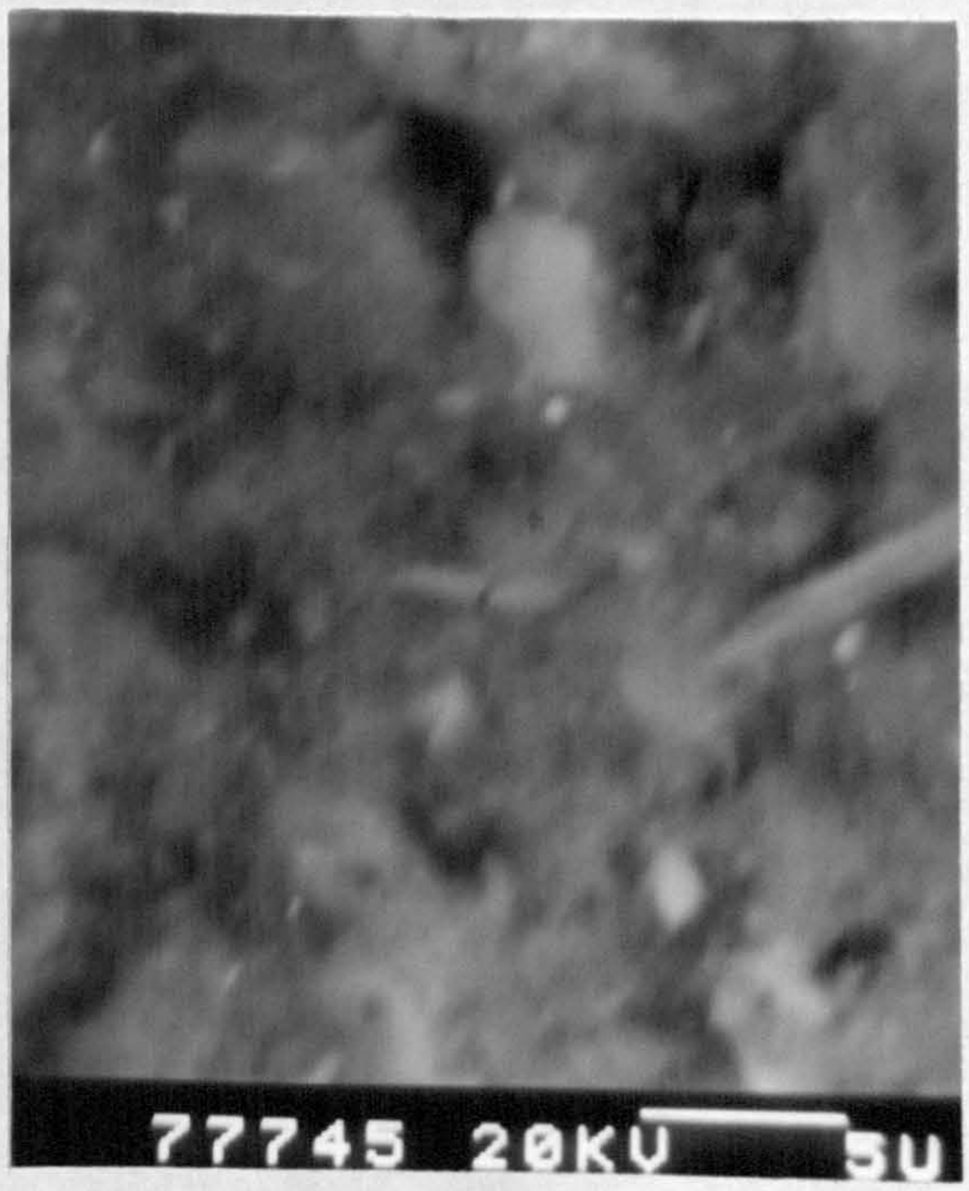

Plate 8.14-Residual soil fired at 800°C. Partial coalescence of grains. Traces of glass.

Plate 8.15-Residual soil fired at 800°C: etched fracture surface. Fibrous matrix. High degree of interparticle bonding.

Plate 8.16-Residual soil fired at 850°C. Change in morphology. Low degree of coalescence of grains.

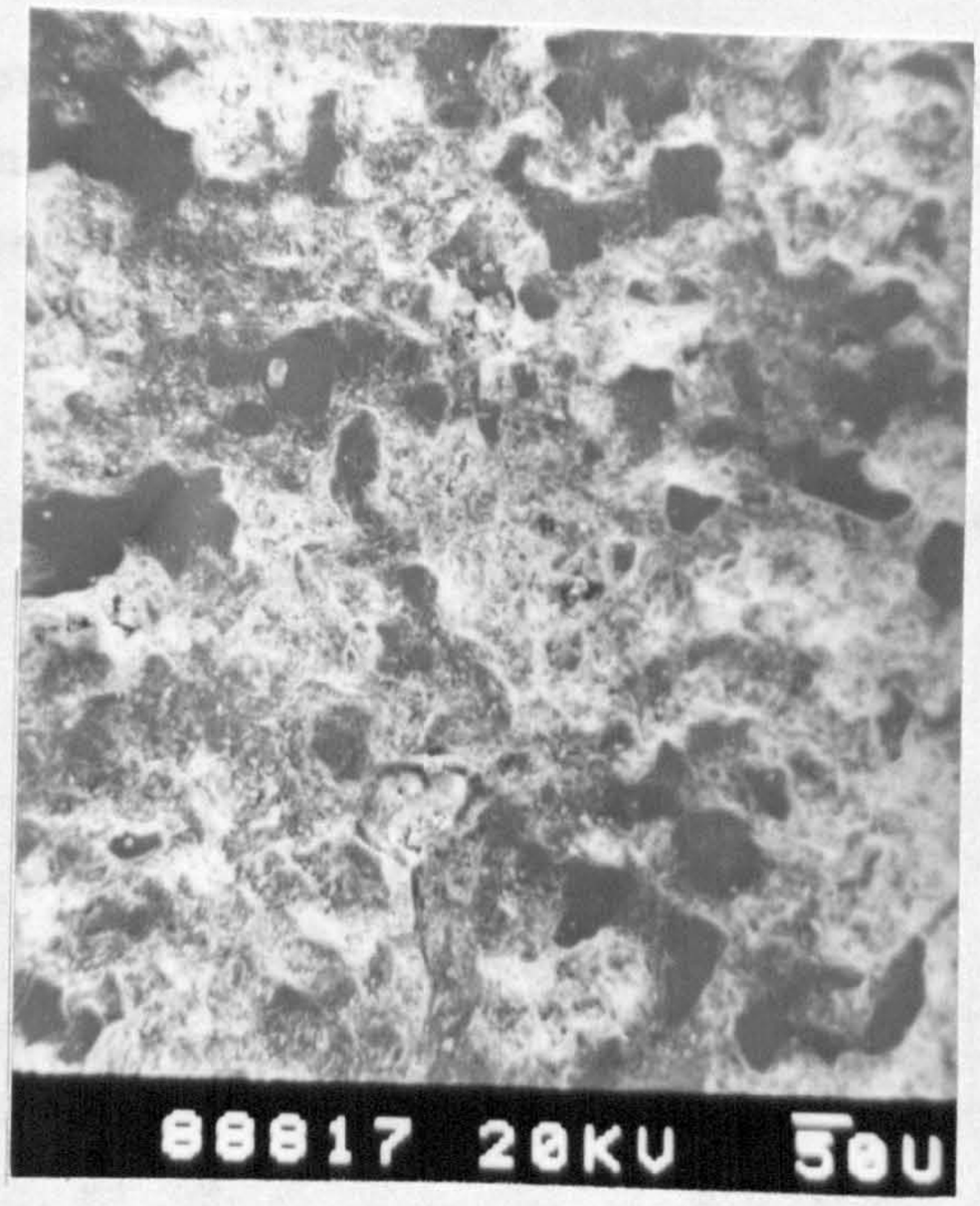

Plate 8.17-Back scattered photomicrograph of residual soil fired at 850°C. High concentration of coarse pores.

Plate 8.18-Residual soil containing 4 wt% $CaCO_3$ fired at 1000°C. Vitrification well-advanced.

Plate 8.19-Residual soil containing 4wt% $CaCO_3$ fired at 1000°C: etched surface. Absence of mullite needles.

The microprobe analyses of bulk fired material, intergranular glassy phase and regions of primary mullite formation are given in Table 8.2.

Table 8.2-Electron probe microanalyses (normalized) of:
(1) Bulk fired material
(2) Primary mullite
(3) Intergranular glassy phase
for residual soil
(Plate 8.8)

Material	% Oxide								
	SiO_2	Al_2O_3	Fe_2O_3	Na_2O	K_2O	CaO	MgO	TiO_2	MnO
Primary mullite	28.01	26.99	41.98	-	0.01	1.25	0.02	1.51	0.03
Glassy phase	49.64	32.27	11.10	0.31	0.31	4.26	0.67	1.34	0.07
Bulk material	64.04	22.42	7.99	-	0.45	4.04	-	0.77	0.16

The composition of mullite formed at 1000°C in the residual soil specimen approximates to an Al_2O_3:SiO_2 ratio of 1:1.

8.3 OPTICAL MICROSCOPY

According to Insley and Frechette (1955), the use of optical microscope is less common in the structural clay products industry than almost anywhere else in the ceramic field. They believe that there are several factors responsible for this. Because of the competition from other low-cost construction materials, emphasis has been placed on price rather than quality; tackling of production problems have been more pressing than the need to understand phase relationships with a view towards securing greater uniformity, strength, toughness and durability. Nevertheless the microscopy of structural clay wares is complex. The phase relationships are very complicated due to the impure materials used in manufacture, and because firing

temperatures are too low to approach the attainment of equilibrium conditions.

Optical microscopy was used in this investigation to supplement the information obtained from electron microscopy.

8.3.1 Microstructural specimens

Microstructural studies were carried out on broken flexural-strength test-bars of residual soil and podzolic clay bodies which had been subjected to the following heat treatments.

8.3.1.1 Podzolic clay

(i). Maximum firing temperature-800°C, soaking period-2 h.
(ii). Maximum firing temperature-800°C, soaking period-4 h.
(iii).Maximum firing temperature-900°C, soaking period-2 h.
(iv). Maximum firing temperature-1000°C, soaking period-2 h.

8.3.1.2 Residual soil

(i). Maximum firing temperature-800°C, soaking period-2 h.
(ii). Maximum firing temperature-800°C, soaking period-4 h.
(iii).Maximum firing temperature-900°C, soaking period-2 h.
(iv). Maximum firing temperature-900°C, soaking period-4 h.
(v). Maximum firing temperature-900°C, soaking period-6 h.
(vi). Maximum firing temperature-1100°C, soaking period 2 h.

In all cases a uniform heating rate of 5.6°C/min and an oxidizing atmosphere were maintained in a muffle furnace. Thin sections prepared from bars sectioned parallel to adjacent faces were examined under a petrographic microscope. Photomicrographs were taken at a magnification of 35 with plane polarized light. Plates 8.20 to 8.29 show photomicrographs of thin sections of residual soil and podzolic clay bodies subjected to the above heat treatments.

8.3.2 Microstructure versus thermal history - Podzolic clay bodies.

Changes in microstructure with heat treatment are less dramatic in podzolic clay bodies than in residual soil bodies. The microstructures are illutrated in Plates 8.20

to 8.23. A description of the microstructures is given below.

8.3.2.1 Podzolic clay fired at 800°C for 2 h (Plate 8.20)

The structure is relatively more isotropic containing a low concentration of pores. Quartz grains showed no signs of solution although traces of glass can be detected in the matrix material. In Plate 8.20, in the centre, a dark brown area probably arising from the crystallization of hematite can be seen which has been partially separated from the matrix forming an island containing unmelted quartz grains in the middle. The lack of porosity can be expected to contribute to high strength. However, the presence of large isolated areas in the matrix may be harmful to strength properties.

8.3.2.2 Podzolic clay fired at 800°C for 4 h (Plate 8.21)

This specimen showed a slight solution of the quartz grains which are now devoid of sharp outlines. More glassy phase was present in the structure than in the previous case. Hematite was highly dispersed in the matrix. The increased homogeneity has evidently improved the properties.

8.3.2.3 Podzolic clay fired at 900°C for 2 h (Plate 8.22)

This microstructure showed practically all of the smaller quartz and feldspar grains to have been melted with larger grains containing solution rims. There was evidence of diffusion of hematite into the matrix intensifying the brown colour of the specimen. Isolated hematite-rich regions have fused into the body.

8.3.2.4 Podzolic clay fired at 1000°C for 2 h (Plate 8.23)

Hematite-rich regions in this specimen were largely dispersed and combined with the matrix material to form a glassy phase. The general background was dark brown in colour. Coarse particles formed an interlocking mass of bonded particles with fewer pores. The fine grain size of the matrix material made its resolution difficult.

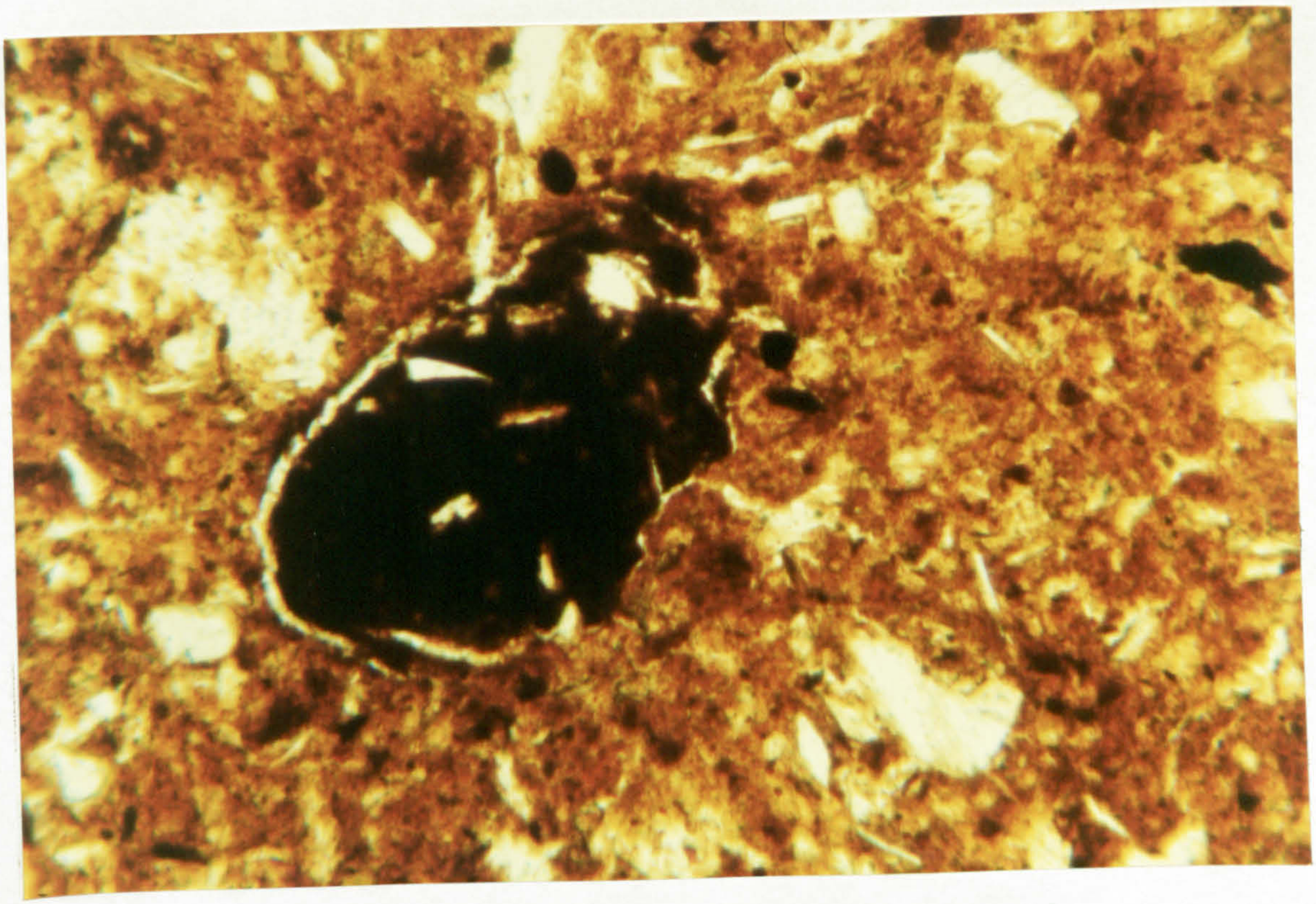

Plate 8.20-Podzolic clay fired at 800°C for 2 h. P.p.l.,35x.

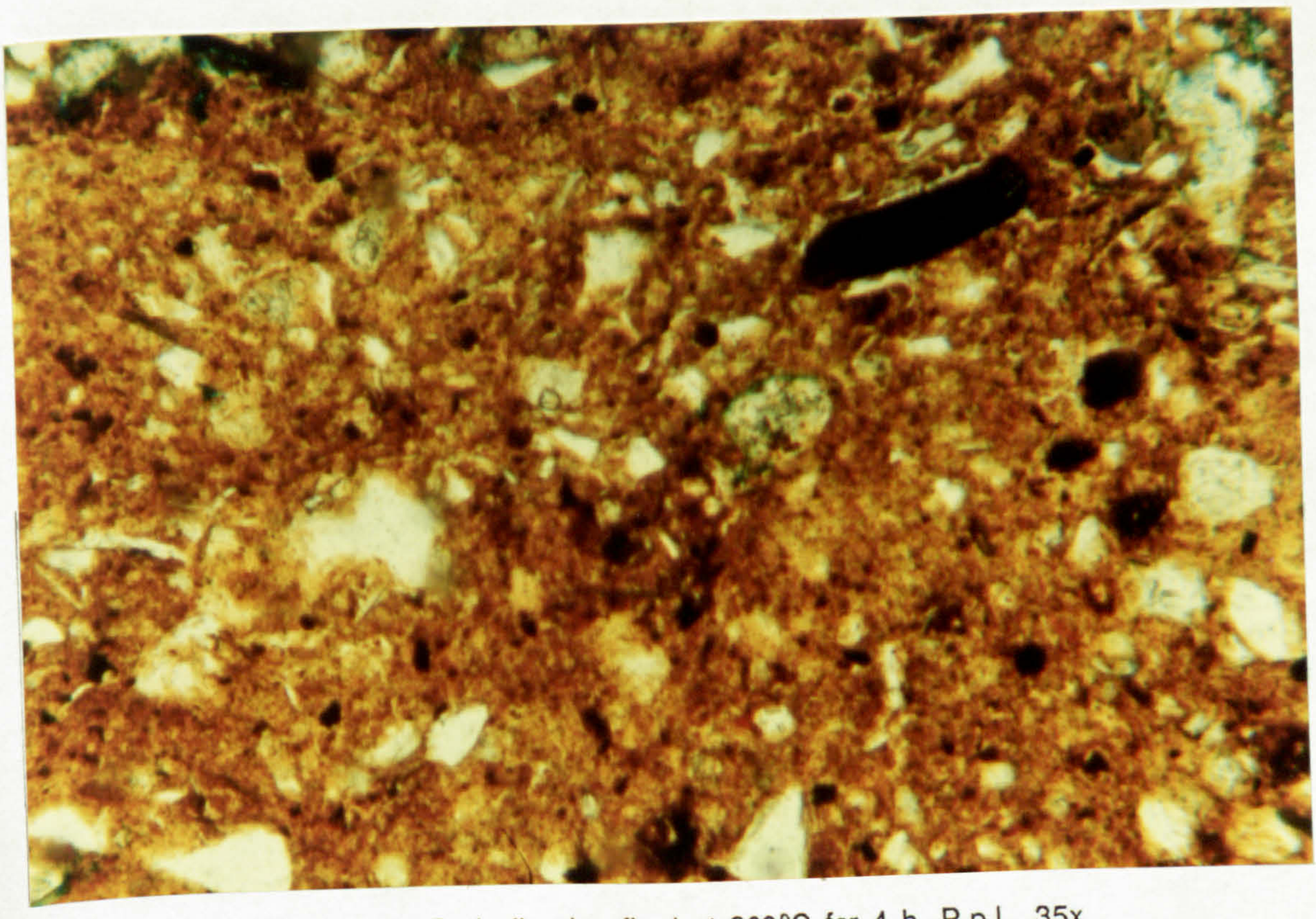

Plate 8.21-Podzolic clay fired at 800°C for 4 h. P.p.l., 35x.

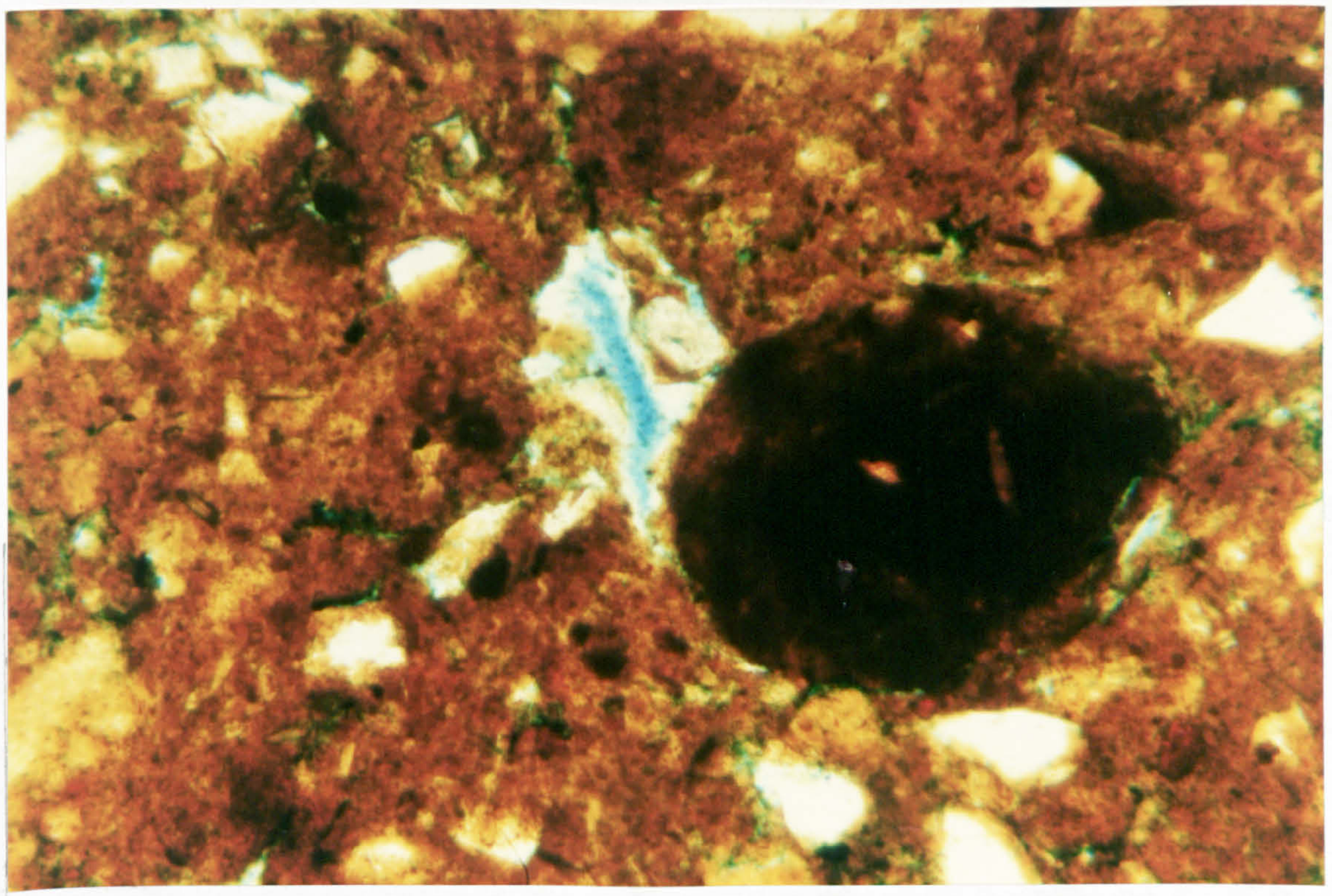

Plate 8.22-Podzolic clay fired at 900°C for 2 h. P.p.l., 35x.

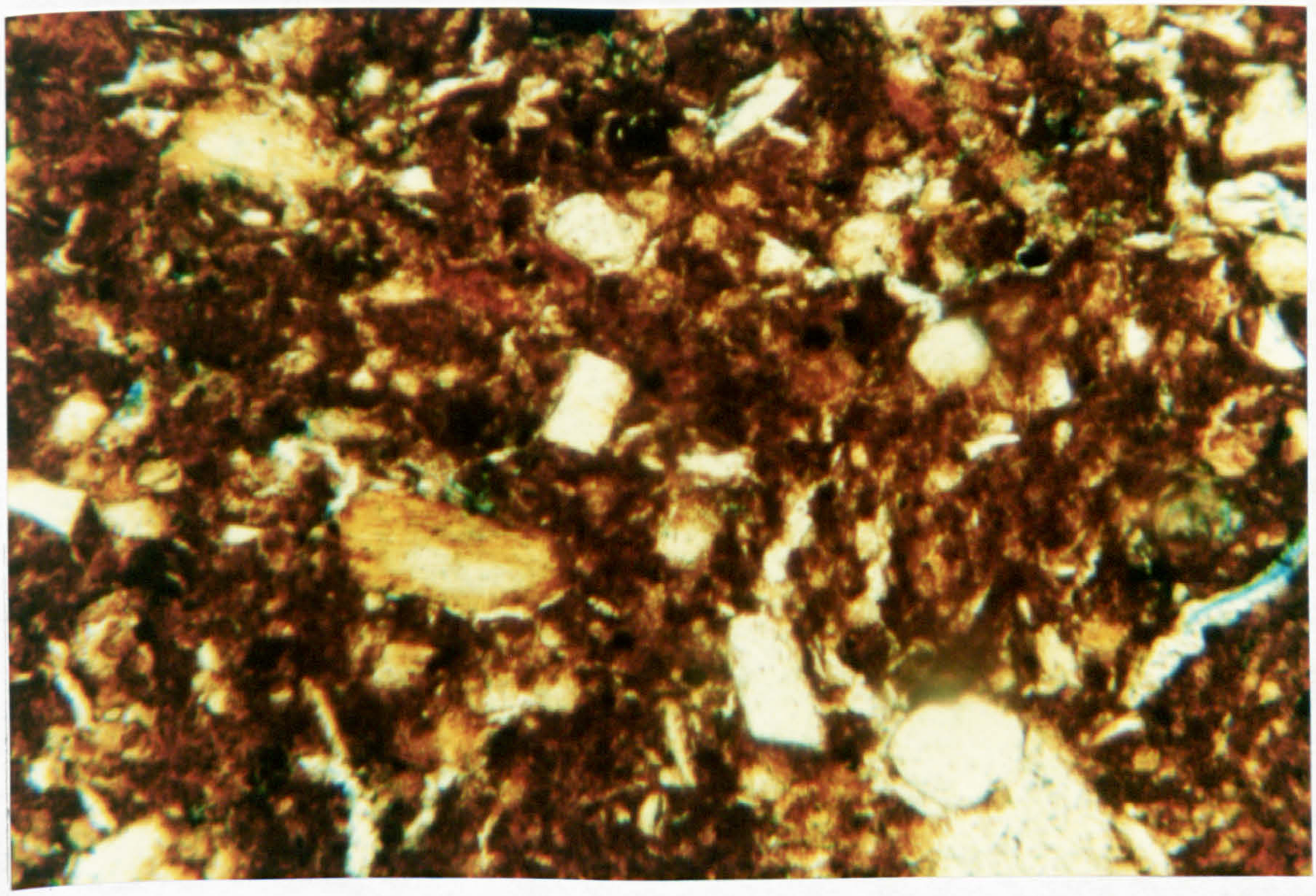

Plate 8.23-Podzolic clay fired at 1000°C for 2 h. P.p.l., 35x.

Nevertheless, it is possible that mullite crystallites were present in the matrix at this temperature as was evident from X-ray diffraction studies. This texture of fired material is favourable for obtaining good properties.

8.3.3 Microstructure versus thermal history - Residual soil bodies

8.3.3.1 Residual soil fired at 800°C for 2 h (Plate 8.24)

The specimen contained unchanged feldspar grains and quartz grains showing only slight solution of edges in a fine-grained clay matrix. Many longitudinal open voids exist adjacent to the edges of large grains leading probably to low strength and unsatisfactory properties.

8.3.3.2 Residual soil fired at 800°C for 4 h (Plate 8.25)

The effect of prolonging firing at 800°C was evident in this microstructure which shows the melting of some feldspar grains in the centre. Partially melted feldspar grains formed isotropic areas resembling a honeycomb-like texture presumably containing bubbles. Smaller grains have almost disappeared by reaction with the surrounding clay. Quartz grains showed signs of solution.

8.3.3.3 Residual soil fired at 900°C for 2 h (Plate 8.26)

The fact that long firing times at lower temperature (4 h at 800°C) may yield better structures than shorter times at higher temperature (2 h at 900°C) is illustrated by Plate 8.26. This specimen showed the striking persistence of micaceous minerals and feldspar grains with clear outlines. This texture is indicative of a low degree of maturing than that described in Section 8.3.3.2.

8.3.3.4 Residual soil fired at 900°C for 4 h (Plate 8.27)

Soaking for 4 h at 900°C caused fissures in feldspar grains and solution rims around quartz grains. Porosity has reduced quite considerably enhancing the strength.

8.3.3.5 Residual soil fired at 900°C for 6 h (Plate 8.28)

This microstructure showed a high degree of melting of feldspar grains with only a few unmelted large grains. The

melted feldspar grains have diffused into the body making the groundmass more homogeneous. Small quartz grains have undergone solution while large grains still retain their rough outlines. A greater reduction in porosity can be seen. There was no evidence of mullite crystallization.

8.3.3.6 Residual soil fired at 1100℃ for 2 h (Plate 8.29)

Micaceous structure was completely destroyed in this specimen. Large feldspar grains have turned to an isotropic glass but they still retain their original outlines. Correlative electron micrographs provided evidence of mullite development in pseudomorphs of such feldspar grains. Plate 8.29 shows in the centre of the microphotograph an area of probable nucleation of mullite although mullite crystals cannot be resolved with the optical microscope used in the investigation. Quartz in this structure shows some solution, particularly on the smaller grains. A counter effect to the deepening of brown colour of the matrix observed in high temperature-fired podzolic clay was found in this specimen. This may be due to high free lime content of residual soil (Table 3.3) which was effective in redissolving most of the brown hematite crystals. No clear indication of porosity could be obtained.

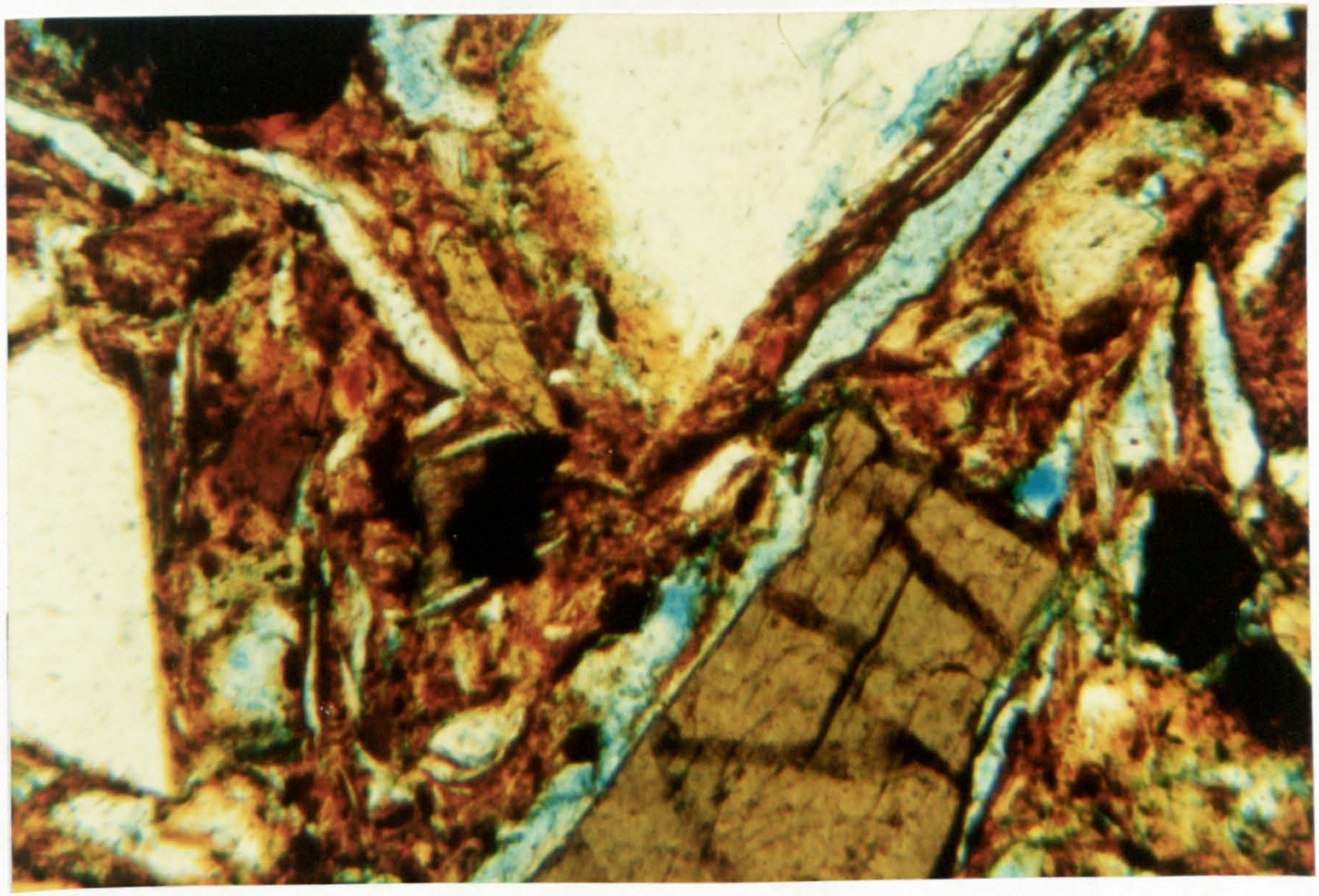

Plate 8.24-Residual soil fired at 800°C for 2 h. P.p.l., 35x.

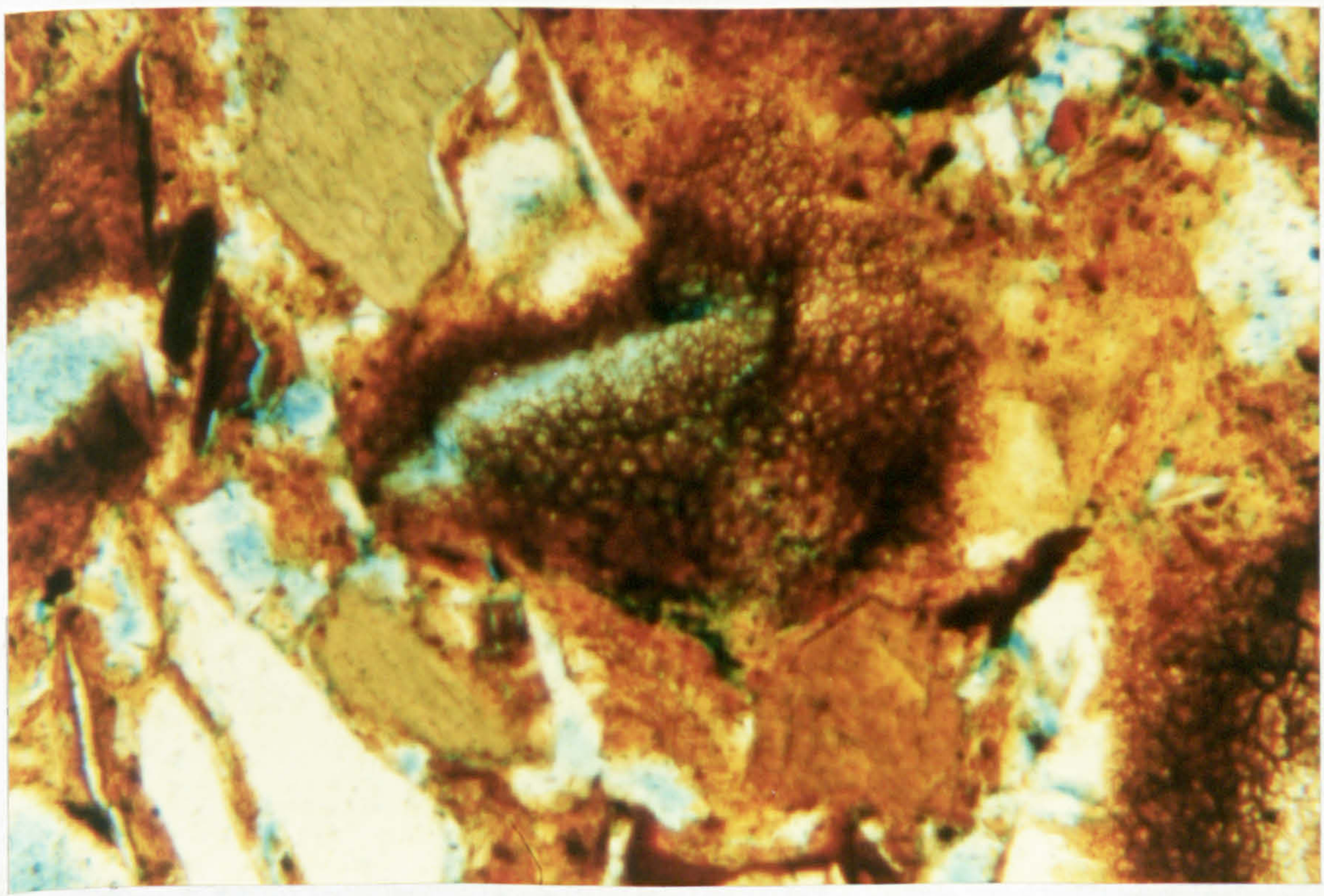

Plate 8.25-Residual soil fired at 800°C for 4 h. P.p.l., 35x.

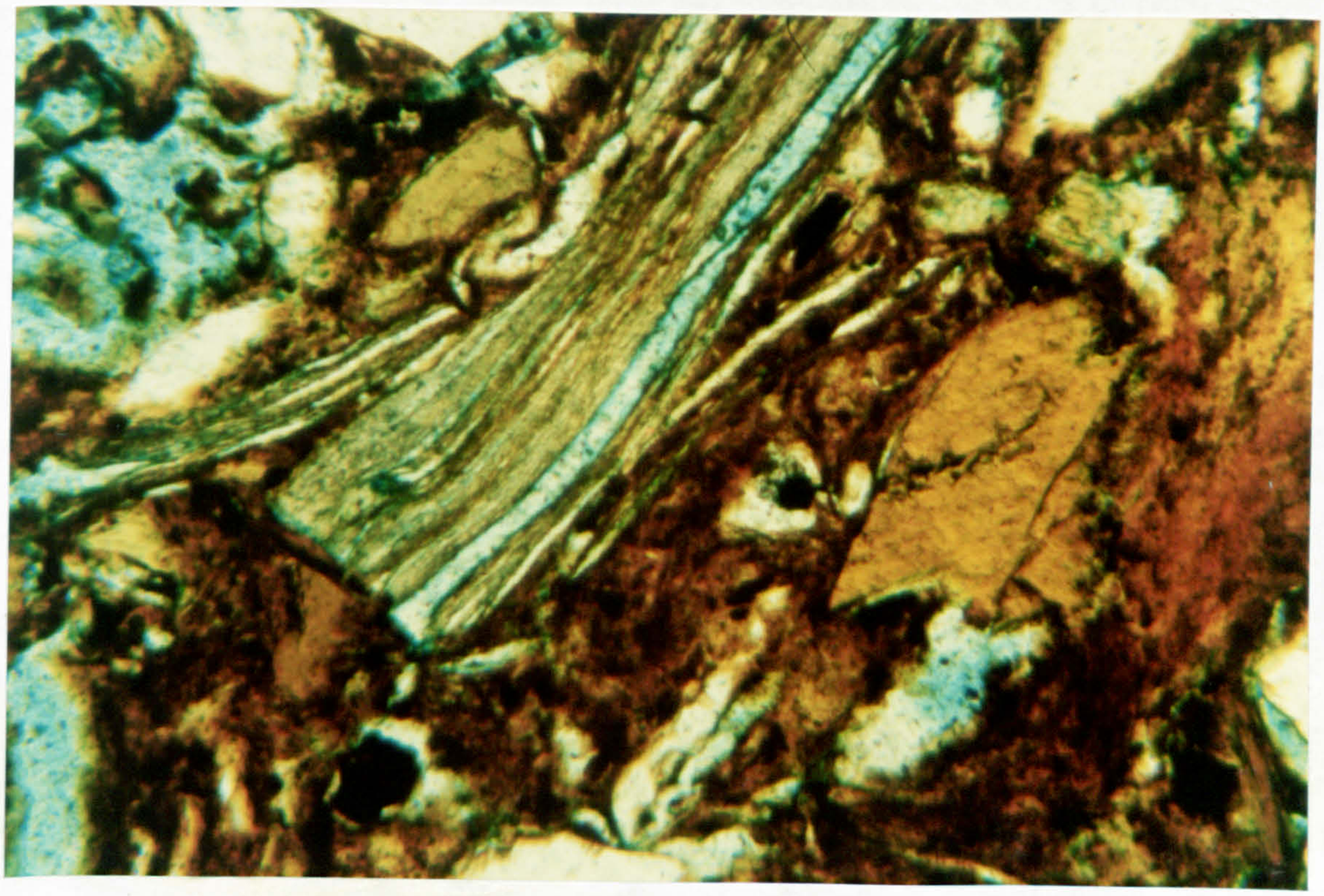

Plate 8.26-Residual soil fired at 900°C for 2 h. P.p.l., 35x.

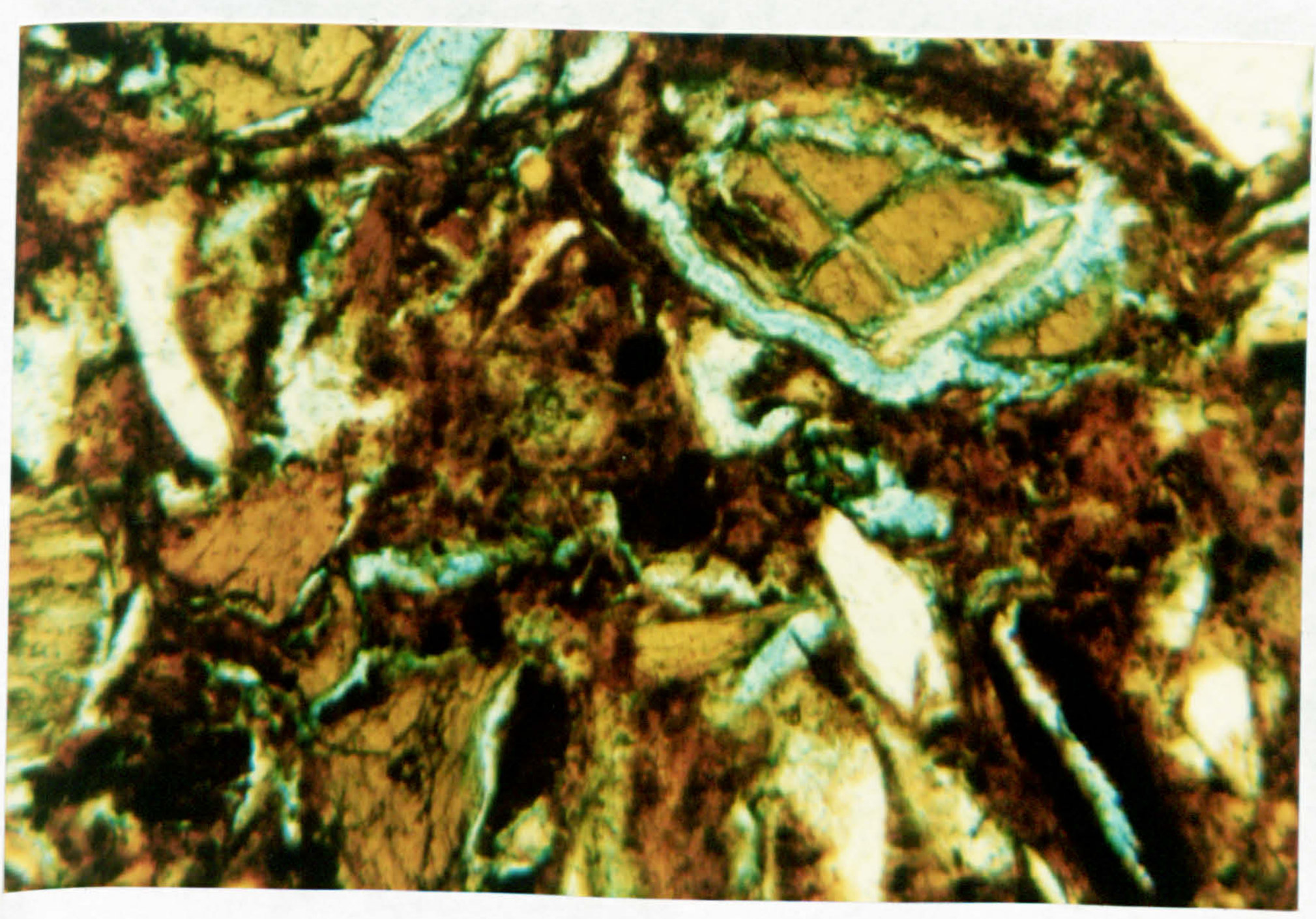

Plate 8.27-Residual soil fired at 900°C for 4 h. P.p.l., 35x.

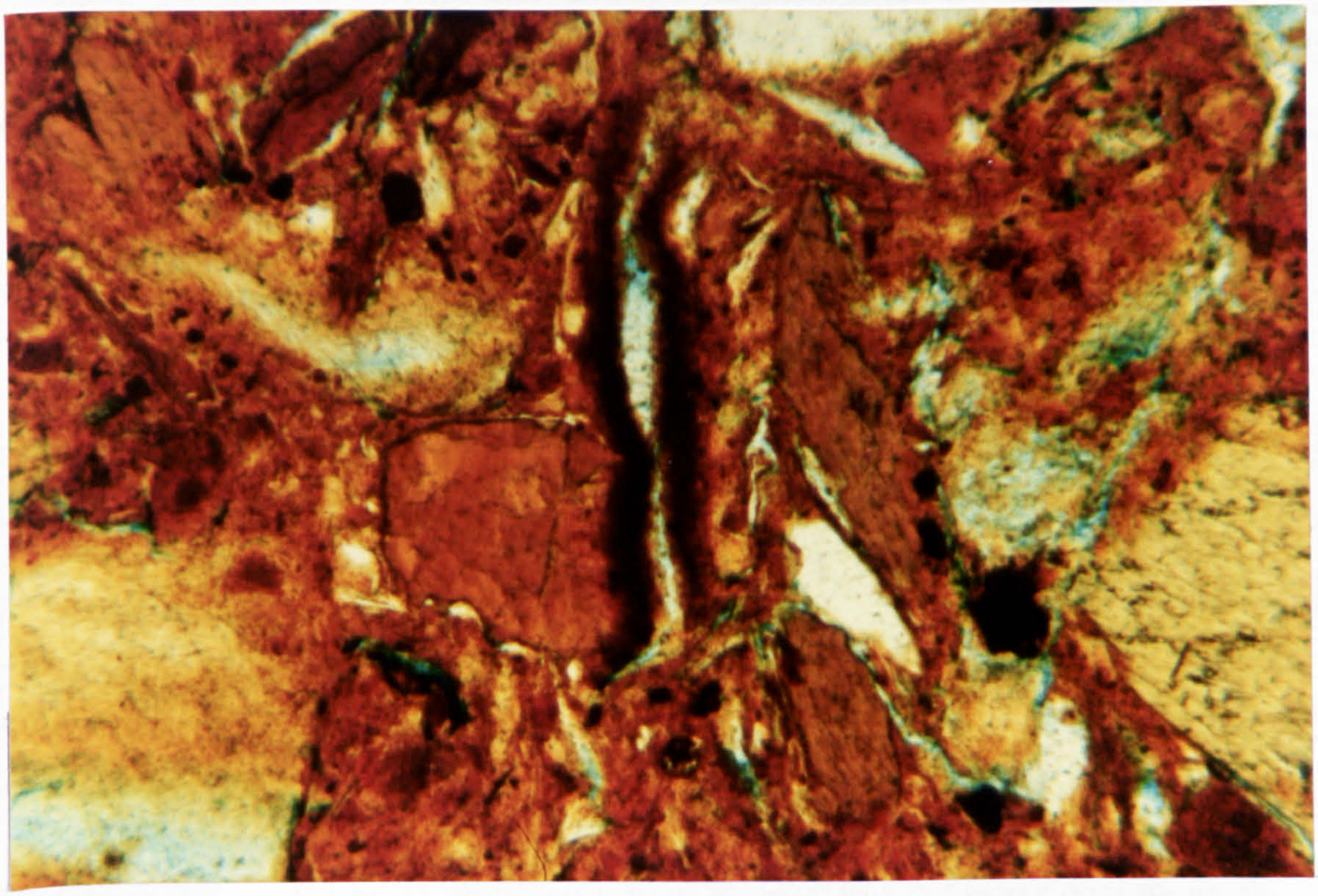

PLate 8.28-Residual soil fired at 900°C for 6 h. P.p.l., 35x.

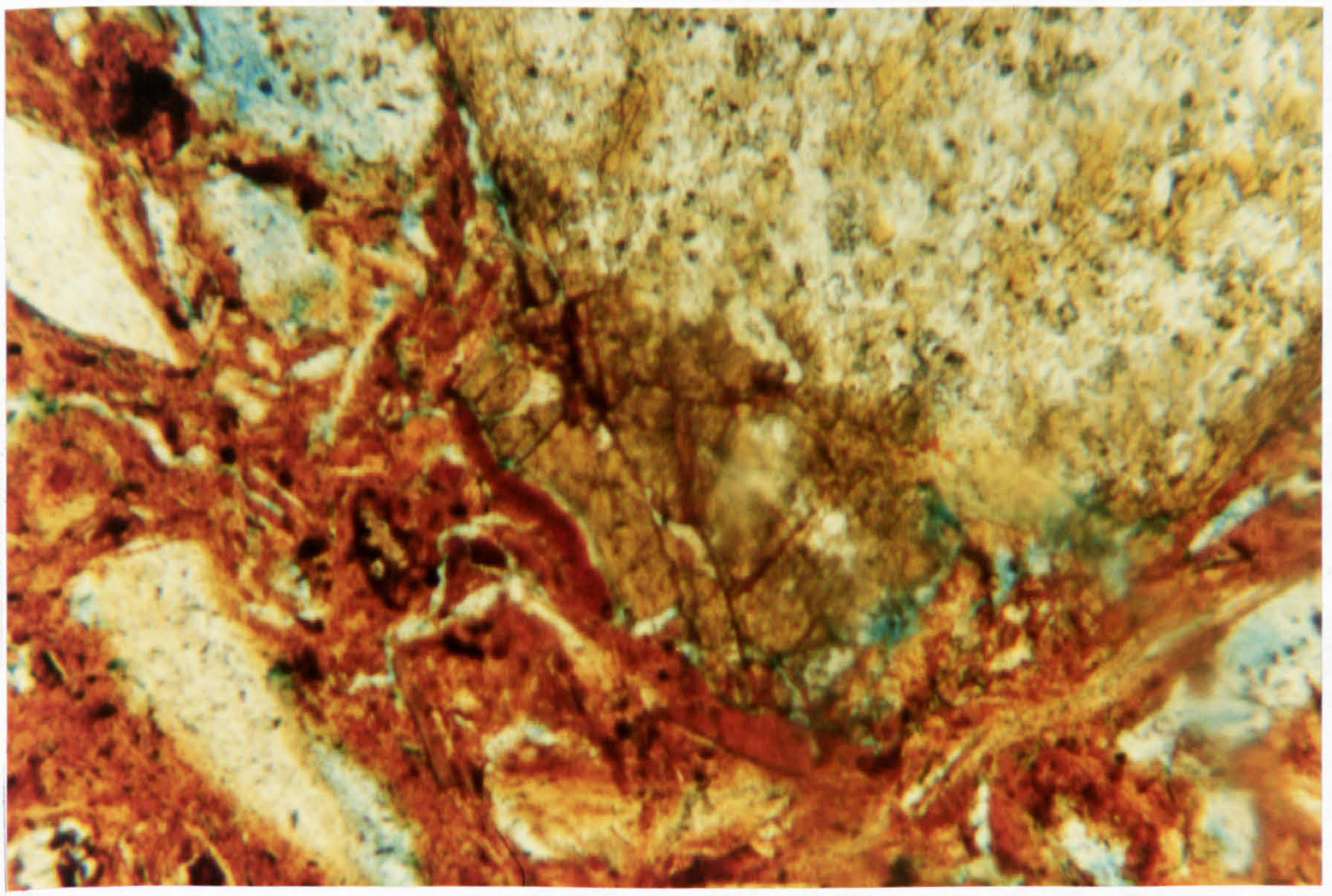

Plate 8.29-Residual soil fired at 1100°C for 2 h. P.p.l., 35x.

CHAPTER 8

8.4 INDUSTRIAL IMPLICATIONS

The technological importance of calcareous clays in clay products industry becomes evident from their ease of vitrification which facilitates firing. Vitrification commences in these clays at a relatively low firing temperature of about 800°C. The resulting morphology remains essentially unchanged up to the stage of bloating (between 1000°and 1150°C). Consequently, the control of firing temperature may not be particularly critical. In contrast, vitrification in non-calcareous clays intensifies with increasing temperature. Therefore the quality of the fired product can vary quite considerably with changes in firing temperature.

8.5 GENERAL FEATURES

Observations of the features of electron micrographs of the clay bodies and their compositions carried out in conjunction with the correlative energy dispersive X-ray analysis led to the following conclusions.

(i). The strength development of bodies fired at relatively low temperatures (of about 800°C) may have resulted from the formation of favourable structures with fibrous matrix hastening intergranular bonding of materials. The presence of traces of glassy phase may also have been beneficial; the layers of glass surrounding the grains probably originated from reactions with original coatings of fluxing materials, particularly iron bearing minerals.

(ii). The presence of lime up to 4 wt% in clay bodies is effective in promoting early vitrification. The development of large amount of glassy phase in lime containing bodies presumably resulted in a homogeneous matrix. This favourable structure with fewer pores had better properties at intermediate firing temperatures (800 -1000°C).

(iii).Well developed long needles of secondary mullite (maximum grain size:20 μm) were formed in $CaCO_3$ compositions fired at 1100°C. Formation of globular primary mullite was inhibited. In contrast, the equivalent lime-free clays

contained both relatively small mullite needles (maximum grain size: 15 μm) and globular primary mullite. It seems probable that $CaCO_3$ promoted the direct growth of secondary mullite crystals. It was apparent, however, that the onset temperature of mullite formation was slightly increased by $CaCO_3$ in the clays studied. The highly viscous lime glasses presumably inhibited the nucleation of mullite. At higher temperatures, however, glasses became sufficiently fluid to permit the recrystallization and grain growth of mullite. A minimum firing temperature of about 1000°C was found to be necessary for the nucleation of mullite. It appeared that the first clusters of mullite crystals developed in the feldspar grains. These grains retained the pseudomorphic outlines of the original feldspar grains. For both types of clay, the composition of secondary mullite approximates to an Al_2O_3:SiO_2 ratio of 2:1 whereas that of primary mullite approaches a ratio of 1:1.

(iv). Interlocking mullite needles having a reinforcing effect on the matrix probably contributed to the strength development of the fired product. The effects of vitrification and porosity, however, cannot be overlooked in drawing conclusions as to the relation of structure to strength.

(v). The essential morphological features identified in lime-containing clays were:

(a) Extensive formation of a continuous layer of glass at 800°C, which indicates their relative ease of vitrification.

(b) Uniform morphology until the stage of bloating is reached at a temperature between 1000°and 1150°C. This is consistent with a low-porous, homogeneous fired body.

(c) Growth of well developed secondary mullite at the expense of primary mullite.

(vi). The occurrence of bloating in the fired material at high temperatures was characterised by the specimens containing isolated ovoid pores which are abundant. Escalation of firing beyond this temperature can be detrimental.

(vii).It is evident from the variations of microstructure that changes in firing schedule are reflected rapidly in the final texture of the product. It may be concluded that both the firing temperature and soaking period are important factors in the development of favourable texture.

CHAPTER 9

THE REACTIONS OF PHOSPHATES WITH NATURAL CLAYS

9.1 THE USE OF PHOSPHATES AS BONDING AGENTS

The literature review (Section 2.4.5) indicates that the bonding property of phosphates has the potential of application in clay products industry. With the emergence of a somewhat clear picture of phosphate-clay mineral reactions, it was deemed desirable, therefore, to examine the effectiveness of phosphate bonding for clay products. The primary objective of the investigation was to develop satisfactory phosphate-bonded clay products with less energy intensive fabrication techniques rather than to the study of sintering mechanisms. Therefore more emphasis was placed upon determining the temperature dependence of strength and other physical and mechanical properties, densification and constitution of experimental clay bodies. The investigation consisted of experiments designed to:

(i). establish conditions most favourable for the phosphate-silicate reaction in relation to the properties of the fired product,

(ii). formulate experimental compositions and conditions for the preparation and firing of clay bodies,

(iii). evaluate the influence of processing variables on the physical and material properties of the fired product,

(iv). investigate the possibility of lowering the normal firing temperature of clay bodies through the low temperature reactions of phosphates and clays,

(v). examine the changes in constitution and microstructure of fired bodies by XRD, SEM and IR spectroscopy,

(vi). clarify the mechanism by which the strength of clay bodies containing phosphates is affected.

CHAPTER 9

9.2 MATERIALS USED

9.2.1 Clay

In view of the wide scope of the investigation, the initial experiments were limited to only one clay, viz. Residual soil LSK2A. The clay is extensively used in the brick industry, particularly in the central highlands of the island. The chemical and mineralogical composition and particle size distribution of the clay are given in Section 3.3.

9.2.2 Phosphatic binders and admixtures

The phosphatic binders and admixtures used individually or in combination were:

(i). Orthophosphoric acid (H_3PO_4 - weight per ml 1.75g).

(ii). Diammonium hydrogen phosphate [$(NH_4)_2HPO_4$].

(iii).Calcium phosphate [$Ca_3(PO_4)_2$].

(iv). Calcium oxide (CaO).

All the materials were of analar grade.

9.3 METHOD OF FABRICATION

9.3.1 Clay bodies constituted with H_3PO_4 and $(NH_4)_2HPO_4$

The effects of phosphate treatment with H_3PO_4 and $(NH_4)_2HPO_4$, and equilibrium pH value of clay mixes prepared under different maturing conditions on the final properties of fired clay products were investigated in relation to the above system. For this purpose, seven clay mixes were prepared under different experimental conditions as described below.

9.3.1.1 Preparation of specimens

1 M solutions of orthophosphoric acid (pH 0.9) and di-ammonium hydrogen phosphate (pH 7.6) were prepared using deionised distilled water and mixed in predetermined proportions to adjust the pH of the bulk solution to desired levels. The levels of pH were such as to give

equilibrium pH values ranging from 3 to 7 to clay mixes when treated with a fixed volume of phosphate solution. This volume which imparts proper moulding consistency to a clay mix was predetermined from blank trials.

It was found from control tests that 750 g of air-dried clay required 250 ml of 1 M phosphate solution to attain the appropriate moulding consistency. The equivalent composition of 3.16 wt% phosphate ion concentration was maintained throughout the initial series of clay mixes.

A weighed sample of air-dried, disaggregated clay was treated with the required volume of phosphate solution and mixed for 15 minutes. The clay mix was then covered and allowed to mature at room temperature for 20 h, 40 h and 90 h to disperse the additives and to initiate reactions. At the end of each period of maturing, the clay mix was puddled again for 10 min. and moulded into a steel mould (160 mm x 30 mm x 15 mm) with a steel plunger. A uniform moulding moisture content of about 20% was maintained in all the mixes. The moulding moisture content and equilibrium pH of the clay mix were determined according to BS 1377:1975 (Methods of test for civil engineering purposes). All pH determinations were carried out using a WPA-C10 bench type pH meter fitted with glass and calomel electrodes.Three batches of specimens were prepared from a clay mix of equilibrium pH 5, under maturing times of 20 h, 40 h and 90 h. A second series consisting of four batches of specimens were prepared from clay mixes of equilibrium pH 3 and 7; times of maturing corresponding to each level of pH were 20 h and 90 h. A total of seven batches of specimens were thus prepared under identical composition (3.16 wt% phosphate ion concentration) to investigate the effect of binders, the variation of equilibrium pH and the time of maturing on the fired properties of phosphate-bonded clay bodies. Control specimens were also prepared from an untreated clay mix for comparison purposes. Each batch consisted of at least 12 rectangular bars. The composition of the experimental mixes are presented in Table 9.1.

Table 9.1-Composition of experimental mixes prepared to investigate the effects of equilibrium pH and time of maturing on fired properties

(Moulding moisture content - 20%, Phosphate ion concentration - 3.16 wt%)

Designation of specimens	Weight of clay (g)	Volume of 1M phos. soln. (ml)	Mix proportions-H_3PO_4: $(NH_4)_2HPO_4$	Initial pH of phos. soln.	Initial pH of clay mix	Equil. pH of clay mix	Time of mat. (h)
K13/1,..,6	750	250	1.5:1	2.9	6.7	5.1	90
K13/7,..,12	750	250	1.5:1	2.8	6.7	5.0	40
K13/13,..,18	750	250	1.5:1	2.8	6.8	4.7	20
K11/1,..,6	720	240	14:1	1.5	6.8	3.0	20
K11/7,..,12	705	235	14:1	1.4	6.8	3.3	90
K17/1,..,6	705	235	1:18	7.5	6.8	7.4	90
K17/7,..,12	705	235	1:18	7.6	6.8	7.4	20

The experimental bars were first air-dried and then oven-dried at 105°C for 24 h and later fired in a laboratory electric muffle furnace in air at temperatures from 400° to 900°C. The temperature difference between the different firings being typically 100°C. The heating rate was 5.6°C/min. with a soaking period of 2 h at the peak temperature.

9.3.1.2 Optimisation of processing conditions

Having determined the critical equilibrium pH value, time of maturing and minimum firing temperature required to obtain an acceptable product, the second part of the study was designed to ascertain the optimum concentration of phosphate.

Four clay mixes were prepared incorporating 1 M, 2 M, 2.5 M and 3 M solutions of orthophosphoric acid and di-ammonium hydrogen phosphate at the optimum equilibrium pH determined in the first part of the study. The preparation of clay mixes and specimens were similar to that described in Section 9.3.1.1. The experimental bars were fired at

500°C with 2 h soaking at the maturing temperature. Table 9.2 presents the composition of the experimental mixes and the modulus of rupture values of fired bars.

Table 9.2-Composition of experimental mixes prepared to investigate the effect of the amount of binders on the modulus of rupture of fired bars

(Moulding moisture content - 20%)

Designation of specimens	Clay (LSK2A) (parts by weight)	Phosphate ion concentration (parts by wt.)	Average M.O.R of bars fired at 500°C (N/mm^2)
K17	100	3.16	2.55
K27	100	6.32	3.57
K2.57	100	7.90	4.00
K37	100	9.48	4.25

9.3.2 Clay bodies constituted with $Ca_3(PO_4)_2$

9.3.2.1 Outline of the experiment

Since some X-ray diffraction patterns of the clay mixes treated with phosphate solution exhibited features similar to an apparent increase in silica content in the system, an experiment was designed to investigate the effect of incorporation of phosphate as $Ca_3(PO_4)_2$. It was anticipated that if silica is released as a reaction product, Ca would interfere in phosphate-clay reactions leading to the formation of amorphous cementitious phases.

This part of the study consisted of experiments to:

(i). determine the level of pH at which the above effect is pronounced, in order to suppress the probable formation of silica by establishing appropriate conditions.
(ii). remove any undesirable silica which may transform to tridymite on heating, resulting in volume expansion and loss of strength.

(iii).utilize cold-setting reactions which possibly occur between Ca^{2+} and silica, if any, for low temperature strengthening of clay products.

9.3.2.2 Preparation of the clay mixes

Two clay mixes with the same total phosphate ion concentration as the first series but part of the phosphate incorporated as $Ca_3(PO_4)_2$ were prepared in the following manner. The initial pH of the 0.004 M phosphoric acid solution was adjusted to the desired level (5.6) by dilution with water. This level of pH was found to give an equilibrium pH of about 7 in the treated clay mix. The phosphate ion concentration of the prepared solution was ascertained. The compensating amount of $Ca_3(PO_4)_2$ required to bring the total phosphate ion concentration to 3.16 wt. % was then calculated from the difference. After proportioning, the constituents [clay and $Ca_3(PO_4)_2$] were dry mixed in a mechanical mixer for 15 min. The mix was finally treated with phosphoric acid solution, puddled for 10 min. and allowed to mature for 20 h to 90 h.

In compounding the third clay mix, it was hypothesized that if silica is released as a phosphate-clay reaction product, the ensuing Ca-silica reaction would proceed in equimolecular proportions. An additional amount of $Ca_3(PO_4)_2$ calculated on the above basis was therefore incorporated into a clay mix (maintained at equilibrium pH 5) to induce the secondary reaction. Table 9.3 presents the compositions of the prepared experimental batches.

Table 9.3-Composition of experimental mixes containing calcium phosphate

Designation of specimens	Weight of clay (g)	Volume of phosphate soln. (ml)	Mix proportions of phosphate solution	Weight of $Ca_3(PO_4)_2$ (g)	Wt % of PO_4 in clay mix	Wt % of Ca^{2+} in clay mix	Initial pH of phosphate solution	Initial pH of clay mix	Eq. pH of clay mix	Time of mat of clay mix (h)
K26/1,...,6	750	280	0.004M H_3PO_4 only	38.75	3.18	2.00	5.6	6.7	6.6	20
K23/1,...,6	750	280	210 ml 0.5M H_3PO_4+ 70 ml 1M $(NH_4)_2HPO_4$	16.46	3.56	0.85	2.8	6.8	5.1	20
K43/1,...,6	750	280	175 ml 1M H_3PO_4+ 105 ml 1M $(NH_4)_2HPO_4$	25.62	5.64	1.32	2.7	6.7	4.9	20

Rectangular bars moulded from each clay mix were subjected to the firing schedule described in Section 9.3.1.1.

9.3.3 Clay bodies constituted with H_3PO_4, $(NH_4)_2HPO_4$ and CaO

In this series, an attempt has been made to initiate reactions between potential phosphate-clay mineral reaction products and externally added CaO. For this purpose, two clay mixes of equilibrium pH 7 and 9 were prepared. They were of the same composition as the mixes described in Section 9.3.2.2 except that $Ca_3(PO_4)_2$ has now been replaced with CaO providing an equivalent amount of Ca^{2+}. The mix proportions are presented in Table 9.4. Specimens were prepared as described in the foregoing sections.

9.4 PROPERTY MEASUREMENTS

9.4.1 Modulus of rupture

Modulus of rupture was determined in accordance with ASTM designation C674-77 (Standard test methods for flexural properties of ceramic materials). The details of the test are given in Section 6.6.2.1. Mean on 6 determinations on each material was recorded.

9.4.2 Linear firing shrinkage

The linear firing shrinkage was determined according to the procedure described in Section 7.3.1.1. An average of three values was used for each reported value.

9.4.3 Absorption (24-h immersion)

The test was carried out according to the procedure specified in ASTM designation C67-78 (Standard methods of sampling and testing brick and structural clay tile). The details of the test are given in Section 5.3.1.3.

Table 9.4-Composition of experimental mixes containing phosphates and lime

Designation of specimens	Weight of clay (g)	Volume of phosphate soln. (ml)	Mix proportions of phosphate solution H_3PO_4: $(NH_4)_2HPO_4$	Weight of CaO added (g)	Wt % of PO_4 in clay mix	Wt % of Ca^{2+} in clay mix	Initial pH of phosphate solution	Initial pH of clay mix	Eq. pH of clay mix	Time of mat of clay mix (h)
K33/Blank	40	17	1.72:1	-	4.19	-	2.7	6.7	4.4	66
K33/1,...,6	750	330	1.72:1	14.0	4.19	1.33	2.7	6.7	7.2	66
K31/1,...,6	750	330	1M H_3PO_4 only pH adjusted w 50% HCl	14.0	4.19	1.33	1.2	6.8	5.4	44

9.4.4 Durability under laboratory conditions

9.4.4.1 5-h boiling test

The durability test (5-h boiling test) was carried out according to the procedure described in ASTM designation C67-78. The test specimens used in the 24-h cold water submersion test were used for the 5-h boiling test.

The specimens subjected to the 24-h submersion test were returned to the bath and submerged in distilled water at 20°C in such a manner that free circulation of water on all sides of the specimens was possible. Water in the bath was then brought to boiling within 1 h and boiling was continued for 5 h. After allowing to cool to room temperature, the specimens were wiped off with a damp cloth and weighed within 5 minutes. The absorption of each specimen was calculated as follows:

$$\text{Absorption, \%} = 100(W_b - W_d)/W_d$$

where W_d = dry weight of the specimen, and

W_b = saturated weight of the specimen after submersion in boiling water.

Average absorption of all the specimens tested was reported as the absorption of the lot.

9.4.4.2 Saturation coefficient

The saturation coefficient is the ratio of absorption by 24-h submersion in cold water to that after 5-h submersion in boiling water. It was calculated for each specimen as follows.

$$\text{Saturation coefficient} = (W_c - W_d)/(W_b - W_d)$$

where W_c = saturated weight of the specimen after 24-h submersion in cold water

9.4.5 Bulk density

The bulk density was determined according to the procedure described in ASTM designation C373-72 (Standard test method for water absorption, bulk density, apparent porosity and apparent specific gravity of fired whiteware

products). The method of determination is described in Section 7.3.1.2. The bulk density was calculated as follows.

$$\text{Bulk density (B)} = W_d/V = W_d/(W_b - W_s)$$

where V = exterior volume

W_s = weight of specimen while suspended in water

An average of three values was used for each reported value.

9.5 EFFECT OF PHOSPHATE ADDITION ON THE FIRED PROPERTIES

9.5.1 Phosphate-bonded clay bodies without other additives

9.5.1.1 Strength

Modulus of rupture as a function of firing temperature (Table 9.5) is shown for the three clay mixes in Fig. 9.1, which also depicts the effect of variation of maturing time of each clay mix.

Table 9.5-Modulus of rupture of fired phosphate-bonded clay bars

Conditions of preparation		Modulus of Rupture in N/mm^2 at firing temperatures shown					
Eq. pH of mix	Mat. time (h)	400°C	500°C	600°C	700°C	800°C	900°C
3	20	1.40	1.19	0.70	1.09	1.15	1.14
(K11)	90	1.54	1.53	1.37	1.24	1.19	1.17
	20	1.92	2.08	1.71	1.24	1.66	1.96
5	40	1.15	1.42	1.19	1.17	1.18	1.34
(K13)	90	0.57	1.32	0.96	0.67	0.72	0.92
7	20	1.98	2.32	1.94	2.01	1.56	1.72
(K17)	90	2.41	2.55	2.10	1.86	1.99	1.85

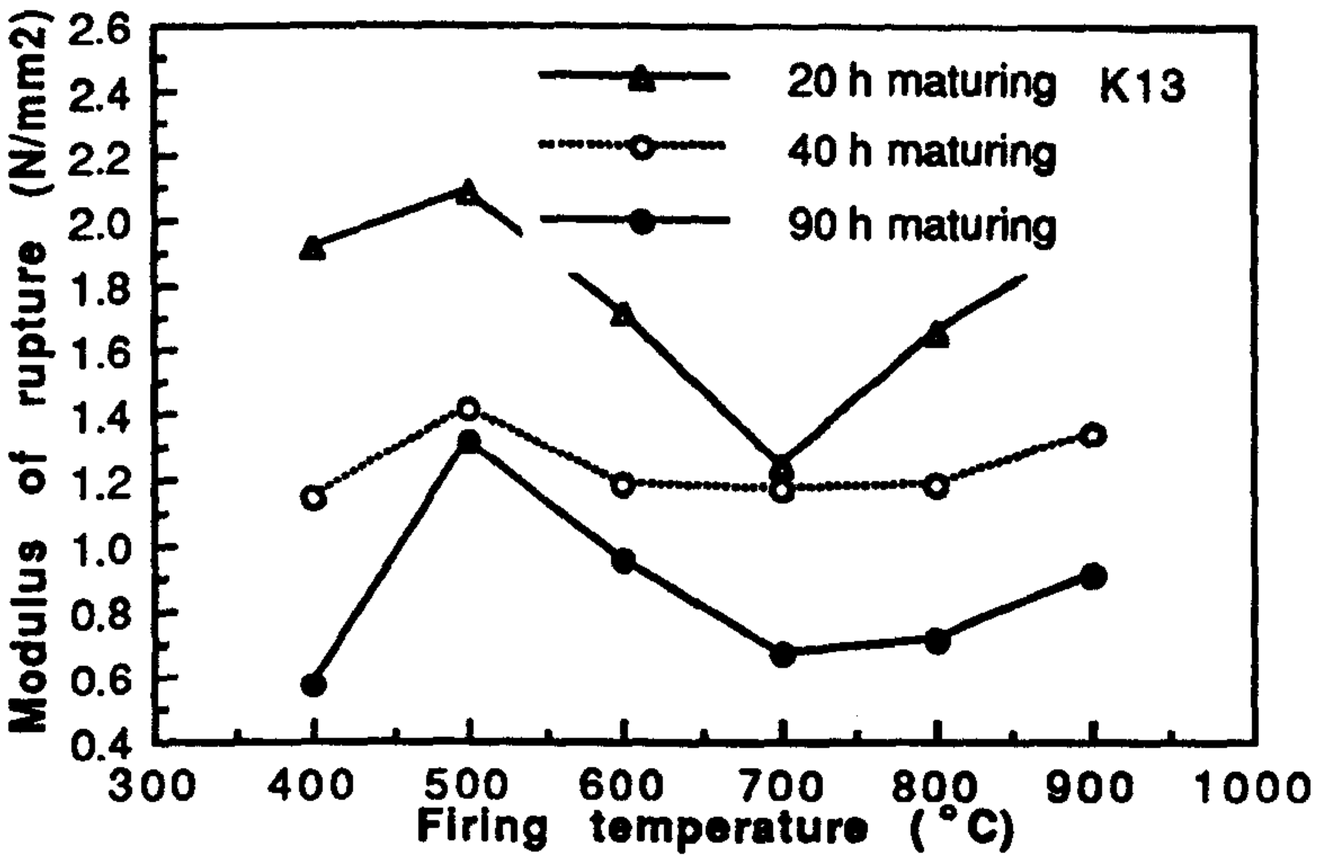

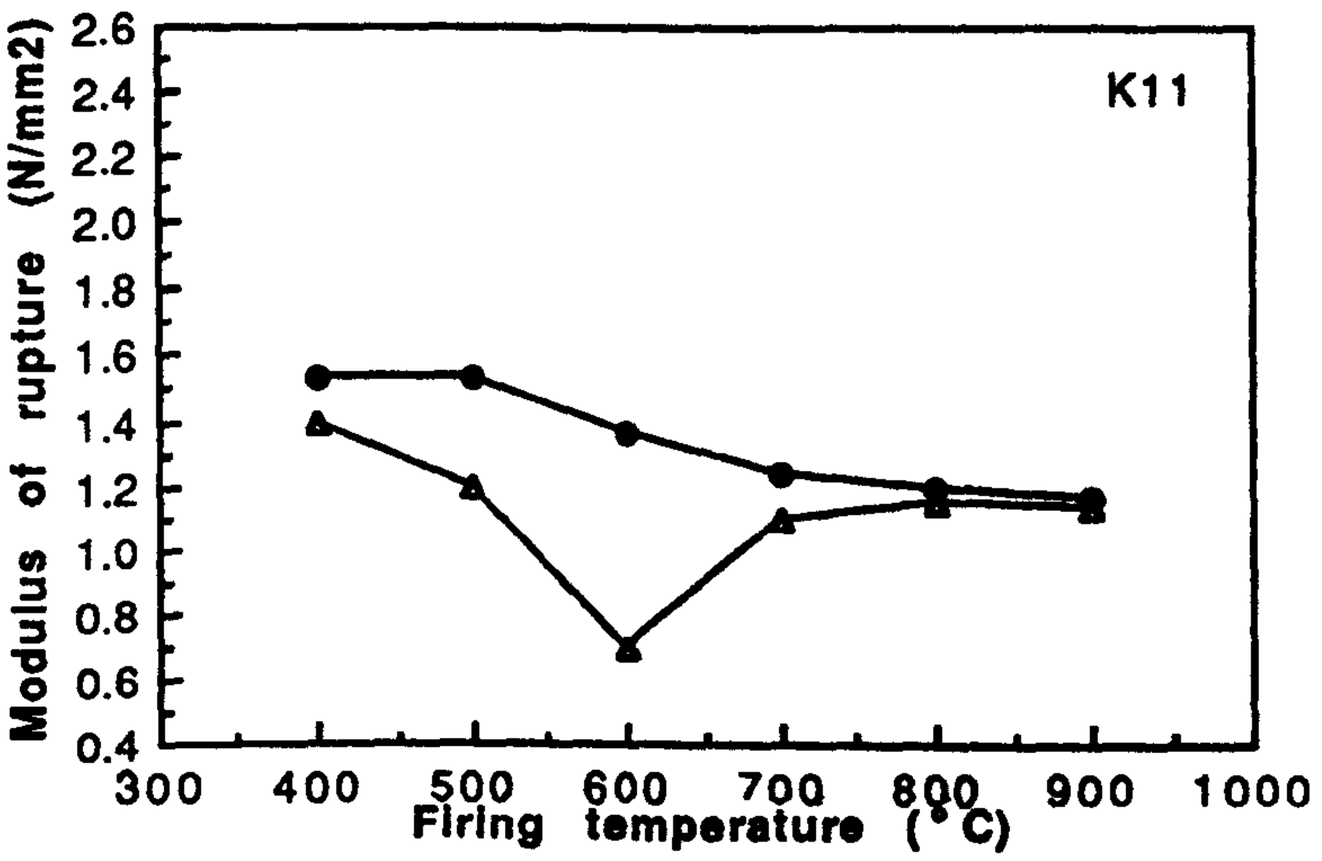

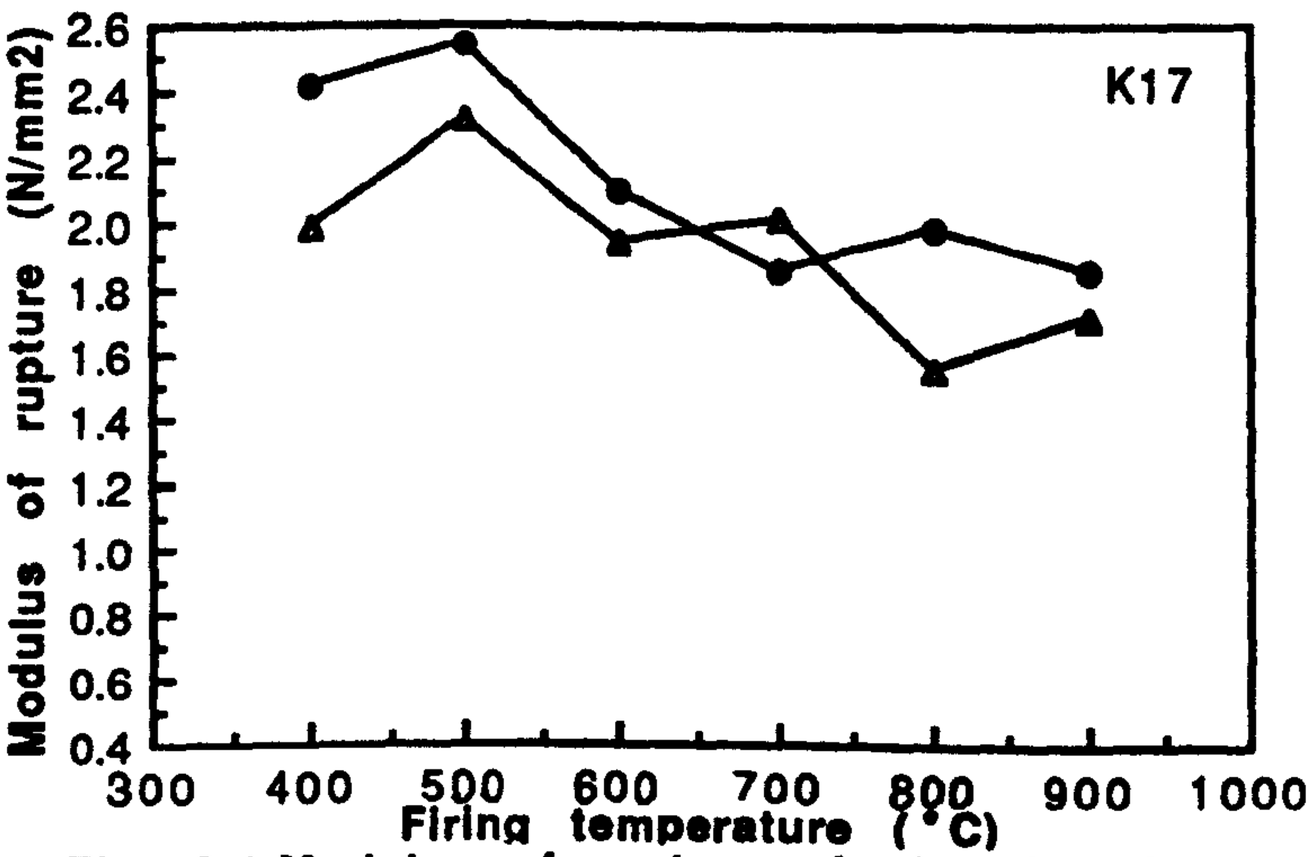

Fig. 9.1-Modulus of rupture of phosphate-bonded bars fired at various temperatures.

CHAPTER 9

Marked changes in modulus of rupture with equilibrium pH of the clay mix were shown by the clay bodies. Highest fired strengths (2.32-2.55 N/mm^2) were associated with clay bodies prepared at an equilibrium pH 7.4 (K17). Bars representing the clay mix of equilibrium pH 5 (maturing time 20 h) had intermediate strengths whereas an analogous set of bars from the clay mix of equilibrium pH 3 had the lowest strengths. In general, the modulus of rupture increased sharply when the firing temperature was raised from 400° to 500°C, at which a maximum was attained. Above this temperature, modulus of rupture of both K17 and K13 bodies dropped steeply while that of the K11 body dropped gradually as the firing temperature was increased to about 600-700°C. An apparent increase in strength above 700°C was discernible in the K13 body. Bodies fired at the optimum temperature of 500°C gave strengths of the order of 60% higher than the normal clay bodies fired at 800°C (1.6 N/mm^2). Clay mixes within each batch exhibited similar trends irrespective of their extent of maturing

The effect of variation of maturing time of clay mix on the modulus of rupture of fired bars is also illustrated in Fig. 9.1. A substantial increase in modulus of rupture with increasing maturing time from 20 h to 90 h was evident in the two clay bodies K17 and K11. The gain in strength due to prolonged maturing of the K17 body fired at 500°C was approximately 10%. In contrast, the strength of the clay body prepared at the equilibrium pH 5, deteriorated gradually on maturing; the strength dropped from 2.08 N/mm^2 to 1.32 N/mm^2 on prolonging the maturing from 20 h to 90 h.

The influence of the amount of binders on the modulus of rupture at a constant firing temperature (500°C) is illustrated in Fig. 9.2, which shows that a curvilinear relationship with a gradual approach of a maximum exists for mixes containing up to 9.5 parts by weight of phosphate concentration (Table 9.2).

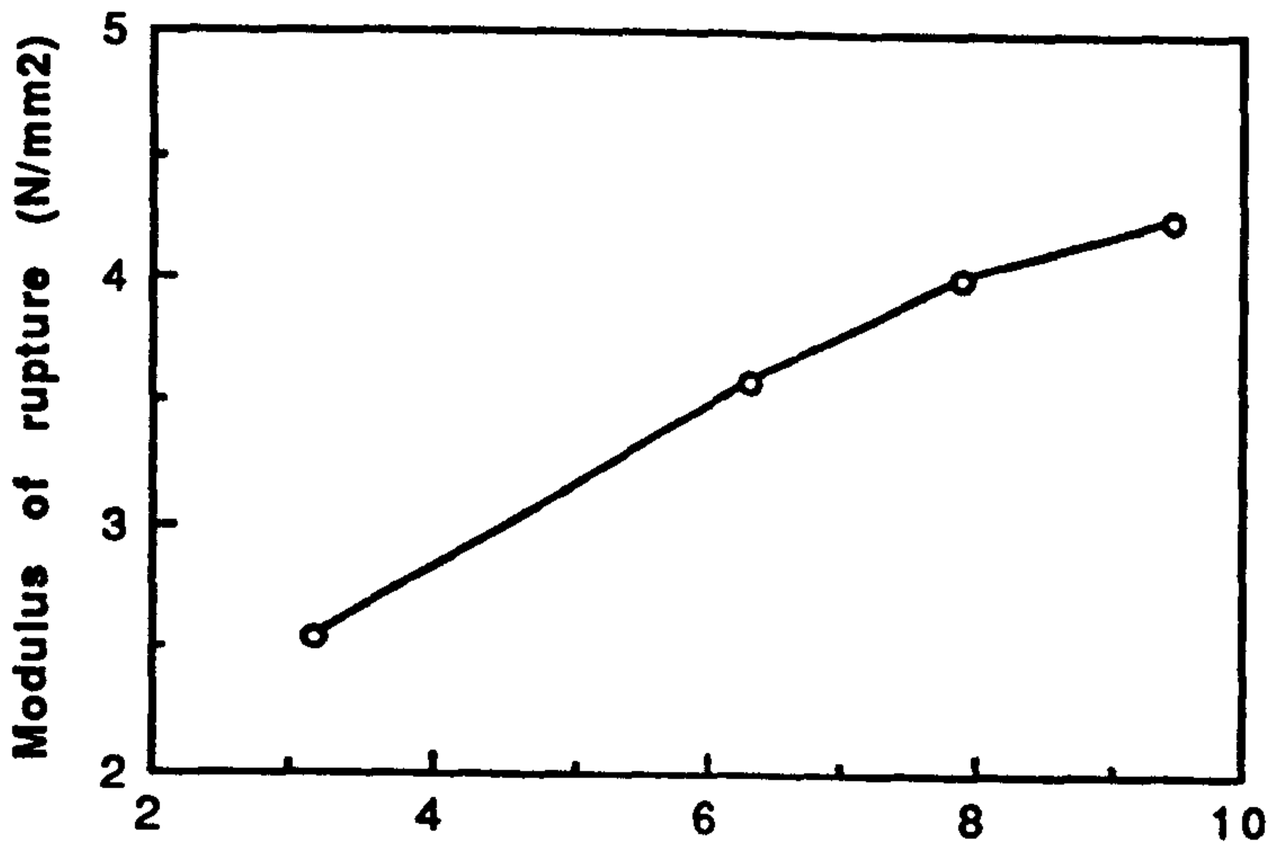

Fig. 9.2-Relationship between modulus of rupture and phosphate ion concentration.

It can thus be deduced from the above that admixture bodies containing 3.16 wt% phosphate prepared from clay mixes of equilibrium pH 7.4 when matured for 90 h give promising strengths; the optimum firing at 500°C with a soaking period of 2 h seems adequate for such bodies.

The clear pH dependence of strength can be interpreted in terms of the relative abundance of OH groups available for structure formation and the extent of collapse of kaolinite lattices at different levels of pH. The optimum strength achieved on firing at 500°C may be attributed to the favourable structures formed by reactions of phosphates with clay minerals. Preferential structure formation probably occurred at different levels of pH. Rearrangement of these metastable structures at temperatures above 500°C, however, resulted in loss of strength. Supporting evidence for the above was obtained from the DSC, XRD, IRA and SEM studies.

9.5.1.2 Bulk density

The bulk density results on each batch presented in Table 9.6 are plotted in Fig. 9.3 for various firing temperatures.

Table 9.6-Physical properties of fired phosphate-bonded clay bars

Designation of clay mix	Property		Average value of property at temperatures shown					
			400°C	500°C	600°C	700°C	800°C	900°C
K11	Bulk density (g/cm3)	20 h mat	1.52	1.45	1.50	1.49	1.45	1.47
		90 h mat	1.52	1.51	1.50	1.48	1.48	1.45
	% Absorption (24 h)	20 h mat	19.22	20.06	20.23	21.24	22.40	21.41
		90 h mat	18.64	19.51	20.52	21.40	21.78	21.39
	% Absorption (5 h b)	20 h mat	23.24	24.60	25.03	25.70	26.75	26.32
		90 h mat	22.56	24.06	25.27	25.95	26.29	26.58
	Sat. coefficient	20 h mat	0.83	0.81	0.81	0.82	0.84	0.81
		90 h mat	0.83	0.81	0.81	0.82	0.83	0.82
	% Weight loss	20 h mat	3.15	4.38	5.24	6.67	7.33	7.38
		90 h mat	3.09	4.43	5.69	6.81	7.29	7.58
	% Drying shrinkage	20 h mat			Average=6.25			
		90 h mat			Average=6.45			
	% Firing shrinkage	20 h mat	-	-	-	-	1.33	-
		90 h mat	-	-	0.67	-	-	0.67
K13	Bulk density (g/cm3)	20 h mat	1.54	1.46	1.46	1.48	1.48	1.46
		40 h mat	1.52	1.49	1.49	1.45	1.43	1.49
		90 h mat	1.48	1.46	1.41	1.46	1.46	1.43
	% Absorption (24 h)	20 h mat	19.68	20.85	21.87	22.33	22.51	21.60
		40 h mat	19.28	20.92	21.83	22.12	22.92	21.83
		90 h mat	20.37	21.79	21.99	22.68	23.10	22.79
	% Absorption (5 h b)	20 h mat	23.65	25.43	26.53	26.89	27.04	26.80
		40 h mat	23.03	25.69	26.79	26.93	27.46	26.96
		90 h mat	24.28	26.71	26.48	27.29	27.45	27.72
	Sat. coefficient	20 h mat	0.83	0.82	0.82	0.83	0.83	0.83
		40 h mat	0.84	0.81	0.81	0.82	0.83	0.81
		90 h mat	0.84	0.81	0.83	0.83	0.84	0.82
	% Weight loss	20 h mat	3.40	5.15	6.70	7.56	7.86	8.23
		40 h mat	3.16	4.88	6.18	7.16	7.49	7.76
		90 h mat	3.34	5.86	6.28	7.05	7.57	7.93
	% Drying shrinkage	20 h mat			Average=7.29			
		40 h mat			Average=6.77			
		90 h mat			Average=6.25			
	% Firing shrinkage	20 h mat	0.67	-	0.67	-	0.67	1.33
		40 h mat	-	-	-	-	-	1.34
		90 h mat	-	0.67	-	-	0.67	0.67
K17	Bulk density (g/cm3)	20 h mat	1.63	1.62	1.58	1.56	1.56	1.57
		90 h mat	1.61	1.60	1.58	1.53	1.52	1.57
	% Absorption (24 h)	20 h mat	16.46	17.07	18.44	18.74	19.17	19.10
		90 h mat	16.60	17.48	18.37	19.05	19.30	19.11
	% Absorption (5 h b)	20 h mat	20.82	21.44	23.36	23.53	23.74	24.21
		90 h mat	20.78	21.86	23.24	23.72	23.65	23.89
	Sat. coefficient	20 h mat	0.79	0.80	0.79	0.80	0.81	0.79
		90 h mat	0.80	0.80	0.79	0.80	0.81	0.80
	% Weight loss	20 h mat	3.42	4.18	6.76	7.50	7.74	8.30
		90 h mat	3.64	4.98	6.87	7.71	7.99	8.37
	% Drying shrinkage	20 h mat			Average=8.65			
		90 h mat			Average=8.75			
		20 h mat	0.68	0.68	0.68	-	0.68	0.68
		90 h mat	0.68	0.68	0.68	-	-	0.68

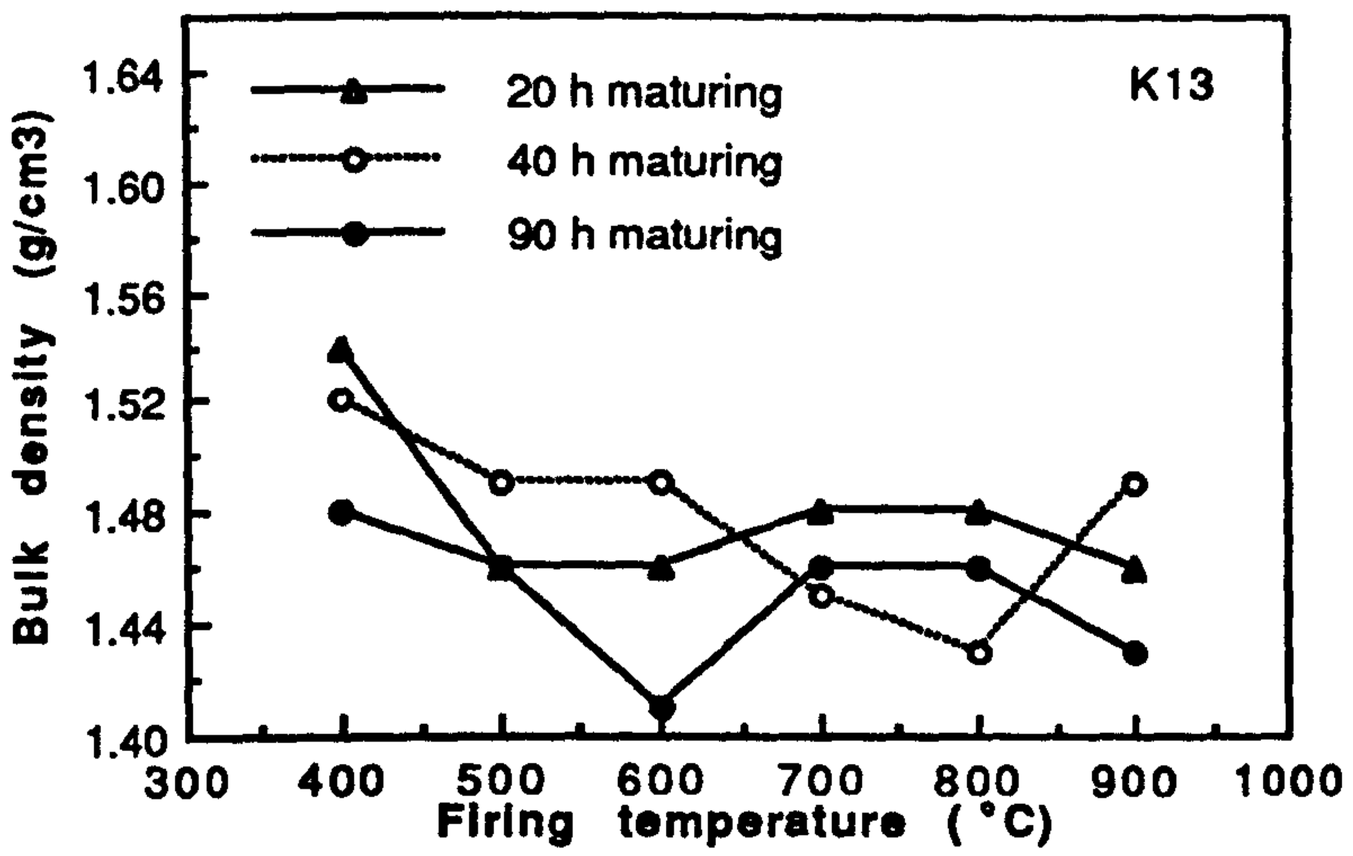

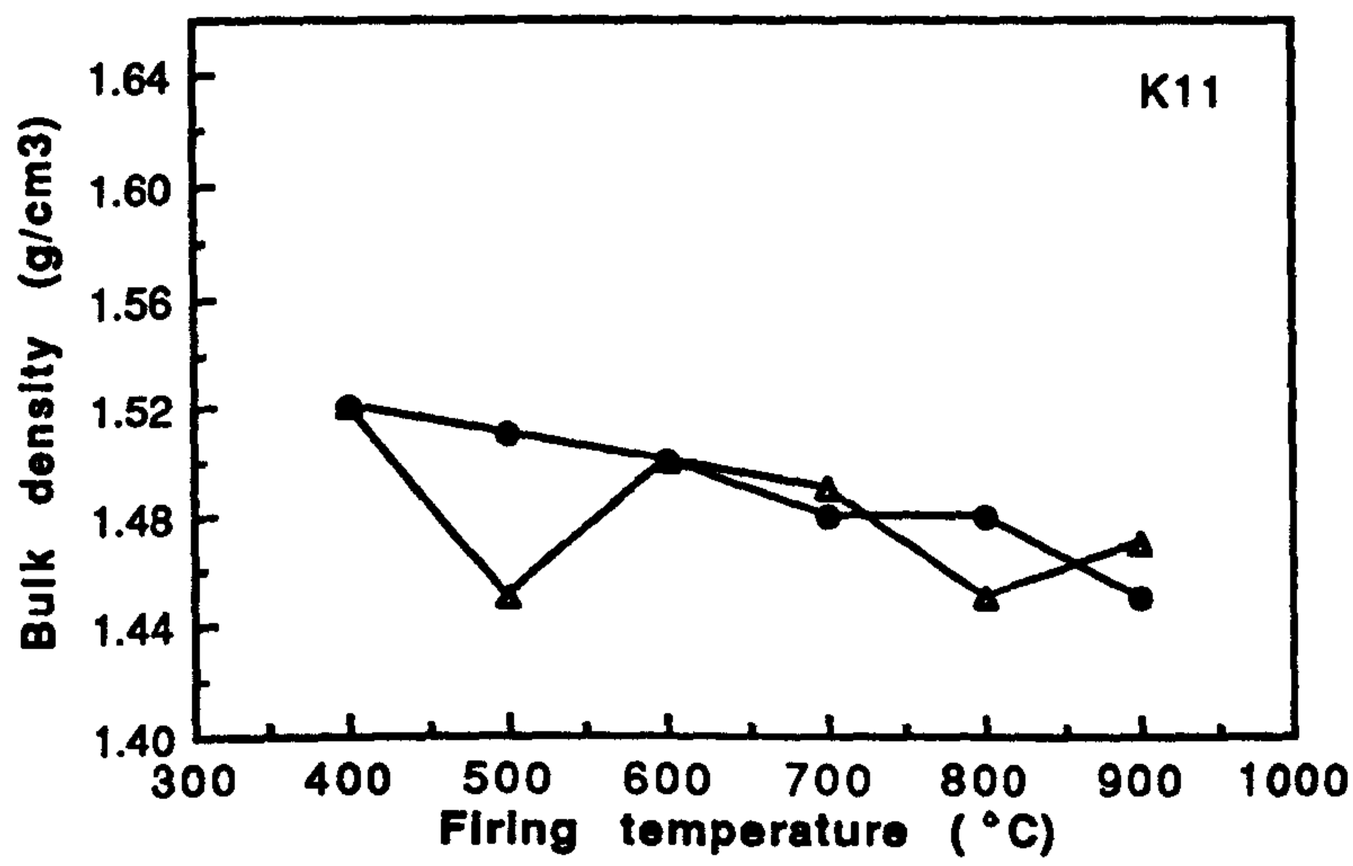

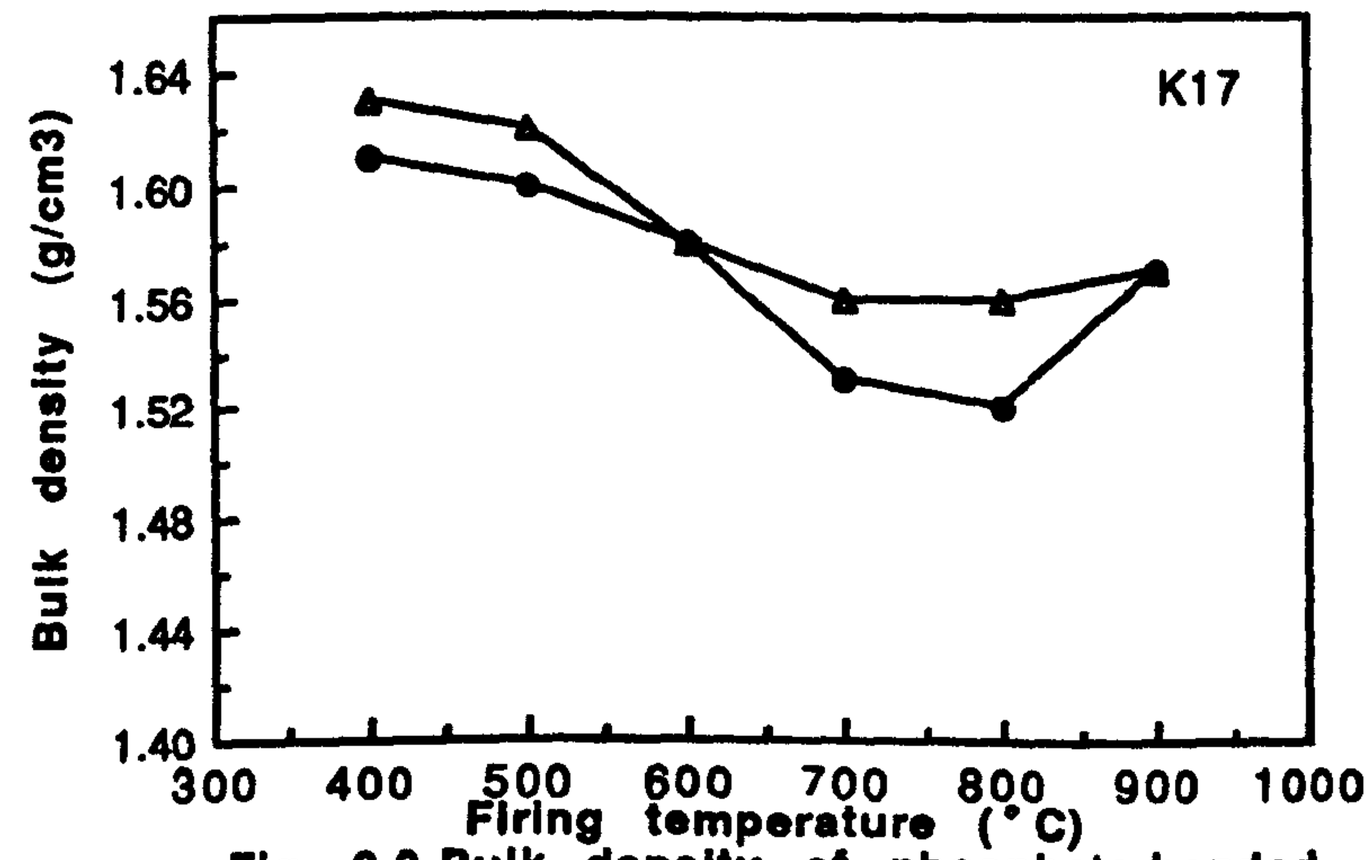

Fig. 9.3-Bulk density of phosphate-bonded bars fired at various temperatures.

A comparison of the data given on Figs. 9.1 and 9.3 shows the similar trends displayed by the two parameters, modulus of rupture and bulk density. However, an irregularity was noted; between 700° and 800°C, the densification curve of the K13 body showed an arrest in slope not observed in the corresponding trend in strength.

The modulus of rupture and bulk density show consistent changes with increasing firing temperature. Fig. 9.4 shows the plot of modulus of rupture versus bulk density of bars made from the three clay mixes and fired at various temperatures. Each point on the curve represents an average of at least 3 determinations. Although results show a considerable scatter which was not unexpected owing to the small cross-section of the specimens and the consequent relative increase in the effect of surface flaws, there seems to be a reasonable correlation between these two parameters over the range of temperature 400 -900°C.

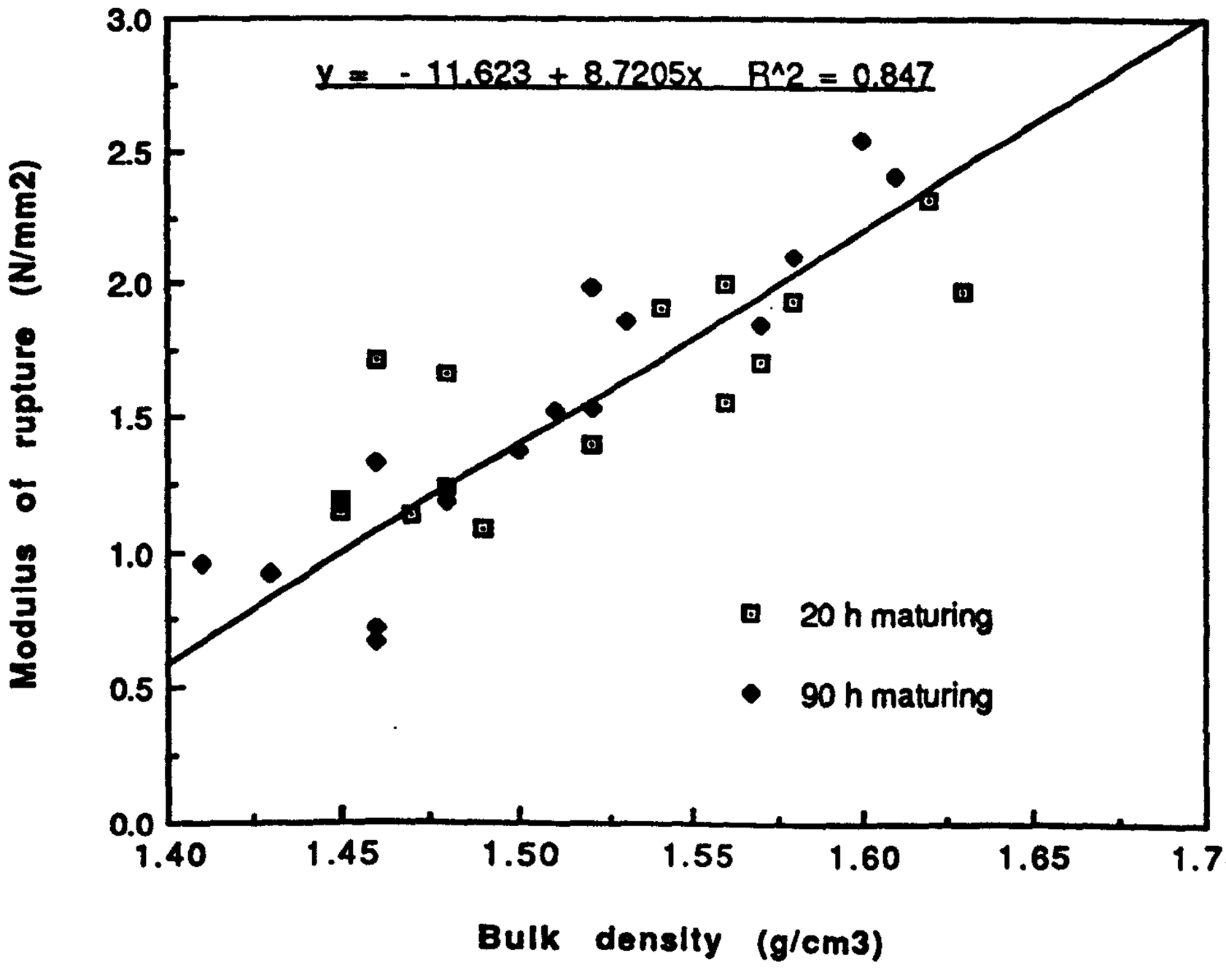

Fig. 9.4-Relationship between modulus of rupture and bulk density.

The regression equation is given by: M.O.R =8.72 B.D - 11.62

The correlation coefficient has a value of 0.92. This also raises the possibility that the bulk density could serve as a useful site acceptance test similar to the slump test in structural concrete.

9.5.1.3 % Absorption (24-h immersion)

The 24-h absorption for the bodies (Table 9.6) versus firing temperature is shown in Fig. 9.5. All the bodies, in particular the K17 body of promising strength initially had low absorption values (low porosities). Increase in firing temperature caused a progressive increase in porosity up to 800°C, followed by a steep drop. This contrasts with the situation for normal clay bodies where a rapid approach of a minimum at high temperature was seen (Fig. 7.3). Relatively low porosities of phosphate-bonded clay bodies fired at low temperatures (400 -500°C) suggest the possibility of compound formation by precipitation infilling the pores. This effect was more pronounced in the K17 body. The dissociation of compounds at higher temperatures probably caused evolution of gaseous matter resulting in increased porosity. Above 800°C, the decrease in porosity suggests the onset of sintering process, evidence of which could be seen on the fired samples.

9.5.1.4 Shrinkage

The wet-to-dry shrinkage of bars (Table 9.6) from the demoulded stage (moisture content-15%) to the oven-dry stage (105°C, 24 h) depended on the composition of the clay mix. Experimental bars made from the three clay mixes K11, K13 and K17 had wet-to-dry shrinkages of 6.3%, 6.8% and 8.7% respectively. The favourable composition (K17) had a comparatively high shrinkage at the green stage.

Phosphate-bonded bodies had remarkably low firing shrinkages when compared with those of conventional clay bodies. The clay body K17 had a consistently low firing shrinkage of 0.67% over the range of firing temperature from 400°to 900°C. Although the firing shrinkages of the two clay bodies K11 and K13 were somewhat high, the three bodies

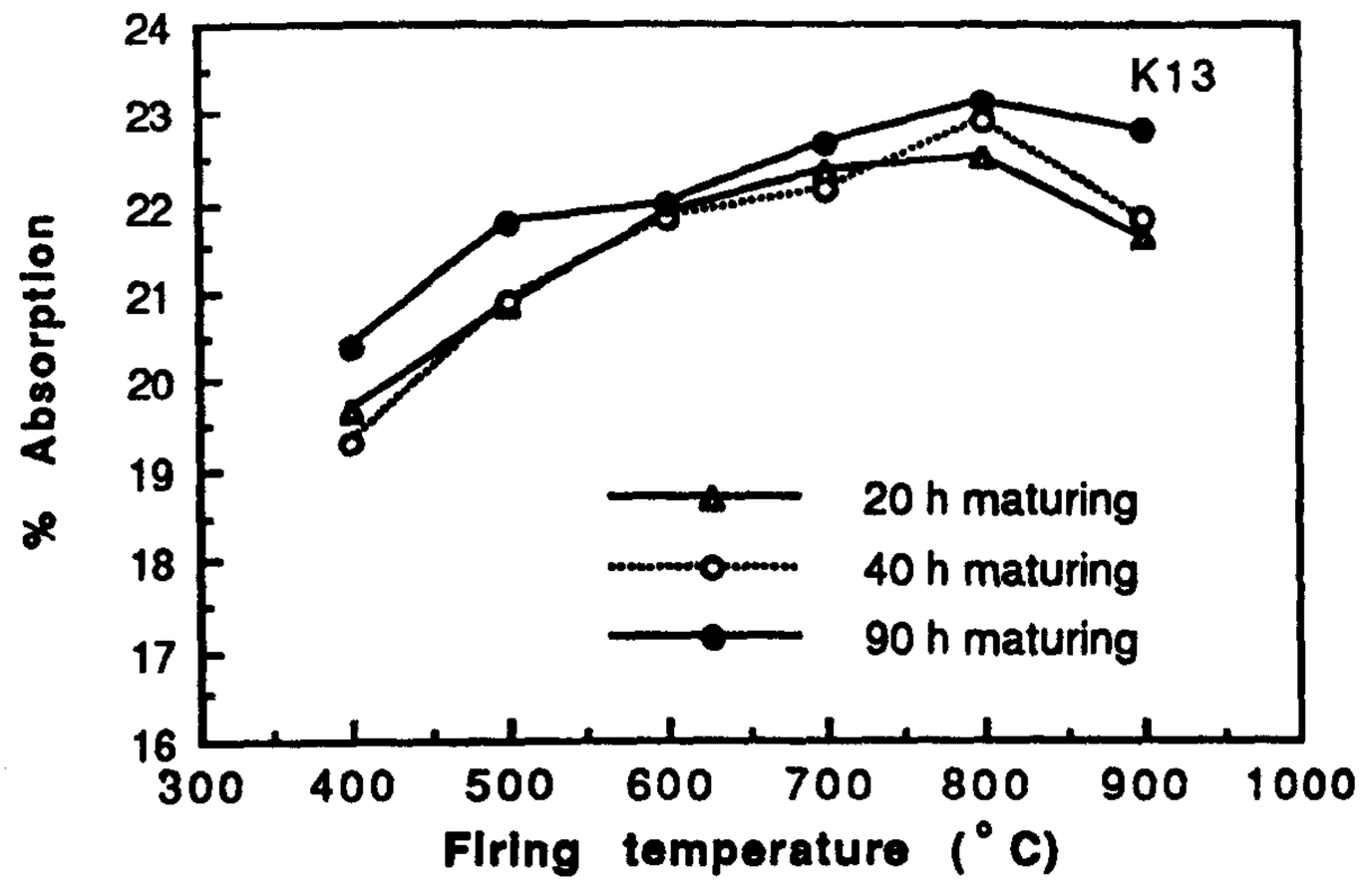

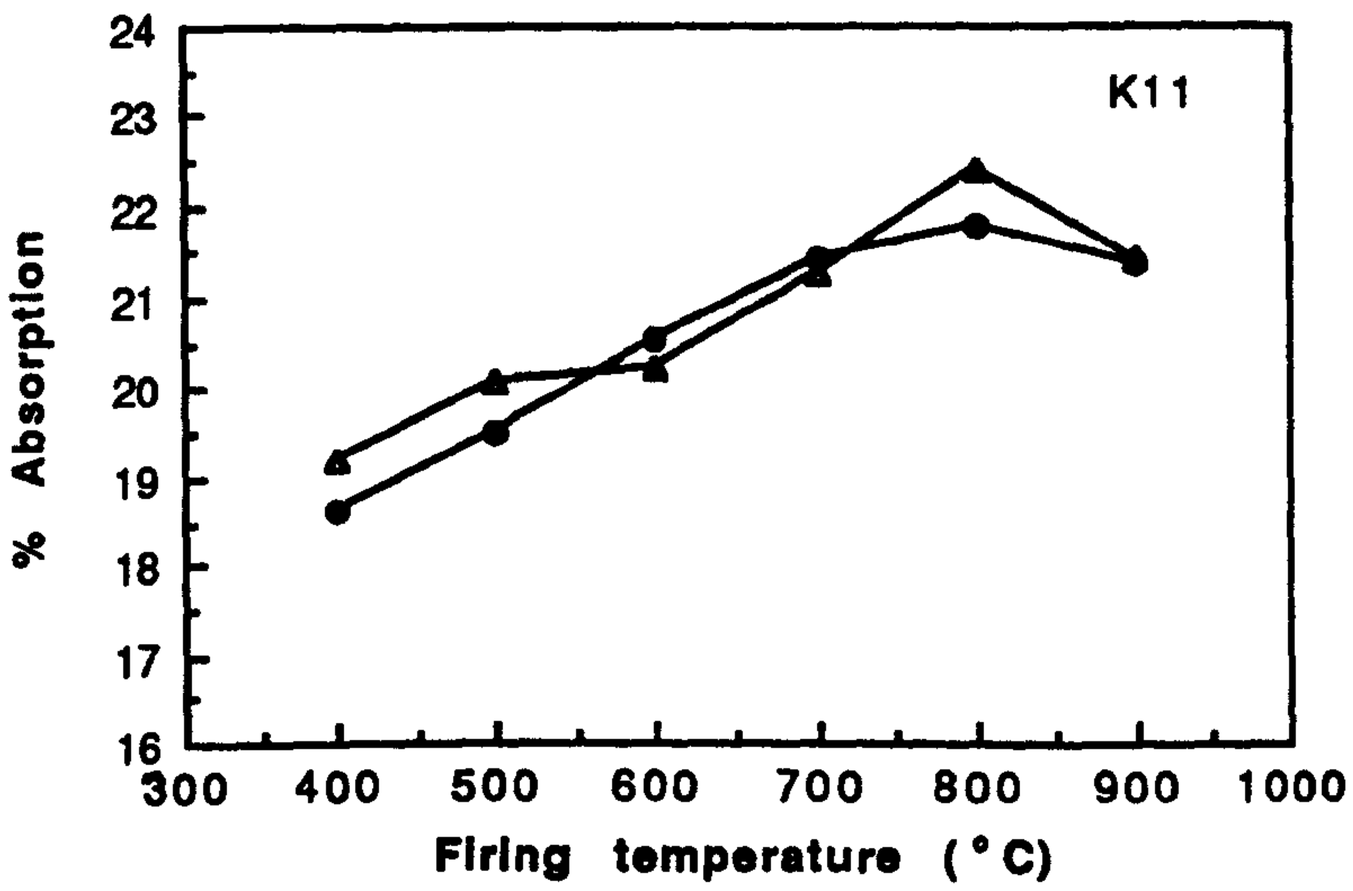

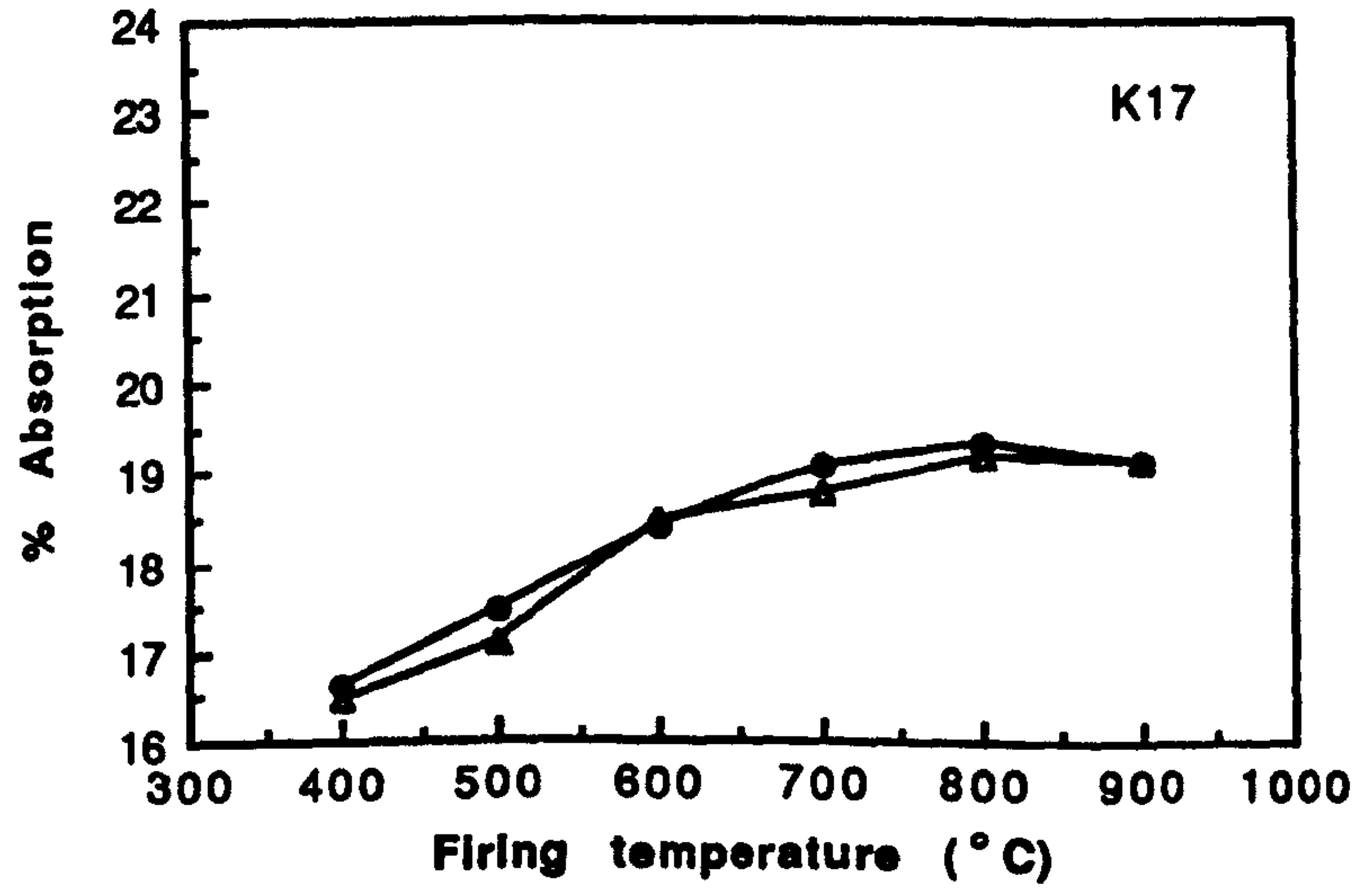

Fig. 9.5-%Absorption of phosphate-bonded bars fired at various temperatures.

were of better dimensional stability. It is conceivable that the low shrinkage of phosphate-bonded bodies is due to the quartz type inversions of aluminium phosphate which are believed to occur at lower temperatures than in silica (Section 2.4.5.3, Beck 1949). The samples fired at 500°C yielded DSC and SEM evidence of the formation of such amorphous products. Differential shrinkage behaviour of the three clay bodies indicate varying degree of formation of reaction products in them. On the other hand, the experimental systems do not support the possibility of retardation of the sintering process which may also cause a reduction in shrinkage in showing signs of sintering at about 800°C (Figs. 9.1 and 9.3).

9.5.1.5 Redevelopment of strength on boiling

Phosphate-bonded clay bars fired at various temperatures were tested for flexural strength after boiling in water for 5 h followed by oven-drying at 105°C for 24 h. Control bars made from a clay mix without any admixture and fired together with the test samples were also tested under similar conditions for comparison purposes. The modulus of rupture values and percentage gain in strength for different clay mixes are presented in Table 9.7. (Percentage gains within a range of experimental error of 10% have been excluded in the tabulation). The change in strength of the promising composition, K17, is depicted graphically in Fig. 9.6.

It is evident from the experimental results that clay bars made from the three mixes showed appreciable gain in strength when fired at specific temperatures between 400°and 900°C followed by boiling. Those fired at the optimum temperature (500°C) showed a substantial gain in strength. The highest modulus of rupture of 500°C fired clay bars made from the K17 clay mix was increased to 2.94 N/mm^2 on boiling showing an overall improvement of 27%. The limits of overall strength improvement of bars fired at 500°C ranged from 10% to 27% for various clay mixes. On the other hand, the critical firing temperature corresponding to the maximum

Table 9.7-Modulus of rupture of fired phosphate-bonded clay bars before and after boiling

(Gains/losses within 10% 0mitted)

Designation of clay mix	Modulus of rupture in N/mm^2 at firing temperatures shown																	
	400°C			500°C			600°C			700°C			800°C			900°C		
	fired	fired & boiled	% gain /loss	fired	fired & boiled	% gain /loss	fired	fired & boiled	% gain /loss	fired	fired & boiled	% gain /loss	fired	fired & boiled	% gain /loss	fired	fired & boiled	% gain /loss
K11-20 h maturing	1.40	1.47	-	1.19	0.70	-41.2	0.70	0.95	35.7	1.09	1.19	-	1.15	1.21	-	1.14	0.95	-16.7
K11-90 h maturing	1.54	1.54	-	1.53	1.89	23.5	1.37	1.55	13.1	1.24	1.31	-	1.19	1.31	10.1	1.17	1.45	23.9
K13-20 h maturing	1.92	2.00	-	2.08	2.50	20.2	1.71	1.73	-	1.24	1.91	54.0	1.66	1.79	-	1.96	1.82	-
K13-40 h maturing	1.15	1.34	16.5	1.42	1.77	24.6	1.19	1.08	-	1.17	1.17	-	1.18	1.35	14.4	1.34	1.42	-
K13-90 h maturing	0.57	1.09	91.2	1.32	1.53	15.9	0.96	0.87	-	0.67	0.88	31.3	0.72	1.13	56.9	0.92	1.05	14.1
K17-20 h maturing	1.98	2.10	-	2.32	2.94	26.7	1.94	2.28	17.5	2.01	2.26	12.4	1.56	1.95	25.0	1.72	1.82	-
K17-90 h maturing	2.41	2.59	-	2.55	2.81	10.2	2.10	2.37	12.8	1.86	2.18	17.2	1.99	1.92	-	1.85	1.79	-

gain in strength on boiling depended on the consistency of the clay mix. The bars representing the clay mix K13 showed 91% and 57% overall improvement in strength when boiled after firing at 400°and 800°C respectively. An overall deterioration in strength on boiling, however, was seen in bars made from the K11 clay mix matured for 20 h, which in many respects behaved anomalously. The general strength enhancement was apparent from the plot for the K17 bodies (Fig. 9.6).

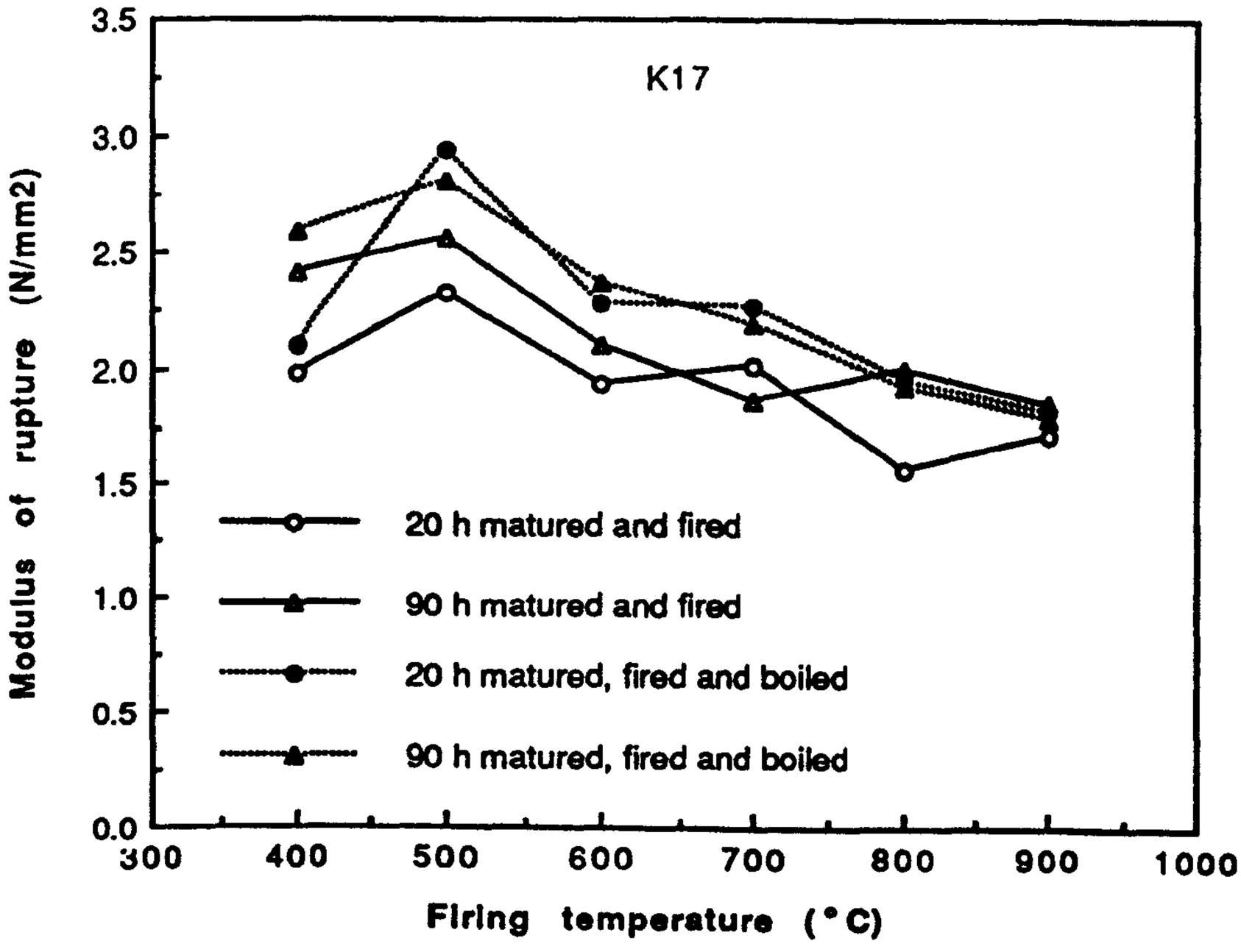

Fig. 9.6-Effect of boiling on modulus of rupture of bars made from the K17 clay mix fired at various temperatures

Bars fired between 500° and 700°C showed a consistent strength improvement on boiling. They reached values comparable to those for the unboiled samples when fired at 800°to 900°C. However, the variation in changes in strength between different batches and also within the individual batches are so wide that no definite conclusions on the

redevelopment of strength on boiling can be drawn at this stage.

The observed redevelopment of strength on boiling of phosphate-bonded clay bars may be attributed to the formation of amorphous phosphates and phosphate-silicate compounds (Section 2.4.5.3) which on hydration set to materials of high strength. It is also plausible that on firing at 500°to 700°C, disordered metakaolinite domains are formed (Brindley and Nakahira 1959) wherein an Al-O(OH)-phosphoric acid complex may readily form contributing to the strength improvement.

9.5.1.6 Durability

(i).Accelerated durability test

Phosphate-bonded bars prepared from the most promising composition (K17) and fired under the optimum conditions (500°C for 2 h) were randomly sampled for testing the durability under laboratory conditions. Bars made from a clay mix without any phosphate binder and fired at the same temperature and samples of engineering brick (LBC) satisfying BS specifications were also taken to compare the behaviour of the respective bodies under similar conditions of accelerated weathering. Twelve specimens from each batch were subjected to the test.

The procedure used in the present work was first to dry (110°C, 24 h) and cool the samples. They were then immersed in water for 2 h and after removal placed in an oven overnight at 105-110°C. The following morning the samples were cooled in a desiccator and the cycle repeated. A total of 60 cycles of alternate wetting and drying were completed within a period of three months. After the last cycle, specimens were carefully examined for cracks, disintegration and leaching of compounds.

The accelerated durability test showed that both the test and control samples did not undergo cracking or disintegration after 60 cycles of test. Weight losses were relatively insignificant. However, there was evidence of

leaching of compounds from the test samples with consequent discoloration of external surfaces.

(ii).5-h boiling test

The test procedure is described in Section 9.4.4.1. A total of 144 samples from three clay mixes (K11, K13 and K17) fired at 400°, 500°, 600°, 700°, 800° and 900°C were subjected to the test. The boiling test showed that none of the specimens disintegrated during test indicating the adequacy of the heat treatment and bonding to impart sufficient durability to fired clay. However, water absorption of the specimens increased on boiling and the resulting values of saturation coefficient are summarised in Table 9.6. The lowest saturation coefficient is associated with the K17 bars fired at 600°C.

9.5.2 Bodies containing other admixtures

Six compositions prepared in two batches (Tables 9.3 and 9.4) in order to study the effects of different phosphate admixtures on otherwise similar bodies were dried and fired in the following manner. Pressed bars made from the clay mixes according to the procedure described in Section 9.3.1.1 were first air-dried for 3 days and then oven-dried at 110°C for 24 h before firing in an electric furnace according to two firing schedules. Peak firing temperature in each case was 500°C (optimum firing temperature ascertained for the first series of clay bodies).

The two firing schedules were:

(i). <u>Normal firing</u>

Rate of heating up to 500°C - 10°C/min

Soaking period at the peak temperature - 2 h

(ii).<u>Modified firing</u>

Rate of heating up to 200°C - 10°C/min

Rate of heating from 200° to 250°C - 1.6°C/min

Rate of heating from 250° to 500°C - 8.0°C/min

Soaking period at the peak temperature - 3 h

The firing schedules are schematically represented in Fig. 9.7. The fired bars were tested for modulus of rupture. The results are summarized in Table 9.8.

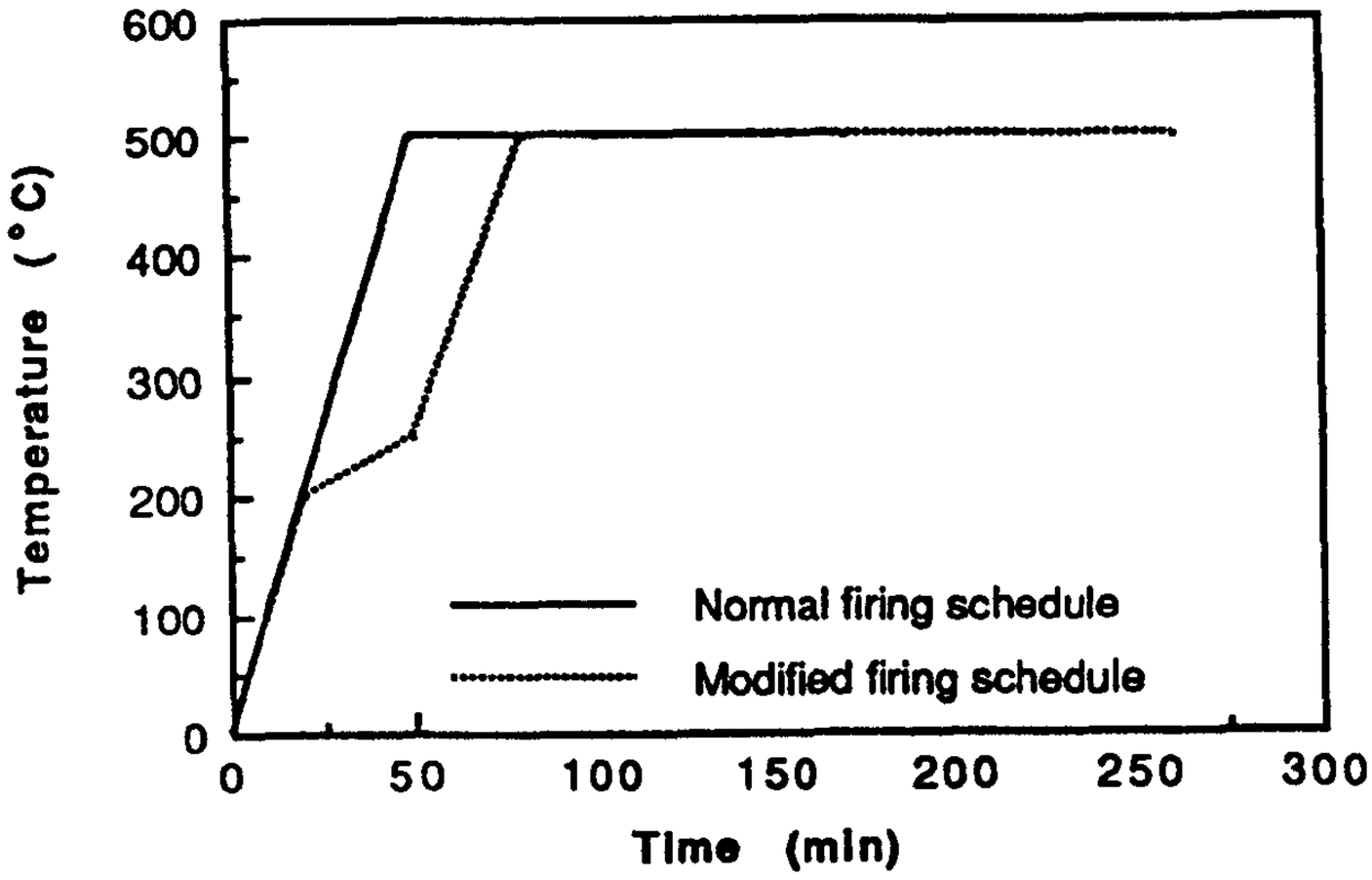

Fig. 9.7-Firing schedules used in the investigation.

Table 9.8-Modulus of rupture of fired clay bars bonded with: (1) calcium phosphate
(2) phosphates and lime

Designation of initial clay mix	Average M.O.R. (N/mm^2) for the heat treatment shown	
	Normal	Modified
K23	1.96	2.00
K26	2.53	2.50
K33	2.07	2.41
K43	2.08	2.14
K31	1.88	2.03

CHAPTER 9

It was apparent that the introduction of calcium phosphate and lime was not effective in improving the strength of clay bodies fired at 500°C. In bodies containing these admixtures, no favourable change in physical properties took place as a result of the modified heat treatment.

9.6 X-RAY DIFFRACTION ANALYSIS

XRD was used to detect any new crystalline phases formed. Fired products were investigated using finely ground randomly orientated samples. Analyses were carried out on a Philips diffractometer using CuK_{α} radiation.

9.6.1 Unfired material

9.6.1.1 Clay-phosphoric acid-diammonium hydrogen phosphate system

Phosphate treated clays exhibited dramatic changes in their diffraction patterns with changes in equilibrium pH of the original mix. Some of the diffractograms (Appendix 10) are reproduced in Fig. 9.8. Two additional reflections appeared in the trace made with phosphate treated clay at equilibrium pH 3 (K11). The reflection of medium intensity at 2.71 Å probably arose from aluminium phosphate hydrate-$AlPO_4.2H_2O$ (ASTM Index 15-311). The weak reflection at 2.80 Å can only be ascribed to a new phosphate hydroxide phase involving calcium ions derived from the Ca-rich clay (ASTM Index 6-0454).

A striking feature of the diffractogram obtained with the clay mix of equilibrium pH 4.7 (K13) was the appearance of a very strong reflection at 4.02 Å with simultaneous reduction in intensity of the characteristic quartz reflection (3.34 Å). The relative intensities of the two hypersthene/hornblende type of reflections increased considerably shifting slightly the d-spacings to 3.18 and 3.12 Å. In addition, a series of equally weak diffuse reflections arose at 2.81, 2.74, 2.70 and 2.52 Å. Positive identification of the additional reflection at 4.02 Å is difficult due to limited information available on the

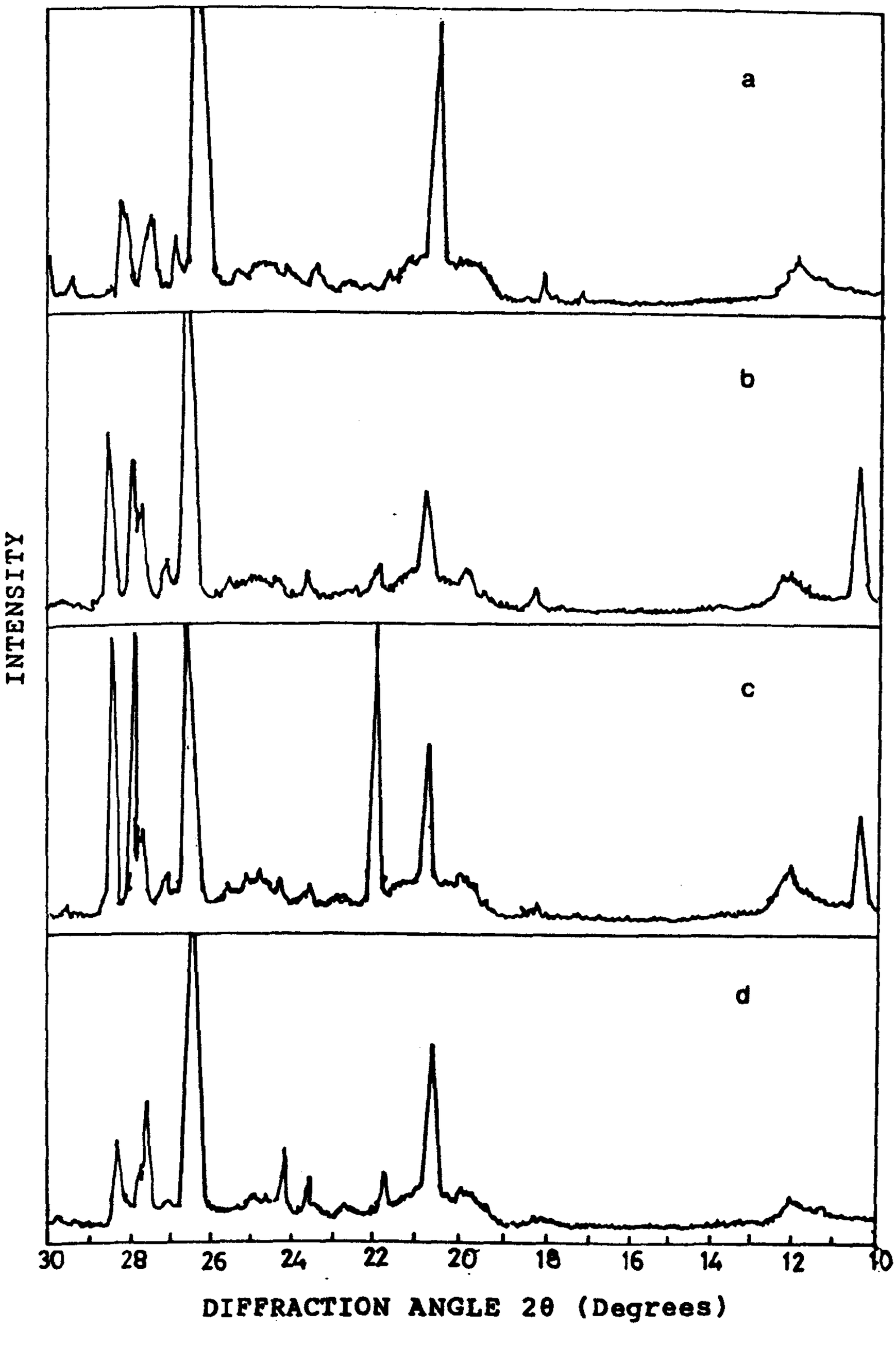

Fig. 9.8-X-ray diffraction patterns of residual soil LSK2A showing the effects of phosphate treatment a-Clay mix, eq. pH 7.4 b-Clay mix, eq. pH 3.1 c-Clay mix, eq. pH 4.7 d-Clay mix, eq. pH 3.1 matured for 30 days.

SiO_2-P_2O_5-Al_2O_3 system. Robinson et al. (1964) quote X-ray data from the work of Jacoby (1957) and Tien and Hummel (1962) relating to the existence of a binary compound $3SiO_2.2P_2O_5$ within the ternary system having a d-spacing of 4.02 Å. The binary compound was detected at 500°C, the lowest temperature employed by previous workers. They further state that ternary compound formation is unlikely below 50 mole % P_2O_5. It seems probable therefore that the additional reflection at 4.02 Å observed in the experimental clay-phosphate system arise from a SiO_2-P_2O_5 binary compound. However, no further X-ray data to substantiate this circumstantial evidence were found. Nevertheless this observation leads to the possibility that binary compounds of the type SiO_2-P_2O_5 can exist in natural clay-phosphate systems at room temperature depending on the level of pH at which structural collapse of the clay lattice would probably occur. The existence of such compounds in temperature ranges lower than that covered by Jacoby has not been reported in the literature.

The trace obtained with the above clay mix (pH 4.7) after maturing for 30 days was free from the reflection at 4.02 Å. It was replaced by a very strong reflection at 3.11 Å corresponding to a complex Mg, Fe, aluminium silicate hydroxide probably involving phosphate (ASTM Index 21-149). The characteristic quartz reflection remained relatively weak. This shows the metastable nature of the new phases which undergo transformation into hydrated products on maturing in aqueous medium. In addition, a series of very weak, diffuse reflections appeared at 3.00, 2.94, 2.53, 2.16 and 2.01 Å. Increasing disorder of kaolinite was reflected by the disruption of the characteristic groups of triplets (2.49-2.25 Å) and by the simultaneous weakening of the characteristic kaolinite reflections. These modifications of the diffraction pattern suggest a partial collapse of the kaolinite lattice as a consequence of the phosphate treatment.

The diffraction pattern resulting from the clay mix of equilibrium pH 7.4 (K17) exhibits a few significant changes. A strong reflection had appeared at 8.40 Å. This was attributed to a new phase identified as aluminium phosphate hydroxide hydrate ($Al_3(PO_4)_2(OH)_3.5H_2O$) by reference to the ASTM Index 2-75. The intensity of the hornblende reflection at 3.12 Å was diminished. The quartz reflection remained dominant while a series of additional weak reflections appeared at 2.94, 2.70, 2.60, 2.55 and 2.53 Å. It seems that the disorder of the kaolinite structure had increased.

It is interesting to note that the evidence of formation of aluminium phosphate hydroxide hydrate was apparent only in the slightly basic clay-phosphate system with an equilibrium pH of 7.4 (K17). This system was the most promising from the strength standpoint. The system with an equilibrium pH of 4.7 favoured the initial formation of a SiO_2-P_2O_5 binary compound while the highly acidic system with equilibrium pH 3 contained calcium phosphate hydroxide. The latter had no favourable properties. X-ray data also indicated that lattice destruction had occurred to different extent in the clay-phosphate systems investigated. It seems probable that phosphates reacted with the disordered kaolinite crystals, extracting aluminium to form different phosphate compounds.

Table 9.9 records a summary of the phases identified by X-ray diffraction in the phosphate treated (H_3PO_4 + $(NH_4)_2HPO_4$) clay mixes prepared under different conditions.

9.6.1.2 <u>Clay-phosphoric acid-tricalcium phosphate system</u>

Clay mix designated K26

There were no significant differences between samples of untreated clay and experimental clay mix. The 3.12 Å hornblende type silicate hydroxide reflection appeared much stronger than the neighbouring 3.17 Å reflection. Relative intensities of the characteristic quartz and kaolinite reflections were reduced.

Table 9.9-Summary of reaction products formed in unfired clay mixes treated with $(NH_4)_2HPO_4$ and H_3PO_4

Designation of clay mix	Max.aggregate size of clay (mm)	Eq. pH of clay mix	Period of mat. of clay mix (h)	Diffraction characteristics			
				Phases identified (effects observed in parenthesis)	Intensity	d-spacing	Reference
K11	3.35	3.1	20	$AlPO_4.2H_2O$ Ca-phosphate hydroxide phase	Medium Weak	2.71 Å 2.80 Å	ASTM 15-311 ASTM 6-0454
K13	3.35	4.7	20	$3SiO_2\ 2P_2O_5$ (or $SiO_2\ P_2O_5$) New phases (Diminution of quartz peak)	Strong Weak	4.02 Å 2.80, 2.74, 2.70, 2.52 Å	(i).Jacoby (ii).Tien et al.
K13	3.35	4.7	30 days	Na,Mg,Fe,Al silicate hydroxide New phases	Very strong Weak	3.11 Å 3.00, 2.94, 2.53, 2.16, 2.01 Å	ASTM 21-149
K13	-125 um	4.7	20	(Enhancement of quartz peak) New phases	Very weak	3.00, 2.92, 2.81, 2.70 Å	
K17	3.35	7.4	20	Aluminium phosphate hydroxide hydrate-$Al_3(PO_4)_2(OH)_3.5H_2O$ New phases	Very strong Weak	8.40 Å 2.94, 2.70, 2.60, 2.55, 2.53 Å	ASTM 2-75

9.6.1.3 Clay-phosphoric acid-diammonium hydrogen phosphate-calcium phosphate system

Clay mix designated K23

The feldspar reflection at 3.72 Å observed in the diffractogram of the K26 clay mix had disappeared. Relative intensities of the 3.12 and 3.17 Å reflections were reversed. Both the characteristic quartz and kaolinite reflections showed considerable diminution in intensity.

Clay mix designated K43

A sample containing the same ingredients but with a higher phosphate concentration maintained at pH 4.9 showed an increase in intensity of the quartz signal. The 3.12 Å twin reflection appeared more dominant than the other (3.17 Å).

9.6.1.4 Clay-phosphoric acid-lime system

Clay mix designated K31

An additional reflection appeared in the trace at 7.52 Å. However, the data are so scanty to enable positive identification. Relatively weak silicate hydroxide reflections were both present at 3.17 and 3.12 Å; the 3.12 Å peak reduced in intensity relative to the other.

9.6.1.5 Clay-phosphoric acid-diammonium hydrogen phosphate-lime system

Clay mix designated K33

The resulting diffractogram was essentially similar to that described in Section 9.6.1.4 except for the increase in intensity of the new reflection at 7.52 Å and the shifting of the kaolinite reflection to 7.22 Å. The shifting of basal spacing probably indicate partial collapse of the lattice.

The results of X-ray diffraction analyses of clay samples containing phosphates and Ca-bearing admixtures (Appendix 11) are summarised in Table 9.10.

Table 9.10-Phases and characteristics observed in unfired clay mixes containing: (1) calcium phosphate (2) phosphates and lime

Designation of clay mix	Wt% phosphate ion in clay mix	Wt% lime added	Eq. pH of clay mix	Phases/characteristics observed
K26	3.18 (3.14 by $Ca_3(PO_4)_2$)	-	6.6	Reduction in intensity of quartz and kaolinite reflections
K23	3.56 (1.34 by $Ca_3(PO_4)_2$)	-	5.1	Reduction in intensity of quartz and kaolinite reflections
K43	5.64 (2.08 by $Ca_3(PO_4)_2$)	-	4.9	Slight enhancement of quartz reflection
K31	4.19	1.87	5.4	Significant increase in intensity of quartz reflection;appearance of an additional ref. at 7.52 Å
K3	4.19	1.87	7.2	Additional reflection at 7.52 Å

9.6.2 Fired bodies

X-ray diffraction patterns of phosphate-bonded clay bodies showed that no new crystalline compounds were formed up to 400°C. In specimens fired at 800°C, however, two crystalline compound showing weak diffuse reflections at 2.67 and 2.48 Å were present.

Fired clay bodies containing different types of phosphatic binders showed that reactions on firing result in loss of intensity of the characteristic quartz (3.34 Å) reflection and in the general weakening of the pattern. These modifications are perhaps associated with the formation of amorphous compounds in the fired bodies. The above effects were most pronounced in the K17 clay mix and were hardly observable in the K13 clay mix. On the other hand, extensive structure collapse of kaolinite as evidenced by ill-defined reflections and the appearance of a

continuous band in the 35-40 (2θ) range were seen in the diffraction pattern of the K11 clay mix. It is interesting to note that the K17 clay mix gave higher overall values for the modulus of rupture than the K11 clay mix. It is therefore conceivable that the formation of amorphous compounds probably involving phosphate is more likely the cause of high strengths in phosphate-bonded bodies than the development of a collapsed structure.

9.7 INFRARED ANALYSIS OF UNFIRED MATERIAL

Infrared analysis of unfired phosphate treated clay was carried out on a Unicam SP1100 spectrophotometer using KBr disc technique to detect the presence of amorphous phases. The infrared analysis of the untreated residual soil is given in Section 3.3.4. The infrared spectrum of the unfired, phosphate treated residual soil, K17, (Appendix I2) is reproduced in Fig. 9.9.

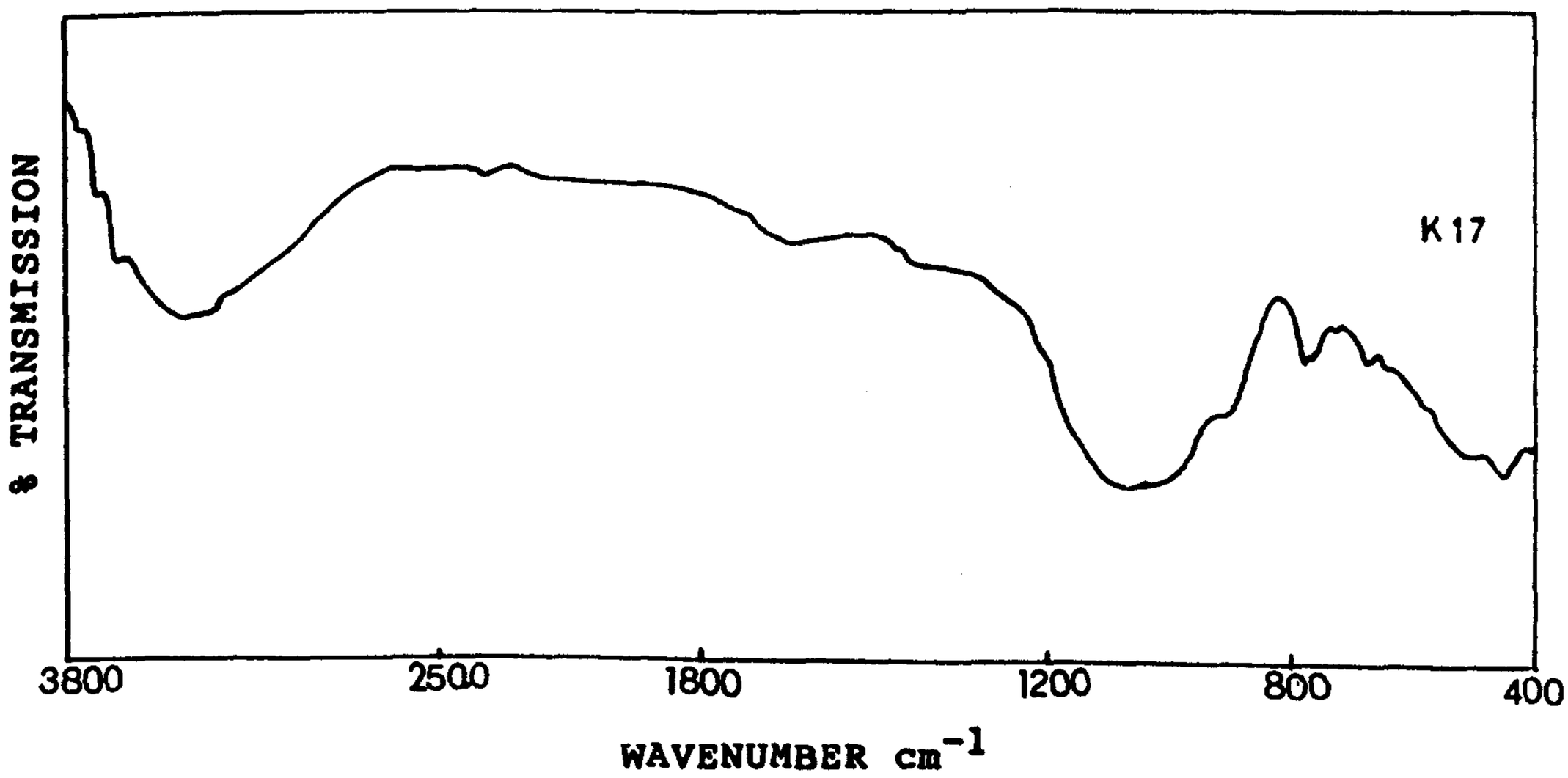

Fig. 9.9-Infrared spectrum of phosphate treated clay (K17).

The main features of the spectrum are, a broad band at 3450 cm^{-1} corresponding to adsorbed water and two shoulders at 3620 and 3700 cm^{-1} attributed to free hydroxyl and hydrogen bond hydroxyls respectively. The two bands due to quartz at 790 and 465 cm^{-1} stand out sharply against the shoulder for biotite at 685 cm^{-1}. The H--O--Al stretching frequency of kaolinite at 910 cm^{-1} remains unchanged.

A plateau appears between approximately 1000 and 1100 cm^{-1} in contrast to the sharp bands due to microcline, kaolinite and muscovite present in the spectrum of raw clay. It seems probable that this modification represents a reduction in the amount of condensed silicate material present in the raw clay. This is consistent with the appearance of a broad band at 1640 cm^{-1} corresponding to a hydrated amorphous phase probably involving silica and phosphate. The additional sharp band at 770 cm^{-1} can be assigned to PO_4^{3-}—O--H vibrations of $Na_2HPO_4.2H_2O$ arising from hydrogen bonding with water (Chapman and Thirlwell 1964). Thus the spectral differences in the two spectra point to the development of amorphous silicate phase and hydrogen bonding involving phosphates in the treated residual clay.

9.8 CLAY-PHOSPHATE BOND

SEM techniques were employed to follow changes in microstructure and constitution. A Hitachi electron microscope was used to examine fracture surfaces of the fired clay-phosphate composites, and these were vacuum-coated with a thin film of carbon prior to examination.

Scanning electron micrographs, Plate 9.1, revealed several characteristics regarding the physical nature of phases developed in the clay-phosphate bond.

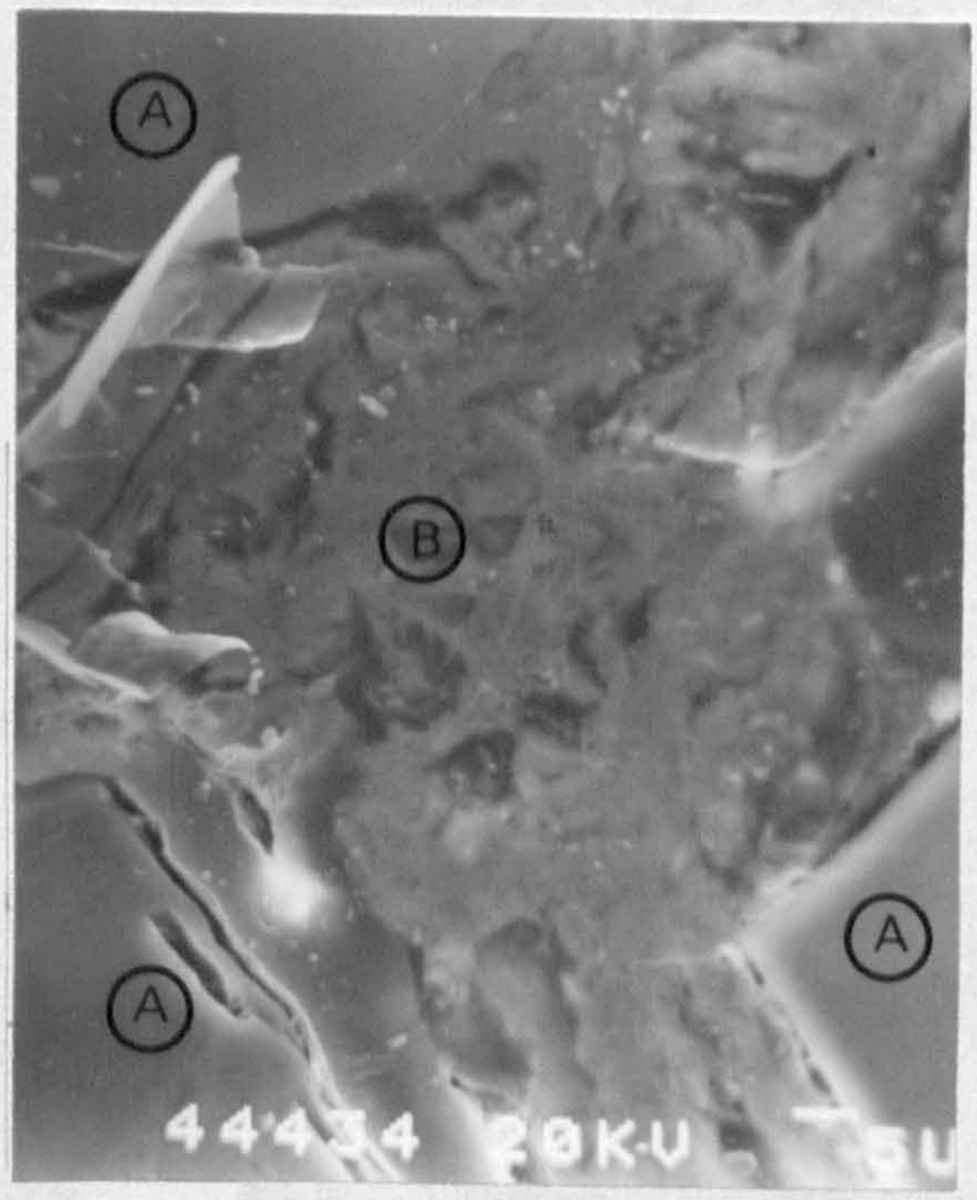

Plate 9.1-Scanning electron micrograph showing clay-phosphate reaction phases produced by firing at 500°C. A-Amorphous phases B-Clay substrate

Bond materials developed at 500°C on specimens consisted of three distinct types: large regions which appeared to be amorphous, an intermediate phase of large particle size and fine particles of clay. The large regions are most likely the hydrated aluminium-phosphate phases. Correlative electron probe microanalysis shows the grains of intermediate size to be rich in silica.

9.9 DIFFERENTIAL SCANNING CALORIMETRY (DSC)

Physico-chemical changes produced by phosphate treatment of residual soil were studied by differential scanning calorimetry. The DSC scans (Appendix 13) were obtained using a Perkin-Elmer 7 series thermal analysis system at a heating rate of 10°C/min with nitrogen flow rate of 60 cm^3/min. Samples of raw and treated clay (~ 9 mg) were placed in a flat aluminium pan and heated in nitrogen alongside an empty pan as reference. A set of scans is illustrated in Fig. 9.10.

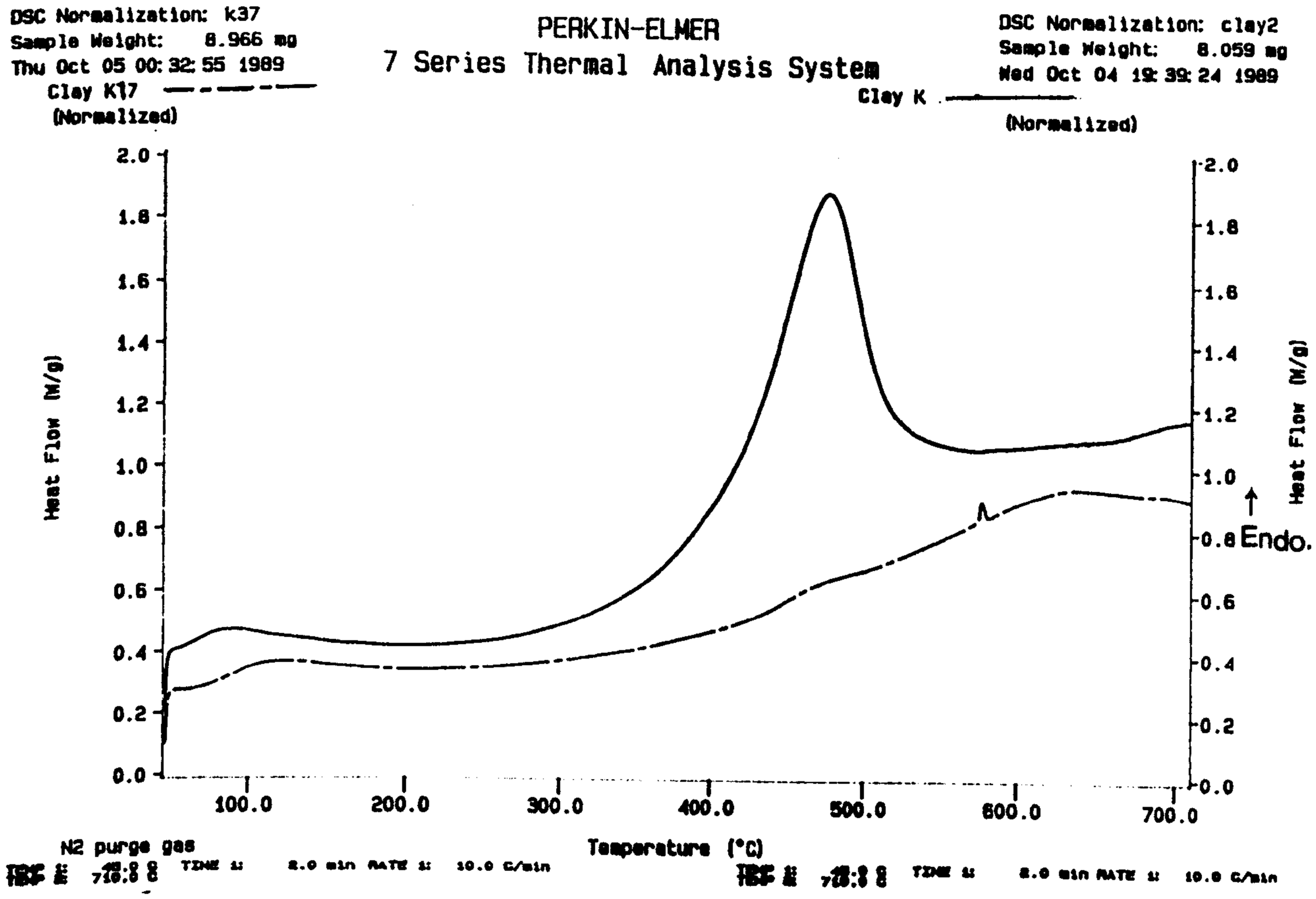

Fig. 9.10-DSC curves of: (1) K (2) K17.

The untreated clay, K, showed a small endotherm at about 100°C probably due to the loss of interlayer water of vermiculite followed by the dehydroxylation endotherm in the range 400-500°C with a peak temperature at 475°C. The total areas of the dehydration and dehydroxylation peaks correspond to heats of reaction of 15.5 and 445.4 J/g respectively. The striking feature of the DSC scan of phosphate-treated residual soil, K17, is the absence of both endotherms in the thermograms. There appears to be a very broad endotherm above 550°C with a peak temperature at 630°C. It is possible that the phosphate treatment destroyed the original clay mineral structure of the clay giving rise to compounds which undergo physico-chemical changes above 550°C. It is also likely that this critical change corresponded to the decomposition of hydrated aluminium-phosphate phases. The loss strength of bars fired at temperatures above 500°C is probably a direct consequence of such changes in the bonding phases.

CHAPTER 9

9.10 PHASE RELATIONS

On the basis of experimental evidence obtained, an attempt was made to elucidate the phase relations in the region not explored in the system SiO_2-Al_2O_3-P_2O_5.

The compositions studied were equivalent to approximately 15:1 molar mixtures of SiO_2 and P_2O_5. Free Al_2O_3 available initially was assumed to be small when compared with the total amount of the other two constituents. The slightest destruction of kaolinite lattice releases Al_2O_3 and therefore, the experimental composition (represented by the point X in Fig. 9.11) with a very low proportion of Al_2O_3, would produce hydrated aluminium phosphate microcrystalline powder (A) as the stable solid phase at 25°C. The experimental data for the clay-phosphate system-K17, are in moderate agreement with this phase equilibrium.

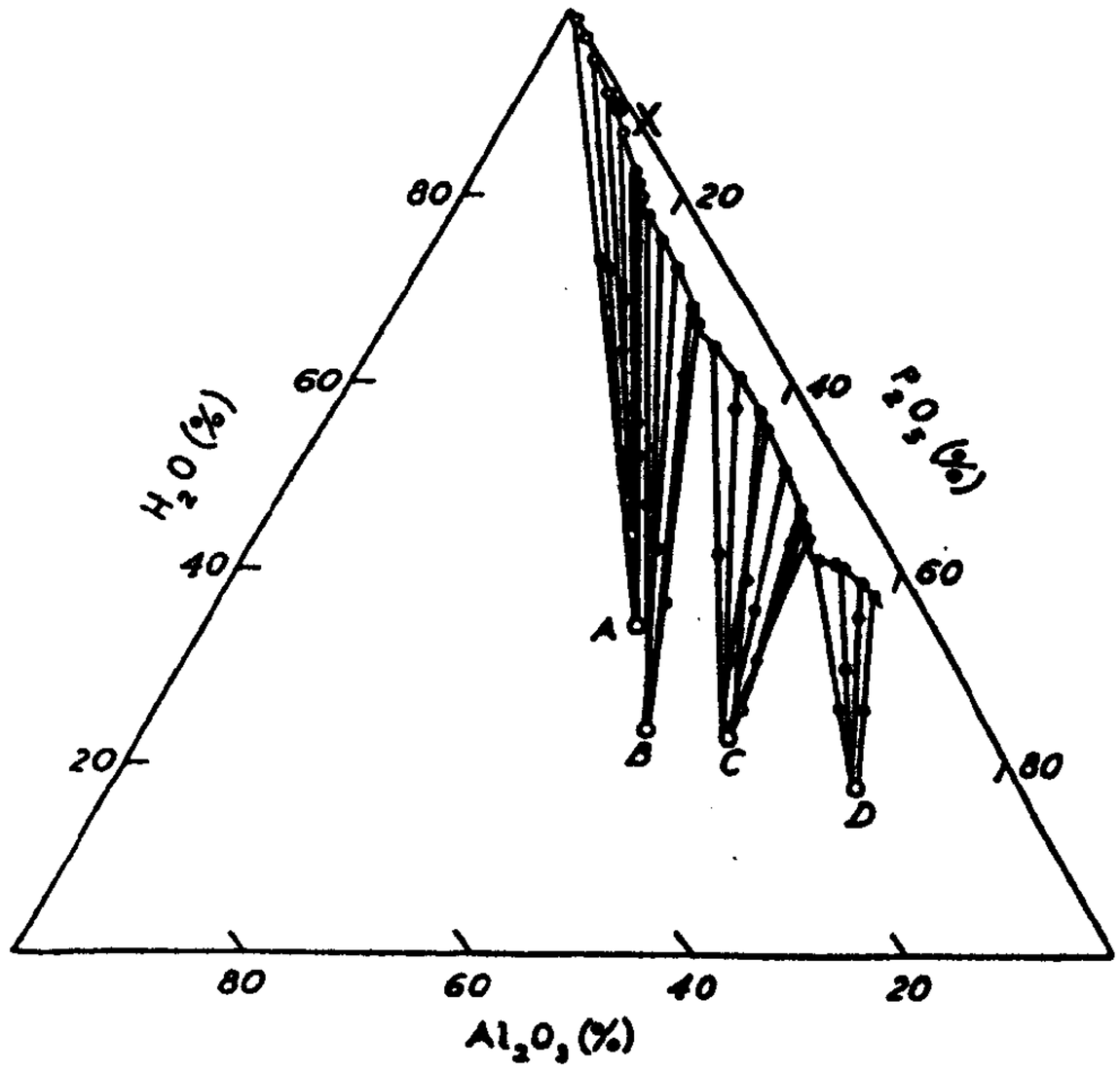

Fig. 9.11-Stable equilibria in the system Al_2O_3-P_2O_5-H_2O at 25°C (after Jameson and Salmon 1954).
[A-$Al_2O_3.P_2O_5.7H_2O$, B-$Al_2O_3.P_2O_5.4H_2O$, C-$2Al_2O_3.3P_2O_5.10H_2O$, D-$Al_2O_3.3P_2O_5.6H_2O$].

CHAPTER 9

The phase relations at subsolidus temperatures were determined in relation to the ternary system SiO_2-Al_2O_3-P_2O_5 proposed by Robinson et al. (1964). The nominal composition studied is represented by the point Y in the compatibility triangle (Fig. 9.12). It lies in the region not explored by the previous investigators.

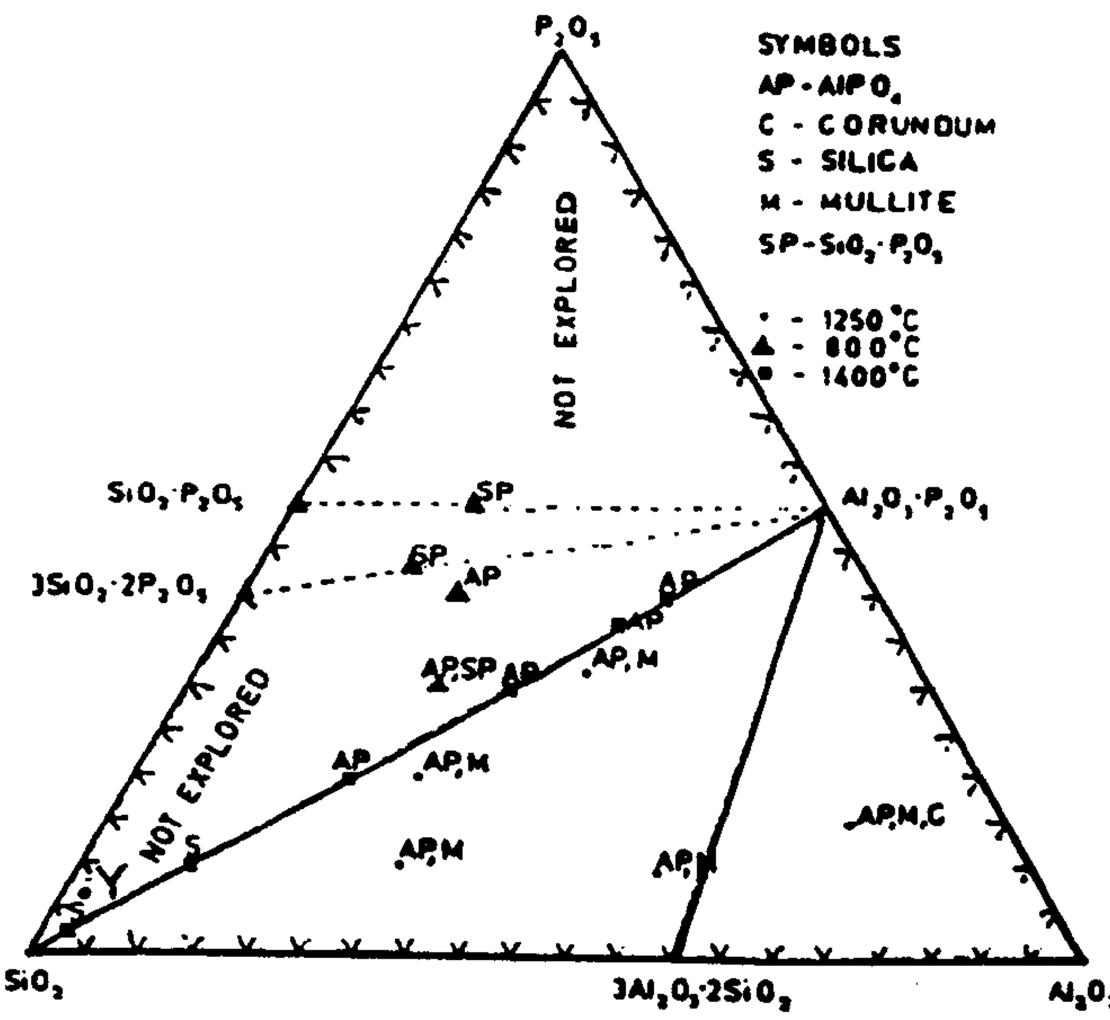

Fig. 9.12-Compatibility relations in the system SiO_2-P_2O_5-Al_2O_3 at 800°, 1250° and 1400° C (after Robinson and McCartney 1964).

Robinson et al. who studied the phase relations in the part of the system SiO_2-Al_2O_3-P_2O_5 below 50 mole% P_2O_5 reported that no ternary compound forms at subsolidus temperatures. In the present work, therefore, the only crystalline compounds to be expected are $3SiO_2 \cdot 2P_2O_5$ and $AlPO_4$. The binary compound $3SiO_2 \cdot 2P_2O_5$ was tentatively identified in the unfired acidic clay-phosphate systems during this present study, but its X-ray data agree only moderately. However, its preferential formation to $AlPO_4$ in acidic systems was inferred from the shrinkage data; relatively high linear firing shrinkage of specimens was inconsistent with the presence of $AlPO_4$. The above binary

compound, on the other hand, was not detected in basic clay-phosphate systems. In these systems, it was possible to detect the presence of aluminium phosphate hydroxide hydrate at room temperature. The fired products, however, gave inconclusive evidence as to the presence of crystalline $AlPO_4$. Nevertheless, they had exceptionally low thermal shrinkage values compatible with the presence of $AlPO_4$. It seems probable therefore that in basic systems phosphate hydrate on heating yielded amorphous $AlPO_4$ not detected by X-ray diffraction. According to Robinson et al., $3SiO_2.2P_2O_5$ decomposes rapidly at temperatures below 1000°C whereas $AlPO_4$ is stable up to 1400°C. Since there were also signs of a probable decomposition reaction in the experimental specimens above 500°C as was evident from the DSC scans, it was believed that both $3SiO_2.2P_2O_5$ and amorphous aluminium phosphates were formed in the fired clay-phosphate bodies; the relative proportions of the constituents presumably varied according to the pH of the system and the ultimate fired product contained both the decomposition products of $3SiO_2.2P_2O_5$ and amorphous $AlPO_4$. This concept agrees with the compatibility relations established for the SiO_2-Al_2O_3-P_2O_5 system, as the experimental composition lies within the $SiO_2.P_2O_5$ binary and the SiO_2-$AlPO_4$ join in the system.

9.11 REACTION MECHANISM

Literature presents a confusing picture of the mechanism involved in clay mineral-phosphate reactions. Some compare this to a physical adsorption, others to a chemical reaction. The experimental evidence points to the latter.

The model proposed by Hsu and Bates (1964) for reactions of phosphates with aluminium hydroxide and iron oxides can be extended to the experimental system involving kaolinite.

In a slightly basic medium (such as pH 7.4), aluminium in the kaolinite lattice is available in the form of Al^{3+} and the reaction may take place in the following manner:

$$6Al^{3+} + 6H_2PO_4^- \text{ --- } Al_6(OH)_{12}(H_2PO_4)_6 + 12H^+$$

$$[Al_6(OH)_{12}]^{6+} + 6H_2PO_4^- \text{ --- } Al_6(OH)_2(H_2PO_4)_6$$

In acidic medium (such as pH 3.1), however, the availability.of Al^{3+} from lattice destruction is low and phosphates may form polymers of aluminium silicate hydroxide phases by hydroxyl bonding. In moderately acidic medium (such as pH 4.7) the formation of a metastable binary phase is initially favoured but subsequent hydrolysis and polymerisation on ageing produces stable aluminium silicate hydroxide phases. Thus, precipitation may occur giving rise to aluminium phosphate hydrate hydroxide when phosphate removes discrete Al^{3+} ions from the lattice. When phosphate breaks only part of the Si--O--AL bonds, aluminium silicate hydroxides may form. Since the OH/Al ratio is different in the various phases, the activity of aluminium in these phases may also be different.

The proposed mechanism accords the porosity and shrinkage data of the clay bodies examined. The DSC and SEM examinations also support the underlying constitutional and morphological changes.

9.12 GENERAL SUMMARY

The following conclusions are drawn from this work.

(i).The strength of phosphate-bonded fired clay products is to large extent related to the equilibrium pH of the initial clay mix. The equilibrium pH of about 7.4 seems to be the most favourable for the attainment of high fired strengths. The pronounced increase in strength at this level of pH is probably due to the formation of amorphous aluminium phosphate phases involving new and stronger bonds as evidenced by the IRA, DSC and SEM examinations. There is circumstantial XRD evidence to indicate the formation of metastable phosphate-silicate phases. The substantial reduction in porosity and shrinkage is consistent with the development of these new phases.

(ii).Clay mixtures which are promising from a strength standpoint contained 3.16 wt% phosphate ion. The highest strengths were obtained at the 500°C firings where increases as high as 60% were observed compared to the unbonded bars fired at 800°C. The average modulus of rupture of such bodies was 2.55 N/mm^2.

(iii).A mixture of phosphoric acid and diammonium hydrogen phosphate are more effective than calcium phosphate alone in maintaining the critical equilibrium pH in the clay mixes. There is no evidence to suggest that calcium phosphate contributes to the strength development of the clay bodies examined.

(iv).Indications are that the normal firing temperature of clay products can be effectively reduced by more than 450°C. Firing at a minimum peak temperature of 500°C followed by boiling is sufficient to impart durability and adequate strength (2.9 N/mm^2) to experimental bars. [The minimum compressive strength stipulated for load-bearing applications (SLS 39:1978) is 2.8 N/mm^2].

(v).Boiling for 5 h further improves the strength of products by at least 10%.

(vi).Phosphate addition improves workability of raw clays, reduces firing shrinkage and porosity and improves the dimensional stability of the fired product.

(vii).The limited laboratory accelerated durability test showed no evidence of disintegration. There was slight discoloration of external surfaces due to leaching.

(viii).The economic aspects of phosphate bonding in clayware ceramics appear to be favourable but can be fully ascertained only when the industrial requirements are determined.

CHAPTER 10

CONCLUSIONS AND IMPLICATIONS

Specific conclusions on the aspects of strength enhancement considered in this study are given in the relevant sections. Broad conclusions drawn from the foregoing review of results are summarised below. The implications of research findings are also outlined.

10.1 METHODS OF STRENGTH IMPROVEMENT

The present study has identified several potential areas where it is possible to improve the strength of fired clay bodies made from the Sri Lankan clays studied.

10.1.1 Optimum heat treatment

(i). The optimum conditions of firing consistent with the maximum mechanical strength of a clay body can be estimated from a consideration of the kinetic analysis based on the first order kinetics.

(ii). The kinetic analysis also yields the critical heat treatment beyond which further firing only causes deterioration of the properties of the fired product.

The industrial implication of the above is that any combination of two of the following conditions of firing,

(a) Maximum firing temperature
(b) Rate of heating
(c) Soaking period

can be transposed to give the optimum combination to satisfy economic and industrial requirements.

This procedure shows promise as a method of determining the conditions required to produce a technically acceptable product from a given raw material. Heat treatments that are favourable from an energy conservation standpoint can also be determined.

10.1.2 Phosphate bonding

This part of the study has shown that it is possible to produce fired clay products by phosphate bonding at lower firing temperatures. The strength characteristics and dimensional stability of phosphate bonded clay bodies are comparable with and in most cases better than those of normal clay bodies fired at temperatures 400-450°C higher. The following effects on fabrication were noted.

(i). To obtain the optimum strength characteristics, the equilibrium pH of a clay mix must be maintained at about 7.4. A mixture of phosphoric acid and diammonium hydrogen phosphate can be used for this purpose. DSC, XRD and SEM studies and also porosity and shrinkage data indicate that the strength improvement is consistent with the formation of a new mineral phase, probably aluminium phosphate, in the clays examined.

(ii). Strength development is dependent on the concentration of phosphates; addition of 3.16 wt% phosphate to a clay body is effective in increasing the M.O.R by at least 60% for bars fired at 500°C compared to unbonded bars fired at 800°C.

(iii).Indications are that the normal firing temperature may be reduced by at least 450°C. A minimum firing temperature of 500°C is sufficient to impart adequate durability and strength to clay bodies.

(iv). Low levels of phosphate addition have been shown to improve workability of the raw clays, reduce firing shrinkage and porosity and also improve the dimensional stability of the fired product.

It is thought that the increase in the cost of production associated with the use of phosphate additive may be offset by the economy in energy consumption brought about by the reduction in firing temperature. However, the economic aspects of phosphate bonding can be fully ascertained only when plant trials are performed.

There was no evidence of favourable reactions between the clay particles and phosphate at pH values other than those within the critical range where the sudden increase in strength occurred. This indicates the necessity of maintaining a rigorous process control in the fabrication of clay bodies.

10.1.3 Use of a lime mineralizer

(i). Within the limits of the formulation it has been shown that an optimum amount of lime determined by the type of clay has an influence on the strength. The strength increases were,

6% for podzolic clay (containing 2 wt% lime),
36% for residual soil (containing 3 wt% lime),
60% for latosol (containing 4 wt% lime).

(ii). There is circumstantial evidence to suggest that the marginal improvement of the fired strength in low-lime clay bodies is probably attributed to the liquid phase sintering rather than to the induced mullitization of kaolinite.

(iii).The lime mineralizer widens the maturing range of clays, thus reducing the tendency to overfire.

The results of this study justify greater attention to the use of lime in clay bodies. Importance should be attached to ensuring sufficient fineness in the grain size of lime and to thorough mixing with the clay in order to achieve full effectiveness. Localized concentration of particles of lime results in a heterogeneous body of poor mechanical strength.

Some clay deposits in the dry zone of Sri Lanka still remain unexploited in view of lime contamination. In spite of certain misgivings in the industry that have directed it away from the use of calcareous clays, these materials have the potential of improving processing and product characteristics when treated properly. It is to be hoped that the results of these studies will point to additional means of reducing or eliminating the firing problems connected with high-lime materials.

Lime is considerably more expensive than clay, being about Rs.2500 (£40)/tonne ex-producer compared to Rs.625 (£10) for clay. This adds to material costs. A cost benefit analysis would be necessary to justify its use with non lime-bearing clays.

10.1.4 Mullite content and porosity

(i). It is probable that the nucleation of mullite begins at temperatures above 800°C in the podzolic clays and residual soils. Latosol requires a minimum temperature of 1100°C for mullite formation. Within the range of temperature of mullite development, M.O.R increases progressively with the mullite content in the fine-grained soils. On the other hand, porosity obeys an inverse linear relationship with M.O.R over the range of 20-40% porosity.

The combined effects of both mullite content and porosity on the M.O.R of fine-grained clay bodies are in substantial agreement with the empirical equation:

$$M.O.R = M_0[(1-0.03A.P)(1+0.02I_m)]^{\frac{1}{2}}$$

The experimentally determined values of M.O.R, A.P and I_m of specimens fired at various temperatures gave a calculated value of 15 N/nm^2 for M_o. This indicates that the maximum strength (M.O.R) attainable with the specimens of podzolic clay fired to temperatures below the formation of mullite is 15 N/nm^2. The above equation thus provides a basis for the characterization of clays with respect to strength.

(ii). There is circumstantial evidence to suggest that the total mullite content rather than the interlocking arrangement of mullite crystals is a better indicator of the strength development in these bodies.

10.1.5 Surface coating

(i). Self-coated clay products maturing at 900°C can be developed from suitable compositions in the Na_2O-Al_2O_3-SiO_2 ternary system formulated according to the mineralogy of clays. The fabrication requirements necessary to develop the surface coating determined in this laboratory are;

(a) The SiO_2/Al_2O_3 ratio of clay must be within the range 1.5-2.0.

(b) The optimum granulometric composition of clay:

3.35-1.18 mm. fraction- 9-11%

600-212 μm fraction- 47-54%

< 212 μm fraction- 20-25%

(c) Optimum amount of additive required to activate efflorescence deposition and subsequent sintering of coating:

1 wt% solution of Na_2CO_3 (anhydrous)

(d) Pre-moulding moisture content of clay mix-13-29%.

(e) Air-drying of moulded specimens at room temperature for 6 days followed by oven-drying at 50°C for 24 h.

(f) Firing at a peak temperature of 900°C for 2 h.

(ii). Surface coating improves both the yielding and strength behaviour of fired clay bodies. The coating increased the load at the elastic limit by 30% and the ultimate failing load by 19% for the clays used. The measured increases in modulus of rupture and modulus of elasticity were over 33% and 40% respectively.

(iii).The surface coating does not appear to have any detrimental effect on the overall durability of brick specimens.

CHAPTER 10

The technique of producing the surface coated clay product may be a potential alternative to the current method of producing facing bricks by harmful salt glazing. The alternative system is more environmentally attractive. The induced deposition of surface material as an efflorescence obviates the need for glazing. The product is aesthetically more satisfying than a normal brick.

The new fabrication technique developed in this study necessitates the introduction of process modifications, the most important of which are the adjustment of drying conditions and the use of $NaCO_3$ additive and ground silica. Good quality control is essential since crazing of the surface coating may occur if the expansion mismatch between the body and the coating is high.

10.1.6 Texture

The following textural features associated with the development of strength of clay bodies have been recognized:

(i). The strength development of bodies fired to low temperatures (about 800°C) corresponds to the development of favourable structures with fibrous matrix hastening intergranular bonding of materials. The presence of traces of a glassy phase also contributes to this.

(ii). The strength development at temperatures above the onset of mullite formation is probably attributed to the desirable properties of mullite. There was insuffi-cient evidence to substantiate the commonly accepted belief that the strength development is associated with the interlocking network of secondary mullite.

(iii). At intermediate firing temperatures (800-1000°C), lime mineralizer is effective in promoting early vitri-fication. The development of large amount of glassy phase produces a texture with a heterogeneous matrix, fewer pores and slightly improved strength.

(iv). It is possible that lime mineralizer favoured the direct formation of secondary mullite and its subsequent grain growth. The onset temperature of mullite formation, however, is slightly increased by the presence of lime.

(v). The occurrence of bloating of the fired material at temperatures above 1000°C is characterized by the specimens containing isolated ovoid pores which are abundant. This critical stage is identifiable with deterioration of properties.

(vi). Microstructural analyses of the experimental surface coatings on bricks indicate that marked improvements in properties can be expected from finer surface finish.

The high temperature mineral phases present in brick include mullite, cristobalite, and hematite. It is possible that under the normal oxidizing conditions of firing used in the investigation, the iron present in the clay partly forms hematite and partly enters into solid solution with mullite. Mullite begins to develop from residual feldspar at about 800°C. The composition of primary mullite approximates to an Al_2O_3:SiO_2 ratio of 1:1 whereas that of secondary mullite approximates to the ratio of 2:1.

It seems probable that the main factors in improving strength of the bodies are the elimination of defects (pores, cracks) and development of favourable structures and phases. However, improved homogeneity cannot be discounted as insignificant.

10.2 SUGGESTIONS FOR IMPROVEMENT OF STANDARD SPECIFICATIONS

The present SLS specification for clay bricks is incomplete because it does not include durability requirements. the current specification might be improved with the incorporation of 5-h boiling test. However, statistically significant test results on a large number of commercially marketed bricks must be obtained to re-evaluate

the relation between the physical properties and durability of bricks.

An accelerated durability test based on the heat-quench procedure designed for testing the surface coated clay product will be suitable for facing bricks.

10.3 SUGGESTIONS FOR FURTHER RESEARCH

The present study indicates the scope and limitations of the fabrication techniques developed in enhancing the mechanical strength of bricks made from Sri Lankan brick clays. However, in order to evaluate the true significance of the results it would be of value to have a thorough and critical appraisal of the results and their interpretations coupled to the service behaviour of the materials. It is perhaps appropriate to close this report of the present study with the following suggestions for further research in this area. In particular research should be directed towards:

(i). The performance of materials in service under known design conditions in order to relate it to the properties investigated.

(ii). The strength characteristics of a wide cross-section of clays to establish their effectiveness as potential alternative building materials.

(iii).The long term durability of the alternative materials.

REFERENCES

Abdel, F., Hussein, W.I. and Gad, G.N., (1972), "Preparation and characteristics of mullite corundum porcelains." Ber. Deut. Keram. Ges., 49, 391-95.

ASTM C67-78 (1980) "Standard methods of sampling and testing brick and structural clay tile." American Society for Testing and Materials, Philadelphia. Part 16, 45-53.

ASTM C373-72 (1982) "Standard test method for water absorption, bulk density, apparent porosity and apparent specific gravity of fired whiteware products." American Society for Testing and Materials, Philadelphia. Vol. 15 .02, 105-106.

ASTM C674-77 (1978) "Standard test methods for flexural properties of ceramic materials." American Society for Testing and Materials, Philadelphia. Part 17, 672-673.

ASTM C674-81 (1988) "Test methods for flexural properties of ceramic whiteware materials." American Society for Testing and Materials, Philadelphia. Vol. 15.02, 196.

Bain, J.A. and Morgan, D.J., (1970), "Role of thermal analysis in the evaluation of impure clay deposits." Clay Miner., 8, 171-192.

Bannerjee, J.C., De, S.K. and Nandi, D.N., (1964), "Sintered alumina." Central Glass Ceram. Res. Inst. Bull. (India), 11, 93-100.

Bar-Yosef, B., Kafkafi, V., Rosenberg, R. and Sposito, G., (1988), "Phosphorous adsorption by kaolinite and montmorillonite." Soil. Sci. Soc. Am. Proc., 52, No.6, 1580-1585.

Barnes, I.D. and Palmour, H., (1966), "Rate controlled hot pressing of spinel." Am. Ceram. Soc. Bull., 45 [9], 805.

Barrett, L. R., (1976), "High temperature chemistry of inorganic and ceramic materials." edited by F.P. Glasser and P.E. Potter, 90-91.

Bartha, P., Lehmann, H. and Koltermann, M., (1971), "Untersuchungen zur binding keramischer werkstoffe mit H_3PO_4." Ber. Deut. Keram. Ges., 48, 111-115.

Beck, W. R., (1949), "Crystallographic inversions of the aluminium orthophosphate polymorphs and their relation to those of silica." J. Am. Ceram. Soc., 32 [4], 147-151.

Beutelspacher, H. and Van Der Marel, H.W., (1961), Univ. Carolina Geol. Suppl. 1, 97-114.

Bien, A. and Keyser, W.L.De., (1962), "The effects of aluminium fluoride on the thermal behaviour of kaolin." Clay. Miner., 5, 81-89.

Binns, D.B., (1965), "The testing of alumina ceramics for engineering applications." J. Br. Ceram. Soc., 2, 294-308.

REFERENCES

Black, C. A., (1941), "The penetration of phosphate into the kaolinite crystal." Soil Sci. Soc. Am. Proc.,6, 157-161.

Brindley, G.W. and Brown, G., (1980), "Crystal structures of clay minerals and their X-ray identification." Minerelogical Society, London.

Brindley, G.W. and Nakahira, M., (1957), "Kinetics of dehydroxylation of kaolinite and halloysite." J. Am. Ceram. Soc., 40, 346-356.

Brindley, G.W. and Nakahira, M., (1959), "Kaolinite-mullite reaction series; I." J. Am. Ceram. Soc., 42 [7], 311-364.

BS 1377 (1975) "Methods of test for soils for civil engineering purposes." British Standards Institution.

BS 3921 (1985) "Specification for clay bricks." British Standards Institution.

Carniglia, S.C., (1965), "Petch relation in single phase oxide ceramics." J. Am. Ceram. Soc., 48 [11], 580-83; "Working model for porosity effects on the uniaxial strength of ceramics." ibid, (1972), 55 [12], 610-18.

Chandler, B.A. and Fryxell, R.E., (1963),"Physical properties of sintered BeO as influenced by micro-structure." Ann. Mtg. Am. Ceram. Soc., Pittsburgh.

Chang, S.C. and Jackson, M.L., (1957), "Solubility product of iron phosphate." Soil Sci. Soc. Am. Proc., 21, 265-269.

Chapman, A.C. and Thirlwell, L.E., (1964), "Spectra of phosphate compounds: 1. IR spectra of orthophosphates." Spectrochim. Acta., 20, 937-947.; ibid, 27 A, 425-439.

Chung, D.H., (1963), "Elastic moduli of single crystal and polycrystalline MgO." Phil. Mag., 8, 833.

Clark, J. S. and Peech, M., (1955), "Solubility criteria for the existence of calcium and aluminium phosphates in soils." Soil Sci. Soc. Am. Proc., 19, 171-174.

Coble, R.I. and Aitken, E.A., (1966), "Powder processing and sintering of non fissionable ceramics." Proc. Conf. Nuclear Applications of Non Fissionable Ceramics. 347-358.

Cole, C.V. and Jackson, M.L., (1950), "Colloidal dihydroxy dihydrogen phosphate of aluminium and iron with crystalline character established by electron and X-ray diffraction." J. Phys. Chem., 54, 128-142.

Cole,C.V. and Jackson, M.L., (1951),"Solubility equilibrium constant of dihydroxy aluminium dihydrogen phosphate relating to a mechanism of phosphate fixation in soils." Soil Sci. Soc. Am. Proc., 15, 84-89.

Coleman, R., (1944), "The mechanism of phosphate fixation by montmorillonite and kaolinitic clays." Soil Sci. Soc. Am. Proc., 9, 72-78.

REFERENCES

Coleman, N.T., Thorupand, J.T. and Jackson, W.A., (1960), "Phosphate sorption reactions that involve exchangeable aluminium." Soil Sci., 90, 1-7.

Copley, S.M. and Pask. J.A., (1965), "Deformation of polycrystalline magnesia at elevated temperatures." J. Am. Ceram. Soc., 48 [12], 636-42.

Davidge, R.W. and Evans, A.D., (1970), "The strength of ceramics." Mat. Sc. Eng., 6, 281-298.

Day, R.D. and Stoke, R.J., (1966), "Mechanical behaviour of polycrystalline magnesia at high temperatures." J. Am. Ceram. Soc., 49 [7], 345-54.

Dayton, J., (1978), "Minerals Metals Glazing and Man." Harrup, London.

Dietzel, A., (1953), "Significance of equilibrium diagrams for ceramics." Sprechsaal, 86 [10], 251-52.

Duckworth, W., (1953), Discussion on compression strength of porous sintered alumina and zirconia. J. Am. Ceram. Soc., 36, 68.

Duke, D.A., Megles, J.E. Jr., Macdowell, J.F. and Bopp, H.F. (1968), "Strengthening glass-ceramics by application of compressive glazes." J. Am. Ceram. Soc., 51, 98-102.

Emrich, A., (1964), "Technology of new devitrified ceramics, A Literature review." Tech. Report No. ML. TDR 64, 203.

Eudier, M., (1962), "Mechanical properties of sintered low-alloy steels." Powder Met., No.9, 278-90.

Farmer, V.C., (1974), "The infrared spectra of minerals." Mineralogical Society, London.

Forest, J., (1964), "Contribution a la connaissance de ciments lies par lacid orthophosphorique et a letude de certains phosphate d'aluminium." Revue Mater. Contr. Trav. Publ., 580, 1-12.

Freeman, J.L. and Rayment, D.L., (1975), "Scanning electron micrographs of some structural ceramic materials." Trans. J. Br. Ceram. Soc., 74, 611-618.

Gannon, R.E., Harris, G.M. and Vasilos, T., (1965), "Effect of porosity on mechanical, thermal and dielectric properties of fused silica." Am. Ceram. Soc. Bull., 44 [5], 460-62.

Genin, L.G., (1958), "Influence of quartz on the strength of porcelain." Steklo i Keram., 15 [4], 35-38.

Gentile, A.L. and Foster, W.R., (1961), "System $CaO-Al_2O_3-SiO_2$." Phase diagrams for ceramists, Fig. 631, The Am. Ceram. Soc., Ohio.

German, W.L., (1952), "Observations on the properties of pottery fired on rapid schedules in some types of tunnel ovens." Trans. Br. Ceram. Soc., 51, 198-202.

Griffith, A.A., (1920), "The phenomenon of rupture and flow in solids." Phil. Trans. Roy. Soc., London. A221(4), 163.

REFERENCES

Grofcsik, Janos, (1966), "The strength increase of electrical porcelain." Chem. Abstr., 65, 10302 h.

Harrison, W.B., (1964), "Influence of surface condition on the strength of polycrystalline magnesium oxide." J. Am. Ceram. Soc., 47 [11], 574-79.

Harward, M.E. and Coleman, N.T., (1954), "Some properties of H- and Al-clays and exchange resins." Soil Sci., 78, 181-188.

Haseman, J.F., Brown, E.H. and Whitt, C.D., (1950), "Some reactions of phosphate with clays and hydrous oxides of iron and aluminium." Soil Sci., 70, 257-71.

Hasselman, D.P.H., (1962), "On the porosity dependence of the elastic moduli of polycrystalline refractory materials." J. Am. Ceram. Soc., 45, 452-453.

Hasselman, D.P.H. and Fulrath, R.M., (1964), "Effect of small fraction of spherical porosity on elastic moduli of glass." J. Am. Ceram. Soc., 47 [1], 52-53.

Hemwall, J.B., (1957), "The role of soil clay minerals in phosphorous fixation." Soil Sci., 83, 101-108.

Herath, J.W., (1973), "Industrial clays of Sri Lanka." Econ. Bull. No. 1, Geol. Survey Dept., Sri Lanka.

Hsu, Pa Ho and Bates, T.F., (1964), "Formation of X-ray amorphous and crystalline aluminium hydroxides." Mineral. Mag., 33, 749-768.

Inglis, C.E., (1913), "Stresses in a plate due to the presence of cracks and sharp corners." Trans. Inst. Nav. Arch., 55, 219-229.

Insley, H. and Frechette, C.D., (1955), "Microscopy of ceramics and cements." Academic Press, New York.

Jacoby, W.R., (1957), "Equilibrium relations in a portion of the system SiO_2-P_2O_5." Publ. No. 22528, 119 pp.; Dissertation Abstr., 17, 2233.

Jameson, R.F. and Salmon, J.E., (1954), "Phase diagram and ion-exchange studies of the system aluminium oxide-phosphoric oxide-water at 25 C." J. Chem. Soc., 4013-4015.

Jones, J.T., Maitra, P.K. and Cutler, I.B., (1958), "Role of structural defects in the sintering of alumina and magnesia." J. Am. Ceram. Soc., 41 [9], 353-57.

Jorgensen, P.J., (1965), "Modification of sintering kinetics by solute segregation in alumina." J. Am. Ceram. Soc., 48 [3], 207-210.

Jorgensen, P.J. and Westbrook, J.H., (1964), "Role of solute segregation at grain boundaries during final stage of sintering of alumina." J. Am. Ceram. Soc., 47 [7], 332-38.

Kingery, W.D., (1950), "Fundamental study of phosphate bonding in refractories: Part I." J. Am. Ceram. Soc., 33 [8], 239-241.

REFERENCES

Kingery, W.D., (1952), "Fundamental study of phosphate bonding in refractories: Part IV." J. Am. Ceram. Soc., 35 [3], 61-63.

Kingery, W.D. and Berg, M., (1955), "Study of the initial stages of sintering solids by viscous flow, evaporation-condensation, and self-diffusion." J. Appl. Phys., 26 [2], 1205-1212.

Kingery, W.D., (1959), "Devitrification during sintering in the presence of a liquid phase." J. Appl. Phys., 30 [3], 301-306.

Kingery, W.D., (1960), "Introduction to ceramics." First edition , Wiley and sons, London.

Kingery, W.D., (1962), "The physics and chemistry of ceramics." Proc. of Symp. held at Pennsylvania State Univ. May 28-30, edited by Cyrus Klingsberg.

Kingery, W.D., (1986), "Ancient technology to modern science." Vol. 1, Am. Ceram. Soc.

Kittrick, J.A. and Jackson, M.L., (1956), "Electron-microscope observations of the reaction of phosphate with minerals, leading to a unified theory of phosphate fixation in soils." J. Soil Sci., 7, 81-89.

Knudsen, F.P., (1959), "Dependence of mechanical strength of brittle polycrystalline specimens on porosity and grain size." J. Am. Ceram. Soc., 42 [8], 376-87.

Koch, H., (1970), "The influence of kaolin and clays on the mechanical strength of porcelain." Ber. Deut. Keram. Ges., 47, 538-44.

Kodama, H. and Oinuma, K., (1963), "Identification of kaolin minerals in the presence of chlorite by X-ray diffraction and infrared absorption spectra." Clays Clay Miner., 11, 236-249.

Krause, Otto and Ursala, Klempin, (1942), "Relationships between grain size of quartz and properties of hard porcelain." Sprechsaal, 75 [23-24], 229-31; [25-26], 251-55; [27-28], 273-76; [47-48], 480.

Kriegel, W.W., Hayne, Palmer III and Choi, D.M., (1965), "Special ceramics." 167-86, edited by P. Popper, Academic press, New York.

Kuczynski, G.C., (1949), "Self-diffusion in sintering metal powders." Trans. AIME., 185, 169.

Lach, V., (1974), "The formation mullite on the temperature range above 1000 C." Inter. Ceram., 23 [1], 27-29.

Laws, W.D. and Page, J.B., (1946), "Changes produced in kaolinite by dry grinding." Soil Sci., 62, 319-336.

Layden, G.K. and McQuarrie, M.C., (1959), "Effect of minor additions on sintering of magnesia." J. Am. Ceram. Soc., 42 [2], 89-92.

Leach, Bernard (1976), "A potters book." Faber and Faber, London.

REFERENCES

Ledoux, R.L. and White, J.L., (1964), "Infrared study of selective deuteration of kaolinite and halloysite at room temperature." Science, New York. 145, 47-49.

Lindsay, W.L. and Stephenson, H.F., (1959), "Nature of the reactions of mono-calcium phosphate monohydrate in soils." Soil Sci. Soc. Am. Proc., 23, 18-22.

Low, P.F., (1955), "The role of aluminium in the titration of bentonite." Soil Sci. Soc. Am. Proc., 19, 135-139.

Low, P.F. and Black, C.A., (1948), "Phosphate induced decomposition of kaolinite." Soil Sci. Soc. Am. Proc., 12, 180-184.

Mackenzie, J.K. and Shuttleworth, R., (1949), "Phenomenological theory of sintering." Proc. Phys. Soc., (London), 62, 833-52.

Mallinder, F.P. and Proctor, B.A., (1966), "The strengths of flame-polished sapphire crystals." Phil. Mag., 13, 197-207.

Maniatis, Y. and Tite, M.S., (1975), "A scanning electron microscope examination of the bloating of fired clays." Trans. J. Br. Ceram. Soc., 74, 229-232.

Marel, H.W. Van Der, (1966), "Quantitative analysis of clay minerals and their admixtures." Contrib. Miner. Petrol., 12, 96-138.

Mattyasovszky-Zsolnay, Laszlo, (1957), "Mechanical strength of porcelain." J. Am. Ceram. Soc., 40 [9], 299-306.

McKee, W.D. and Alestrin, E., (1963), "Aluminium oxide-titanium oxide solid solution." J. Am. Ceram. Soc., 46 [1], 54-58.

McKenzie, J.E., (1950), "The elastic constants of a solid containing spherical holes." Proc. Phys. Soc., (London), 63B, 2.

McKenzie, K.J.D., (1969) "The effects of impurities on the formation of mullite from kaolinite type minerals." Trans. Br. Ceram. Soc., 68 [3], 97-101.

Metcalfe, B.L. and Sant, J.H., (1975), "The synthesis, microstructure and physical properties of high purity mullite." Trans. J. Br. Ceram. Soc., 74, 193-201.

Meyer, W.W., (1938), "Computation of heat treatments for whiteware bodies." J. Am. Ceram. Soc., 21, 75-79.

Meyer, W.W. and Shelton, G.R., (1938), "Nature of the glass phase in heated clay minerals." J. Am. Ceram. Soc., 21, 371-385.

Mitchell, B.D., Farmer, V.C. and McHardy, W.J., (1964), "Amorphous inorganic materials in soils." Advances in Agronomy, 16, 327-383.

Morley, J.G. and Proctor, B.A., (1962), "Strengths of sapphire crystals." Nature, 196, 1082.

REFERENCES

Mukherjee. J.N., Chatterjee, B. and Bannerjee, B.M., (1948), "Liberation of H^{+}, Al^{3+} and Fe^{3+} ions from hydrogen clays by neutral salts." J. Colloid Sci., 3, 437-445.

Neal, M. and Worrall, W.E., (1977), "Mineralogy of fireclays -Part 1: The crystallinity of kaolinite in fireclays." Trans. Br. Ceram. Soc., 76, 57-61.

Niesper, A.A., (1958), "Uber das Trocknen von Ziegeltonen." 153 S, Diss. ETH Zurich.

Norton, C.L., (1931), "The influence of time on the maturing temperature of whiteware bodies." J. Am. Ceram. Soc., 14, 192-206.

Norton, F.H., (1970)," Fine ceramics". McGraw-Hill, Book Co., New York. 269.

Norton, F.H. and Hodgdon, F.B., (1931), "Influence of time on maturing temperature of whiteware bodies." J. Am. Ceram. Soc., 14 [3], 177-91.

Oinuma, K. and Hayashi, H., (1968), "Infrared spectra of clay minerals." J. Tokyo Univ., Gen. Educ. (Nat. Sci.) 9, 57-97.

Osborn, E.F. and Muan, Arnulf, (1964), "Phase diagrams for ceramists." Am. Ceram. Soc.

Orowan, E., (1948), "Fracture and strength of solids." Rep. Progr. Phys., 12, 186-232.

Parikh, N.M., (1966), "Fracture mechanisms in poly-crystalline non-metallic materials." Illinois Inst. of Tech. Res. Inst. Rep. No. II TRI B6057-6.

Parker, T.W., (1969), "A classification of kaolinite by infrared spectroscopy." Clay Miner., 8, 135-141.

Parmalee, C.W., (1973), "Ceramic glazes". Cahners Publishing Co., Inc. Massachusetts.

Parmelee, C.W. and Rodriquez, A.R., (1942), "Catalytic mullitization of kaolinite by metallic oxide." J. Am. Ceram. Soc., 25 [1], 1-10.

Passmore, E.M., Spriggs, R.M. and Vasilos, T., (1965), "Strength-grain size porosity relations in alumina." J. Am. Ceram. Soc., 48 [1], 1-7.

Paver, H. and Marshall, C.E., (1934), "The role of aluminium in the reaction of the clays." Chem. Ind., 12, 750-760.

Perkins, A.T., (1948), "Kaolins and treated kaolins and their reactions." Soil Sci., 65, 185-191.

Petch, N.J., (1953), "Cleavage strength of polycrystals." J. Iron Steel Inst., London. 174 [1], 25-28.

Poncelet, G.M. and Brindley, G.W., (1967), "Experimental formation of kaolinite from montmorillonite at low temperatures." Am. Miner., 52 [2], 1161-1173.

Poole, A.B., (1970), "Application of X-ray fluorescence to silicate analysis." Proc. Br. Ceram. Soc., 16, 41-51.

REFERENCES

Redfern, S.A.T., (1987), "The kinetics of dehydroxylation of kaolinite." Clay miner., 22, 447-456.

Ries, H., (1947), "Clays, their occurrence, properties and uses." Chapman and Hall, London. 281.

Robinson, P. and McCartney, E.R., (1964), "Subsolidus relations in the system SiO_2-Al_2O_3-P_2O_5." J. Am. Ceram. Soc., 47, 587-592.

Robinson, P. and Segnit, E.R., (1967), "The influence of phosphoric acid on the forming, constitution, and properties of dry pressed steatite bodies." J. Aust. Ceram. Soc., Vol.3, No.1, 9-17.

Russell, G.C. and Low, P.F., (1954), "Reaction of phosphate with kaolinite in dilute solutions." Soil Sci. Soc. Am. Proc., 18, 22-25.

Schofield, R.K., (1939), "The electrical charges on clay particles." Soils and Fertilizers, 2, 1-5.

Schuster, P., Gugel, E. and Hennicke, H.W., (1972), "Investigations on texture and properties of stonewares: II formation and mode of occurrence of mullite in a stoneware body." Ber. Deut. Keram. Ges., 49 [9], 291-94.

Secor, R.B., and Radke, C.J., (1985), "Spillover of the diffuse double layer on montmorillonite particles." J. Colloid Interface Sci., 103, 237-244.

Segnit, E.R. and Anderson, C.A., (1972), "Scanning electron microscopy of fired illite." Trans. J. Br. Ceram. Soc., 71, 85-88.

Segnit, E.R. and Gelb, T., (1971), "Kaolinite-$CaCO_3$ reactions below 1000 C." J. Aust. Ceram. Soc., Vol. 7, No. 1, 1-6.

Shelton, G.R. and Meyer, W.W., (1938), "Nature of the glass phase in heated clay minerals." J. Am. Ceram. Soc., 21, 371-385.

Shepard, F.P., (1954), "Nomenclature based on sand-silt-clay ratios." J. Sed. Pet., 24, 151-158.

Singer, F. and Singer, S.S., (1963), "Industrial ceramics." Chapman and Hall Ltd., London.

Skinner, K.G., Cook, W.H., Potter, R.A. and Palmour, H., (1953), J. Am. Ceram. Soc., 36 [11], 349-56.

SLS 39 (1978) "Specification for common burnt clay building bricks." Sri Lanka Standards Institution.

Smith, A.N., (1954), "Investigations on glaze body layers. II-Influence of the layer on crazing and peeling." Trans. Br. Ceram. Soc., 53, 220.

Smothers, W. J. and Reynolds, H.J., (1954), "Sintering and grain growth of alumina." J. Am. Ceram. Soc., 37, 588-95.

Smykatz-Kloss, W., (1974), "Differential thermal analysis." Springer-Verlog, New York. 69.

REFERENCES

Spriggs, R.M., (1962), "Effect of open and closed pores on elastic moduli of polycrystalline alumina." J. Am. Ceram. Soc., 45 [9], 454.

Spriggs, R.M., (1961), "Expression for effect of porosity on elastic modulus of polycrystalline refractory materials, particularly aluminium oxide." J. Am. Ceram. Soc., 44, 628.

Spriggs, R.M., Mitchell, J.B. and Vasilos, T., (1964), "Mechanical properties of pure dense aluminium oxide as a function of temperature and grain size." J. Am. Ceram. Soc., 47 [7], 323-27.

Srbek, F., Kunes, K. and Hanykyr V., (1972), Silikaty, 16, 295.

Stokes, R.J., Johnston, T.L. and Li, C.H., (1959), "The relationship between plastic flow and the fracture mechanism in magnesium oxide single crystals." Phil. Mag., 920-932.

Stokes, R.J. and Li, C.H., (1963), "Dislocations and the tensile strength of magnesium oxide." J. Am. Ceram. Soc., 46 [9], 423-34.

Stout, P.R., (1940), "Alterations in the crystal structure as a result of phosphate fixation." Soil Sci. Soc. Am. Proc., 4, 177-182.

Stubican, V. and Roy, R., (1961), "A new approach to the assignment of infrared absorption bands in layer silicates." Z. Kristallogr., 115, 200-214.

Studt, P.C. and Fulrath, F.M., (1962), "Mechanical properties and chemical reactivity in mullite-glass systems." J. Am. Ceram. Soc., 45 [3], 182-88.

Stull, T. and Johnson, P.V., (1942), "Low-cost glazes for structural clay products." U.S. Nat. Bureau of Stds., 1-20.

Sudakas, L.G. and Sinina, L.M., (1971), "Regulation of the time of binding and hardening of phosphate binders." Inorg. Mater., 7, 537-538.

Symmers, C., Ward, J.B. and Sugarman, B., (1962), "Studies of the mechanical strength of glass." Phys. Chem. Glasses. 3, 76-83.

Tauber, E., Pepplinkhouse, H.J., Crook, D.N. and O'Brien, R.J., (1972), "Phosphate-bonded zircon refractories." Proc. Aust. Inst. Min. Met., No. 244 47-55.

Taylor, A.W. and Gurney, E.L., (1961), "Solubilities of potassium and ammonium taranakites." J. Phys. Chem., 65, 1613-1616.

Taylor, J.R. and Bull, A.C.,(1986), "Ceramic glaze technology." The Institute of Ceramics, London.

Thurn, H.L., (1945),"Use of wood ash in a low fire mat glaze." J. Am. Ceram. Soc., 28, 261-264.

REFERENCES

Tichane, R., (1986), "Ashes and glazes-scientific and technological insights on ancient chinese pottery and porcelain." Shanghai Inst. of Ceram., China, 265-268.

Tien, T.Y. and Hummel, F.A., (1962), "System SiO_2-P_2O_5." J. Am. Ceram. Soc., 45 [9], 422-424.

Tite, M.S. and Maniatis, Y.,(1975), "Scanning electron microscopy of fired calcareous clays." J. Br. Ceram. Soc., 74, 19-22.

Turner, W.E.S., (1956), "Studies in ancient glasses and glass-making processes." J. Soc. Glass Tech., 40, 270-300.

Uhlman, D.R. and Kreidl, N.J., (1980), Glass science and technology, Vol.5, Academic Press, London. 22.

Van Vlack, L.H., (1960), "Microstructure of silica in the presence of iron oxide." J. Am. Ceram. Soc., 43, 140-145.

Van Vlack, L.H. and Riegger, O.K., (1962), "Microstructures of magnesiowustite,(Mg, Fe)O in the presence of silica." Trans. AIME,, 224, 957-65.

Vasilos, T., Mitchell, J.B. and Spriggs, R.M., (1964), "Mechanical properties of pure dense magnesium oxide as a function of temperature and grain size." J. Am. Ceram. Soc., 12, 606-10.

Veith, J.A. and Sposito, G., (1977), "Reactions of aluminosilicates, aluminium hydrous oxides and aluminium oxide with o-phosphate: The formation of X-ray amorphous analogs of variscite and montebrasite." Soil. Sci. Soc. Am., 41, 870-876.

Vernetti, R.A. and Cook, R.I., (1966), "Effect of metal oxide additions on the high-temperature electrical conductivity of alumina." J. Am. Ceram. Soc., 49 [3], 194-99.

Wada, K., (1959), "Reaction of phosphate with allophane and halloysite." Soil Sci., 87, 325-330.

Walsh, J.N. and Howie, R.A., (1980), "An evaluation of the performance of an inductively coupled plasma source spectrometer for the determination of the major and trace constituents of silicate rocks and minerals." Mineral. Mag., 43, 967-974.

Warshaw, S.I. and Seider, R., (1967), "Comparison of strength of triaxial porcelains containing alumina and silica." J. Am. Ceram. Soc., 50 [7] , 337-343.

Weil, N.A.,(1963), "Parametric effects governing the mechanics of ceramic materials." Proc. Int. Symp. High Temperature Technology, California, 1963, Edited by N.K. Hiester.

Westwood, A.R.C., (1960), "The effects of surface condition on the mechanical properties of lithium fluoride crystals." Phil. Mag., 5, 981-990.

REFERENCES

White, J. and Murray, P.,(1949), "Kinetics of the thermal dehydration of clays." Trans. Br. Ceram. Soc., 48, 187-197.

Wiedmann, T., (1959), "Strength carriers in porcelain." Sprechsaal, 92 [1], 2-5; [2], 29-30; [3], 52-55.

Wild, A., (1953), "The effect of exchangeable cations on the retention of phosphate by clay." J.Soil Sci., 4, 72-85.

Wilson, J., (1966), "The weathering of biotite in some Aberdeenshire soils." Mineral. Mag., 35, 1080-1093.

Winkler, H.G.F., (1954), "Bedeutung der Korngrosenverteilung und des Mineral bestandes von tonen fur die horstellung grobkeramischer erzeugnisse." Ber. Deut. Keram.Ges., 31, 337-343.

Wright, B.C. and Peech, M., (1960), "Characterization of phosphate reaction products in acid soils by the application of solubility criteria." Soil Sci., 90, 32-43.

APPENDIX 1

X-RAY DIFFRACTION PATTERNS OF THE RAW CLAYS

APPENDIX 1

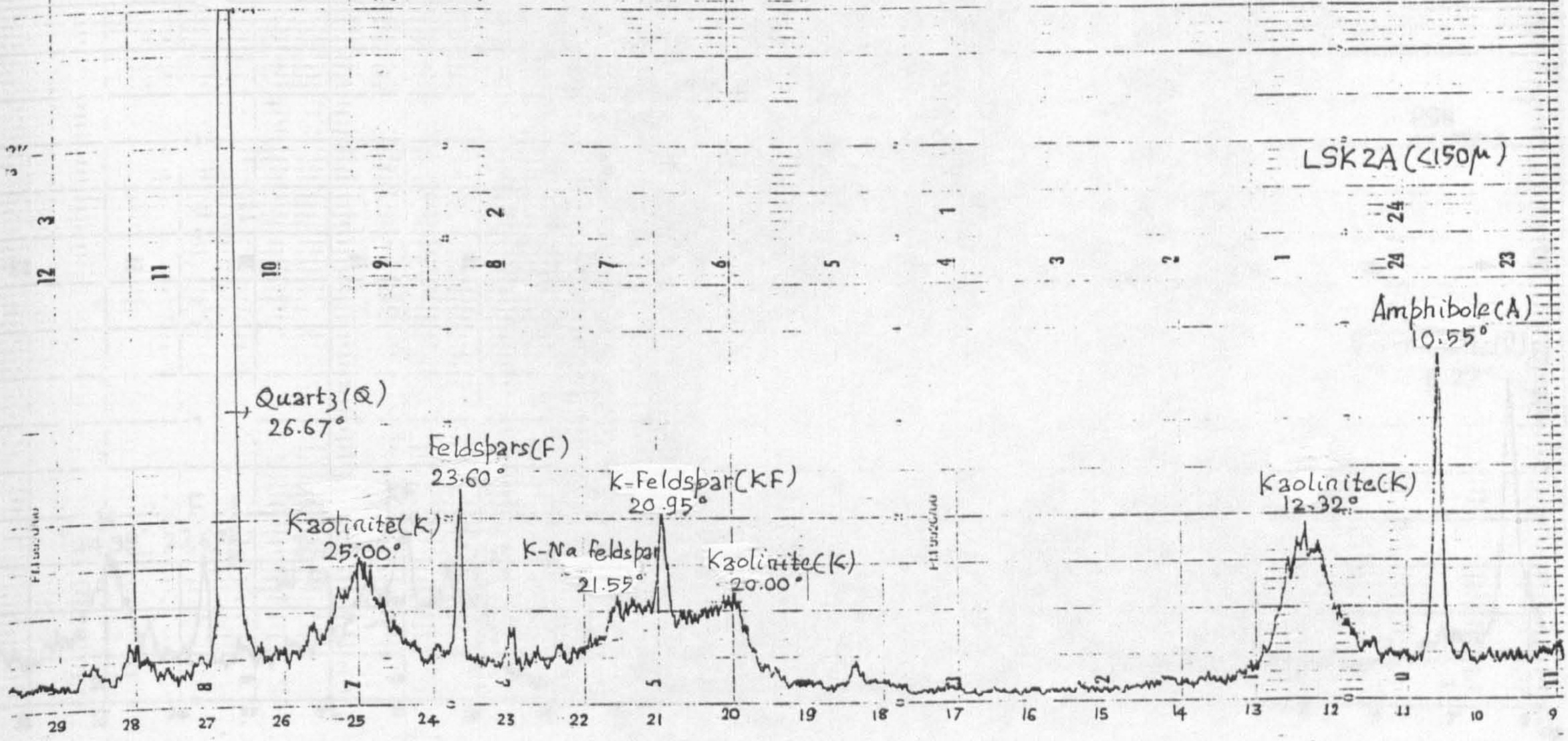
LSK2A (<150μ)
Amphibole(A)
10.55°
Quartz(Q)
26.67°
Feldspars(F)
23.60°
K-Feldspar(KF)
20.95°
Kaolinite(K)
12.32°
Kaolinite(K)
25.00°
K-Na feldspar
21.55°
Kaolinite(K)
20.00°

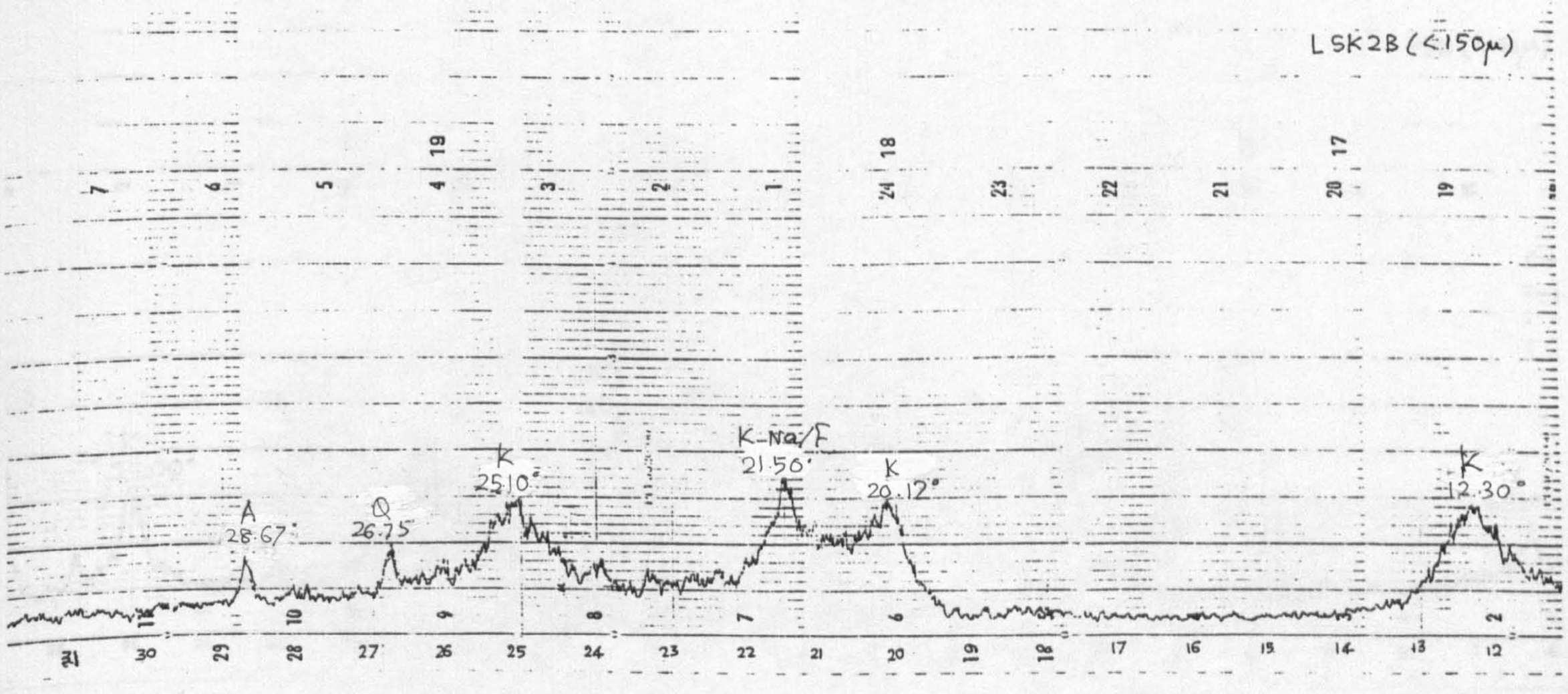
LSK2B (<150μ)
A
28.67°
Q
26.75°
K
25.10°
K-Na/F
21.50°
K
20.12°
K
12.30°

APPENDIX I

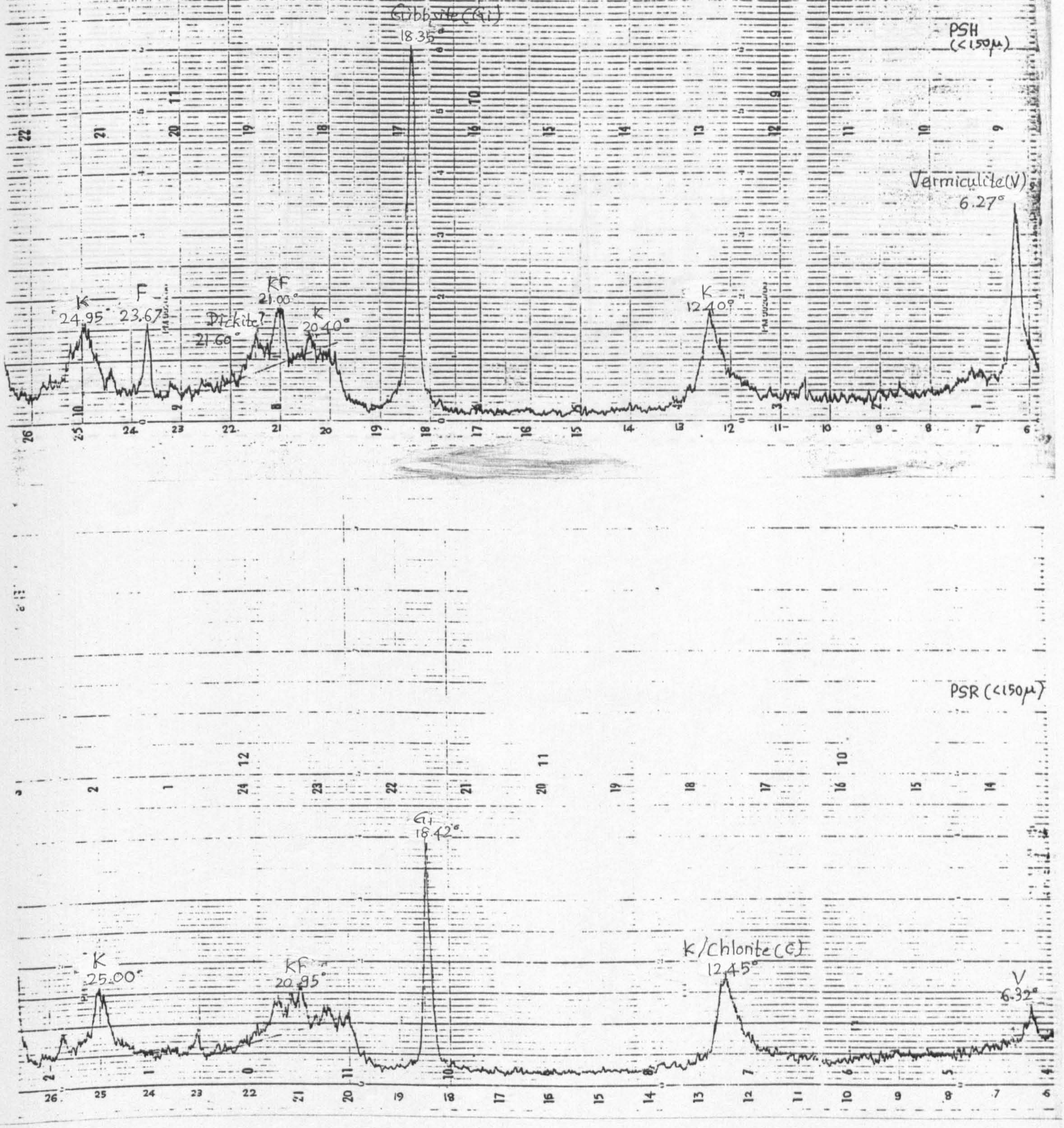
Gibbsite(G1)
18.35°
PSH
(<150μ)
Vermiculite(V)
6.27°
K
24.95°
F
23.67°
Dickite?
21.60°
KF
21.00°
K
20.40°
K
12.40°
PSR (<150μ)
G1
18.42°
K
25.00°
KF
20.95°
K/Chlorite(CI)
12.45°
V
6.32°

APPENDIX 1

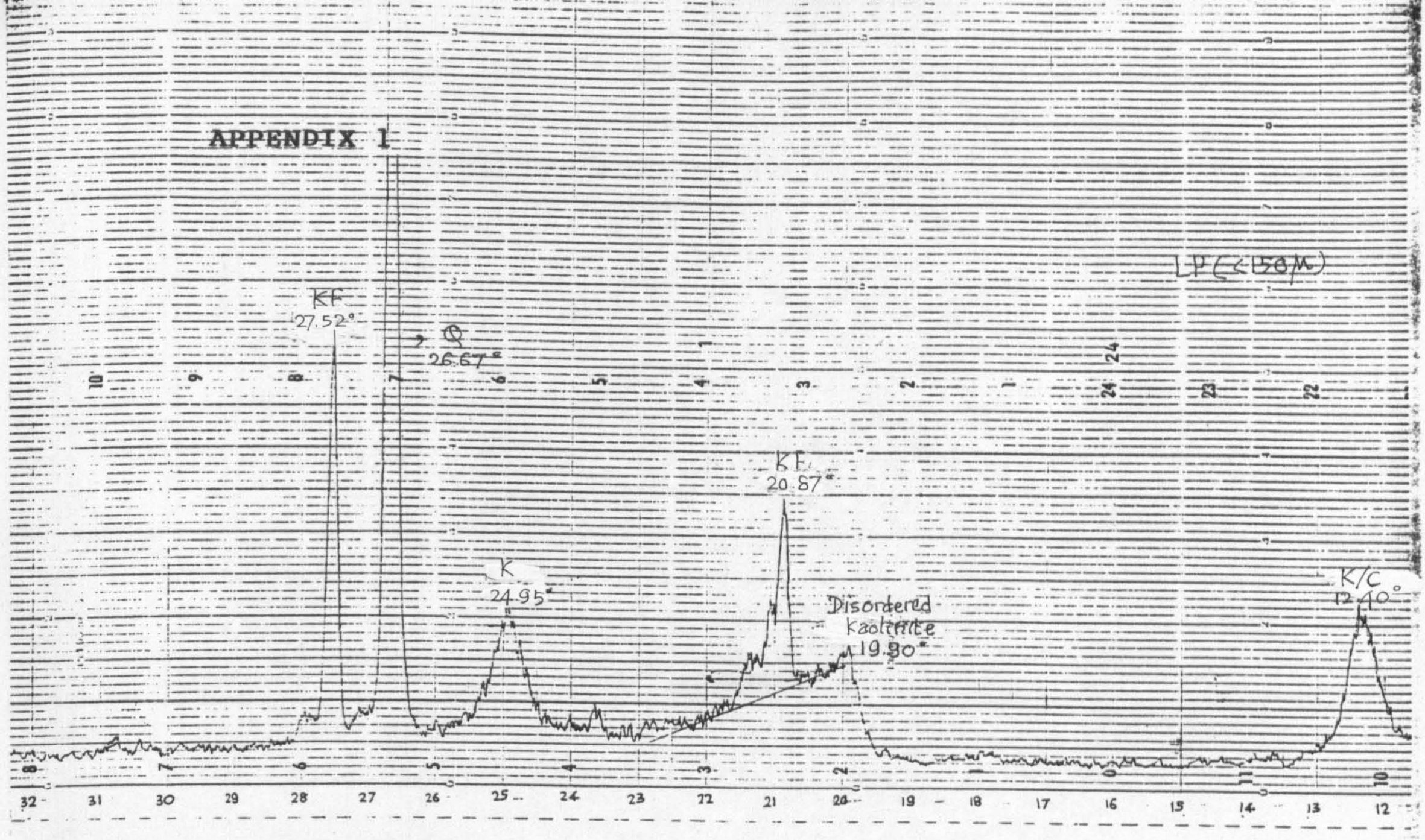
LP(≤150μ)
KF
27.52°
26.67°
KF
20.87°
K
24.95°
Disordered
kaolinite
19.90°
K/C
12.40°
32
31
30
29
28
27
26
25
24
23
22
21
20
19
18
17
16
15
14
13
12

APPENDIX 2

DTA CURVES OF THE CLAYS

APPENDIX 2

DATE: 8/2/90	SAMPLE LSK2A	DTA/TG

ATMOSPHERE: ARGON/65		CRUC/PREPn: PT/AL203 REF.	
EXPERIMENT Nº: 1	TEMP. PROGRAMME: HEAT	MIN. UTP TEMP (°C): 25	WEIGHT RANGE (mg): 30.4
SAMPLE WEIGHT (mg): 30.4	HEATING RATE (°C/min): 10	MAX. UTP TEMP (°C): 1150	WEIGHT SENSITIVITY: × 1
OPERATOR: RS	Nº OF CYCLES: 1	DTA RANGE (µV): 80	DTG RANGE (µg/min): 4000

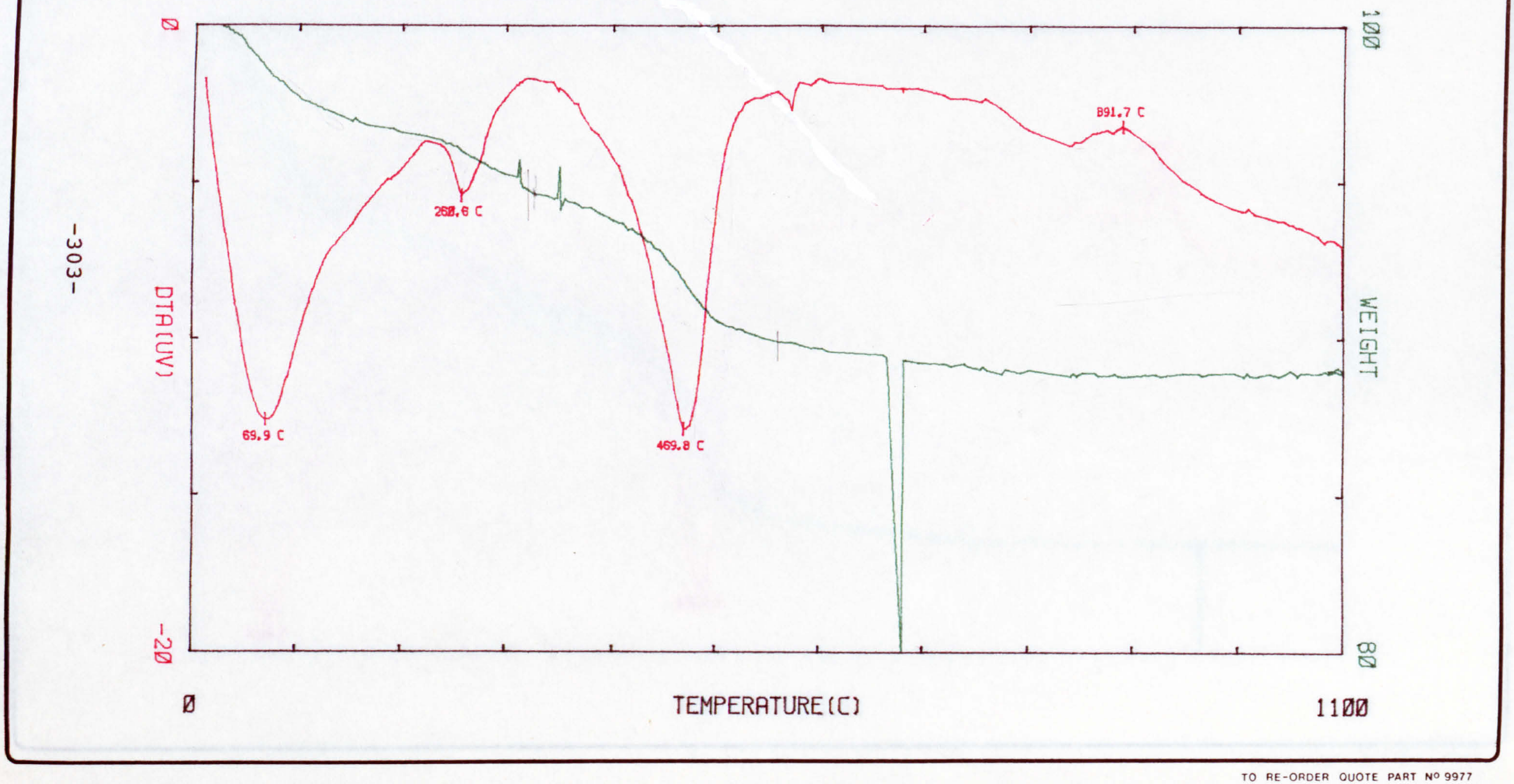

DATE: 23/4/90	SAMPLE: L5K2B	DTA/TG

ATMOSPHERE: AIR/65		CRUC/PREPn: PT/AL2O3 REF.	
EXPERIMENT Nº: 3	TEMP. PROGRAMME: HEAT	MIN. UTP TEMP (°C): 25	WEIGHT RANGE (mg): 32.76
SAMPLE WEIGHT (mg): 32.76	HEATING RATE (°C/min): 10	MAX. UTP TEMP (°C): 1150	WEIGHT SENSITIVITY: × 1
OPERATOR: RS	Nº OF CYCLES: 1	DTA RANGE (µV): 50	DTG RANGE (µg/min): 1000

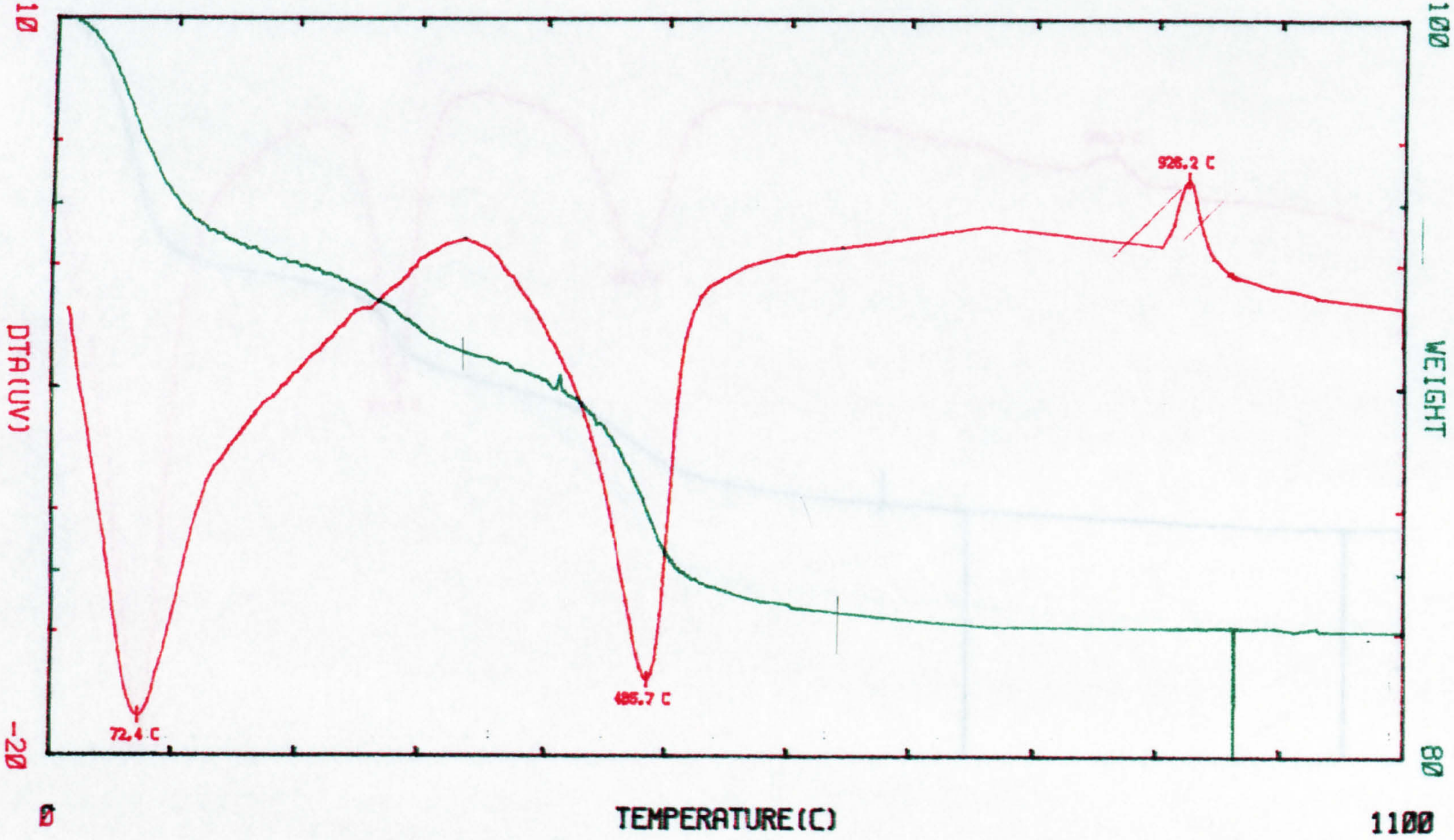

DATE: 8/2/90	SAMPLE: PSH	DTA/TG

ATMOSPHERE: ARGON/65		CRUC/PREPn: PT/AL203REF	
EXPERIMENT No: 2	TEMP. PROGRAMME: HEAT	MIN. UTP TEMP (°C): 25	WEIGHT RANGE (mg): 34.81
SAMPLE WEIGHT (mg): 34.81	HEATING RATE (°C/min): 10	MAX. UTP TEMP (°C): 1150	WEIGHT SENSITIVITY: × 1
OPERATOR: RS	No OF CYCLES: 1	DTA RANGE (µV): 50	DTG RANGE (µg/min): 4000

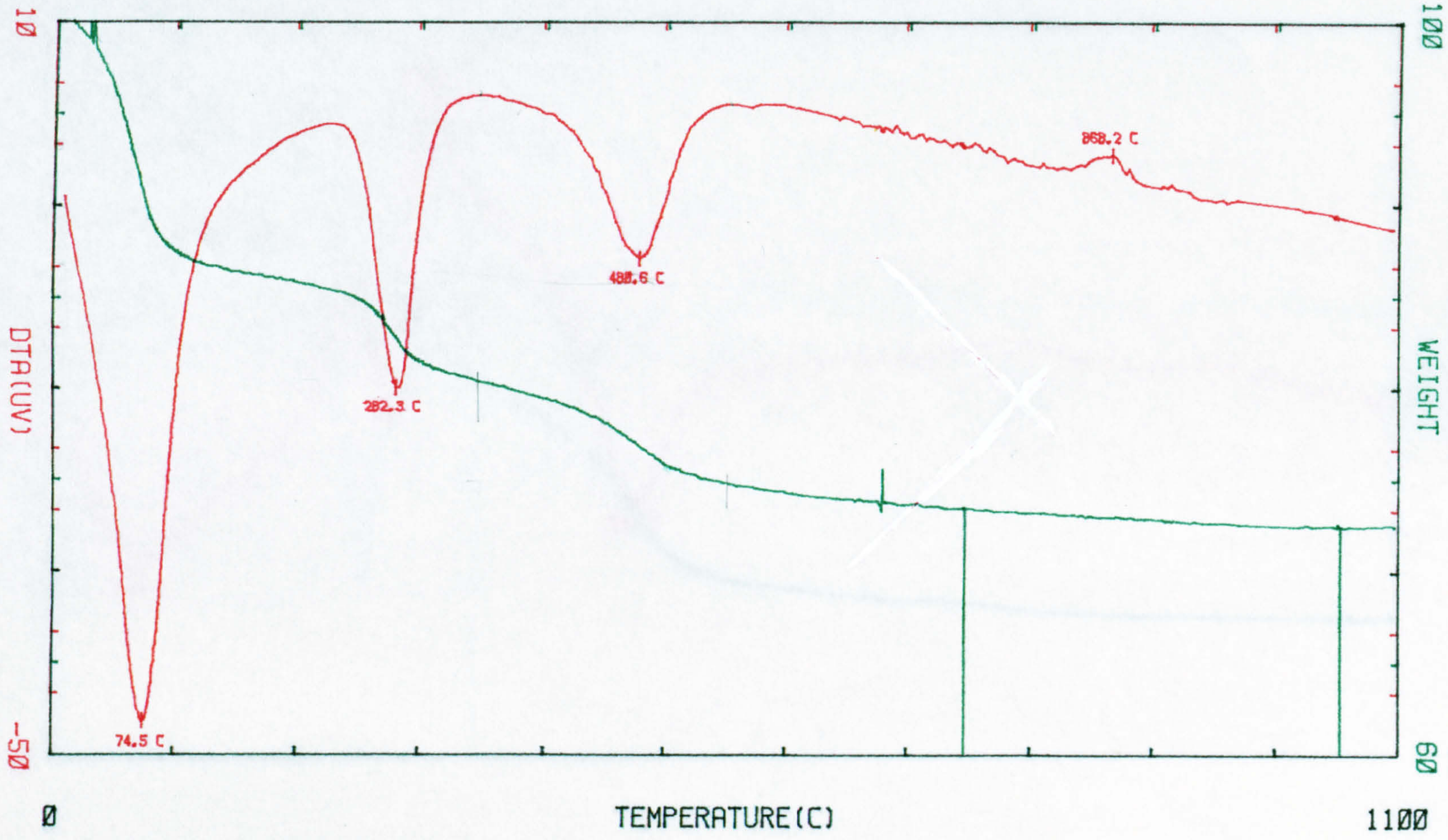

DATE: 23/4/90	SAMPLE: PSR	DTA/TG

ATMOSPHERE: AIR/65		CRUC/PREPn: PT/RL203 REF.	
EXPERIMENT Nº: 1	TEMP. PROGRAMME: HEAT	MIN. UTP TEMP (°C): 25	WEIGHT RANGE (mg): 27.95
SAMPLE WEIGHT (mg): 27.95	HEATING RATE (°C/min): 10	MAX. UTP TEMP (°C): 1150	WEIGHT SENSITIVITY: × 1
OPERATOR: RS	Nº OF CYCLES: 1	DTA RANGE (µV): 50	DTG RANGE (µg/min): 1000

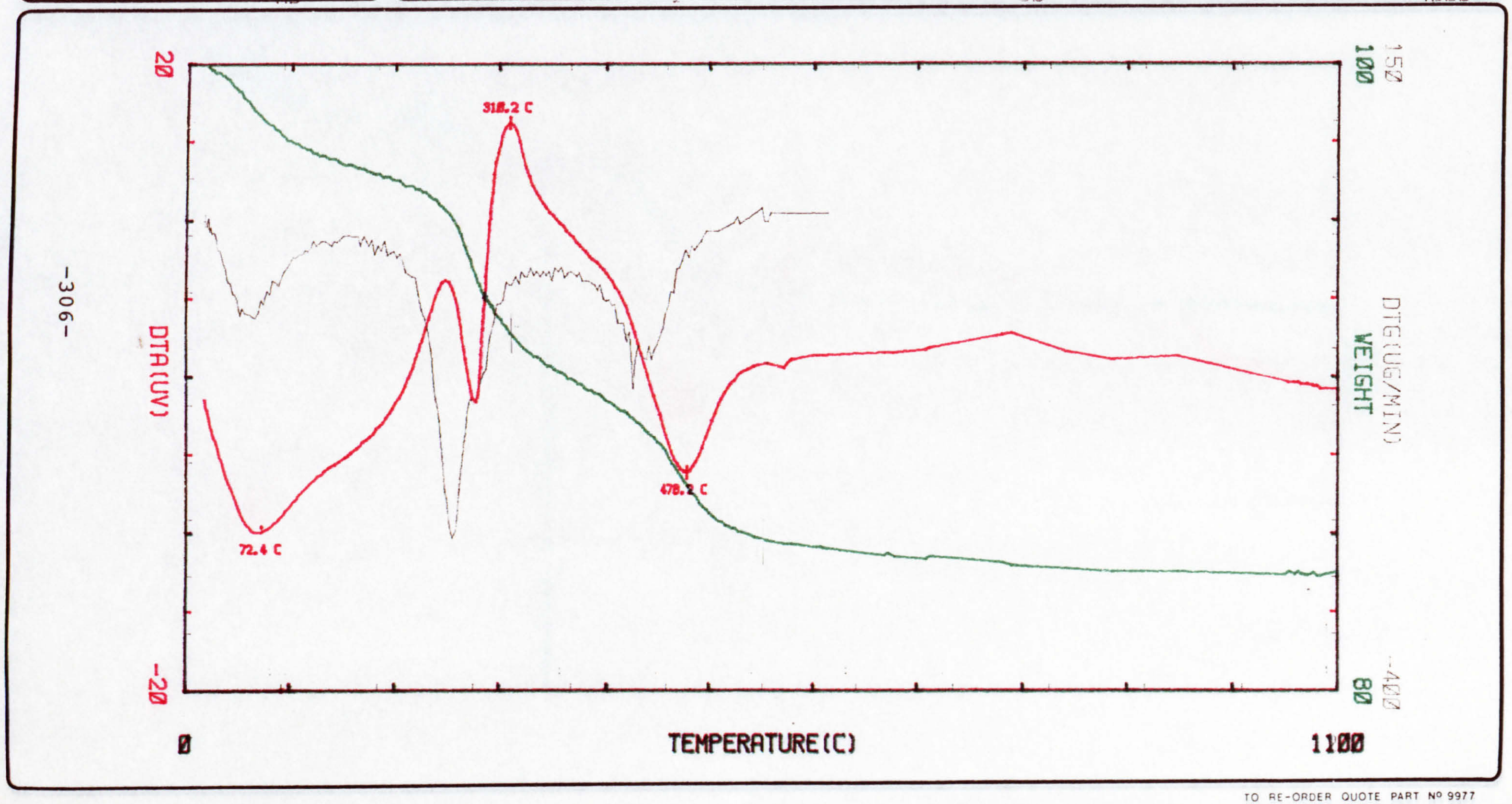

DATE: 24/4/90	SAMPLE: I P	DTA/TG

ATMOSPHERE: AIR/65		CRUC/PREPn: PT/Al2O3 REF	
EXPERIMENT No: 5	TEMP. PROGRAMME: HEAT	MIN. UTP TEMP (°C): 25	WEIGHT RANGE (mg): 20 22
SAMPLE WEIGHT (mg): 30.22	HEATING RATE (°C/min): 10	MAX. UTP TEMP (°C): 1150	WEIGHT SENSITIVITY: ×
OPERATOR: RS	No OF CYCLES: 1	DTA RANGE (µV): 50	DTG RANGE (µg/min): 1000

APPENDIX 2

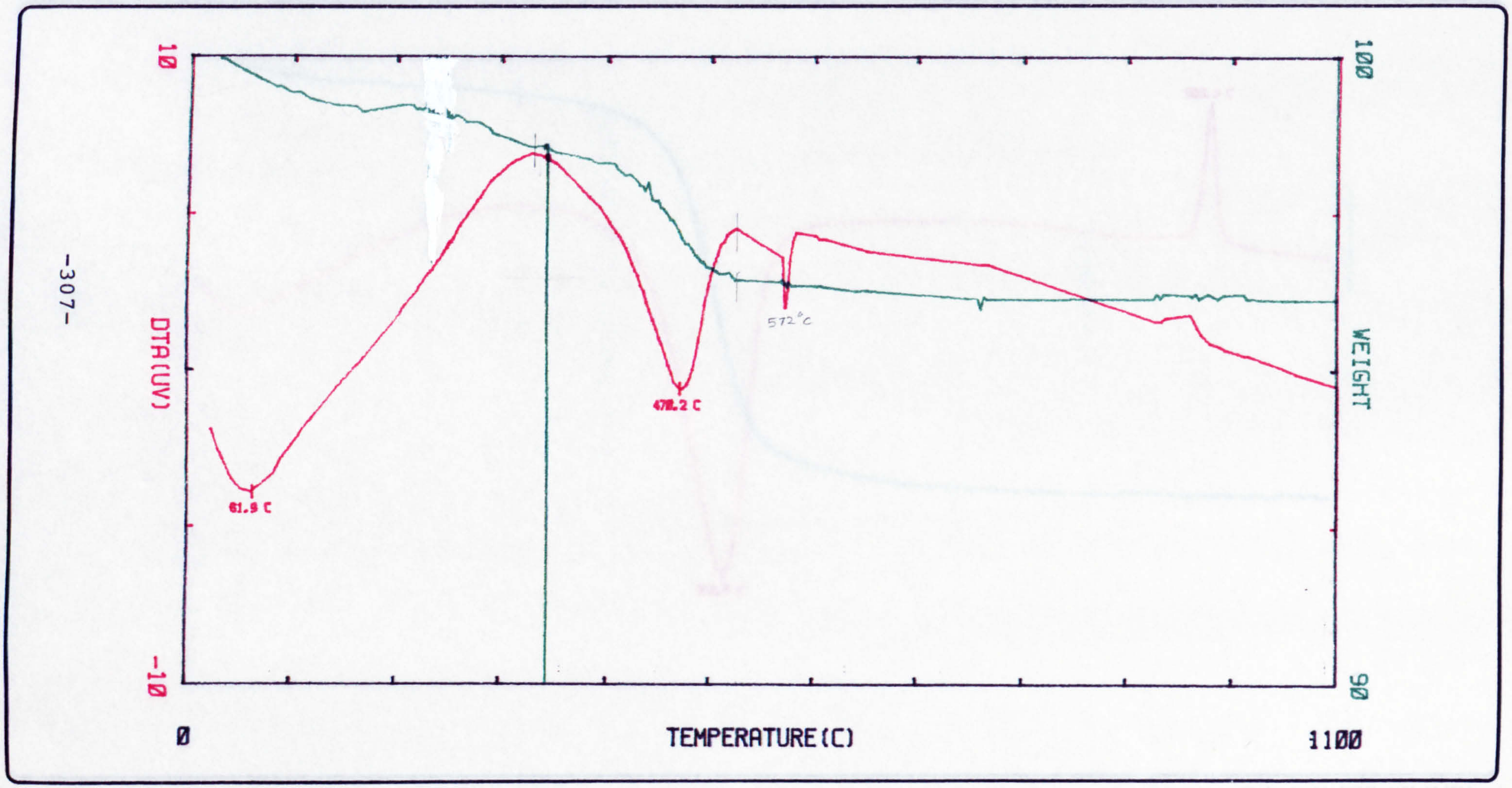

DATE: 24/4/90	SAMPLE: SK	DTA/TG

ATMOSPHERE: AIR/65		CRUC/PREPn: PT/AL2O3 REF	
EXPERIMENT Nº: 6	TEMP. PROGRAMME: HEAT	MIN. UTP TEMP (°C): 25	WEIGHT RANGE (mg): 33.61
SAMPLE WEIGHT (mg): 33.61	HEATING RATE (°C/min): 10	MAX. UTP TEMP (°C): 1150	WEIGHT SENSITIVITY: × 1
OPERATOR: RS	Nº OF CYCLES: 1	DTA RANGE (µV): 50	DTG RANGE (µg/min): 4000

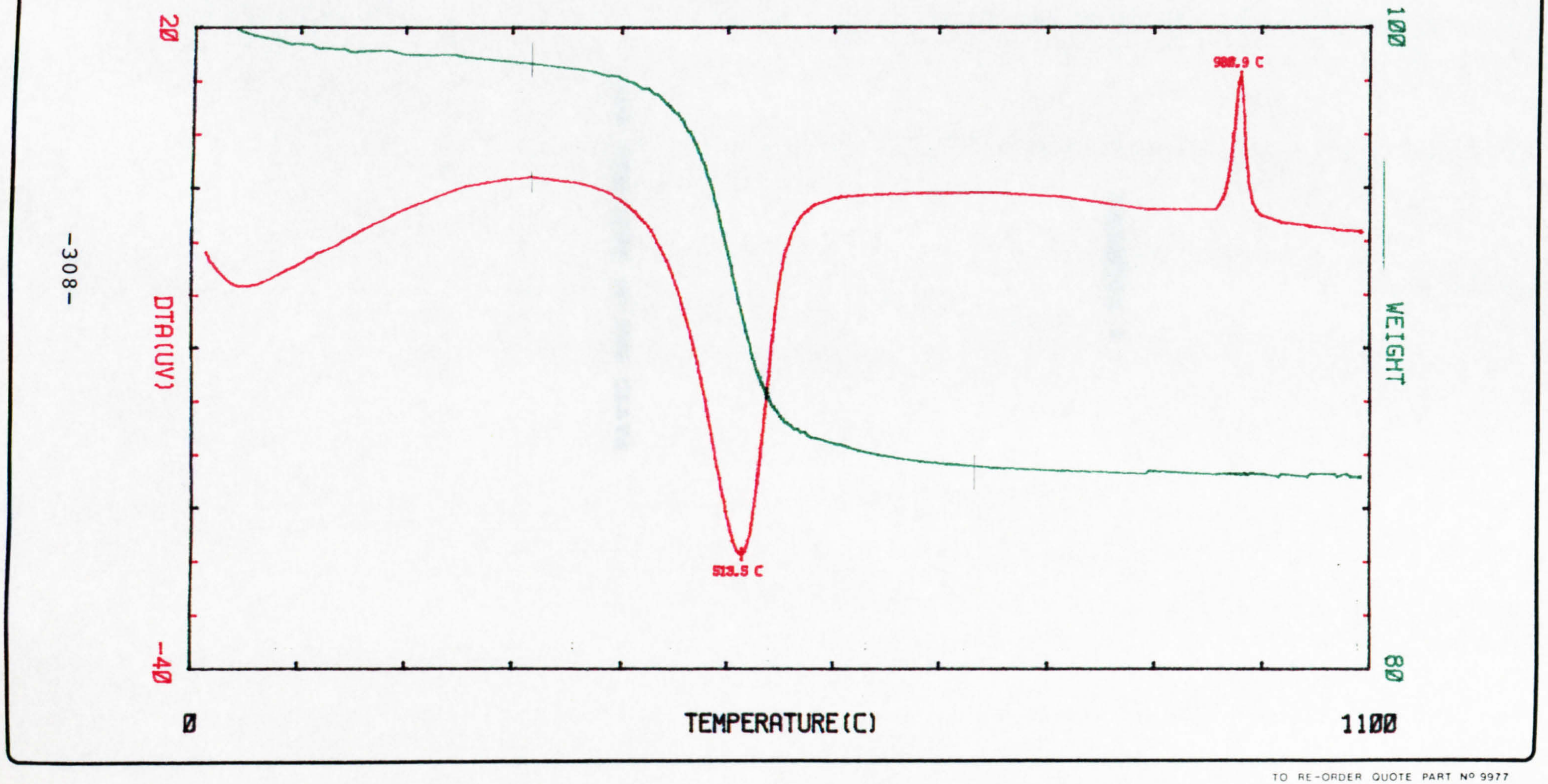

APPENDIX 3

ICP ANALYSES OF THE CLAYS

APPENDIX 3

Royal Holloway and Bedford New College 12-JAN-89 11:49
Sample: LSK 1(1) AP: TRACES 12-JAN-89 11:49
Concentrations

Al2O3	Fe2O3	MgO	CaO	Na2O
22.57 %		1.08 %	0.66 %	0.15 %

K2O	TiO2	P2O5	MnO	Ba
0.64 %	1.03 %	0.12 %	0.25 %	764 ppm

Co	Cr	Cu	Li	Mo
59 ppm	303 ppm	83 ppm	15 ppm	-15 ppm

Nb	Ni	Sc	Sr	V
14 ppm	79 ppm	36 ppm	103 ppm	239 ppm

Y	Zn	Zr	La	Ce
48 ppm	88 ppm	34 ppm	63 ppm	202 ppm

Nd	Sm	Eu	Dy	Yb
123 ppm	18.9 ppm	2.9 ppm	11.3 ppm	5.1 ppm

Fe
14.40 %

Royal Holloway and Bedford New College 12-JAN-89 11:50
Sample: LSK 1 2 AP: TRACES 12-JAN-89 11:50
Concentrations

Al2O3	Fe2O3	MgO	CaO	Na2O
22.22 %	15.63 %	1.07 %	0.66 %	0.15 %

K2O	TiO2	P2O5	MnO	Ba
0.62 %	1.02 %	0.12 %	0.25 %	754 ppm

Co	Cr	Cu	Li	Mo
59 ppm	278 ppm	82 ppm	18 ppm	-15 ppm

Nb	Ni	Sc	Sr	V
15 ppm	78 ppm	35 ppm	101 ppm	237 ppm

Y	Zn	Zr	La	Ce
46 ppm	88 ppm	35 ppm	61 ppm	201 ppm

Nd	Sm	Eu	Dy	Yb
120 ppm	18.8 ppm	2.8 ppm	11.2 ppm	4.9 ppm

Fe
14.24 %

Royal Holloway and Bedford New College 12-JAN-89 11:52
Sample: LSK 2B 1 AP: TRACES 12-JAN-89 11:52
Concentrations

Al2O3	Fe2O3	MgO	CaO	Na2O
22.86 %	17.36 %	0.89 %	0.84 %	0.12 %

K2O	TiO2	P2O5	MnO	Ba
0.24 %	1.30 %	0.12 %	0.19 %	411 ppm

Co	Cr	Cu	Li	Mo
50 ppm	330 ppm	83 ppm	19 ppm	-17 ppm

Nb	Ni	Sc	Sr	V
15 ppm	104 ppm	37 ppm	54 ppm	263 ppm

Y	Zn	Zr	La	Ce
31 ppm	81 ppm	42 ppm	34 ppm	104 ppm

Nd	Sm	Eu	Dy	Yb
102 ppm	13.2 ppm	1.9 ppm	8.7 ppm	4.1 ppm

Fe
15.48 %

Royal Holloway and Bedford New College 12-JAN-89 11:54
Sample: LSK 2B 2 AP: TRACES 12-JAN-89 11:54
Concentrations

Al2O3	Fe2O3	MgO	CaO	Na2O
21.83 %	16.45 %	0.85 %	0.81 %	0.11 %

K2O	TiO2	P2O5	MnO	Ba
0.23 %	1.24 %	0.12 %	0.19 %	389 ppm

Co	Cr	Cu	Li	Mo
48 ppm	308 ppm	81 ppm	19 ppm	-15 ppm

Nb	Ni	Sc	Sr	V
14 ppm	101 ppm	35 ppm	50 ppm	251 ppm

Y	Zn	Zr	La	Ce
29 ppm	81 ppm	40 ppm	33 ppm	100 ppm

Nd	Sm	Eu	Dy	Yb
97 ppm	13.2 ppm	1.8 ppm	8.4 ppm	3.9 ppm

Fe
14.81 %

APPENDIX 3

Royal Holloway and Bedford New College 12-JAN-89 12:01
Sample: PSR 1 AP: TRACES 12-JAN-89 12:01
Concentrations

Al2O3	Fe2O3	MgO	CaO	Na2O
22.02 %	12.22 %	0.46 %	0.50 %	0.23 %

K2O	TiO2	P2O5	MnO	Ba
1.01 %	1.06 %	0.16 %	0.09 %	479 ppm

Co	Cr	Cu	Li	Mo
23 ppm	270 ppm	53 ppm	24 ppm	-11 ppm

Nb	Ni	Sc	Sr	V
18 ppm	92 ppm	23 ppm	106 ppm	161 ppm

Y	Zn	Zr	La	Ce
34 ppm	109 ppm	159 ppm	64 ppm	149 ppm

Nd	Sm	Eu	Dy	Yb
98 ppm	14.4 ppm	1.7 ppm	8.7 ppm	4.0 ppm

Fe
11.61 %

Royal Holloway and Bedford New College 12-JAN-89 12:03
Sample: PSR 2 AP: TRACES 12-JAN-89 12:02
Concentrations

Al2O3	Fe2O3	MgO	CaO	Na2O
22.72 %	11.14 %	0.46 %	0.42 %	0.24 %

K2O	TiO2	P2O5	MnO	Ba
1.02 %	1.05 %	0.15 %	0.09 %	488 ppm

Co	Cr	Cu	Li	Mo
20 ppm	233 ppm	56 ppm	20 ppm	-15 ppm

Nb	Ni	Sc	Sr	V
14 ppm	82 ppm	22 ppm	106 ppm	151 ppm

Y	Zn	Zr	La	Ce
32 ppm	95 ppm	143 ppm	58 ppm	134 ppm

Nd	Sm	Eu	Dy	Yb
93 ppm	11.2 ppm	1.5 ppm	7.7 ppm	3.6 ppm

Fe
10.56 %

Royal Holloway and Bedford New College 12-JAN-89 12:05
Sample: LSK 2 1 AP: TRACES 12-JAN-89 12:05
Concentrations

Al2O3	Fe2O3	MgO	CaO	Na2O
22.63 %	16.29 %	1.44 %	1.30 %	0.27 %

K2O	TiO2	P2O5	MnO	Ba
0.35 %	1.32 %	0.17 %	0.11 %	394 ppm

Co	Cr	Cu	Li	Mo
37 ppm	263 ppm	83 ppm	17 ppm	-17 ppm

Nb	Ni	Sc	Sr	V
12 ppm	84 ppm	35 ppm	88 ppm	258 ppm

Y	Zn	Zr	La	Ce
35 ppm	79 ppm	43 ppm	38 ppm	92 ppm

Nd	Sm	Eu	Dy	Yb
107 ppm	11.9 ppm	2.0 ppm	8.3 ppm	4.2 ppm

Fe
14.45 %

Royal Holloway and Bedford New College 12-JAN-89 12:07
Sample: LSK 2A 2 AP: TRACES 12-JAN-89 12:07
Concentrations

Al2O3	Fe2O3	MgO	CaO	Na2O
22.52 %	16.26 %	1.42 %	1.28 %	0.26 %

K2O	TiO2	P2O5	MnO	Ba
0.34 %	1.32 %	0.17 %	0.11 %	390 ppm

Co	Cr	Cu	Li	Mo
37 ppm	254 ppm	85 ppm	19 ppm	-18 ppm

Nb	Ni	Sc	Sr	V
12 ppm	85 ppm	35 ppm	85 ppm	258 ppm

Y	Zn	Zr	La	Ce
35 ppm	80 ppm	43 ppm	38 ppm	91 ppm

Nd	Sm	Eu	Dy	Yb
106 ppm	11.8 ppm	2.0 ppm	8.2 ppm	4.2 ppm

Ce

APPENDIX 3

Royal Holloway and Bedford New College 12-JAN-89 11:56
AP: TRACES 12-JAN-89 11:56

Sample: PSH 1
Concentrations

Al2O3	Fe2O3	MgO	CaO	Na2O
23.73 %	12.31 %	0.77 %	0.43 %	0.24 %

K2O	TiO2	P2O5	MnO	Ba
1.11 %	1.09 %	0.18 %	0.07 %	449 ppm

Co	Cr	Cu	Li	Mo
22 ppm	189 ppm	56 ppm	26 ppm	-12 ppm

Nb	Ni	Sc	Sr	V
19 ppm	76 ppm	25 ppm	75 ppm	177 ppm

Y	Zn	Zr	La	Ce
38 ppm	115 ppm	91 ppm	49 ppm	111 ppm

Nd	Sm	Eu	Dy	Yb
90 ppm	13.6 ppm	1.7 ppm	9.4 ppm	4.4 ppm

Fe
11.70 %

Royal Holloway and Bedford New College 12-JAN-89 11:58
AP: TRACES 12-JAN-89 11:58

Sample: PSH 2
Concentrations

Al2O3	Fe2O3	MgO	CaO	Na2O
23.60 %	12.61 %	0.77 %	0.43 %	0.24 %

K2O	TiO2	P2O5	MnO	Ba
1.14 %	1.12 %	0.19 %	0.08 %	458 ppm

Co	Cr	Cu	Li	Mo
22 ppm	180 ppm	56 ppm	28 ppm	-13 ppm

Nb	Ni	Sc	Sr	V
20 ppm	81 ppm	25 ppm	76 ppm	182 ppm

Y	Zn	Zr	La	Ce
38 ppm	116 ppm	95 ppm	48 ppm	110 ppm

Nd	Sm	Eu	Dy	Yb
91 ppm	13.6 ppm	1.8 ppm	9.4 ppm	4.4 ppm

Fe
11.90 %

Royal Holloway and Bedford New College 12-JAN-89 11:59
AP: TRACES 12-JAN-89 11:59

Sample: KC 11 TILAK
Concentrations

Al2O3	Fe2O3	MgO	CaO	Na2O
14.82 %	8.62 %	3.64 %	6.77 %	2.66 %

K2O	TiO2	P2O5	MnO	Ba
1.80 %	1.03 %	0.32 %	0.14 %	443 ppm

Co	Cr	Cu	Li	Mo
26 ppm	140 ppm	92 ppm	322 ppm	-9 ppm

Nb	Ni	Sc	Sr	V
16 ppm	281 ppm	22 ppm	334 ppm	204 ppm

APPENDIX 3

Royal Holloway and Bedford New College

Sample: FB
Concentrations

12-JAN-89 12:10
AP: TRACES 12-JAN-89 12:10

Al2O3 38.97 %	Fe2O3 2.58 %	MgO 0.52 %	CaO 0.34 %	Na2O 0.08 %
K2O 0.44 %	TiO2 1.11 %	P2O5 0.07 %	MnO 0.01 %	Ba 876 ppm
Co 16 ppm	Cr 200 ppm	Cu 41 ppm	Li 455 ppm	Mo -19 ppm
Nb 22 ppm	Ni 93 ppm	Sc 23 ppm	Sr 196 ppm	V 187 ppm
Y 45 ppm	Zn 115 ppm	Zr 86 ppm	La 54 ppm	Ce 111 ppm
Nd 62 ppm	Sm 9.8 ppm	Eu 1.7 ppm	Dy 10.8 ppm	Yb 4.1 ppm
Fe 2.87 %				

Royal Holloway and Bedford New College

Sample: LP 1
Concentrations

12-JAN-89 12:12
AP: TRACES 12-JAN-89 12:12

Al2O3 21.76 %	Fe2O3 10.21 %	MgO 0.40 %	CaO 0.45 %	Na2O 0.17 %
K2O 0.91 %	TiO2 3.38 %	P2O5 0.08 %	MnO 0.16 %	Ba 297 ppm
Co 17 ppm	Cr 133 ppm	Cu 40 ppm	Li 30 ppm	Mo -18 ppm
Nb 46 ppm	Ni 58 ppm	Sc 24 ppm	Sr 79 ppm	V 173 ppm
Y 60 ppm	Zn 79 ppm	Zr 286 ppm	La 133 ppm	Ce 281 ppm
Nd 151 ppm	Sm 21.3 ppm	Eu 2.2 ppm	Dy 12.0 ppm	Yb 6.2 ppm
Fe 9.76 %				

Royal Holloway and Bedford New College

Sample: LP 2 CLOUDY
Concentrations

12-JAN-89 12:14
AP: TRACES 12-JAN-89 12:14

Al2O3 21.61 %	Fe2O3 10.39 %	MgO 0.39 %	CaO 0.41 %	Na2O 0.17 %
K2O 0.91 %	TiO2 2.59 %	P2O5 0.06 %	MnO 0.16 %	Ba 291 ppm
Co 17 ppm	Cr 158 ppm	Cu 40 ppm	Li 30 ppm	Mo -17 ppm
Nb 19 ppm	Ni 60 ppm	Sc 25 ppm	Sr 80 ppm	V 146 ppm
Y 64 ppm	Zn 81 ppm	Zr 286 ppm	La 129 ppm	Ce 265 ppm
Nd 147 ppm	Sm 21.0 ppm	Eu 2.3 ppm	Dy 12.2 ppm	Yb 6.5 ppm
Fe 9.91 %				

Royal Holloway and Bedford New College

Sample: ~~LP 2~~ ACB-1
Concentrations

12-JAN-89 12:16
AP: TRACES 12-JAN-89 12:15

Al2O3 20.14 %	Fe2O3 9.13 %	MgO 0.94 %	CaO 0.69 %	Na2O 0.48 %
K2O 1.09 %	TiO2 1.05 %	P2O5 0.08 %	MnO 0.06 %	Ba 753 ppm
Co 17 ppm	Cr 155 ppm	Cu 62 ppm	Li 28 ppm	Mo -13 ppm
Nb 13 ppm	Ni 53 ppm	Sc 24 ppm	Sr 127 ppm	V 158 ppm
Y 37 ppm	Zn 87 ppm	Zr 44 ppm	La 50 ppm	Ce 99 ppm
Nd 81 ppm	Sm 10.0 ppm	Eu 1.6 ppm	Dy 7.8 ppm	Yb 3.7 ppm
Fe 8.90 %				

Royal Holloway and Bedford New College

Sample: ACB 2
Concentrations

12-JAN-89 12:17
AP: TRACES 12-JAN-89 12:17

APPENDIX 4

INFRARED SPECTRA OF THE CLAYS

APPENDIX 4

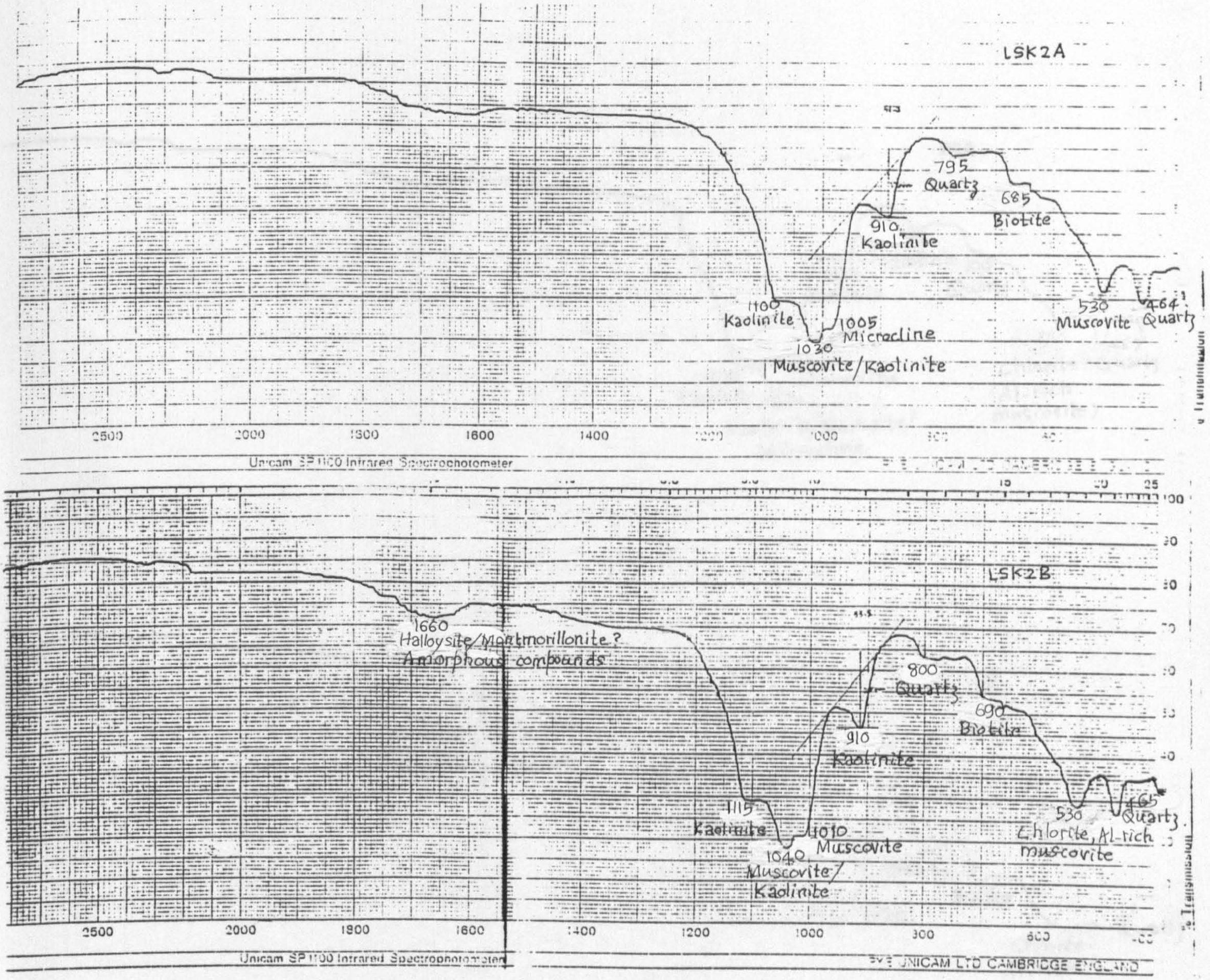
LSK2A
795
Quartz
685
Biotite
910
Kaolinite
1100
Kaolinite
1030
1005
Microcline
Muscovite/Kaolinite
530
Muscovite
464
Quartz
2500
2000
1500
1600
1400
Unicam SP1100 Infrared Spectrophotometer
LSK2B
1660
Halloysite/Montmorillonite?
Amorphous compounds
800
Quartz
690
Biotite
910
Kaolinite
1115
Kaolinite
1040
Muscovite/
Kaolinite
1010
Muscovite
530
Chlorite, Al-rich
muscovite
465
Quartz
2500
2000
1800
1600
1400
1200
1000
800
Unicam SP1100 Infrared Spectrophotometer
UNICAM LTD CAMBRIDGE ENGLAND
PSH
1650
Halloysite/Montmorillonite?
Amorphous compounds

APPENDIX 4

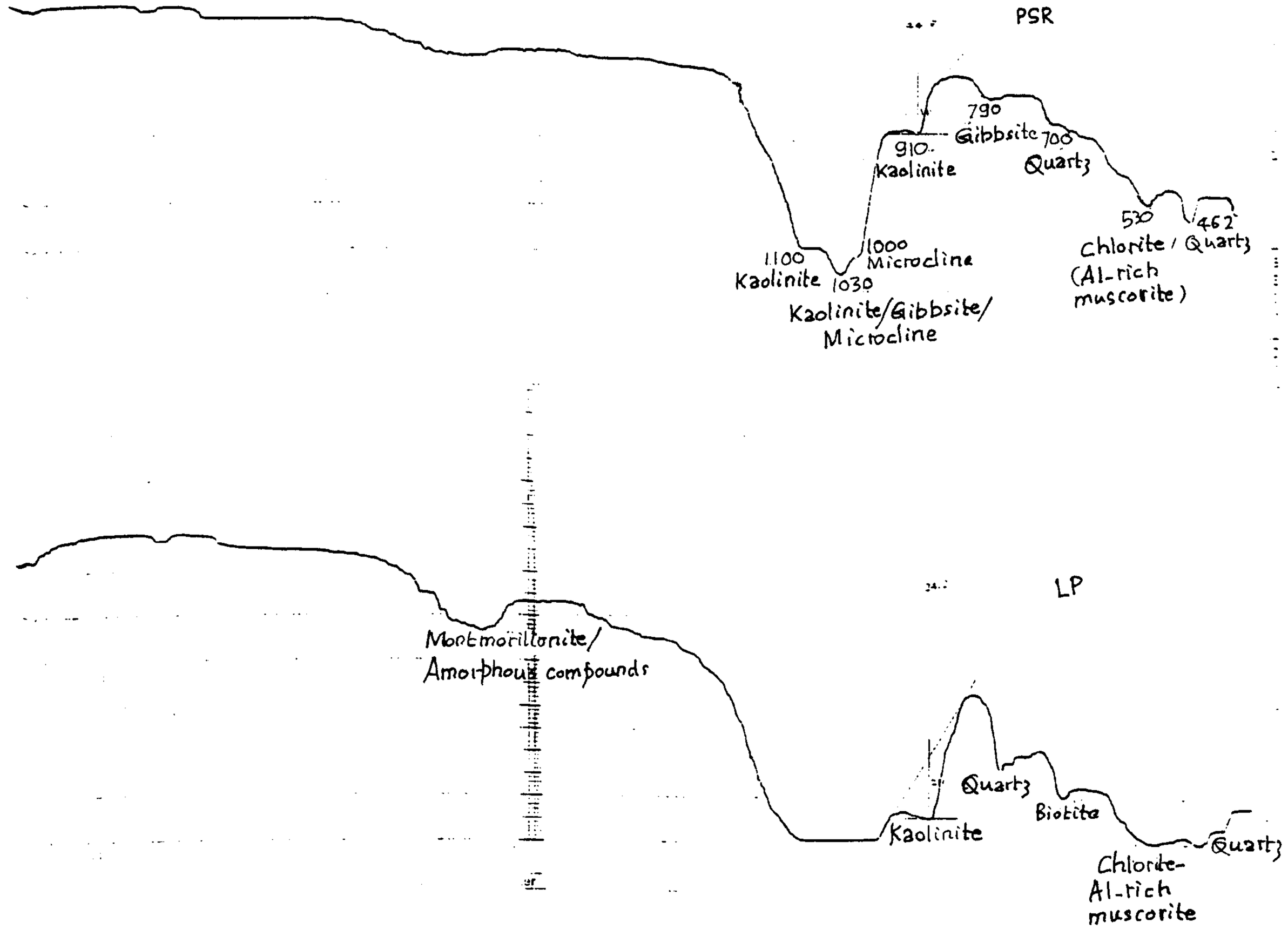
PSR
790
Gibbsite
910
700
Kaolinite
Quartz
530
462
1100
1000
Microcline
Kaolinite
1030
Chlorite / Quartz
(Al-rich
muscorite)
Kaolinite/Gibbsite/
Microcline
LP
Montmorillonite/
Amorphous compounds
Quartz
Biotite
Kaolinite
Quartz
Chlorite-
Al-rich
muscorite

APPENDIX 5

LOAD-DEFLECTION CURVES FOR FLEXURAL TESTS ON BARS

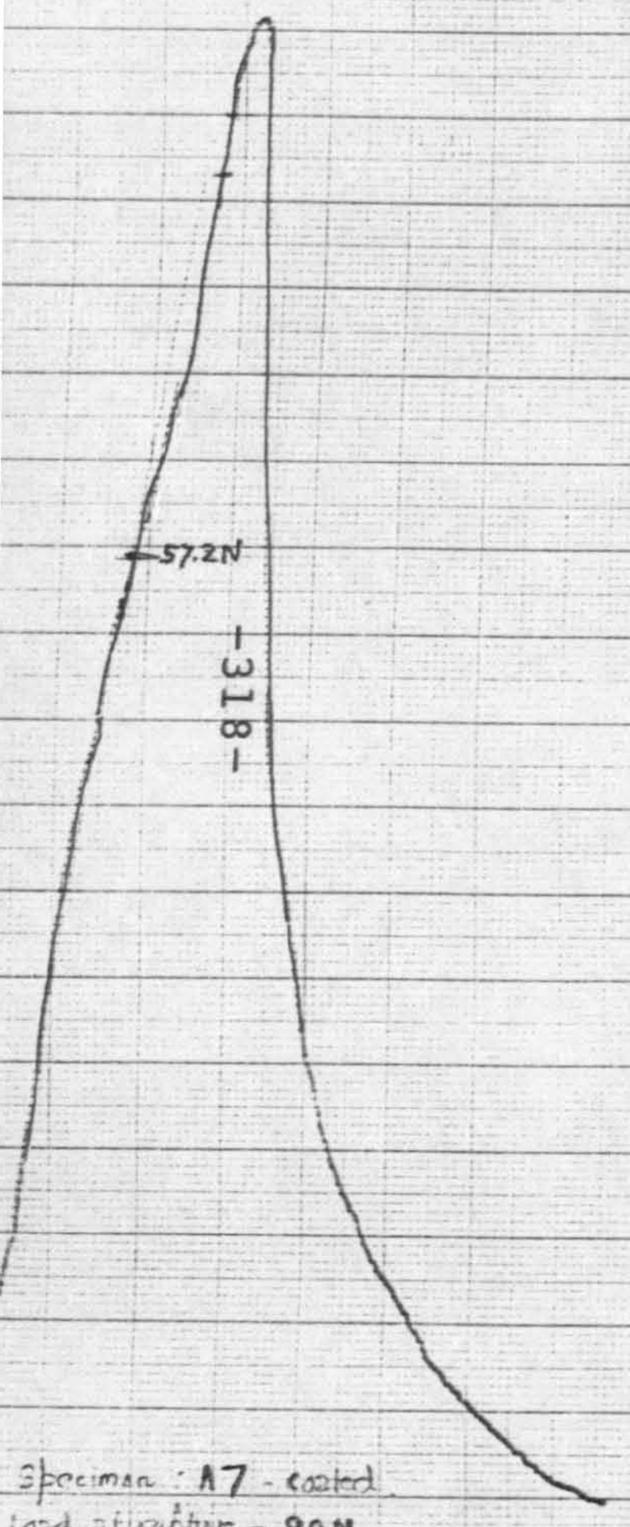

Specimen : A7 - coated
Load at rupture = 90N
Tested w coated surface at the top

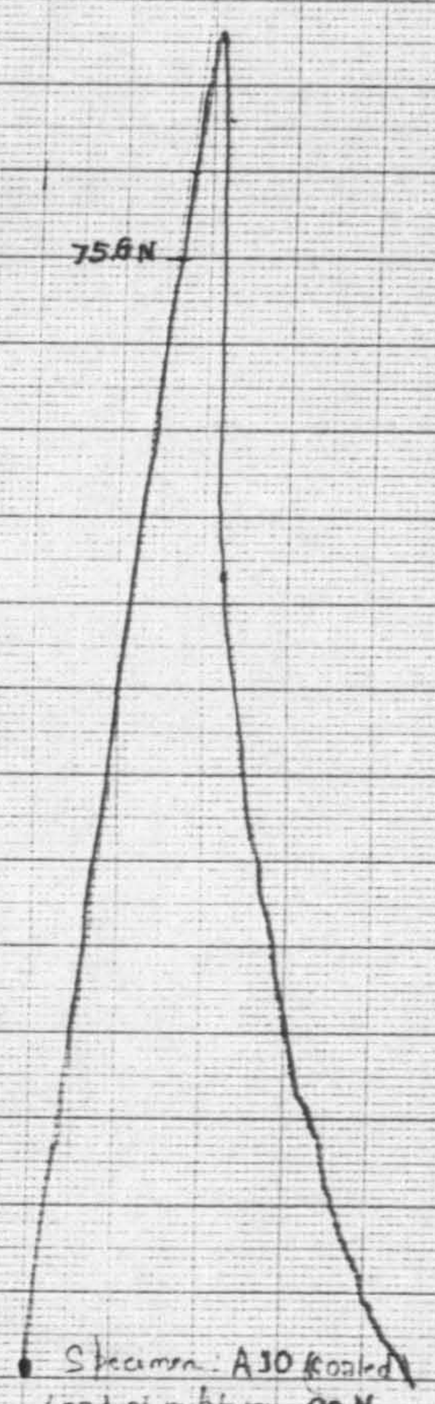

Specimen : A10 (coated)
Load at rupture = 90N
Tested w coated surface at the top

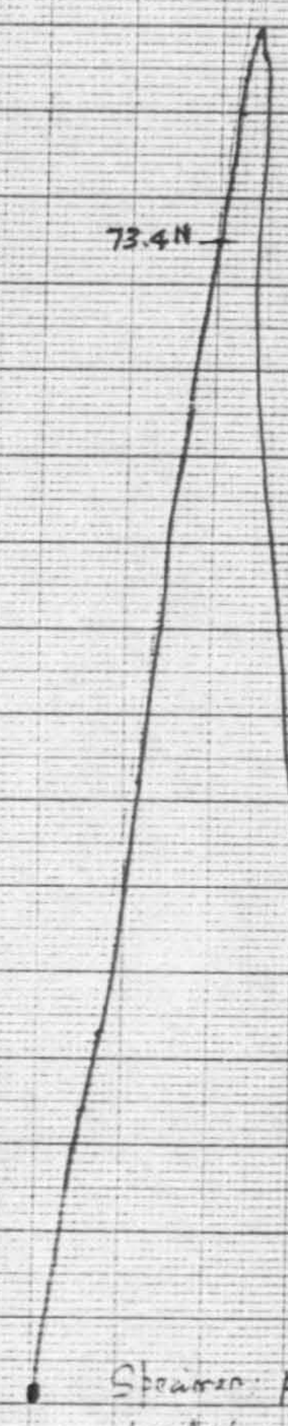

Specimen : A8 (coated)
Load at rupture = 87N
Tested w coated surface at the top.

Specimen : KC (uncoated)
Load at rupture = 59N

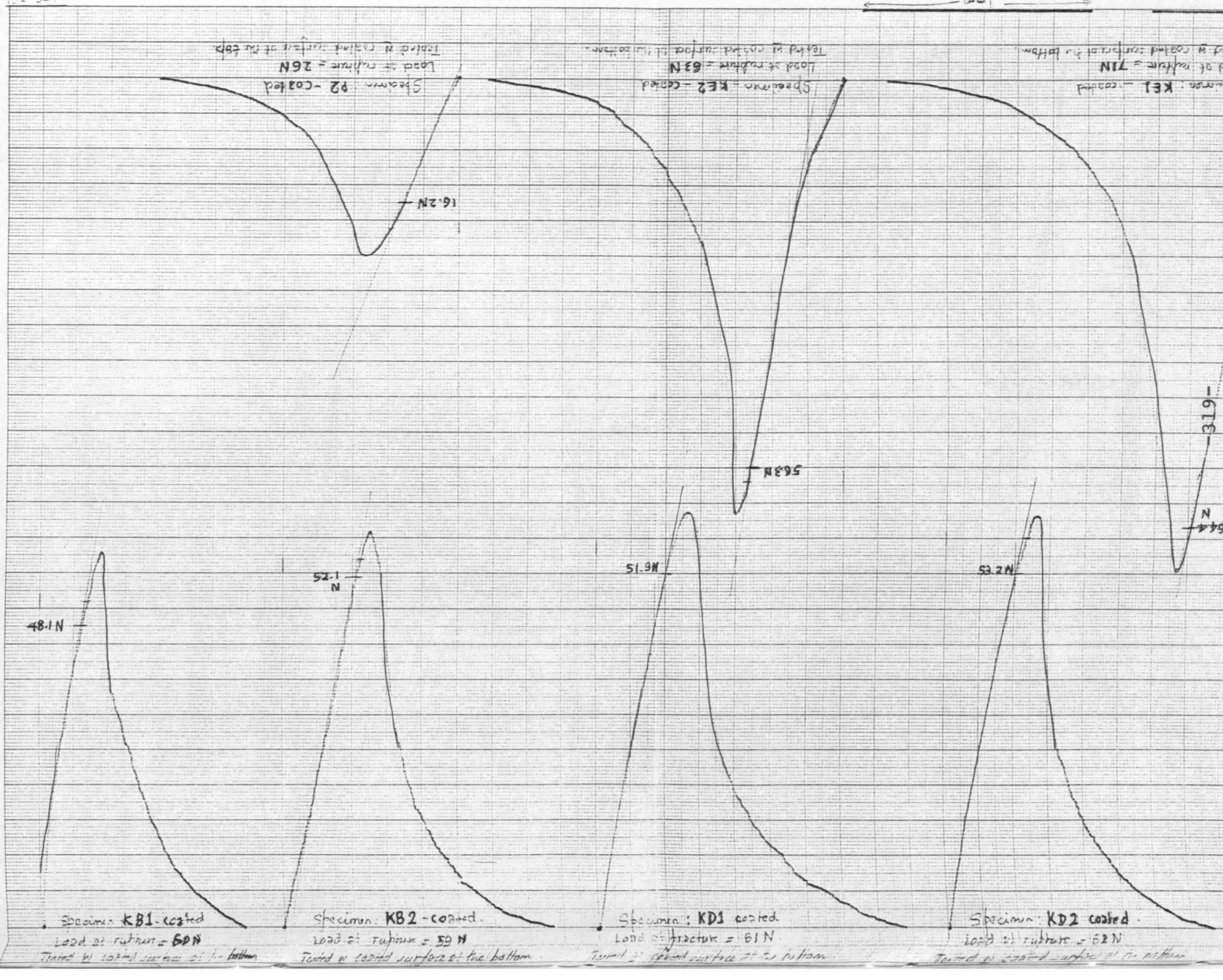
Specimen : KB1 - coated
Load at rupture = 60N
Tested w coated surface at the bottom
48.1N
Specimen : KB2 - coated.
Load at rupture = 59 N
Tested w coated surface at the bottom.
52.1 N
Specimen : KD1 coated
Load at fracture = 61 N
Tested w coated surface at the bottom
51.9N
Specimen : KD2 coated.
Load at rupture = 62 N
Tested w coated surface at the bottom
53.2N
Specimen : KE1 - coated
Load at rupture = 71N
Tested w coated surface at the bottom.
56.3N
Specimen : KE2 - coated
Load at rupture = 63N
Tested w coated surface at the bottom.
16.2N
Specimen : P2 - coated
Load at rupture = 26N
Tested w coated surface at the bottom.
644 N
319

Max load 0.061 kgf

1 mm on CH → 34 mm on chart.

-320-

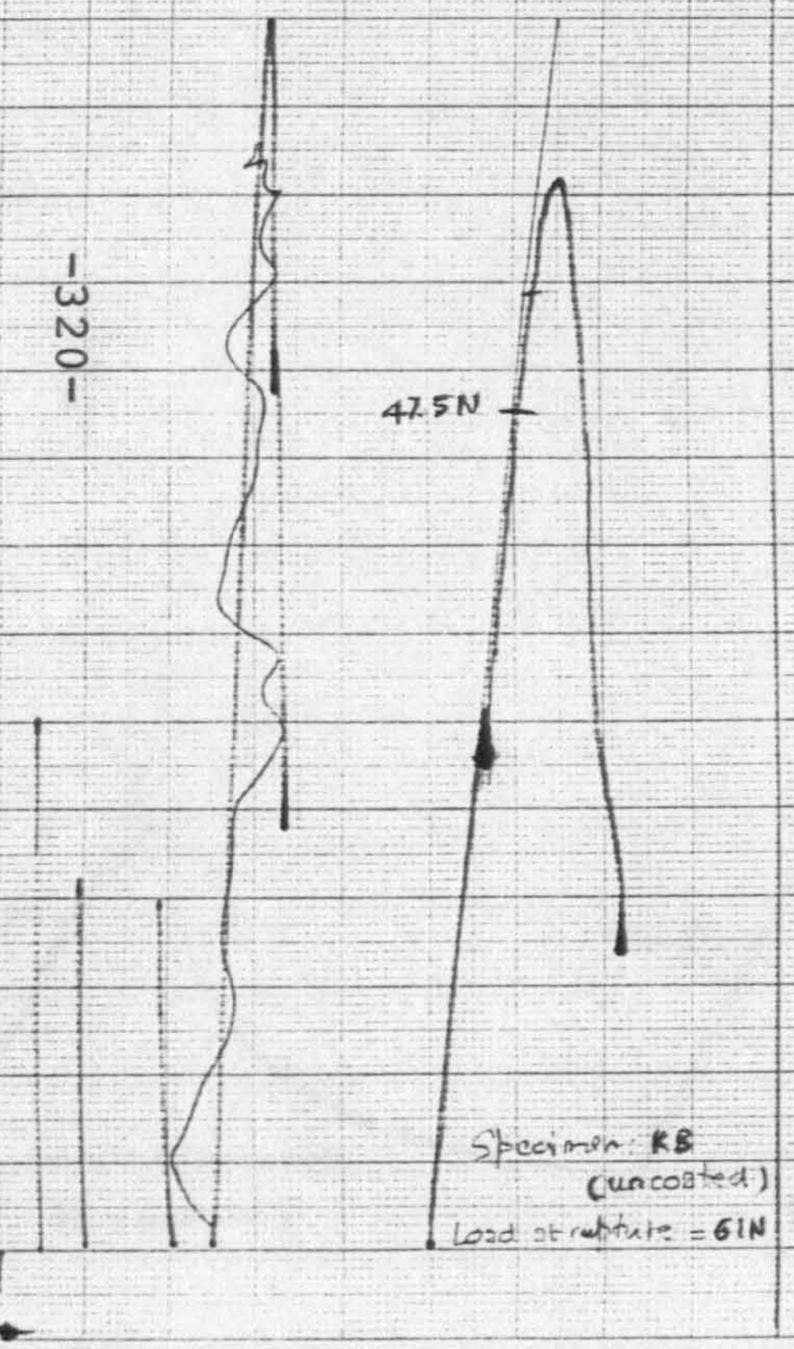

Specimen: KB
(uncoated)
Load at rupture = 61N

1 mm

Specimen: KE
(uncoated)
Load at rupture = 63N

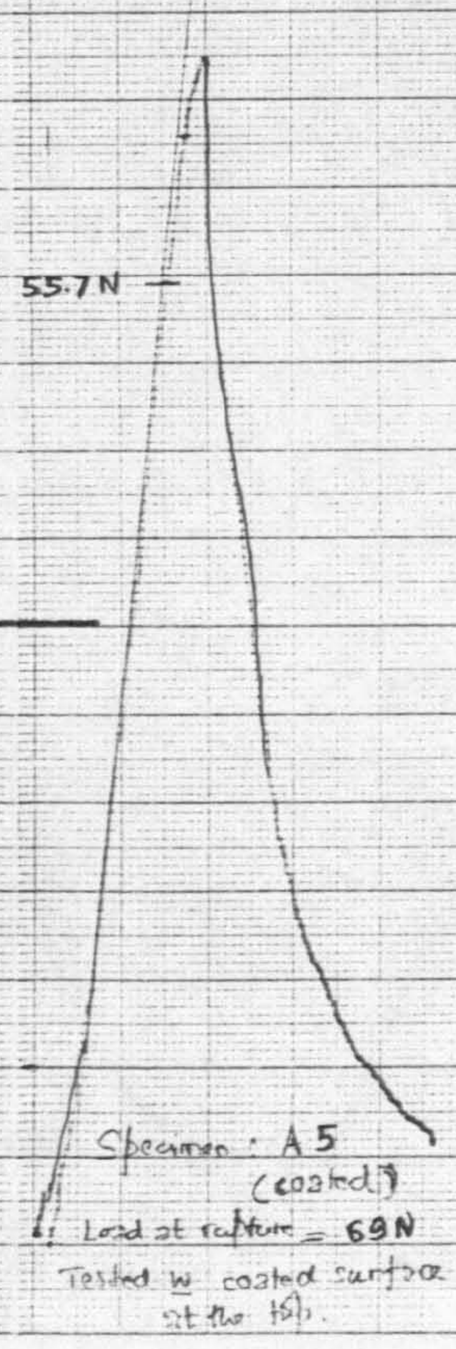

Specimen: A5
(coated)
Load at rupture = 69N
Tested w coated surface at the top.

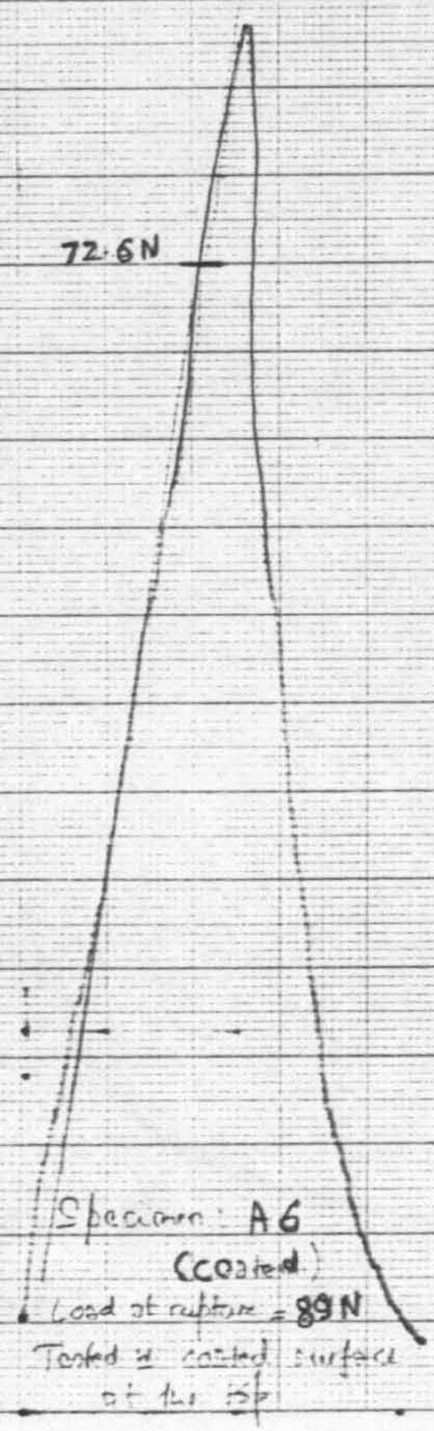

Specimen: A6
(coated)
Load at rupture = 89N
Tested w coated surface at the bottom

Chartwell

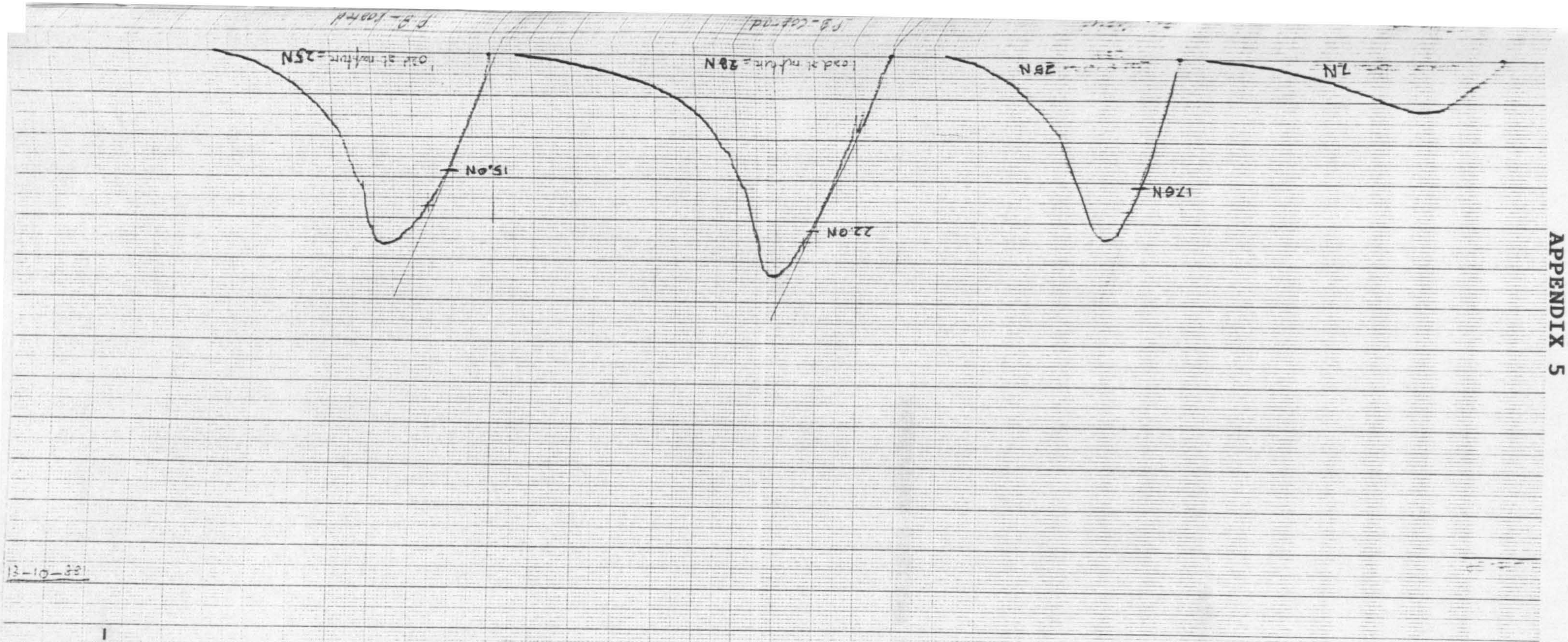
15.0N
Load at rupture = 25N
22.0N
Load at rupture = 28N
17.6N
28N
7N

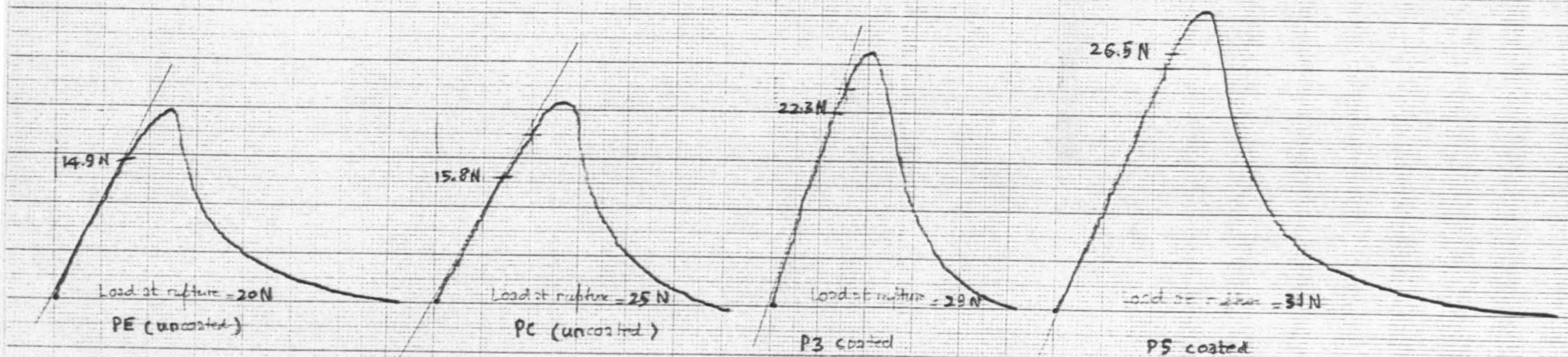
14.9N
Load at rupture = 20N
PE (uncoated)
15.8N
Load at rupture = 25 N
PC (uncoated)
22.3N
Load at rupture = 28 N
P3 coated
Tested w adhered surface at the top
26.5N
Load at rupture = 31 N
P5 coated

APPENDIX 6

INFRARED SPECTRA OF SURFACE COATINGS

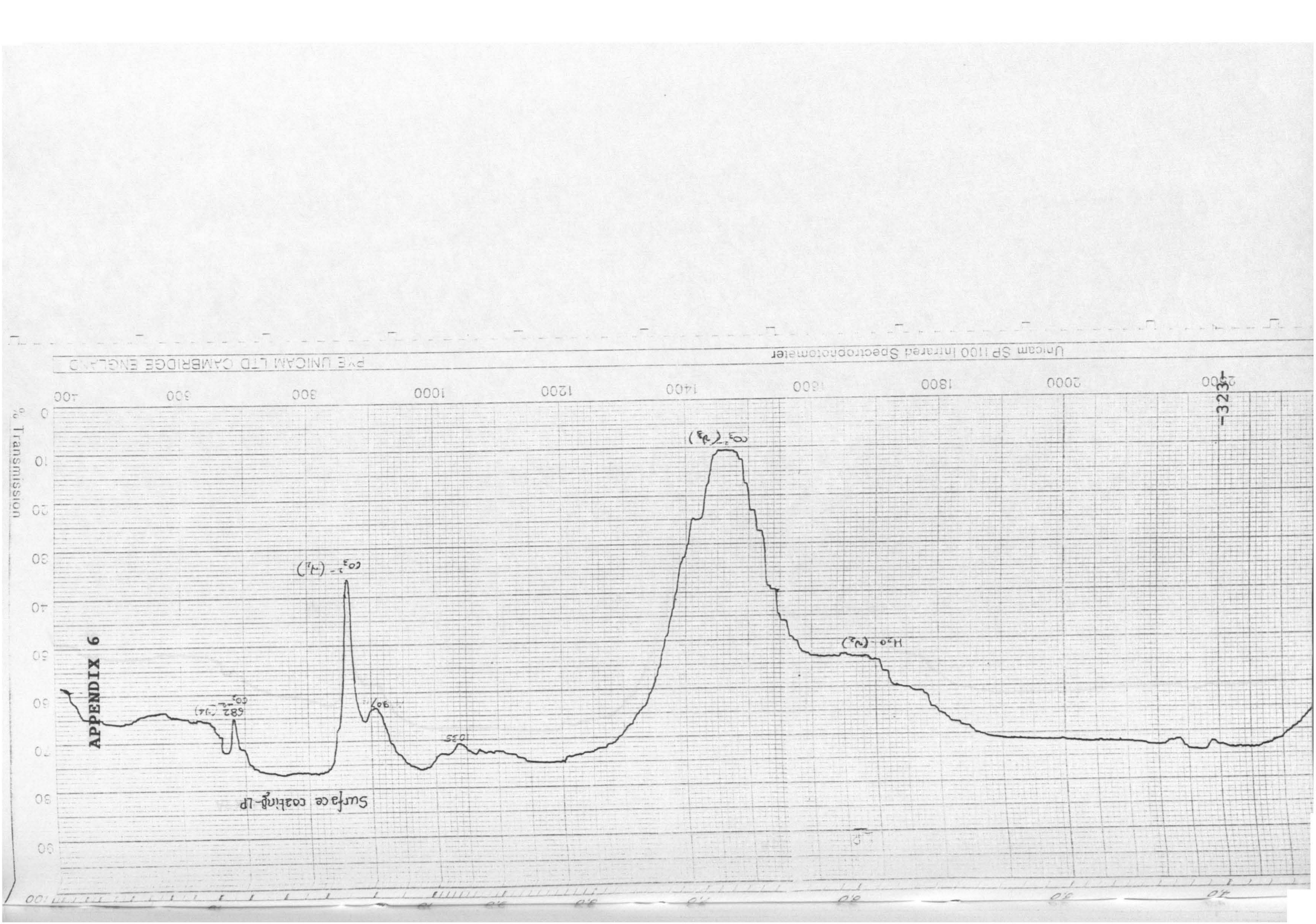
Unicam SP 1100 Infrared Spectrophotometer
PYE UNICAM LTD CAMBRIDGE ENGLAND
% Transmission
Surface coating-LP
CO_3^{2-} (ν_1)
CO_3^{2-} (ν_4)
H_2O (ν_2)
1035
2000
1800
1400
1200
1000
800
600
400
3234

KA

Surface coating-LSK 2A

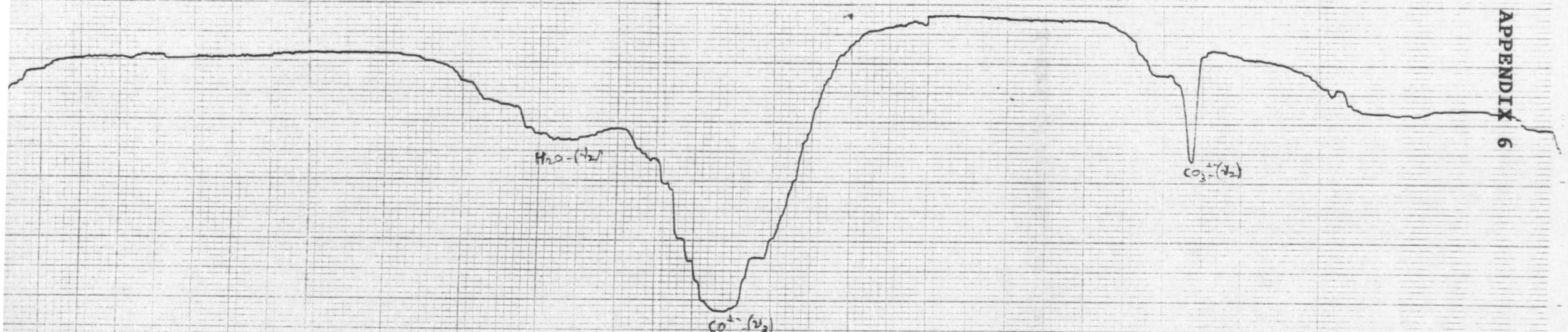

-3241-

2400 2000 1800 1600 1400 1200 1000 800 600 400

Unicam SP1100 Infrared Spectrophotometer

PYE UNICAM LTD CAMBRIDGE ENGLAND

APPENDIX 6

APPENDIX 7

X-RAY DIFFRACTION PATTERNS OF PODZOLIC CLAY COMPOSITIONS

APPENDIX 7

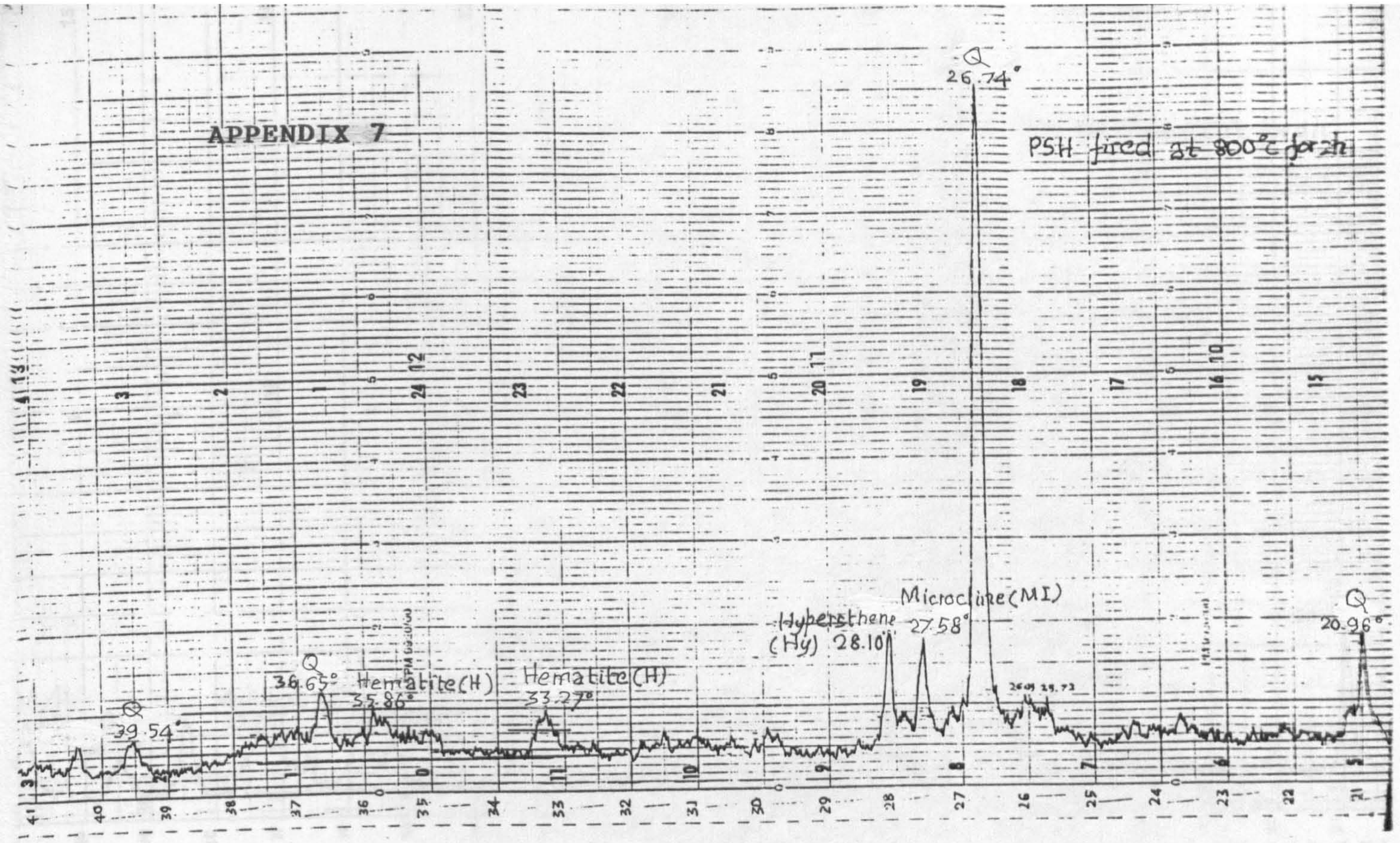
PSH fired at 800°C for 2h
Q 26.74°
Microcline(MI) 27.58°
Hypersthene (Hy) 28.10°
Q 20.96°
Q 39.54°
Q 36.65°
Hematite(H) 35.86°
Hematite(H) 33.27°

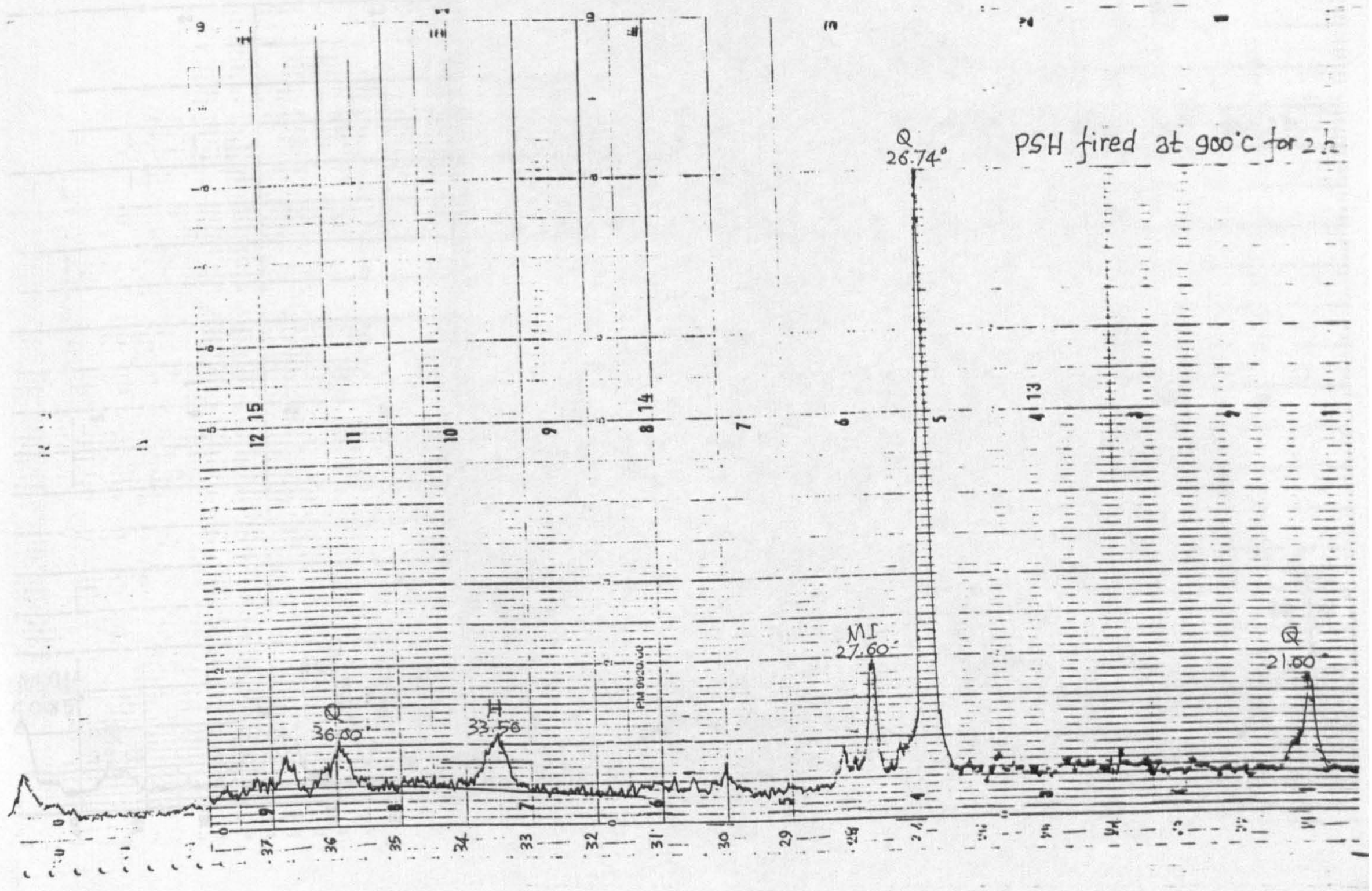
PSH fired at 900°C for 2h
Q 26.74°
MI 27.60°
Q 21.80°
Q 36.88°
H 33.56°

APPENDIX. 7

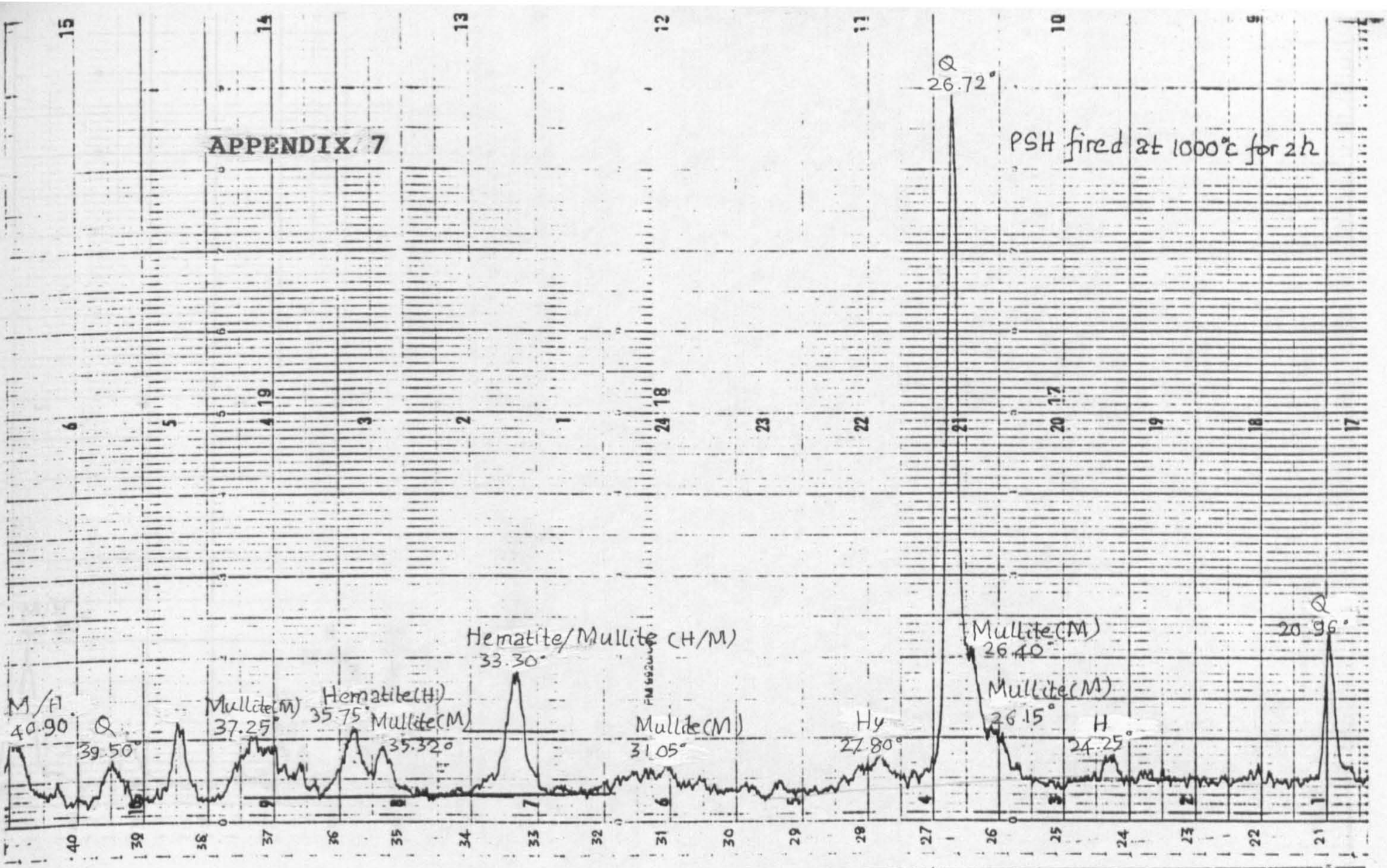
Q
26.72°
PSH fired at 1000°C for 2h
M/H
40.90°
Q
39.50°
Mullite(M)
37.25°
Hematite(H)
35.75°
Mullite(M)
35.32°
Hematite/Mullite (H/M)
33.30°
Mullite(M)
31.05°
Hy
27.80°
Mullite(M)
26.40°
Mullite(M)
26.15°
H
24.25°
Q
20.96°

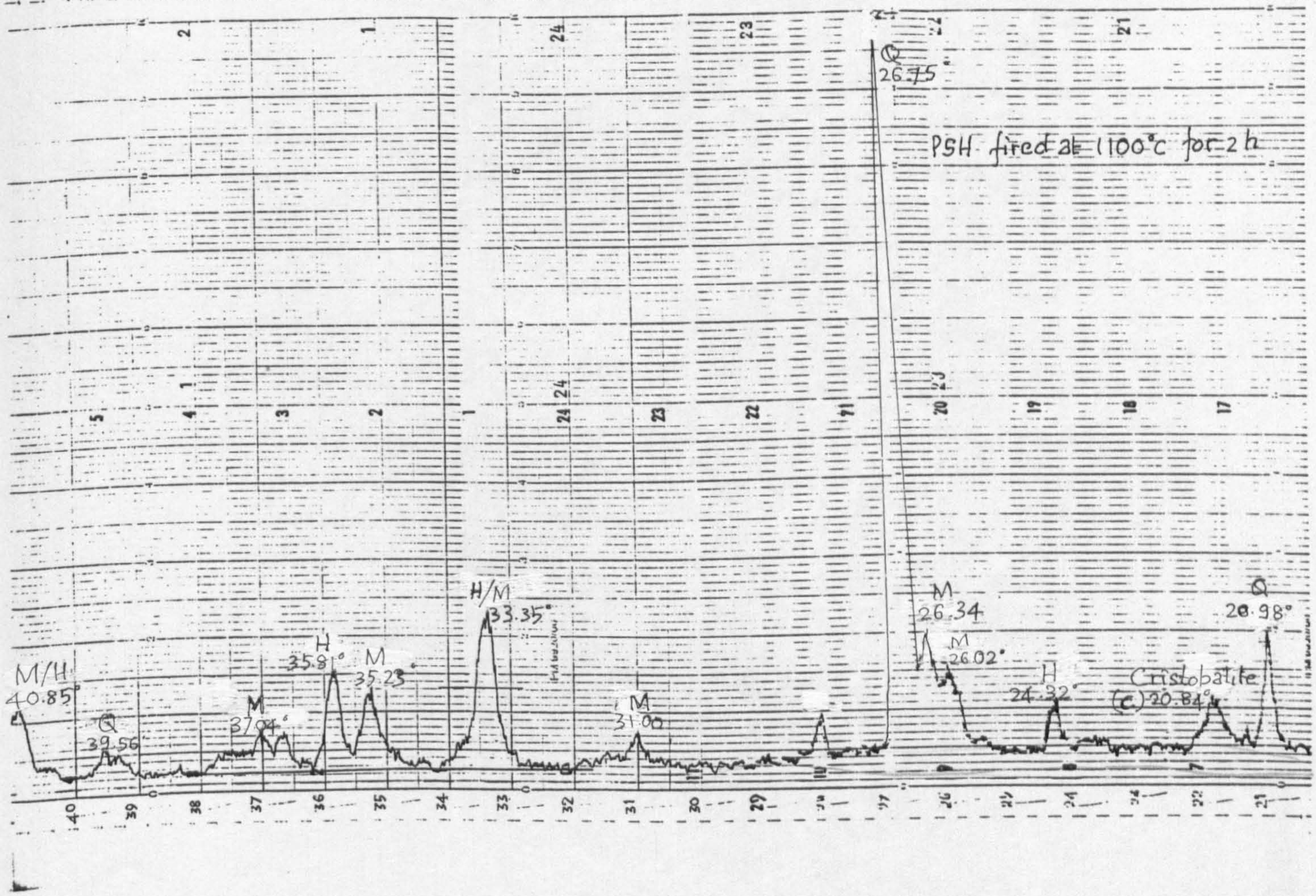
Q
26.75°
PSH fired at 1100°C for 2h
H/M
33.35°
M/H
40.85°
Q
39.56
M
37.84°
H
35.8°
M
35.23°
M
31.00
M
26.34
M
26.02°
H
24.32°
Q
20.98°
Cristobalite
(c) 20.84°

APPENDIX 7

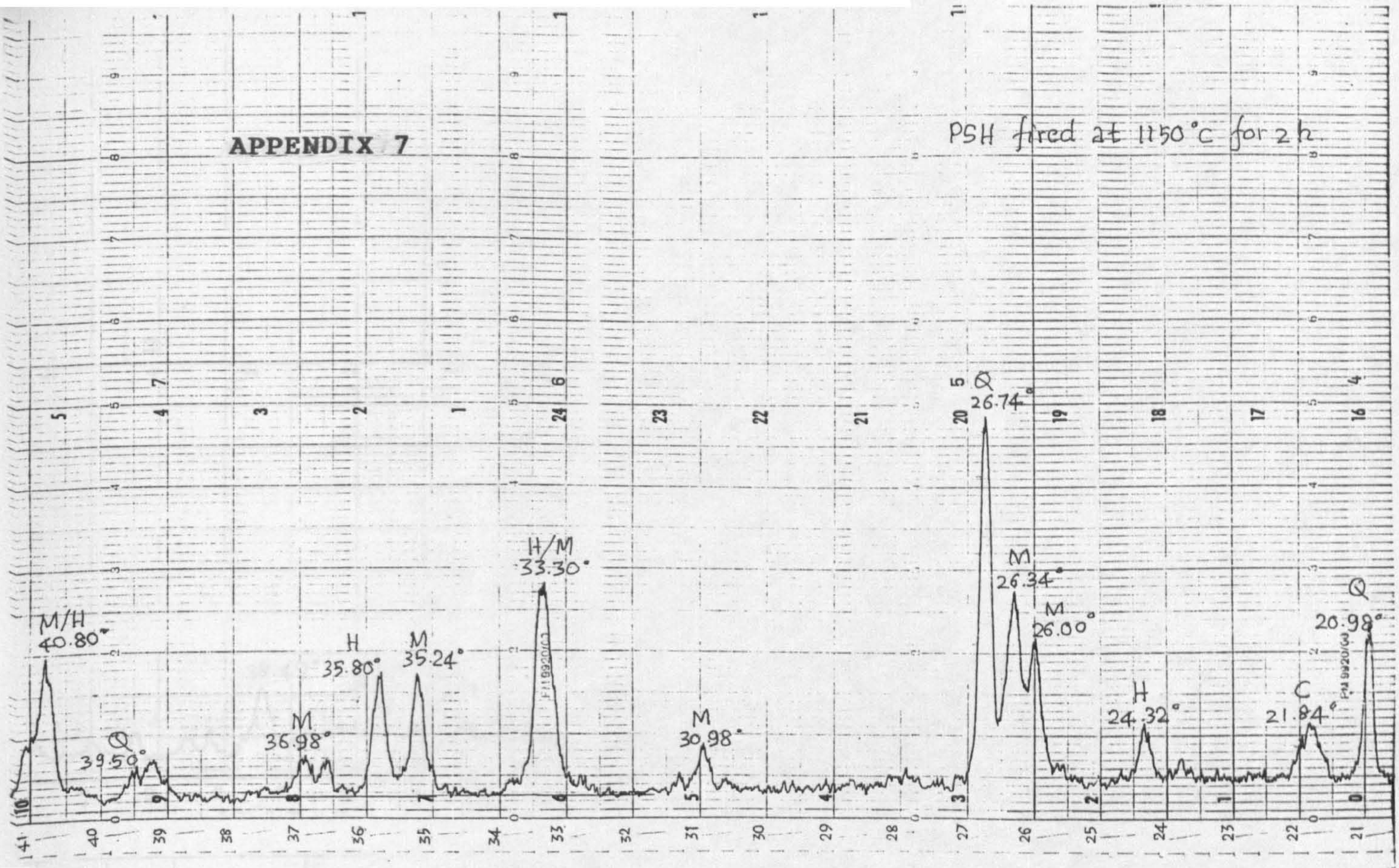
PSH fired at 1150°C for 2h
M/H
40.80°
Q
39.50°
M
36.98°
H
35.80°
M
35.24°
H/M
33.30°
M
30.98°
Q
26.74°
M
26.34°
M
26.00°
H
24.32°
C
21.84°
Q
20.98°

APPENDIX 7

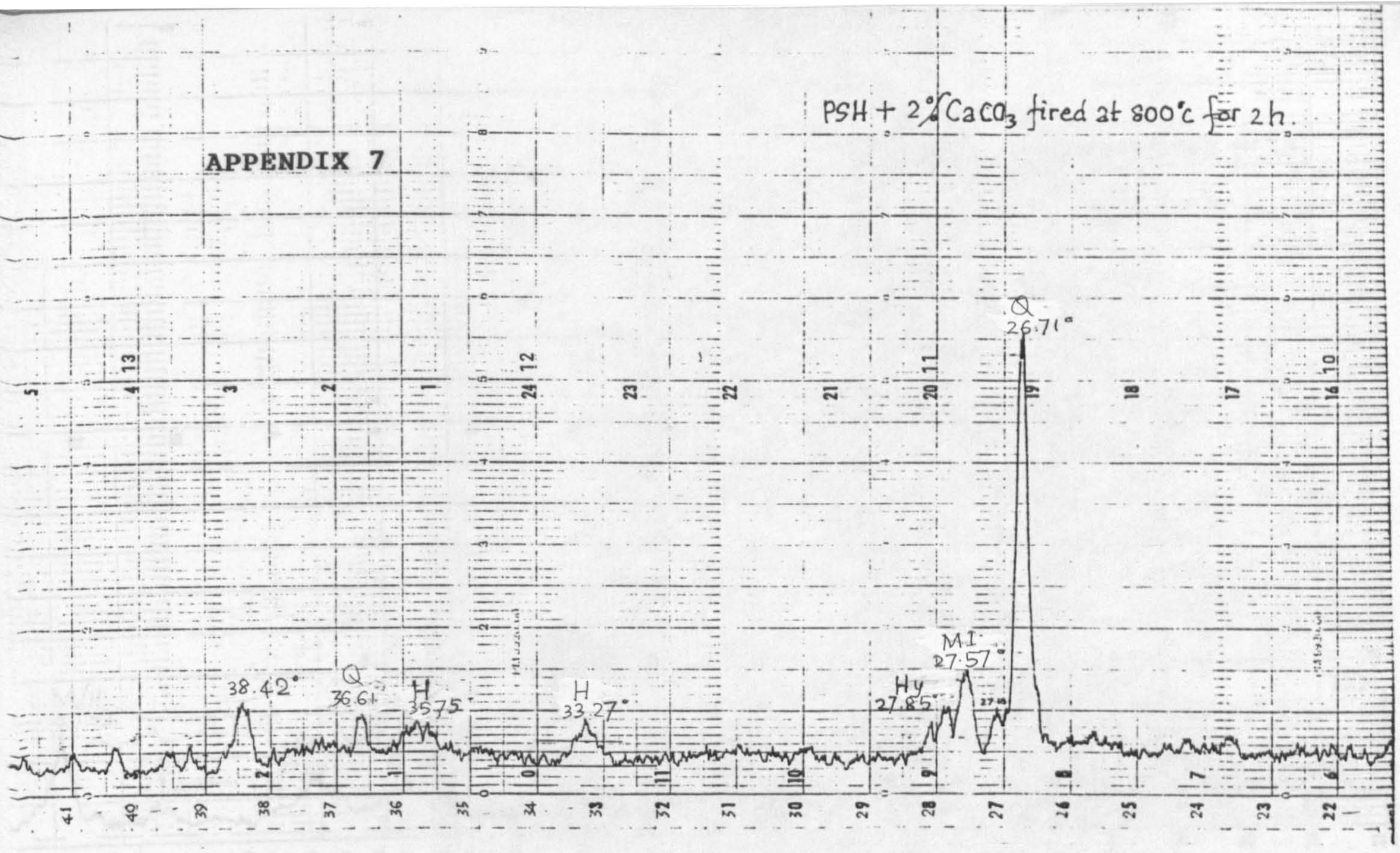
PSH + 2% CaCO3 fired at 800°c for 2h.
Q 26.71°
MI 27.57°
Hy 27.85°
H 33.27°
H 35.75°
Q 36.61°
38.42°

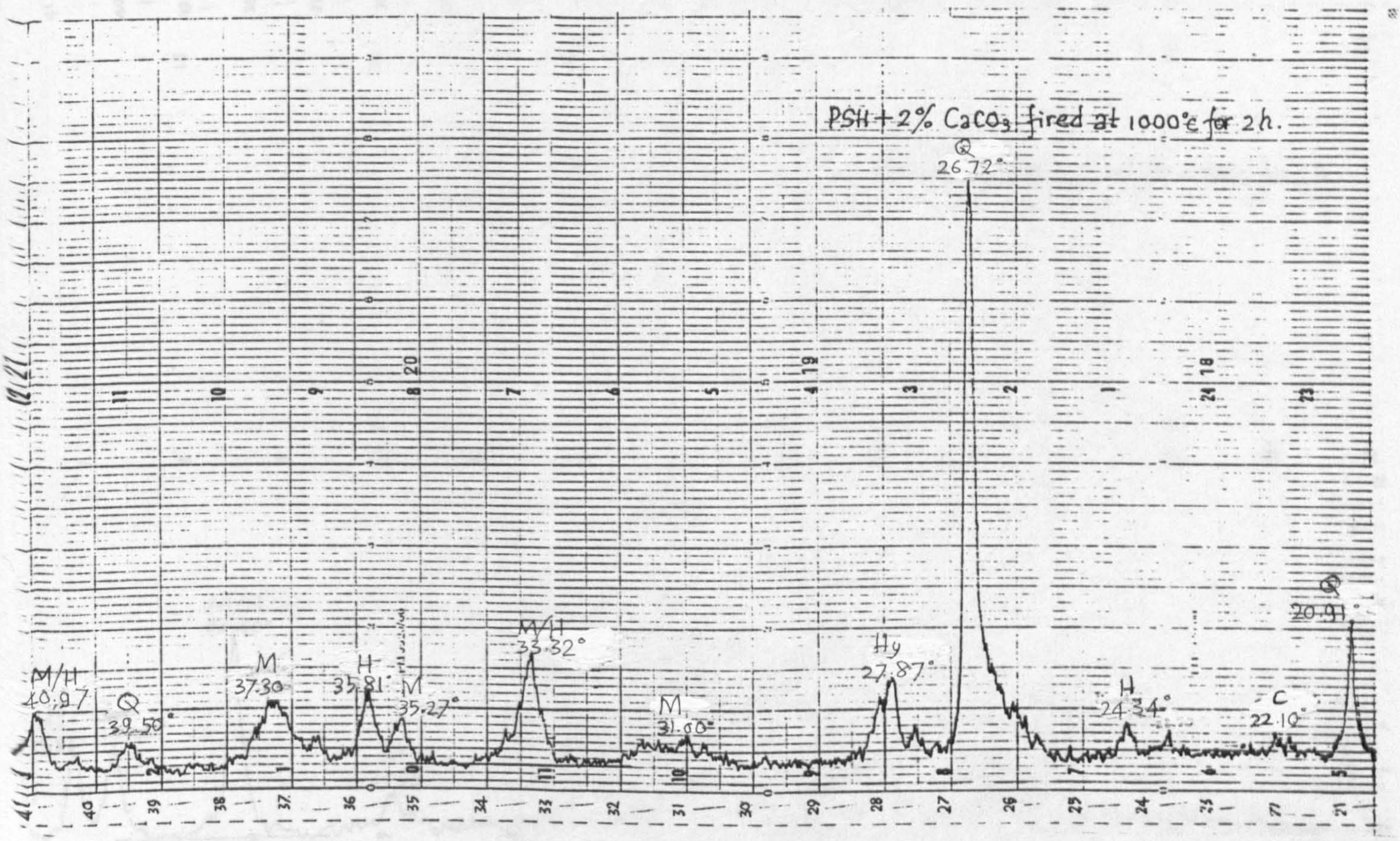
PSH + 2% CaCO3 fired at 1000°c for 2h.
Q 26.72°
M/H 40.97
Q 39.50°
M 37.30
H 35.81°
M 35.27°
M/H 33.32°
M 31.00°
Hy 27.87°
H 24.34°
C 22.10°
Q 20.91°

APPENDIX 7

PSH + 2% $CaCO_3$ fired at 1100°C for 2h.

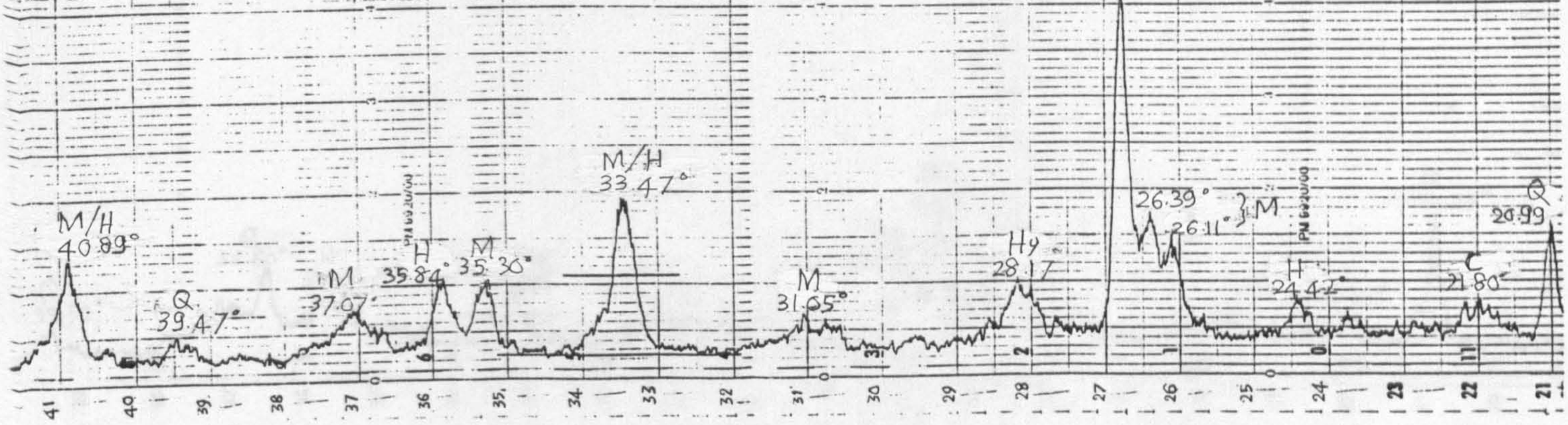

PSH + 2% $CaCO_3$ fired at 1150°C for 2 h.

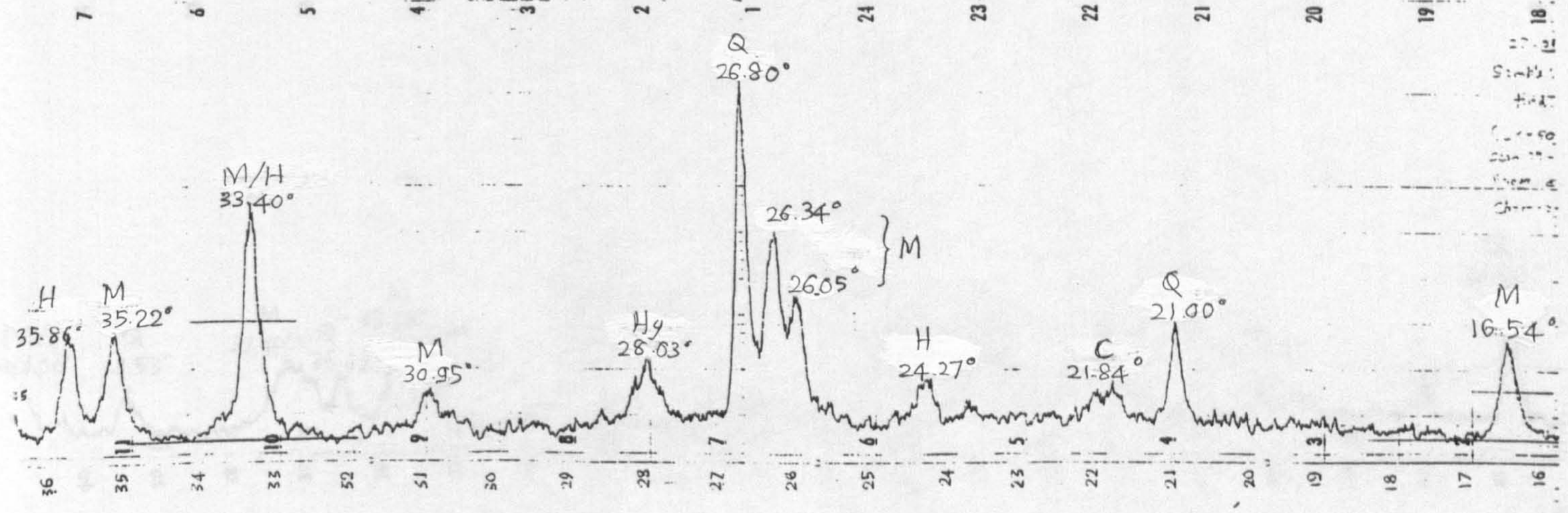

APPENDIX 7

PSH +3% $CaCO_3$ fired at 800°c for 2h.

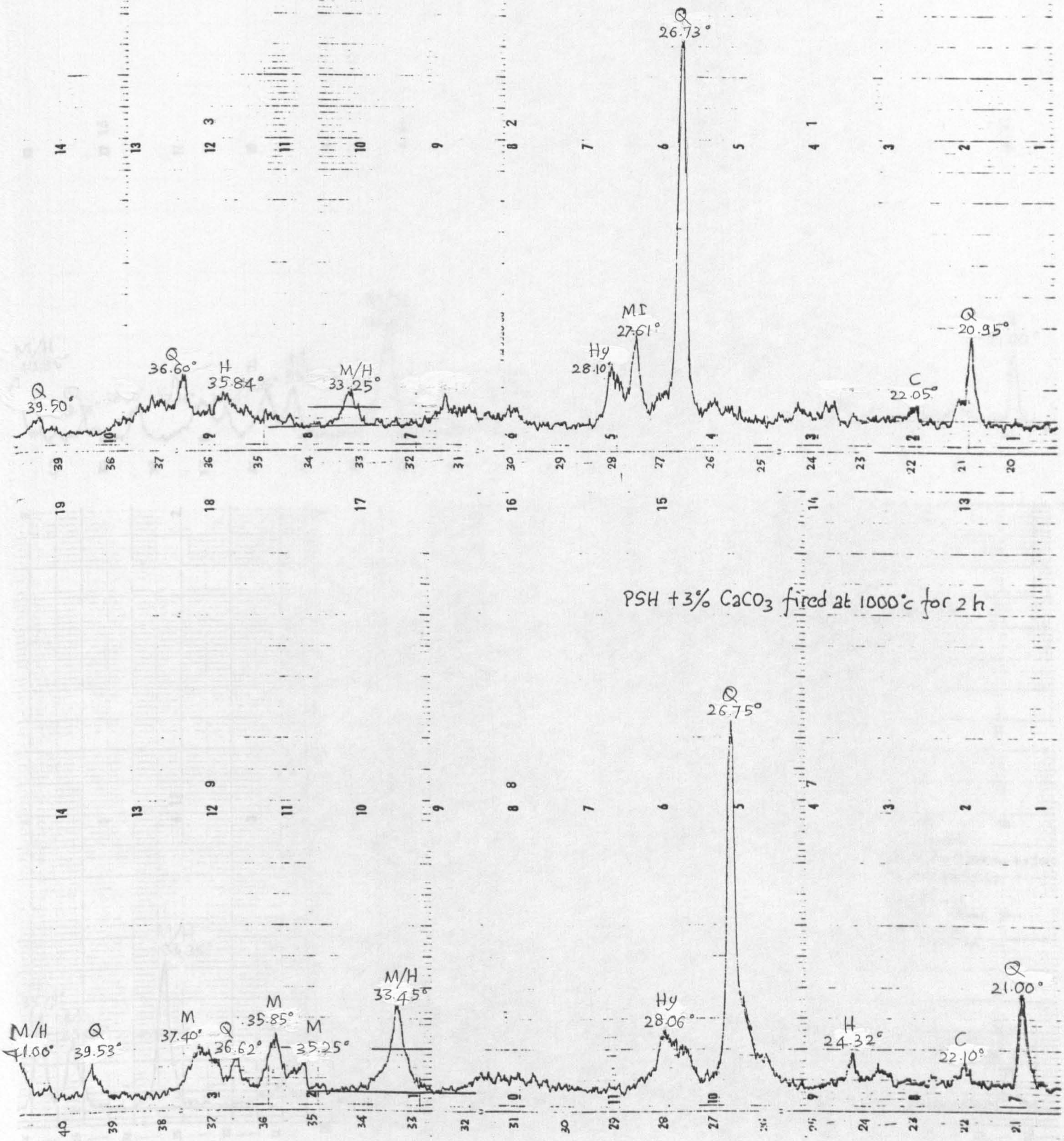

PSH +3% $CaCO_3$ fired at 1000°c for 2h.

APPENDIX 7

PSH + 3% $CaCO_3$ fired at 1100°C for 2h.

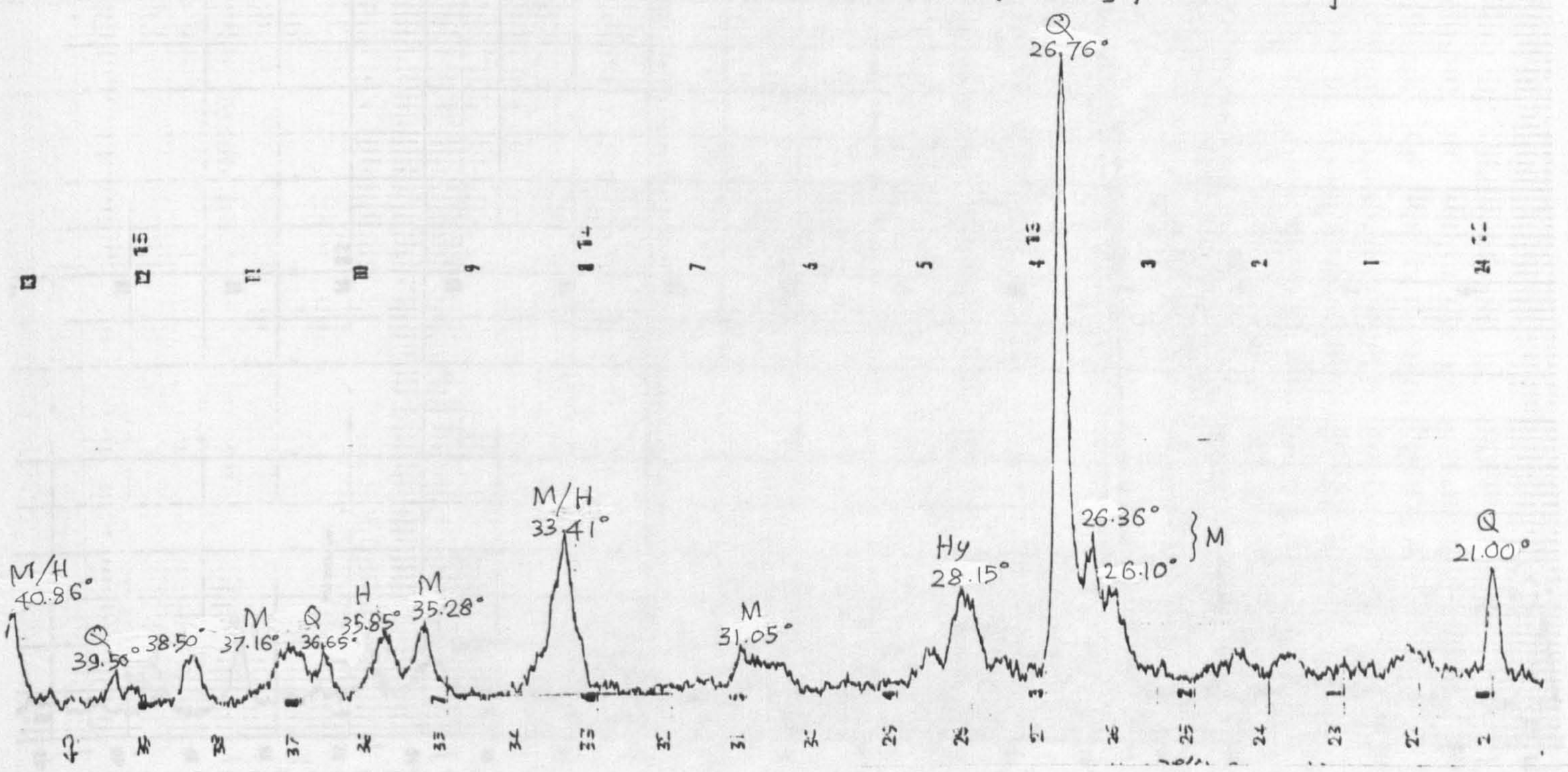

PSH + 3% $CaCO_3$ fired at 1150°C for 2h.

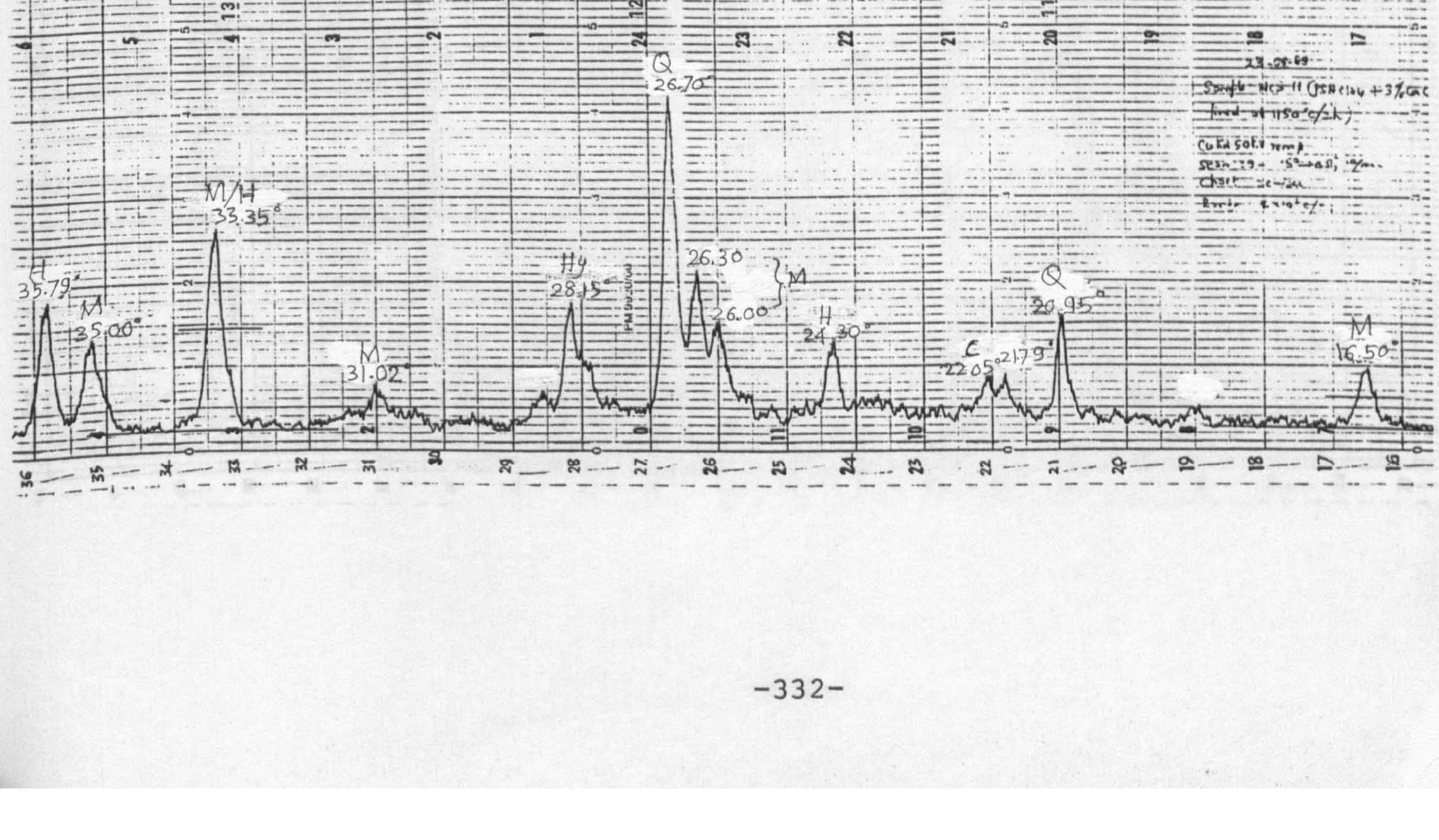

APPENDIX 7

PSH + 4% $CaCO_3$ fired at 800°C for 2 h.

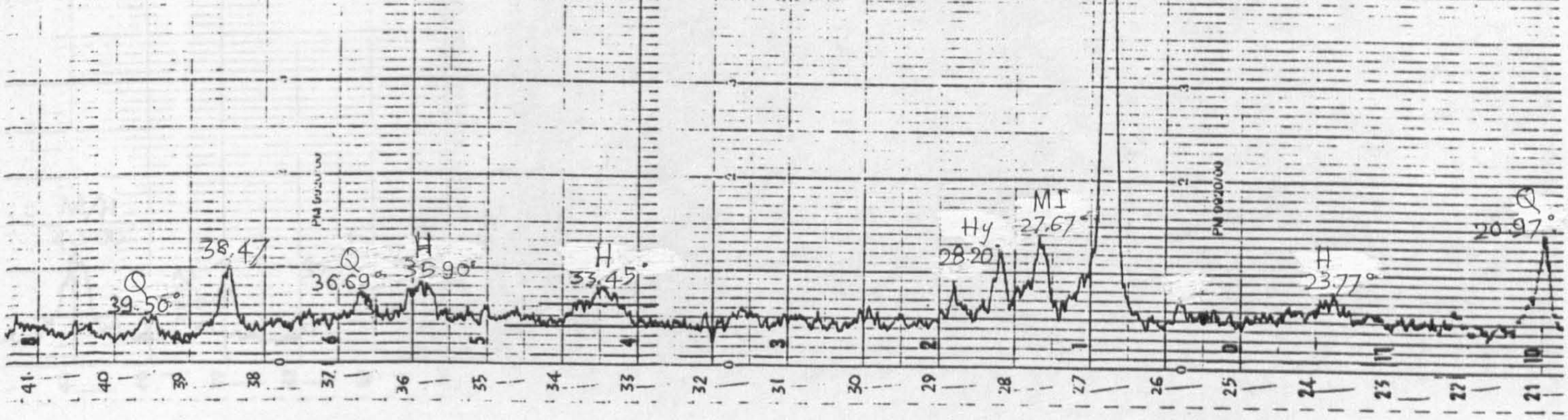

PSH + 4% $CaCO_3$ fired at 1000°C for 2 h.

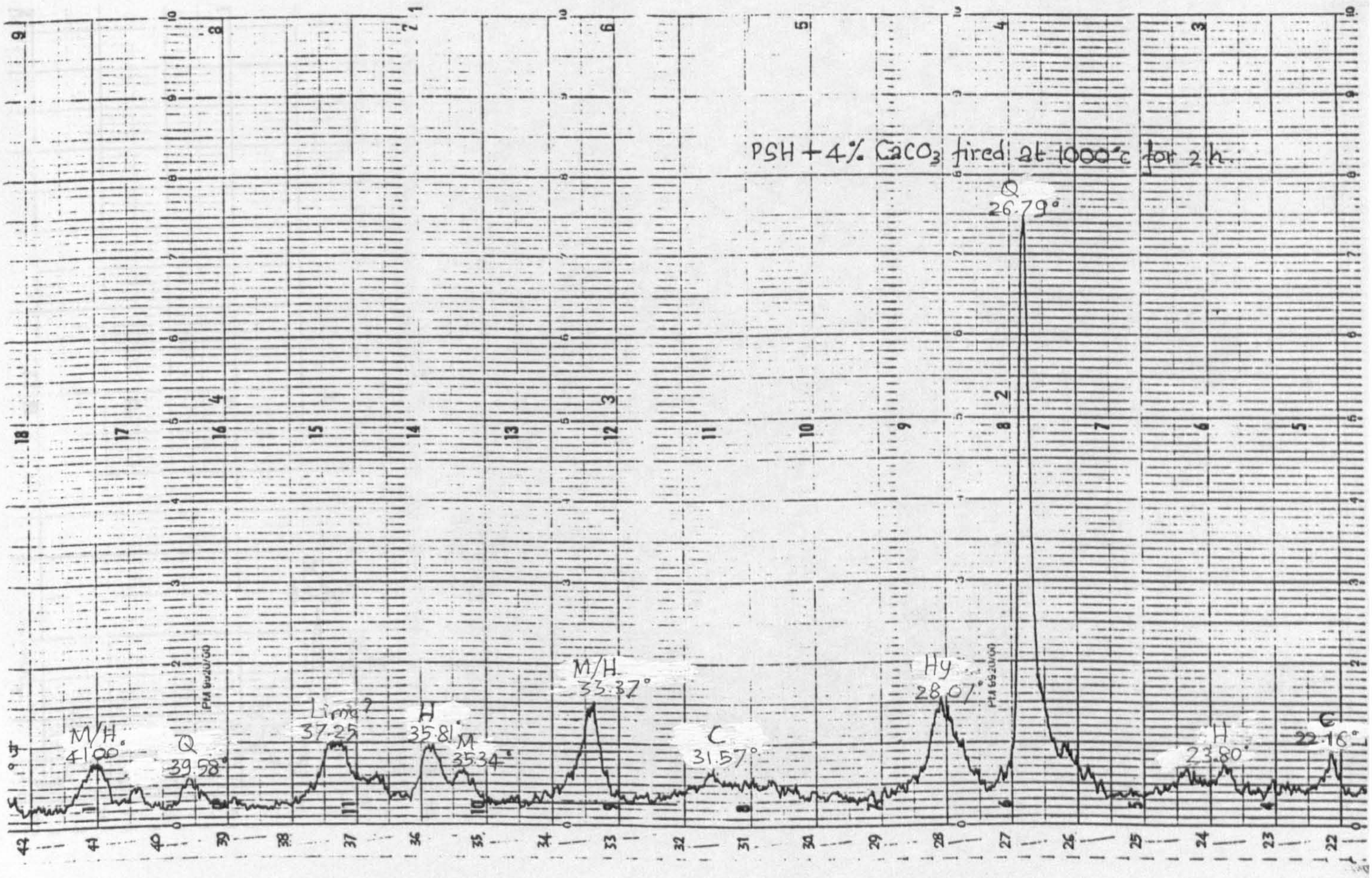

APPENDIX 7

PSH + 4% $CaCO_3$ fired at 1100°C for 2h.

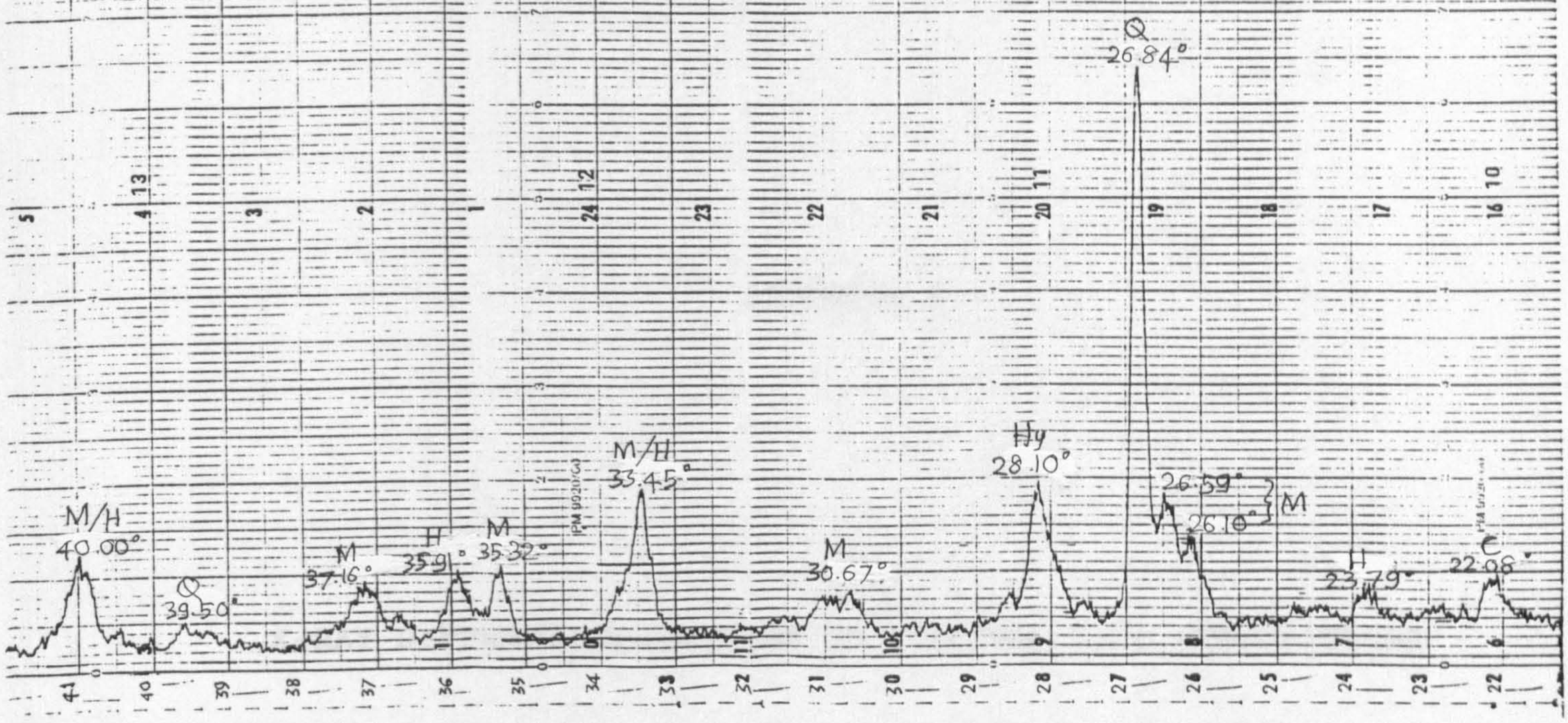

PSH + 4% $CaCO_3$ fired at 1150°C for 2h.

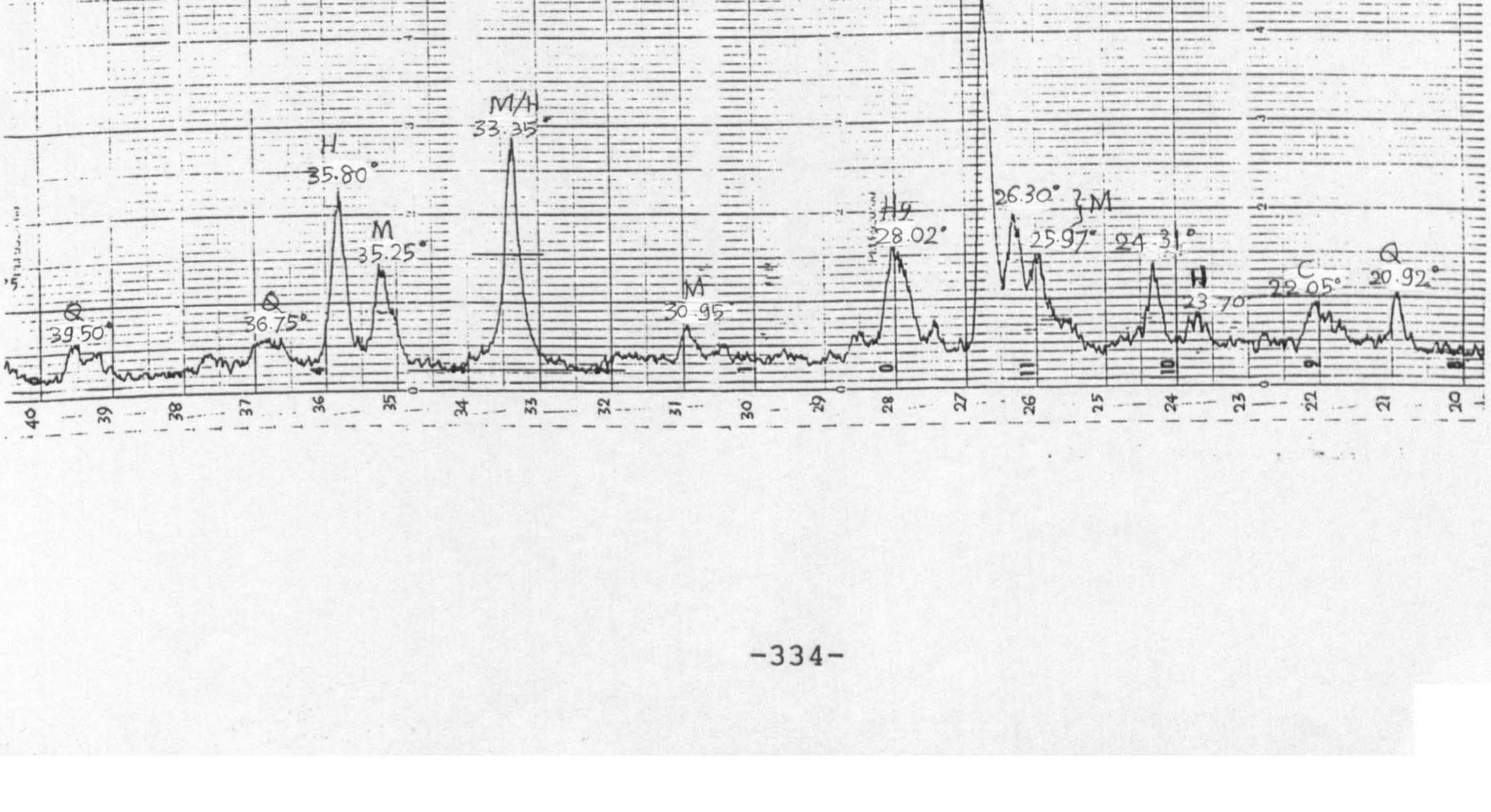

APPENDIX 8

X-RAY DIFFRACTION PATTERNS OF RESIDUAL SOIL COMPOSITIONS

APPENDIX 8

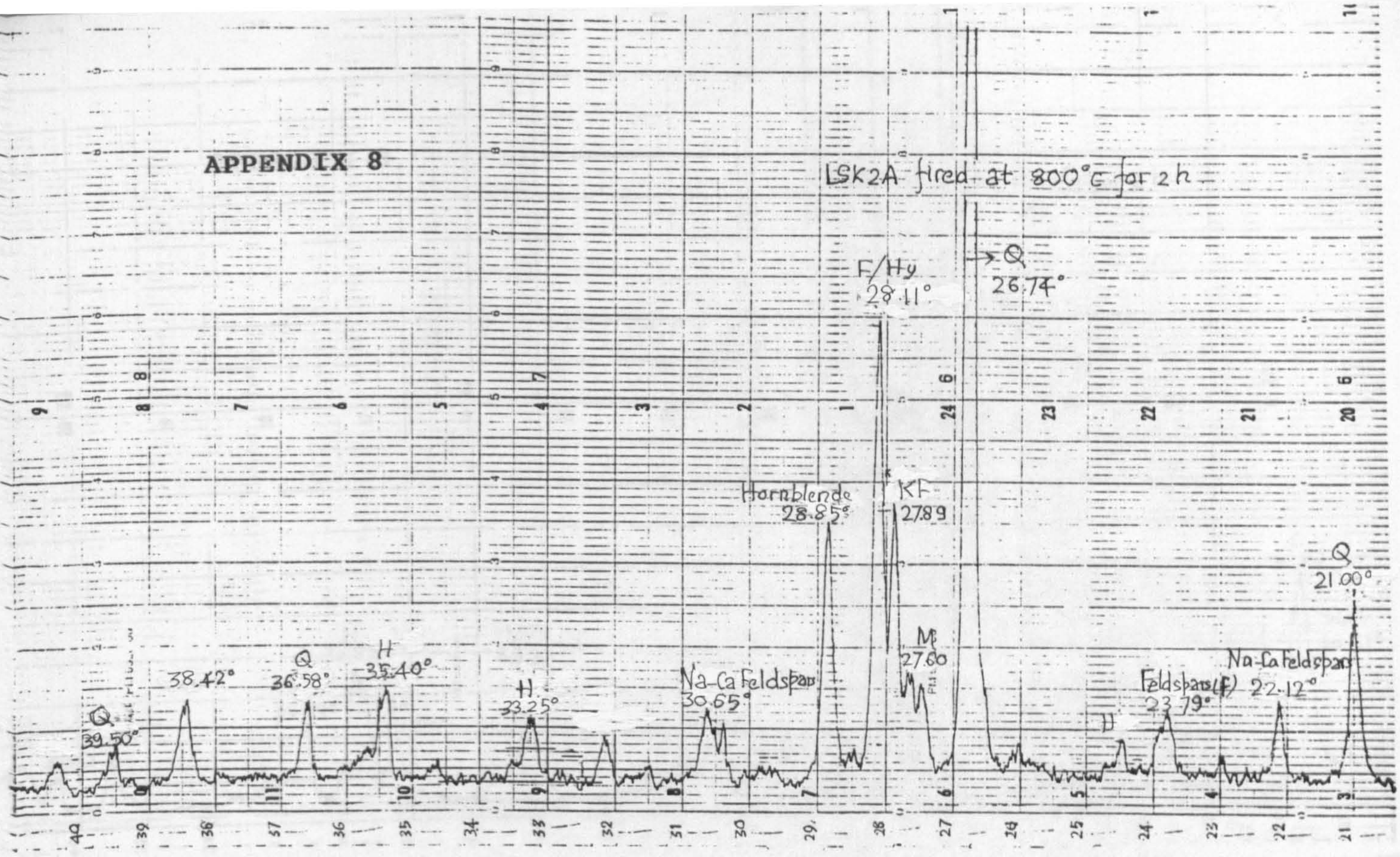
LSK2A fired at 800°C for 2h
F/Hy
28.11°
Q
26.74°
Hornblende
28.85°
KF
27.89
Q
21.00°
M
27.60
Na-Ca Feldspar
30.65°
H
33.25°
Q
36.58°
H
35.40°
38.42°
Q
39.50°
Feldspars(F)
23.79°
Na-Ca Feldspar
22.12°

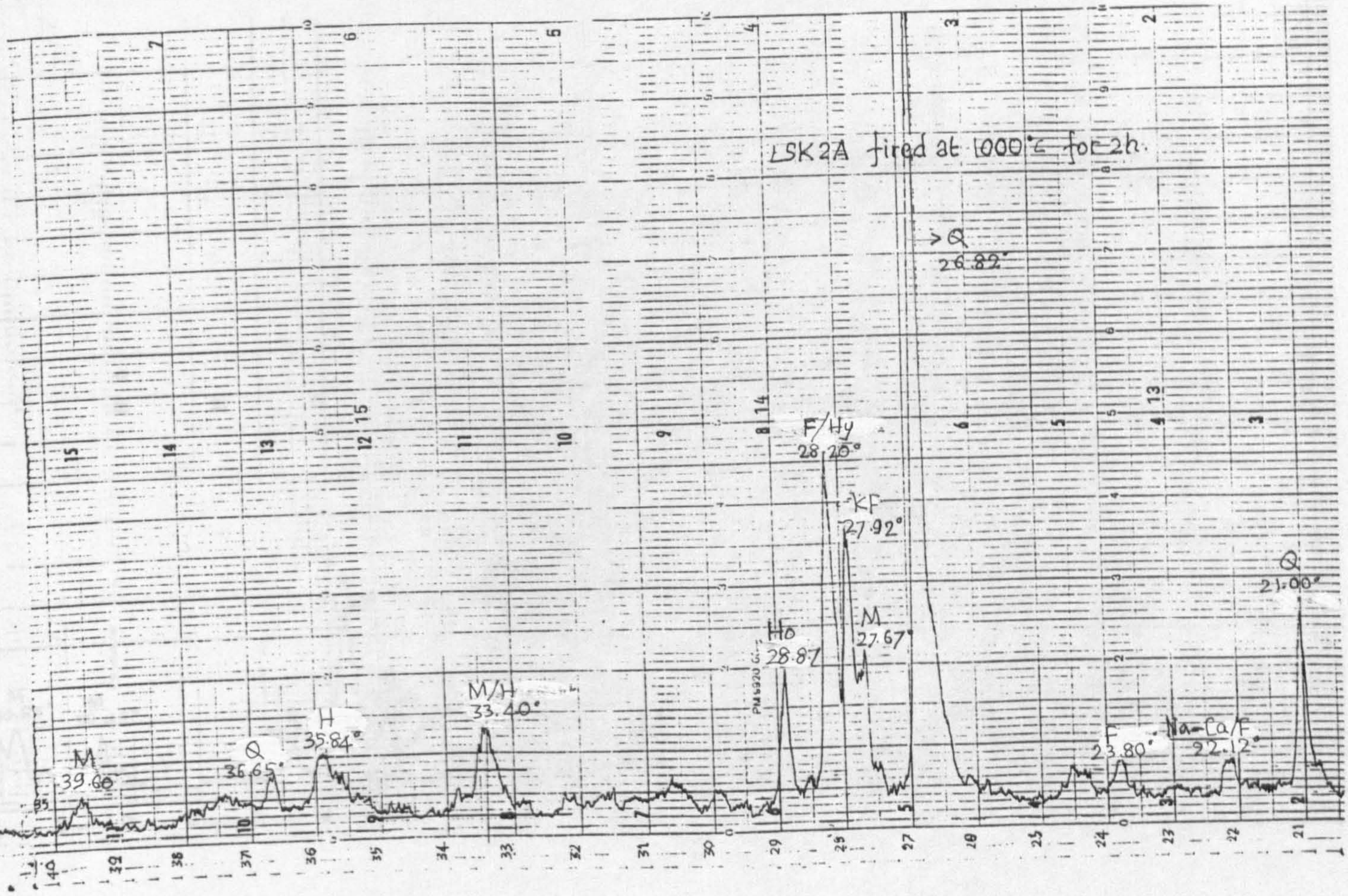
LSK2A fired at 1000°C for 2h.
Q
26.82°
F/Hy
28.20°
KF
27.92°
Ho
28.87
M
27.67°
Q
21.00°
M/H
33.40°
H
35.84°
Q
36.65°
M
39.60
F
23.80°
Na-Ca/F
22.12°

APPENDIX 8

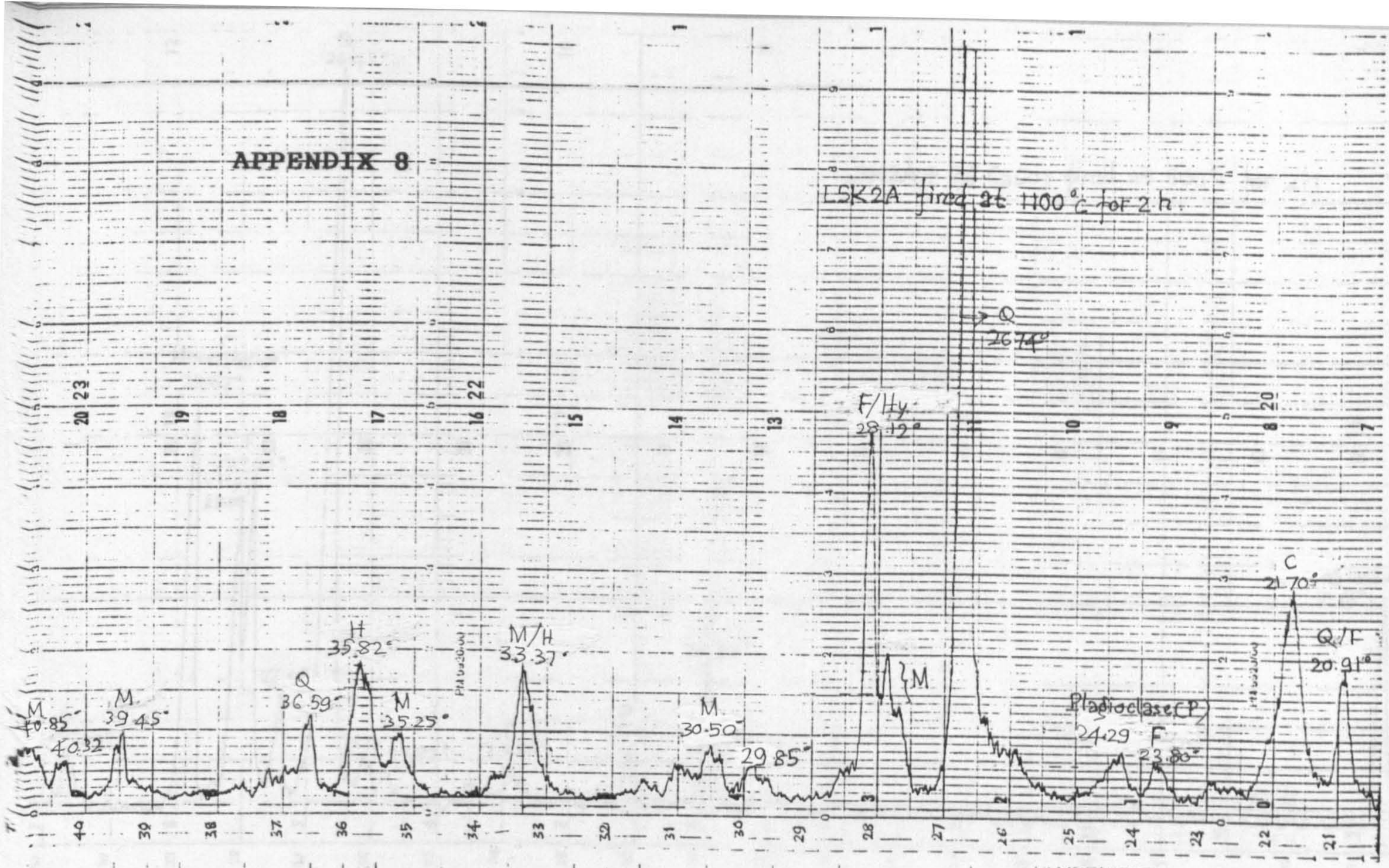
LSK2A fired at 1100°C for 2 h.
Q
26.74°
F/Hy
28.12°
C
21.70°
Q/F
20.91°
M
Plagioclase(CP)
24.29
F
23.80°
H
35.82°
M/H
33.37°
Q
36.59°
M
35.25°
M
30.50°
29.85°
M
40.85°
40.32
M
39.45°

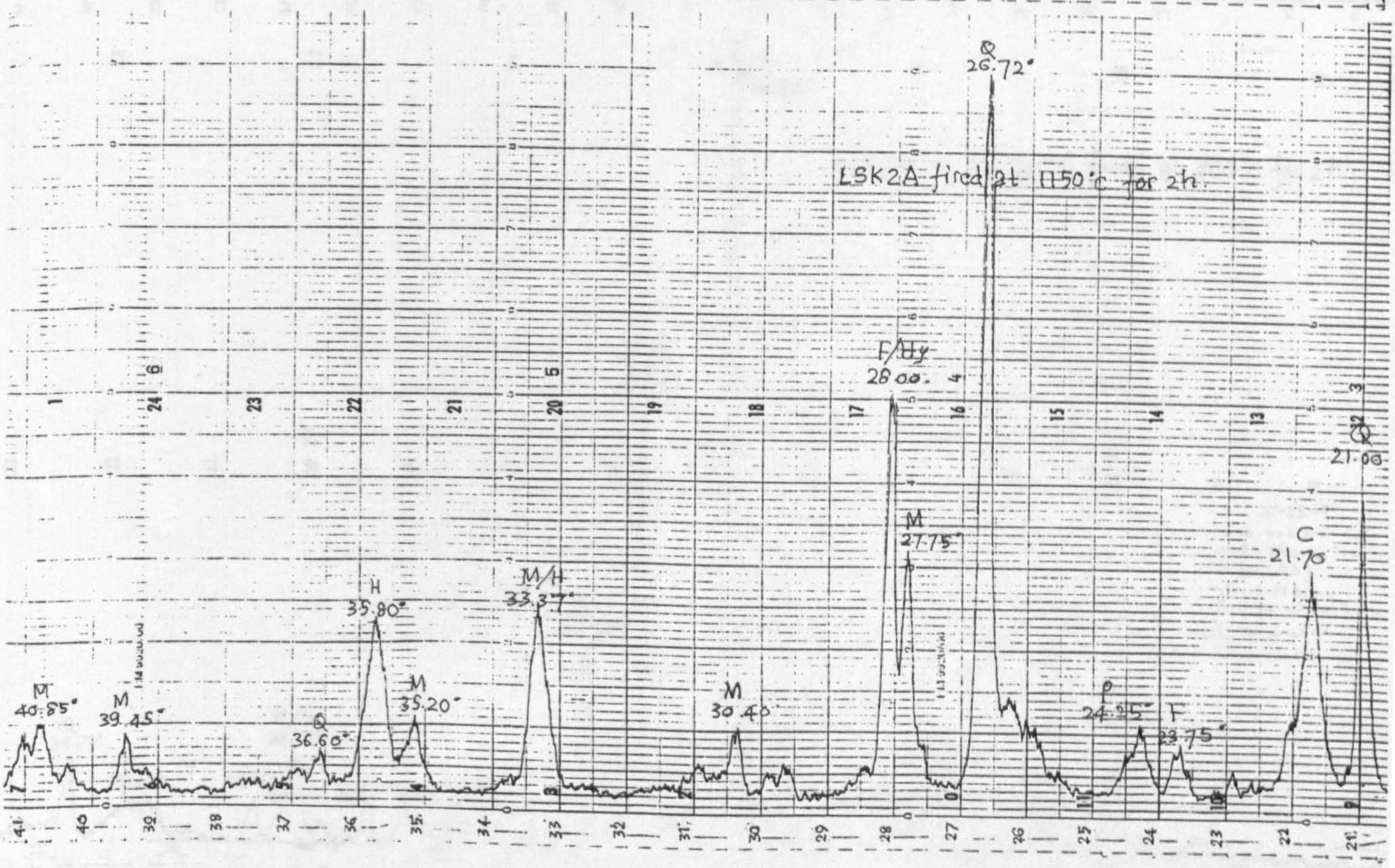
LSK2A fired at 1150°C for 2h.
Q
26.72°
F/Hy
28.00.
M
27.75°
C
21.70
Q
21.00
H
35.80°
M/H
33.37°
M
35.20°
Q
36.60°
M
30.40
M
40.85°
M
39.45°
P
24.25
T
23.75°

APPENDIX 8

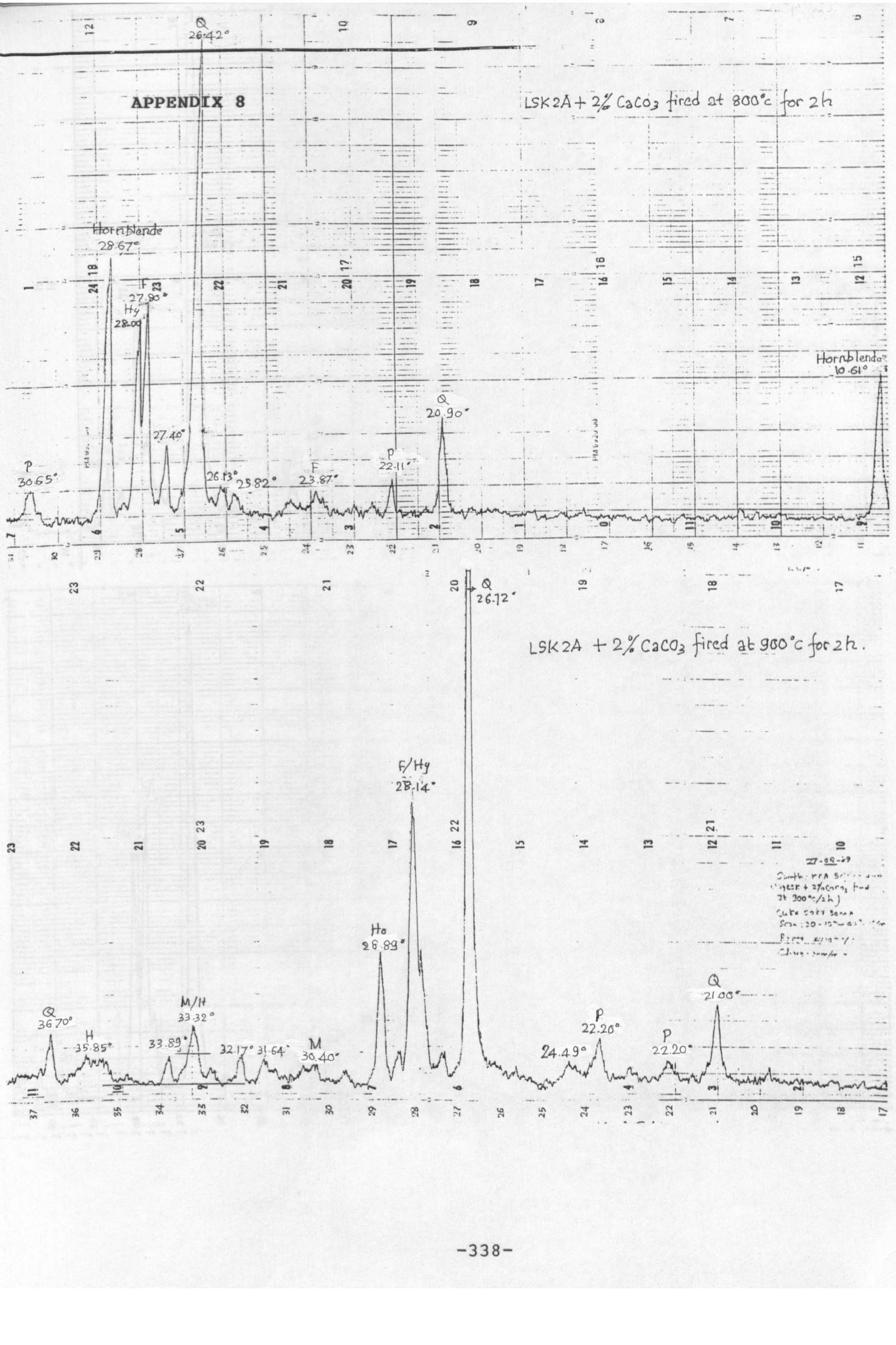
LSK2A + 2% CaCO3 fired at 800°c for 2h
Q 26.42°
Hornblende 28.67°
Hy 28.00
27.80
27.40°
P 30.65°
26.13°
25.82°
F 23.87°
P 22.11°
Q 20.90°
Hornblende 10.61°
Q 26.72°
LSK2A + 2% CaCO3 fired at 900°C for 2h.
F/Hy 28.14°
Ho 28.89°
Q 36.70°
H 35.85°
M/H 33.32°
33.89°
32.17°
31.64°
M 30.40°
24.49°
P 22.20°
P 22.20°
Q 21.00°

APPENDIX 8

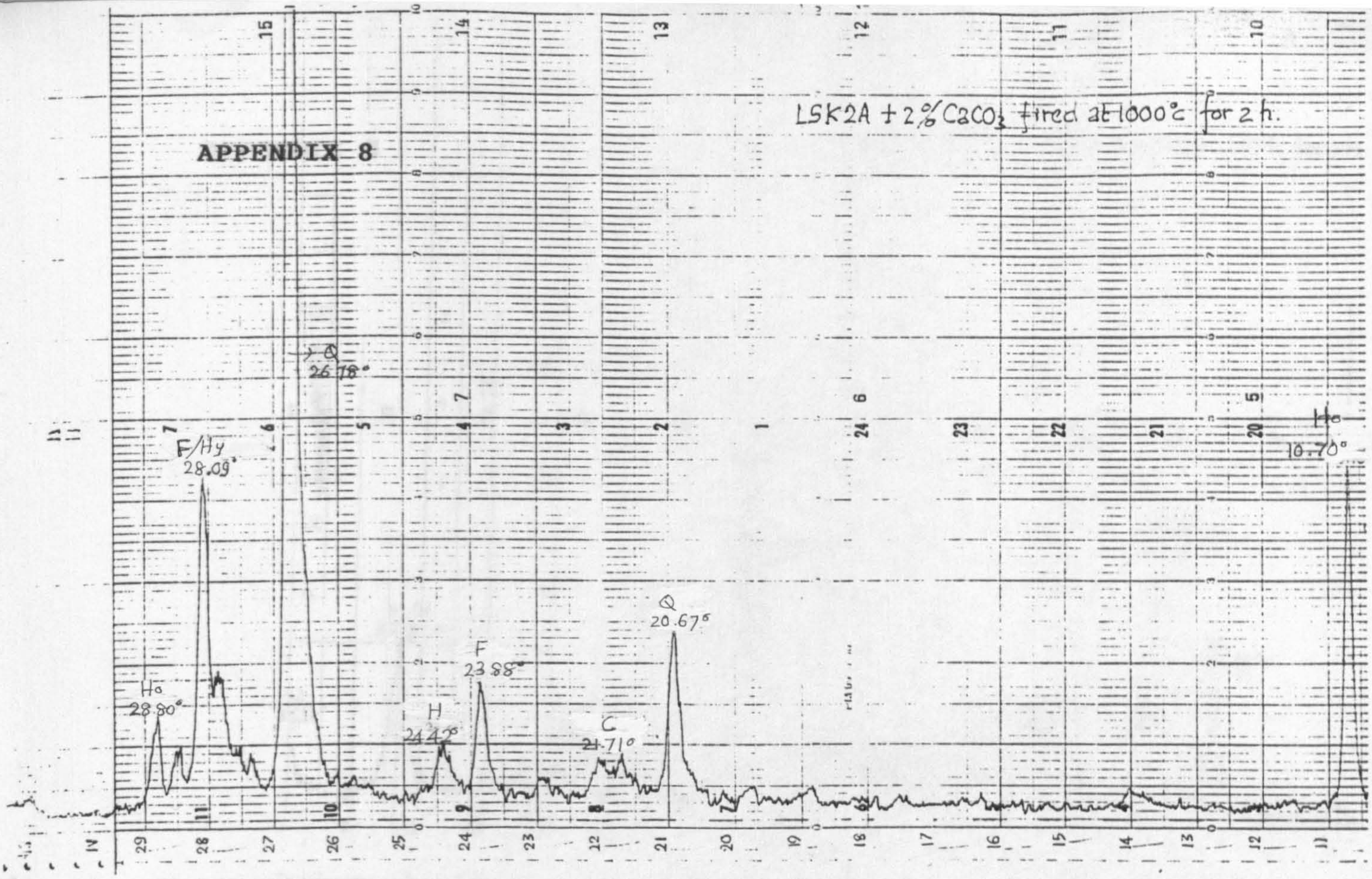

LSK2A + 2% $CaCO_3$ fired at 1100°C for 2 h.

APPENDIX 8

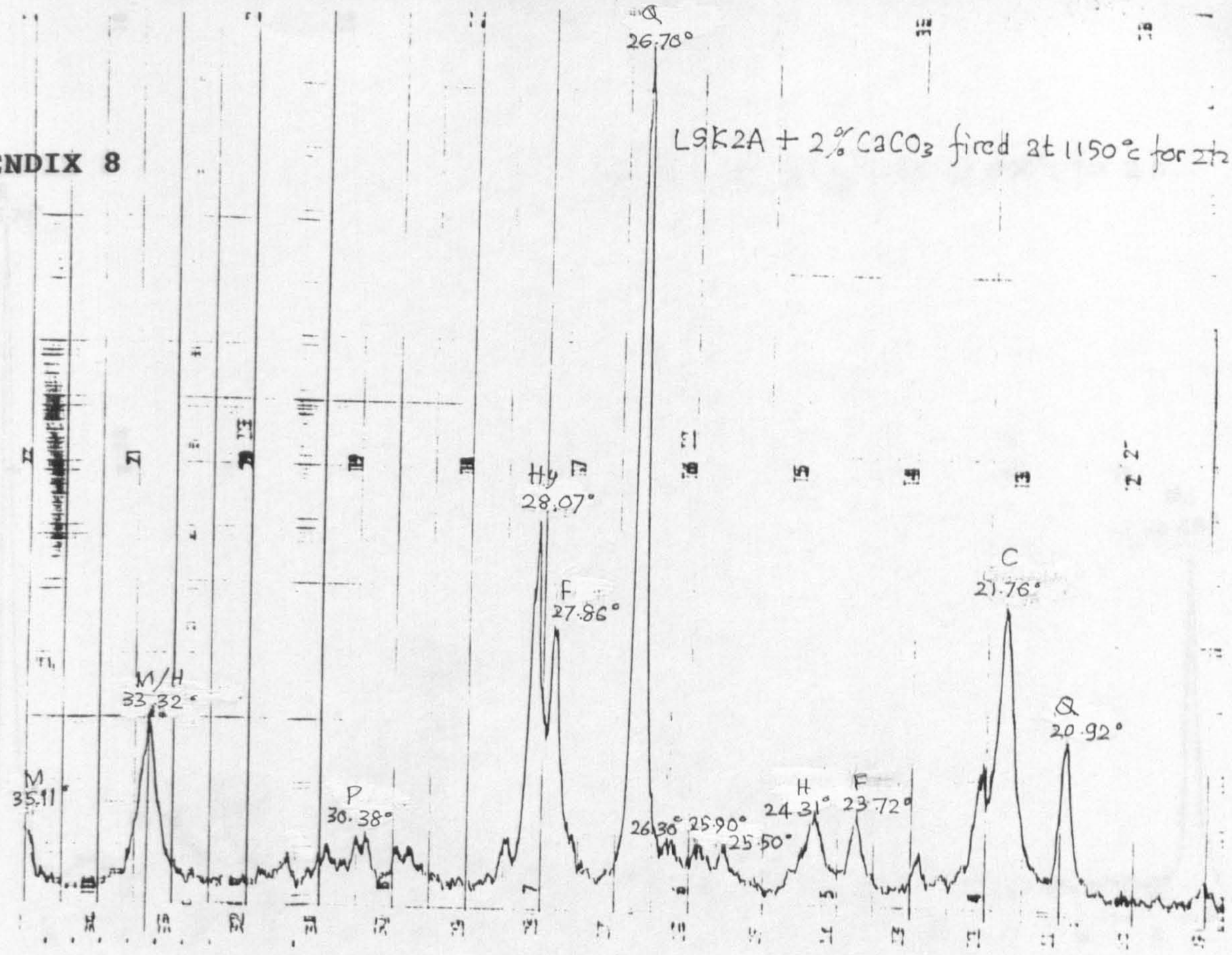
LSK2A + 2% CaCO3 fired at 1150°C for 2h
Q 26.70°
Hy 28.07°
F 27.86°
C 21.76°
M/H 33.32°
Q 20.92°
M 35.11°
P 30.38°
H 24.31°
F 23.72°
26.30° 25.90° 25.50°

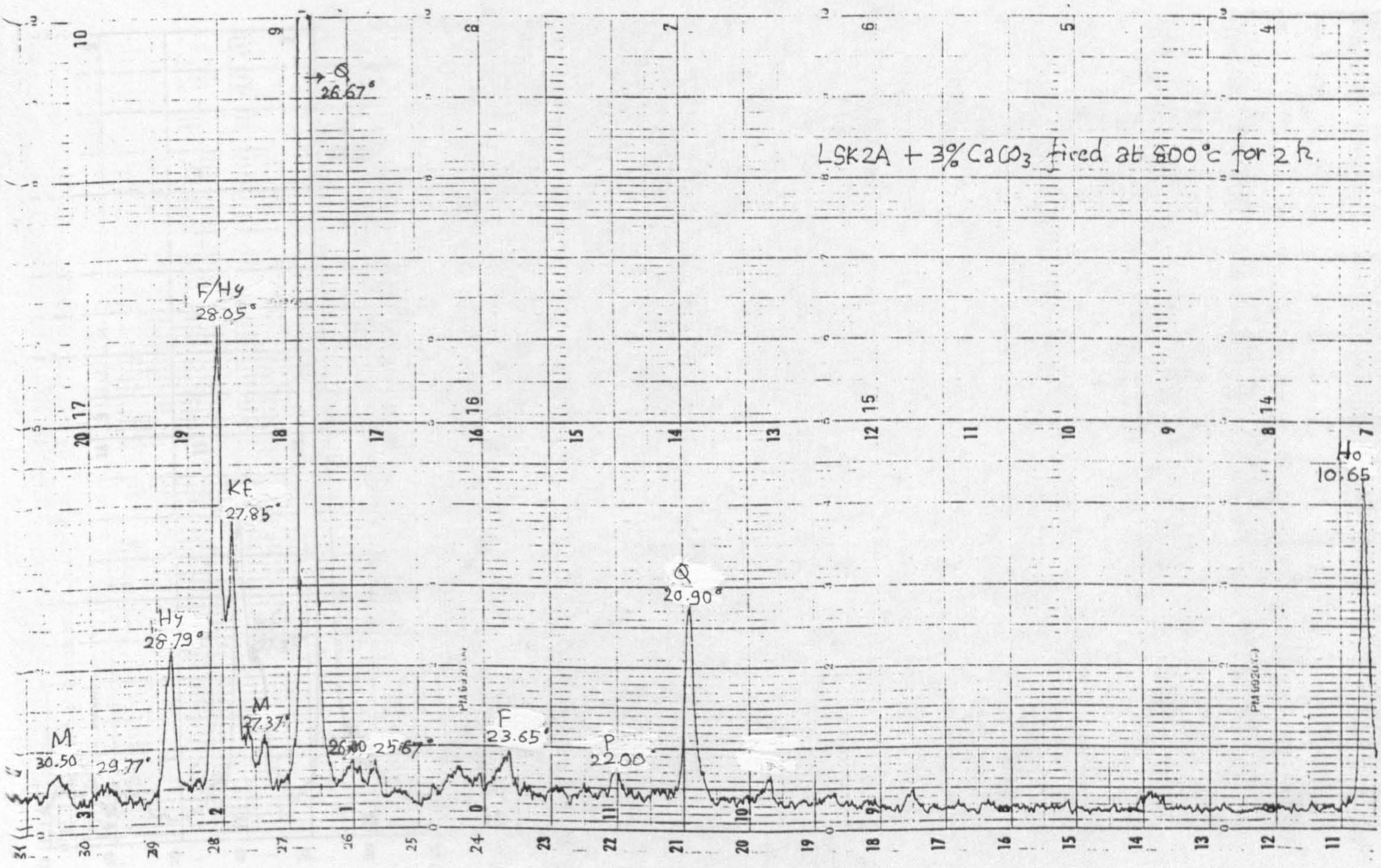
LSK2A + 3% CaCO3 fired at 800°C for 2 h.
Q 26.67°
F/Hy 28.05°
KF 27.85°
Hy 28.79°
M 30.50
29.77°
M 27.37°
26.80 25.67°
F 23.65°
P 22.00
Q 20.90°
Ho 10.65

APPENDIX 8

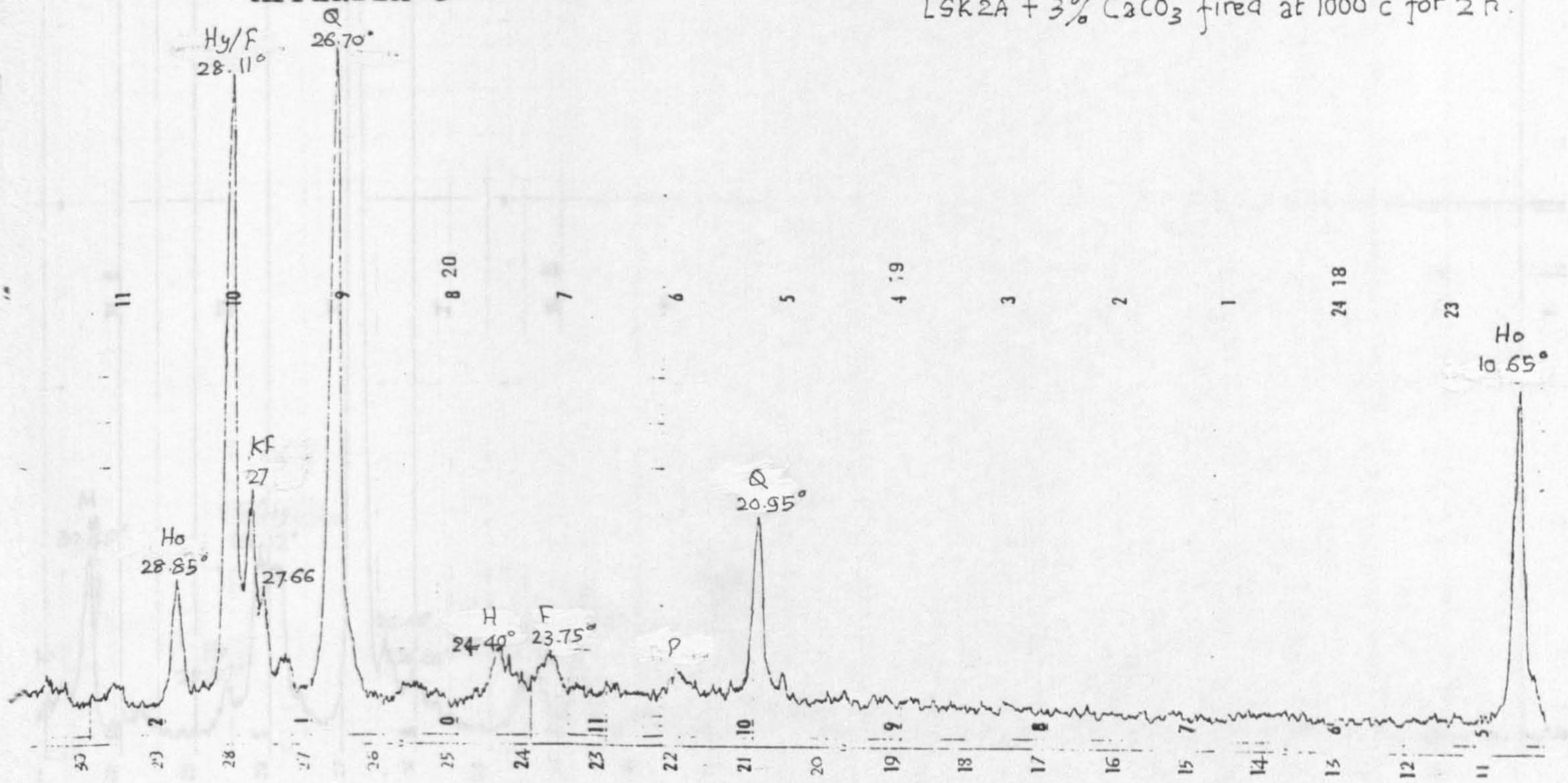

LSK2A + 3% $CaCO_3$ fired at 1000°c for 2 h.

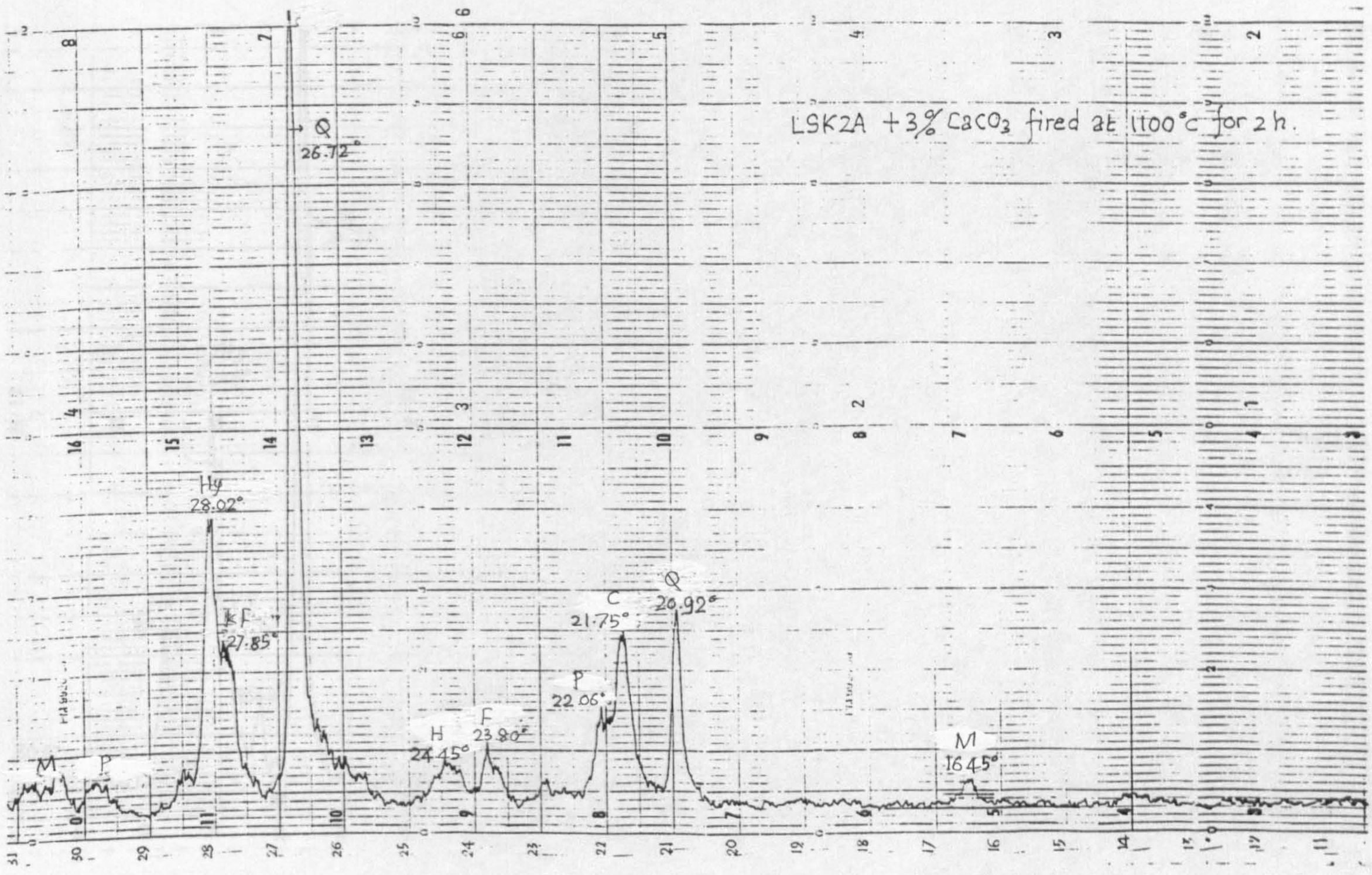

LSK2A + 3% $CaCO_3$ fired at 1100°c for 2 h.

APPENDIX 8

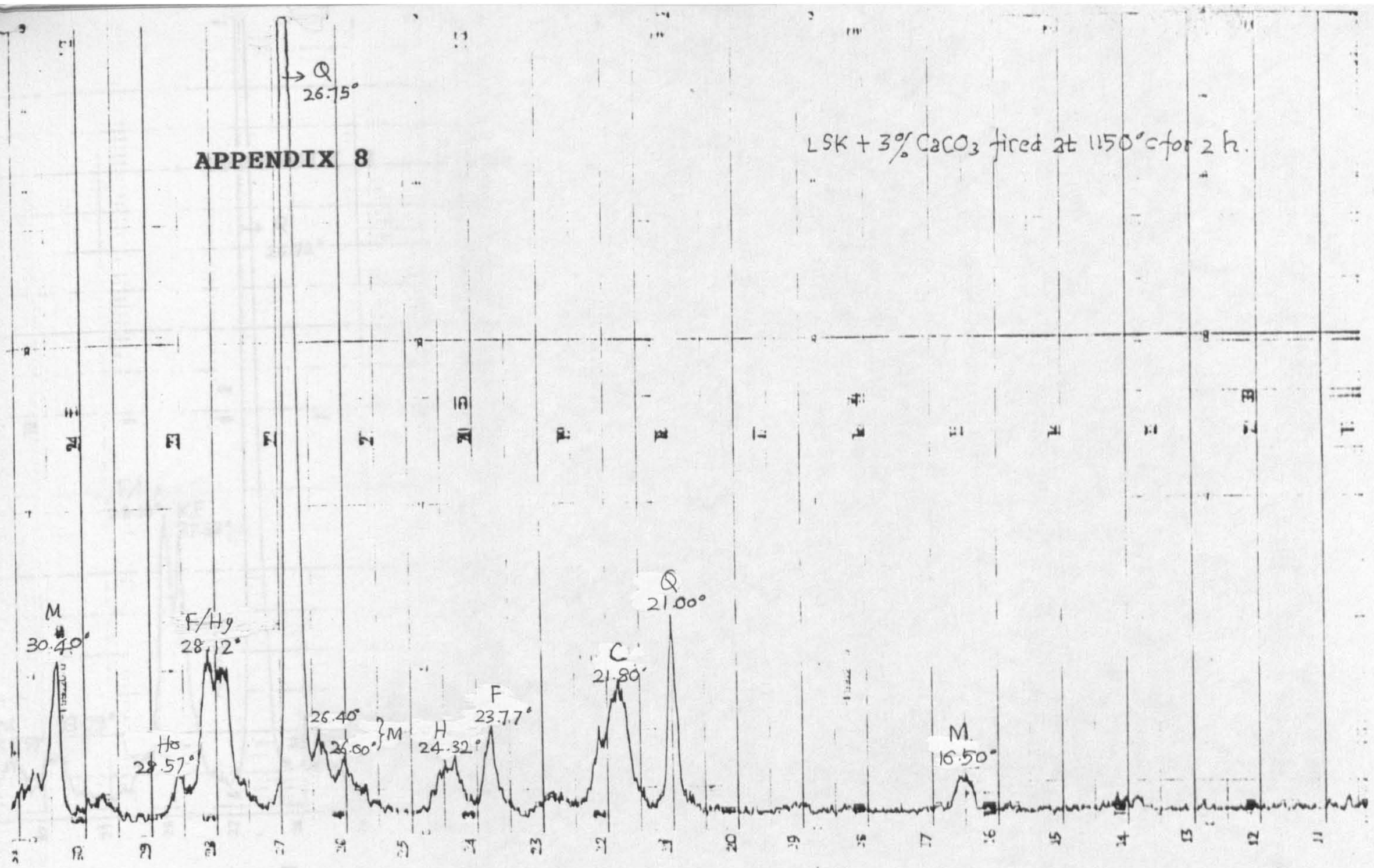
LSK + 3% CaCO3 fired at 1150°c for 2 h.
Q
26.75°
M
30.40°
F/Hg
28.12°
Hα
28.57°
26.40°
26.00°
M
H
24.32°
F
23.77°
C
21.80°
Q
21.00°
M
16.50°

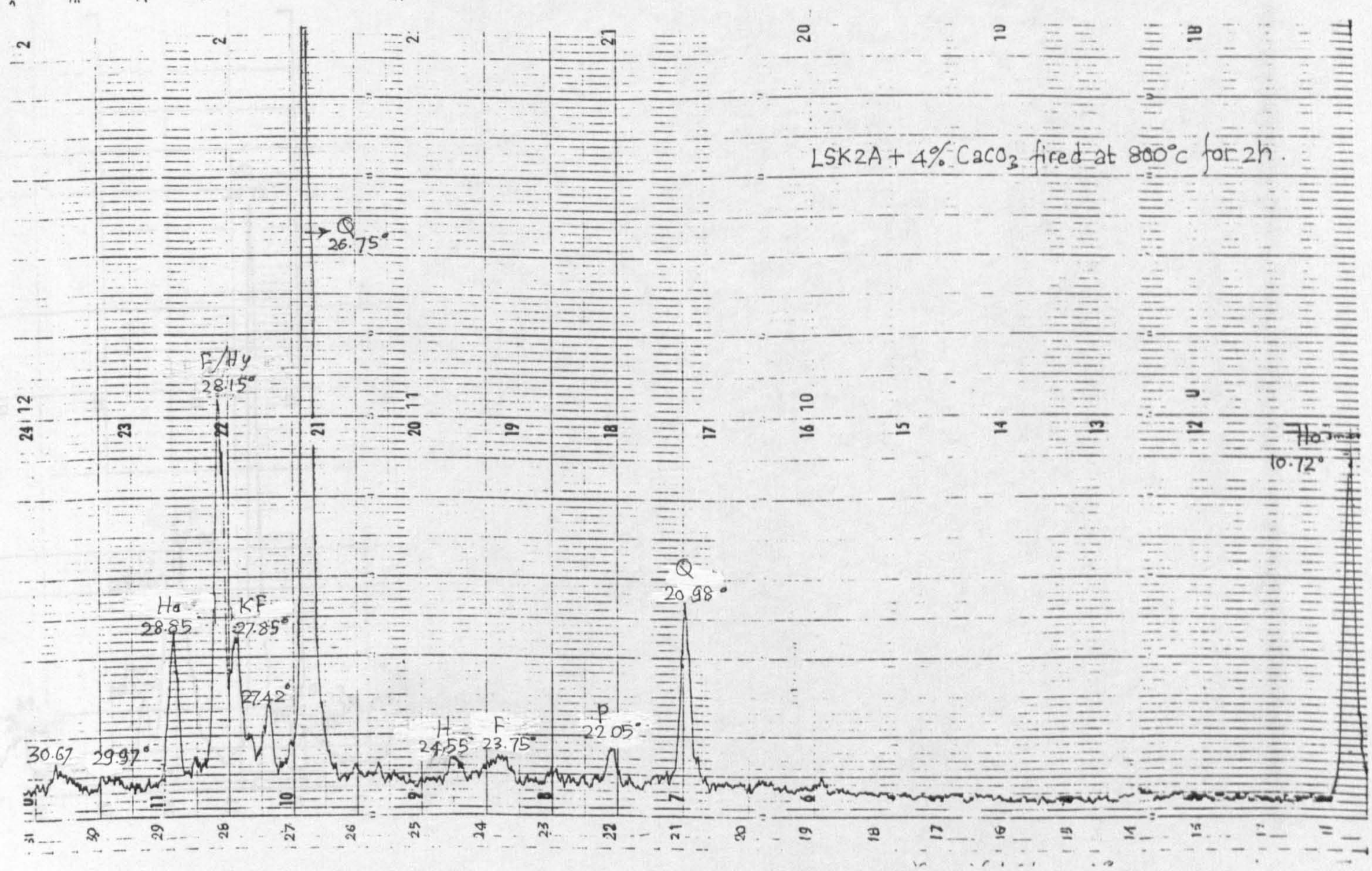
LSK2A + 4% CaCO3 fired at 800°c for 2h.
Q
26.75°
F/Hg
28.15°
Hα
10.72°
Q
20.98°
Hα
28.85
KF
27.85°
27.42°
30.67
29.97°
H
24.55°
F
23.75°
P
22.05°

APPENDIX 8

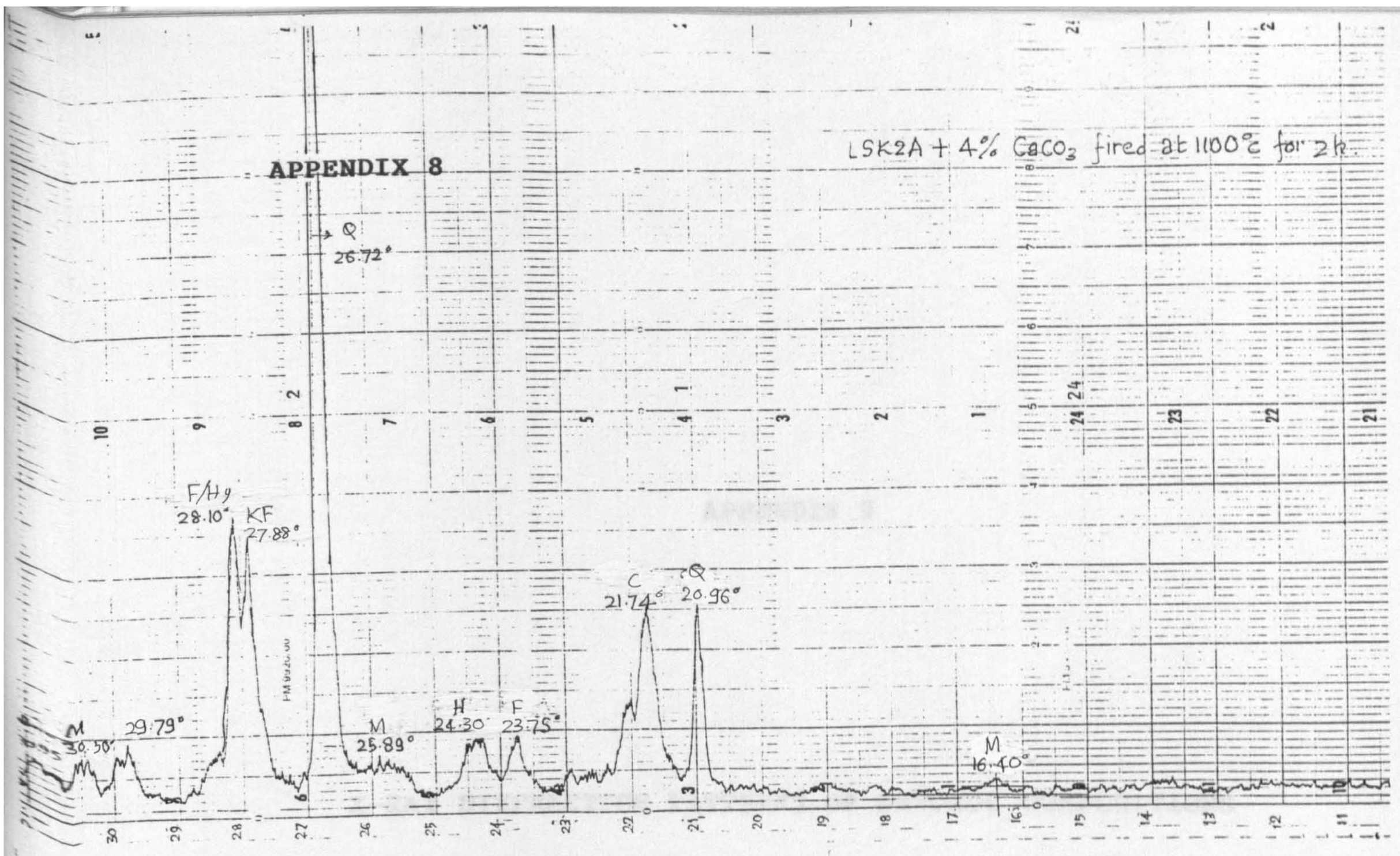
LSK2A + 4% CaCO3 fired at 1100°C for 2h
Q
26.72°
F/Hg
28.10°
KF
27.88°
C
21.74°
Q
20.96°
M
30.50°
29.79°
M
25.89°
H
24.30°
F
23.75°
M
16.40°

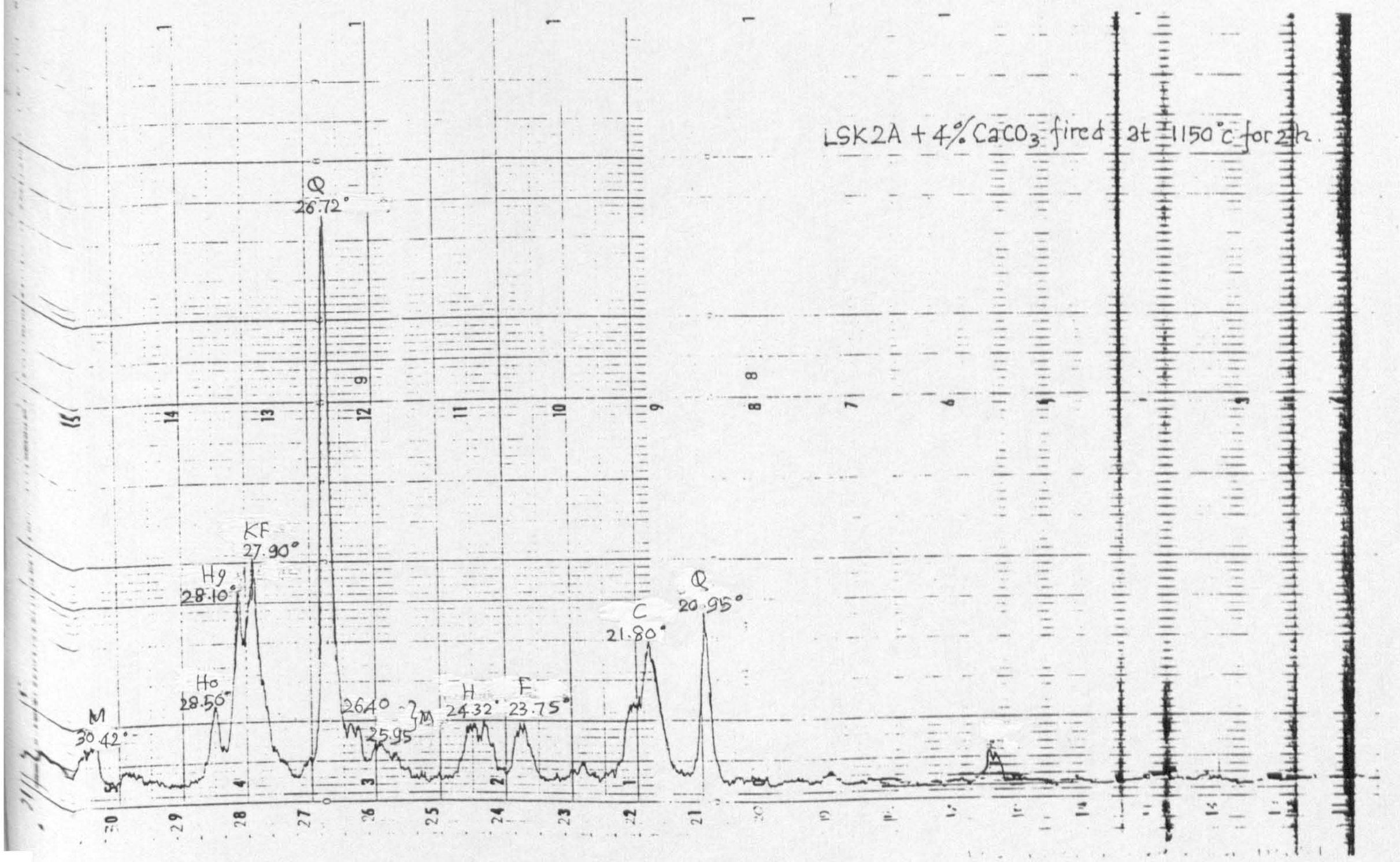
LSK2A + 4% CaCO3 fired at 1150°C for 2h.
Q
26.72°
KF
27.90°
Hg
28.10°
C
21.80°
Q
20.95°
Ho
28.50°
M
30.42°
26.40
M
25.95
H
24.32°
F
23.75°

APPENDIX 9

X-RAY DIFFRACTION PATTERNS OF LATOSOL COMPOSITIONS

APPENDIX 9

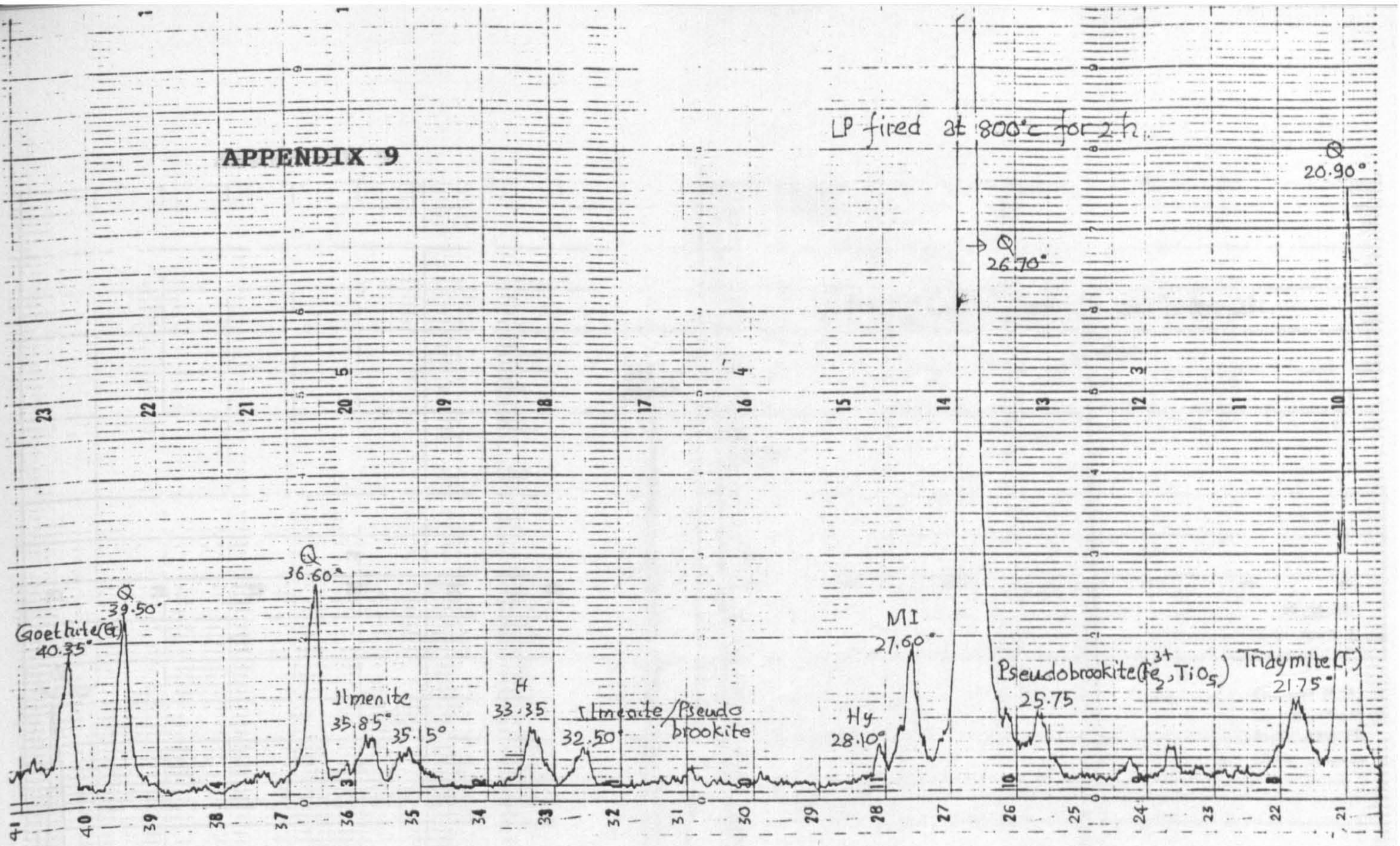
LP fired at 800°c for 2h.
Q 20.90°
Q 26.70°
Goethite(G) 40.35°
Q 39.50°
Q 36.60°
Ilmenite 35.85°
35.5°
H 33.35
Ilmenite/Pseudo brookite 32.50°
Hy 28.10°
MI 27.60°
Pseudobrookite($Fe_2^{3+}TiO_5$) 25.75
Tridymite(T) 21.75°

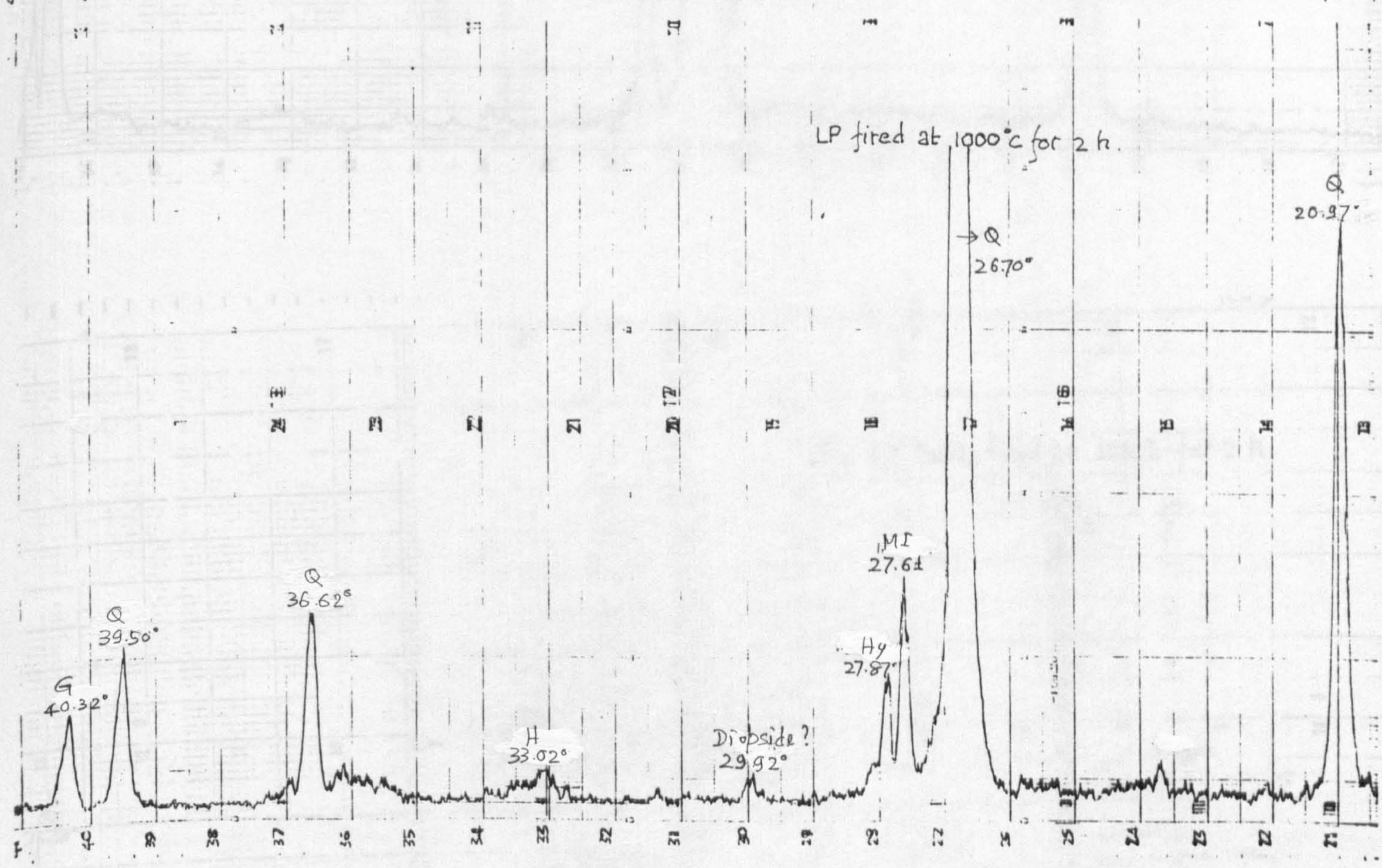
LP fired at 1000°c for 2 h.
Q 20.97°
Q 26.70°
MI 27.61°
Hy 27.87°
Q 36.62°
Q 39.50°
G 40.32°
H 33.02°
Diopside? 29.92°

APPENDIX 9

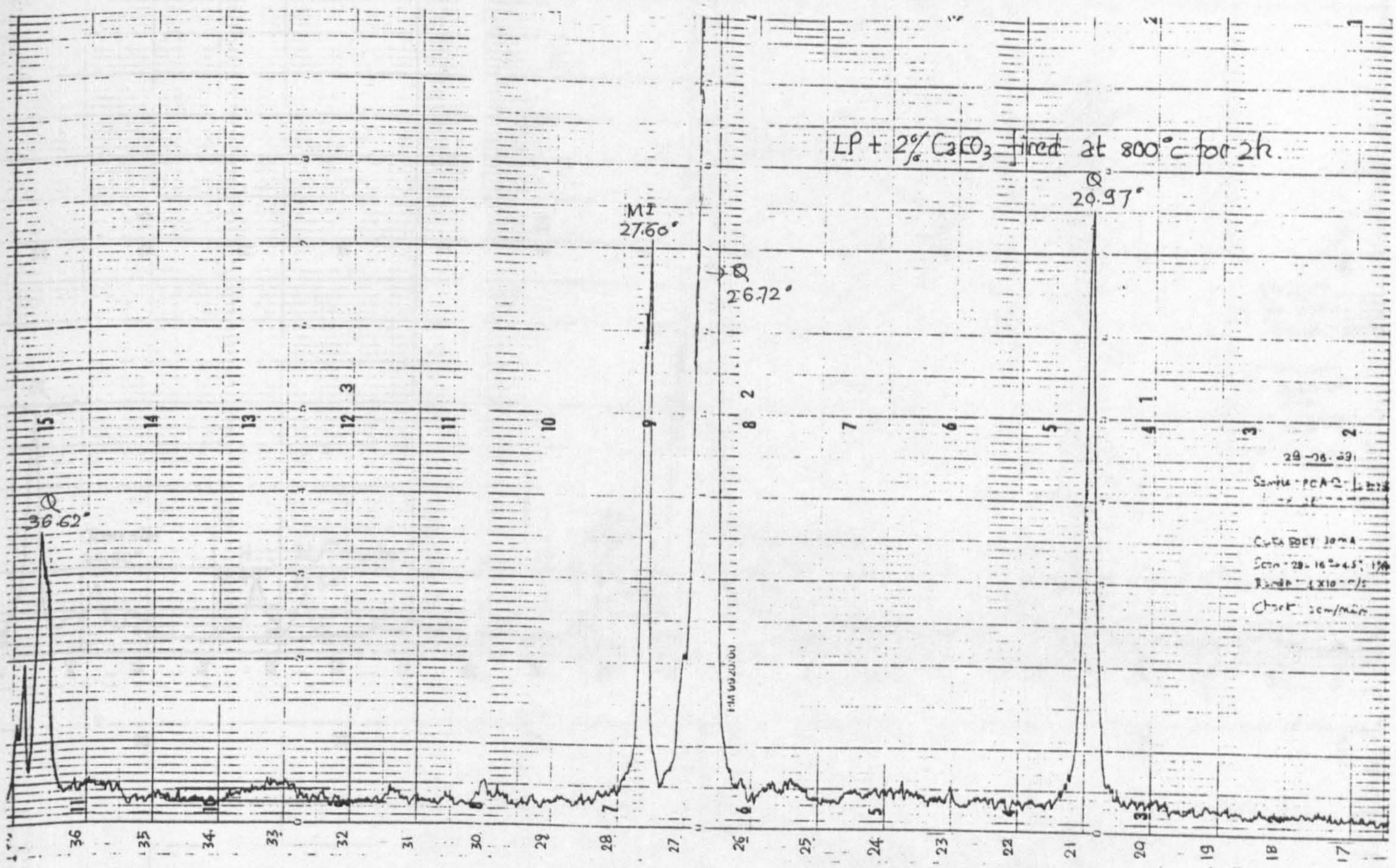
LP + 2% CaCO3 fired at 800°c for 2h.
MI
27.60°
26.72°
20.97°
36.62°

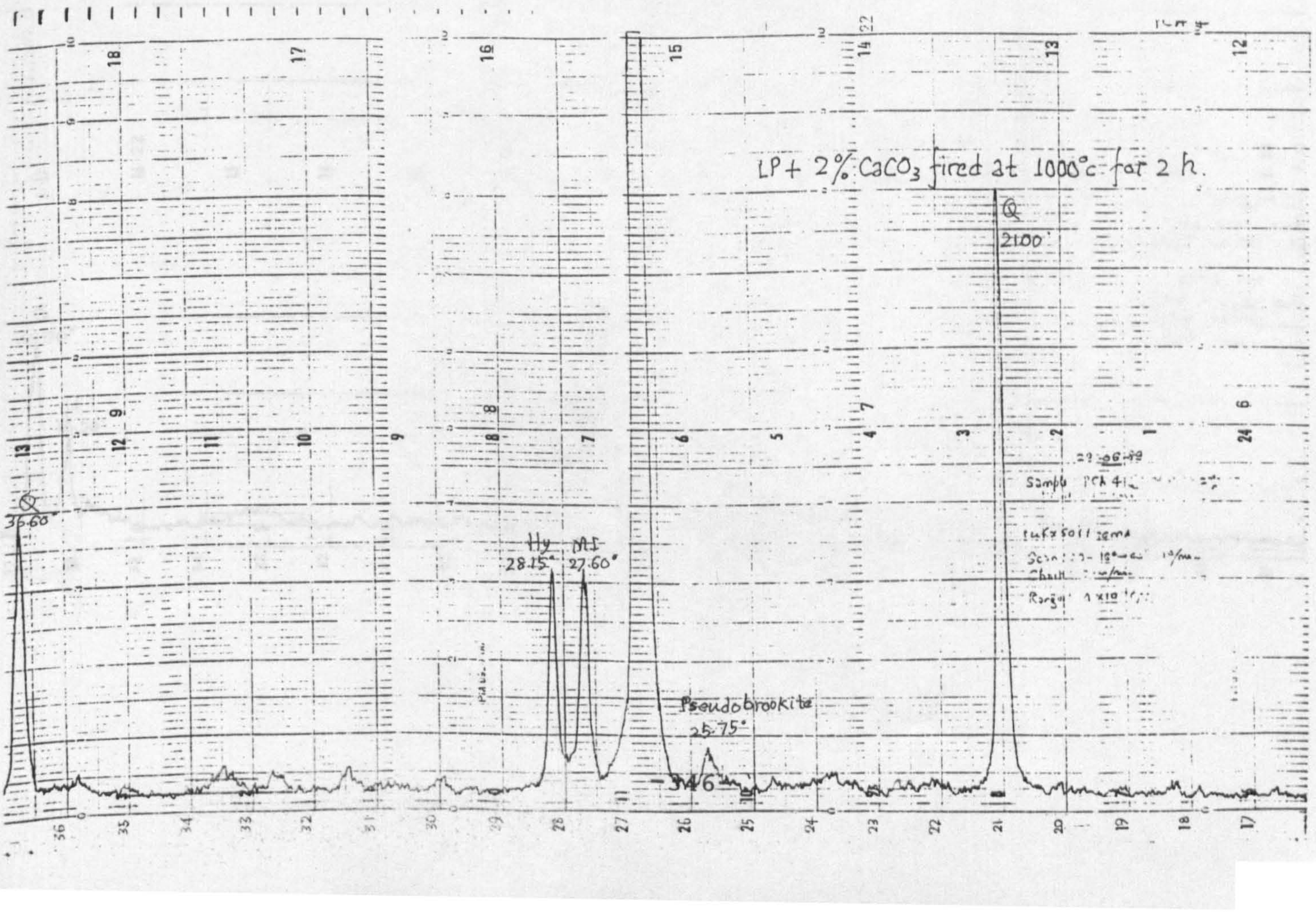
LP + 2% CaCO3 fired at 1000°c for 2 h.
2100
Hy
28.15°
MI
27.60°
Pseudobrookite
25.75°
35.60°
34.6°

APPENDIX 9

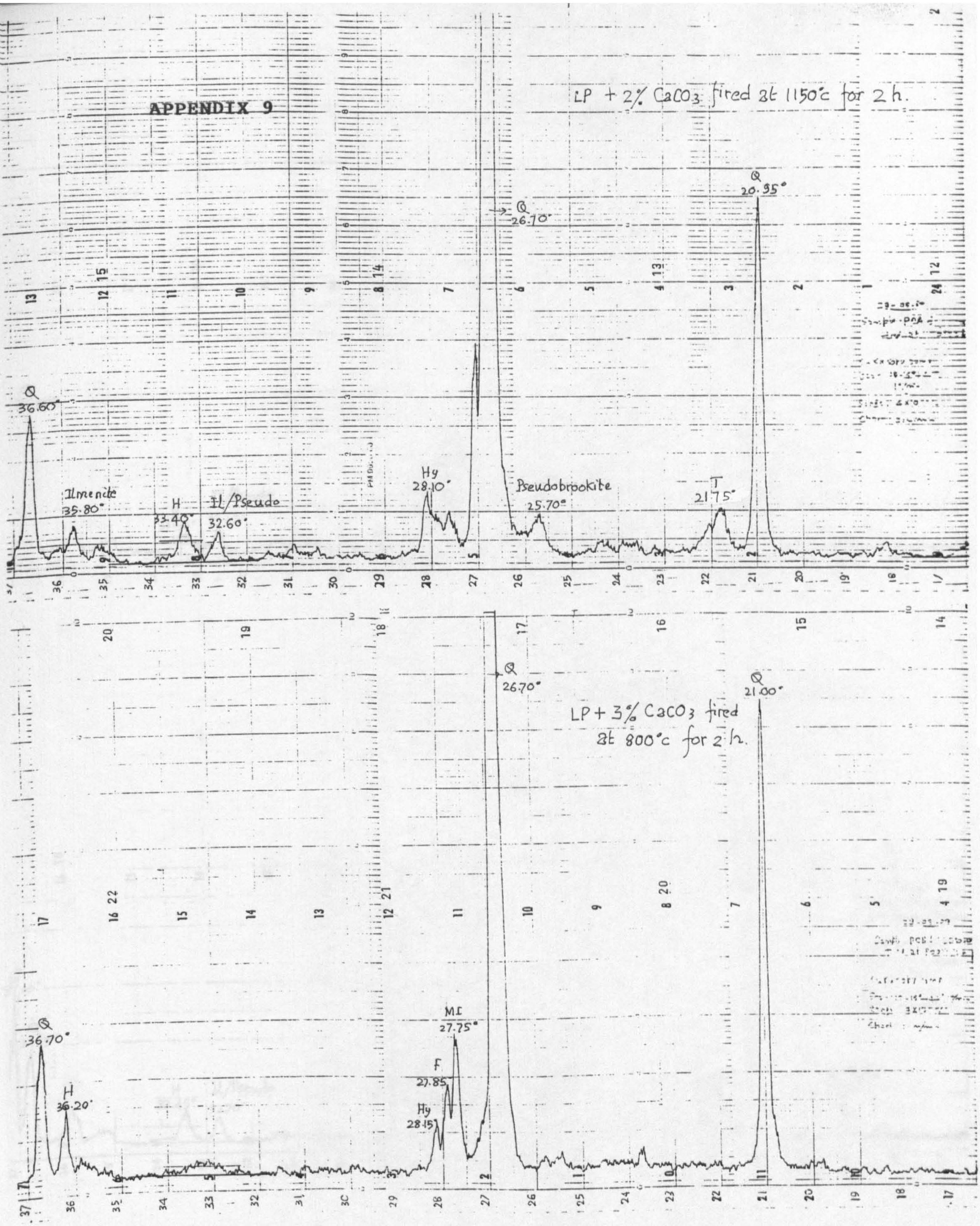
LP + 2% CaCO3 fired at 1150°c for 2 h.
Q 20.95°
Q 26.70°
Q 36.60°
Ilmenite 35.80°
H 33.40°
Il/Pseudo 32.60°
Hy 28.10°
Pseudobrookite 25.70°
T 21.75°
Q 26.70°
Q 21.00°
LP + 3% CaCO3 fired at 800°c for 2 h.
Q 36.70°
H 36.20°
TM 27.75°
F 27.85°
Hy 28.15°

APPENDIX 9

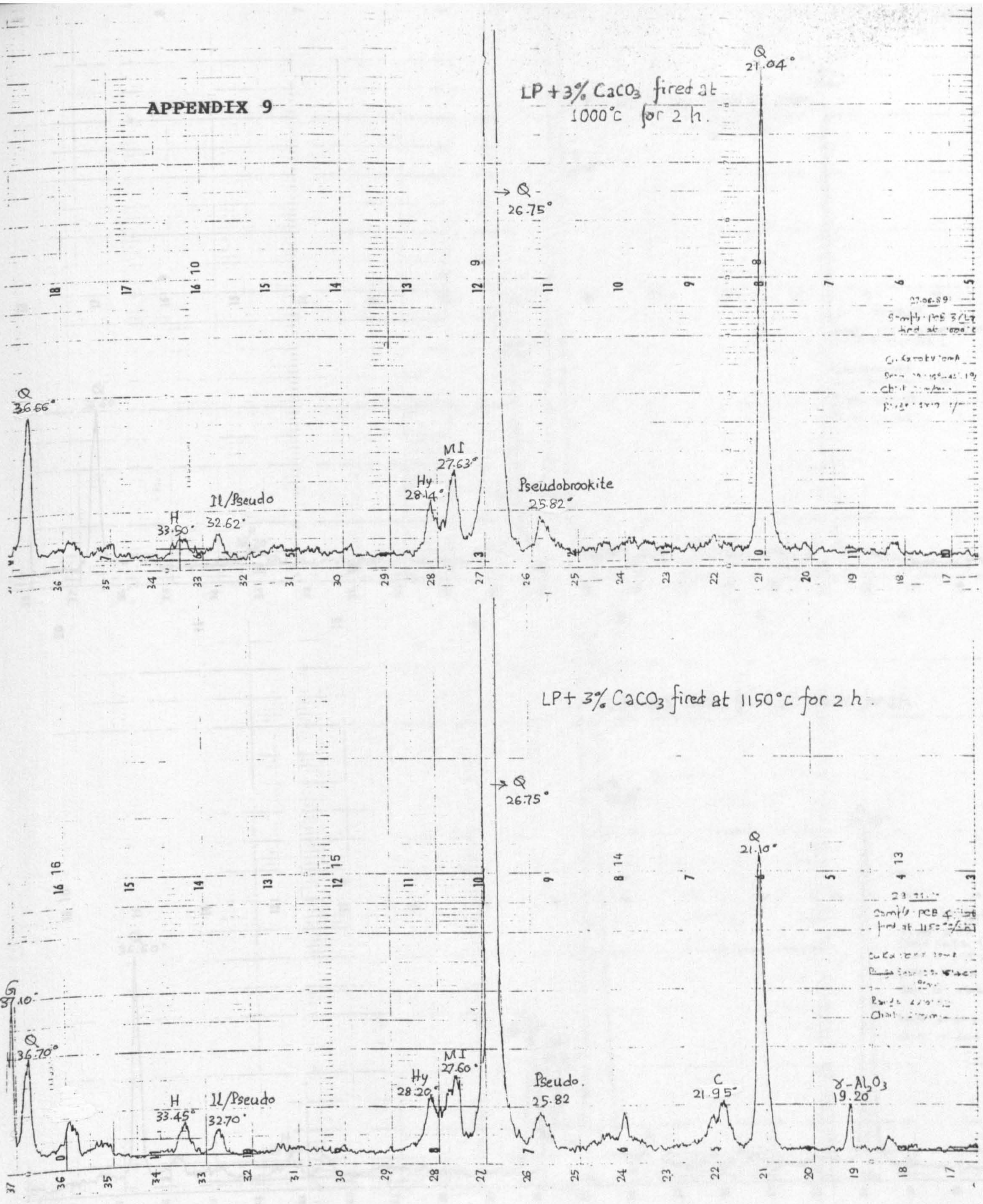
LP + 3% CaCO3 fired at 1000°C for 2 h.
Q 21.04°
Q 26.75°
Q 36.66°
MI 27.63°
Hy 28.14°
Il/Pseudo 32.62°
H 33.50°
Pseudobrookite 25.82°
LP + 3% CaCO3 fired at 1150°C for 2 h.
Q 26.75°
Q 21.10°
Q 36.70°
MI 27.60°
Hy 28.20°
H 33.45°
Il/Pseudo 32.70°
Pseudo. 25.82
C 21.95°
γ-Al2O3 19.20

APPENDIX 9

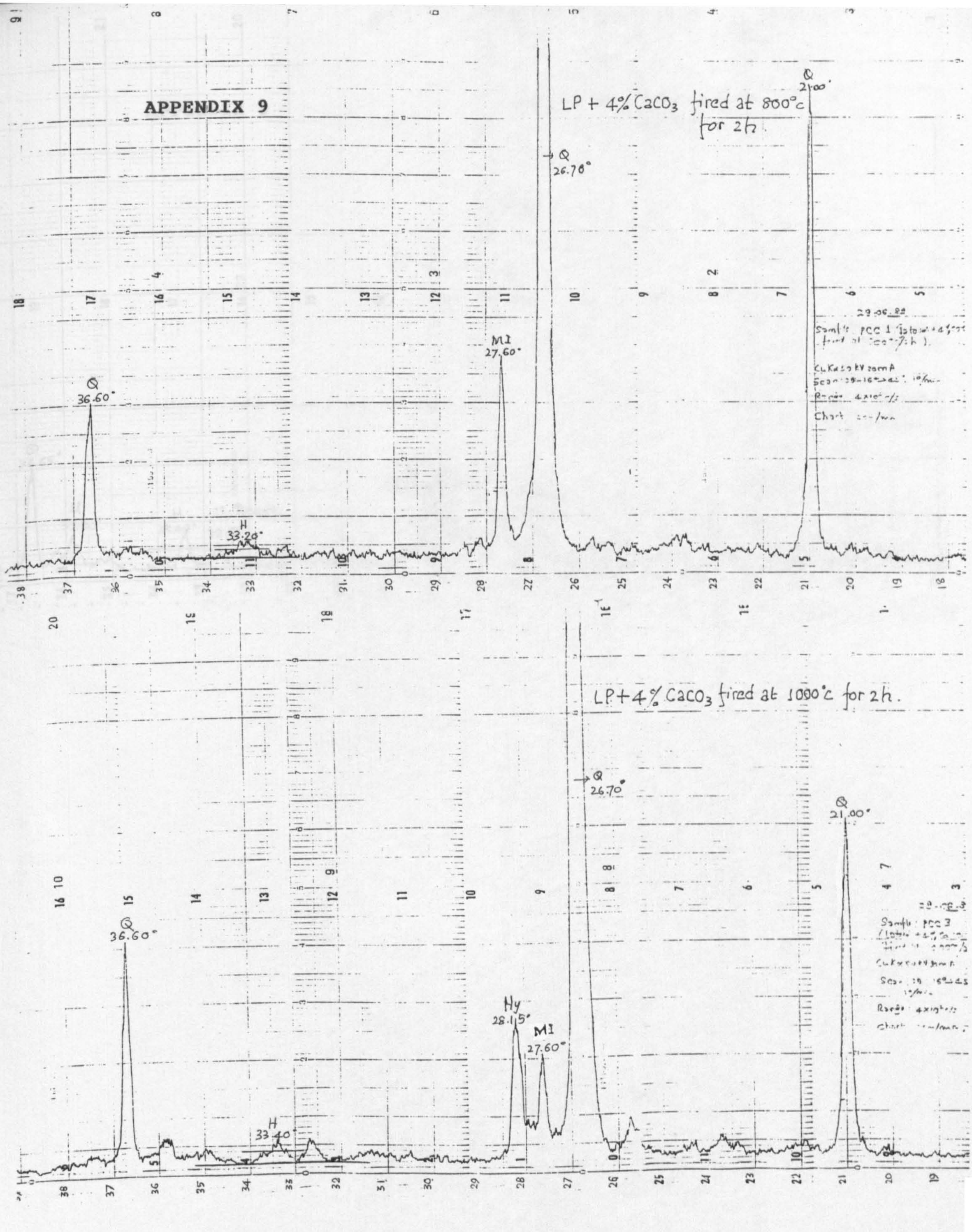
LP + 4% CaCO3 fired at 800°c for 2h.
Ø 26.70°
Ø 21.00°
M1 27.60°
Ø 36.60°
H 33.20°
Sample: PCC 1
CuKα 30 kV 20mA
Scan: 28-16°→2θ°, 1°/min
Chart: cm/min
LP+4% CaCO3 fired at 1000°c for 2h.
Ø 26.70°
Ø 21.00°
Hy 28.15°
M1 27.60°
Ø 36.60°
H 33.40°
Sample: PCC 3
CuKα 30 kV 20mA
Scan: 28-16°→2θ°, 1°/min
Chart: cm/min

APPENDIX 9

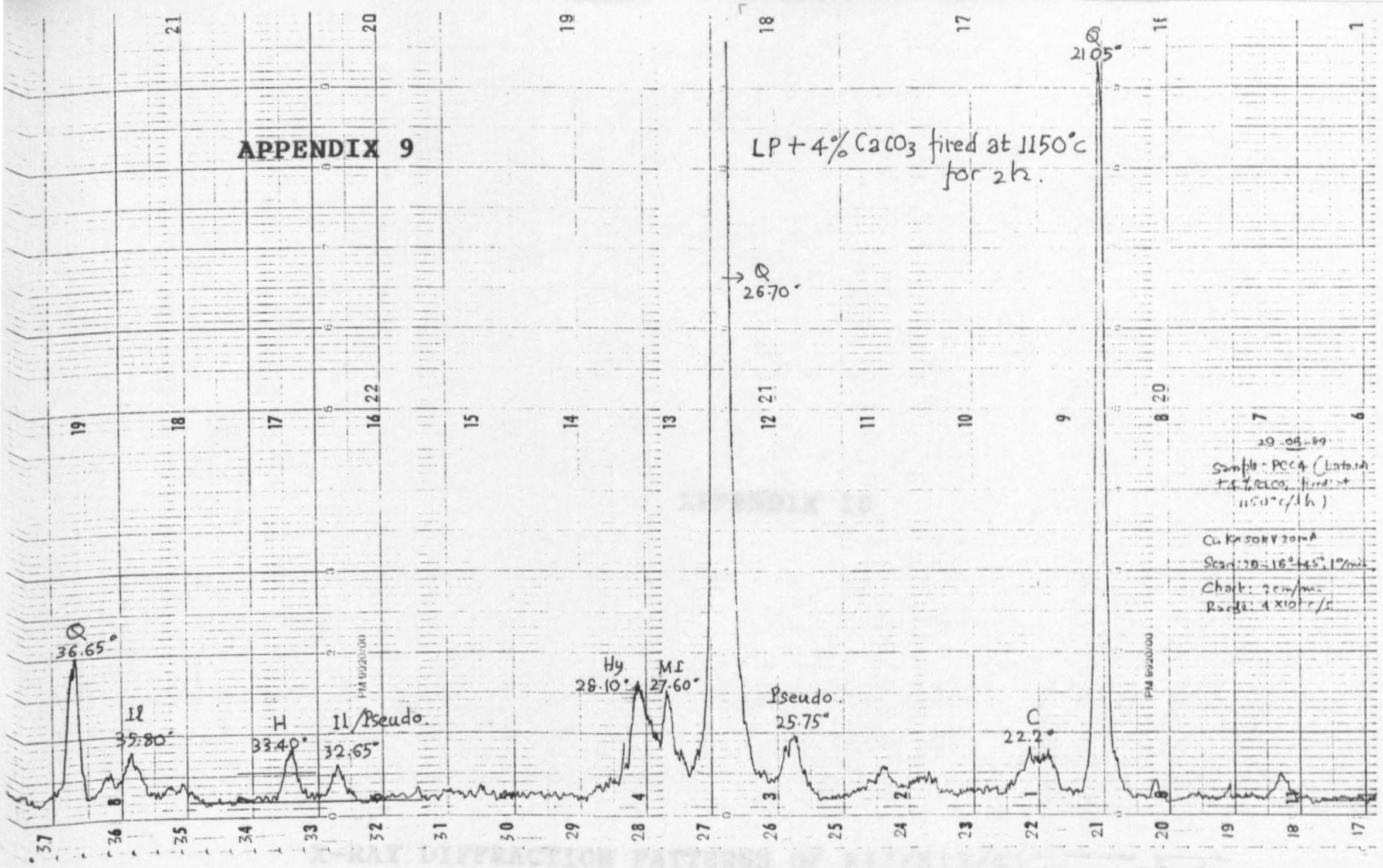
LP + 4% CaCO3 fired at 1150°C for 2h.
Q 21.05°
Q 26.70°
29-06-89
Sample: PCCA (Latosol + 4% CaCO3 fired at 1150°C/1h)
Cu Kα 50KV 30mA
Scan: 2θ-16°-45°, 1°/min
Chart: 2cm/min
Range: 4x10² c/s
Q 36.65°
Il 35.80°
H 33.40°
Il/Pseudo. 32.65°
Hy 28.10°
Ml 27.60°
Pseudo. 25.75°
C 22.2°
PM 9920/00

APPENDIX 10

X-RAY DIFFRACTION PATTERNS OF K11/K13/K17 CLAY MIXES

APPENDIX 10

LSK2A (Raw) treated with 1M phosphate (Eq. pH = 7.4)

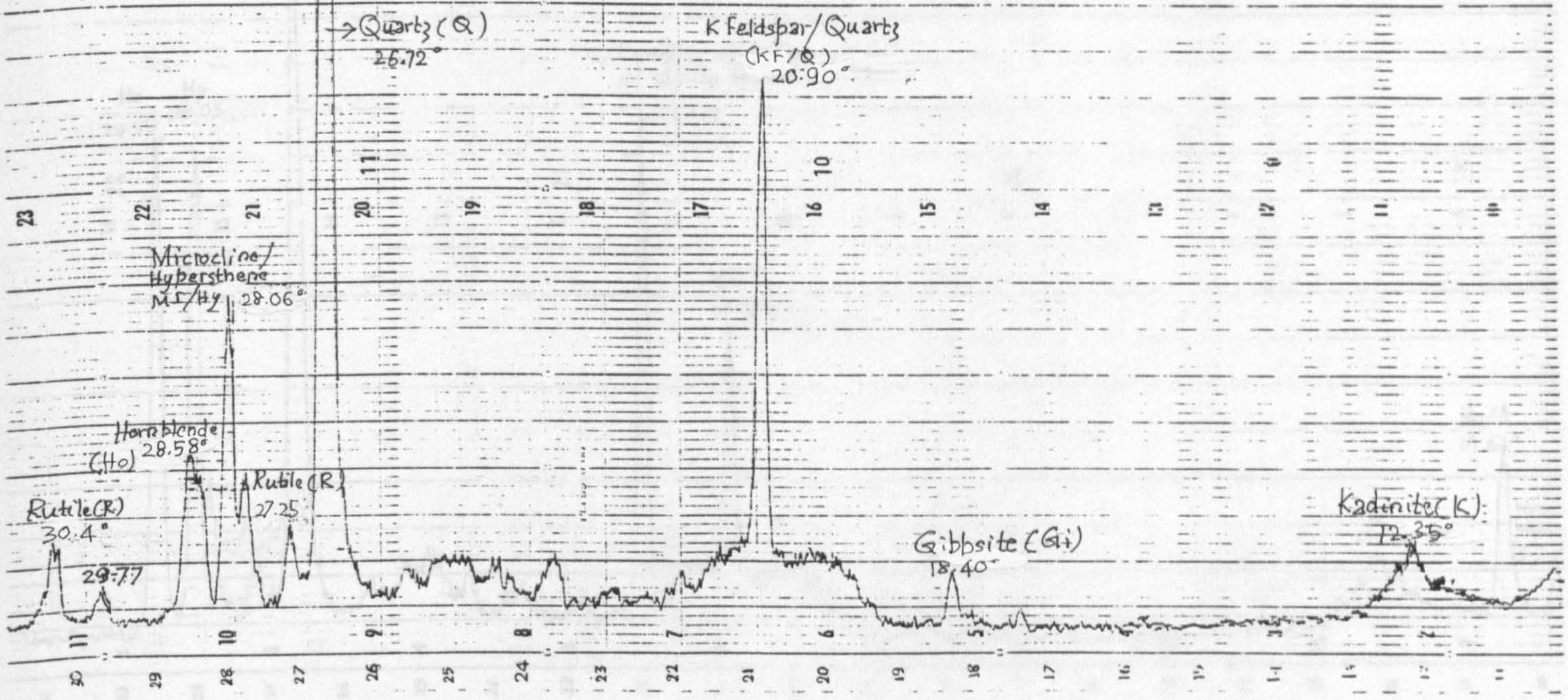

LSK2A (Raw) treated with 1M phosphate (Eq. pH = 3.1)

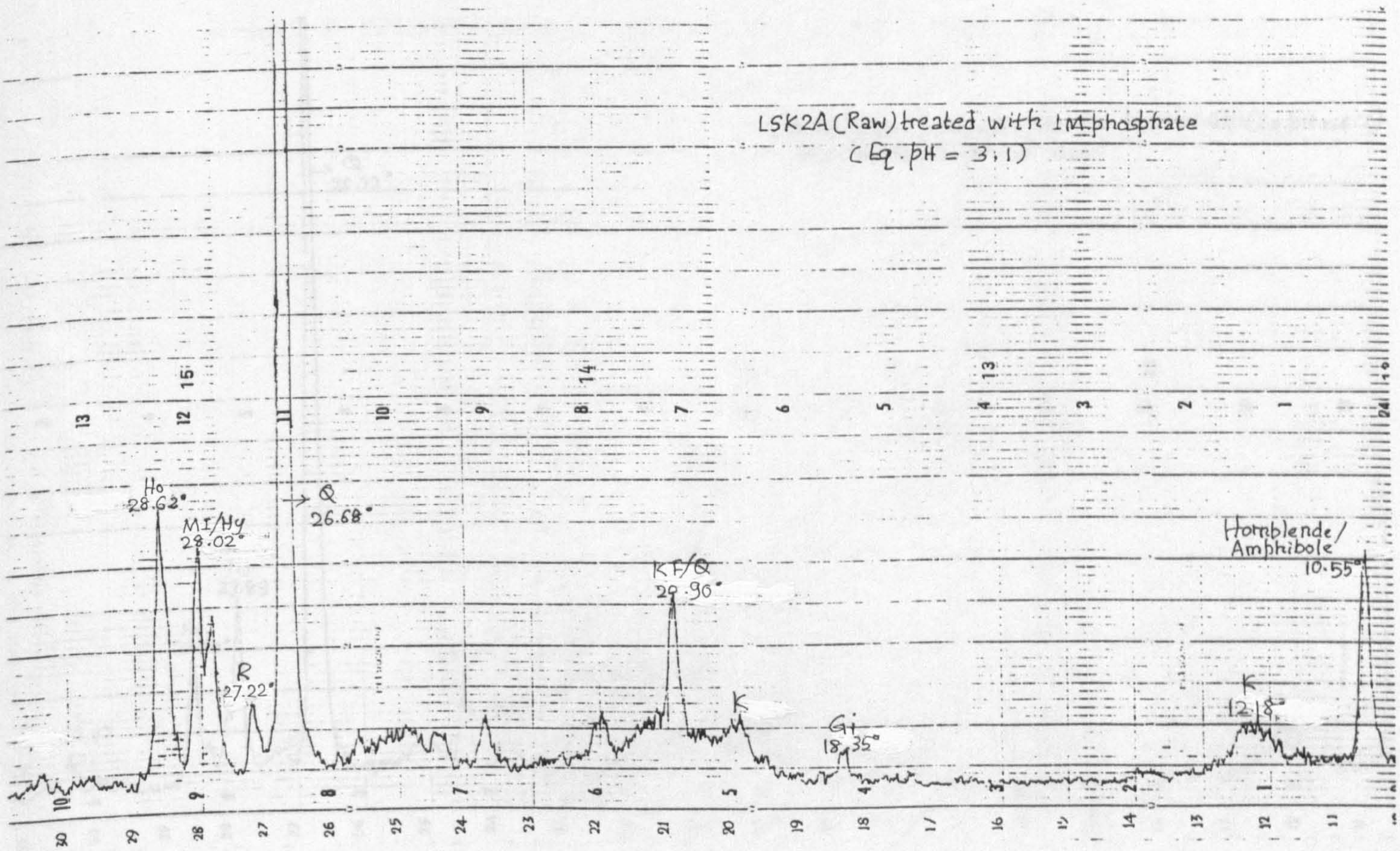

APPENDIX 10

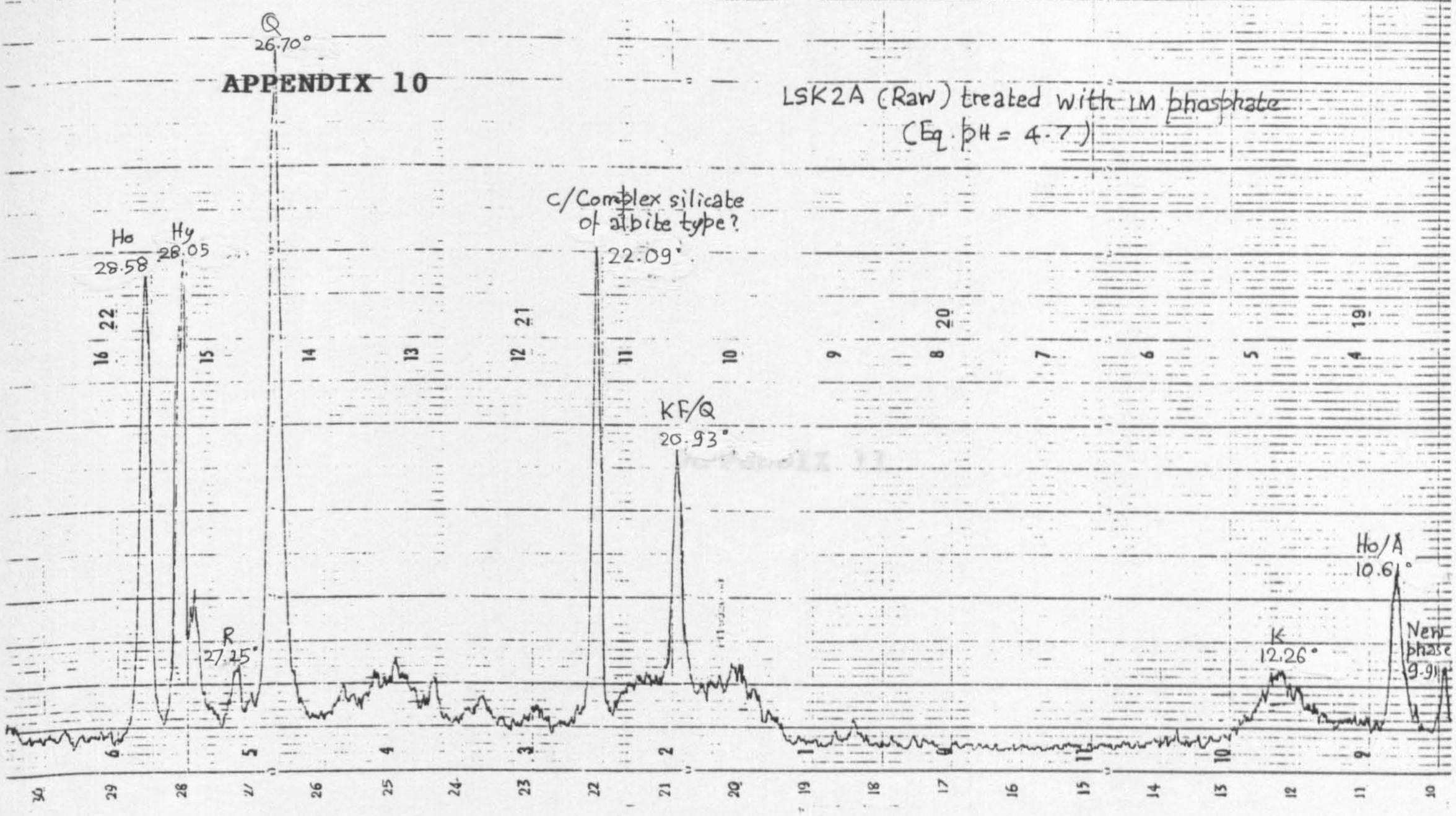
LSK2A (Raw) treated with 1M phosphate (Eq. pH = 4·7)
Q 26·70°
Ho 28·58
Hy 28·05
c/Complex silicate of albite type?
22·09°
KF/Q 20·93°
R 27·25°
Ho/A 10·61°
K 12·26°
New phase 9·91°

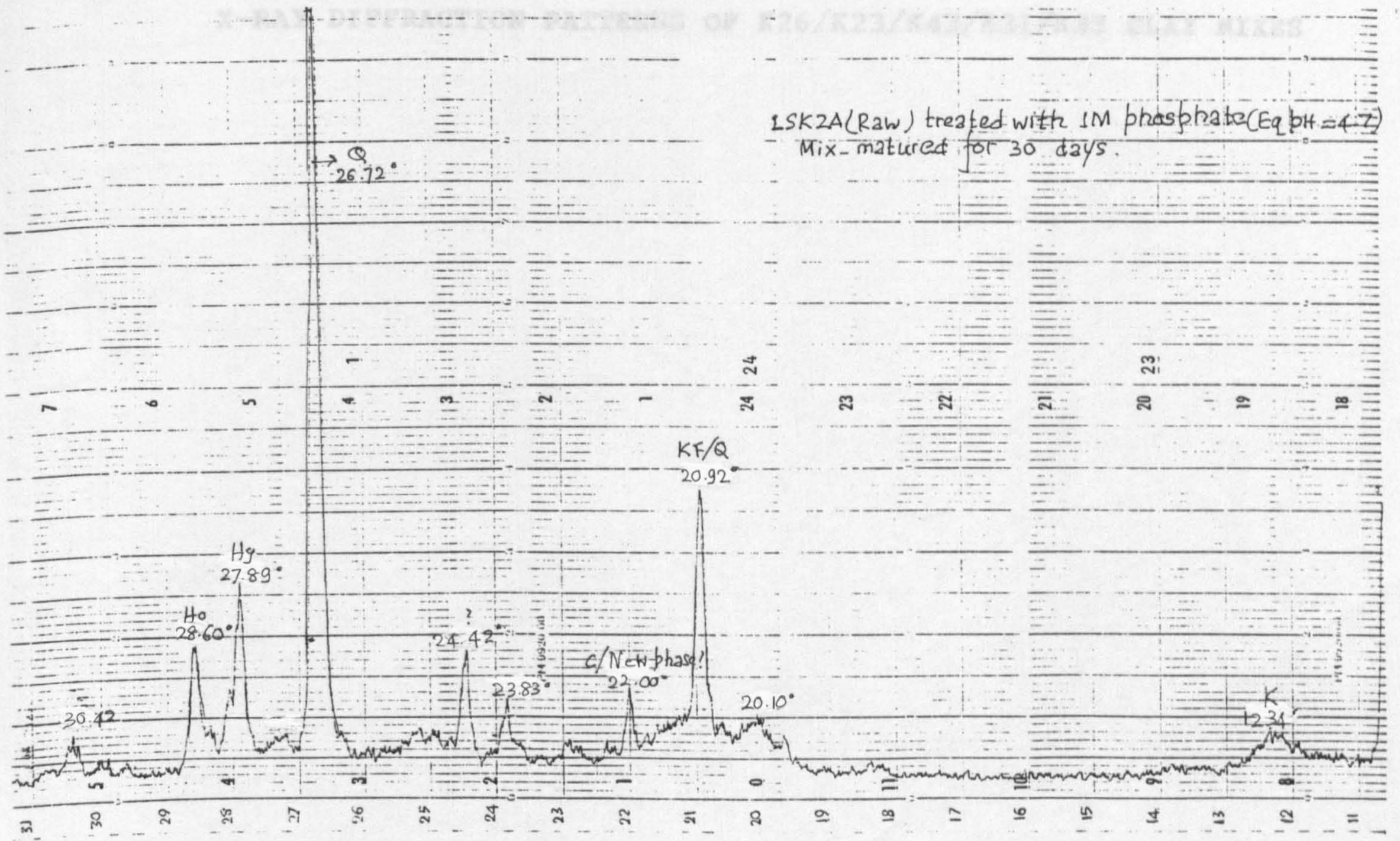
LSK2A(Raw) treated with 1M phosphate(Eq pH=4·7) Mix-matured for 30 days.
Q 26·72°
Hy 27·89°
Ho 28·60°
30·42
24·42°
23·83°
c/New phase? 22·00°
KF/Q 20·92°
20·10°
K 12·31°

APPENDIX 11

X-RAY DIFFRACTION PATTERNS OF K26/K23/K43/K31/K33 CLAY MIXES

APPENDIX 11

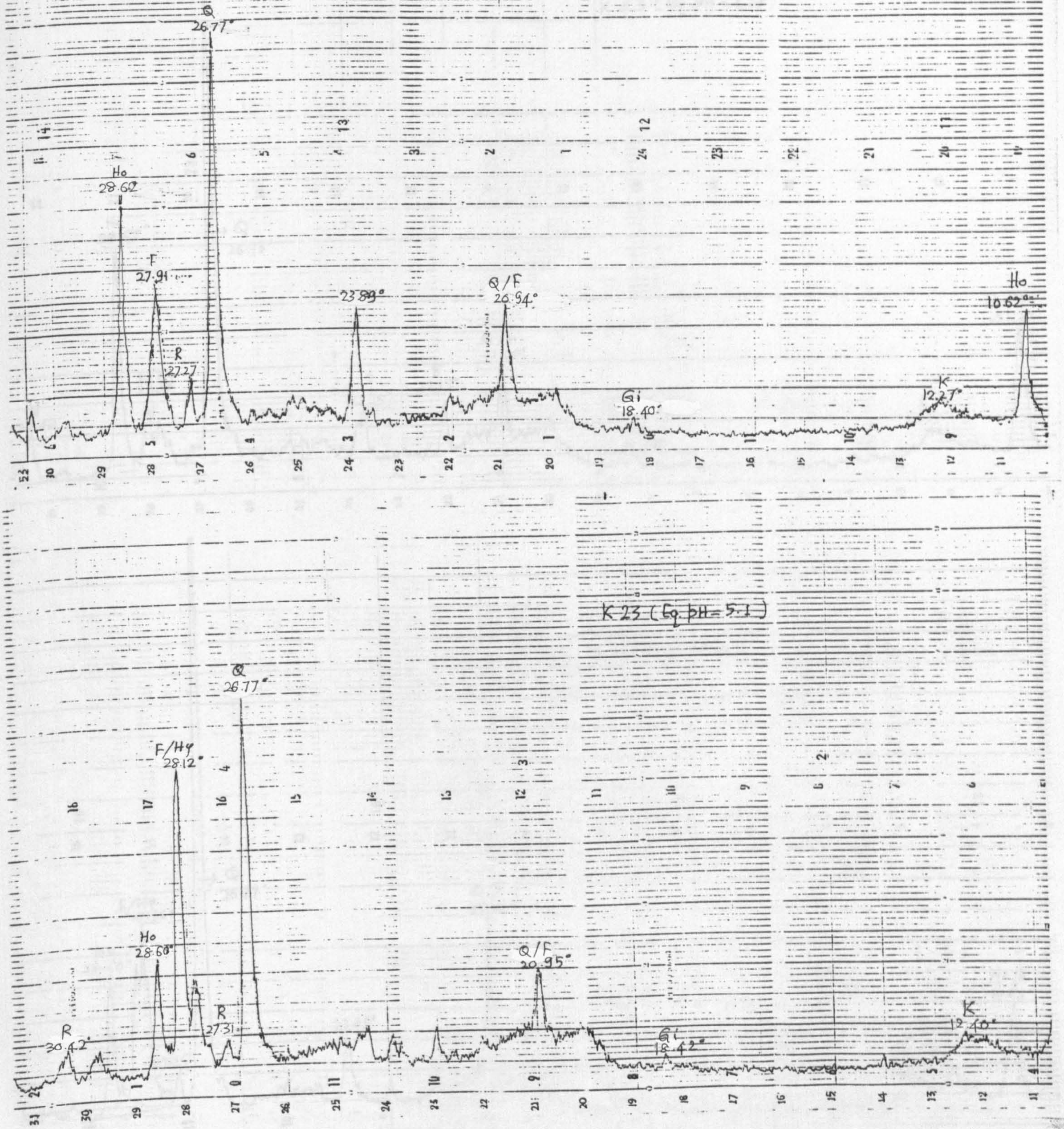
K 26 (Eq. pH = 6.6)
Q
26.77°
Ho
28.62°
F
27.91°
R
27.27°
23.89°
Q/F
26.94°
Gi
18.40°
Ho
10.62°
K
12.27°
K 23 (Eq. pH = 5.1)
Q
26.77°
F/Hq
28.12°
Ho
28.60°
R
30.42°
R
27.31°
Q/F
20.95°
Gi
18.42°
K
12.40°

APPENDIX 11

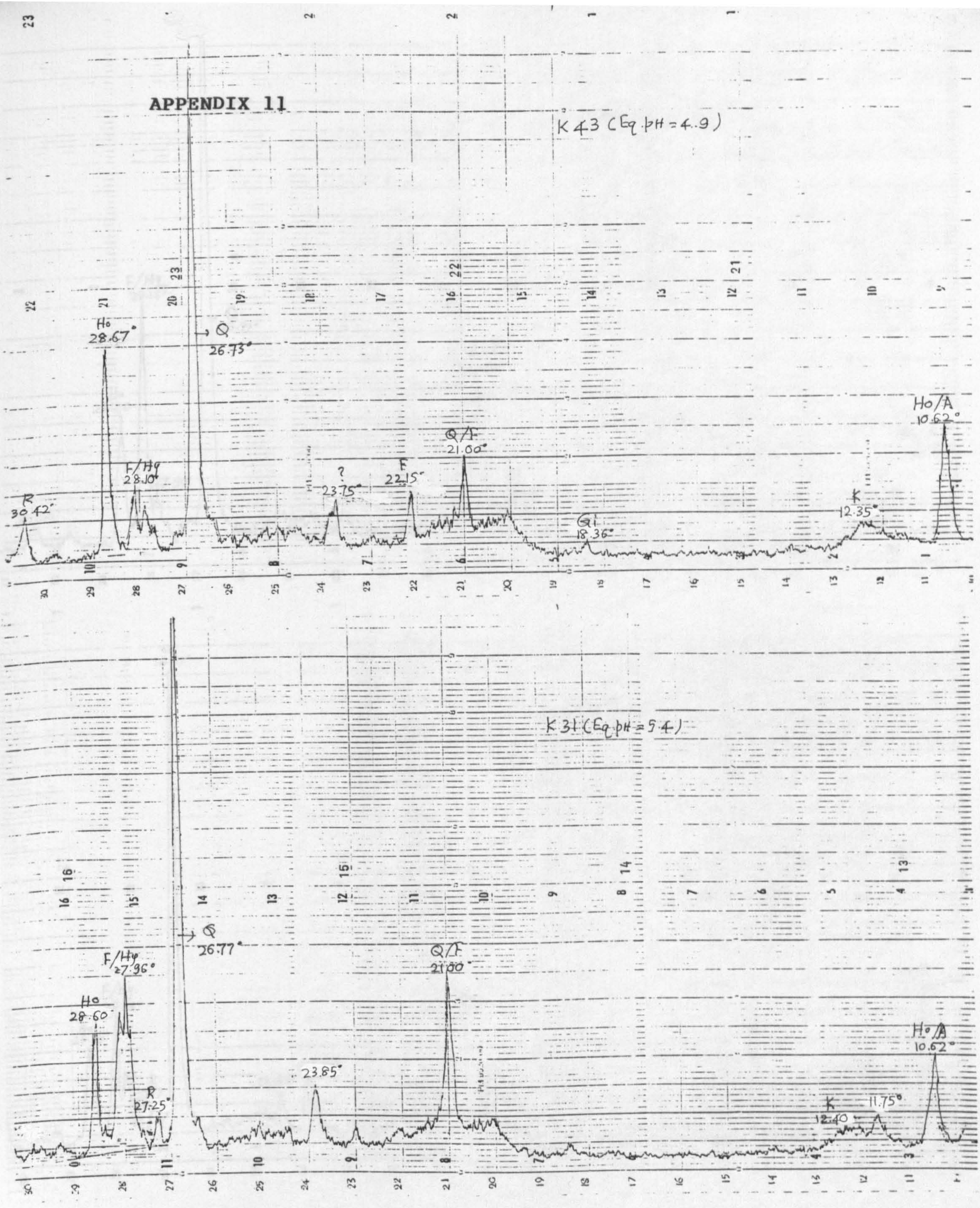
K43 (Eq pH = 4.9)
Ho
28.67°
Q
26.73°
F/Hg
28.10°
R
30.42°
?
23.75°
F
22.15°
Q/F
21.00°
G1
18.36°
K
12.35°
Ho/A
10.62°
K31 (Eq pH = 5.4)
F/Hg
27.96°
Ho
28.60°
R
27.25°
Q
26.77°
23.85°
Q/F
21.00°
K
11.75°
12.40°
Ho/A
10.62°

APPENDIX 11

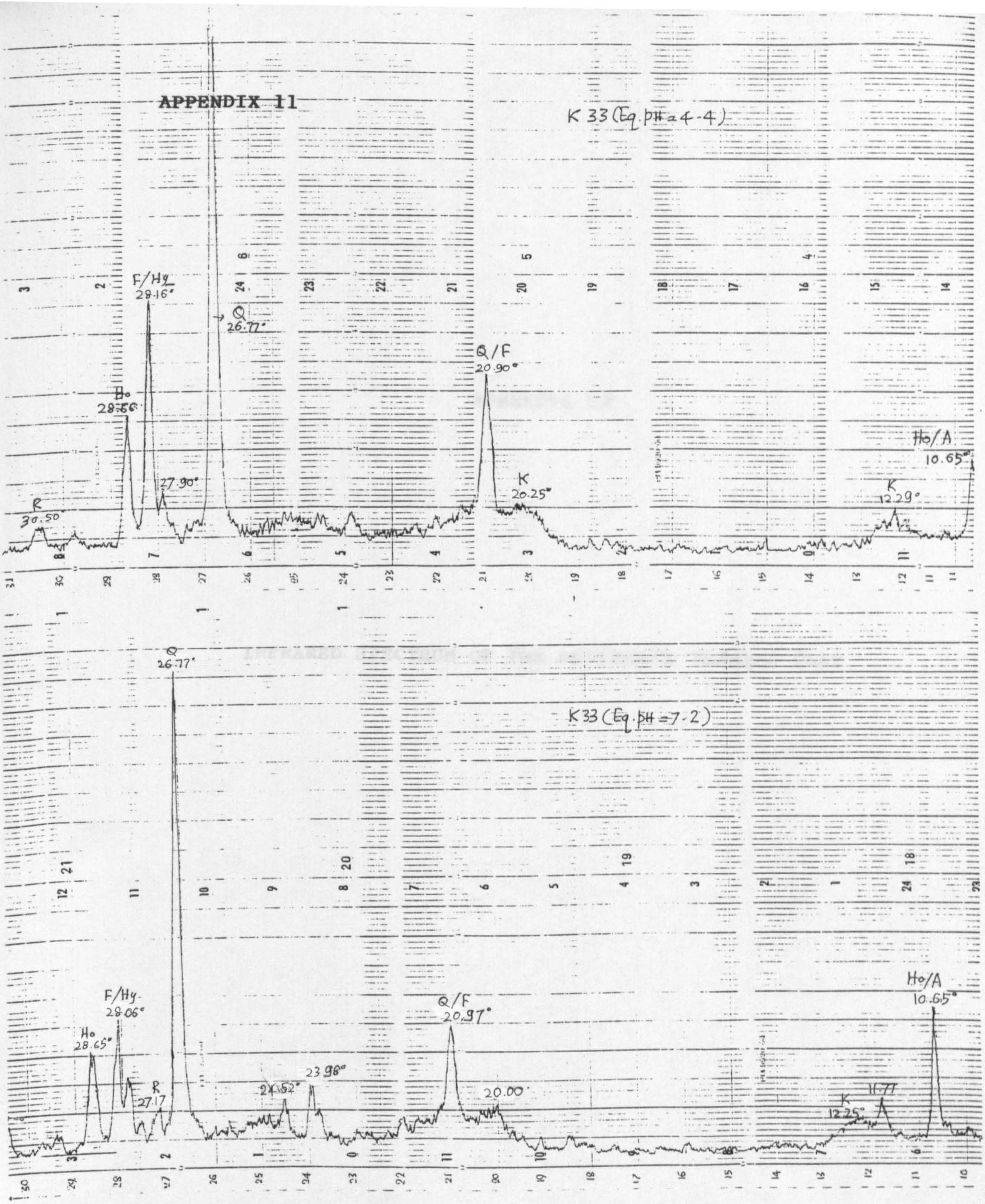
K 33 (Eq. pH = 4-4)
F/Hy
28.16°
Q
26.77°
Ho
28.56°
27.90°
R
30.50°
Q/F
20.90°
K
20.25°
Ho/A
10.65°
K
12.29°
K 33 (Eq. pH = 7-2)
Q
26.77°
F/Hy
28.06°
Ho
28.65°
R
27.17°
24.52°
23.98°
Q/F
20.97°
20.00°
K
12.25°
Ho/A
10.65°

APPENDIX 12

INFRARED SPECTRUM OF THE PHOSPHATE TREATED CLAY

K17


Halloysite / Amorphous material
79.8
790
Quartz
770
P-O-H
685
Biotite
18μm
810
Kaolinite
530
Chlorite - Mica/
Muscovite
465
Quartz
Kaolinite
90
80
70
60
50
40
30
20
10
0
Transmission
2500
2000
1800
1600
1400
1200
1000
800
600
400
Unicam SP1100 Infrared Spectrophotometer
PYE UNICAM LTD CAMBRIDGE ENGLAND

APPENDIX 13

DSC CURVES OF THE PHOSPHATE TREATED CLAYS

Fig 1

DSC Normalization: kclay
Sample Weight: 8.641 mg
Tue Oct 03 22:27:19 1989
Clay K – (untreated)
(Normalized)

PERKIN-ELMER
7 Series Thermal Analysis System

DSC Normalization: k17
Sample Weight: 8.966 mg
Thu Oct 05 00:32:55 1989
Clay K17 treated
(Normalized)

APPENDIX 13

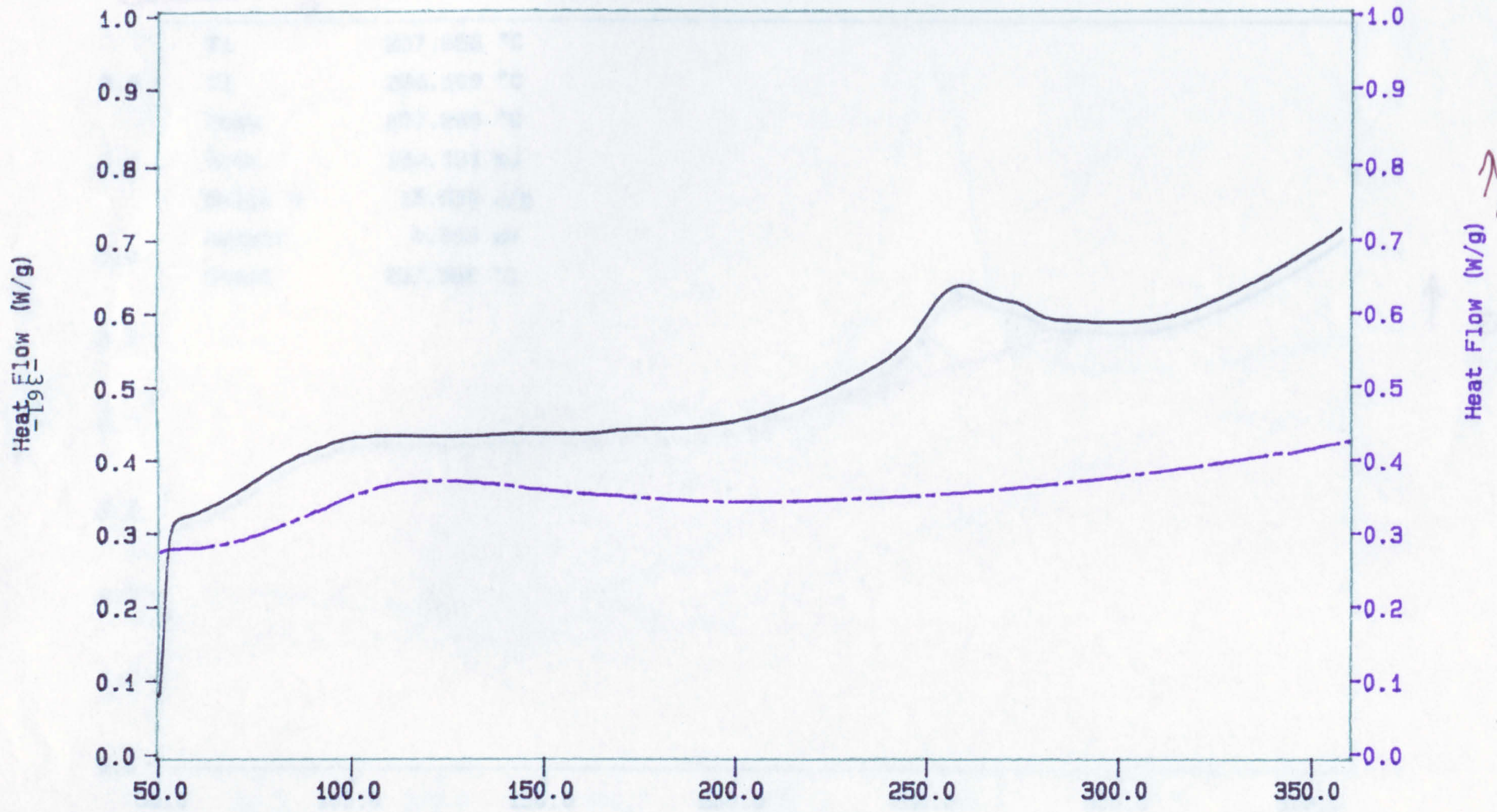

N2 purge gas 60cm3/min

TEMP 1: 50.0 C TIME 1: 2.0 min RATE 1: 10.0 C/min
TEMP 2: 710.0 C

TEMP 1: 45.0 C TIME 1: 2.0 min RATE 1: 10.0 C/min
TEMP 2: 710.0 C

Fig 2

DSC Data File: kclay
Sample Weight: 8.641 mg
Tue Oct 03 22:27:19 1989
Clay K (untreated)

PERKIN-ELMER
7 Series Thermal Analysis System

Calculation of Delta H (enthalpy) value

T1	207.666 °C
T2	286.100 °C
Peak	257.266 °C
Area	134.191 mJ
Delta H	15.530 J/g
Height	0.803 mW
Onset	237.522 °C

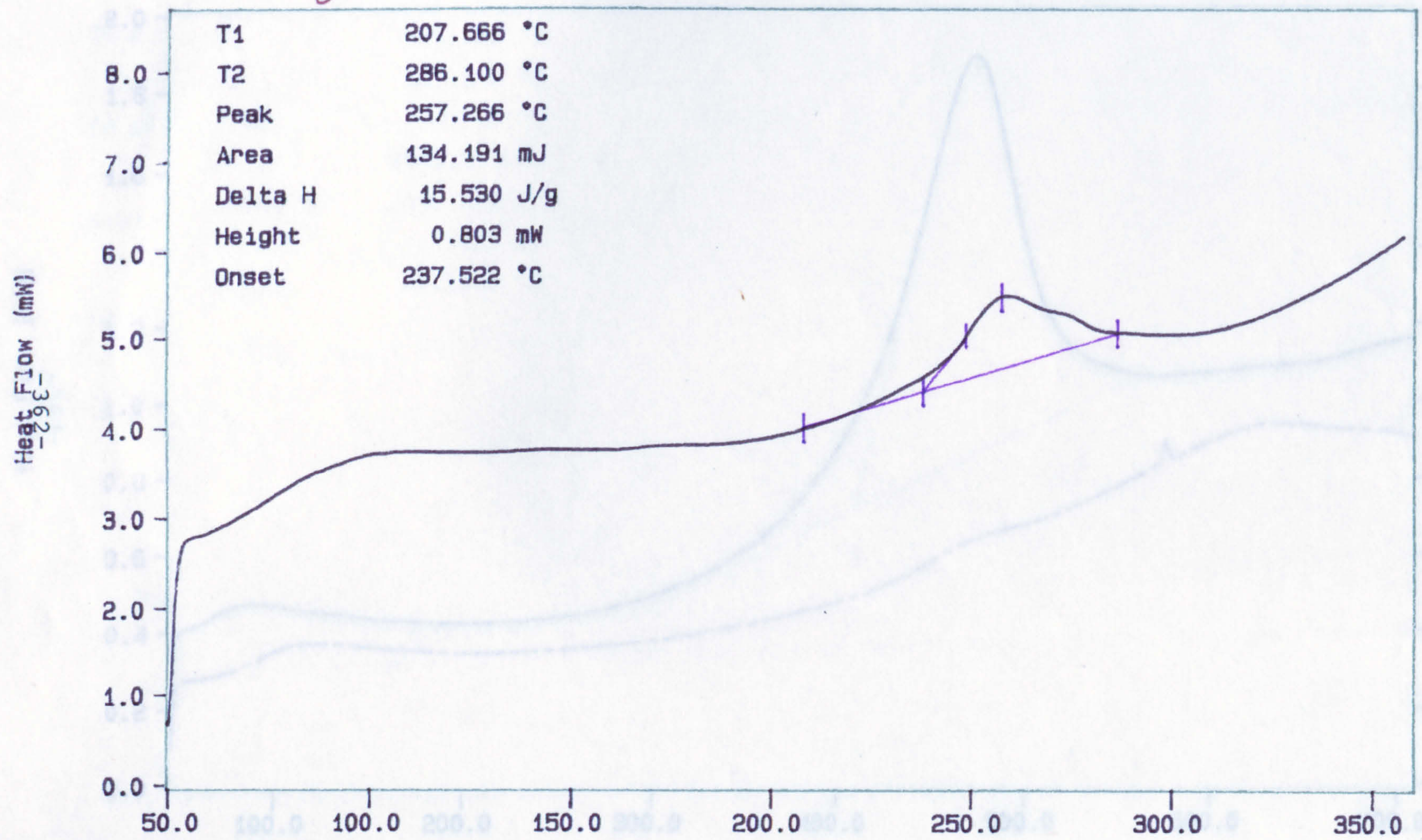

N2 purge gas 60cm3/min

TEMP 1: 50.0 C TIME 1: 2.0 min RATE 1: 10.0 C/min
TEMP 2: 710.0 C

APPENDIX 13

Fig3

DSC Normalization: k17
Sample Weight: 8.966 mg
Thu Oct 05 00:32:55 1989
Clay K17
(Normalized)

PERKIN-ELMER
7 Series Thermal Analysis System

DSC Normalization: clay2
Sample Weight: 8.059 mg
Wed Oct 04 19:39:24 1989
Clay K after heating to 357C in N2
(Normalized)

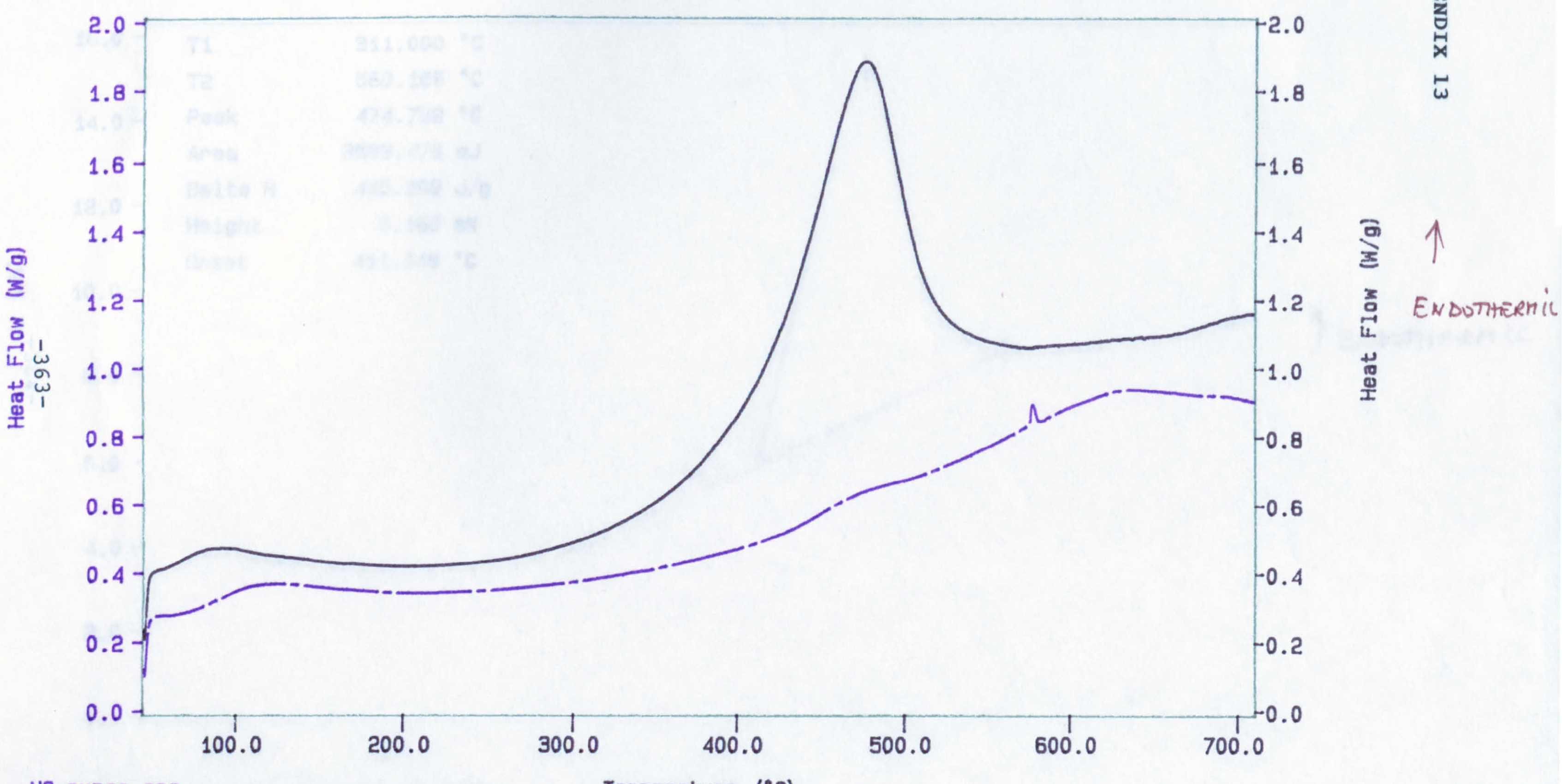

N2 purge gas

TEMP 1: 45.0 C TIME 1: 2.0 min RATE 1: 10.0 C/min
TEMP 2: 710.0 C

TEMP 1: 45.0 C TIME 1: 2.0 min RATE 1: 10.0 C/min
TEMP 2: 710.0 C

APPENDIX 13

↑ ENDOTHERMIC

Fig 4

DSC Data File: clay2
Sample Weight: 8.059 mg
Wed Oct 04 19:39:24 1989
Clay K after heating to 357C in N2

PERKIN-ELMER
7 Series Thermal Analysis System

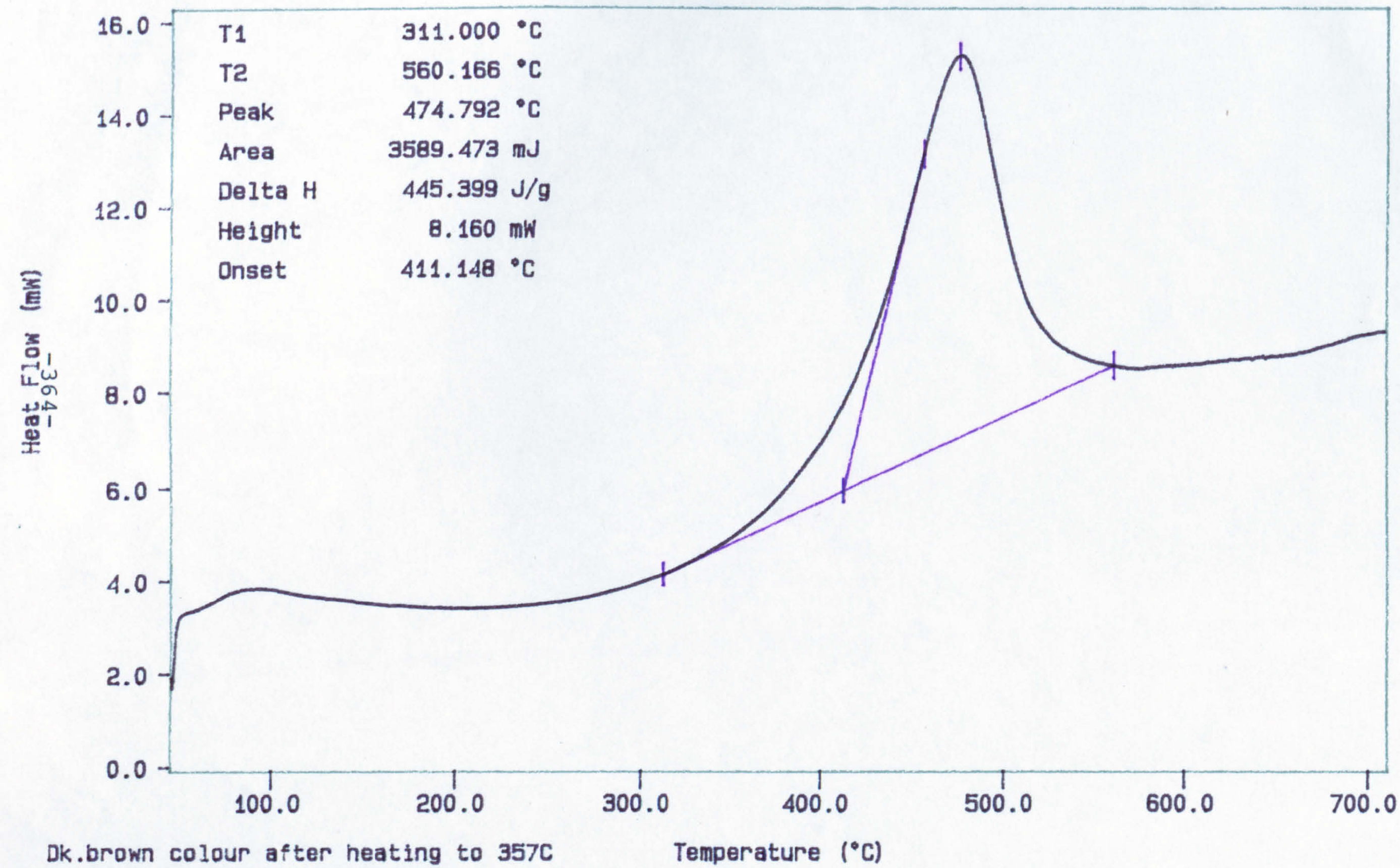

↑ ENDOTHERMIC

Dk.brown colour after heating to 357C

TEMP 1: 45.0 C TIME 1: 2.0 min RATE 1: 10.0 C/min
TEMP 2: 710.0 C

APPENDIX 13